BEST COPY

AVAILABLE

Variable print quality

PAGE
NUMBERS
CUT OFF
IN
ORIGINAL

PAGE NUMBERING AS ORIGINAL

PAGE

MISSING

IN

ORIGINAL

DYNAMIC RECRYSTALLISATION IN A MAGNESIUM ALLOY

A Thesis submitted for the degree of
Doctor of Philosophy of the University of London

by

Susan Elizabeth Burrows

Department of Metallurgy and Materials Science
Royal School of Mines
Imperial College of Science and Technology
London, SW7

October 1979

DIBL.
LONDIN.
UNIV.

ABSTRACT

The development of microstructure and texture in polycrystalline Magnox A180, deformed to high strains at low strain rates and high temperatures, has been followed using optical microscopy, X-ray goniometry and electron microscopy. Particular attention has been paid to the formation of dynamically recrystallised grains at the old grain boundaries during deformation and to the development of zones of heterogeneous high local strain (shear zones).

Specimens of the polycrystalline magnesium alloy have been deformed in uniaxial compression, in the temperature range 150-370^{o}C, at strain rates in the range 10^{-6}-$10^{-1}s^{-1}$, to strains between 0-94%. The effects of preferred orientation of the starting material and of temperature on the nature of the deformation have been studied in detail.

It has been found that at temperatures below 320^{o}C the deformation is very heterogeneous. Slip on the basal system and $\{10\bar{1}2\}$ twinning are important at low strains (< 16% ε at 260^{o}C). Lattice rotations which occur as a consequence of grain boundary constraints and limited slip and recovery lead to dynamic recrystallisation at the old grain boundaries, just before the peak in the stress-strain curve.

The envelopes of dynamically recrystallised grains which develop around the old grains as strain increases are texturally softer than the old grains and strain softening occurs as subsequent deformation is accommodated in the recrystallised bands. This results in heterogeneity on a macroscopic scale and the development of shear zones.

The microstructures of the deformed magnesium have been compared with those observed in naturally deformed minerals. Certain aspects of their deformation have been found to be common and it is suggested that in view of its anisotropy and heterogeneous deformation behaviour, magnesium is a more suitable metal for comparison with deformed minerals than the isotropic cubic metals previously referred to by geologists.

CONTENTS

	Page
Chapter 1. LITERATURE REVIEW	14
1.0. Introduction	15
1.1. Creep and Hot Working	15
1.1.1. Introduction	15
1.1.2. Deformation Mechanisms	19
1.1.2.1. Dislocation Glide	19
1.1.2.2. Recovery Creep	20
1.1.2.3. Diffusion Creep	22
1.1.2.4. Harper Dorn Creep	24
1.1.3. Microstructural Aspects of High Temperature Deformation	24
1.1.3.1. Dynamic Recovery	24
1.1.3.2. Dynamic Recrystallisation	25
1.1.3.3. Grain Boundary Sliding	34
1.2. Deformation of Magnesium	42
1.2.1. Introduction	42
1.2.2. Deformation Mechanisms	43
1.2.2.1. Twinning	43
1.2.2.2. Slip Systems	47
1.2.3. Creep of Magnesium	48
1.2.3.1. Dislocation Creep	48
a) Activation energies	49
b) Microstructural aspects of dislocation creep	50
1.2.3.2. Diffusion Creep	50
1.2.3.3. Grain Boundary Sliding and Cavitation	52

	Page
Chapter 2. EXPERIMENTAL TECHNIQUES	56
2.1. The Material	57
2.2. Mechanical Testing	58
2.3. Specimen Preparation	60
2.4. Colour Technique	60
2.5. X-ray Goniometry	62
2.6. Electron Microscopy	65
a) Transmission	65
b) Scanning	67

	Page
Chapter 3. RESULTS	68
3.1. Introduction	69
3.2. Mechanical Properties	69
3.2.1. Introduction	69
3.2.2. Stress-Strain Behaviour of Material Unfavourably Oriented for Basal Slip	73
3.2.3. Stress-Strain Behaviour of Material favourably Oriented for Basal Slip	78
3.3. Development of Microstructure with Increasing Strain	78
3.3.1. Introduction	78
3.3.2. Deformation of Samples Unfavourably Oriented for Basal Slip	80
3.3.2.1. Introduction	80
3.3.2.2. Microstructural Development at Low Temperatures	83
3.3.2.2.1. Optical microscopy at 150°C	83
3.3.2.2.2. Determination of the nature of the crystallographic features in the old grains using a Laue Back Reflection Technique	85
3.3.2.2.3. Electron microscopy	88
3.3.2.2.4. Macroscopic heterogeneous deformation	88
3.3.2.3. Microstructural Development at Intermediate Temperatures	95
3.3.2.3.1. General observations at 260°C	95
3.3.2.3.2. Microscopic heterogeneity on the grain scale	102
i) Behaviour in the cores	102
ii) Behaviour in the mantles	110
iii) The recrystallised grains	114
3.3.2.3.3. The orientation relationships between old and new grains	114
3.3.2.3.4. Heterogeneity of deformation on the bulk scale as determined from the microscopy of deformed polished surfaces	118
i) Optical microscopy	123
ii) Scanning electron microscopy	123
3.3.2.4. Microstructural Development at High Temperatures	128
3.3.2.4.1. General observations at 370°C	128
3.3.2.4.2. The observation of deformed polished surfaces to investigate the homogeneity of deformation at 370°C	132
3.3.2.5. Effect of Strain Rate on Microstructural Development	132

		Page
3.4.	Development of Texture with Increasing Strain	138
	3.4.1. Introduction	138
	3.4.2. Textural Development at 150°C	138
	3.4.3. Textural Development at 260°C	138
	3.4.4. Textural Development at 300°C	144
	3.4.5. Textural Development at 370°C	144
3.5.	Summary of Microstructural and Textural Development in Samples Unfavourably Oriented for Basal Slip	144
3.6.	Microstructural Development with Increasing Strain at 260°C in Material Favourably Oriented for Basal Slip	145
3.7.	Shear Zones in Magnesium	150
	3.7.1. Introduction	150
	3.7.2. Study of Shear Zones at 260°C	150
	3.7.2.1. Stress Strain Behaviour	150
	3.7.2.2. X-ray Goniometry	153
	3.7.2.3. Optical Microscopy	153
	3.7.2.4. Electron Microscopy	157
	3.7.3. Macroscopic Heterogeneous Deformation Due to the Operation of a Shear Zone	157
	3.7.4. Effect of Temperature on Shear Zone Development	161

	Page
Chapter 4. DISCUSSION	169
4.1. Introduction	170
4.2. Mechanisms of Dynamic Recrystallisation Reported in the Literature	170
4.3. High Temperature Deformation Behaviour	173
4.3.1. Homogeneous Nature of the Deformation	173
4.3.2. Mechanism of Dynamic Recrystallisation	173
4.4. Low Temperature Deformation Behaviour	177
4.4.1. Mechanical Properties	177
4.4.1.1. Effect of Temperature	177
4.4.1.2. Effect of Orientation	177
4.4.1.3. Estimation of Q and n from Mechanical Data	178
4.4.2. Twinning	180
4.4.3. Voids	181
4.4.4. Dynamic Recrystallisation	182
4.4.4.1. Microstructural Observations at low T	182
4.4.4.2. A Qualitative Model for Dynamic Recrystallisation below 320^{o}C	183
4.4.4.3. Experimental Evidence for the Model	188
4.4.4.4. Kinking	190
4.4.5. Shear Zones	194
4.4.5.1. Formation of Shear Zones	194
4.4.5.2. Strain Rate Acceleration in Shear Zones	196
4.4.5.3. Mechanisms of Deformation Within Shear Zones	197
4.4.5.4. Effect of Temperature	198
4.4.5.5. Effect of External Constraints	199

		Page
Chapter 5.	GEOLOGICAL IMPLICATIONS OF THE DEFORMATION BEHAVIOUR MAGNESIUM	202
5.1.	Introduction	203
5.2.	Calcite	205
	5.2.1. Introduction	205
	5.2.2. Single crystal studies	205
	5.2.3. Polycrystalline aggregates	206
	5.2.4. The effect of preferred orientation on the deformation of calcite	207
	5.2.5. Comparison between magnesium and experimentally deformed calcite	208
5.3.	Quartzite	210
	5.3.1. Introduction	210
	5.3.2. Single crystal studies	212
	5.3.3. Experimental deformation of quartz aggregates	213
	5.3.4. Microstructures of naturally deformed quartz aggregates	214
	5.3.5. Comparison between magnesium and naturally deformed quartzites	215
5.4.	Shear Zones	217
	5.4.1. Introduction	217
	5.4.2. Comparison of shear zones in magnesium with geological shear zones	221
	5.4.3. Shear zone development during in-situ deformation of camphor	222
5.5.	Paleo Stress Estimates	225
	5.5.1. Introduction	225
	5.5.2. Relationships commonly used in paleo stress estimates	225
	5.5.3. Estimation of the flow stress in magnesium using paleo stress techniques	228
5.6.	Conclusions	230

		Page
Chapter 6.	CONCLUSIONS	231
6.1.	Conclusions	232
6.2.	Suggestions for Further Work	232
	6.2.1. Magnesium	232
	6.2.2. Other Materials	233
BIBLIOGRAPHY		234
ACKNOWLEDGEMENTS		250
APPENDIXES		251
Appendix A	Analysis of Mechanical Data	252
Appendix B	Burgers Vector Analysis	253
Appendix C	Kikuchi Line Analysis	256
Appendix D	Experiments Carried Out on the Alloy Zr55	259
D.1.	Introduction	259
D.2.	The Material	259
D.3.	Experimental Methods	259
D.4.	Results and Discussion	260
	D.4.1. Low Temperature Behaviour	260
	D.4.2. High Temperature Behaviour	260
Appendix E	In-Situ Studies of the Deformation and Dynamic Recrystallisation of Rhombohedral Camphor	264
E.1.	Introduction	264
E.2.	The Material	264
E.3.	Experimental Methods	265
	E.3.1. Apparatus	264
	E.3.2. Specimen Preparation	265
	E.3.3. Reproducibility and Validity of the Tests	267
E.4.	Results and Discussion	267
	E.4.1. Low Temperature Tests	267
	E.4.1.1. Slip	267
	E.4.1.2. Kinking	270
	E.4.1.3. Deformation Twinning	270
	E.4.1.4. Dynamic Recrystallisation	272
	E.4.1.5. The Development of Microstructure with Strain	272
	E.4.2. High Temperature Tests	278
E.5.	Conclusions	281

LIST OF FIGURES

Figure 1.1. Schematic diagram of a deformation mechanism map.
Figure 1.2. Schematic diagrams of flow curves produced during creep and hot working.
Figure 1.3. Schematic diagrams of mechanisms of superplasticity.
Figure 1.4. Geometry of $(10\bar{1}2)$ twinning.
Figure 1.5. Geometry of double twinning mechanisms.

Figure 2.1. Partial phase diagram of the Mg-Al system.
Figure 2.2. Specimen orientation relationships.
Figure 2.3. X-ray goniometry of starting material.
Figure 2.4. Schematic diagram of electropolishing bath.

Figure 3.1. Table of results from mechanical tests.
Figure 3.2. Graph of yield stress vs. temperature.
Figure 3.3. Graph of stress strain curves at 3 temperatures for samples unfavourably oriented for basal slip.
Figure 3.4. Table for basal slip of peak stress vs. temperature.
Figure 3.5. Table of peak stress vs. strain rate.
Figure 3.6. Graph of log peak stress vs. log strain rate.
Figure 3.7. Table of Q and n values.
Figure 3.8. Graph of stress strain curves for samples favourably oriented for basal slip.
Figure 3.9. Schematic diagram to illustrate the development of microstructure with increasing strain.
Figure 3.10. Micrograph of initial microstructure.
Figure 3.11. Microstructure after 10% ε at $150^{o}C$.
Figure 3.12. Microstructure after 22% strain at $150^{o}C$.
Figure 3.13. Macroscopic view of a specimen deformed 22% at $150^{o}C$
Figure 3.14. Crystallographic features visible under polarised light.
Figure 3.15. Laue back reflection photograph to determine the nature of the crystallographic features.
Figure 3.16. Electron micrograph of twins at $150^{o}C$.
Figure 3.17. Electron micrograph of substructure at $150^{o}C$.
Figure 3.18. Microstructure after 55% strain at $150^{o}C$.
Figure 3.19. Shadow masks illustrating the macroscopic heterogeneity at $150^{o}C$.
Figure 3.20. Microstructure after 2% strain at $260^{o}C$.
Figure 3.21. Microstructure after 8% strain at $260^{o}C$.

Figure 3.22. Colour micrograph at 8% strain.
Figure 3.23. Electron micrograph of a twin at 260°C.
Figure 3.24. Microstructure after 14% strain at 260°C.
Figure 3.25. Microstructure after 16% strain at 260°C.
Figure 3.26. Optical determination of the misorientation in the mantles.
Figure 3.27. Duplex microstructures at 35 and 47% strain.
Figure 3.28. Microstructure at 55% strain.
Figure 3.29. Colour metallograph illustrating optical strain features.
Figure 3.30. Electron micrograph of Core and Mantle structure.
Figure 3.31. Electron micrograph of elongated subgrains in the cores.
Figure 3.32. 'Picket fence' sub-boundary.
Figure 3.33. Subgrain widths and misorientations in the cores.
Figure 3.34. Electron micrograph to illustrate lattice bending.
Figure 3.35. Electron micrograph to illustrate grain boundary bulging.
Figure 3.36. Electron micrograph to illustrate lattice rotations at the old grain boundaries.
Figure 3.37. Lattice misorientations in the mantles.
Figure 3.38. Electron micrograph of substructure within the recrystallised grains.
Figure 3.39. Series of colour micrographs of a specimen deformed 20% at 230°C.
Figure 3.40. do. 20% at 300°C.
Figure 3.41. do. 55% at 230°C.
Figure 3.42. do. 55% at 300°C.
Figure 3.43. Surface deformation at 260°C.
Figure 3.44. Diagram to illustrate lattice rotations.
Figure 3.45. Behaviour of grids at a grain boundary.
Figure 3.46. Diagram of rotations in the region of the grain boundary.
Figure 3.47. Microstructure of specimen deformed 1.5% at 370°C.
Figure 3.48. Microstructure of specimen deformed 25% at 370°C.
Figure 3.49. Determination of misorientations across deformation band boundaries.
Figure 3.50. Microstructure of specimen deformed 55% at 370°C.
Figure 3.51. Surface deformation at 370°C.
Figure 3.52. Microstructure at a strain rate of 3×10^{-3} s^{-1}.
Figure 3.53. Quantitative determination of misorientation.
Figure 3.54. X-ray goniometry of starting material.
Figure 3.55. X-ray goniometry at 150°C.
Figure 3.56. do. 260°C.
Figure 3.57. do. 300°C.
Figure 3.58. do. 370°C.

Figure 3.59. Microstructure of material deformed 5% in an orientation favourable for basal slip at 260°C.
Figure 3.60. Microstructure at 10% strain.
Figure 3.61. Microstructure at 30% strain.
Figure 3.62. Microstructure at 70% strain.
Figure 3.63. Cross-section of a shear zone at 260°C.
Figure 3.64. Stress strain curves to compare samples with and without shear zones at 260°C.
Figure 3.65. X-ray goniometry of sample containing a shear zone.
Figure 3.66. Macroscopic view of a shear zone.
Figure 3.67. Schematic diagram of misorientations in a shear zone.
Figure 3.68. Electron micorgraphs of grains in a shear zone.
Figure 3.69. Electron micrograph of an old grain at the edge of a shear zone.
Figure 3.70. Colour metallograph illustrating a shear zone.
Figure 3.71. Schematic diagram to illustrate the behaviour of superimposed grids on a sample containing a shear zone.
Figure 3.72. Scanning electron micrographs of the surface of a sample containing a shear zone.
Figure 3.73. Internal microstructure of sample after the superimposed grid had been removed.
Figure 3.74. Specimen profiles over a range of temperatures.
Figure 3.75. Colour metallograph of fine recrystallised grains within a low temperature shear zone.
Figure 3.76. Macroscopic view of sample deformed 55%.

Figure 4.1. Micrographs illustrating in-situ observations of SIGBM in camphor.
Figure 4.2. Stress strain curves to illustrate effect of orientation on work hardening behaviour.
Figure 4.3. Orientation dependence of the flow stress.
Figure 4.4.)
Figure 4.5.) Schematic diagrams of the recrystallisation process.
Figure 4.6. Deformation of a model composite.
Figure 4.7. Schematic diagrams of kinking.
Figure 4.8. Schematic diagram of shear zone "initiation.
Figure 4.9.) Shadow masks of specimens deformed with PTFE as a lubricating
Figure 4.10.) material at the piston contacts.

Figure 5.25.1. Deformation of calcite.
Figure 5.25.2. Heterogeneity in deformed polycrystalline calcite.
Figure 5.35.1. Elongated subgrains in Mg and quartzite.
Figure 5.35.2. Micrographs illustrating undulatory extinction.
Figure 5.35.3. Dynamic recrystallisation at the old grain boundaries in quartzite and magnesium.
Figure 5.35.4. Duplex microstructures in quartzite and magnesium.
Figure 5.4.3.1. In-situ shear zone formation in camphor.

Figure B1 Burgers vector analysis.
Figure C1 Kikuchi line analyses.
Figure D1 Heat treated Zr55.
Figure D2 Deformed Zr55 (low temperature)
Figure D3 Micrographs of a shear zone in Zr55.
Figure D4 High temperature deformation of Zr55.

Figure E1 The deformation apparatus
Figure E2 Deformation sequence at 300K.
Figure E3 Deformation twinning at 293K.
Figure E4 Twinned microstructure after deformation at 319K.
Figure E5 Dynamic recrystallisation originating at deformation twins during deformation at 293K.
Figure E6 Dynamic recrystallisation at the old grain boundaries during deformation at 310K.
Figure E7 Development of microstructure with increasing strain at 310K.
Figure E8 Deformation in the "High temperature" range at 335K, showing growth of elongated grains.
Figure E9 Schematic diagram of high temperature grain growth.

CHAPTER 1

Literature Review

1.0. INTRODUCTION

In spite of the large amount of literature published on the hot deformation of metals, very few serious attempts have been made to systematically characterize microstructures with increasing strain. Whilst the behaviour of fcc and bcc metals during creep and hot working is well documented, if not well understood, there is little relevant data concerning metals of lower structural symmetry. As part of a current research programme into plastic deformation and in particular dynamic recrystallisation, a study of the deformation behaviour of a polycrystalline magnesium alloy has been undertaken to try and ascertain some of the mechanisms responsible for the accommodation of deformation during experiments at elevated temperatures in this hexagonal metal.

Firstly a general review of creep and hot working will be presented, followed by a review of the deformation characteristics of magnesium at elevated temperatures.

1.1. CREEP AND HOT WORKING

1.1.1. Introduction

There are a number of reviews which cover the broad aspects of creep deformation, (Garafalo 1965; Weertman 1968, 72, 75; Sherby and Burke 1968; Lagneborg 1972; Mukherjee 1975; Takeuchi and Argon 1976). Normally, creep is the name applied to a slow strain rate, $\dot{\varepsilon} \sim 10^{-10} - 10^{-4}\ s^{-1}$, deformation at constant stress, or for practical situations, constant load, and elevated temperatures (McQueen and Jonas 1975). Strain hardening is slow and is accommodated at low stresses by recovery processes, leading to a steady state deformation after strains of a few percent. A steady state can also be reached in hot working where the strain hardening may be balanced by dynamic recrystallisation as well as dynamic recovery. Hot working usually refers to a high, constant strain rate deformation, $\dot{\varepsilon} \sim 10^{-4} - 10^{3}\ s^{-1}$ at high temperatures ($\gtrsim$ 0.5 Tm) and recrystallisation tends to occur more often in this situation as recovery processes cannot keep pace with the deformation. To some extent recovery and recrystallisation can be considered to be competing processes, the driving force for both being a reduction in the intracrystalline strain energy. In the current work, the strain rates used are in the main within the creep range, although the mode of deformation is constant strain rate rather than constant stress.

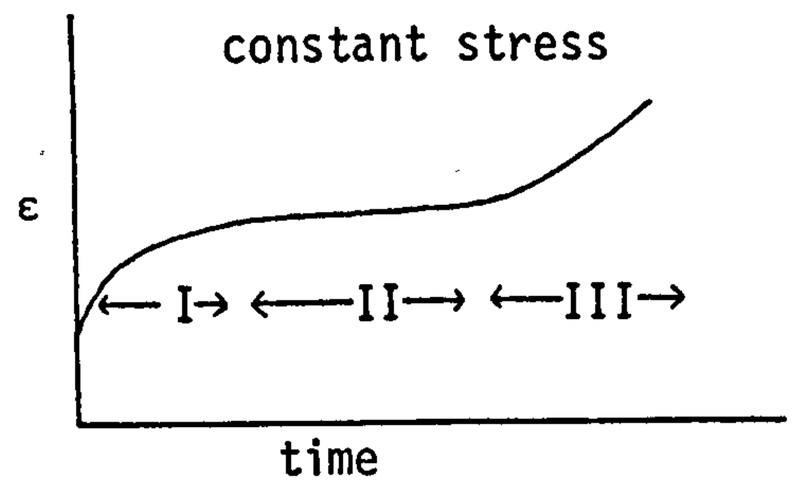
The strain energy built up in the initial stages of deformation can be relieved in more than one way.

a) If deformation is halted and the material annealed, then the strain is relieved by static recovery or static recrystallisation.

b) If the temperature of deformation is high enough then the material may dynamically recover or dynamically recrystallise, i.e. the processes whereby strain is relieved take place as deformation continues.

It is the dynamic restoration processes which are the concern of the current work and which occur in creep and hot working in general. However, since many of the theories advanced in the literature, particularly for recrystallisation, have been formulated from static studies, these will be reviewed where necessary as well as those involving dynamic processes.

Creep is normally divided into 3 stages as shown schematically in a typical creep curve below:



I. Primary creep

This is the first part of the creep curve and it can occur in the absence of thermal activation (Honeycombe 1968). During primary creep high densities of tangled dislocations are produced by interacting glide systems and work hardening exceeds recovery.

II. Secondary creep

This type of creep only takes place when the temperature is high enough to enable dynamic restoration processes to occur. It is often referred to as steady-state creep because the work hardening rate is zero. Work hardening is counterbalanced by recovery.

III. Tertiary creep

Tertiary creep occurs just prior to specimen failure. In a constant stress tensile test, it represents a region of rapidly increasing strain rate which finally ends in creep rupture. Voids which form at

the grain boundaries extend as grain boundary sliding occurs leading to intergranular creep fracture.

It is the secondary creep regime which will be examined in detail, since the dynamic restoration processes which take place during this type of deformation enable large plastic strains to be accommodated. The microstructural changes which take place during secondary creep will be discussed, as will be the main theoretical arguments put forward to account for their origin. Many constitutive equations have been put forward to account for creep data, but as pointed out by Lubahn (1961), no equation has universal applicability. Recently, it has become common to represent data in the form of a deformation mechanism map and this will now be considered.

In metallic systems, the maps have been used to predict deformation mechanisms in engineering materials and the effect of strengthening mechanisms, as well as to study the effect of crystal structure and atomic bonding on plastic flow and assist in the identification of missing mechanisms.

Plastic flow in crystalline solids is accommodated by a number of different mechanisms viz dislocation glide, dislocation creep, diffusional flow, mechanical twinning, grain boundary sliding, and by combinations of these mechanisms. Each mechanism is capable of allowing steady state flow and to a first approximation can operate independently of the others. Each may accommodate the strain over a particular range of stress and temperature (Frost and Ashby 1975, Ashby 1972). This behaviour can be represented by deformation mechanism maps which display fields of stress and temperature over which a particular mechanism is dominant for a given grain size. The maps are plotted on normalised axes - normalised shear stress σ/μ and homologous temperature T/Tm so that materials with the same crystal structure and bonding and in the same microstructural state are described by similar diagrams. Constant strain rate contours are superimposed on the fields so that the maps show the relationship between the 3 variables σ, T and $\dot{\varepsilon}$. Given 2 of these variables a map can be used to determine the third. The maps are constructed by using the equation relating stress, temperature and strain rate for each mechanism but require a great wealth of experimental data backed by sound theoretical models to define the predominant creep processes for any particular combination of σ, T and $\dot{\varepsilon}$. Another form of representation is to plot normalised grain size d/b against normalised stress σ/G for a particular temperature (Mohammed and Langdon 1974).

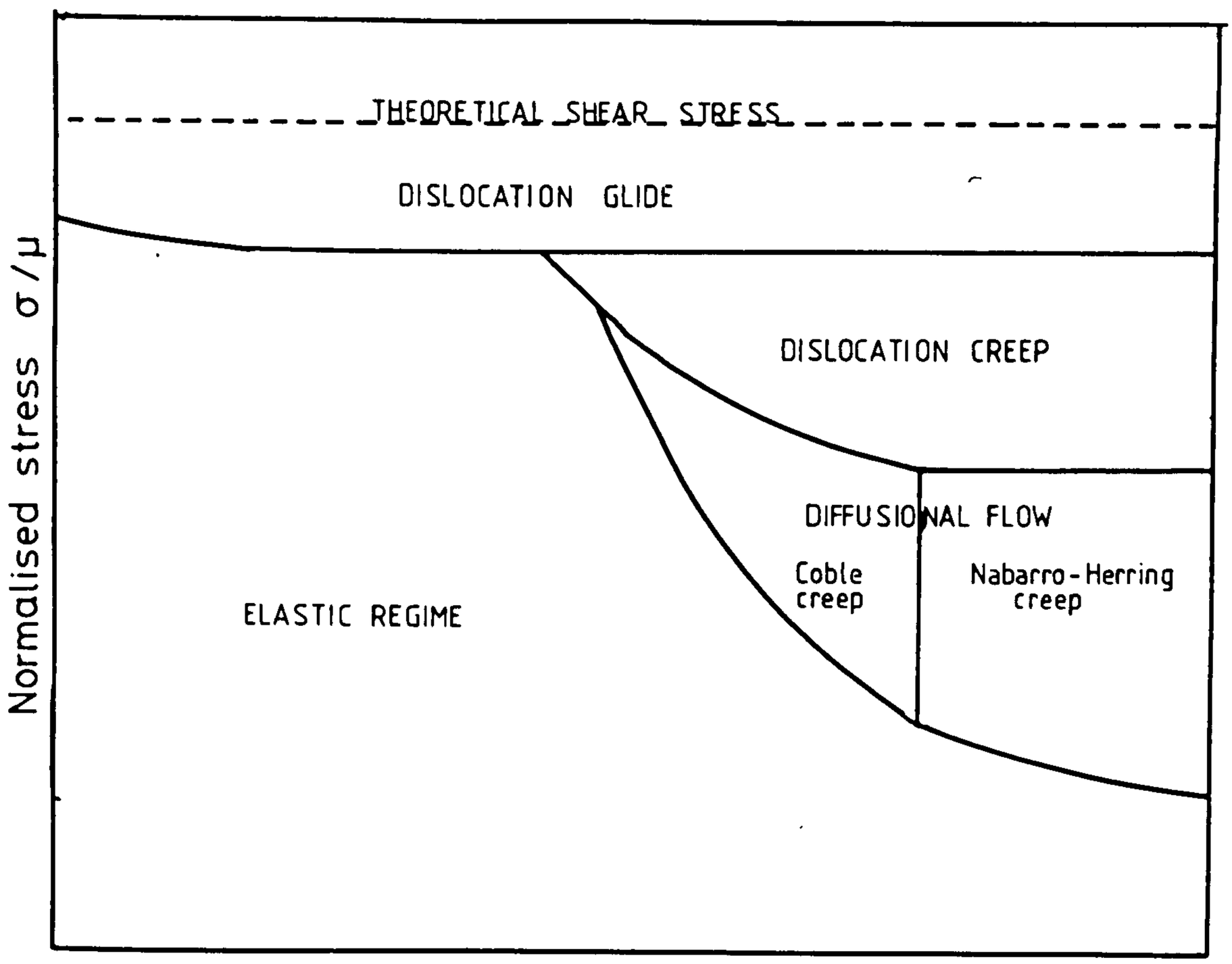


Figure 1.1 Schematic diagram of a deformation mechanism map (Ashby 1972).

In this case the map is divided into fields of grain size/stress space within which the creep behaviour is dominated by a single mechanism. It is necessary then to obtain constitutive equations for each of the possible creep processes. Therefore deformation mechanism maps are only as reliable as the data and model on which they are based. Another drawback is that the assumption is made that all mechanisms operate independently and the strain rates produced by each can be added together to produce the total resultant strain rate. The dominating mechanism at a given stress temperature point is the one which yields the greatest strain rate. In the centre of a field one particular mechanism usually dominates and experiment and theory fit well together. Near to boundaries the situation is not as clear cut and the behaviour observed suggests interaction between mechanisms. The maps are very microstructure dependent due to the very nature of the flow laws used to predict their boundaries, and they do not account for microstructural changes which occur as a result of straining.

A schematic diagram of a deformation mechanism map illustrating the usual mechanisms found in crystalline solids is shown in Figure 1.1. In spite of the reservations which must be attached to the interpretation of results from deformation mechanism maps they have produced valuable information in the past (Frost and Ashby 1975).

The mechanisms of dislocation glide, recovery creep, diffusion creep and Harper-Dorn creep will be summarized before microstructural aspects of high temperature deformation are examined in more detail. Other mechanisms such as mechanical twinning and in particular grain boundary sliding are known to play an important part in creep but they are not normally included on the deformation mechanism maps because of the lack of suitable rate equations to describe them. A further problem is that sliding is not an independent mechanism. It occurs in conjunction with either climb or diffusional creep, therefore attempts to treat it as an independent process result in an overestimation of the sliding contribution to the overall deformation (Langdon 1975). Sliding and grain boundary deformation will be reviewed in a separate section.

1.1.2. Mechanisms of deformation

I. Dislocation Glide

When an applied stress exerts a force on a dislocation and if there is a glide plane available, the dislocation will be able to move and propagate a shear strain on the slip plane. Dislocation glide is

limited by

a) The Peierls stress, which is the interaction between the crystalline lattice and a mobile dislocation and is an intrinsic property of the material.

b) Discrete obstacles, viz. point defects, impurity atoms, other dislocations and grain boundaries.

The mechanism is most important at temperatures less than 0.3Tm and the strain rate depends on the thermally activated motion of dislocations over these short range barriers.

The strain rate is proportional to the number of dislocations and their mean velocity and is described by the following equation put forward by Orowan (1947)

$$\dot{\varepsilon} = \rho b \bar{v}$$

$\dot{\varepsilon}$ = the strain rate

ρ = the density of mobile dislocations

b = the Burgers vector of the dislocations

$\bar{v}$ = the mean dislocation velocity.

II. Recovery Creep

Deformation in the recovery creep regime is possible at lower stresses than would be needed for glide alone because of the extra degree of freedom which allows dislocations to move out of their slip plane. Although dislocation creep usually occurs at temperatures above 0.5Tm, it may occur at lower temperatures if the strain rate is very slow.

The secondary creep rate of most metals and many solid solution alloys is controlled by the recovery of the dislocation substructure. Early models proposed to describe the processes taking place (e.g. Weertman 1968) were based mainly on the climb of edge dislocations and were of the general form

$$\dot{\varepsilon} = A \sigma^n \exp\left(-\frac{Q}{RT}\right)$$

$\dot{\varepsilon}$ = strain rate

A = a constant

σ = the applied stress

n = the stress exponent

Q = the activation energy for the creep process

R = universal gas constant

T = temperature in degrees absolute.

Dislocation climb is limited by the diffusion of vacancies to or from a dislocation thus the creep rate is proportional to the diffusion coefficient of the atoms.

$$\dot{\varepsilon} \alpha D = Do \exp - \frac{Q^{D*}}{RT}$$

where Q^{D*}= the activation energy for self diffusion

Do = a constant.

Since the creep rate is proportional to the diffusion coefficient then the activation energy for the creep process should be approximately equal to that for self diffusion.

As well as predicting that Q should equal Q^{D*}, the Weertman model also predicts that the stress exponent n should have a value of 3. The former relation has been verified for a number of pure metals and compounds, where the temperature dependence of creep at a given stress is nearly equal to the temperature dependence of self diffusion, but the correlation is not always obeyed especially in the case of some hcp metals (Sherby and Burke 1968). Magnesium has been shown to have 2 activation energies (Tegart 1961) so has zinc (Tegart and Sherby 1958). It is thought that two or more mechanisms of creep operate each one contributing separately to the creep process. Q has also been found to be stress dependent (Poirier 1978). The power dependence of the stress has been obtained empirically and found to be between 3 and 7 but no satisfactory explanation for a more exact value has been put forward. The power law theory breaks down at high stresses and the strain rate assumes an exponential dependence on stress. Another equation has been used to describe the data in both the power law and the breakdown region (Garafalo 1965)

$$\dot{\varepsilon} = A''(\sinh\alpha\sigma)^n$$

where A" and α are constant at constant temperature.

In this case there is only a gradual deviation from linearity at high stresses and no abrupt change in mechanism. Weertman (1975) attributed the breakdown of the power law theory at high stresses to the pile up of dislocations at points where dislocation climb occurred. This idea and an earlier model involving jog climb in screw dislocations (Barrett and Nix 1965) rely on the climb velocity being higher at higher stresses due to the excess vacancy concentration (Sherby and Burke 1968).

The major flaw in the recovery theories, which have been formulated for static recovery, is that they fail to correctly predict the value of the stress exponent n in the creep process. One suggestion is that

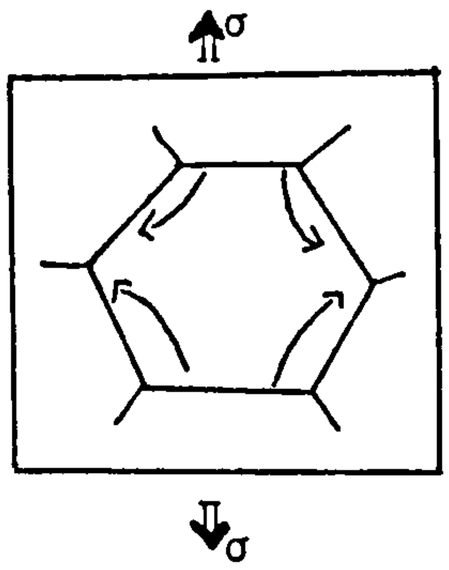
during steady state creep, recovery processes occur dynamically, i.e. recovery is accelerated by simultaneous glide of dislocations (Hausselt and Blum 1976) in which case the steady state stress exponent n and the activation energy Q will be averages of the glide and recovery-hardening parameters (Kocks 1975). Poirier (1978) has also cast doubt on the general acceptance that power law creep is diffusion controlled. The facts that n rarely has a value of 3 and Q has been found to be stress dependent together with the upward curve of the Arrhenius plot suggest the operation of parallel concurrent mechanisms, the one with the highest creep rate being dominant. Poirier intimated that although diffusion controlled climb may be important other mechanisms such as cross slip should not be ruled out. Thermally activated cross slip is a well known mechanism at intermediate temperatures (< 0.5 Tm) (Jaffe and Dorn 1962) and it is possible that.at high stresses the temperature where creep is diffusion controlled may be greater than 0.5Tm, i.e. at high stresses the behaviour would be similar to that found at lower temperatures and stresses (Lagneborg 1972).

Microstructural studies also support the view that the operation of one mechanism is an over simplification. For example, experiments on 316 stainless steel (Kestenbach et al 1978) and copper (Barrett 1965) resulting in the limited formation of substructure at high stresses support the idea that under these conditions climb occurs as a parallel mechanism to dislocation glide. In the steel most dislocations had not left their primary glide plane and sub-boundaries formed parallel to the glide planes. Kestenbach et al suggested that thermally activated cross slip and not diffusion controlled climb was the predominant recovery process.

III. Diffusion Creep

This type of creep occurs at high temperatures and low stresses and is due to a stress directed atom migration process rather than to dislocation motion and climb.

A creep model based on the stress directed migration of vacancies was developed by Nabarro (1948) and Herring (1950). It is now known as the Nabarro-Herring mechanism and is shown schematically below.



Under a tensile stress vacancies flow in the direction of the single arrows. Atoms flow in the opposite direction leading to grain elongation in the direction of the applied stress.

The type of creep relation obtained is

$$\dot{\varepsilon} = \frac{A\, D_V\, \sigma\, b^3}{KT\, L^2}$$

D_V = the lattice diffusion coefficient
L = the grain diameter
b^3 = the volume of a vacancy
σ = the applied stress
T = the absolute temperature
K = Boltzmann's constant
A = a constant

Thus the creep rate is proportional to the inverse of the diameter of the grains squared and is controlled by the diffusion of vacancies in the lattice. A fine grained specimen will creep faster than a coarse grained specimen.

A different type of diffusion creep was investigated by Coble (1963) who proposed a model whereby the creep rate was dependent on the inverse of the third power of the grain diameter and on the grain boundary diffusion coeffient $D_{g.b}$. The creep rate in this case was controlled by the diffusion of the vacancies in the grain boundaries.

$$\dot{\varepsilon} = \frac{A'\, D_{g.b.}\, \sigma\, b^3}{KT\, L^3}$$

A' = a constant.

Both the Nabarro-Herring and Coble equations imply that the strain rate is very grain size dependent. On a deformation mechanism map both these fields expand into the dislocation creep field as the grain size is decreased. Nabarro-Herring creep and high temperature dislocation creep have the same dependence on D_V and therefore the boundary between them is a line of constant stress. A similar relation exists between Coble creep and low temperature dislocation creep.

More sophisticated modifications of the above models have been proposed subsequently to account for experimental results (see e.g. Raj and Ashby 1971).

IV. Harper-Dorn Creep

This type of creep behaviour was first observed by Harper and Dorn in 1957 and has been reported in some metals and alloys at high temperatures and low stresses. It has a strain rate which is linearly dependent on the applied stress and independent of grain size; it also differs from normal diffusional processes in that the strain rate is several orders of magnitude higher than that predicted by the Nabarro-Herring model for a particular grain size. The activation energy for the process is close to that for self diffusion (Mohamed et al 1975). Harper-Dorn creep has been found in pure aluminium, silver, lead and tin (Barret et al 1972, Mohamed et al 1973, 1975). As yet, the details of the mechanism or mechanisms are not known: suggested mechanisms include:- glide of jogged screw dislocations (Harper et al 1958); Nabarro-Herring creep acting across subgrains (Friedel 1964); unsaturated climb of jogged screw dislocations (Burton 1972) and creep via climb of saturated dislocations (Mohamed et al 1975).

1.1.3. Microstructural aspects of high temperature deformation

1. Dynamic Recovery

The dislocations may begin to form a cell structure during the work hardening phase. The dislocation density is reduced by recovery processes involving the overcoming of barriers by cross slip and climb and by viscous glide. The remaining mobile dislocations migrate to form low energy configurations such as tilt and twist walls. Dynamic recovery takes place more readily in materials with a high stacking fault energy where cross slip and climb can occur more easily. By the time the secondary creep stage is reached, the substructure is well developed. The subgrain morphology, i.e. size, shape and misorientation, depends on the deformation conditions (Jonas et al 1969). Most work has been carried out on aluminium where it has been found that in the steady state regime the substructure is stable, i.e. has constant dimensions and density and is independent of strain (McQueen and Jonas 1975; Jonas et al 1969). The constant dislocation density is attributed to the attainment of dynamic equilibrium between dislocation generation and annihilation. Since the subgrains do not become elongated in compression tests, a process of repolygonisation, whereby sub-boundaries repeatedly unravel and

reform at sites which keep their average spacing and density constant, has been suggested to account for the way in which the grains reflect the overall macroscopic strain whilst the subgrains do not (McQueen, Wong and Jonas 1970). It is the formation of subgrains and their subsequent movements which dominate the microstructural changes occurring during recovery, although the exact mechanisms involved in subgrain formation are still not well established (Sherby et al 1977).

Subgrains are often associated with slip bands (Servi and Grant 1951) and grain boundaries are preferred nucleation sites for subgrains (Lytton et al 1965). It is well known that the subgrain size is empirically related to the steady state stress in the following way

$$\sigma_{ss} = \sigma_1 + k_1 d^{-1}$$

σ_1 = a constant
σ_{ss} = steady state stress
k_1 = a constant
d = the subgrain size
(Sherby and Burke 1968; Bird et al 1969; McQueen and Baudelet 1979).

The higher the stress, the smaller the subgrain size. Subgrains tend to be larger and more perfect at higher temperatures or lower strain rates (McQueen 1979). The determination of the subgrain size does present difficulties (Sherby et al 1977) as the subgrains are often difficult to detect optically and their size when measured by this method tends to be larger than the size measured in the TEM - this fact is well documented in the geological literature (White 1979). One point worth noting at this stage is that high temperature creep is highly structure sensitive and steady state creep theories rely on the attainment of a constant substructure whereas at 'steady state' the microstructure is likely to be in a state of flux.

2. Dynamic Recrystallisation

Most of the information available about dynamic recrystallisation has been obtained during the course of hot metal-working experiments (see e.g. McQueen and Jonas 1975, Sellars 1978, McQueen and Baudelet 1979) The following paragraphs deal with the important microstructural aspects of the process.

a) Materials which undergo dynamic recrystallisation

It is generally agreed that dynamic recrystallisation occurs in those metals in which dynamic recovery is limited, i.e. those which have a low

stacking fault energy, for example, Ni, Cu and austenitic steels. It had been stated that Al, Zn, Mg, Sn, low purity α-iron and ferritic steels do not undergo dynamic recrystallisation (Sellars 1978), but more recently it has been shown that some of these materials may exhibit the phenomenon if the conditions for its occurrence are favourable; for example in hot deformation of aluminium (Gardner and Grimes 1979) and as will be shown for magnesium.

At high temperatures the stability of a dislocation cell structure depends upon the recovery and recrystallisation characteristics of the material. Metals which show limited dynamic recovery tend to exhibit dynamic recrystallisation during creep and hot working. As dynamic recovery involves the occurrence of cross slip, climb and node unpinning, it therefore tends to take place more readily in materials with a high stacking fault energy. As the stacking fault energy is lowered, the separation between dislocation partials becomes wider and consequently cross-slip and climb are more difficult. The reported value of the s.f.e. of magnesium is high-300 ergs/cm^2 (Harris and Masters 1966)~125 MJ/m^2 (Sestak 1979) - a similar value to that found in aluminium of 130 MJ/m^2 - it therefore would be expected to fall into the class of materials which undergo dynamic recovery, but the fact that it is hexagonal and therefore has fewer slip systems may also prove to be an important consideration.

b) <u>The flow curve</u>

There are two types of curve usually referred to, viz. that at constant strain rate obtained during hot working and that at constant stress where the mode of deformation studied is creep. Schematic diagrams of these flow curves are shown in Figure 1.2. Curves plotted for constant strain rate give two results. At higher strain rates, the material strain hardens to a peak stress, dynamic recrystallisation leads to work softening and the curve reaches a steady state level where continuous dynamic recrystallisation results in stable flow. At low strain rates successive cycles of recrystallisation result in a periodic flow curve. (Fig. 1.2a).

In creep tests (Fig.1.2b) a rapid increase in strain rate accompanies the onset of dynamic recrystallisation. This terminates primary creep before the steady state deformation has been attained. A new stage of primary creep occurs after the acceleration; this is also likely to end with dynamic recrystallisation. The resulting stress-strain curve has a saw-tooth appearance but is not often observed.

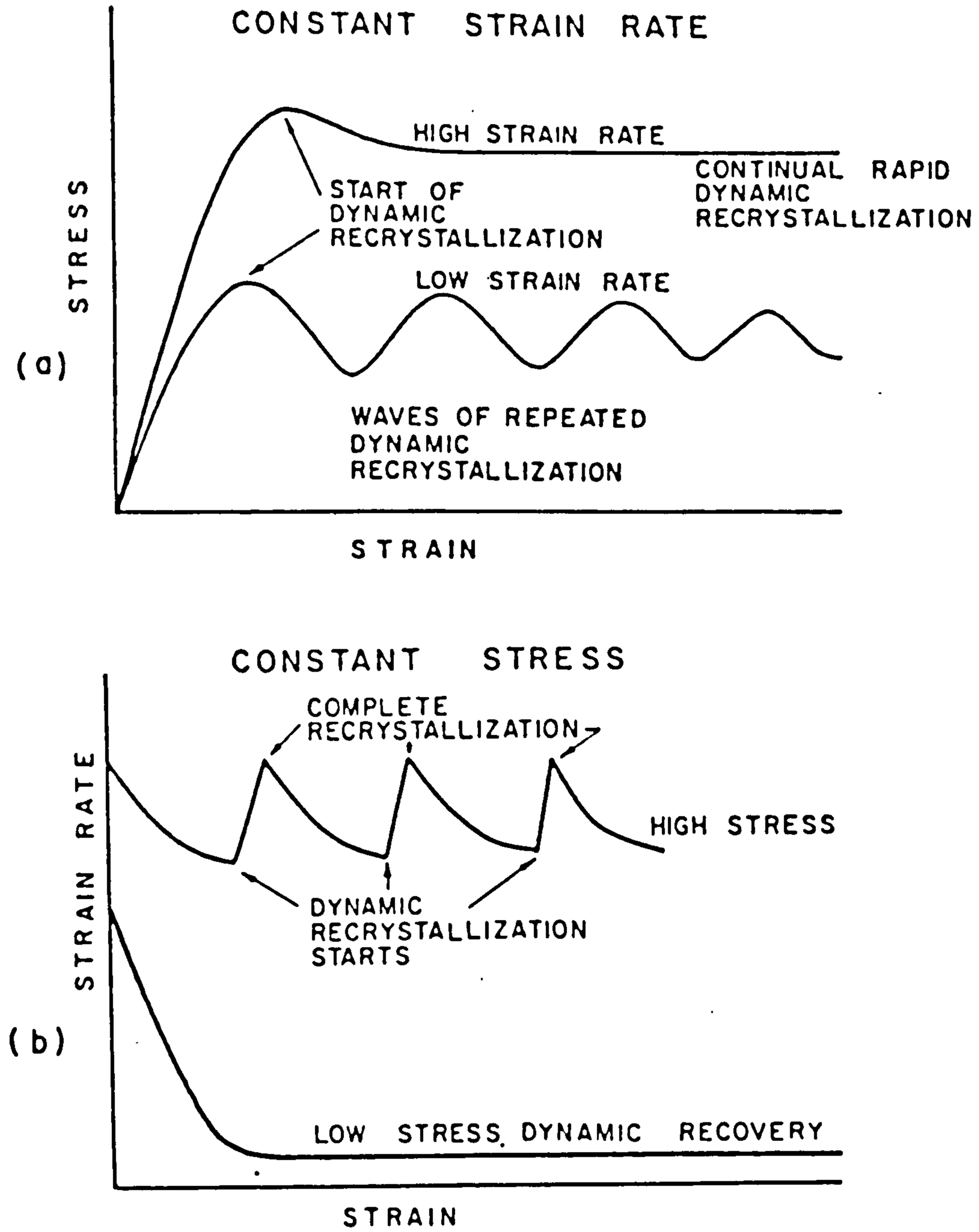


Figure 1.2 (after McQueen and Jonas 1975).
(a) Hot working at a slow rate leads to a cyclic stress strain curve caused by waves of recrystallisation. At high strain rates recrystallisation starts at higher strains causing the drop in stress after the peak.
(b) At low creep stresses tne amount of dynamic recovery is sufficient to keep the dislocation density below critical levels. At high stresses the substructure becomes so dense that recrystallised nuclei form and grow rapidly to engulf the whole specimen. The specimen then begins to creep at high rates as it did initially.

Richardson et al (1966) found that in studies of recrystallisation during creep of nickel the phenomenon occurred only at high stresses in the creep range at temperatures above 0.77 Tm.

Luton and Sellars (1969) explained the difference in stress/strain behaviour at high and low strain rates in terms of the relative values of the critical strain ε_c to cause dynamic recrystallisation and the strain required to recrystallise a large fraction of the material ε_x. They noticed a similarity between the curves at low strain rate and those for the critical strain to recrystallisation in creep (Richardson et al 1966) where the flow curve is periodic. Luton and Sellars stated that as recrystallisation proceeds, the flow stress in the material just recrystallised should drop to the critical yield stress, while the unrecrystallised material continues to work harden and the previously recrystallised material work hardens again. Thus, the distribution of dislocation substructures maintains the steady state value of the flow stress at a value intermediate between the yield stress of the statically annealed material and the peak stress; i.e. the balance between the rate of work hardening and the rate of recrystallisation determines the net stress/strain curve. As summarised by Roberts and Ahlblom (1978) at low $\dot{\varepsilon}$, $\varepsilon_x < \varepsilon_c$ and therefore, once recrystallisation is initiated it goes rapidly to completion before those regions which transformed initially can harden sufficiently to effect nucleation a second time. This results in a periodic stress/strain curve. On the other hand at high strain rates, then $\varepsilon_x > \varepsilon_c$ and several recrystallisation cycles can occur simultaneously resulting in a smooth stress strain curve. A more theoretical approach to this idea has been developed by Stuwe and Ortner (1974) in their review of recrystallisation in hot working and creep. They developed a model for recrystallisation and discussed the influence of the process on the stress strain curves at high strain rates and also the dependence of strain on time at low strain rates (and hence creep).

c) Onset of recrystallisation

Dynamic recrystallisation is initiated at a critical strain which is just below the strain corresponding to the peak in the stress strain curve. It is generally stated that the flow stress decreases as recrystallisation spreads through a specimen and is the result of the restored regions having a lower flow stress. The critical strain for the onset of recrystallisation is less than the strain at the peak stress because whilst the first nuclei are softening the material locally the

remaining material is still work hardening. Luton and Sellars (1969) showed that the critical strain for recrystallisation increases with increasing strain rate and decreasing temperature. This is attributed to the decreased rate of recovery and therefore nucleation at lower T (McQueen and Jonas 1975). Roberts and Ahlblom (1978) have developed a nucleation criterion for dynamic recrystallisation during hot working. One of their main conclusions is that the initiation of dynamic recrystallisation requires a critical dislocation density irrespective of whether dynamic recovery is occurring simultaneously or not. For high deformation temperatures and low strain rates, however, the stress/strain curves are rather flat. Gottstein et al (1979) suggested that since small deviations would cause a large scatter of strain at which a certain flow stress was reached, predictions based on ε_c for dynamic recrystallisation would be of limited use. They carried out tensile experiments on Cu single crystals and suggested dynamic recrystallisation is triggered off by a critical value of the flow stress rather than at a critical strain.

d) Sites

The most common sites for the nucleation of dynamically recrystallised grains are grain boundaries, although at lower strain rates and of course in single crystals intragranular sites such as deformation bands and subgrain boundaries become important (Roberts and Ahlblom 1978, Guillopé and Poirier 1979). Sah, Richardson and Sellars (1974) examined recrystallisation in nickel tested in hot torsion in the range 800-1000^{o}C at twisting rates of 0.03 to 50 rev/min. i.e. shear strain rates of 6.55×10^{-4} - 6.55×10^{-1} s^{-1}. They found that dynamically recrystallised grains formed in the old grain boundaries before the peak torque. Continuing the deformation resulted in further nucleation of recrystallised grains at the old grain boundaries until these sites were saturated. Thereafter, further recrystallised grains deposited on those already formed. The process continued until recrystallisation was complete. In studying coarser grained material and material showing prominent deformation bands, Sah Richardson and Sellars found that intragranular nucleation occurred but only when the original grain boundary sites were saturated. Similar results have been reported for stainless steel (Roberts and Ahlblom 1978, 1979). Once the nucleation sites at the original grain boundaries are exhausted the reaction proceeds via nucleation at the interface between recrystallised and unrecrystallised

material, until the transformed regions emanating from opposing grain boundaries impinge at the centres of pre-existing grains. This condition corresponds to the attainment of steady-state on the stress/strain curve.

e) Relationship between recrystallised grain size and steady state stress

It is well documented (see e.g. Sellars 1978) that the size of the recrystallised grains follows the phenomenological relationship

$$\sigma_s = \sigma_o + AD^{-n}$$

σ_s is the steady state stress

D the recrystallised grain size

σ_o, A and n are empirical constants - n varying between 0.5 and 1. Sah et al 1974 reported a value of 0.5 in Ni, Glover and Sellars (1973) obtained a value of n = 0.71 in zone refined iron and Luton and Sellars (1969) found n = 0.75 in Ni-Fe alloys, although they did point out that the data did give an almost equally good correlation with n = 0.5 or 1. It has been stated that throughout the steady state region, the grains remain constant in size and equiaxed in shape. Sah et al (1974) found that after the first few percent grains recrystallised there was no change in grain size and concluded that the grains grow very rapidly to their final size and do not grow thereafter. They attributed this lack of growth to the fact that the newly formed grains become rapidly work hardened and lose their driving force for further growth, while other regions of the specimen achieve enough strain for nucleation elsewhere. This lack of growth is in sharp contrast to the behaviour in static recrystallisation where growth of the recrystallised grains continues throughout recrystallisation. Also in contrast to static recrystallisation where the material is completely recovered, dynamically recrystallised grains do contain substructures. The recrystallised grains undergo deformation as they are growing and substructures are evident within them.

Sah et al found that the dynamically recrystallised grain size is independent of the original grain size although the kinetics of the first cycle of recrystallisation are affected by the original grain size being accelerated as grain size is decreased. A similar result was obtained by Roberts et al (1979), who monitored the dynamic recrystallisation reaction in two austenitic stainless steels. Four main points extracted from Roberts et al are that:

i) the critical strain for dynamic recrystallisation ε_c and the strain to the stress maximum show a significant increase with an increase in D_o the original grain size for a given temperature and strain rate.

ii) the maximum stress is virtually independent of D_o.

iii) Once the peak stress is passed the steady state is attained more rapidly with decreasing D_o. Prior to the onset of dynamic recrystallisation, an increased work hardening rate is promoted by a reduction in D_o.

iv) the dynamically recrystallised grain size D and the steady state stress are independent of D_o.

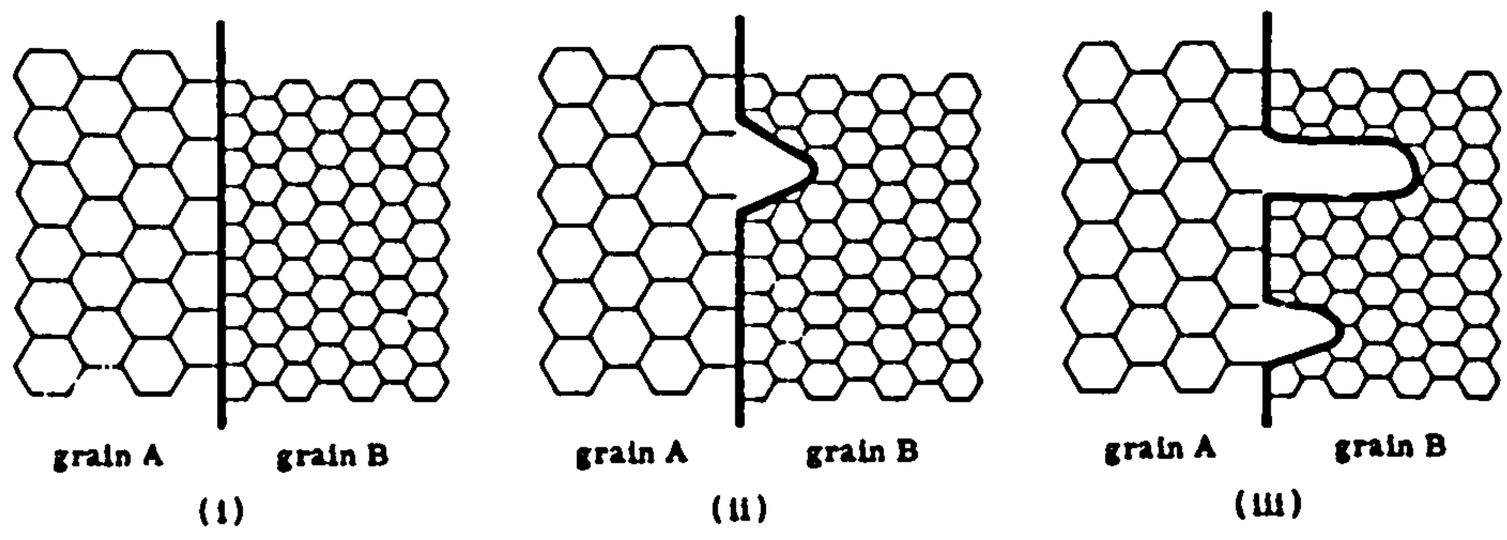
McQueen and Jonas 1975 suggest that since the subgrain size d is formed by dynamic recovery and is causally related to strain rate and temperature and therefore to σ_s then the dynamically recrystallised grain size will be related to the nucleus density and therefore the density of subgrains present, i.e. as suggested by Luton and Sellars (1969) the recrystallised grain size, D, is proportional to the sub-grain size, d, therefore σ_s can be correlated with D as well as d. McQueen and Jonas do however, point out that it is a correlation rather than a causal relationship since there are added hardening contributions due to the sub-boundaries and the dislocation density within the subgrains.

f) Nucleation mechanisms

Two theories have been advanced for the nucleation of dynamic recrystallisation in metals; firstly nucleation by bulging and migration of a pre-existing grain boundary and secondly by the formation of high angle boundaries by the accumulation of dislocations in sub-boundaries. The strain rate is thought to be the factor which determines the operating mechanism (McQueen 1977). The former mechanism is more frequently reported; it occurs at low strain rates. Bulging of grain boundaries also occurs in materials which have a high rate of dynamic recovery, but in this case the process does not lead to recrystallisation. It has been noted that in low recovery metals, grain boundaries are effectively pinned by highly tangled cell walls and that there is a greater difference in strain energy between the region within the bulge and that in front of it, the high dislocation density being on the side of the boundary into which bulging is taking place. Luton and Sellars (1969) examined dynamic recrystallisation in Ni-Fe alloys at high temperatures. They found that the old grain boundaries were markedly irregular and that there was evidence of localised bulging and the formation of recrystallised grains in the boundary region. Sah et al (1974) also

presented evidence for nucleation of recrystallisation from a bulge in a pre-existing grain boundary: the mechanism is also supported by work on stainless steel (Roberts and Ahlblom 1978). All these authors cite the mechanism of strain induced grain boundary migration as an integral part of dynamic recrystallisation, but the theory was originally formulated for static recrystallisation (Beck and Sperry 1955) and developed by Bailey and Hirsch (1962).

In static recrystallisation the phenomenon of boundary migration followed by recrystallisation is well known. The most common site for recrystallisation particularly at low strains is at the old grain boundaries. Beck and Sperry (1955) gave the first detailed description of this phenomenon in polycrystalline high purity Al after 40% deformation by rolling. They found the formation of "new" nuclei on annealing to be rare and that strain induced migration of existing boundaries resulted in volume elements that were relatively free from substructure. A schematic representation of Beck and Sperry's mechanism is shown below.



Schematic diagram of Strain Induced Grain Boundary Migration (SIGBM) (after Beck and Sperry 1955).
It is assumed that the boundary is capable of high mobility by virtue of a large misorientation between the two grains A and B, which it separates and secondly that there is a significant strain difference (represented by different subgrain sizes in the two grains). The direction of migration is from the lesser strained grain (A) into the more heavily strained grain (B). The driving force for the process is the difference in stored energy values for the two grains.

The advancing boundary had an irregular jagged front which was made up of a series of curved sections, each one moving away from its centre of curvature. Laue back reflection techniques showed that the bulge region had a similar orientation to that of the original grain from which it was moving away. The mechanism does not propose nucleation as such, merely that an existing grain advances into its neighbouring area and becomes strain free in the process. Recent work on aluminium by Bellier and Doherty (1977) using a Kossel pattern technique to determine

grain misorientations has shown that although the new grains growing from a single grain have different orientations these lie within the spread of orientations of the old grain. An extension to Beck and Sperry's original idea was developed by Bailey and Hirsch (1962) with the advent of EM which enabled the examination of bulges on a much finer scale.

It is worthwhile examining the Bailey and Hirsch model of bulge nucleation in some detail since it is widely referred to in papers discussing dynamic as well as static recrystallisation. Bailey and Hirsch developed a theory of recrystallisation by grain boundary migration and used it to correlate recrystallisation kinetics and electron microscope observations made on copper, nickel and silver. Polycrystalline Ni and Cu were deformed in tension and the dislocations were found to be arranged in a cell structure closely resembling that observed in silver polycrystals and copper single crystals in previous work. The cell boundaries consisted of complex tangles of dislocations and large numbers of small loops. Misorientations across the walls were $\sim 2^{o}$. Evidence was presented for grain boundary migration and it was suggested that recrystallisation occurred by the migration of the original grain boundaries, the driving force stemming from a difference in the dislocation density across the boundary. Recrystallisation would only occur if there was a difference in stored energy across a sufficiently large region of a grain boundary and the process would therefore depend on the inhomogeneity of the dislocation distribution. It was suggested that the size of the bulge might depend on the dislocation structure and that the anchoring of the boundary at the edges of the bulge might be due to a large local density of dislocations ending in the boundary which tend to prevent migration in the same direction as for the bulge. The operative value of the bulge radius would be of the order of the cell size since this is similar to the spacing of the dense regions of dislocations.

Bailey and Hirsch did not attempt to account for the nucleation of recrystallisation or to explain the formation of the boundary which must occur behind the bulge before it becomes a recrystallised grain.
This paper is frequently cited in the literature as a mechanism of dynamic recrystallisation, whereas in fact it merely acknowledges the formation of grain boundary bulges and carries out a detailed investigation into the kinetics of bulge nucleation and growth for static recrystallisation.

SIGBM would seem to be firmly established but details of the recrystallisation mechanism are still far from clear. More recent work by King and Smith (1979) proposes a mechanism for the formation of a bulge on a grain boundary by the separation of grain boundary dislocations with steps at their cores, but once again the work is microscopically detailed without consideration of the macroscopic result.

The second mechanism of nucleation which has been reported during high strain rate torsion experiments on copper (McQueen and Bergerson 1972) is theformation of high angle boundaries by the accumulation of dislocations in sub-boundaries. The authors presented evidence to suggest that as strain is increased some of the tangles build up to high misorientations giving rise to nuclei throughout each grain and pointed out that since the strain is higher near the grain boundaries as a result of plastic anisotropy the density of nuclei is higher in these regions. This result contrasts with those reported for metals with high recovery rates, e.g. Al, where the subgrain misorientation remains constant during steady state flow (Takeuchi and Argon 1976). In this case the constant misorientation is attributed to the process of continuous dynamic recovery.

A similar process to that reported by McQueen and Bergerson has been frequently described in the geological literature in studies of the microstructures of deformed minerals (Hobbs 1968, White 1973, Poirier and Nicolas 1975). These authors suggested that recrystallisation was an integral part of the recovery sequence and that it occurred by progressive misorientation of subgrains as strain increased.

1.1.3.3. Grain Boundary Sliding

Grain boundary sliding has been well documented in the deformation of magnesium and it is worthwhile reviewing the current literature referring particularly to the theories and mechanisms put forward more recently to account for the phenomenon in general. Grain boundary sliding has often been observed in metals and ceramics deformed at elevated temperatures. It is recognised that this must be accompanied by grain accommodation if sample continuity is to be maintained. Beere (1978) in a review covering stresses and deformation at grain boundaries placed the sliding and accommodating processes into 3 categories which are summarised below.

1. Grain boundary sliding during diffusion creep.
   Material is redistributed by a stress directed atom migration process

resulting in a displacement of adjacent grain centres normal to their common boundary. Sliding accompanies this process to prevent gaps appearing at the grain boundaries and no deformation takes place in the interior of the grains. Boundary shear forces during this type of deformation are low.

2. Grain boundary sliding during rigid grain creep.

When the boundary shear forces are large, grain rotation becomes important. The interior of the grain does not deform but frictional forces developed on the boundary rotate the atomic lattice.

3. Grain boundary sliding during dislocation creep.

Deformation of the grain interior occurs when the applied stress is sufficiently large and the grain centre displacement is accommodated by shear inside the grain and by grain boundary sliding.

Beere suggested that the first and second categories included the phenomenon of superplasticity which will be reviewed in more detail in the following subsection. The third form of accommodating process will be dealt with separately.

Superplasticity

Superplasticity, the phenomenon whereby materials can deform extensively without fracture, has been a subject of considerable interest in view of its potential applications in metal working and fabrication. In spite of the large volume of literature reporting the phenomenon the modes and mechanisms of superplasticity have yet to be established with some certainty. A review of superplasticity by Johnson (1970) covered most of the relevant experimental results in metals, alloys and ceramics and went some way to summarising the theories suggested up to that time but many of the important advances in understanding the deformation mechanisms involved in superplasticity and in exploiting it to advantage have been made in more recent years. A comprehensive review by Edington, et al (1976) provides an up-to-date assessment of the mechanisms thought to be important in superplasticity backed up by references to experimental observations carried out on materials exhibiting superplastic behaviour. The review deals with mechanical properties, metallographic studies and texture measurements before examining the mechanisms involved in superplasticity. The first three will be briefly summarised before the different mechanisms are examined in more detail.

The characteristics of superplastic materials are:

1. Superplastic materials have a high strain rate sensitivity of the flow stress which opposes the development of necking and consequently are able to undergo elongations up to 1000%.
2. They undergo little work hardening so deformation is possible at low stresses.
3. Superplastic materials exhibit a characteristic sigmoidal relation between log σ vs log $\dot{\varepsilon}$.
4. The phenomenon has only been reported in high temperature (>0.5Tm) experiments..
5. It is normally observed in materials with a small grain size ($\leqslant 10\mu$).
6. There is no evidence for slip lines and channelling patterns from grain interiors remain sharp indicating absence of strain. EM foils in general reveal dislocation free grains.
7. Grain boundary sliding is important and since offsets are sharp confirms that there is little grain deformation. Grain boundary slipping is thought to be the cause of cavitation encountered in superplastic deformation.
8. New surfaces are created at grain boundaries.
9. The grains remain equiaxed even after very large strains (100's of %).
10. Limited grain growth occurs after superplastic deformation. It is enhanced by deformation.
11. The overall level of texture is generally reduced by superplastic deformation, though all components do not decrease at the same rate.

Mechanisms of Superplasticity

Edington et al (1976) point out that there is no 'unique' theory of superplasticity. Indeed there is still considerable controversy over mechanisms and although many researchers have attempted to describe the phenomenon in terms of a single theory, the bulk of experimental evidence indicates that several processes are involved. These include grain boundary sliding, diffusional and dislocation processes and dynamic recrystallisation. An elegant technique involving in-situ tensile deformation of the Pb-Sn eutectic in an S.E.M. has shown that grain boundary sliding and large grain rotations occur extensively during superplastic flow (Geckinli and Barrett 1976). Attempts have been made to account for superplasticity in terms of N-H and coble creep, but it is generally agreed that creep is not the rate controlling mechanism, as predicted strain rates are usually several orders of magnitude too low,

insufficient grain elongation occurs to account for the overall specimen elongation and the mechanism is inconsistent with the large rotations observed during superplastic deformation. Similarly slip based mechanisms for superplasticity (Chaudhari 1967) are also unlikely as they do not explain the retention of an equiaxed grain structure, the large amount of grain boundary sliding or the randomising of texture observed experimentally. Dynamic recrystallisation during diffusional creep (Karim 1969) was put forward as a means whereby an equiaxed grain size could be maintained, but there are objections to this mechanism in that the lack of deformation within grains means that the driving force is low and the randomisation in texture generally observed would not be expected if dynamic recrystallisation were occurring.

It is likely then, that as is the case for deformation in general, different mechanisms will predominate under different conditions and the phenomenon of superplasticity will thus be due to the operation of more than one of them. The main theories discussed in the literature, i.e. those advanced by Ball and Hutchinson (1969), Ashby and Verrall (1973) and Gifkins (1976,78) will be examined in more detail.

1. Grain boundary sliding with accommodation by dislocation processes

Ball and Hutchinson (1969) examined the superplastic behaviour of the Al-Zn eutectoid. They found that grain boundary sliding was frequently accompanied by dislocation motion within the grains. The activation energy derived from their results indicated that superplastic flow was controlled by grain boundary diffusion and they suggested that it also controlled the rate of absorption of the intragranular dislocations into the grain boundaries. The Ball and Hutchinson model proposed that groups of grains with suitably aligned boundaries would slide as units and that when an obstruction to sliding was encountered, the shear stress on the whole group would be concentrated at the point of contact. Pile-ups of dislocations would be generated at the opposite boundary in the blocking grain by this localised stress until the resulting back stress prevented further dislocations being generated. Sliding would then be halted at this point unless the dislocations at the head of the pile up could climb into the grain boundary, in which case further grain boundary sliding could occur at a rate controlled by the kinetics of dislocation climb along grain boundaries. Ball and Hutchinson suggested that the absence of grain elongation in superplastic flow could be accounted for by the progressive rotations of grains to accommodate the movement of their

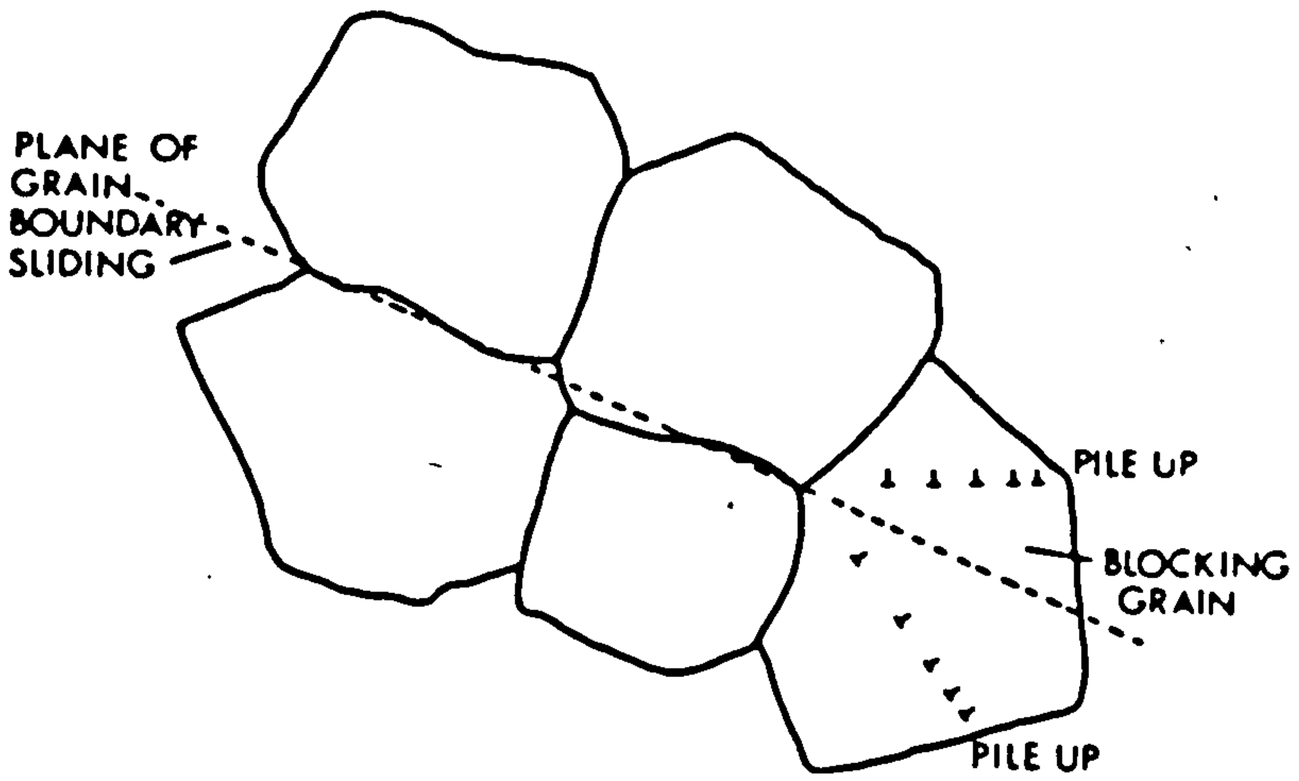


Figure 1.3a Schematic diagram of the Ball and Hutchinson (1969) model (after Edington et al 1976).

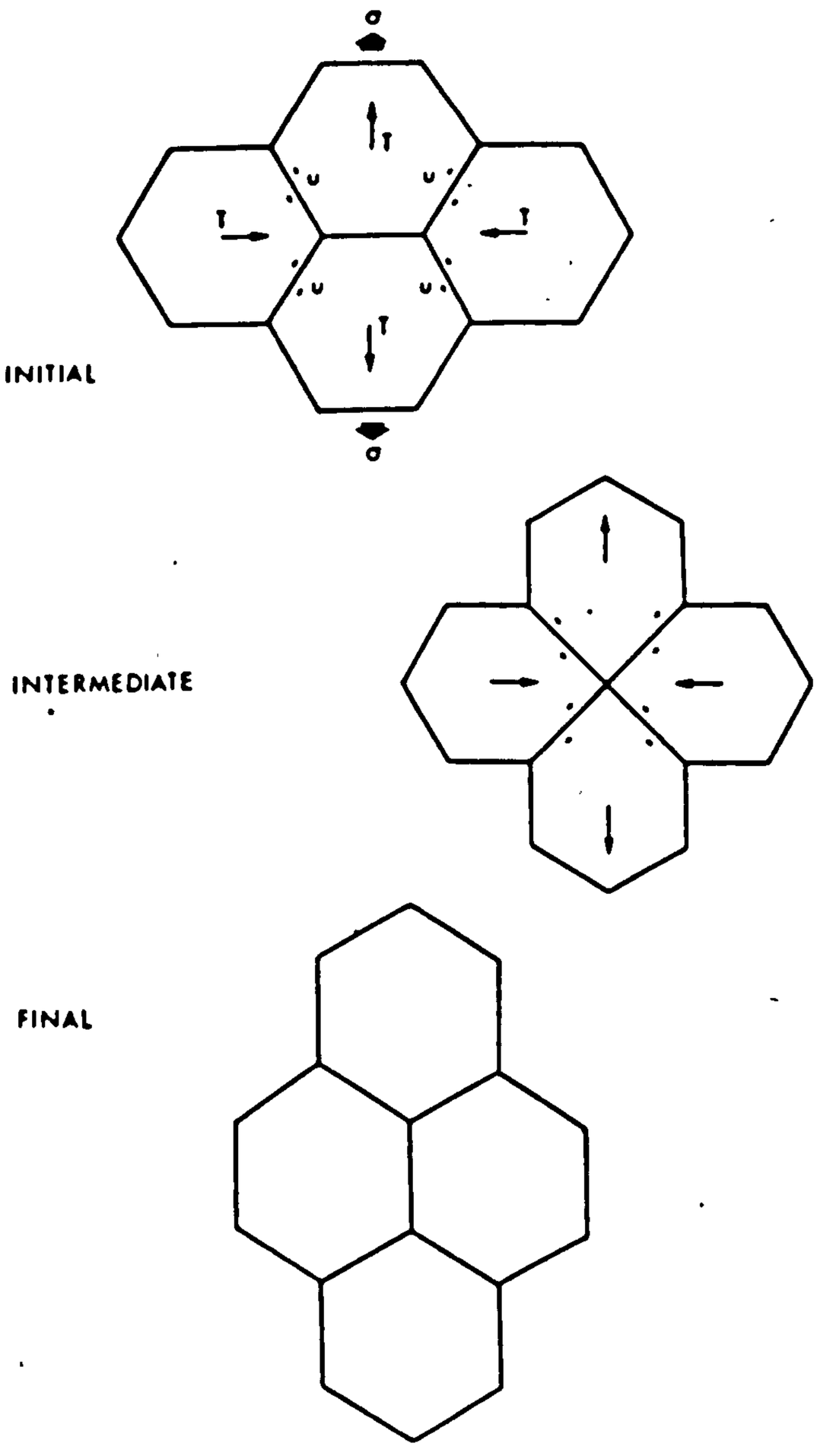


Figure 1.3b Schematic diagram of the Ashby-Verrall (1973) model (after Edington et al 1976).

neighbours and hence changes in the operating slip system. One important conclusion the authors drew from their deliberations was that it is a necessary condition for superplasticity that the grain size in the superplastic state is stable and smaller than the equilibrium cell structure which would form under the same conditions of stress and temperature for the non-superplastic state. This is because their model requires dislocations to cross yielded grains and be absorbed at the opposite grain boundaries. This is only possible if the cell size is larger than, or of the order of the grain size, i.e. once dislocations are prevented from crossing grains by tangles or cell walls, then superplasticity ceases. Figure 1.3a shows a schematic diagram of their model.

Mukherjee (1971) put forward a similar model to Ball and Hutchinson, whereby the grains rotate individually rather than in groups. In this case the dislocations are generated by ledges and bulges in the grain boundaries.

Both models have been criticised because of doubt over the formation of pile ups (Edington et al 1976). In the Ball and Hutchinson case it is thought that dislocations would be annihilated during climb and cross slip whilst in Mukherjee's model since the ledges move during sliding, the dislocations do not start on the same plane and pile ups are unlikely. A further criticism is that dislocation models do not automatically give large strains and inyolve large amounts of dislocation motion across grains.

2. Grain boundary sliding with diffusion accommodated flow

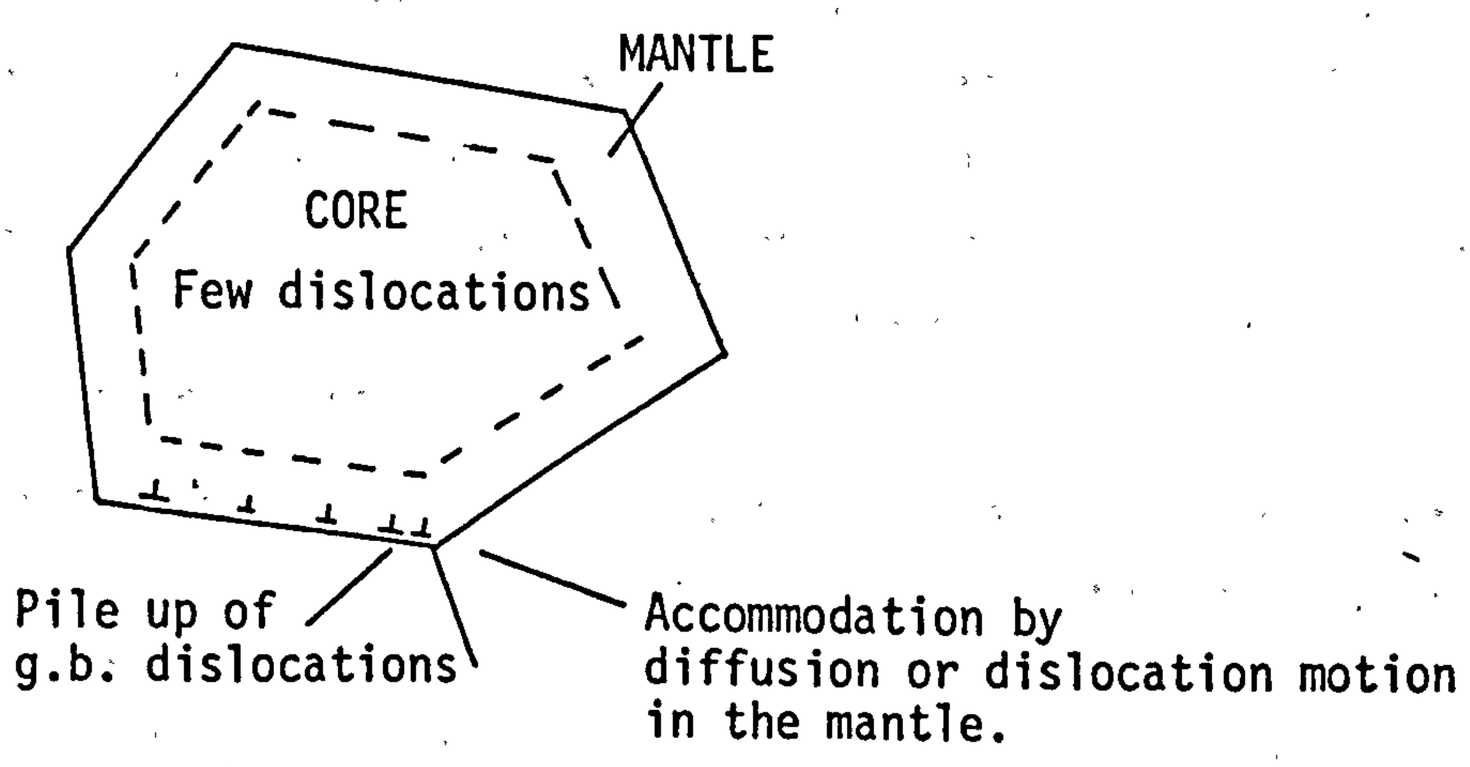
This theory was put forward by Ashby and Verrall to account for large strains at temperatures high enough to permit diffusion. They derived a theory and formulated a constitutive equation to account for the characteristics of superplastic flow. The mechanism was fundamentally different from N-H and Coble creep in that the grains did not elongate significantly and underwent switching of neighbours. This grain switching had been observed during in-situ deformation of the Zn-Al eutectoid alloy in the HVEM (Naziri et al 1975), although it has been pointed out that the specimen used was essentially two dimensionsl (Gifkins 1978) - a criticism of the model in general. Another criticism is that the strain rates predicted by the model are too low and give a dependence of σ/d^3 rather than the experimentally observed σ^2/d^2. The model considered the relative motion of a group of four grains which caused the cluster as a whole to change shape. This is shown schematically in Figure 1.3b. Whilst this was occurring, the grains would suffer accommodation strains which would

be accomplished by diffusion. Ashby and Verrall stated that the accommodating mechanism was driven by four irreversible processes:-

1. The diffusive process which inserts or removes material into the boundary separating two grains, i.e. normal displacements occur and both bulk and boundary diffusion are involved.
2. An interface reaction where grain and phase boundaries are considered to be imperfect sinks or sources for point defects.
3. Grain boundary sliding where work is done against the boundary viscosity. Shear displacements occur in the boundary plane as well as the normal displacements caused by diffusion. It is this shear displacement which enables the grains to translate past each other. The energy needed to drive the large sliding displacements which occur is small.
4. The fluctuation of grain boundary area. As a cluster of four grains moves from the initial to the intermediate state there is an increase in area and as it moves to the final state the boundary area and hence the energy decreases. However, since this local release of energy cannot be made available to another cluster of grains, it is dissipated as heat. No deformation is possible below a threshold stress because the external stress has to do enough work to supply the energy which is temporarily stored as new boundary.

3. <u>Grain boundary sliding involving a 'Core and Mantle' structure</u>

This model was first postulated during a study of the behaviour of lead thallium alloys in the creep and superplastic modes of deformation (Gifkins 1976).



Deformation in the centre of a grain (core) is considered to be different from that at the edge of the grain (mantle). Grain boundary sliding (GBS) is accommodated in the mantles by the formation of folds, by dislocation motion or by diffusion depending on the conditions.

For GBS accommodated by dislocation processes it was suggested that grain boundary dislocations pile up at triple points and the leading dislocation dissociates into grain boundary dislocations which can move in either of the other 2 boundaries and/or crystal dislocations which accommodate sliding. This relaxes the stress concentration at the triple point, see above. The process continues with the motion of these 'new' dislocations until they interact with other dislocations and are annihilated or react to form different grain boundary dislocations. The overall concept of the theory is similar to that of Ashby and Verrall excepting that the GBS is accommodated by dislocation climb and glide in the mantles rather than by viscous flow.

Further development of the Core and Mantle theory (Gifkins 1978) led to the suggestion that as well as grain rotation being made possible by flow in the mantle, grains are able to move from one layer to another, i.e. after a small amount of sliding a void is opened up and a grain moves from the layer below to fill the gap. The mechanism maintains the correct specimen surface area and requires less movement in the mantles than the triple point model. It also overcomes the two dimensional model objections. Gifkins presented evidence from the literature to support his theory which predicts the experimentally observed σ^2/d^2 dependence of the strain rate, e.g. in Naziri's thicker specimens grain emergence rather than the Ashby Verrall switching could be detected.

GRAIN BOUNDARY SLIDING DURING RECOVERY CREEP

Grain boundary sliding which often accompanies dislocation creep consists of two interdependent processes, viz. grain boundary shear and grain accommodation. Due to geometrical constraints in a polycrystalline aggregate, boundary shear must always be accompanied by grain accommodation if specimen coherency is to be maintained. The values of n (the stress exponent and Q (the activation energy) in the rate equation will lie between the two processes (Horton 1975).

Most of the studies of grain boundary sliding during high temperature creep have been carried out at low strains (i.e. in the primary creep regime) in order to try and estimate the contribution of GBS to the total deformation. It is recognised as being an important process during the early stages of creep and can account for as much as 70 or 80% of a total creep strain of 2% (Bell and Langdon 1967).

Under conditions which favour intragranular deformation, i.e. higher applied stresses, then sliding occurs as an accommodation mechanism to relieve strain incompatibilities (Speight 1976). The contribution of sliding to the overall deformation is normally determined from the movement of marker lines on the specimen surface at grain interfaces but this is an oversimplification of the real situation.

Various mechanisms have been proposed to account for grain boundary sliding during recovery creep, for example, mechanisms based on boundary defects such as grain boundary dislocations (Gleiter et al 1968), or on the influence of lattice dislocations (Ishida and McLean 1967) or on differences in the number of atomic planes meeting at a boundary (Johannesson and Tholen 1972). Experimental evidence in support of the last mechanism has been obtained during creep of polycrystalline copper at elevated temperatures. TEM of grain boundaries revealed that cavities were always associated with obstacles in the grain boundaries. It was suggested that the mechanism of sliding involved the dissociation of dislocations intersecting high angle grain boundaries at elevated temperatures into mobile boundary dislocations (Johannesson and Tholen 1972). Grain boundary sliding is easy unless the dislocations are halted by obstacles such as triple points and boundary corrugations where stress concentrations build up. These are relieved by plastic flow. The authors suggested that the effect of stress relief at triple points by plastic flow would be reduced at elevated temperatures. This is because dislocation cell structures would develop and the dislocations emitted during plastic flow would easily dissociate on meeting a grain boundary and thus contribute to the sliding. At low temperatures on the other hand they would contribute to the high density of dislocations usually found in boundaries in cold worked metals. At elevated temperatures, although diffusion would also contribute to the stress relief, if it did not occur rapidly enough then cavities and cracks would form at the triple points and kinks and eventually lead to creep fracture.

Grain boundary sliding is known to play an important part in the formation and development of cavities at elevated temperatures. It is particularly important in the creep deformation of magnesium and will be examined in more detail in the context of the deformation characteristics of the metal at a later stage.

1.2. DEFORMATION OF MAGNESIUM

1.2.1. Introduction

Studies of the deformation of magnesium and its dilute alloys have

centred in the main around their use as canning materials for gas cooled thermal reactors. The range of temperatures and stresses imposed on these materials during reactor operation lie in the main in the 'creep' regime of deformation. The macroscopic details resulting from such studies are as follows:-
magnesium is a hexagonal metal and deformation is accommodated by slip, twinning, grain boundary flow, diffusion and the motion of dislocations according to the conditions.

The twinning mechanisms and slip systems known to operate in the metal will be reviewed first, followed by the macro and microscopic aspects of creep deformation. This will include the mechanistic and microstructural aspects of cavity formation and grain boundary sliding during recovery and diffusion creep.

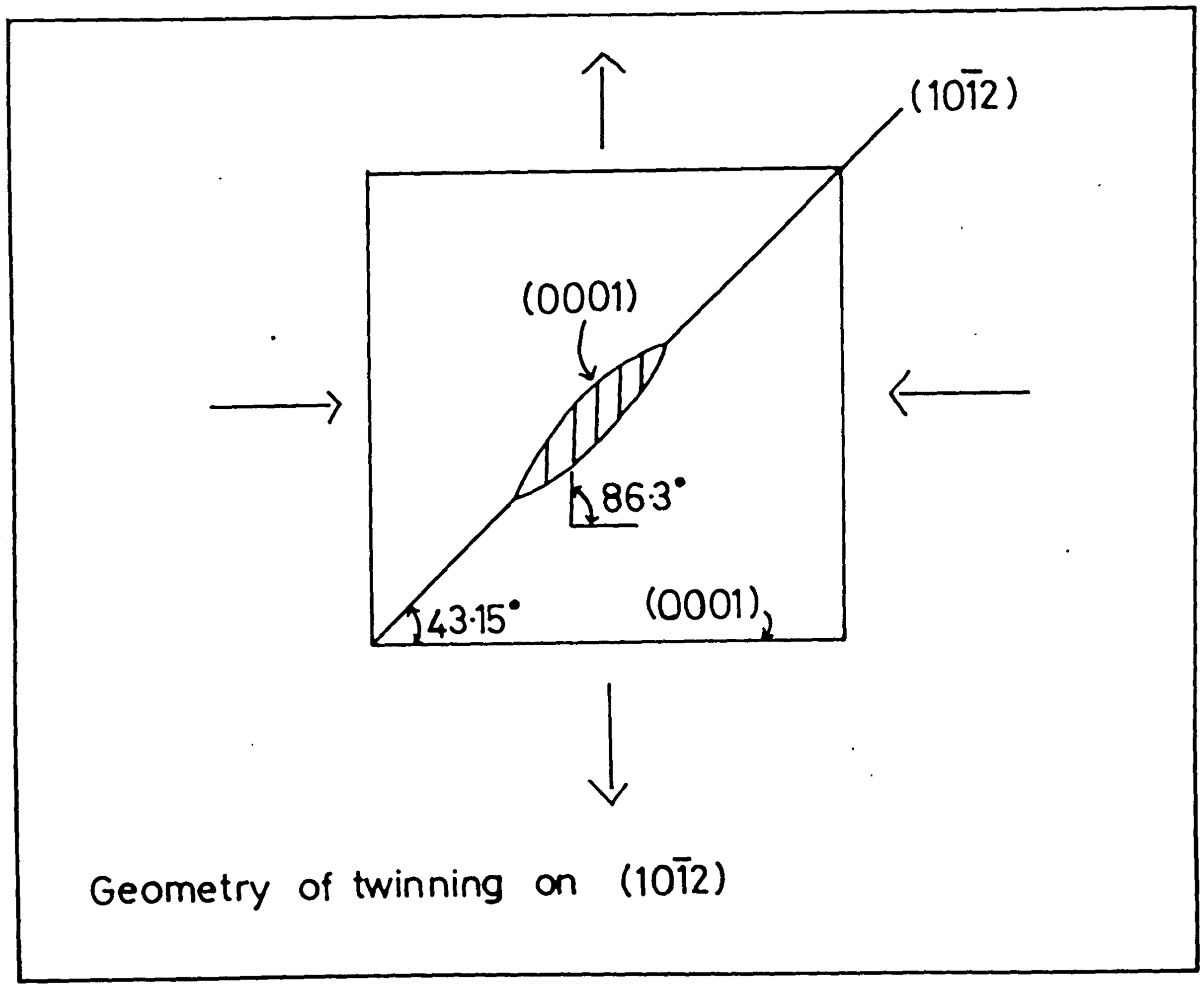
1.2.2. Deformation Mechanisms

1.2.2.1. Twinning

Deformation twinning in both single and polycrystalline samples is a common occurrence and the main aspects of the process are summarized in text books involving the technology of magnesium and its alloys (Raynor 1959, Roberts 1960, Emley 1966).

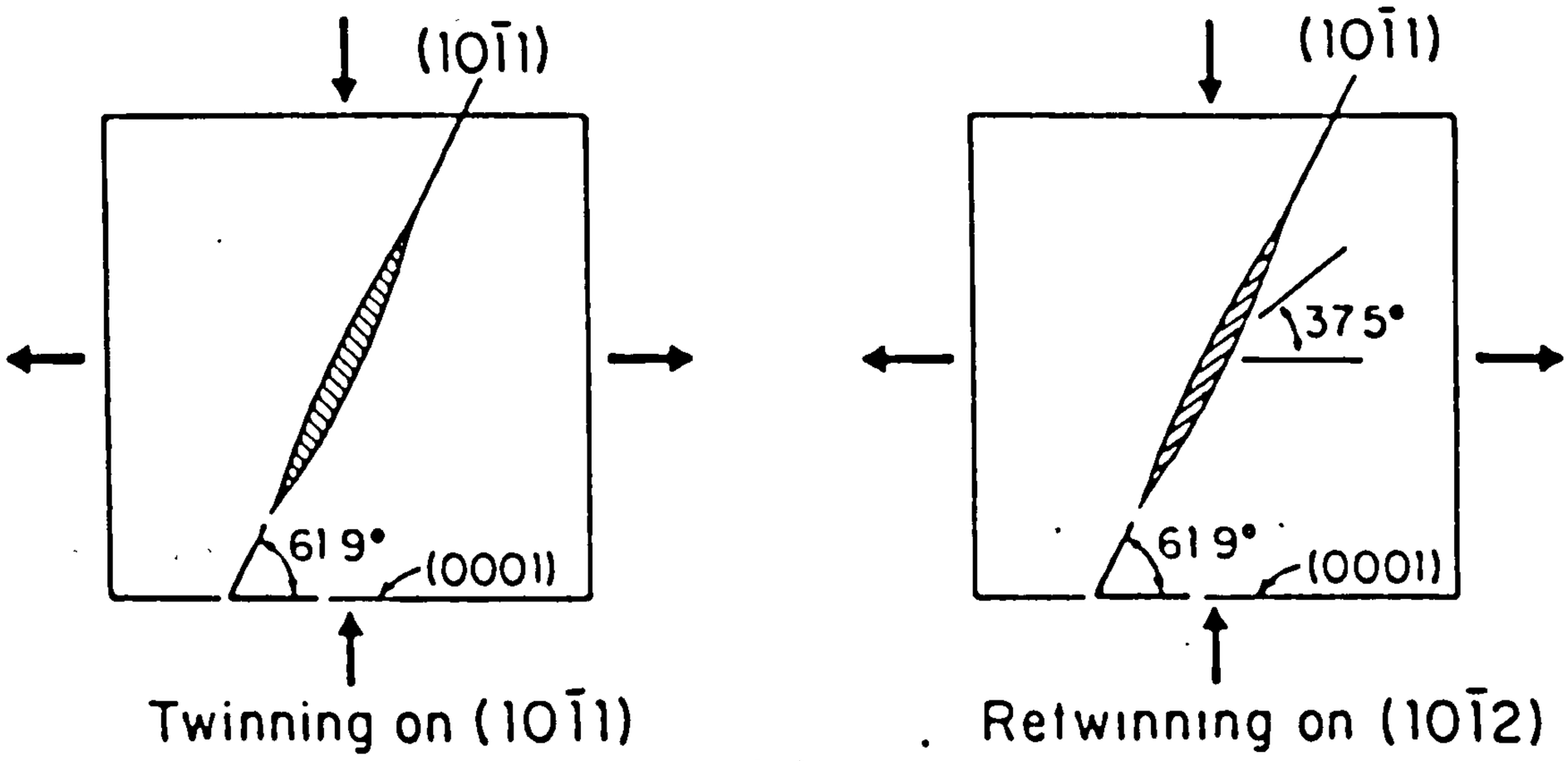
The most common form of twinning is on $\{10\bar{1}2\}$. The geometry of the mechanism is illustrated in Figure 1.4. The shear accommodated is 0.13 and the mechanism results in a reorientation of the basal plane of 86.3^{o}. This means that in single crystals $\{10\bar{1}2\}$ twinning occurs on compression parallel to the basal plane or in tension perpendicular to it. Although it is recognised that $\{10\bar{1}2\}$ twinning is temperature dependent there have been no systematic studies of the phenomenon. Consequently, the fact that twinning in polycrystalline magnesium becomes less important with increasing temperature, cannot be separated from the knowledge that the critical stresses for non-basal slip and other mechanisms decrease markedly at elevated temperatures.

Other types of twinning which have been reported are two mechanisms of double twinning (Figure 1.5.) The mechanisms are $\{10\bar{1}1\}$ followed by $\{10\bar{1}2\}$ which results in a basal plane reorientation of 37.5^{o} (Couling et al 1959) and $\{10\bar{1}3\}$ followed by $\{10\bar{1}2\}$ which results in a basal plane reorientation of 22.2^{o} (Reed-Hill 1960). Both these twinning mechanisms result in a contraction along the C-axis which means they will occur under an opposite system of loading to the $\{10\bar{1}2\}$ mechanism.

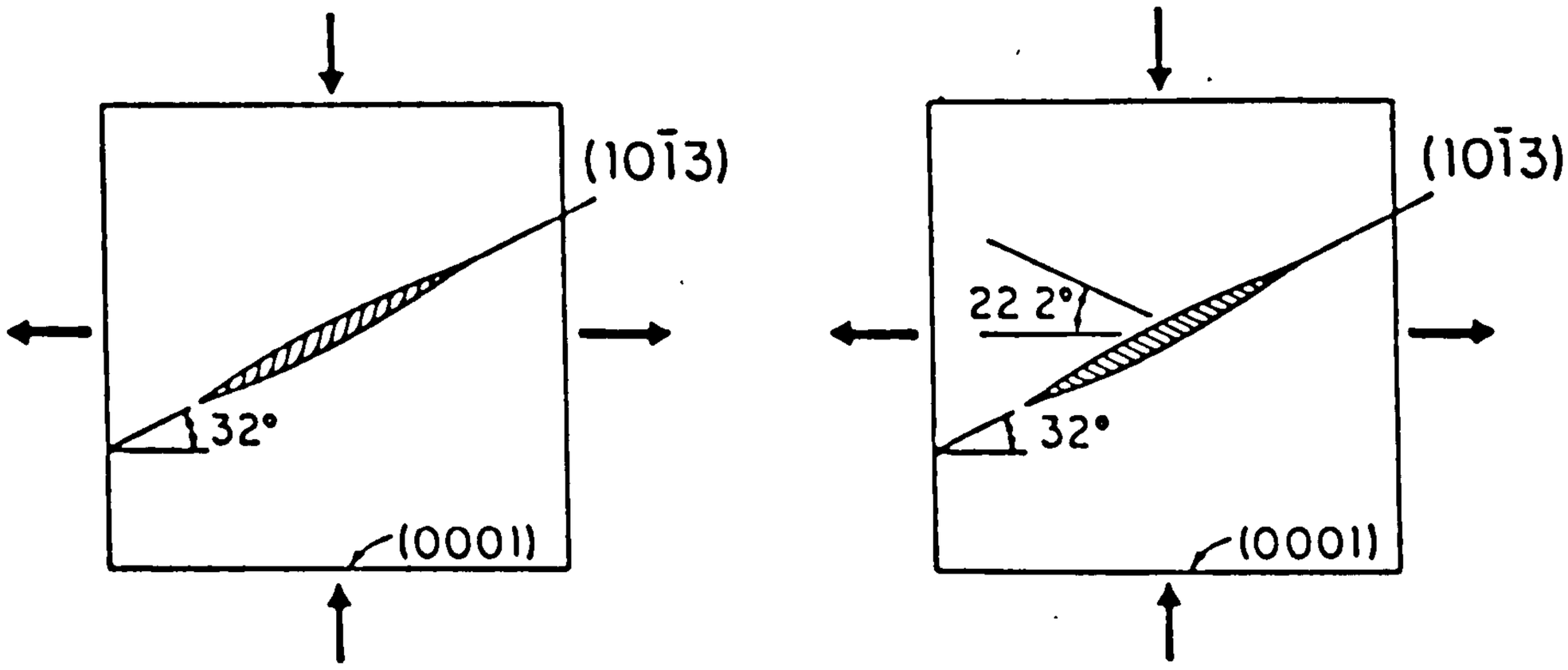


Geometry of twinning on (10$\bar{1}$2)

Figure 1·4



(a)



(b)

Figure 1.5 Two double twinning mecanisms can occur in tension parallel to, or compression perpendicular to the basal plane
i) a $\{10\bar{1}1\}$ twin can form and then retwin on $\{10\bar{1}2\}$
ii) a $\{10\bar{1}3\}$ twin can form and then retwin on $\{10\bar{1}2\}$

In general wrought polycrystalline aggregates have a strong preferred orientation which leads to an anisotropy in mechanical behaviour. This means that in rolled Mg sheet, almost all the grains have their basal planes nearly parallel to the sheet surface. Consequently the $\{10\bar{1}2\}$ twinning is not favoured when such material is later deformed in tension in the plane of the sheet or by cold rolling but the double twinning mechanisms are favoured. In rolled sheet deformed in plane strain compression and in single and polycrystals compressed in plane strain in the temperature range 20°C to 307°C both types of double twinning have been reported (Wonsiewicz and Backofen 1967). These authors concluded that in Mg crystals unfavourably oriented for basal slip twinning occurred in the main by the $\{10\bar{1}1\}$-$\{10\bar{1}2\}$ double mechanism. Large C axis strains were accommodated by this mechanism and basal shear occurred within the doubly twinned volume. The strong temperature dependence of $\{10\bar{1}1\}$ twinning was thought to reflect the temperature dependence of the preliminary non basal slip.

It was found that the double twin was associated with a $\{30\bar{3}4\}$ habit but as reported by Roberts (1960) there were several inconsistencies in the mechanisms proposed for the $\{30\bar{3}4\}$ structure and the experimental evidence obtained. Hartt and Reed-Hill (1967) re-investigated the habit of the double twins. They found that the irrational habit fell close to $\{30\bar{3}4\}$ or 7° away from the primary $\{10\bar{1}1\}$ twin habit and presented evidence to show that the habit shift probably resulted from the need to accommodate the second order twinning shear. It was suggested that this accommodation resulted in an external shear in the matrix and an internal shear in the lamella. The reorientation of the crystal structure by means of the double twinning mechanism would mean that the twin would be well oriented for slip in contrast to the matrix. It had been suggested in previous work by Reed-Hill and Robertson (1957) that since extensive internal deformation was possible whilst the matrix was still virtually underformed, then ductile rupture running the length of the twin could result.

1.2.2.2. Slip Systems

Studies of the deformation behaviour of magnesium which are summarized by Raynor (1959), Suiter (1958), Roberts (1960) and Emley (1966), show that slip on the basal plane (0001) in the close packed $<11\bar{2}0>$ direction is the most common system and occurs up to $\sim 225^{o}C$ whenever the crystal is favourably oriented with respect to the applied stress. At temperatures above $225^{o}C$ the $\{10\bar{1}1\}$ planes also become slip planes, the slip direction again being $[11\bar{2}0]$. Raynor (1959) quotes values for the critical resolved shear stress (CRSS) at $330^{o}C$ for both types of slip, being 0.66MPa for $(0001)[11\bar{2}0]$ and 3.9 MPa for $(10\bar{1}1)[11\bar{2}0]$, i.e. for pyramidal slip to occur the resolved shear stress must reach a value six times that for basal slip. This would normally only be expected to occur when the tension axis is within a small angle of the orientation of the basal planes. However, Burke and Hibbard (1952) detected pyramidal slip at room temperatures stressed in tension when the basal plane was oriented within 6^{o} of the stress axis at a lower value of the CRSS than that found previously by Bakarian and Matthewson (1943). The results of Reed Hill and Robertson (1957) confirmed those of Burke and Hibbard who attributed the behaviour to the constraints imposed by the grips holding their specimens.

An anomaly in the temperature dependence of pyramidal slip in the range 270-375K has been reported in magnesium single crystals (Stohr and Poirier 1973). It was attributed to thermally activated blocking of $\overrightarrow{c + a}$ edge dislocations and their dissociation into partial dislocations.

The resolved shear stress along the basal plane is at a maximum when the basal planes are inclined at 45^{o} to the stress axis and is zero when they are parallel or perpendicular to it. This means that in a polycrystalline sample the behaviour will depend to a large extent on the texture (degree of preferred orientation) of the starting material. As would be expected polycrystalline deformation is much more complex than single crystal deformation because of the considerable stresses which develop between grains which are unfavourably oriented for slip. Hauser et al (1956) undertook a careful examination of polycrystalline behaviour at room temperatures and below. They found that as the temperature was decreased, duplex slip on $\{10\bar{1}0\}$ planes occurred in conjunction with basal slip. This was thought to be due to the fact that at lower temperatures, the highly localised stresses are relieved by non-basal slip rather than by the relative movement of grains.

Much of the recorded data about active slip systems at elevated temperatures was obtained in the course of studies of the creep behaviour of polycrystalline magnesium. Chadhuri et al (1955) extended coarse grained cylindrical specimens in creep at 371°C. Basal slip was observed on initial loading but non-basal slip was seen to occur as deformation proceeded and accounted for a greater part of the total creep strain. A form of cooperative slip, with $\{10\bar{1}0\}$ and $\{10\bar{1}1\}$ being the participating planes, was proposed to account for the experimentally observed wavy slip lines.

It has been reported that at least five independent mechanisms of deformation must be invoked to account for the five independently variable strain components necessary for a general deformation (Von Mises 1928, Taylor 1938). However, it is well known that this criterion is not satisfied in low temperature deformation of magnesium. Pure magnesium exhibits primarily basal slip and twinning, and very localised prismatic slip in regions of high stress concentrations adjacent to grain boundaries and at triple points (Hauser et al 1955). The two types of slip - prism, $\{10\bar{1}0\}\langle 2\bar{1}\bar{1}0\rangle$ and basal, $(0001)\langle 2\bar{1}\bar{1}0\rangle$ - lead to four independent slip systems. It has been stated that twinning on the $(10\bar{1}2)$ plane can account for six additional mechanisms but since its action is limited geometrically and the amount of strain it can account for small, it is thought that this mechanism would not provide the further necessary deformation modes (Hauser et al 1958, Tegart 1963). Thus, in the absence of other additional independent major mechanisms polycrystalline aggregates of magnesium should exhibit brittle behaviour at low temperatures. However small amounts of deformation have been observed prior to brittle fracture of magnesium. Localised grain boundary shearing and minor amounts of prismatic slip together with twinning were thought to provide the necessary accommodation across grain boundaries (Hauser et al 1958). In high temperature deformation of magnesium, although slip and twinning processes are important initially they tend to be overshadowed by the relief of local strain energy, particularly at grain boundaries by subgrain formation and sliding and migration of the grain boundaries as strain is increased (Roberts 1960).

1.2.3. Creep of Mg

1.2.3.1. Dislocation creep

The high temperature dislocation creep of polycrystalline Mg was studied extensively over the last two decades in order to try and obtain a consistent interpretation of creep behaviour over a wide range of temperatures and stresses as part of the development programme for the

magnox reactor. Most of the experiments were carried out in the temperature range 0.5 - 0.8 Tm. on polycrystalline aggregates - although some experiments have been carried out to study dislocation climb in single crystals (Edelin and Poirier 1973).

a) Activation Energies

In common with experiments on the creep of other polycrystalline metals an equation of the form

$$\dot{\varepsilon} = f(s)\sigma^n \exp - \frac{Q}{RT}$$

has been employed to obtain values of the activation energy Q and the stress exponent n.

At slow strain rates characteristic of those used for engineering creep, studies were carried out on the activation energy for the secondary creep of both A180 (Jones and Harris 1963) and pure magnesium (Tegart 1961). In the case of the Magnox AL80 it was found that for creep rates $<10^{-6}s^{-1}$ the activation energy for secondary creep was $\sim$25 Kcal mol^{-1} and was independent of temperature and strain in the range 200 - 415^{o}C. Stress exponents of 4-5 were found under these conditions. For creep rates $>10^{-6}s^{-1}$ it was found that the power law relationship fitted the data less well and that n and Q increased with increasing temperature. This was attributed to non basal cross slip becoming dominant at higher temperatures. A value of 10 for n has been found in the cross slip regime (Crossland and Jones 1972).

Compressive creep data in the range 177 - 577^{o}C yielded two different activation energies. Q had a value of 26-29 Kcal/mol below 0.6 Tm and a value of 50-55 Kcal/mol above 0.75 Tm (Tegart 1961). The result was attributed to non basal cross slip at the higher temperature. Carrying out experiments in the same temperature range as Tegart, Jones and Harris (1963) did not obtain a higher value of Q above 0.6 Tm but as they pointed out the higher creep rates and larger grain sizes used by Tegart would increase the role of cross slip, particularly at higher temperatures. Stress relaxation experiments carried out by Gibbs (1965) led this author to suggest that secondary creep of fine grained polycrystalline magnesium for strain rates greater than $10^{-4}s^{-1}$ was controlled by thermally activated glide of basal dislocations and the rate determining obstacles were jogs in the screw segments.

The theoretical analyses carried out for dislocation creep (e.g. Weertman 1968) require that the activation energy for creep, Q, is equal

to the activation energy for self diffusion and that the stress exponent n has values of 3 and 4.5 for mechanisms controlled by glide and climb respectively. The activation energy for self diffusion of Mg is 32 Kcal/mol (Shewmon and Rhines 1954) which means that the values obtained by Jones and Harris and Tegart are significantly lower. A similar disparity has been observed in copper where the effect was attributed to an enhancement of the lattice self diffusion by a contribution due to rapid pipe diffusion down dislocations (Barrettand Sherby 1964). It has been suggested that a dislocation pipe diffusion process could contribute to the dislocation creep in magnesium below 0.67 Tm (Crossland and Jones 1972). Since the activation energy for pipe diffusion is close to that for grain boundary self diffusion, this would result in an activation energy for dislocation creep in magnesium in the range 20-25 Kcal/mol (these activation energies for grain boundary diffusion have been found from experiments on diffusion creep by Jones 1965 and Crossland and Jones 1972 respectively).

b) Microstructural aspects of dislocation creep

Irregular boundary migration is a common feature reported during dislocation creep of magnesium and has often been associated with the formation of cells in the vicinity of grain boundaries (Suiter and Wood 1953, Stacey 1958). In studies of tensile creep of fine grained electrolytic magnesium in the range 93-316^{o}C and stresses of 16.7 - 139 Pa. (Roberts 1953) it was found that as temperature increased the slip within the grains and subgrain formation gave way to grain boundary deformation. Slip and subgrain formation were related to the transient creep stage whilst grain boundary deformation, in the form of alternate sliding and migration, was related to the steady state portion of the creep curve. It has been suggested that this irregular migration eventually leads to primary recrystallisation at the grain boundaries and this is discussed later.

At temperatures $\sim$200^{o}C basal slip and cell formation are the prominant microstructural features (Roberts 1953, Suiter and Wood 1952, Tegart 1961), although some workers have observed non basal slip bands, e.g. Chaudhuri and Grant(1953,55) and Jones and Harris(1963). As temperature is increased the non basal slip traces grow wider and there is more evidence for cross slip. It has also been found that at the higher temperatures (480^{o}C) when low strain rates are employed, the subgrains are not concentrated at the grain boundaries and grain boundary sliding is very marked (Jones and Harris 1963). Tegart observed that in his higher temperature work

although the main slip was basal, extensive non-basal slip could also be detected and intimated that a large contribution to the overall deformation was probably made by crystallographic slip.

Reports of recrystallisation in Mg during creep have been mainly qualitative in nature consisting merely of observations of the phenomenon with no explanation as to the mechanisms. Harris (1963) reported recrystallisation and grain boundary sliding in a magnesium alloy during tensile deformation in the temperature range 100-350^{o}C. He also reported that cells formed close to the grain boundaries in agreement with Suiter and Wood (1952) (though this observation was based on optical studies) and that this was followed by irregular grain boundary migration, the boundaries being pinned at their intersections with the cell walls. Harris thought that the irregular migration would limit sliding and that eventually primary recrystallisation would occur along the old grain boundaries. He presented evidence for further sliding at the new grain boundaries and suggested that the recrystallisation would lead to improved tensile ductility. This concurs with Stacey(1958)who suggested that enhanced ductility at ~180^{o}C was due to the formation of fine grains at the grain boundaries. Greenwood et al(1954)on the other hand attributed the phenomenon to the occurrence of non-basal slip at the lower strain rates used in their work.

Byrne 1963 studied the effects of elevated temperature deformation in both tension and compression in magnesium. He found that sharp grain boundary corrugations developed during deformation and this was followed by local recrystallisation at higher strains.

1.2.3.2. Diffusion creep

Creep tests carried out on magnesium at high temperatures and low stresses confirmed that diffusion creep was occurring and that it was controlled by either the Nabarro-Herring or the Coble mechanism depending on the temperature (Jones 1965). Coble creep was found to be the more important mechanism in fine grained specimens stressed at lower temperatures.

It is the magnesium alloy Magnox ZR55 which has provided some of the most convincing evidence for the existence of diffusion creep. Annealing this alloy in a hydrogen atmosphere results in extensive precipitation of zirconium hydride in the form of stringers extending throughout the sample. The zirconium hydride precipitates can thus act as internal markers. It was found that during creep tests at 450^{o}C zones denuded of the precipitate formed at grain boundaries perpendicular to the direction of

the applied stress. These zones were attributed to the diffusion of Mg atoms along grain boundaries lying perpendicular to the applied stress (Squires et al 1963). Initially there was some doubt as to whether or not these zones were in fact due to diffusion creep since similar experiments revealed a stress exponent of 4 instead of unity and it was thought that second phase particles might inhibit diffusion creep (Vickers and Greenfield 1967). However, these experiments were carried out at higher stress levels than those of Squires et al, and it has been suggested that the n value of 4 is probably due to dislocation creep becoming more dominant in this region and also to the fact that a true steady state creep rate is not often obtained. (Harris et al 1969). Another theory put forward to account for the precipitate free zones suggested a redistribution of precipitates would result from stress oriented grain boundary migration (Raraty 1966) but since this would lead to an accumulation of precipitates alongside the zones, the proposal was dismissed (Harris et al 1969).

Electron microprobe analyses of Mg ½wt% Zr showed zirconium free zones and also that in compression the zones formed along boundaries approximately parallel to the stress axis suggesting they were formed by diffusional creep (Karim et al 1969). Lee (1969) disagreed with the conclusion noting that there was no accumulation of Zr at the longitudinal boundaries and suggested grain boundary migration caused by shear would result in denuded zones consistent with Karim's observations.

Harris et al (1969) also pointed out that the presence of denuded zones alone was insufficient to infer diffusional creep and that the mechanism would require the accumulation of precipitates along grain boundaries parallel to the stress axis as well as denuded zones normal to the tensile axis. Evidence for such a result has been presented by Pickles (1967) and Harris et al (1969) for creep tests on Zr55 at 500°C.

1.2.3.3. Grain Boundary Sliding and Cavitation

Magnox A180 was accepted as a good canning material due to its ability to comply with the stringent physical requirements of strength and ductility over the temperature range employed for operation of a thermal reactor. However, during its first year of use, expensive delays and losses of power were experienced because of reactor shutdown, as a result of failures in the magnox cans. It was discovered that grain boundary cavities formed and ultimately linked to give ready leakage paths for the fission gases. Dimensional changes in the can during service had given rise to stresses resulting in conditions which caused relatively high local strains of 4% or 5% in a year and at

200-250^{o}C intergranular cavitation had occurred.

The mechanisms of nucleation and growth of the cavities are still the subject of controversy (for a recent review see Goods and Brown 1979) but it is recognised that the process of grain boundary sliding, which is known to take place in magnesium, plays an impcrtant role in this material. Much interest has been centred on trying to measure the magnitude of the grain boundary sliding contribution to the overall creep deformation. The attempts have involved measurements of surface offsets at boundaries usually made parallel or normal to the tensile axis in the plane of the specimen surface; very few measurements have been made normal to the surface. Langdon (1965) investigated the variation of sliding in Magnox A180 with stress and grain size. Measurements were taken of the step height between adjacent surface grains representing the component of sliding perpendicular to the surface at regular strain increments throughout a test. The grain boundary offsets were revealed by interference fringes. It was found that at low strain rates and small grain sizes at temperatures above 0.4 Tm (100^{o}C) sliding accounted for 70-80% of the total deformation during early stages of creep, up to about 2% total strain. Gifkins et al (1968) carried out experiments on polycrystals of lead-thallium, brass, super-pure Al and magnox A180 in conditions of creep at These authors showed that in general the grain boundary sliding is dependent on the resolved shear component of the applied stress and that at the surface the component of sliding which is perpendicular to the surface is influenced by forces arising from the movement of grains in the interior. It must be remembered that experimental investigations of sliding involve the sliding components measured at a free surface and this free surface may affect the value of the components and that the total creep strain recorded rarely exceeds 4%.

Gifkins (1956) had proposed that the cavities occurring at grain boundaries in magnesium were formed as a result of grain boundary sliding during deformation. He suggested that transcrystalline slip produces boundary jogs which create the necessary stress concentrations to cause void formation during any subsequent sliding, thus accounting for the increased cavitation in experiments carried out at slower strain rates where grain boundary glide plays a greater part in the deformation. Chen and Machlin (1957) came to similar conclusions but assumed that the grain boundary ledges were ingrown. However, one objection to the idea that cavities are nucleated at ledges is that it

is unlikely that such barriers can nucleate fracture at stresses below that for triple point cracking. McLean (1963) in attempting to overcome this objection suggested that narrow steps capable of allowing sliding at either side existed at a grain boundary. He carried out a calculation for Magnox A180 and a nimonic alloy which showed that reasonable rates of sliding were capable of opening up a cavity. However, Harris (1965) in a comprehensive review of the nucleation of creep cavities in magnesium showed by using a corrected expression that the opening of a void at even a very small ledge would require unrealistically high rates of sliding. Other mechanisms have been suggested to account for the nucleation of voids these are vacancy condensation and particle induced cavitation.

Greenwood (1952) attempted to explain cavities which occurred at grain boundaries in α-brass at high temperatures and low strain rates. It was suggested that an excess concentration of vacant lattice sites created during deformation within the grains, diffused towards the grain boundaries. The vacancies at boundaries transverse to the stress axis would form stable groups under the applied tensile stress. In later work Greenwood et al (1954) extended their research to include copper and magnesium as well as α-brass. When these metals were strained at elevated temperatures, cavities formed at intercrystalline boundaries being more prevalent in boundaries transverse to the tensile stress axis. Greenwood et al found that ductility decreased as temperature was increased for a given strain rate. They explained the interesting ductility-temperature relationship of Mg by suggesting that as the temperature is raised, new slip systmes begin to operate causing the ductility to increase, whilst the increasing intergranular cavitation with increasing temperature causes the ductility to decrease. Hence the resulting well known minimum in the ductility vs temperature curve. Greenwood's mechanism of cavity nucleation was later shown to be unsatisfactory (Machlin 1956) because the number of vacancies required to form a stable hole by homogeneous nucleation was too large. Machlin predicted that cold work would reduce elongation at fracture and that for a given structure the product of the steady state creep rate and rupture life for pre-annealed metals and single phase alloys is an approximately invariant quantity. However, Machlin's theory also suggested that if a test was halted in the transcrystalline stage of rupture before failure then it would be possible to observe spherical holes within the grains, and that compression tests would produce holes at the grain boundaries by 5% strain. Stacey (1958) carried out such

experiments but failed to obtain experimental verification of Machlin's predictions. Crussard and Friedel (1956) also considered vacancies to be a controlling factor in void formation. They suggested that the necessary excess of vacancies could be produced when dislocations interact with each other on different slip planes or with obstacles during climb. Honeycombe and May (1960) studied the fatigue characteristics of Mg in push-pull experiments for a number of grain sizes from room temperatures to 300^{o}C. Below 250^{o}C they found that transgranular cracks caused failure whilst at temperatures above 250^{o}C cracks initiated in grain boundary regions and were intergranular. They suggested that at higher stresses the intergranular failure is initiated particularly at grain corners by stress concentrations produced either by the restriction of grain boundaries or by the pile up of dislocations on basal slip striae which are very pronounced at 150^{o}C and 250^{o}C.

Brookes et al (1959/60) studied the effects of temperature, strain rate and grain size onductility and investigated the observed cavitation. They found that cavitation increased with strain and also with decreasing strain rate over the range 4×10^{-5} - 6×10^{-6}/hr, and that cavities were less numerous and of smaller average size in finer grained material.

Harris demonstrated that it was possible to nucleate creep cavities heterogeneously at second phase particles at stresses below that necessary for triple-point cracking and further showed that such particles exist in Magnox A180 in sufficient numbers to account for observed cavity frequencies. Harris's theory suggested a critical particle size for cavity nucleation but Intrater and Machlin (1960) suggested that cavity nucleation could be achieved for smaller particles if g.b.s. occurred in rapid bursts many times faster than the overall sliding rate.

The precipitate mechanism for cavity nucleation, unlike the other mechanisms does have supporting experimental evidence, e.g. in copper (Fleck et al 1975) pure iron (Taplin and Wingrove 1967) and in Cr-Ni-Mo steel (Johannesson and Tholen 1970) but the mechanism of void growth is still controversial as evidence in support of both vacancy condensation (Harris 1965) and grain boundary sliding (Evans 1969) has been put forward in the literature.

CHAPTER 2

Experimental Techniques

2.1. THE MATERIAL

Some preliminary experiments were carried out on commercial purity Mg but as found by other workers (e.g. Langdon 1965) problems of inhomogeneous grain growth and severe oxidation were encountered, particularly in the higher temperature tests. For this reason the magnesium alloy Magnox A180 was used for most of the experimental work. In the latter stages of research a small number of experiments were carried out on the alloy Magnox Zr.55 (See Appendix D). Both alloys were supplied by the Magnesium Elektron Company in the form of 9/16" diameter extruded bar. This meant that the starting material had a strong preferred orientation with the basal planes tending to lie preferentially in the extrusion direction (Roberts 1960).

Magnox Al 80 is a single phase magnesium alloy containing 0.8% Al 0.005% Be. It has a close-packed hexagonal structure with a c/a ratio at room temperature of 1.623. This is close to the ideal ratio of 1.633. Its melting temperature is 649^{o}C. A phase diagram showing the alloy composition is presented in Fig. 2.1. ZR 55 is a binary alloy Mg-0.5 wt% Zr. Annealing in a hydrogen atmosphere results in extensive precipitation of zirconium hydride in the form of stringers (Squires et al 1963).

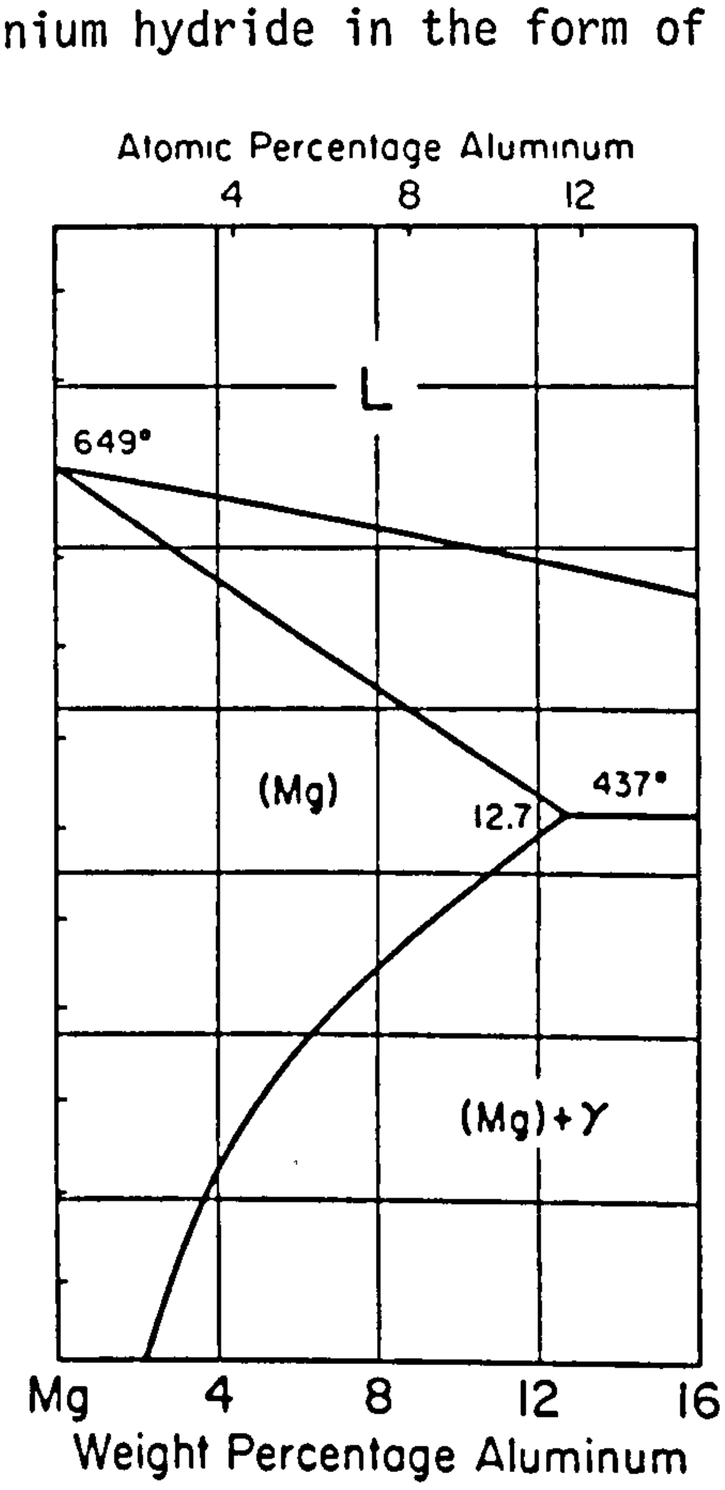


Figure 2.1 Part of the phase diagram of the Mg-Al system.

2.2. MECHANICAL TESTING

The mechanical tests were carried out on a floor model 5000 kg full scale deflection Instron operating in compression. The crosshead speeds utilized in the experimental work lay in the range 0.0005 cm min^{-1} and 0.2 cm min^{-1}, i.e. average plastic strain rates of $\dot{\varepsilon} \sim 10^{-6}s^{-1}$ - $10^{-2}s^{-1}$. The specimens were held inside a furnace which had a constant hot zone of 5 cm. The temperature within the specimen area was continuously monitored by a chromel-alumel thermocouple located at the specimen surface near the midpoint of the test piece. Preliminary experiments were carried out to ensure that the temperature variation over the specimen length was no greater than $\pm 2^{o}C$. It was possible to keep the furnace temperature constant to within $\pm 2^{o}C$. It was the changes in internal structure which were of interest so surface oxidation of the specimens (which was slight even at the higher temperatures) did not prove to be a problem.

The tests were carried out in the temperature range 100-370^{o}C, the majority being at 150, 260, 300 and 370^{o}C. Graphite was used as a lubricant to reduce the friction of the crossheads with the ends of the specimen. PTFE was used for some of the specimens but it proved to be a problem rather than an asset in tests where the sample had a length: diameter ratio of greater than 1.5:1 since the inhomogeneity of the deformation caused the specimen to rotate between the rams.

The tests were carried out at constant rates of compression, i.e. constant crosshead speed. Thus owing to the decrease in specimen length during a test there was a resultant increase in the strain rate. However, this increase was small during the initial stages which meant that the results could be compared directly with those of other workers, many of whom have used similar testing conditions, since it is only recently that Servo-hydraulic constant strain rate machines have become available.

In view of the strong preferred orientation of the starting material and its known anisotropical behaviour (Burke and Hibbard 1952) specimens with two different starting orientations were tested. These are shown in Figure 2.2. One set (Figure 2.2.a) were oriented such that their basal planes were aligned parallel with the extrusion direction of the supplied rod, i.e. in an unfavourable orientation for basal slip. The second set (Figure 2.2.b) were machined such that they were favourably oriented for basal slip.

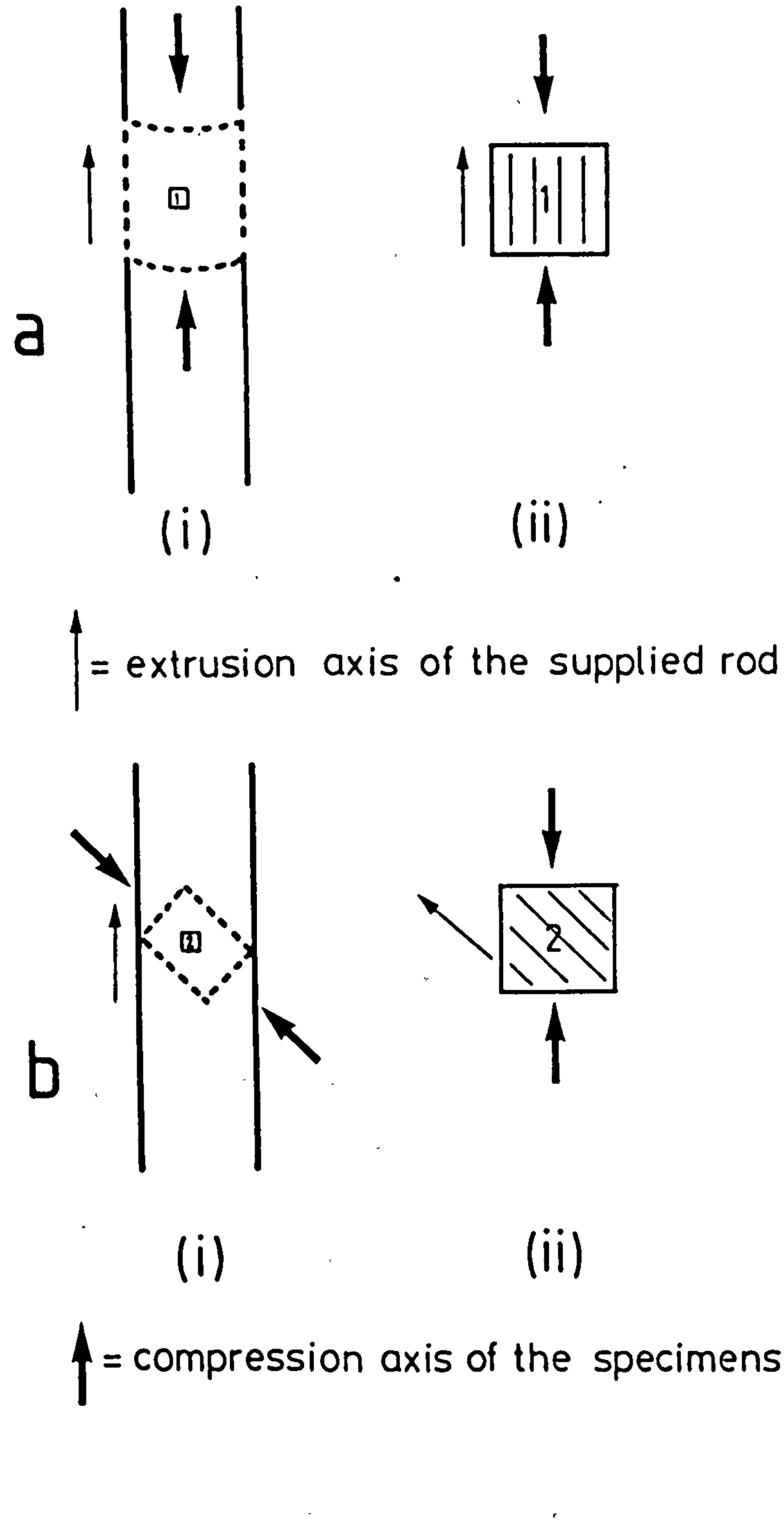


Figure 2.2 Schematic diagram to illustrate the sample orientation
i) with respect to the supplied material
ii) with respect to the compression axis of the specimens
The traces of the basal planes are shown in (ii).

2.3. SPECIMEN PREPARATION

Specimens as shown in Figure 2.2. were machined from the supplied extruded rod. The ends of the specimens were carefully ground parallel to each other and normal to the axis of compression on SiC abrasive paper. They were then polished in 10% HNO_3 to remove any surface deformation before being annealed at 500^{o}C for 24 hours. This heat treatment produced an equiaxed uniform grain size of ~400 μm which was found to be the most suitable. The inhomogeneous secondary grain growth which has been sometimes reported in this material resulting in one or two very large grains was rarely encountered (Higgins 1963). Specimens which did contain the feature were discarded.

After testing, the specimens were water quenched within one minute of the crossheads being reversed. The samples were then sectioned parallel to the compression direction. A slice 1.5 mm thick was removed from the centre of each specimen. The sectioning was carried out using a spark eroder so that a minimum amount of deformation would be introduced. The slices were polished using standard metallographic techniques viz, the surface was ground flat with SiC paper P600A, followed by polishing on 3μ, then on 1μ diamond impregnated cloth. They were immersed in 10% HNO_3 for ~10s to remove any surface deformation which may have been introduced during the mechanical polishing. The surface deformation was easily recognisable optically, occurring in the form of fine scratches marked by very narrow rows of twins.

The final polish was carried out in 30% HNO_3:70% CH_3OH followed by washing in methanol and drying in lab. air. In general this technique resulted in a good polish with the grain boundaries sufficiently revealed to enable preliminary observations of the microstructure to be carried out. For the detailed optical work an acetic picral etch was used to produce a birefringent coating on the specimen surface enabling quantitative metallography to be carried out. This technique is described in detail below. A Vickers Photoplan M41 was the optical microscope used for the work.

2.4. COLOUR TECHNIQUE

A technique first used by Couling and Pearsall (1957) involving the use of colour metallography has been employed to aid with the interpretation of the optical microstructures. It is well known that polarised light can be employed to obtain crystallographic information about anisotropic metals, but quite often the experimental techniques

used are complicated and tedious. In the case of hexagonal metals there are four extinction positions which can be detected when the specimen is rotated about the axis of the microscope. These correspond to alignment of the plane of incident polarised light with the trace of the basal plane or its normal in the grain surface (Hallimond 1953). The magnitude of the basal plane tilt can be estimated from the angular range over which extinction is maintained.

George (1947) showed that the optical anisotropy of magnesium was increased by etching the polished surface in a solution containing picric acid, water, acetic acid and methanol. Other workers (Couling and Pearsall 1957, Williams et al 1969) have reported studies using similar etches but in the present work the following combinations of chemicals was found to give the best results.

4.2 g picric acid
10 ml water
10 ml glacial acetic acid
70 ml ethanol

Freshly polished specimens were immersed in the solution at room temperature for 4-5 secs (until the surface assumed a brown colouration,) were washed in ethanol and allowed to dry in lab. air.

This procedure produced a double-refracting layer on the specimen surface. The metallograph used was one which permitted the insertion of a full wave retardation plate (sensitive tint plate) between the specimen and the polariser. The sensitive tint plate permitted selective wavelength extinction to occur causing the colour of a grain to change from blue to orange when the trace of the basal plane was exactly parallel to a horizontal crosshair in the microscope eyepiece (Williams et al 1969). This meant that the twofold ambiguity in determining the direction of the hexagonal axis, by normal extinction without the waveplate, was eliminated; it was also easier to subjectively detect small misorientations as the human eye is more sensitive to changes in colour than to variations in black/grey/white.

Quantitative measurements were carried out using a photo-cell to determine the extinction position and therefore the direction of the basal plane in any grain to an accuracy of 2-3^{o} providing the basal plane was steeply inclined to the specimen surface. The use of this optical technique made it possible to detect misorientations within the old grains after deformation and to obtain information about the relationship of recrystallised grains to adjacent old grains.

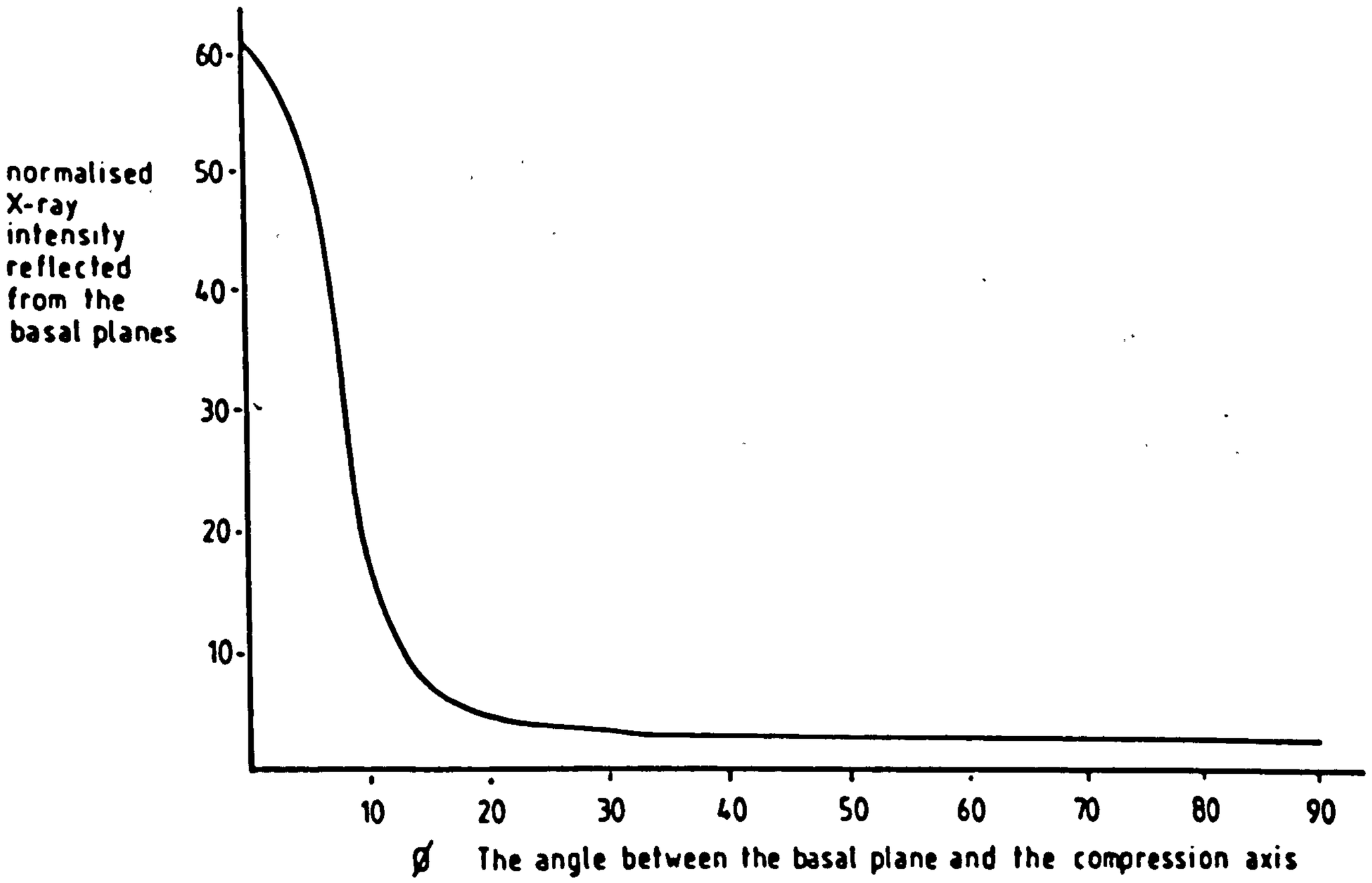
The technique as used in the current work merely located the basal plane trace, it did not define the spatial orientation of the basal pole of individual grains which required a definition of the magnitude of the basal plane tilt as well as the direction of the basal plane trace in the grain surface. The amount of basal plane tilt in any grain can be estimated from the magnitude of the intensity change around the extinction position. The greatest change occurs when the basal plane is perpendicular to the surface and no change occurs when it is parallel. However, in this study the preferred orientation of the specimens was such that the majority of basal planes were steeply inclined to the specimen surface and extinction was limited to $\sim$a 10^{o} range. An absolute description of the basal pole orientation was not necessary; quantitative estimations of misorientations within grains and angular tilt between subgrains and deformation bands could be made since many grains had similar basal plane tilts. Williams, Brown and Healey(1969) describe a method of determining the basal pole orientation and hence the basal plane texture in polycrystalline Magnox A180, but the technique is tedious and a time of $\sim$4 hours per sample is considered necessary for an experienced operator to quantify the basal texture.

2.5. X-RAY GONIOMETRY

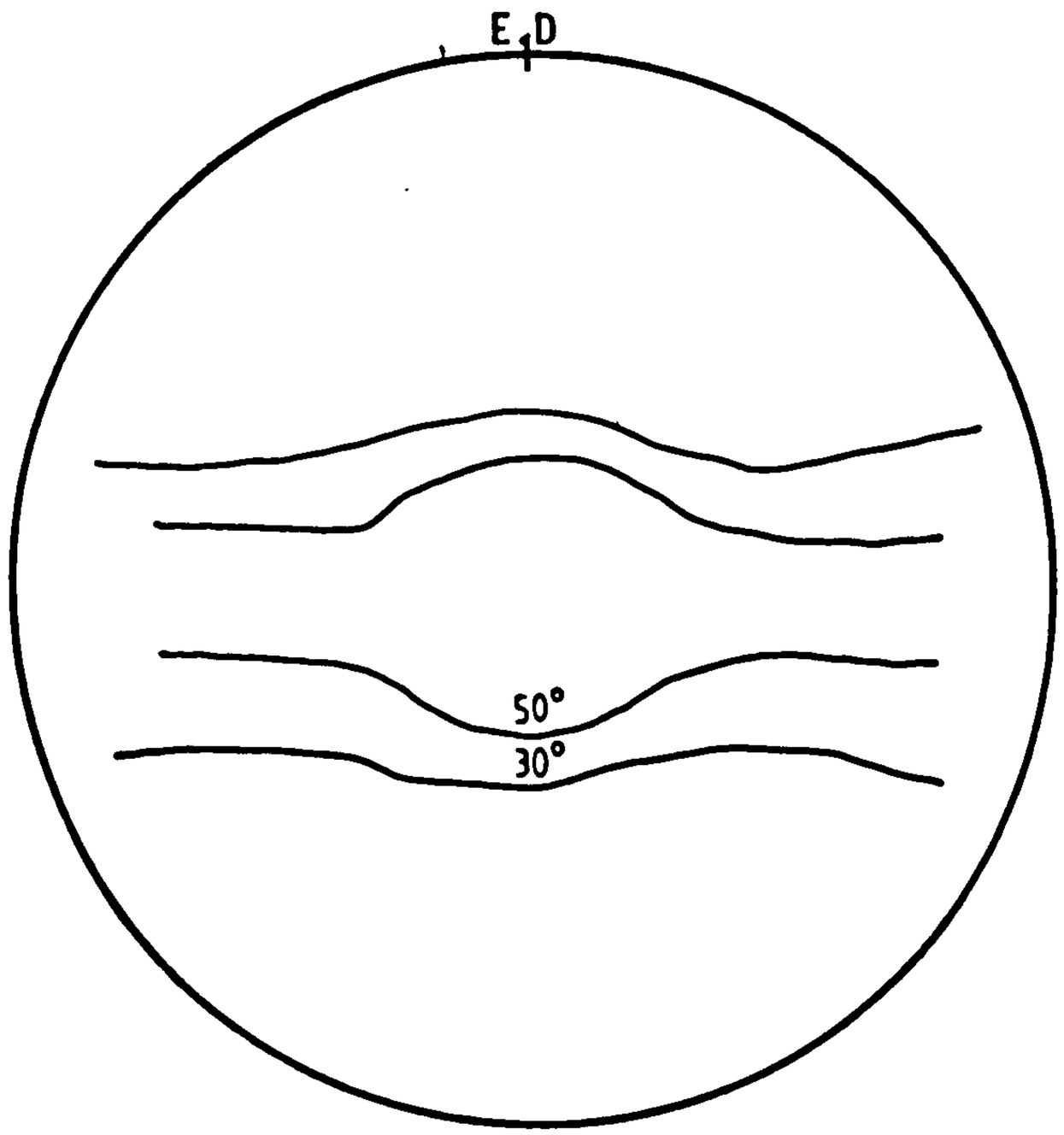
The degree of preferred orientation in a material can be detected in many ways. Practically the most convenient way to determine this texture is by X-ray diffraction. Pole figures provide a convenient and quantitative method for showing the arrangement of crystallographic planes in a polycrystalline material. They are plotted from X-ray diffraction data taken with a known sample alignment with respect to the X-ray beam whilst the sample is tilted at various positions around say its rolling direction and rotated around an axis perpendicular to its rolling plane. The data are usually continuously using a recorder and then transferred to the standard stereographic plot used for pole figures.

In this work a Philips Texture goniometer PW1078 which was developed primarily for studying the texture of metals was used in a reflection mode to determine the preferred orientation of the Mg samples. The design of the PW 1078 is based upon the well known Schulz method (1949).

The slices parallel to the compression axis sectioned from the centre of the deformed samples were used as specimens in the goniometer. Since the machine was being operated in the reflection mode care was taken to ensure that surface polish was not damaged during setting up of



(a)



(b)

Figure 2.3 This figure illustrates the way in which the X-ray data is presented in the experimental results. The basal plane profile is shown in (a), whilst the 0002 pole figure of the starting material is shown in (b). The pole figure is the standard girdle to be expected from an extruded rod and the profile shows that the majority of basal planes are closely aligned with the extrusion axis of the rod.

the specimens. The instructions as laid out in the Astm Book of Standards (1963) were followed to prepare the pole figures. It was found useful to present the information obtained from the X-ray goniometer in the form of basal plane profiles rather than pole figures. The profiles record the intensity of X-rays reflected from the basal plane as a function of ϕ, the angle between the plane and the compression axis. An example of such a profile is shown schematically below (Figure 2.3). The technique enabled easy comparisons to be made of the change in texture which occurred as a function of strain.

2.6. ELECTRON MICROSCOPY

a) Transmission

The slice cut from the centre of a specimen was repolished using 30% HND_3 70% CH_3OH after the optical microscopy and X-ray goniometry had been completed. 3mm discs were cut from the centre of each slice, the spark machine again being the cutting tool to minimise deformation.

A standard electropolishing technique for profiling the discs ready for electron microscopy (see e.g. Briers et al 1963) was employed. The specimens were held in a PTFE holder (Figure 2.4.) as shown. The contact to the specimens was made with a piece of platinum wire and the cathode was made from a piece of stainless steel. The electropolishing solution was 5% HNO_3 and the operating conditions were 20V 1A for ~20s. (A small amount of wetting agent was added to the solution to prevent the adhesion of bubbles to the surface being polished.) A disc was taken from the corner of each slice and profiled until it just perforated in the centre. The time was noted and for subsequent discs the current switched off 3 seconds before perforation was expected. In view of the fact that magnesium undergoes chemical attack in nitric acid, once the specimens had been dished they were quickly removed from the PTFE holder and rinsed in methanol.

The final thinning process was carried out chemically in 30% HNO_3 70% CH_3OH cooled with liquid N_2 to -20°C. The discs were held in CTFE tweezers or steel tweezers coated with Lacomit. A focussed light source illuminated the back of the discs so that a hole could be detected just after it formed. When this occurred the discs were quickly removed and carefully washed in CH_3OH.

Some discs were made on the highly praised Struers Jet Polishing machine, but they were found to be buckled in the thinnest areas at the edge of the foil and this technique was abandoned.

The thinned discs were observed using the AEI EM7 1 MeV high voltage electron microscope at Imperial College. Most microscopy was performed at 500 KeV using the standard double tilt, rear entry state of the EM7. Most standard electron microscopes operate at 100 kV but there are well known advantages to be gained from the use of higher voltages. Thicker foils can be used and much greater areas can be penetrated by the beam making the results obtained more representative of bulk behaviour. A further advantage is that not only do more electrons penetrate the specimen

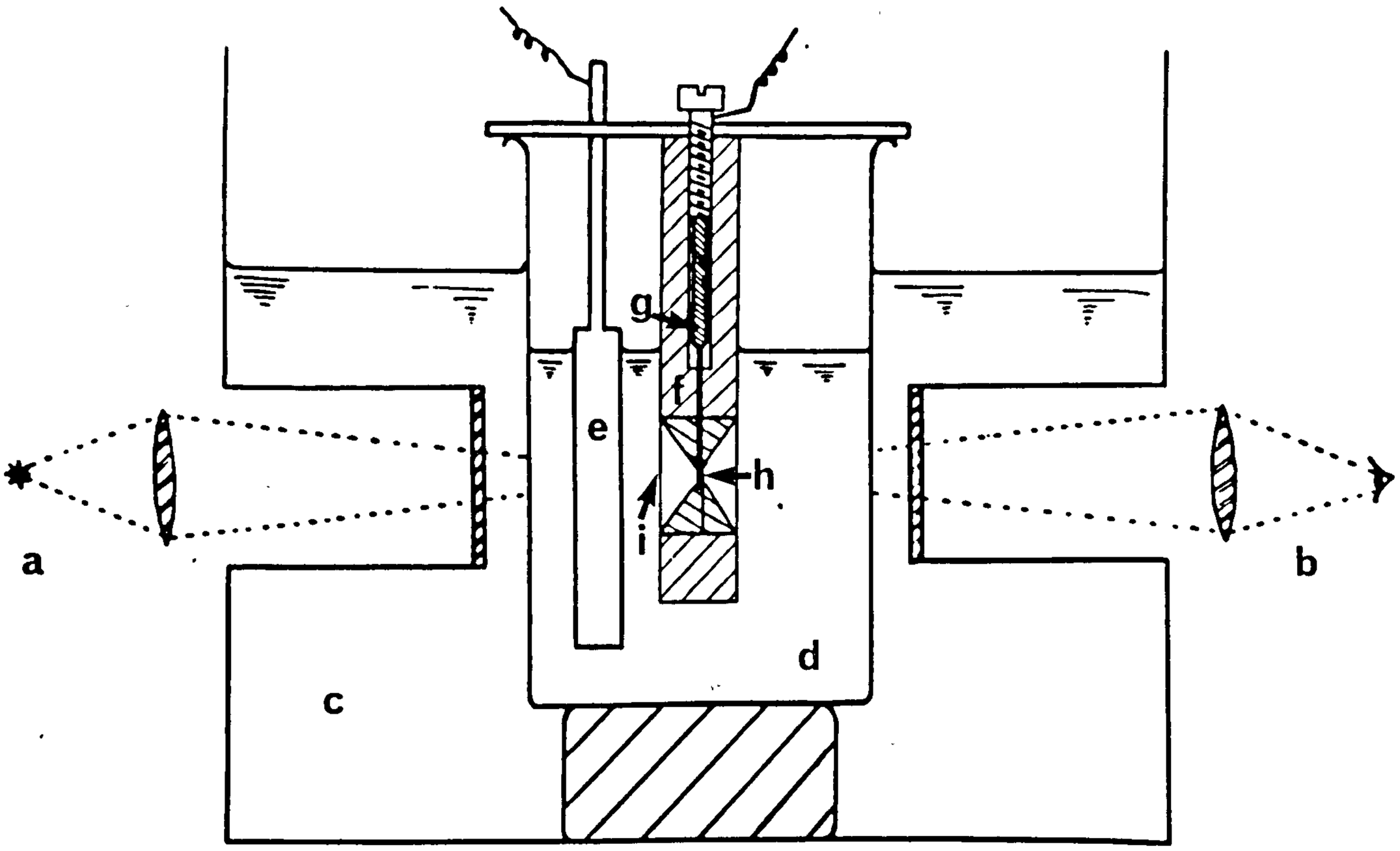


Figure 2.4 Diagram to illustrate electropolishing apparatus.

a Light source
b Viewing monocular
c Temperature control bath
d Electolyte bath
e Cathode
f P.T.F.E.holder
g fully adjustable contact plug
h specimen
i threaded plug

but since the scatter angles decrease with increased kilovoltage, the electron diffraction pattern contains many more orders of diffraction than at lower voltages. The greater specimen thickness also enables the imaging of the crystallographically informative Kikuchi line patterns. (Other advantages are well reviewed by Agar 1974.)

b) Scanning

A Cambridge 600 Stereoscan and a JEOL JSM 35 scanning electron microscope were used to examine the surfaces of the deformed specimens which had been coated with a gold grid prior to testing. An operating voltage of 15 kV was found to give the most satisfactory results.

CHAPTER 3

Results

RESULTS

3.1. INTRODUCTION

Dynamic recrystallisation has been found to play an important part in the deformation of magnesium at elevated temperatures. Its role in the development of microstructure during deformation has been studied in detail. The results will be divided initially into two sections, viz mechanical behaviour followed by microstructural development. The mechanical behaviour will include the variations in stress strain behaviour with T and $\dot{\varepsilon}$ and also the effect of preferred orientation. An estimation of the activation energy Q and the stress exponent n will be made from the stress strain data. The microstructural observations will then be related to specific conditions of stress/strain, strain-rate and temperature.

3.2. MECHANICAL PROPERTIES

3.2.1. Introduction

The specimens tested were all deformed in uniaxial compression. The standard Instron outputs in the form of load vs time curves were converted to stress strain curves by a simple computer programme (see Appendix A). The programme assumed that constant volume was maintained and that the cross-sectional area increased uniformly with increasing strain. At temperatures below $\sim 320^{o}C$ the curves are only accurate up to ~25% strain. Beyond this strain the heterogeneous nature of the deformation, particularly in specimens which contained shear-zones, rendered the interpretation of such curves difficult. At higher temperatures where the deformation is homogeneous then the curves are accurate over the entire range of the tests and the steady state attained after ~25% strain is thought to be a real effect.
A large spectrum of deformed specimens of Magnox A180 has been examined and the data obtained from the mechanical tests is recorded in Figure 3.1. It was found, in agreement with other work carried out on magnesium that the yield stress decreased with increasing temperature (Figure 3.2.)

The peak stress as well as being strongly temperature dependent also depended upon the preferred orientation of the starting material. The behaviour can be divided into two categories; firstly that of material unfavourably oriented for basal slip and secondly that of material favourably oriented for basal slip. The former will be presented first.

Figure 3.1. Table of results of the mechanical testing.
The temperature, peak stress, strain at the peak stress, final stress, final strain, stress at 20% strain and 30% strain and the strain rate are recorded in tabular form.

SAMPLES UNFAVOURABLY ORIENTED FOR BASAL SLIP

$T(^oC)$	σ_p(MPa)	ε_p	σ_f(MPa)	ε_f	σ_{20}(MPa)	σ_{30}(MPa)	$\dot{\varepsilon}$
150			7.00	10			10^{-5}
	12.00	18	6.90	22	10.50		
	14.00	16	8.50	35	12.50	9.50	
	12.25	18	4.50	55	11.90	5.90	
200	11.00	18	10.00	22	10.90		
	11.00	18	3.50	55	10.50	8.00	
230	10.20	17	9.90	22	10.10		
	10.20	17	2.20	55	10.10	9.00	
260			2.69	2			
			4.00	8			
			6.50	9			
			7.88	12			
			8.25	14			
	8.90	16	8.90	16			
	8.25	16	7.90	25	8.00		
	8.00	16	5.50	35	6.67	5.30	
	9.20	16	3.50	47	8.50	5.50	
	10.00	16	4.25	55	9.80	7.90	
	9.00	16	4.30	65	8.50	5.50	
280	7.42	14	4.18	40	6.96	5.07	10^{-5}
300			3.90	9			
	6.60	14	6.34	15			
	6.50	16	5.70	20	5.70		
	6.71	16	5.01	26	6.46		
	6.11	16	3.79	33	5.26	41.6	
	7.20	16	4.00	55	7.00	5.50	
310	5.90	15	2.10	55	4.70	3.20	
	4.60	10	4.50	15			

Figure 3.1. (continued)

T(^{o}C)	σ_p(MPa)	ε_p	σ_f(MPa)	ε_f	σ_{20}(MPa)	σ_{30}(MPa)	$\dot{\varepsilon}$
320	2.50	8	2.50	10			
	2.50	7	2.40	11			
	3.50	9	3.40	13			
	4.00	15	3.50	22	3.80		
	4.00	13	3.00	55	3.60	3.20	
370			0.70	1.5			
	2.00	5	2.20	7			
	2.00	6	1.90	14			
	2.33	6	1.70	25	1.95		
	2.43	7	1.60	38	1.74		
	2.30	8	1.70	55	1.80	1.70	
230	5.50	30	5.20	45	4.50	5.50	
300	4.20	14	2.00	33	3.25	2.00	10^{-6}
	4.80	15	2.00	55	4.70	4.00	
310	3.80	10	1.75	55	3.00	1.75	
370	2.33	6	1.70	27	1.95		
300	7.90	15	5.60	35	6.50	6.20	3×10^{-3}
	7.50	13	3.50	35	5.00	4.00	1×10^{-3}
	5.50	13	3.40	35	4.75	3.50	5×10^{-4}
	4.90	13	3.00	35	4.00	3.25	2×10^{-4}
	4.80	12	2.80	35	3.75	2.90	1×10^{-4}
	4.40	11	2.25	35	3.00	2.40	5×10^{-5}
SAMPLES FAVOURABLY ORIENTED FOR BASAL SLIP							
260			2.90	5			10^{-5}
			3.40	10			
	4.60	25	4.60	30	4.60		
	4.80	26	2.75	70	4.50	4.70	
300			2.20	5			
			3.40	10			
	2.75	12	2.60	30	2.70	2.60	
	2.75	12	2.00	63	2.60	2.50	

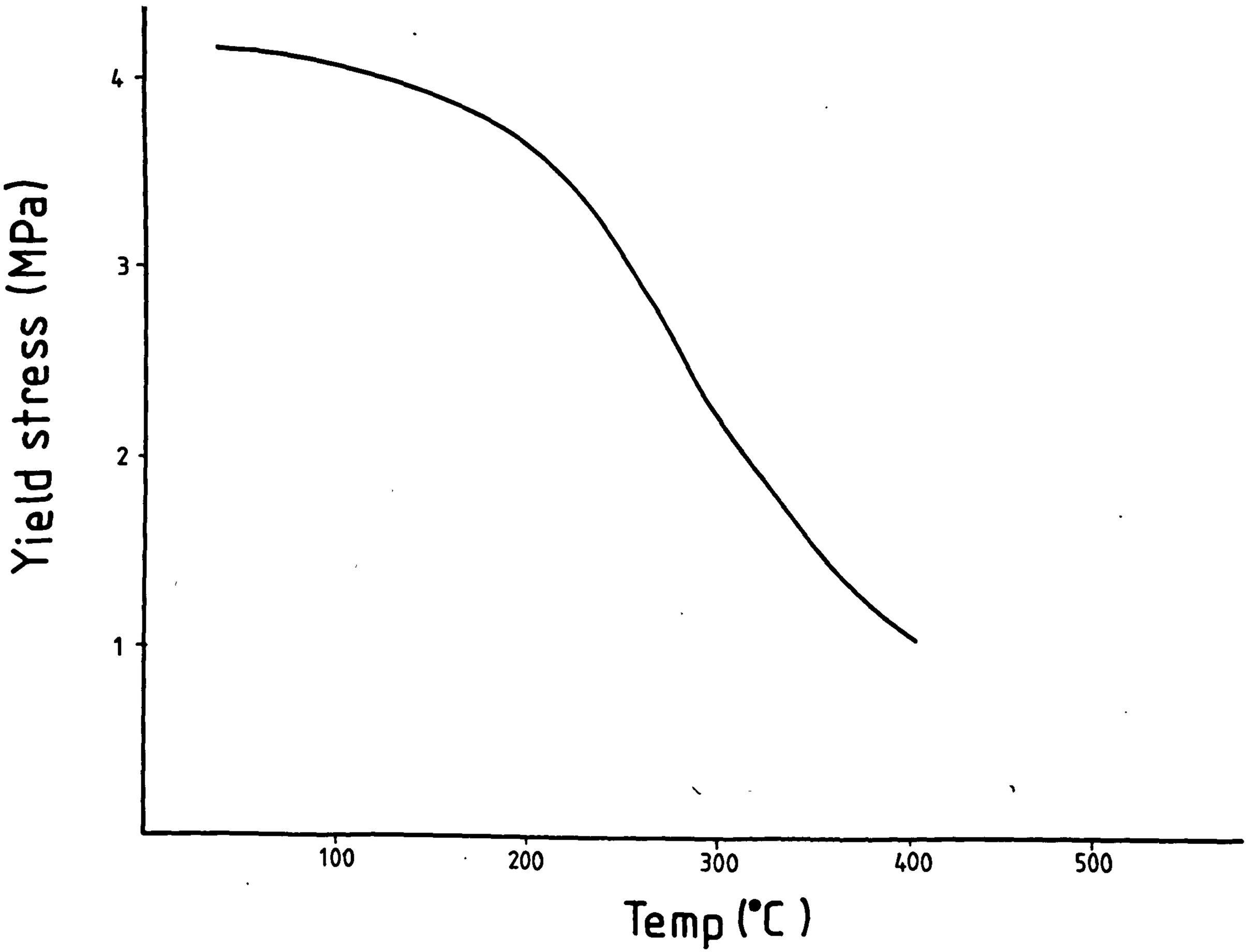


Figure 3.2 Graph of yield stress vs. temperature for samples of polycrystalline Magnox A180.
$\dot{\varepsilon} = 10^{-5} s^{-1}$.

3.2.2. Stress strain behaviour of material unfavourably oriented for basal slip

Typical stress strain curves for tests at three temperatures are shown in Figure 3.3. A peak stress is particularly marked in the 2 lower temperature tests and is followed by marked softening in both cases. At the higher temperatures there is only a slight peak and very little softening thereafter. The peak occurs at higher strains at lower temperatures and the value of the peak stress is dependent on temperature (Figure 3.4) and strain rate (Figure 3.5). The peak decreases with increasing temperature and decreasing strain rate. However, as will be shown later the microstructure of the samples also varied with temperature and strain rate so it was not possible to separate the stress, temperature, strain rate and structure parameters.

In the metallurgical literature (at least for hot working, e.g. Jonas et al 1969) it is common to plotlog steady state stress against log strain rate or log Z where Z is the Zener-Holloman parameter and to calculate the stress exponent n from the gradient. In the current work however, strictly speaking, a steady state was not attained except at high temperatures so the log peak stress was plotted against log strain rate (Figure 3.6). This stress is still a flow stress and since the microstructure was relatively homogeneous it was thought that a value of n could be obtained from the gradient. The gradient of the graph had a value of 0.14.

$$\text{Now gradient} = \frac{1}{n} = 0.14$$

$$\therefore \quad n = 6.89$$

This.figure is in agreement with the values obtained from the strain rate and temperature change experiments described in the next paragraph.

Calculation of Q and n

The activation energy Q and the stress exponent n in the creep equation

$$\dot{\varepsilon} = A\sigma^n \exp\left(-\frac{Q}{RT}\right)$$

where A = a constant

R = universal gas constant

were calculated by fitting data from strain rate and temperature change tests to the above equation. The microstructure was assumed to be constant during the period over which measurements were taken - a point which will be discussed at a later stage.

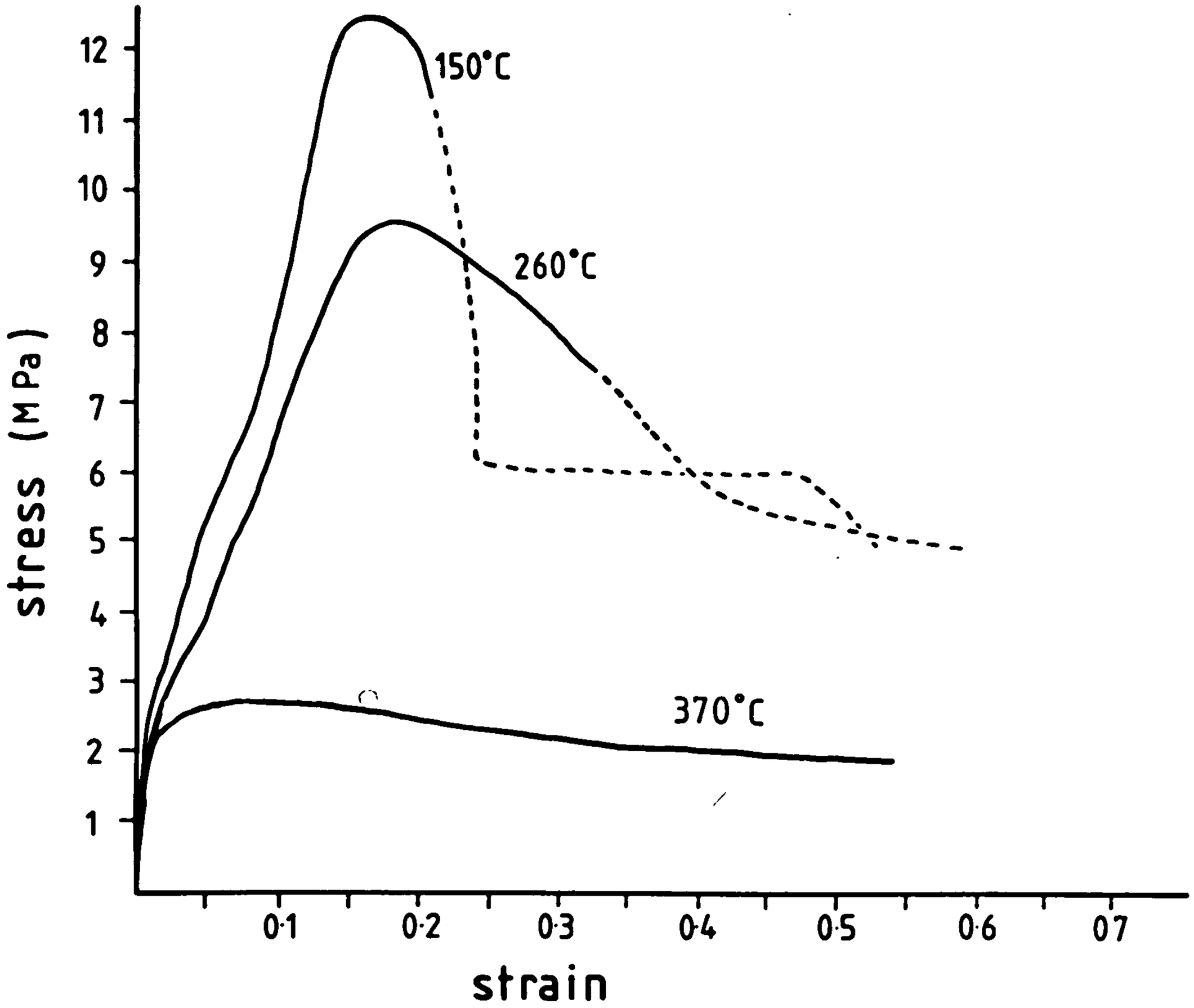


Figure 3.3. Stress strain behaviour of polycrystalline samples with a strong preferred orientation which was unfavourable for basal slip. The three curves illustrate the effect of temperature on the stress strain behaviour at a strain rate of $10^{-5}s^{-1}$.

T(^{o}C)	average peak stress (MPa)
150	12.75
200	11.00
230	10.20
260	8.89
280	7.42
300	6.62
310	5.25
320	3.30
370	2.21

Figure 3.4. Table of peak stress and temperature for material unfavourably oriented for basal slip ($\dot{\varepsilon} = 10^{-5}s^{-1}$)

peak stress (MPa)	strain rate (s^{-1})
7.90	3×10^{-3}
7.50	1×10^{-3}
5.50	5×10^{-4}
4.90	2×10^{-4}
4.80	1×10^{-4}
4.40	5×10^{-5}

Figure 3.5. Table of peak stress and strain rate at 300^{o}C in material unfavourably oriented for basal slip.

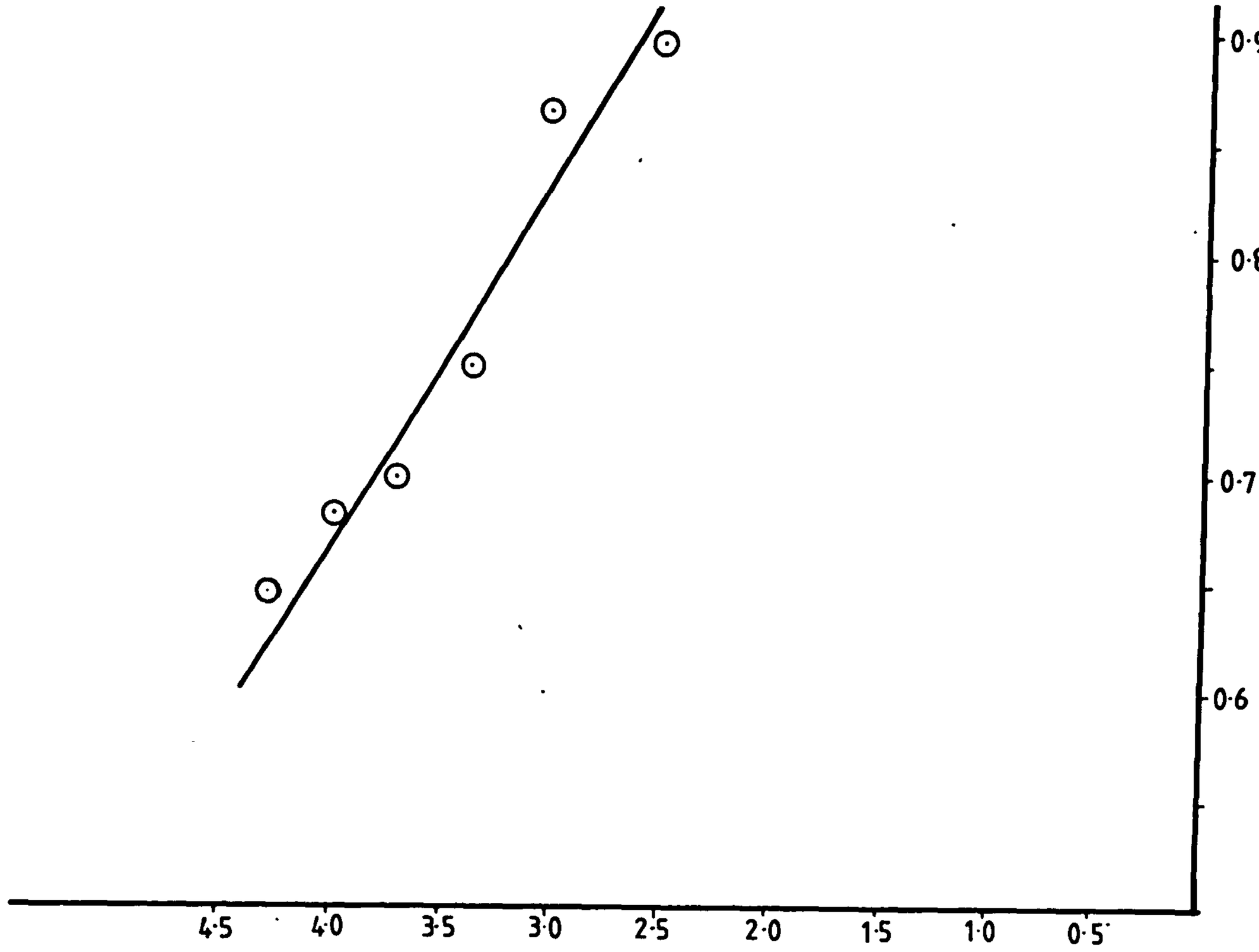


Figure 3.6. Log peak stress vs. log strain rate for specimens deformed in the orientation unfavourable for basal slip. T = 300°C

change of strain rate

$\dot{\varepsilon}$	1 load(kg)	2 load(kg)	3 load(kg)
$10^{-6}s^{-1}$	690	330	255
$10^{-5}s^{-1}$	950	460	355

	Q
$n_1 = 6.9$	24.1
$n_2 = 7.0$	24.5
$n_3 = 7.2$	25.1

change of temperature $\dot{\varepsilon} = 10^{-5}s^{-1}$

$T_1(K)$	$L_1(kg)$	$T_2(K)$	$L_2(kg)$
533	550	463	910

Figure 3.7. Values of the activation energy Q and the stress exponent n.

i) at constant temperature

$$\dot{\varepsilon}_1 = A\sigma_1^n \exp - \frac{Q}{RT}$$

$$\dot{\varepsilon}_2 = A\sigma_2^n \exp - \frac{Q}{RT}$$

$$\frac{\sigma_1^n}{\dot{\varepsilon}_1} = \frac{\sigma_2^n}{\dot{\varepsilon}_2}$$

$$\frac{\log \frac{\dot{\varepsilon}_1}{\dot{\varepsilon}_2}}{\log \frac{\sigma_1}{\sigma_2}} = n$$

ii) at constant $\dot{\varepsilon}$

$$\sigma_1^n \exp - \frac{Q}{RT} = \sigma_2^n \exp - \frac{Q}{RT_2}$$

$$n \ln \frac{\sigma_2}{\sigma_1} = \frac{Q}{R} \left(\frac{T_1 - T_2}{T_1 T_2}\right)$$

$$Q = \frac{n R T_1 T_2}{(T_1 - T_2)} \left(\ln \frac{\sigma_1}{\sigma_2}\right)$$

The results of such experiments are presented in Figure 3.7.
The average value of n was found to be 7.0. $\pm$ 0.2
The average value of Q was found to be 25 Kcal/mol. $\pm$ 4kcal/mol.

3.2.3. Stress-strain behaviour of material favourably oriented for basal slip

The specimens favourably oriented for basal slip exhibited different stress strain behaviour. For equivalent temperatures and strain rates the peak in the stress strain curvewas lower and occurred at a higher strain. Representative curves for two temperatures are shown in Figure 3.8. There was no marked peak and subsequent softening of specimens deformed in this orientation and the effect of temperature was therefore not as evident.

3.3. DEVELOPMENT OF MICROSTRUCTURE WITH INCREASING STRAIN

3.3.1. Introduction

A summary of the development of structure as seen in the optical microscope will first be made with reference to different points along the stress strain curve for specimens unfavourably oriented for basal slip.

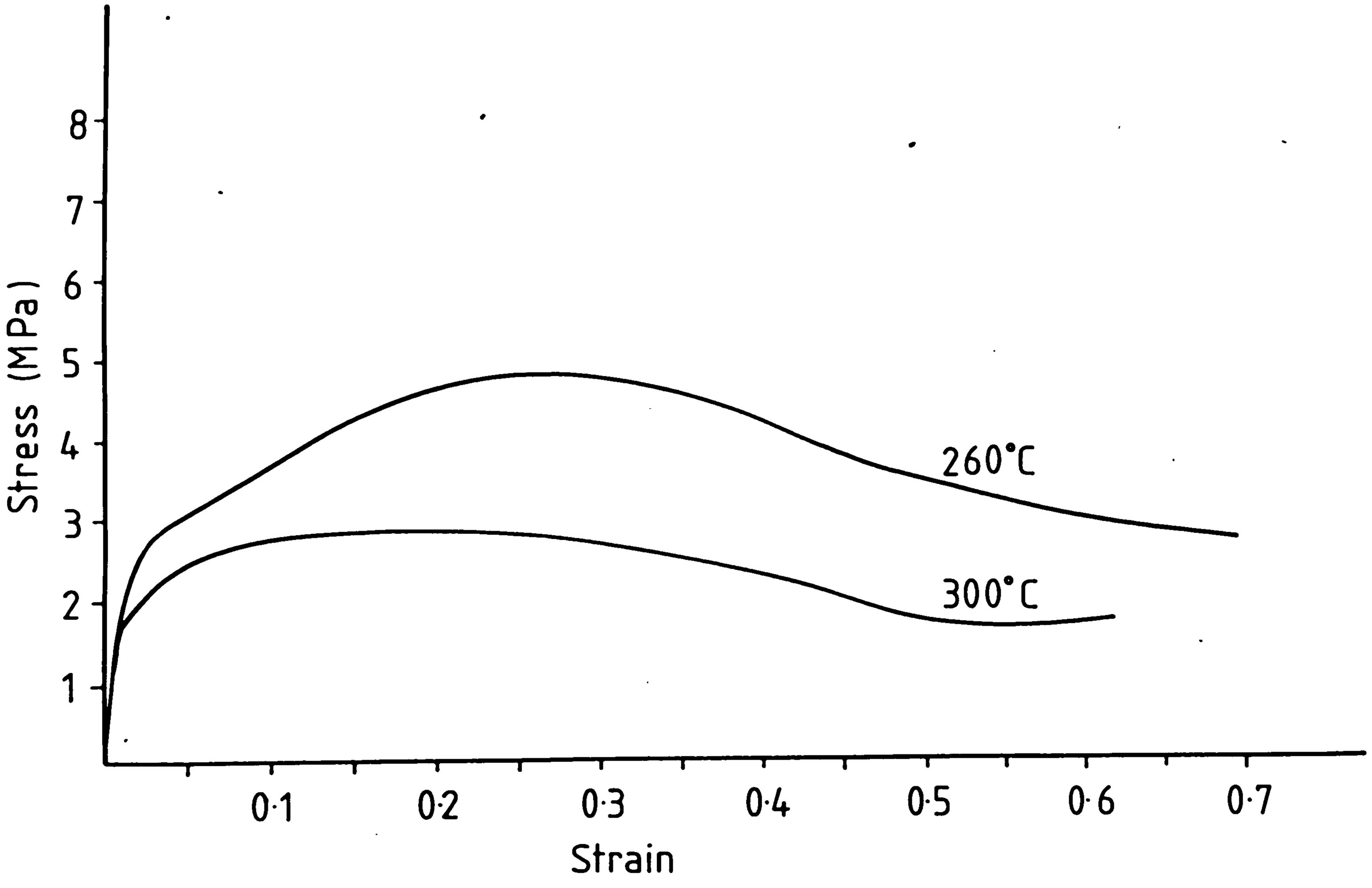


Figure 3.8 Stress-strain behaviour of samples favourably oriented for basal slip.

There are two different types of behaviour which are a result of the relative homogeneity of the deformation. At low (<320^{o}C) temperatures, the deformation is very heterogeneous whilst at temperatures greater than 320^{o}C the deformation is homogeneous.

The detailed study of microstructural and textural development with increasing strain will then be reported for three temperatures, 150^{o}C, 260^{o}C and 370^{o}C at a strain rate of $\dot{\varepsilon} = 10^{-5}s^{-1}$. Studies of the behaviour at these three temperatures give a representative view of the effect of the increase of temperature on deformation. The effect of strain rate on deformation behaviour will also be reported. Particular attention has been paid to the importance of dynamic recrystallisation and the extensive electron microscopy carried out to aid with the microstructural interpretation will also be referred to. The optical microscopy of specimens favourably oriented for basal slip at 260^{o}C and a strain rate of $\dot{\varepsilon} = 10^{-5}s^{-1}$ will then be reported.

The development of shear zones which play an important part in the latter stages (>20% strain) of deformation particularly in unfavourably oriented samples at low temperatures will be treated in detail in a separate section.

3.3.2. Deformation of samples unfavourably oriented for basal slip

3.3.2.1. Introduction

A schematic diagram illustrates the development of microstructure with reference to points along the stress strain curve (Figure 3.9). The initial microstructure (Figure 3.10) had an average grain size of 400μm. The grains were equiaxed and had smooth grain boundaries. A summary of the microstructural development at 150^{o}C, 260^{o}C and 370^{o}C will first be made before the detailed studies at each of these temperatures are presented. Unless otherwise indicated on the figure, the compression axis in all the optical micrographs presented is vertical.

150^{o}C

Twinning occurs during part A of the deformation sequence. At this temperature two types of twinning mechanism have been identified: a first mechanism which consumes the whole of the host material followed by a second mechanism which results in the appearance of fine twins in the final microstructure. Voids are present in samples deformed to just before the peak in the stress strain curve (B). The voids occur mainly at triple points, along boundaries parallel to

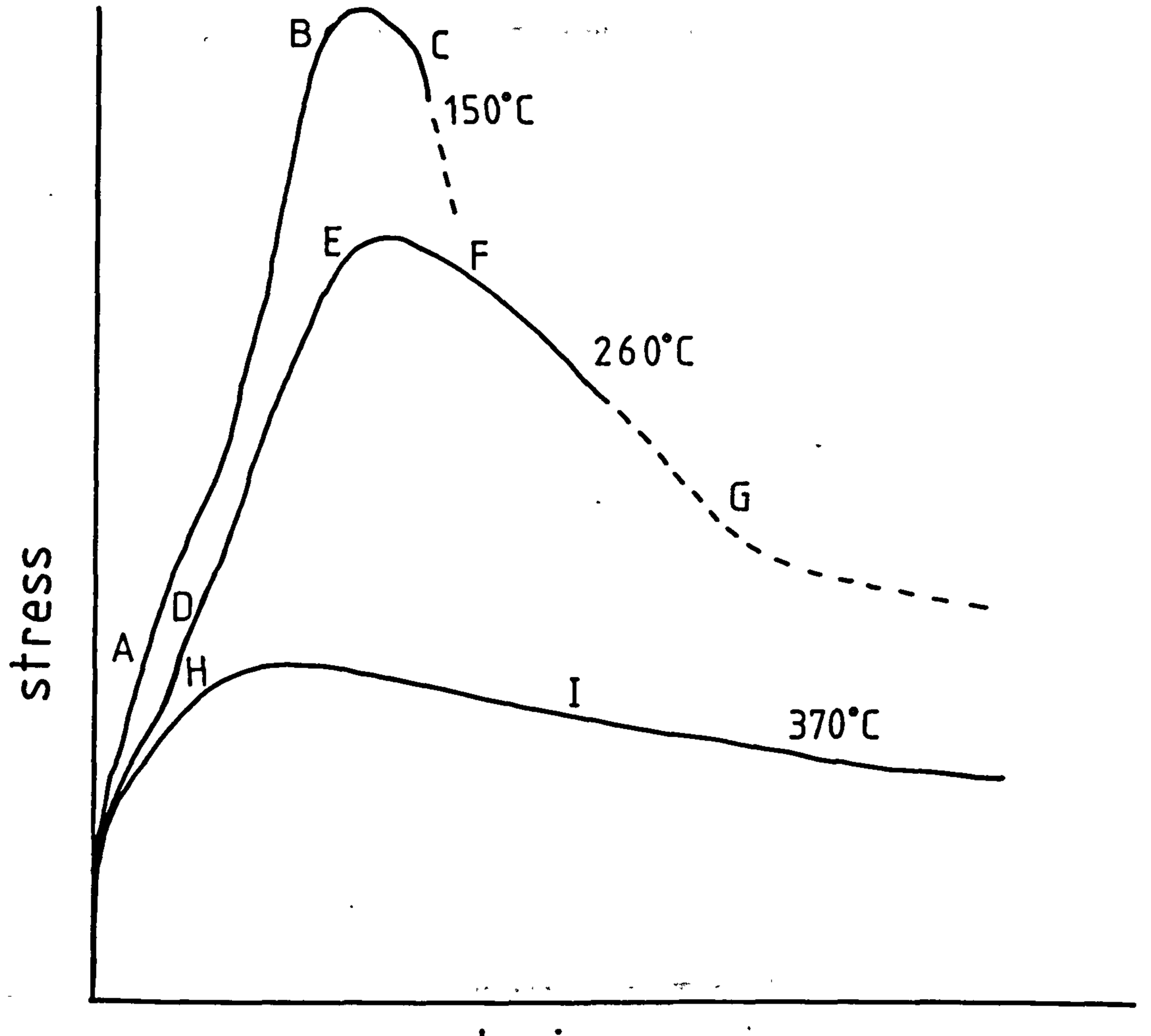


Figure 3.9. Schematic diagram to illustrate the way in which microstructure develops as the strain increases.

A Extensive twinning

B A high percentage of voids at triple points and along boundaries where the shear stress is high.

C Small amounts of recrystallisation in localised regions of heterogeneous high strain

---

D Extensive twinning

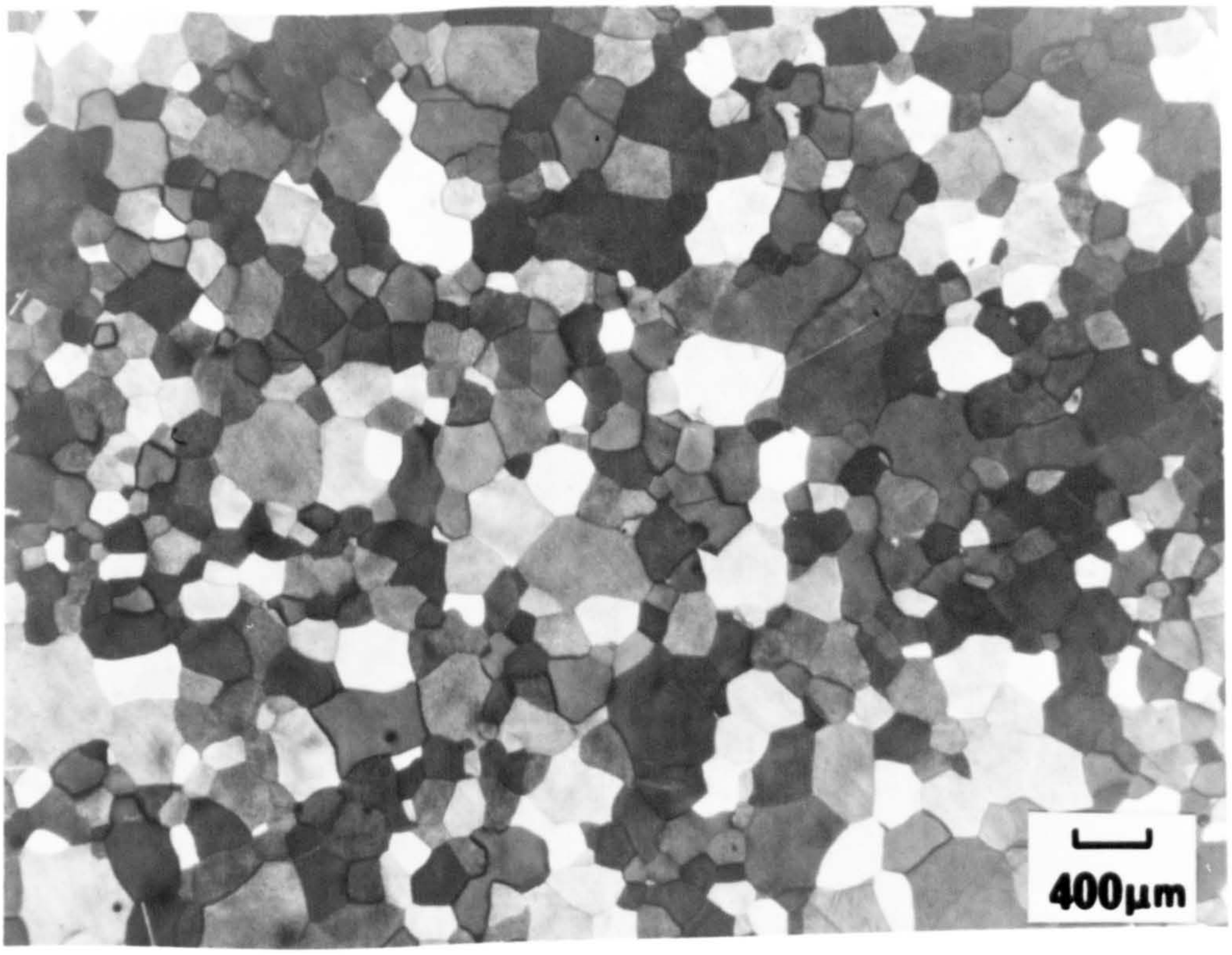
E Dynamic recrystallisation at the old grain boundaries

F Development of a duplex microstructure consisting of old grains surrounded by layers of small recrystallised grains.

G Shear zone development

H Extensive grain boundary bulging and migration leading to recrystallisation by Strain Induced Boundary Migration

I Maintenance of a "steady-state" microstructure by continuous dynamic recrystallisation.



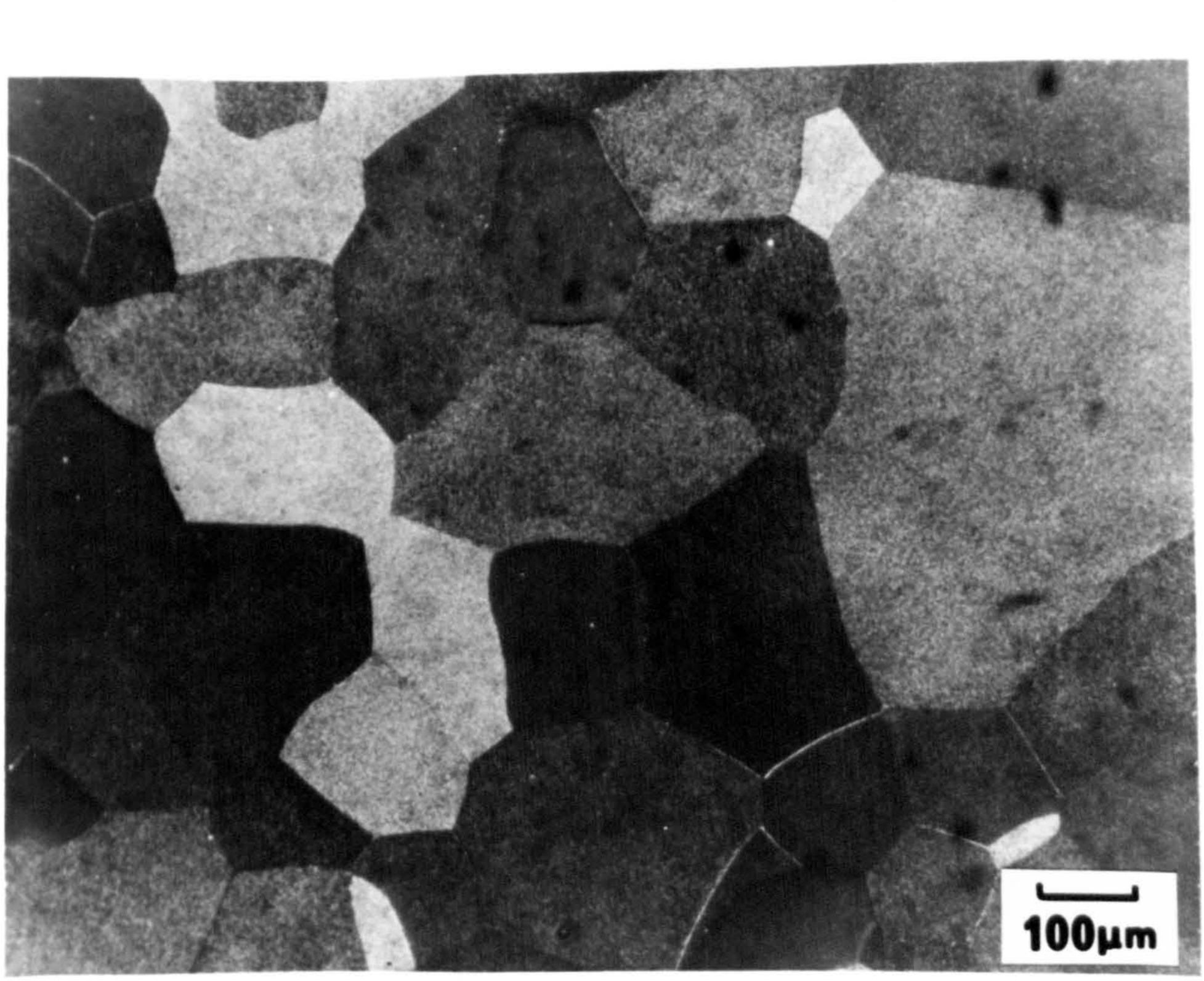


Figure 3.10. Microstructure of the undeformed material. The grains were equiaxed with smooth boundaries and had an average size of 400µm.

the maximum shear stress and less frequently along the fine twins. Small recrystallised grains at the grain boundaries can also be detected at this stage in the deformation but they are barely resolvable optically. Further straining results in the formation of shear fractures and eventual sample failure (C).

260°C

At 260°C extensive twinning followed by twin and grain boundary migration occurs (D). New grains first appear at the old grain boundaries by dynamic recrystallisation just prior to the peak in the stress strain curve (E). Further straining results in the development of a duplex microstructure consisting of old grains surrounded by envelopes of small recrystallised grains (F). These envelopes of recrystallised grains broaden with increasing strain leading to the formation of shear zones (G). The recrystallised grains are associated with bulges and misoriented regions in the grain boundaries. Voids are also present in samples deformed at this temperature. The voids occur at triple points and along boundaries parallel to the maximum shear stress.

370°C

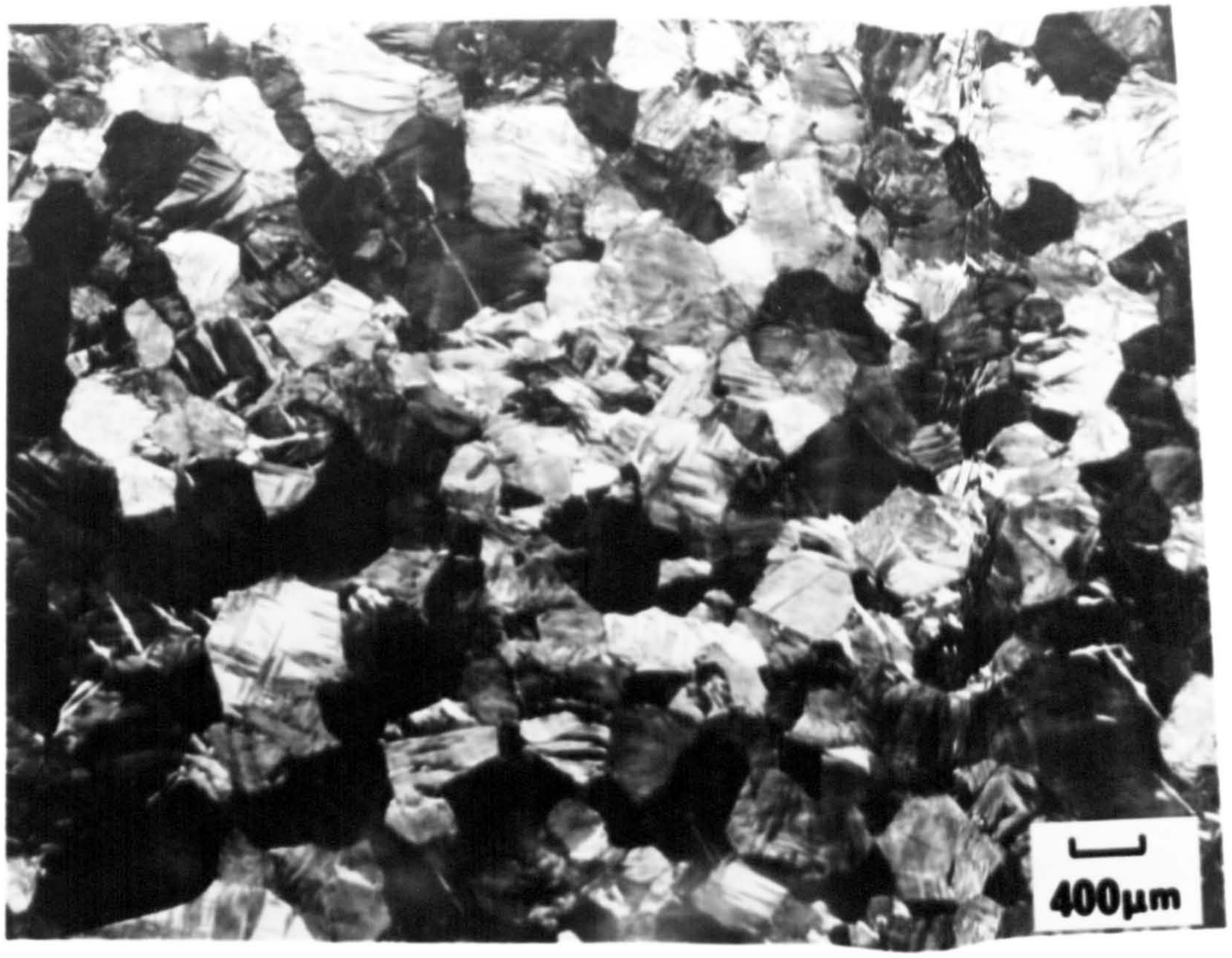
At this temperature the deformation is relatively homogeneous. There is little evidence for twinning and voids are absent. Grain boundary migration is marked at low strains (H) and the recrystallised grains which form at the boundaries are of a size similar to the boundary bulges from which they appear to form. Deformation bands are present in many of the old grains. At higher strains the recrystallised grains exhibit extensive migration and bulging (I)

The detailed microstructural investigation at 150°C, 260°C and 370°C will now be reported.

3.3.2.2. Microstructural development at low temperature

3.3.2.2.1. Optical microscopy at 150°C

At 10% strain twinning was extensive (Figure 3.11). The difference in basal plane orientation between twin and host as estimated from polarised light microscopy was ~90° which suggested that the twins were of the $\{10\bar{1}2\}$ type.



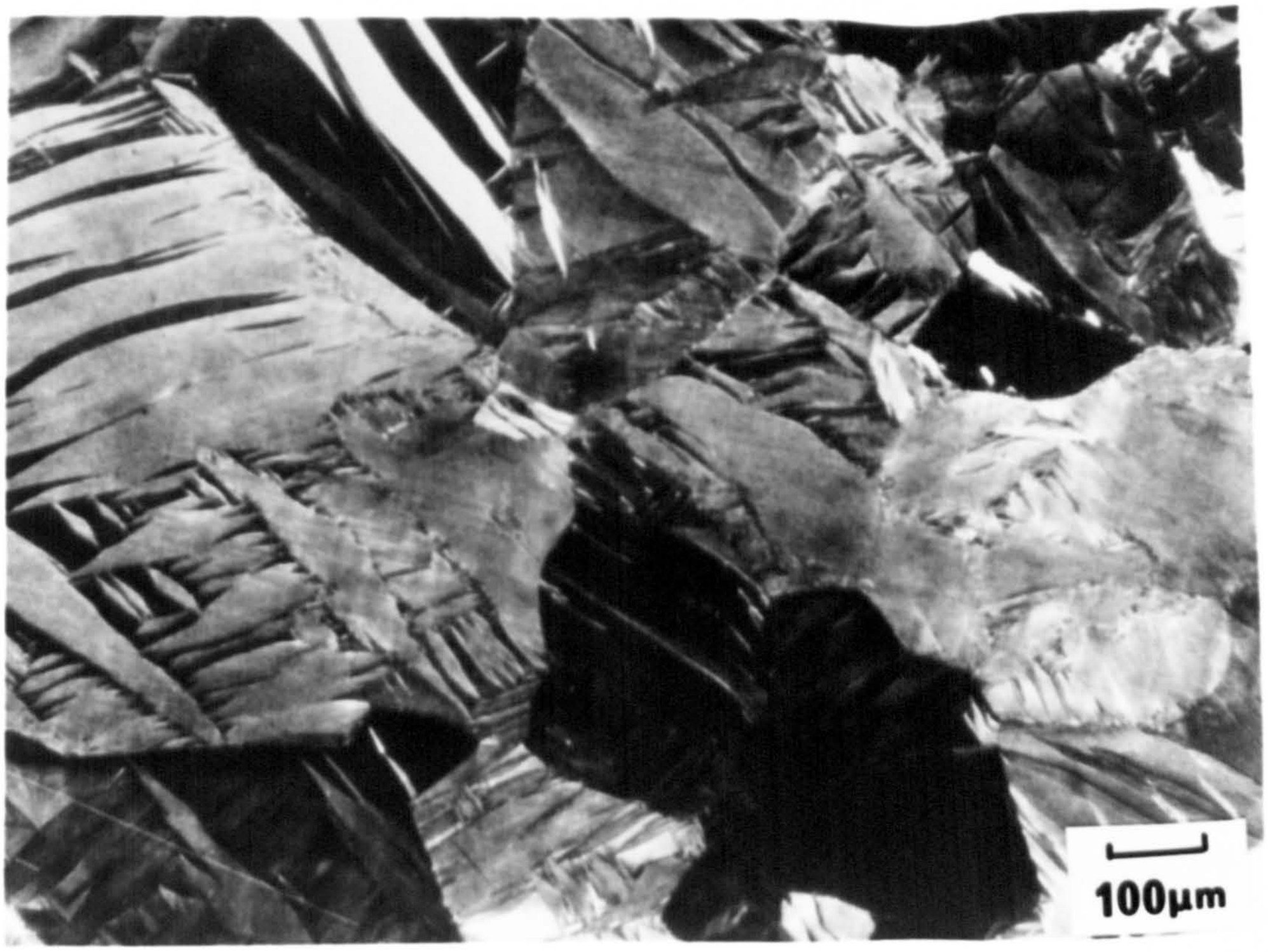


Figure 3.11. This sample had been strained 10% at 150°C $\dot{\varepsilon} = 10^{-5}s^{-1}$ It had undergone extensive twinning. Most grains contained more than one set of twins.

At 22% strain which was just beyond the peak in the stress strain curve the optical microscopy showed that the basal texture was very sharp (Figure 3.12). The basal planes were aligned parallel $\pm 5^{o}$ to the compression plane indicating that they were in the twinned orientation. Only small areas of material in the original orientation were left at grain boundaries. Voiding had occurred at this strain (Figure 3.13). The voids were elongated and had formed mainly at triple points and along boundaries supporting a high shear stress (they tended to be areas of preferential chemical attack during polishing and therefore are over emphasised in the micrograph). Fine twins could be detected in some grains. Voids were present along some of these twins. The twins had their habit plane inclined at $58^{o} \pm 2^{o}$ to the basal plane and were thought to be the result of the $\{10\bar{1}1\}\{10\bar{1}2\}$ double twinning mechanism. Very fine recrystallised grains could be detected at some of the grain boundaries. These were highly misoriented from adjacent old grains - up to 45^{o} and occurred in areas of the specimen where the strain was particularly heterogeneous. The old grains contained fine lines (arrowed in Figure 3.13) which were thought to be the traces of the basal planes. This was confirmed by X-ray microbeam analysis, as described below, of a specimen deformed 35% which exhibited similar features.

3.3.2.2.2. Determination of nature of the crystallographic features in the old grains using a Laue back reflection technique

The back-reflection Laue method is a well known technique in metallurgy (Cullity, 1959) and has been used extensively in the study of single crystals where the orientation of a specimen can be determined from the location of the Laue spots on the film. In this work the Laue microbeam technique was used to determine the orientation of the grains in a polycrystalline sample with respect to the stress axis. Greninger's method of analysis was used for the purpose of facilitating the identification of the crystallographic features visible optically (see e.g. Smallman and Ashbee 1966). The orientation of the basal planes was determined and the results compared with those obtained using the colour technique.

The specimen examined had been deformed 35% at $150^{o}C$. This particular sample was chosen because the optical crystallographic features were well developed and once their origin had been deduced, the results could be related to specimens exhibiting less prominent, but similar features.





Figure 3.12. 22% strain at 150°C, $\dot{\varepsilon} = 10^{-5}s^{-1}$.
The strong texture which had developed in this sample is easily discernible in the upper micrograph.



Figure 3.13. The voids which can be seen in the macroscopic view of this sample had formed mainly at triple points and along boundaries inclined at 45^{o} to the compression direction. They were areas of preferential chemical attack during the polishing and etching process and consequently have an exaggerated size.

The micrographs (Figure 3.14) show the features in one of the grains examined. The orientation of the grain with respect to the stress axis is indicated in each case. It can be seen that the optical strain features are particularly evident when the specimen is rotated 45^{o} on the microscope stage. The line drawn on the micrograph corresponds to a reference line drawn on the X-ray film (Figure 3.15a) and was used when transferring each spot to be indexed onto a stereographic projection (Figure 3.15b).

The fine lines indicated on the micrograph (Figure 3.14) were found to correspond to the basal planes and the less regular vertical features were parallel to the trace of the prism planes. When the colour filter had been inserted into the optical microscope, it was found that the trace of the basal plane was parallel to a horizontal crosswire in the eyepiece when the colour of the grain changed from blue to orange on clockwise rotation of the microscope stage. This result concurs with that obtained by Williams et al (1969).

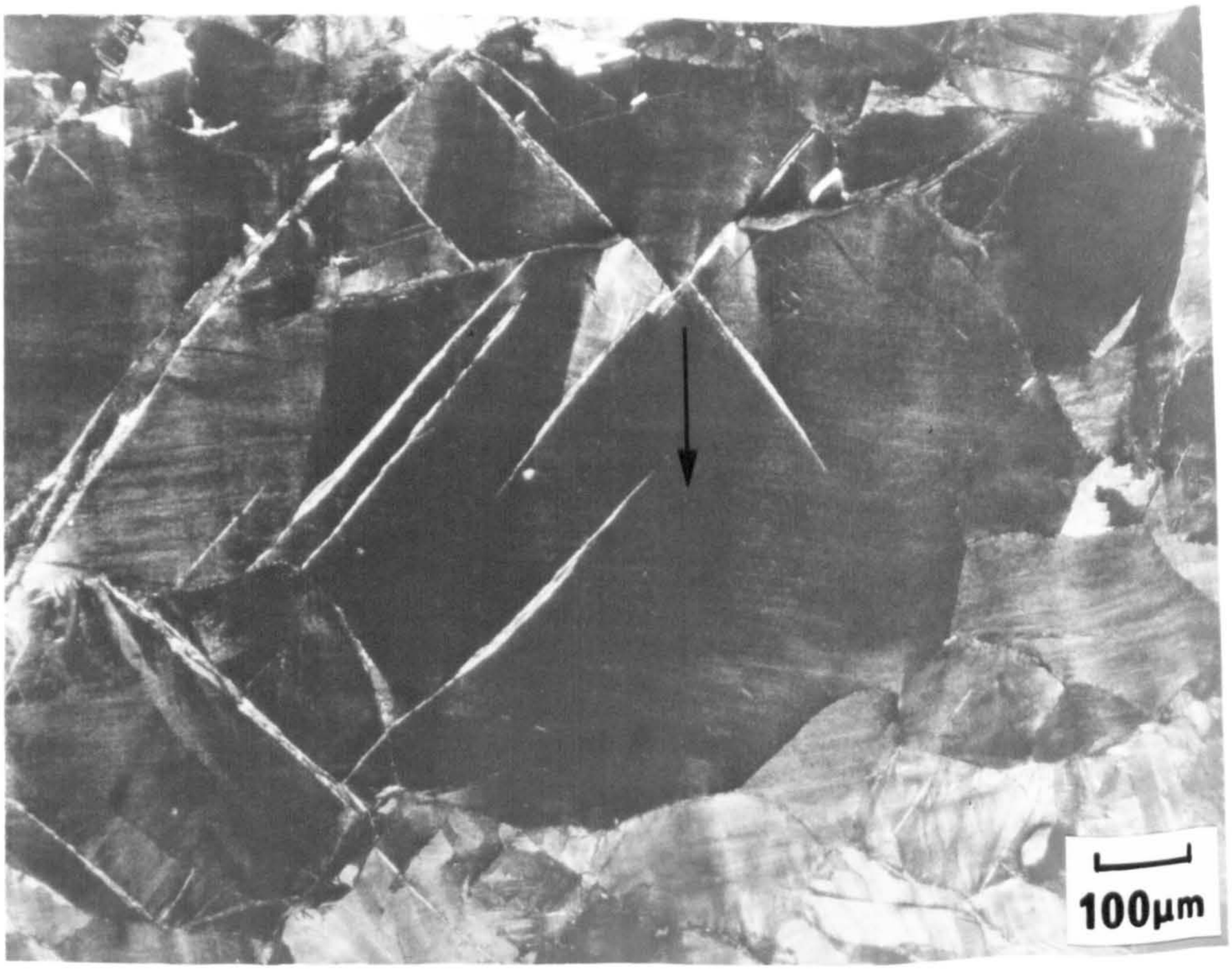
3.3.2.2.3. Electron microscopy

E.M. confirmed the $\{10\bar{1}2\}$ twinning mechanism, Figure 3.16. This micrograph also gives a good indication of the high dislocation density within the old grains at low temperatures. The twin boundary indicated can be seen to be serrated. The serration corresponds to the poorly developed sub-boundaries in the host grain.

The substructure was relatively homogeneous within the old grains consisting mainly of dislocations lying in one plane and poorly developed sub-boundaries. The regions within $\sim 10\mu m$ of a grain boundary exhibited heterogeneous deformation. Subgrains were small $\sim 1\mu$ and more equiaxed. Rotations up to 15^{o} could be detected within $10\mu m$ of the grain boundary - a typical example is shown in Figure 3.17.

3.3.2.2.4. Macroscopic heterogeneous deformation

At higher strains (beyond the peak in the stress strain curve), the deformation was very inhomogeneous being concentrated in a single zone whereas the rest of the sample underwent much less strain (Figure 3.18). Recrystallised grains which were barely resolvable optically could be detected in the zone of high strain. The degree of heterogentity is illustrated in Figure 3.19 where macroscopic shearing can be seen to have occurred. This will be discussed in more detail in the context of shear zones (Section 3.7.)



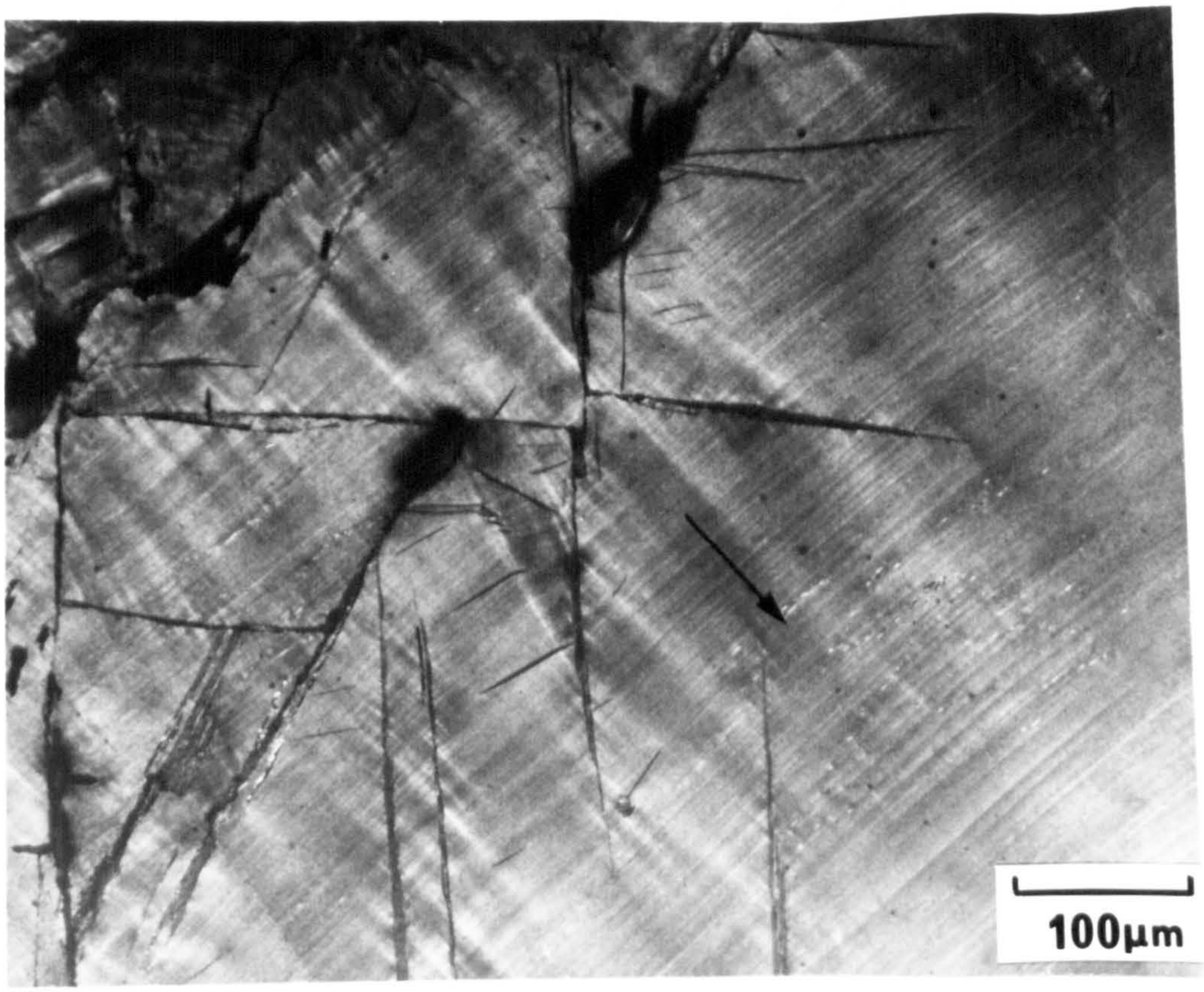


Figure 3.14. The arrows on the two micrographs correspond to the applied stress direction. The fine slip lines in the lower micrograph are the traces of the basal planes. They are more easily discernible in this micrograph which was taken after the specimen had been rotated 45° on the microscope stage.

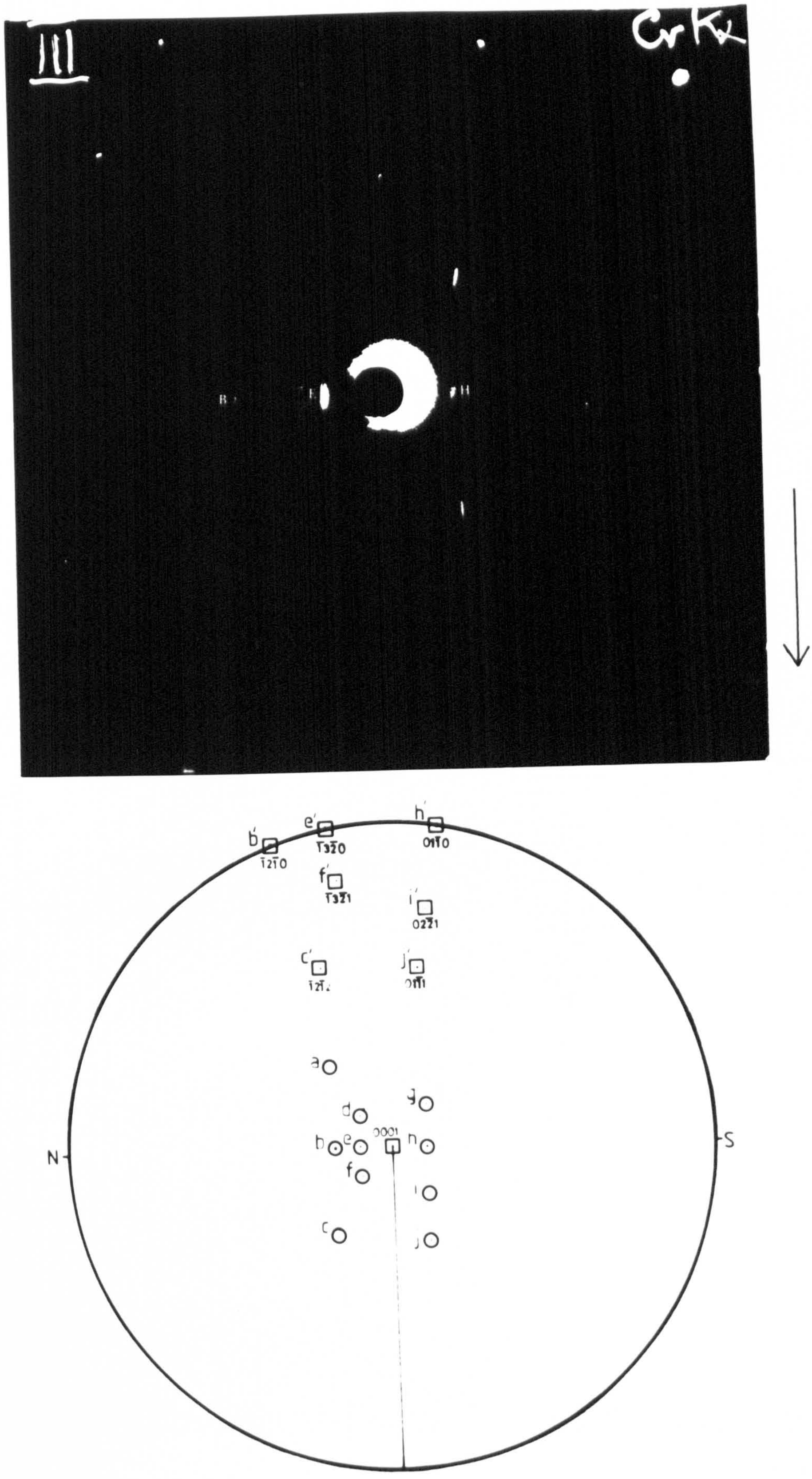


Figure 3.15 Laue back reflection photograph from the central grain in Fig.3.14. and the corresponding stereographic analysis.



Figure 3.16. Dislocation structure at low temperatures in a specimen deformed 10% at 150°C. The twins are easily recognisable and were of the $\{10\bar{1}2\}$ type. Note the serrated nature of the twin boundary indicated. The serrations correspond to intersections of the adjacent perpendicular sub-boundary walls with the twin boundary.

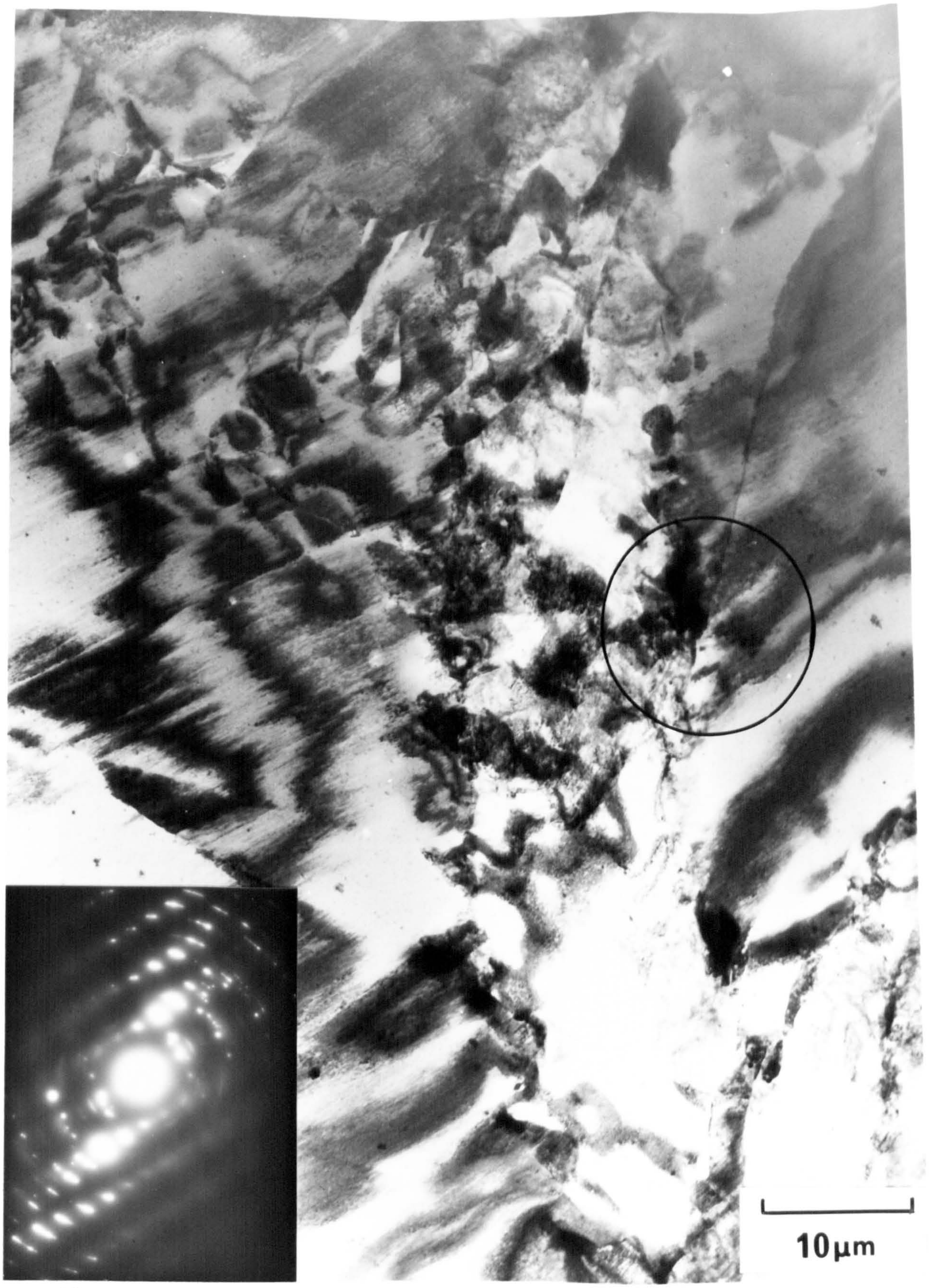
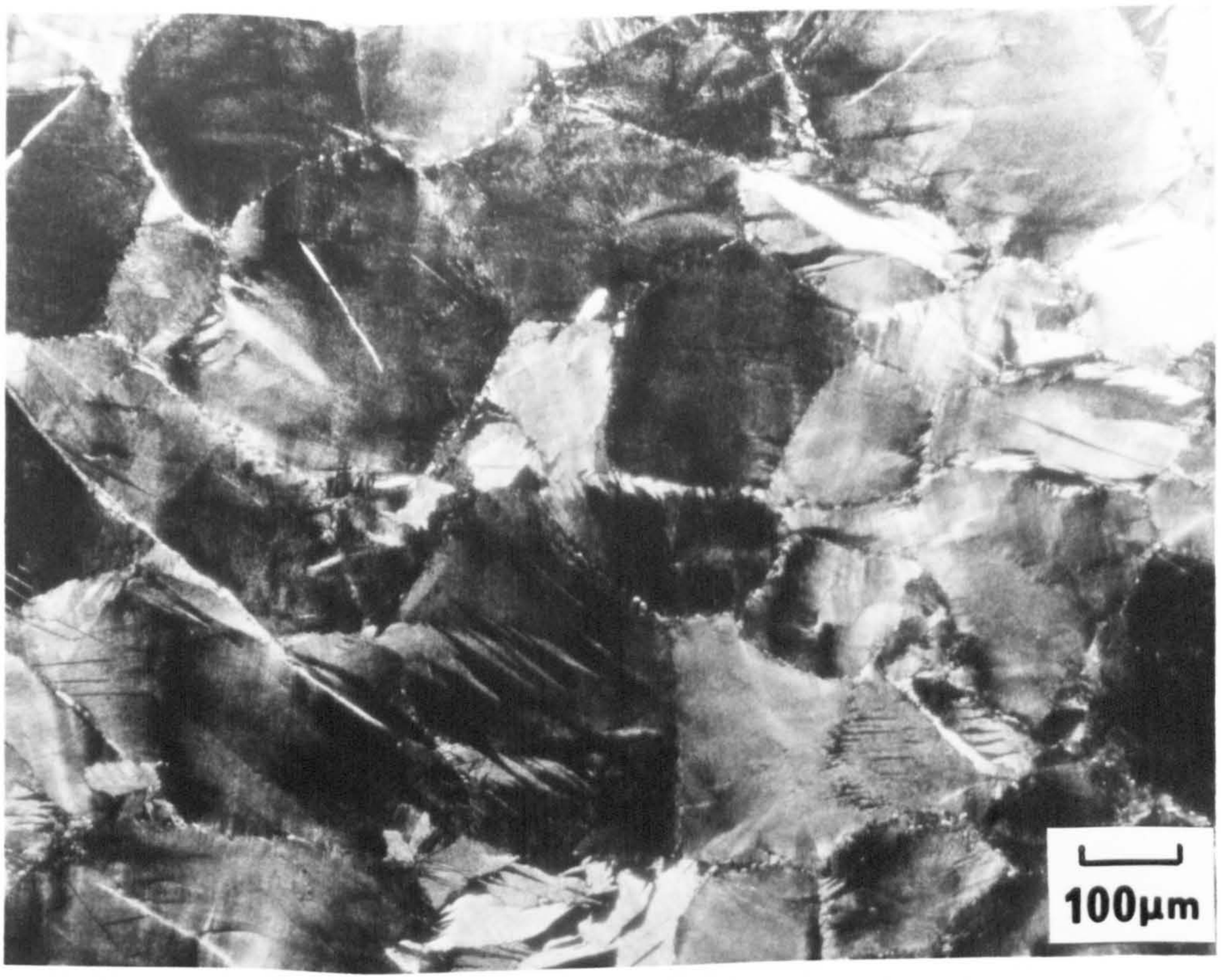


Figure 3.17. Substructure in the grain boundary region of a sample deformed 55% at 150°C. The thin foil was taken from an area near the shear zone (Fig. 3.75) which had developed in the sample. Rotations of up to 15° could be detected in an area within 10µm of the grain boundary from spot streaking in the diffraction pattern (insert).



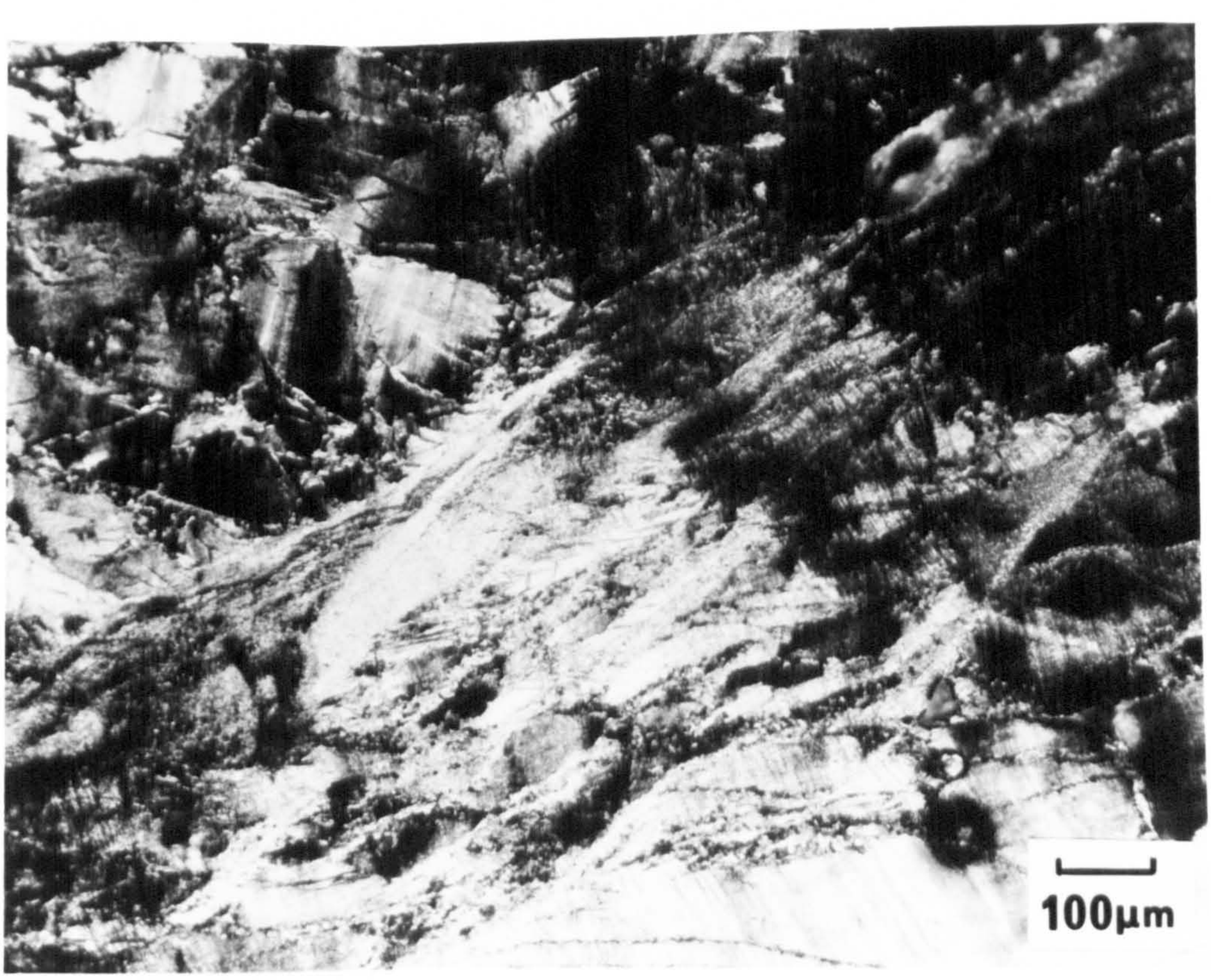


Figure 3.18. These two micrographs are of different areas in the same specimen which had undergone a bulk strain of 55%. The deformation had been very inhomogeneous being concentrated in a shear zone containing fine recrystallised grains (lower micrograph). Away from the zone (upper micrograph), the microstructure resembled that at 22% strain.

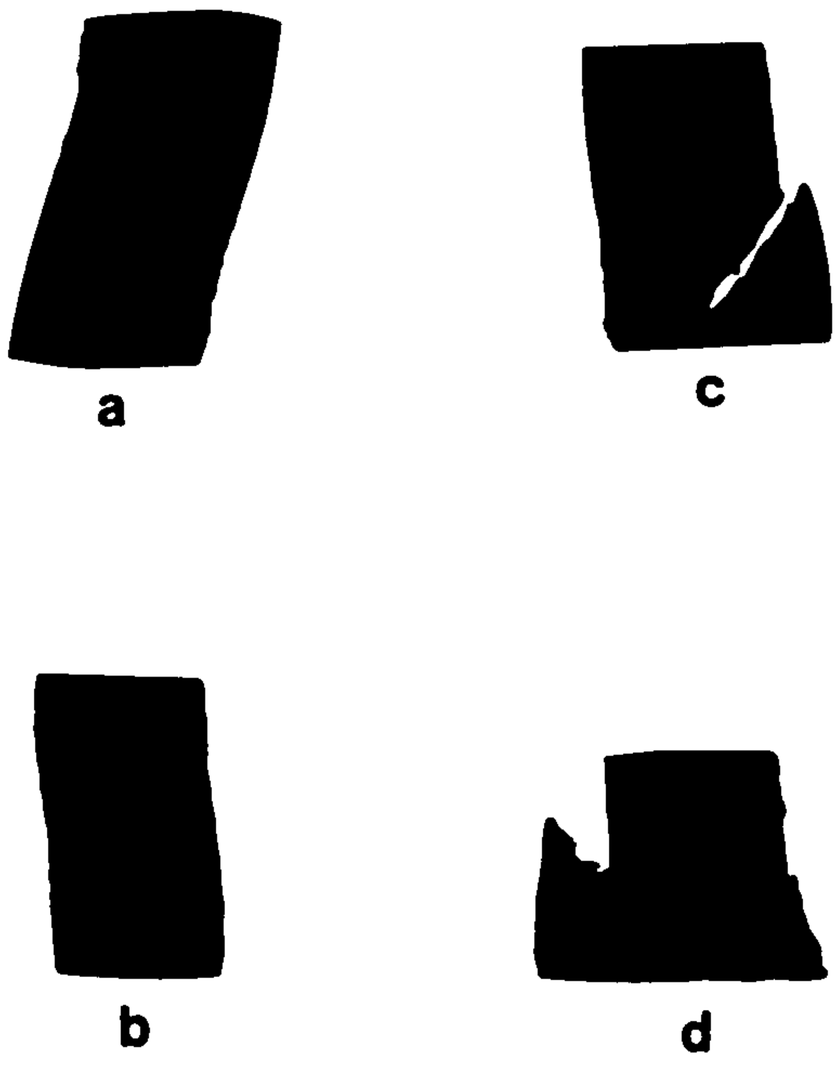


Figure 3.19 Macroscopic heterogeneity of samples deformed at 150^{o}C.
The figure consists of four shadow masks of deformed specimens. The length of (a) and (c) before deformation was 33mm, whilst that of (b) and (d) was 30mm. (c) and (d) underwent 35% and 55% strain respectively, but it can be seen that this has been concentrated into a narrow zone of heterogeneous high strain resulting in macroscopic shear of both specimens.

3.3.2.3. Microstructural Development at Intermediate Temperatures

3.3.2.3.1. General observations at 260°C

At 2% strain Figure 3.20, twinning was present in some of the grains. The twins had a characteristic lenticular morphology. No grain boundary migration could be detected at this early stage. By 8% strain, Figure 3.21, twinning was more extensive. Many grains contained more than one set of twins and twin boundary migration had occurred. Use of the sensitive tint plate facilitated the identification of twin and host material. An indication of the extent of twinning in some areas of the sample is given in Figure 3.22. Only small areas of matrix remain in the form of 'dog-teeth' at the grain boundaries. The reorientation of the basal planes in the twinned volume as determined from the change in colour on rotating the specimen was $\sim 90^{o}$ suggesting that the twins were of the $\{10\bar{1}2\}$ type. This was confirmed from the analysis of twin boundaries in E.M. foils from this specimen. A typical example is illustrated in Figure 3.23 where the two boundaries which were analysed were found to be examples of $(\bar{1}012)$ and $(01\bar{1}2)$ twin boundaries. The strain features within grain A, Figure 3.21 are similar to those analysed in the low temperature specimens. The optical behaviour of the grain upon rotating the specimen under reflected polarised light showed that the fine lines (double arrow) corresponded to the traces of the basal planes, i.e. the basal planes were aligned perpendicular to the stress direction. Grain boundary migration had occurred at this strain. The bulges in the boundary were related in some instances to the twin grain boundary intersections (arrowed). At 14% strain which was just before the peak in the stress-strain curve the microstructure exhibited bulging and migration of the grain boundaries (Figure 3.24). In some areas recrystallised grains could be detected at the grain boundaries. These features were associated with bulges and areas of misoriented lattice at the grain boundaries.

There was more recrystallisation at 16% strain (Figure 3.25) which was just beyond the peak in the stress strain curve. A single layer of recrystallised grains was present around most of the old grains. As will be shown in the next section reflected polarised light microscopy was used to optically determine the relationship of the recrystallised grains to adjacent old grains. The recrystallised grains fell into two categories - those along boundaries perpendicular to the compression

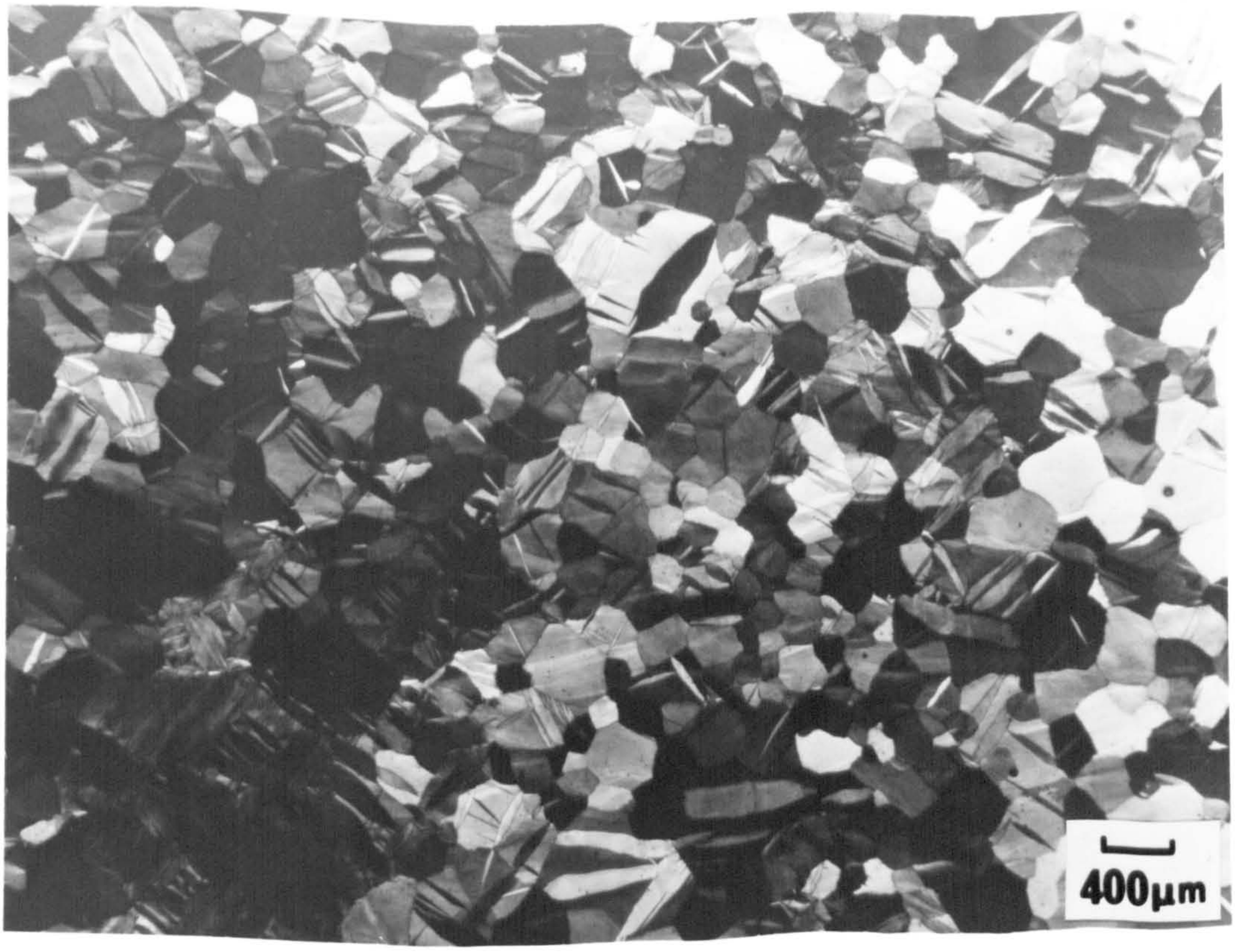




Figure 3.20. Specimen deformed 2% at 260°C. Twinning had occurred in most grains. The twins had a characteristic lenticular morphology which is well illustrated in the micrographs.





Figure 3.21. This specimen had undergone 8% ε at 260^{o}C. Twinning was very extensive and some of the grain boundaries exhibited bulging which coincided with the twin/grain boundary intersections.

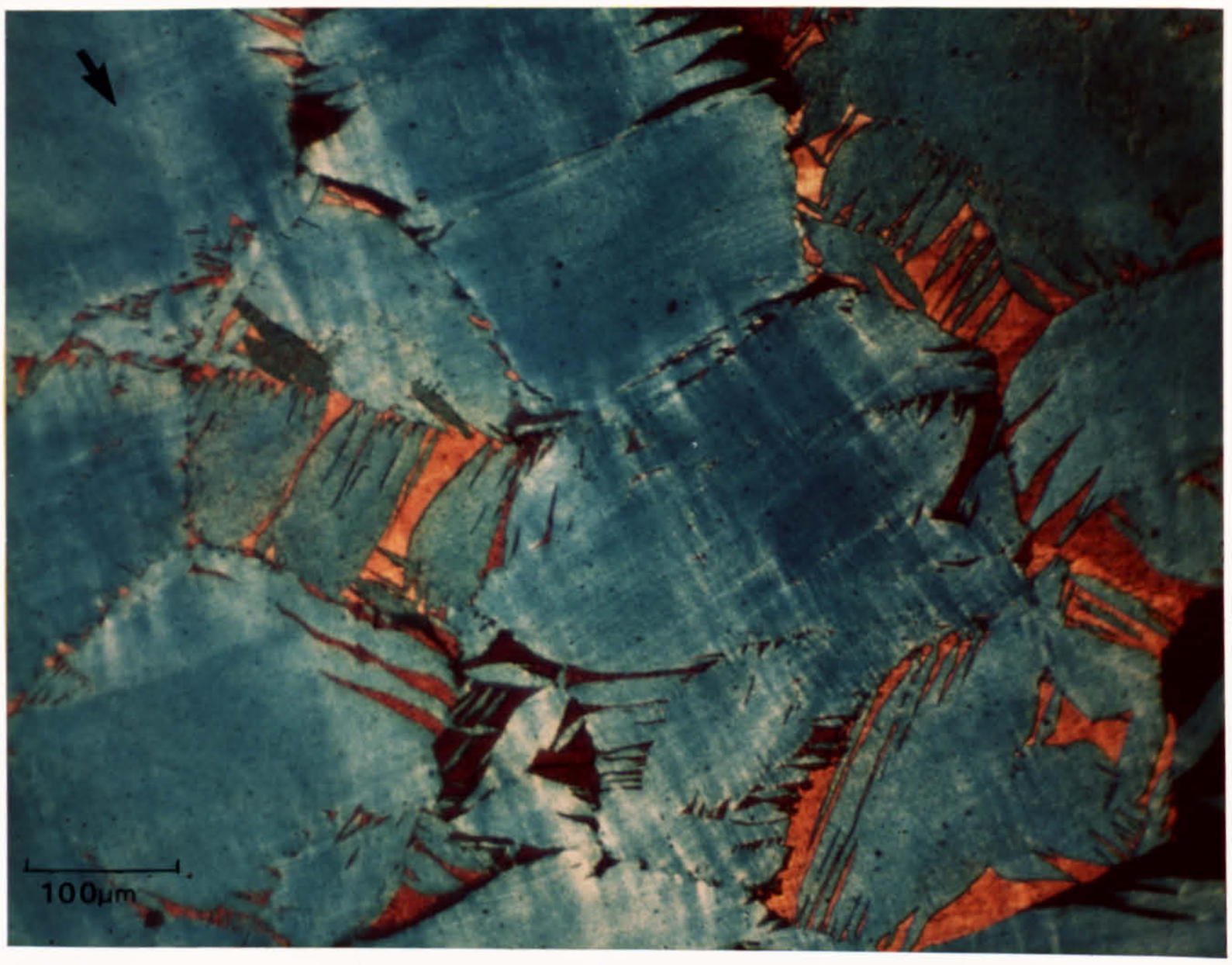
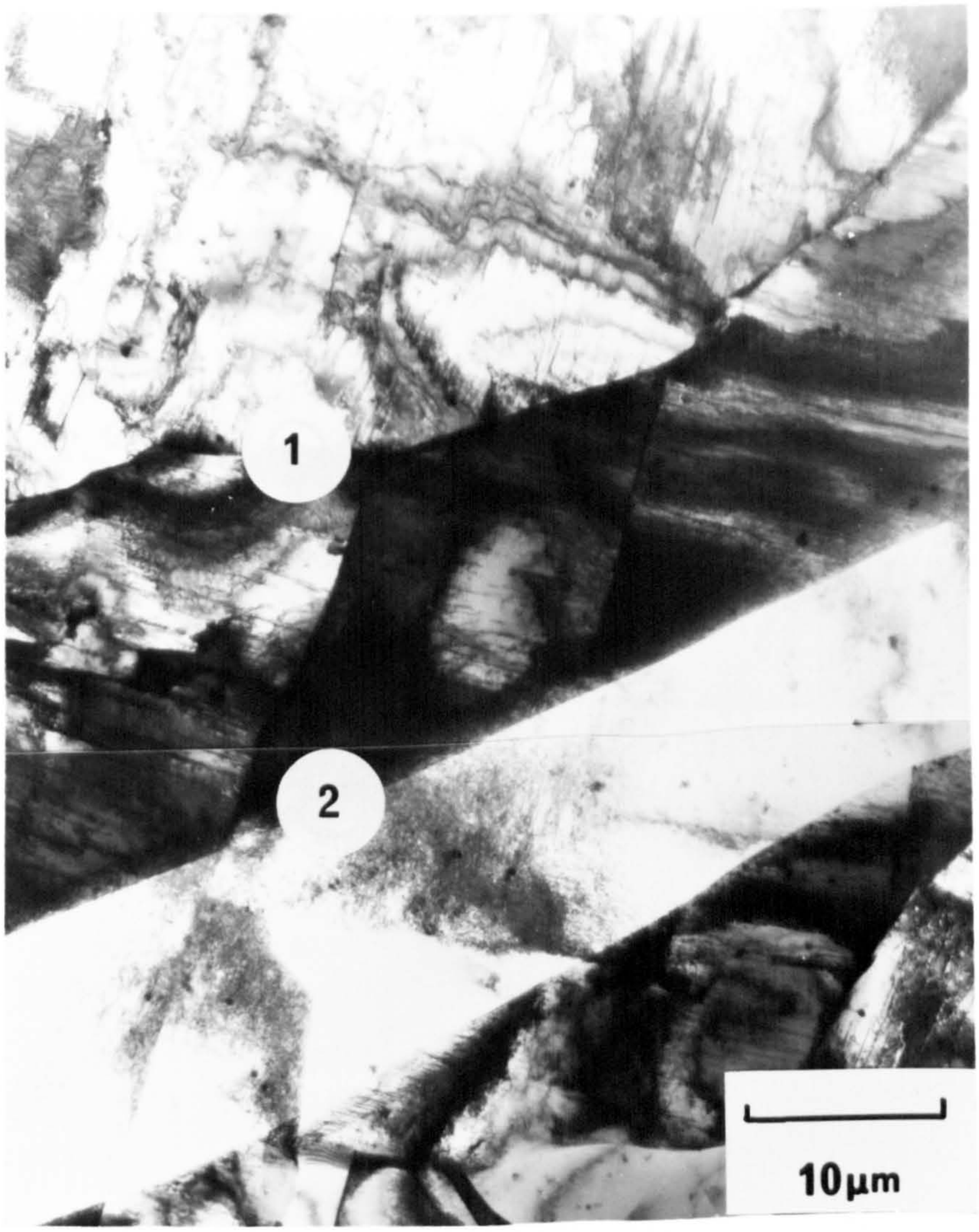


Figure 3.22 This colour metallograph gives a good indication of the extent of twinning in the specimen at 8% strain. The compression direction is indicated by the arrow at the top of the micrograph. The blue material is in the twinned orientation whilst the orange material is the remaining host. It can be seen that many of the grains have been almost consumed by the twins.



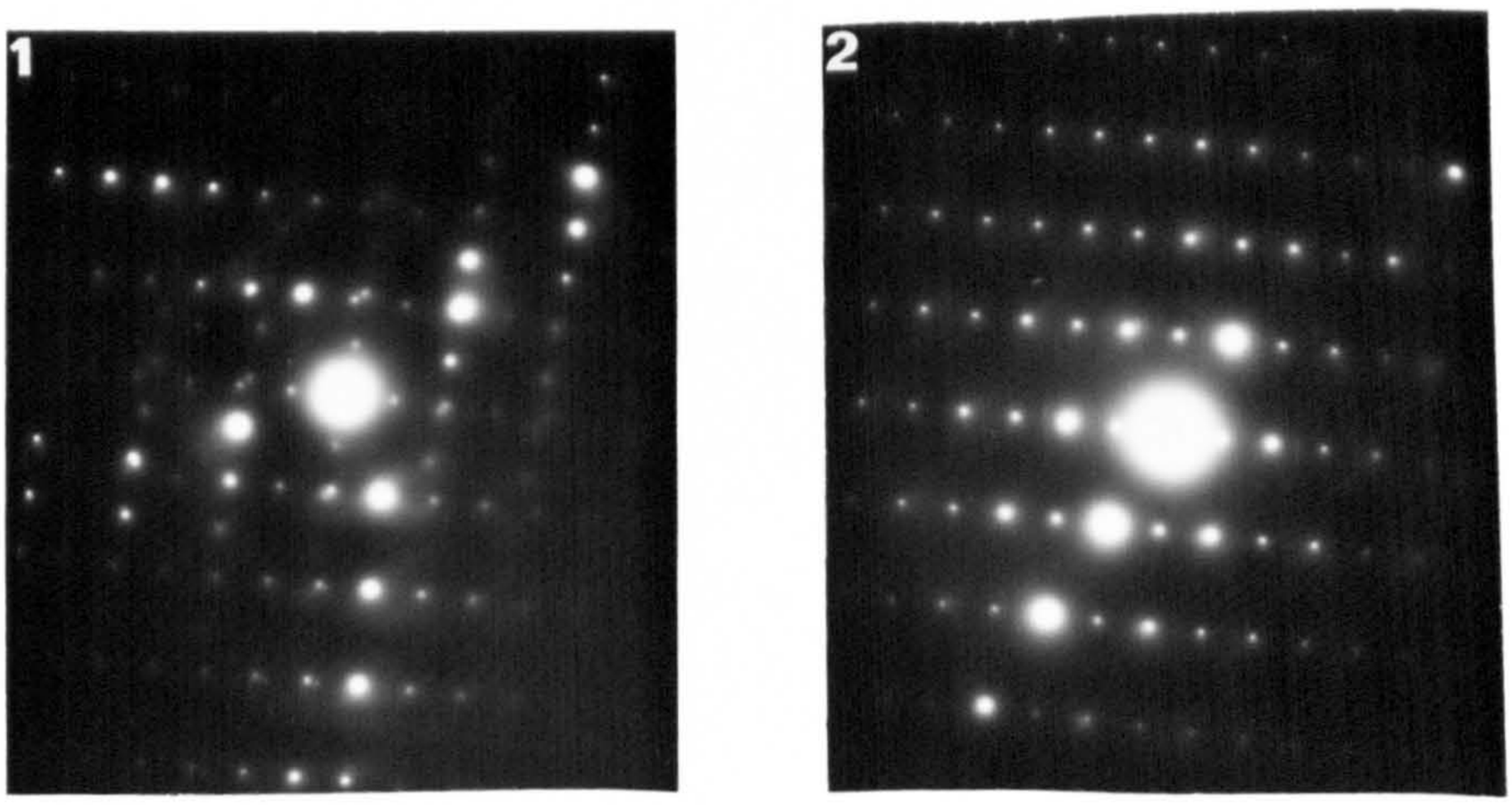


Figure 3.23. Electron micrograph of a twin in a specimen deformed 14% at $\dot{\varepsilon} = 10^{-5}s^{-1}$ at 260°C. The boundaries were analysed and found to be $(\bar{1}012)$ and $(01\bar{1}2)$ respectively.





Figure 3.24. This specimen was deformed to 14% ε at 260^{o}C. Reflected polarised light microscopy indicated that virtually the whole sample had assumed the twin orientation. Many grain boundaries exhibited bulges and migration.



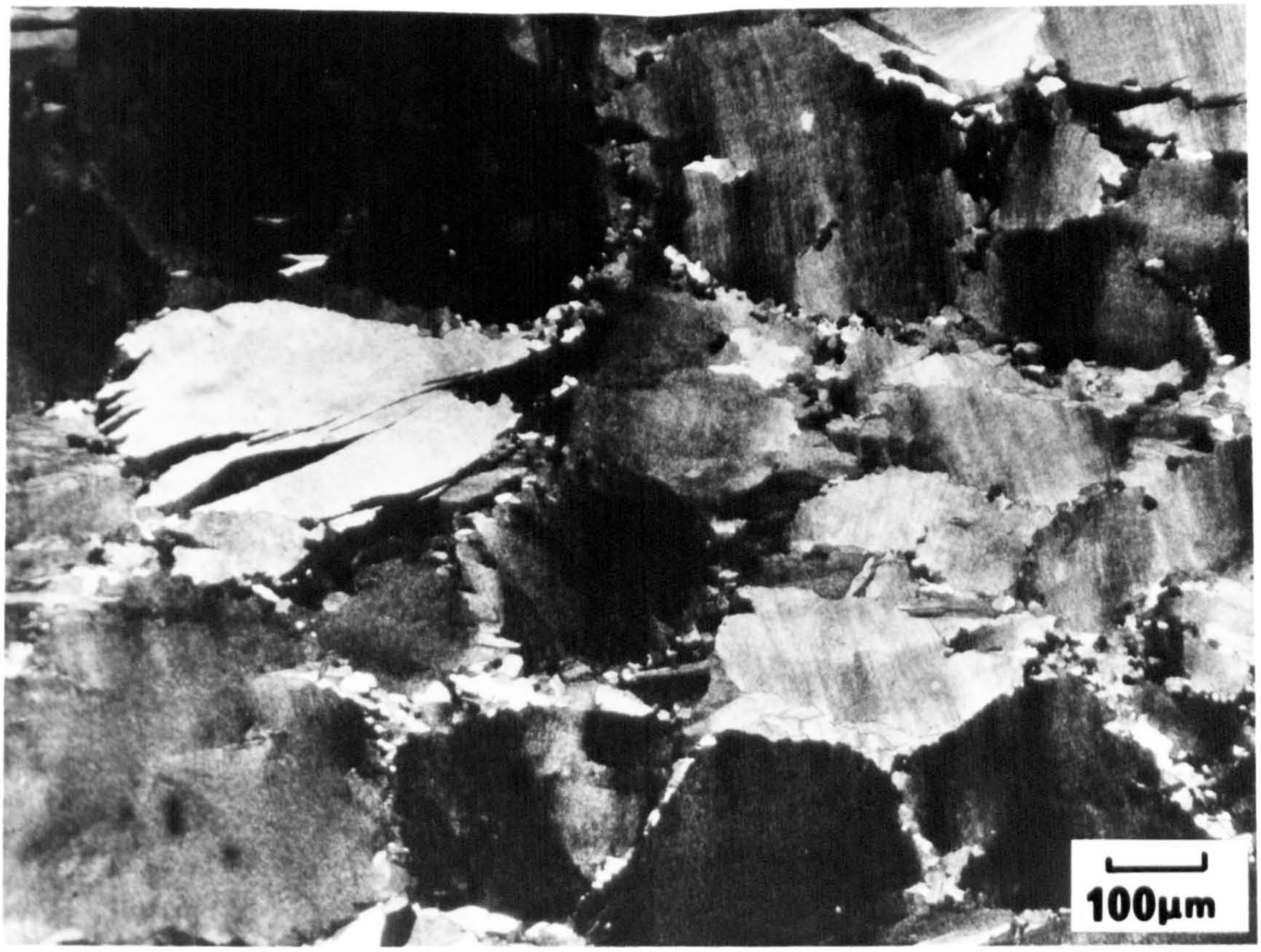


Figure 3.25. This specimen had been deformed 16%. There was more recrystallisation at the grain boundaries.

direction and those along boundaries aligned parallel to the planes of maximum shear stress. The latter were highly misoriented - up to 45^{o} with respect to adjacent old grains, whilst the former showed smaller rotations of the basal planes, i.e. of the order of up to 10^{o}. A sketch to illustrate the rotations is shown in Figure 3.26. Voids could be detected at some of the triple points and along obliquely inclined boundaries.

At higher strains recrystallisation was more extensive. The recrystallised bands were broader particularly along boundaries inclined at 45^{o} to the compression direction resulting in a duplex microstructure with diamond shaped old grains, Figure 3.27. The shape of old grains in general did not reflect the overall strain of the samples examined. The recrystallised grains had not undergone grain growth. It appeared that the deformation was being accommodated in the grain boundary-recrystallised regions. The old grains exhibited strain features similar to those found at lower temperatures (Figure 3.28 - cf. Figure 3.14). They are easily discernible in the colour metallograph, Figure 3.29. The fine lines parallel to the single long arrow are the traces of the basal planes whilst the less regular periodicity perpendicular to these, as determined in the E.M. work, are elongated subgrains with walls parallel to the prism planes.

3.3.2.3.2. Microscopic heterogeneity on the grain scale

T.E.M. carried out on samples deformed 15% and 20% at $300^{o}C$ and 9% and 16% at $260^{o}C$ revealed the presence of a 'Core and Mantle' structure (Figure 3.30). This phrase has been used by Gifkins (1976) in his studies of superplastic behaviour and grain boundary sliding but in the work described here it is used to differentiate between the behaviour in the grain centres (cores) and grain boundary regions (mantles).

i) Behaviour in the cores

Narrow elongated subgrains with walls parallel or perpendicular to the traces of the basal planes (c.f. White 1973) occurred in the core (Figure 3.31). Dislocations in the core had $\vec{a}$ burgers vector and lay in the basal plane. The sub-boundaries tended to be poorly developed and of the 'picket-fence' type. It was thought that these sub-boundaries caused the strain features which were optically visible (Figure 3.29); however, the spacing of the subgrains and the misorientations across individual boundaries were in most cases too small to be optically resolvable. A histogram showing the width of subgrains

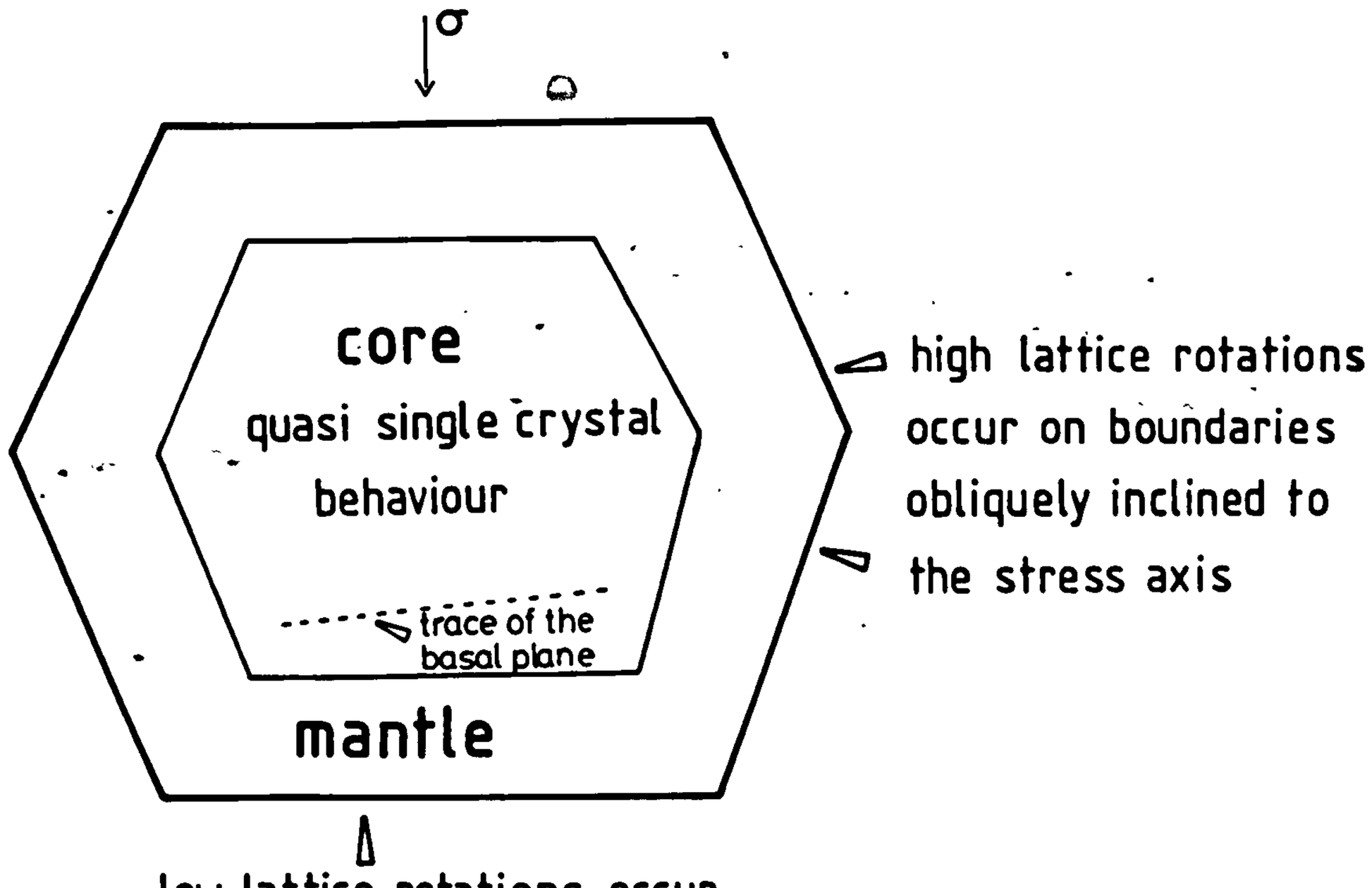
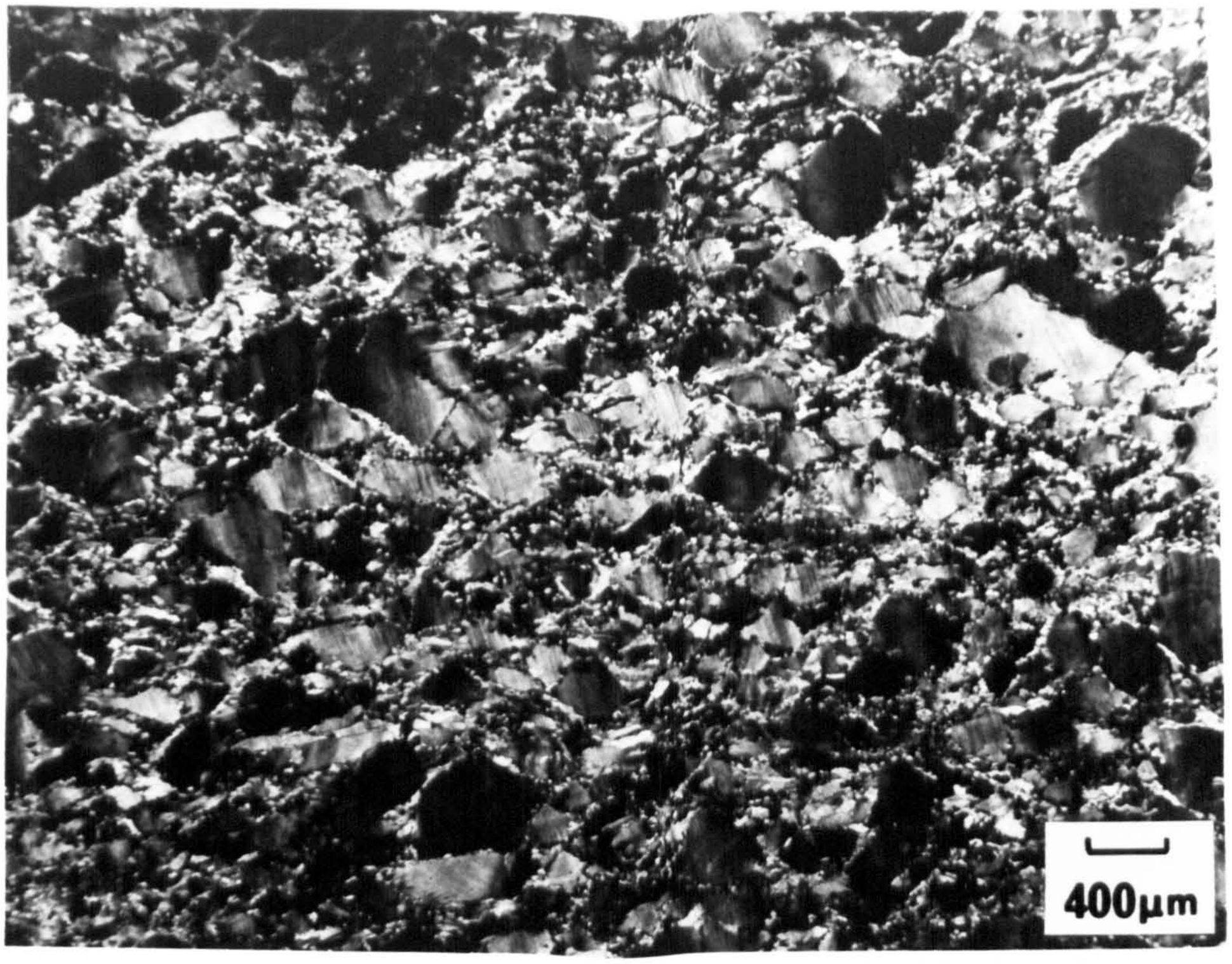


Figure 3.26. Diagram to illustrate the variation in misorientation in the mantles with the inclination of the grain boundaries to the compression axis.



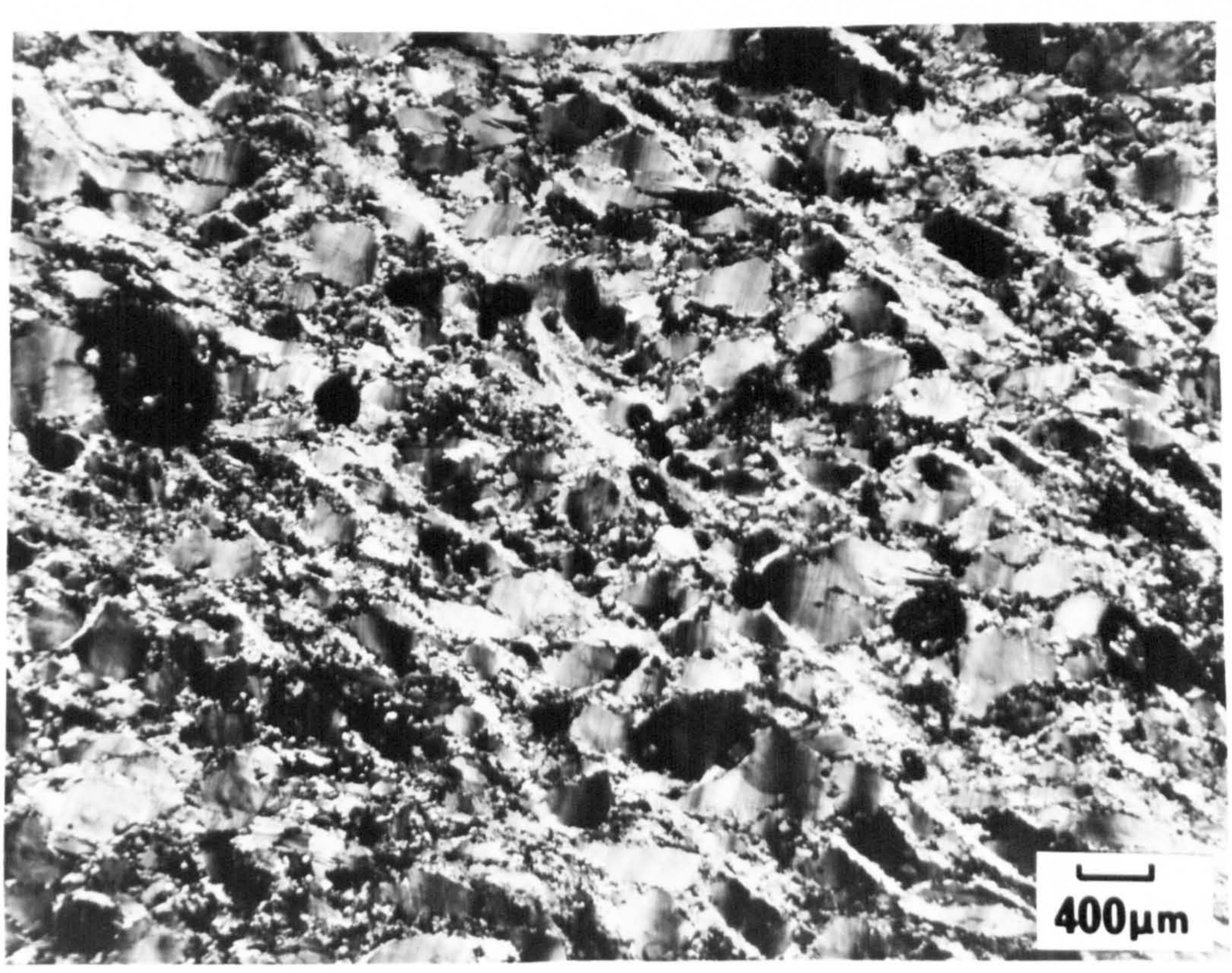


Figure 3.27. Duplex microstructure produced as a result of dynamic recrystallisation at the old grain boundaries. The upper micrograph illustrates the microstructure at 35% ε whilst the lower micrograph (47% ε) illustrates the widening of the recrystallised bands at higher strains.



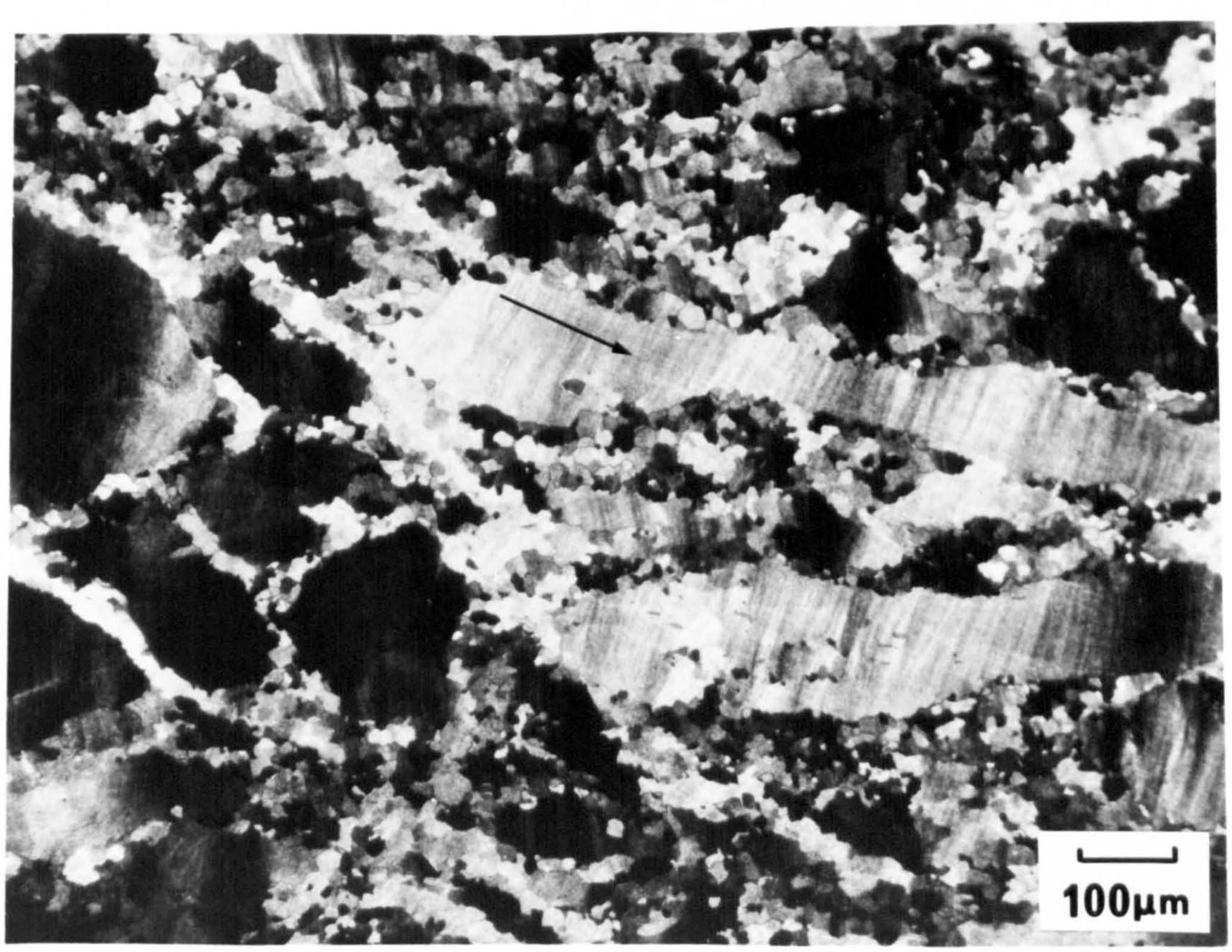


Figure 3.28. This specimen had received a bulk strain of 55% and had developed a zone of preferred deformation. Some of the old grains in this zone were more favourably oriented for slip and had become very elongated.

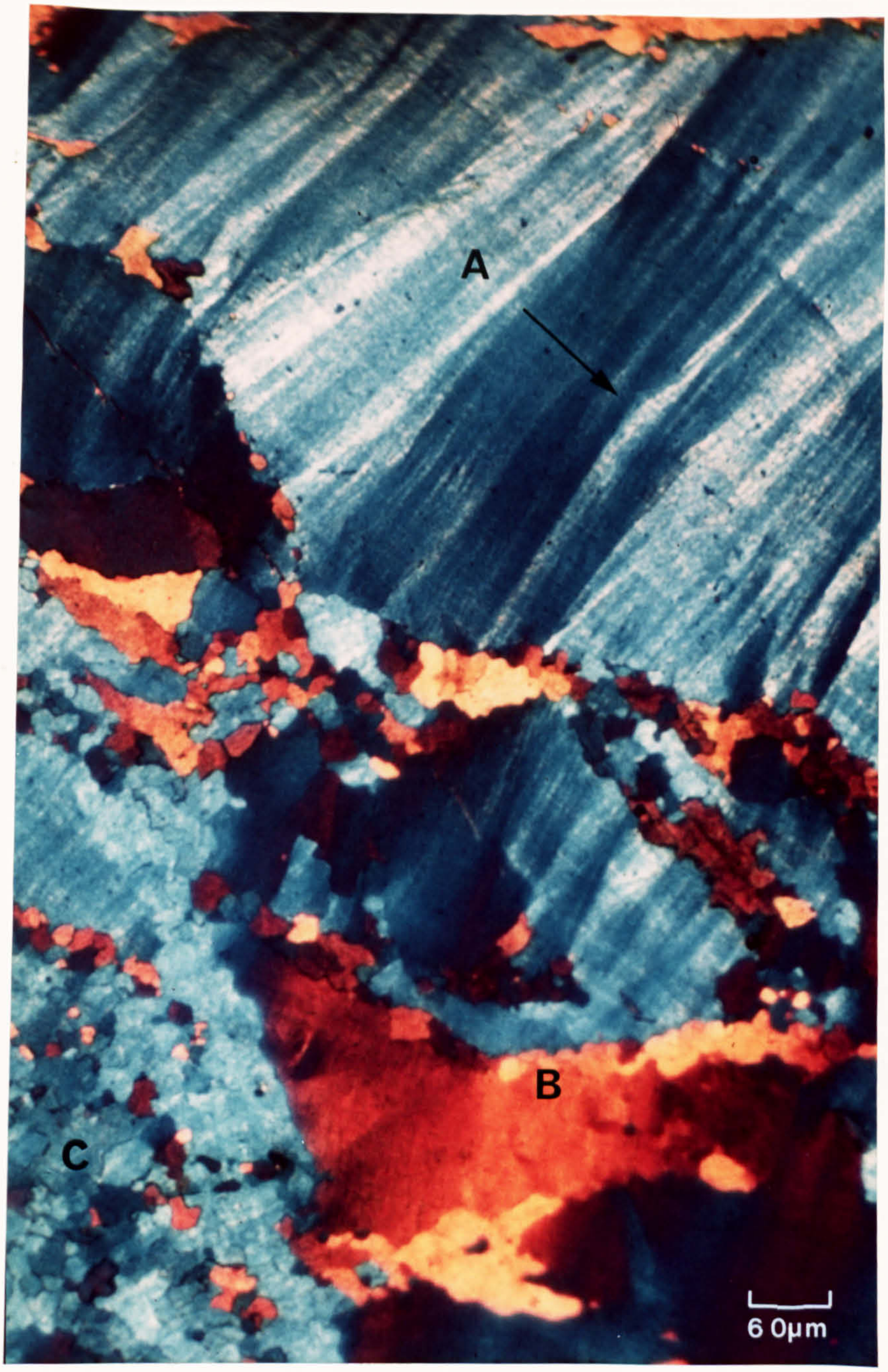


Figure 3.29. Colour metallograph of a sample which had undergone 35% strain at 260^{o}C.
The fine lines parallel to the single long arrow are the traces of the basal planes. The degree of lattice bending within the old grain (A) is clearly discernible from their change in direction across the grain.
Subgrains can be seen at the edges of grain (B).
The recrystallised grains (C) are misoriented from one another by less than 10^{o}.



Figure 3.30. 'Core and Mantle' structure. The change in substructure from Core to Mantle is well illustrated and reflects the heterogeneity of deformation. Elongated subgrains with walls subparallel to the trace of the basal plane give way to more equiaxed subgrains as a grain boundary is approached. Deformation = 16% ε at 260°C; foil plane $(2\bar{1}\bar{1}0)$.

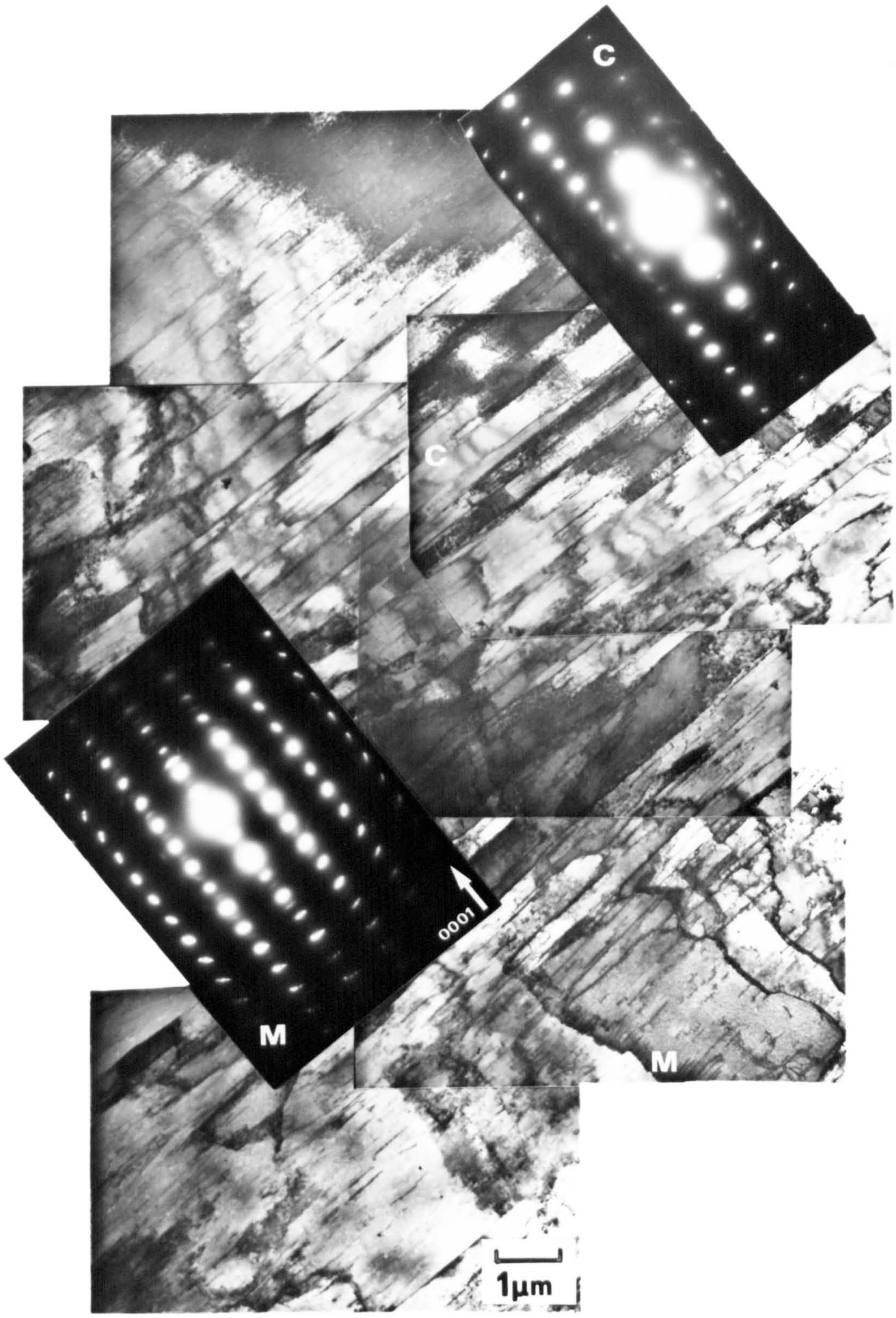
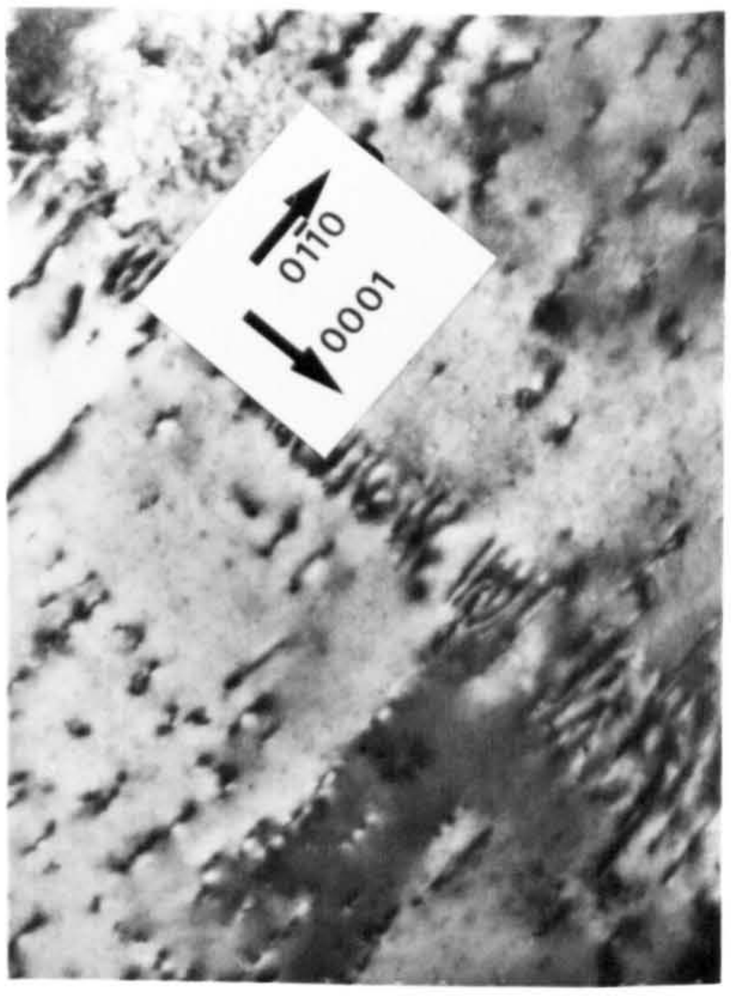
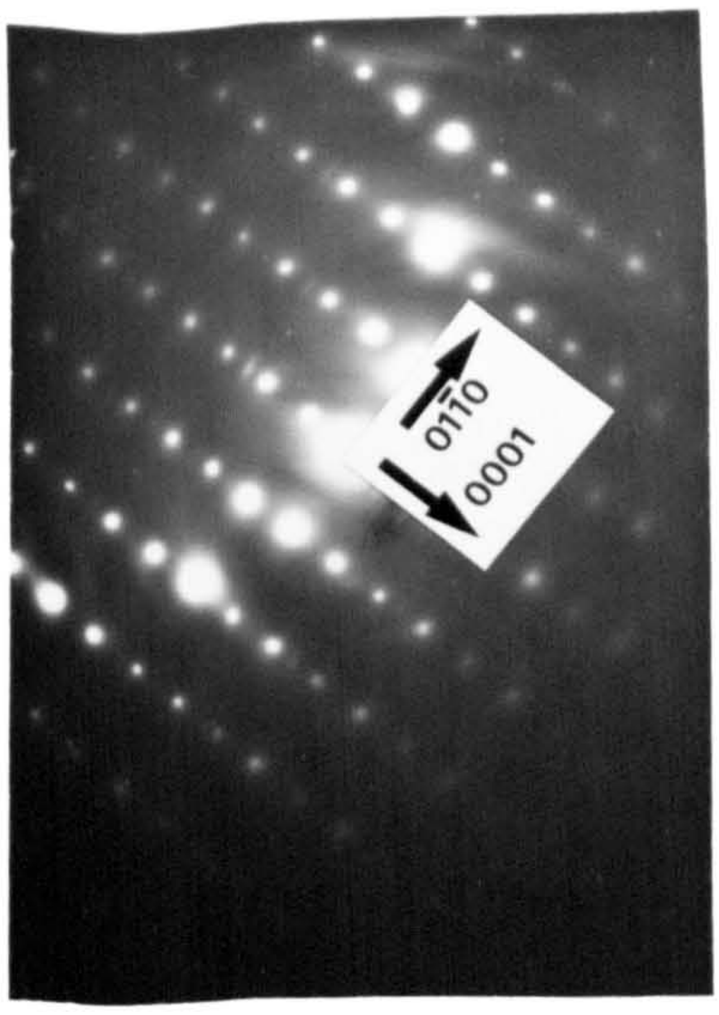


Figure 3.31. Long narrow elongated subgrains in the core (c) of an old grain. The misorientation across the sub-boundaries was 3^{o} rising to 8^{o} as the mantle (m) was approached. The diffraction patterns were taken from the labelled areas (c) and (m) on the micrograph.







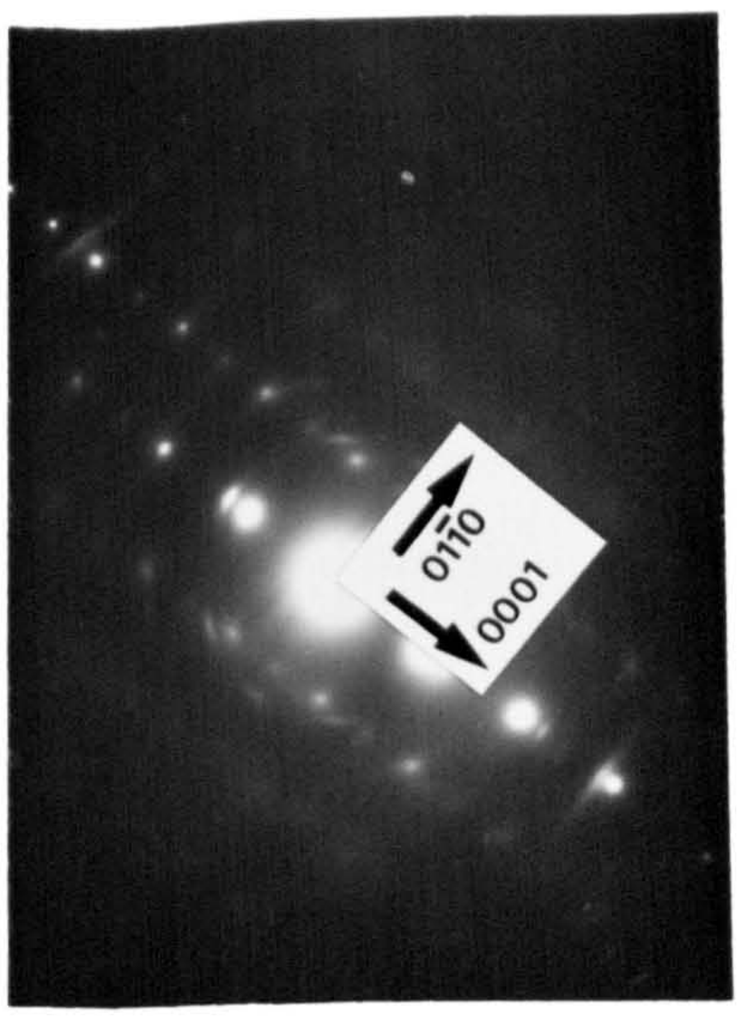
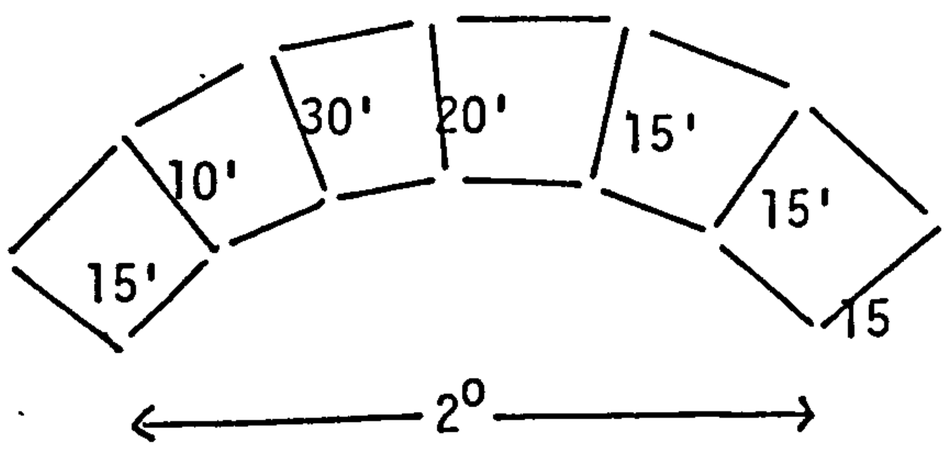


Figure 3.32. The most common type of boundary was the 'picket fence' boundary consisting of edge dislocations of $\vec{a}$ burgers vector: the micrograph is an example of this type of boundary.

in the cores is presented in Figure 3.33. It was found that the subgrains tended to misorientate in groups or clusters. This is shown schematically below.



individual misorientations

collective misorientation

Whilst the individual misorientations would not be detectable, the collective misorientation would be high enough and the collective width of the subgrains of the right order of magnitude to account for the features visible optically.

ii) Behaviour in the mantles

In the mantles the subgrains were more equiaxed and there was evidence for the operation of more than one slip system. Dislocations with $\vec{c + a}$ burgers vector as well as those with $\vec{a}$ burgers vector were analysed in these regions.

Optically the mantles were highly misoriented with respect to the cores. This is reported in detail in the next section. Differences in basal plane orientation between these two regions were as high as 25^{o} in some grains. This was accomplished by gradual bending of the lattice over a distance of up to 200μm, although the degree of bending was higher adjacent to the grain boundaries. This was confirmed in the E.M. work. Figure 3.34. Boundaries aligned close to 45^{o} to the compression axis accommodated the largest rotations whilst the rotations at the horizontal boundaries were smaller. This trend agrees with the orientations of the recrystallised grains at the old grain boundaries as will be shown in the following subsection. The rotations in the mantles were normally associated with grain boundary bulging. One such example is illustrated in Figure 3.35. The bulge in the boundary (X) is misoriented 3^{o} from the centre of the grain and 5^{o} from

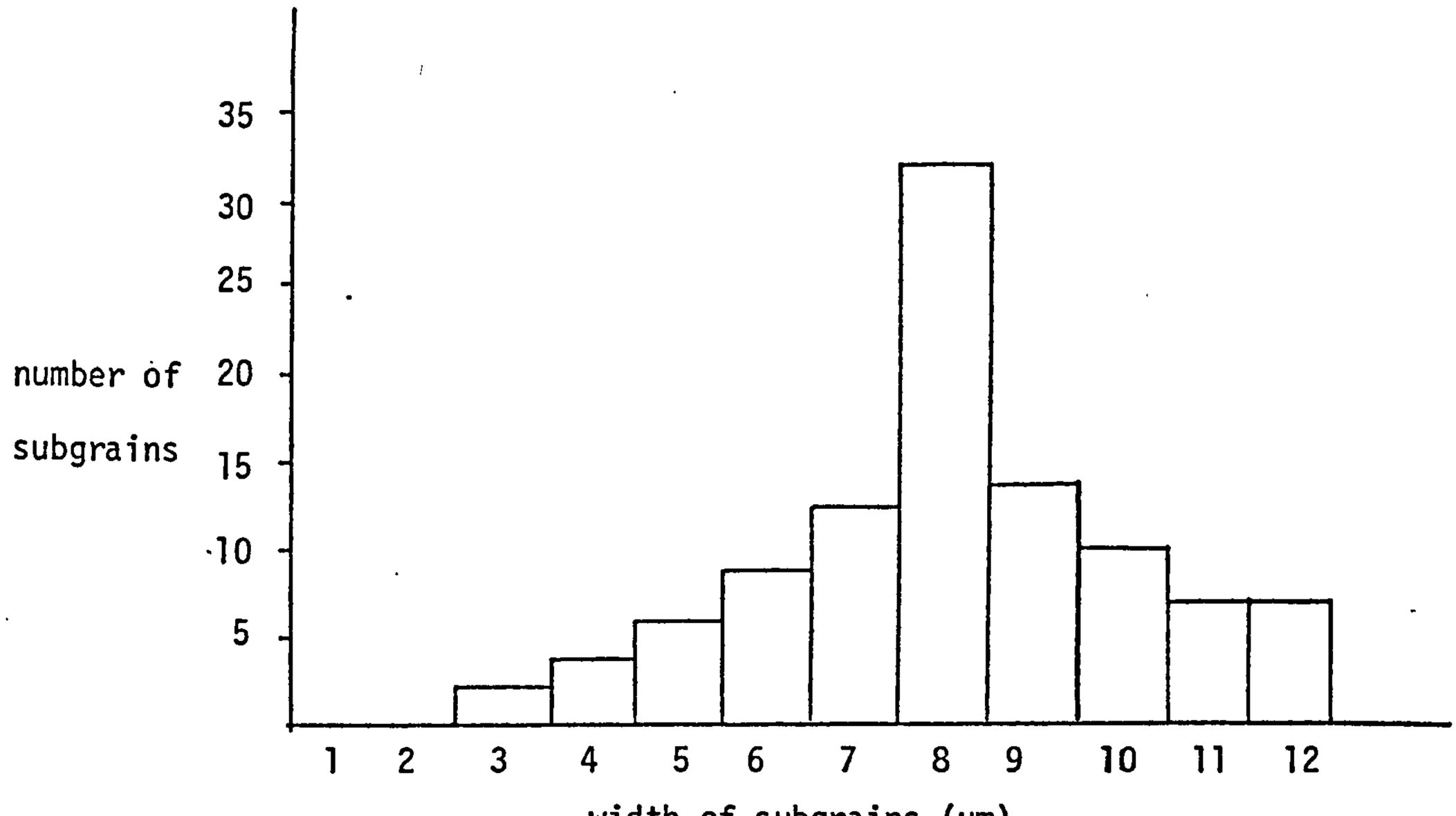


Figure 3.33. Histogram of subgrain sizes in the cores of the old grains.



Figure 3.34. Electron micrograph illustrating the lattice bending near an old grain boundary. A rotation of 18° about a $[2\bar{1}\bar{1}0]$ zone axis can be detected across the arrowed region from which the diffraction pattern was taken. The rotation of the basal planes as the grain boundary is approached is clearly visible. The recrystallised grains A and B are not strain free - merely out of contrast.

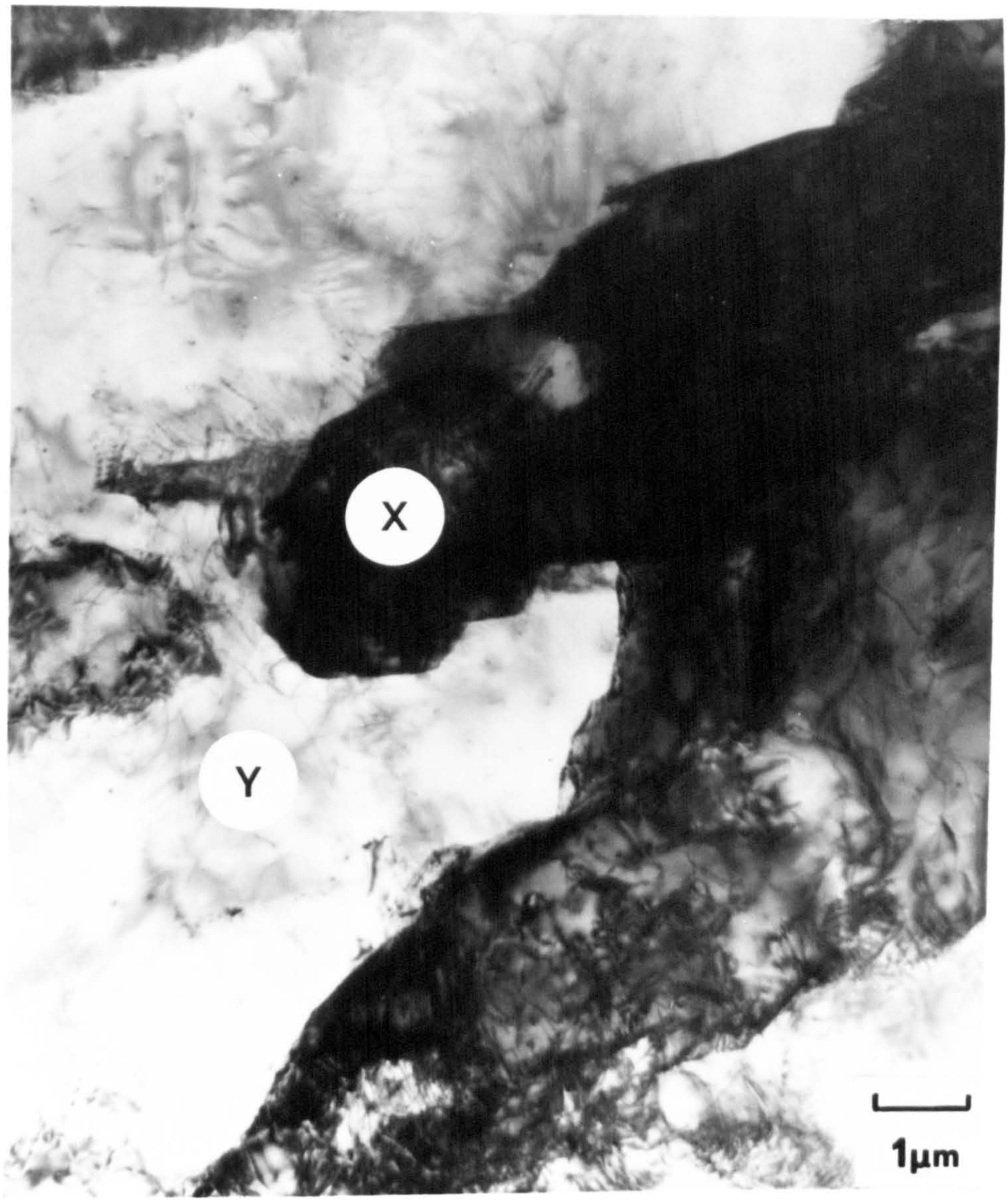


Figure 3.35. Electron micrograph which shows the bulging of a boundary between two old grains. The misorientations in the vicinity of the bulge were determined from an analysis of Kikuchi line shift (see Appendix). The bulge X was found to be misoriented by 3^{o} from its host and by 5^{o} from the adjacent grain which is out of contrast (Y).

the adjacent grain (Y) which is out of contrast. A second example shows the rotations in the mantle of an old grain which is highly misoriented from its neighbour, Figure 3.36. A rotation of 12^{o} about a [21$\bar{1}$0] axis has occurred at boundary A and a zone accommodating a rotation of 10^{o} is evident at B. The subgrains in the mantles tended to be smaller and more equiaxed than those in the cores. A histogram of subgrain sizes is shown in Figure 3.37. It can be seen that there are two peaks which reflected the trend for subgrains to occur alternately wide and narrow.

iii) The recrystallised grains

The recrystallised grains were similar in size to the bulges which could be seen optically and in the electron microscope at the grain boundaries. The bulges and recrystallised grains resolvable in the E.M. were smaller than those resolvable optically. Detailed electron microscopy revealed the existence of dislocation substructures within the new grains showing these to be formed by dynamic rather than post deformation static recrystallisation, Figure 3.38.

3.3.2.3.3. The orientation relationships between old and new grains

Reflected polarised light metallography as described in section 2 enabled misorientations within old grains and also the relationship of recrystallised grains to one another and to adjacent old grains to be determined. The use of the sensitive tint plate facilitated the determination of the basal plane rotation.

Four series of typical micrographs are presented here (Figures 3.39-3.42); the first two are from samples which had been deformed 20% at $230^{o}C$ and $300^{o}C$ and the second two from samples which had been deformed 55% at $230^{o}C$ and $300^{o}C$. Each specimen was rotated 5^{o} on the microscope stage before each micrograph was taken. The traces of basal planes were parallel to a horizontal crosswire in the microscope eyepiece at the point the grain changed colour from blue to orange on clockwise rotation of the microscope stage.

i) 20% ε $230^{o}C$

In Figure 3.39f it can be seen that the seemingly recrystallised grains at the old grain boundary A are in fact remnants of the host material in an almost totally twinned grain. Some rotation of the lattice can be detected at boundary B and in area C.

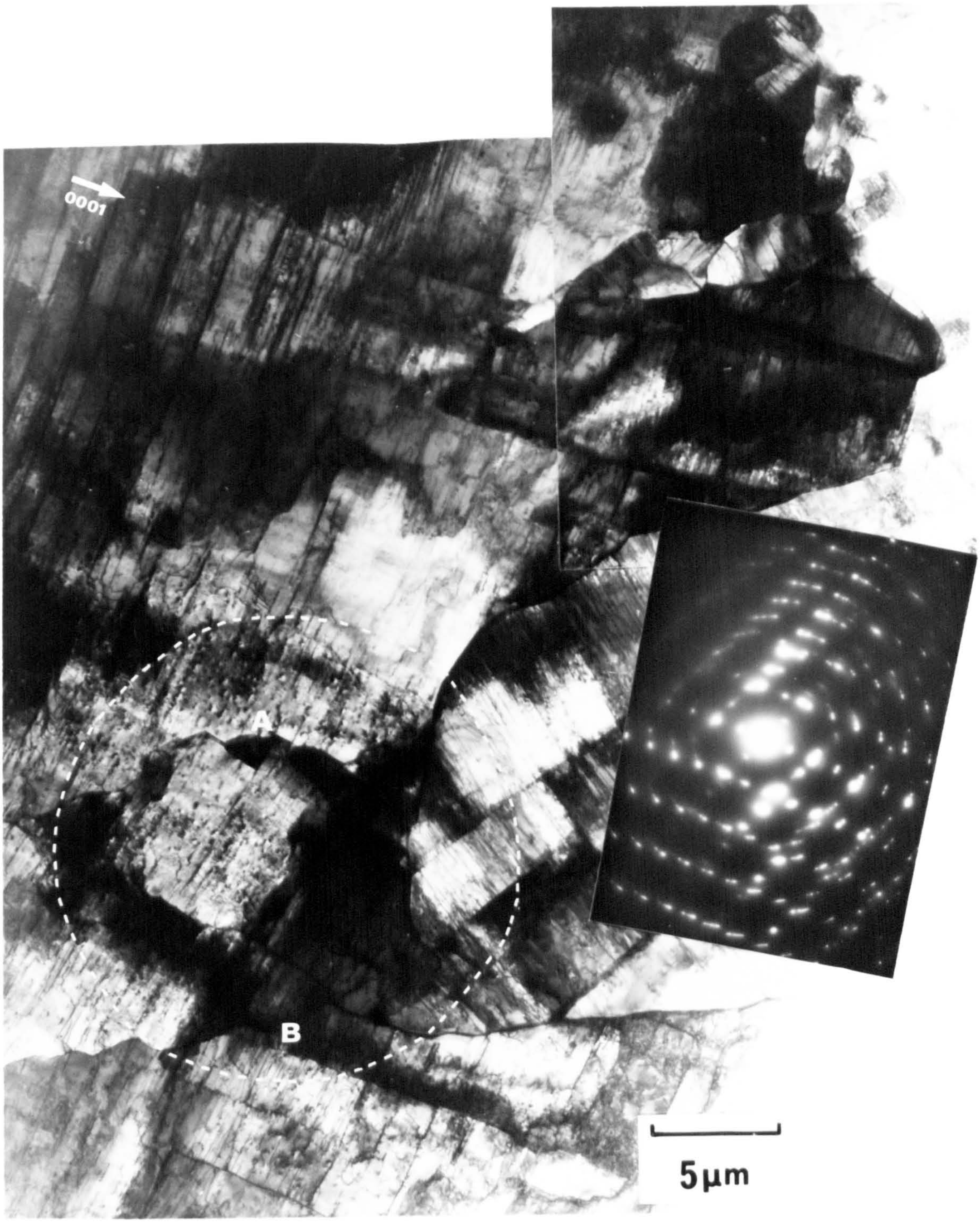


Figure 3.36. Electron micrograph illustrating the large rotations which occurred at the boundary between two old grains in a sample which had been deformed to 14% strain at 260°C. The dotted circle indicates the area from which the diffraction pattern was taken.

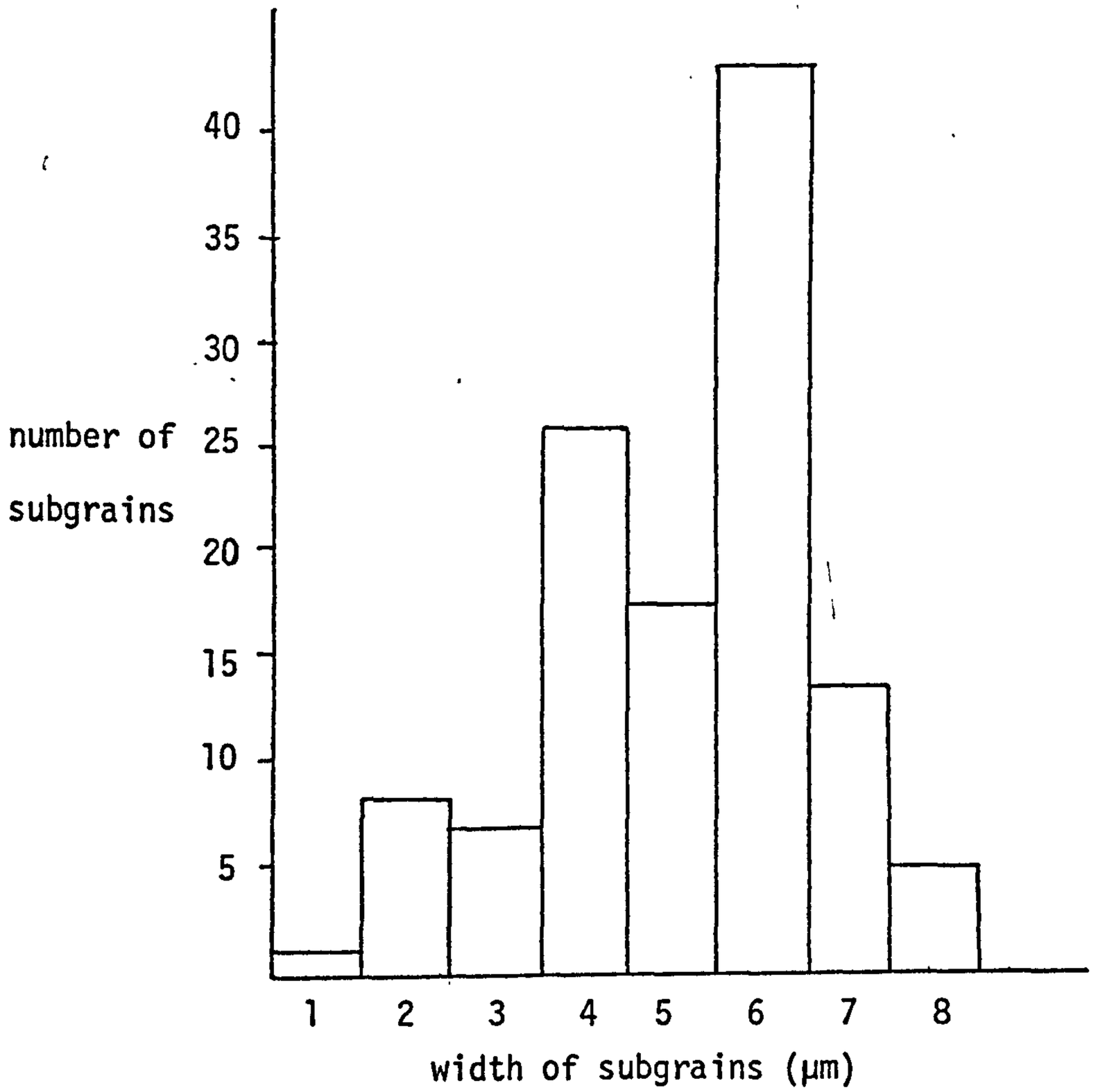


Figure 3.37. Histogram of subgrain sizes in the mantles at 260°C.

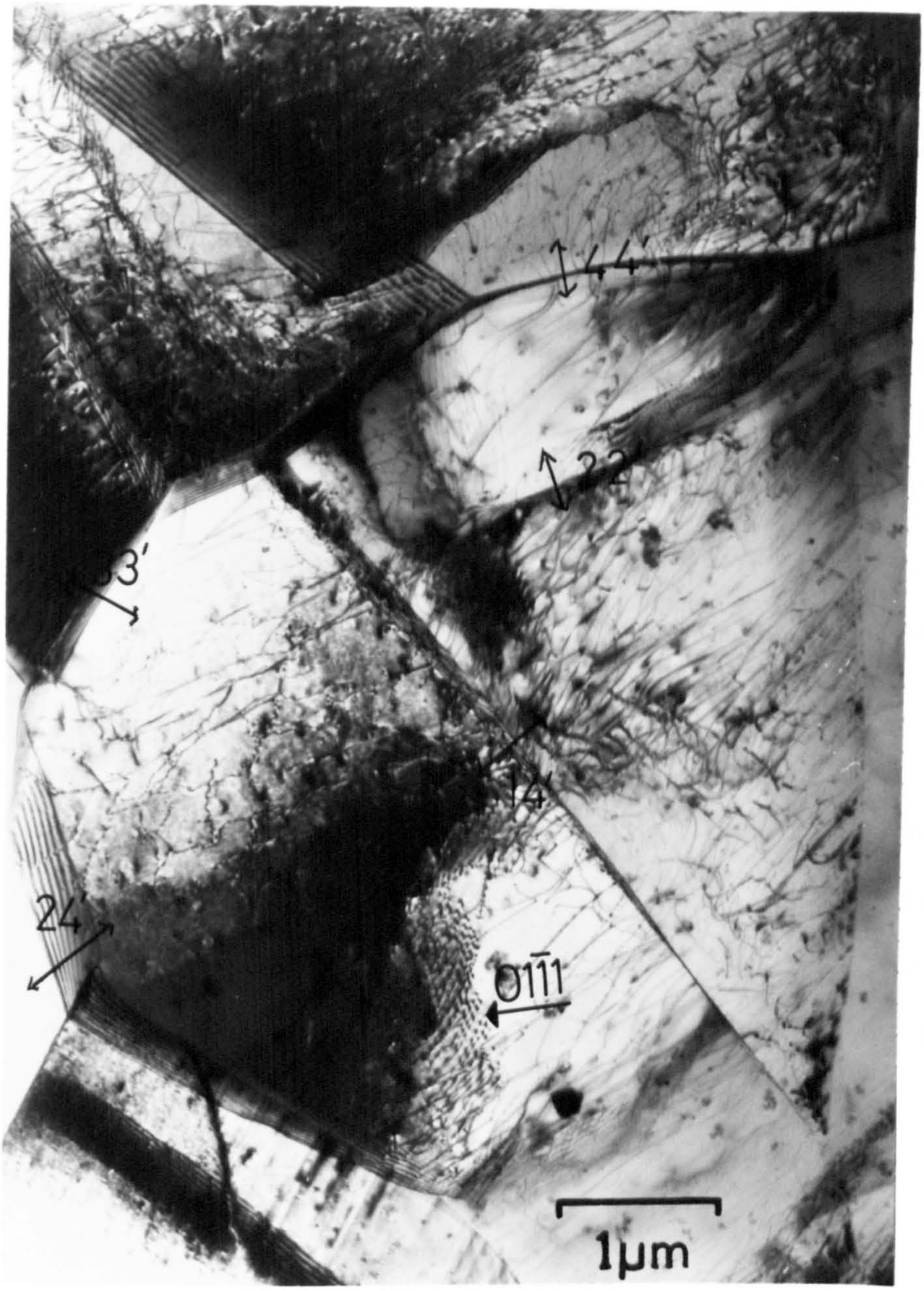


Figure 3.38. Dislocation substructure can clearly be seen in the recrystallised grains. The misorientations across each sub-boundary were determined from the Kikuchi line shift (see Appendix).

ii) 20% ε 300°C

There is more recrystallisation at 300°C (Figure 3.40). The lattice can be seen to be highly bent within the old grains. The misorientation between A and B (Figure 3.40a) is ~25° and is accommodated by gradual bending of the lattice. The recrystallised grains C forming at the boundary between the two old grains can be seen to originate from bulges in the boundary. The recrystallised grains D lie within the spread of orientations in the old grains and those at the edge of the old grain are associated with grain boundary bulges or rotations in the mantle.

iii) 55% ε 230°C

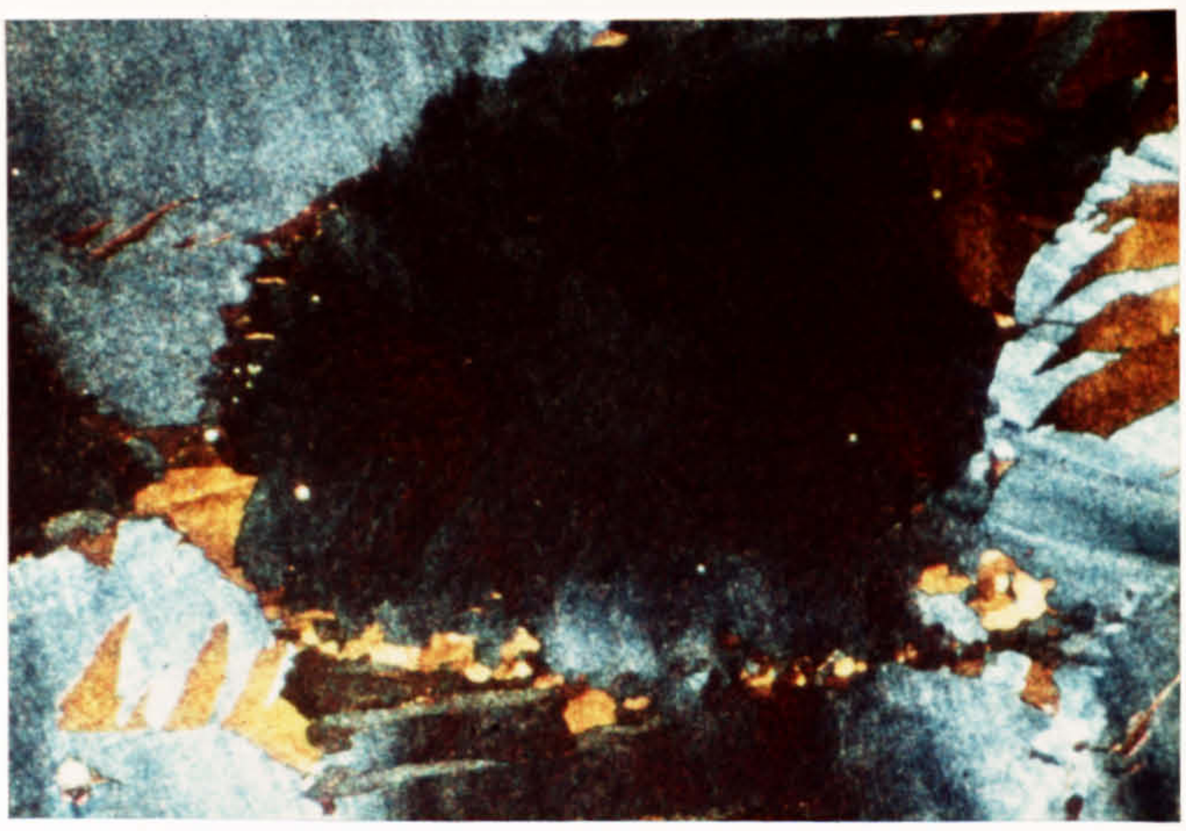
This series of micrographs shows the deformation behaviour within the old grains near a shear zone at 230°C. Features similar to the high temperature deformation bands (Figure 3.48) are visible in grain A, Figure 3.41a. The misorientation across these bands is as high as 15° but they are less regular than those found at high temperatures and the boundaries are not as sharp. Rotations of this order of magnitude are also evident in the recrystallised area B.

iv) 55% ε 300°C

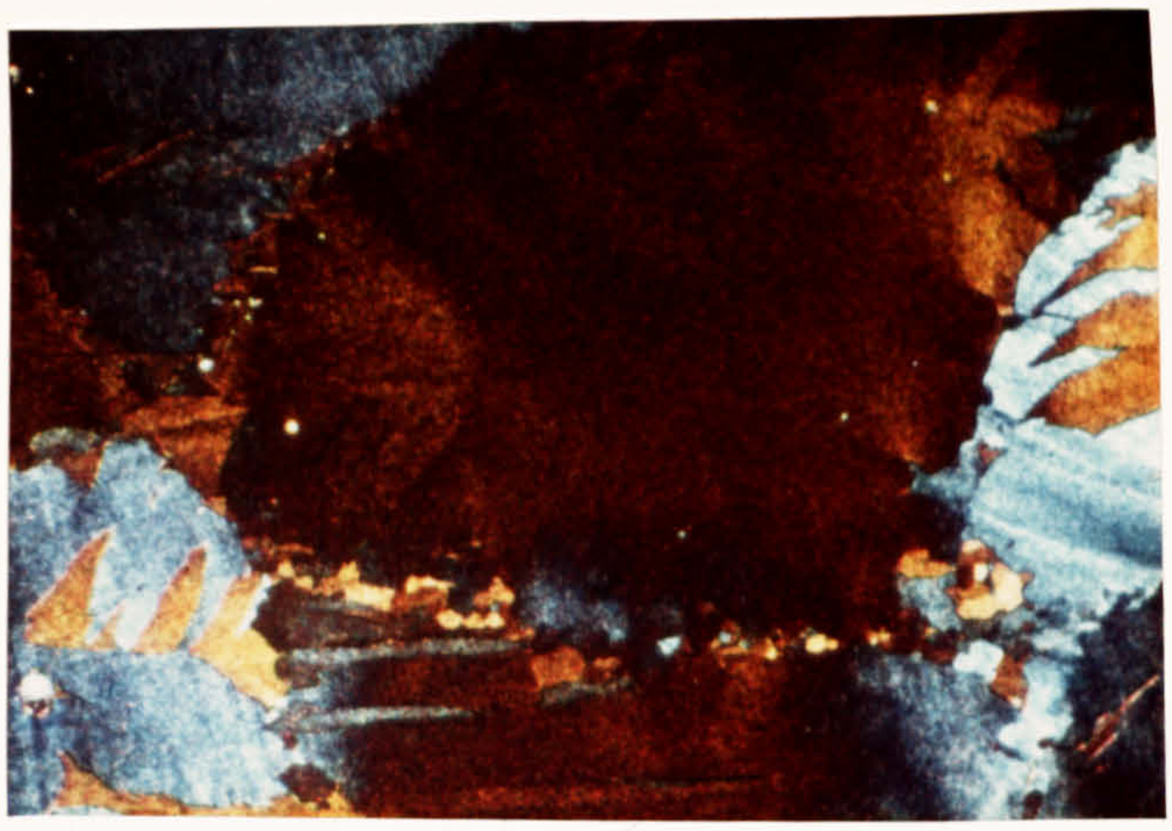
Recrystallisation is more evident in this sample (Figure 3.42). The recrystallised region C consists of small grains misoriented by 1 or 2° and bearing a close relationship to grains A and B. The lattice in grain A shows a large amount of bending. The basal planes at the ends are rotated 15° from each other.
In grain B the two ends are rotated by 15° with respect to the centre. Substructure can clearly be seen in the mantle of grain D; the basal planes in the centre of the grain being rotated by 5° with respect to the basal planes in the subgrains at the edge.

3.3.2.3.4. Heterogeneity of deformation on the bulk scale:- as determined from the microscopy of deformed polished surfaces

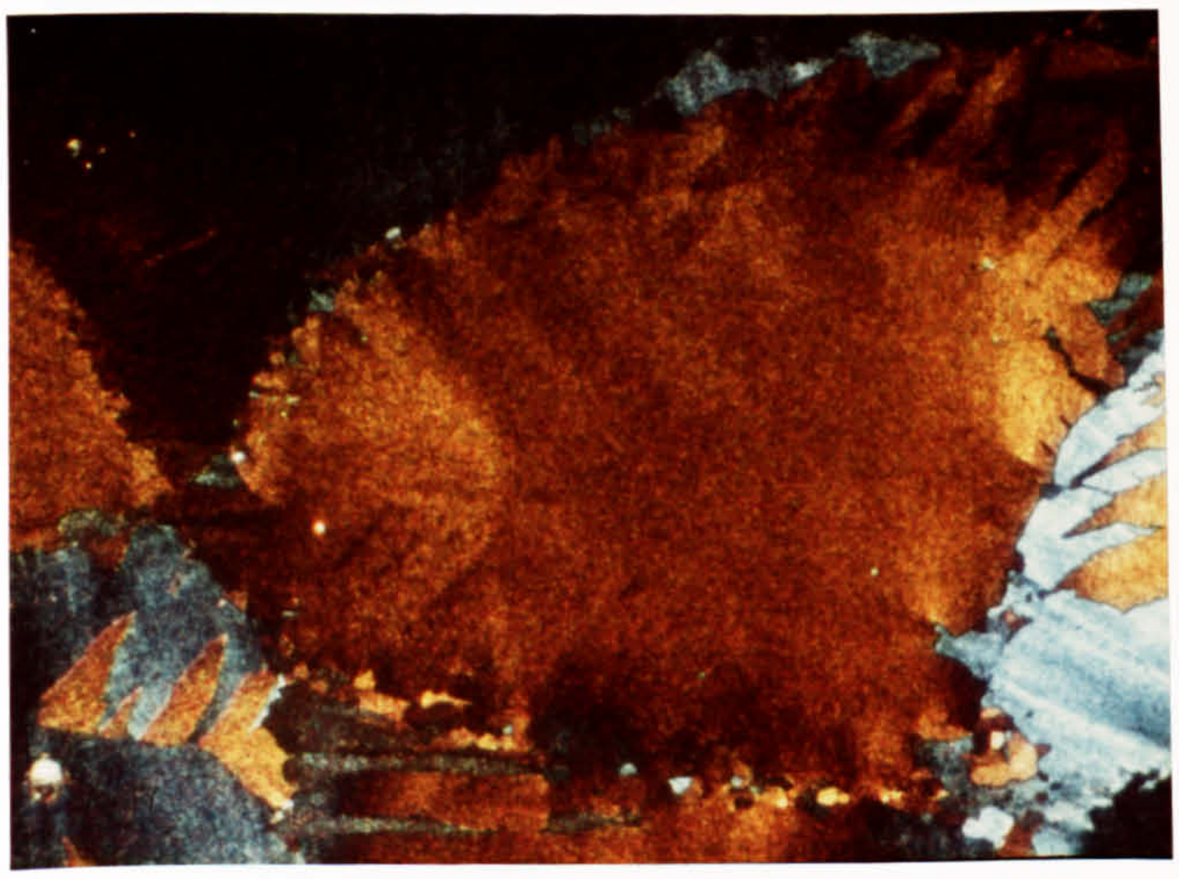
From the forgoing results it was obvious that grain boundary deformation was important. Grain boundary sliding has often been reported in magnesium so experiments were carried out to determine what contribution - if any - it was making to the deformation in the current work. Four specimens were deformed to 5, 9, 16 and 25% strain at $\dot{\varepsilon} = 10^{-5}s^{-1}$ (the latter specimen exhibited a shear zone and will thus be referred to in a subsequent section). A flat surface was



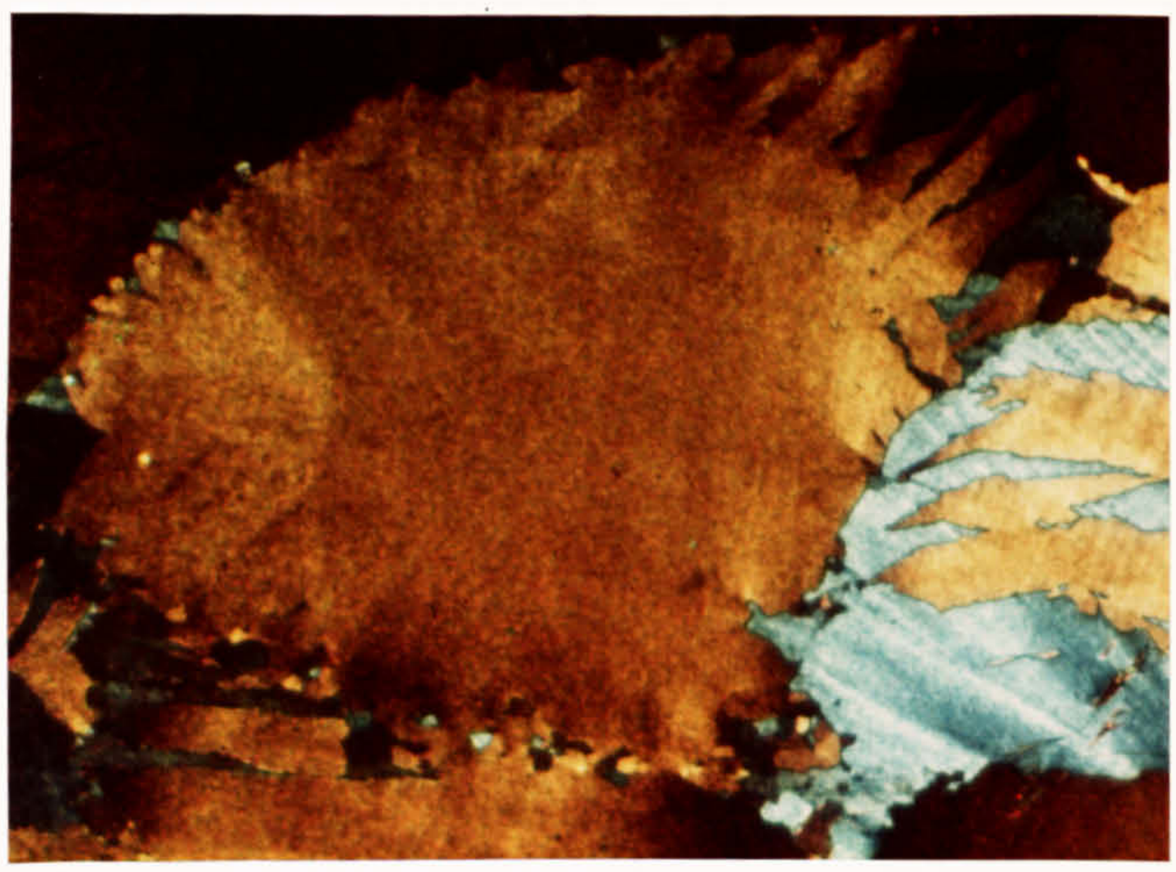
a



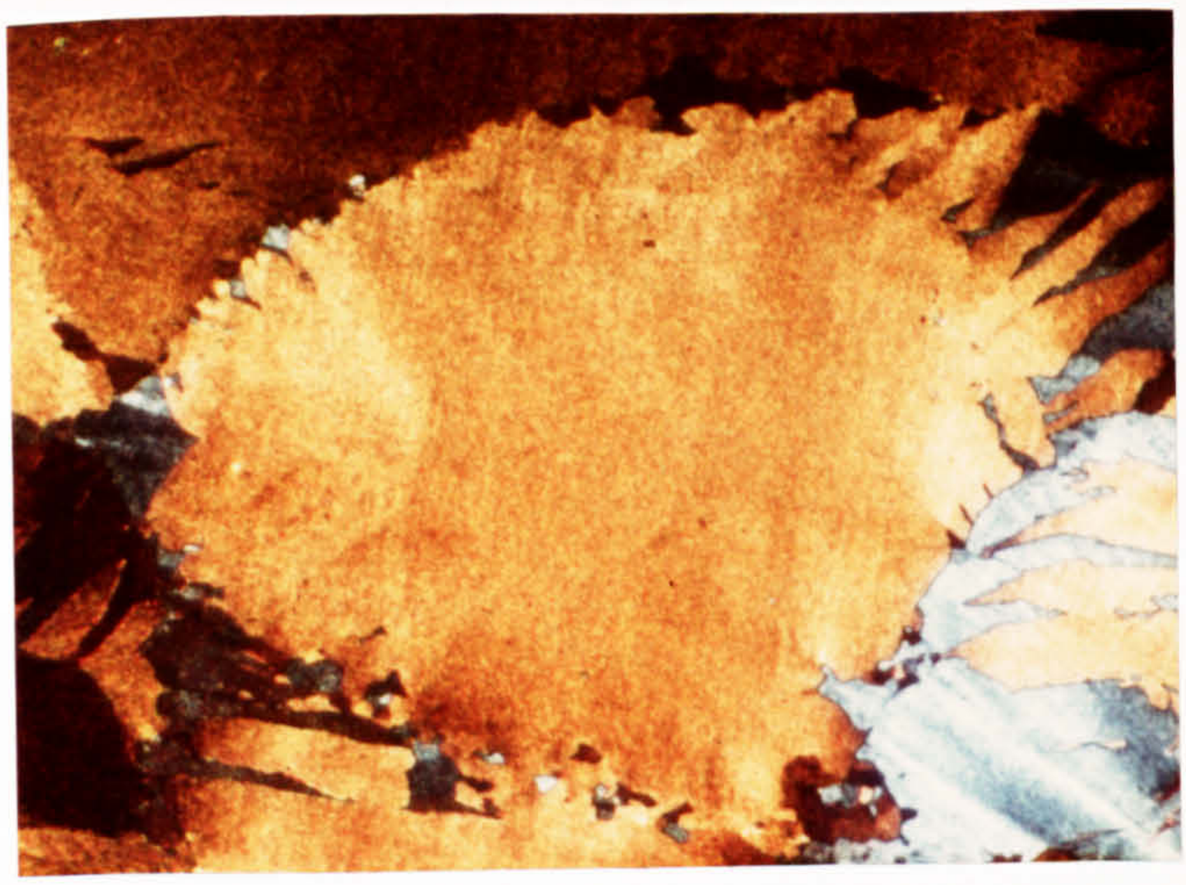
5° b



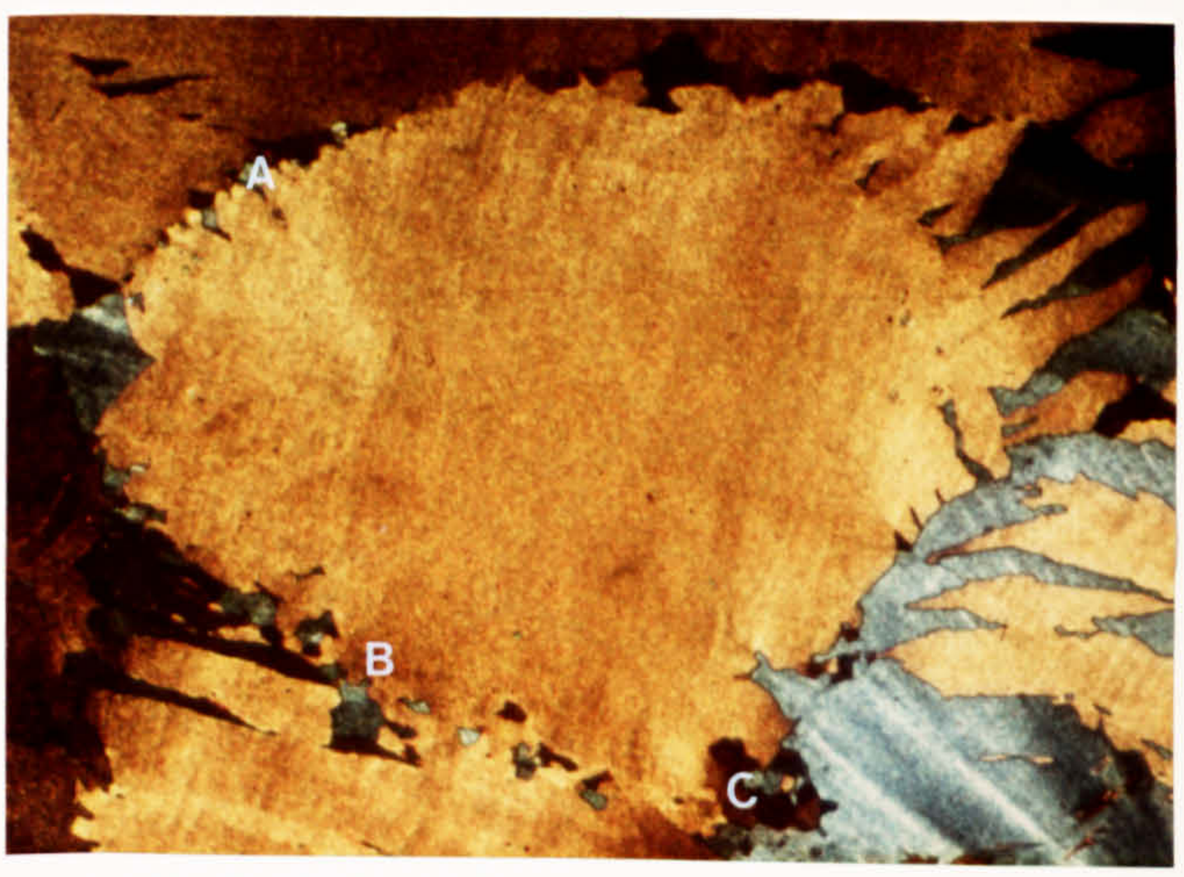
10° c



15° d



20° e



25° f

100μm

Figure 3.39 20% strain at 230°C.

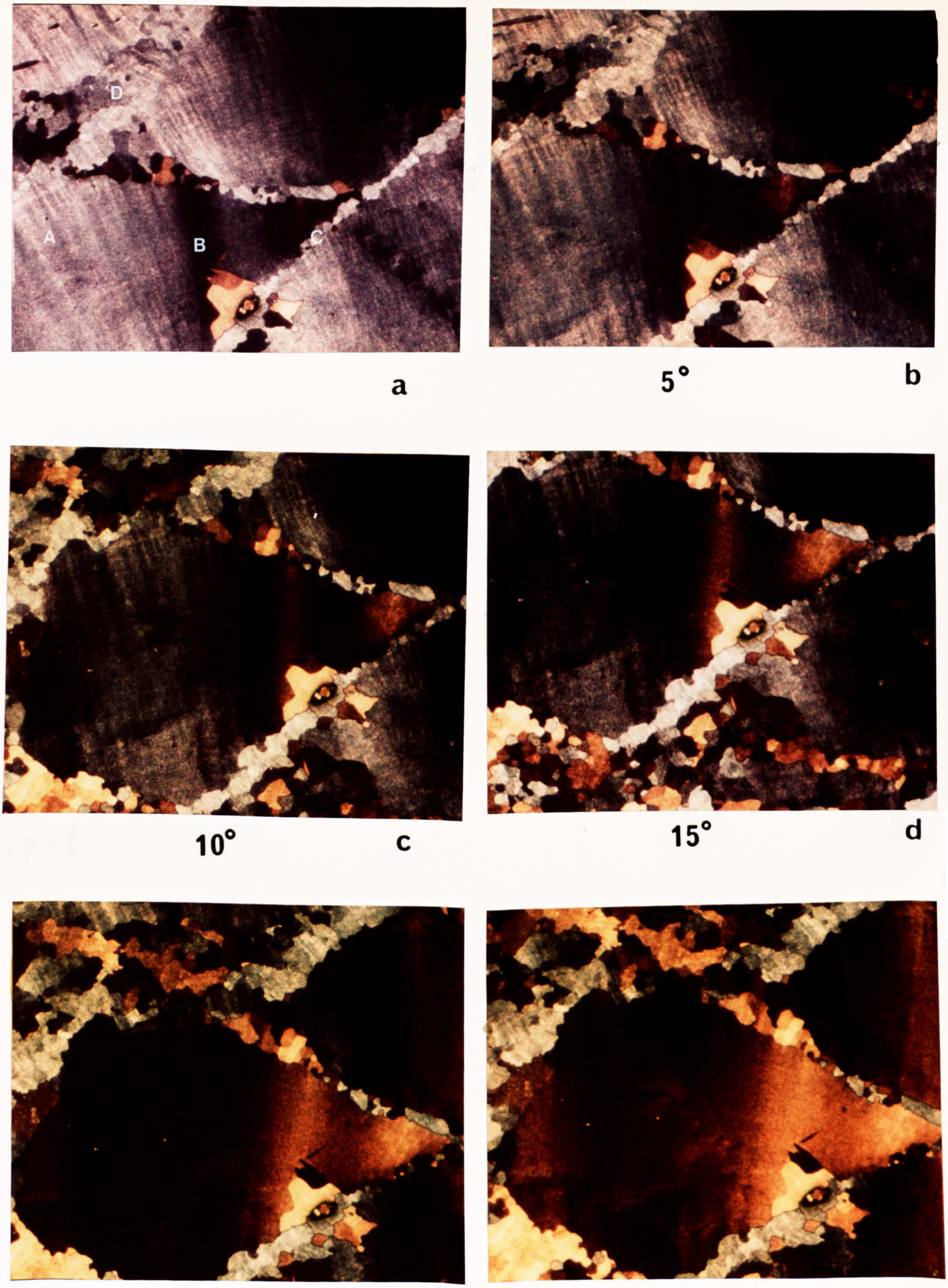
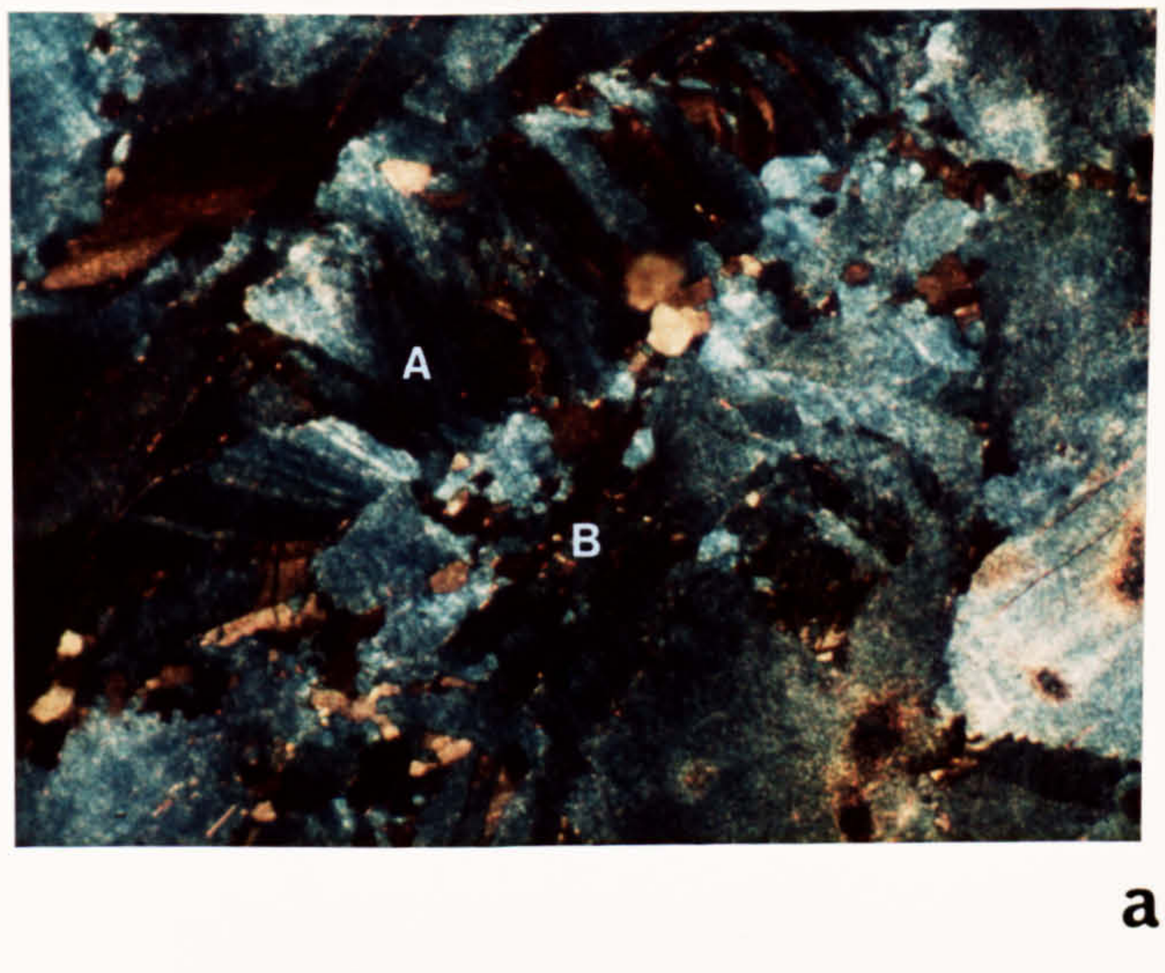
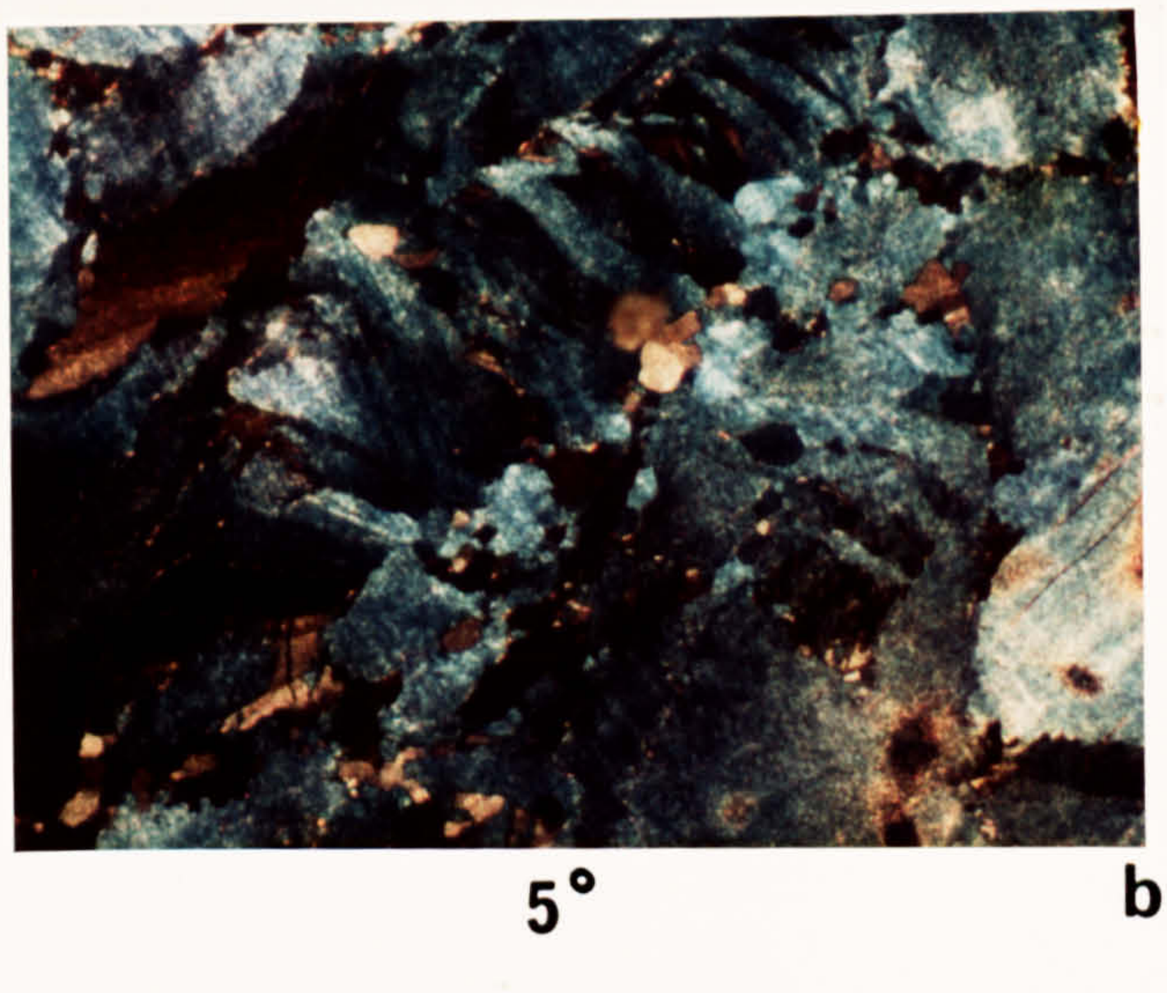


Figure 3.40 20% strain at 300°C.

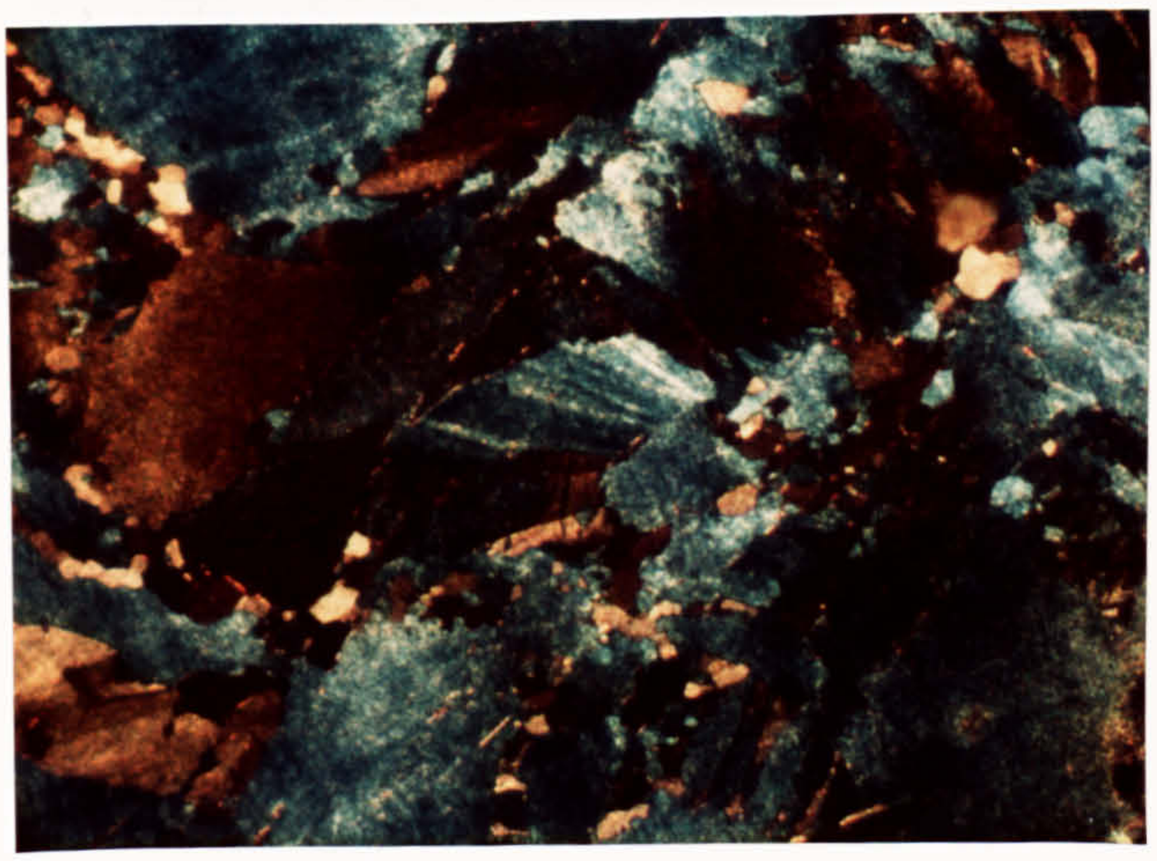


a



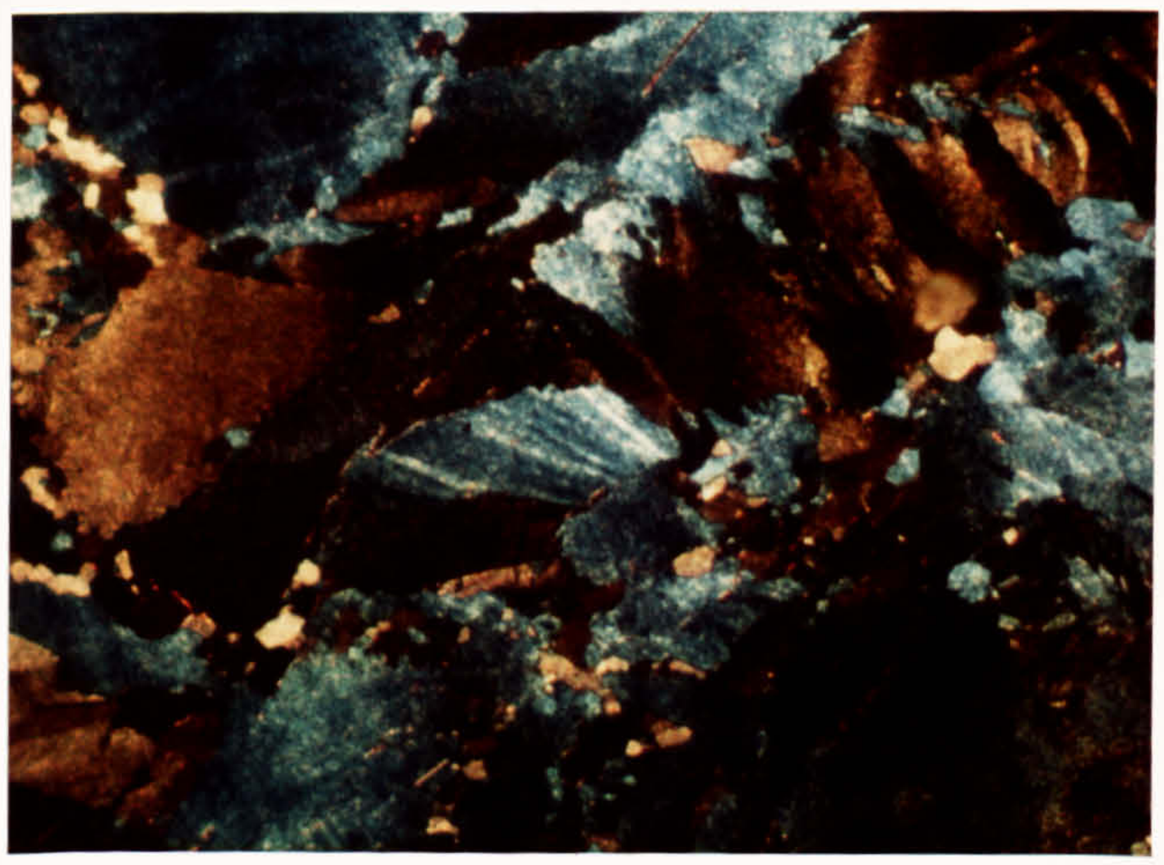
5°

b



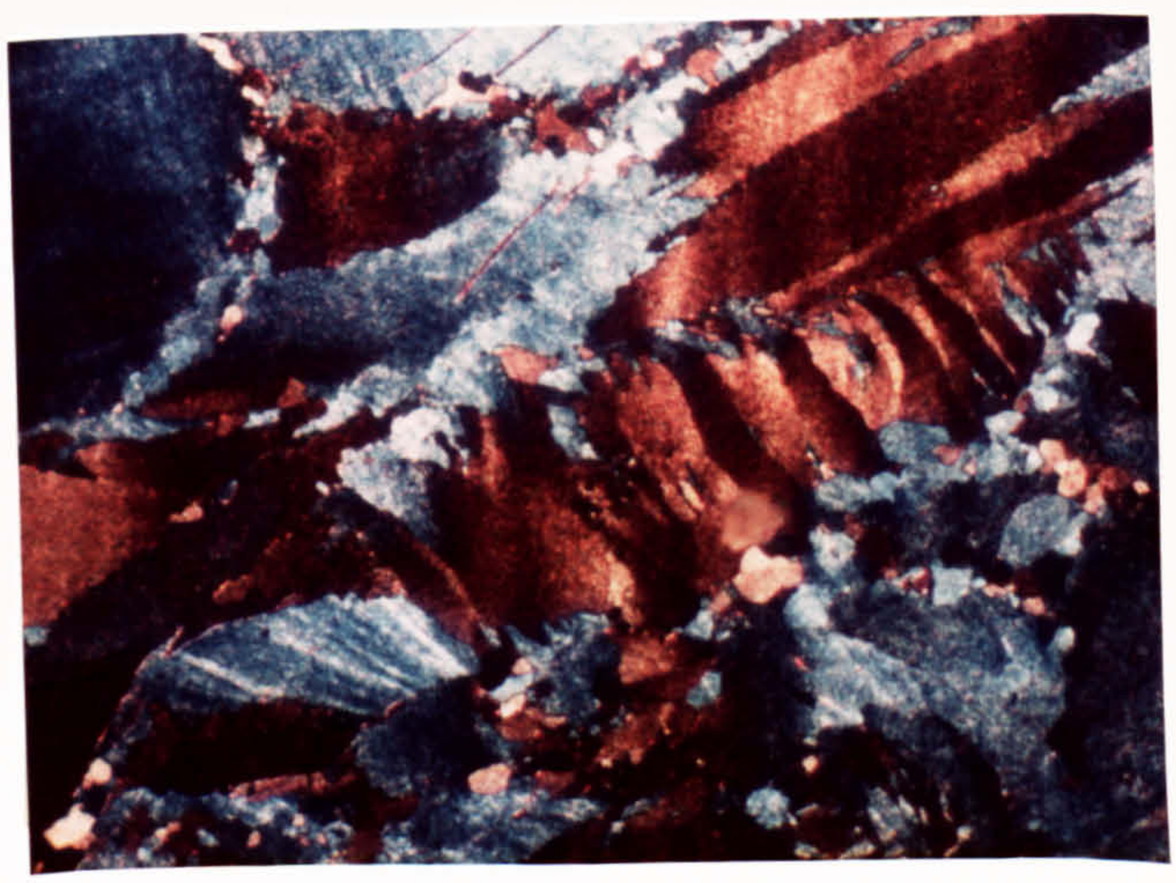
10°

c



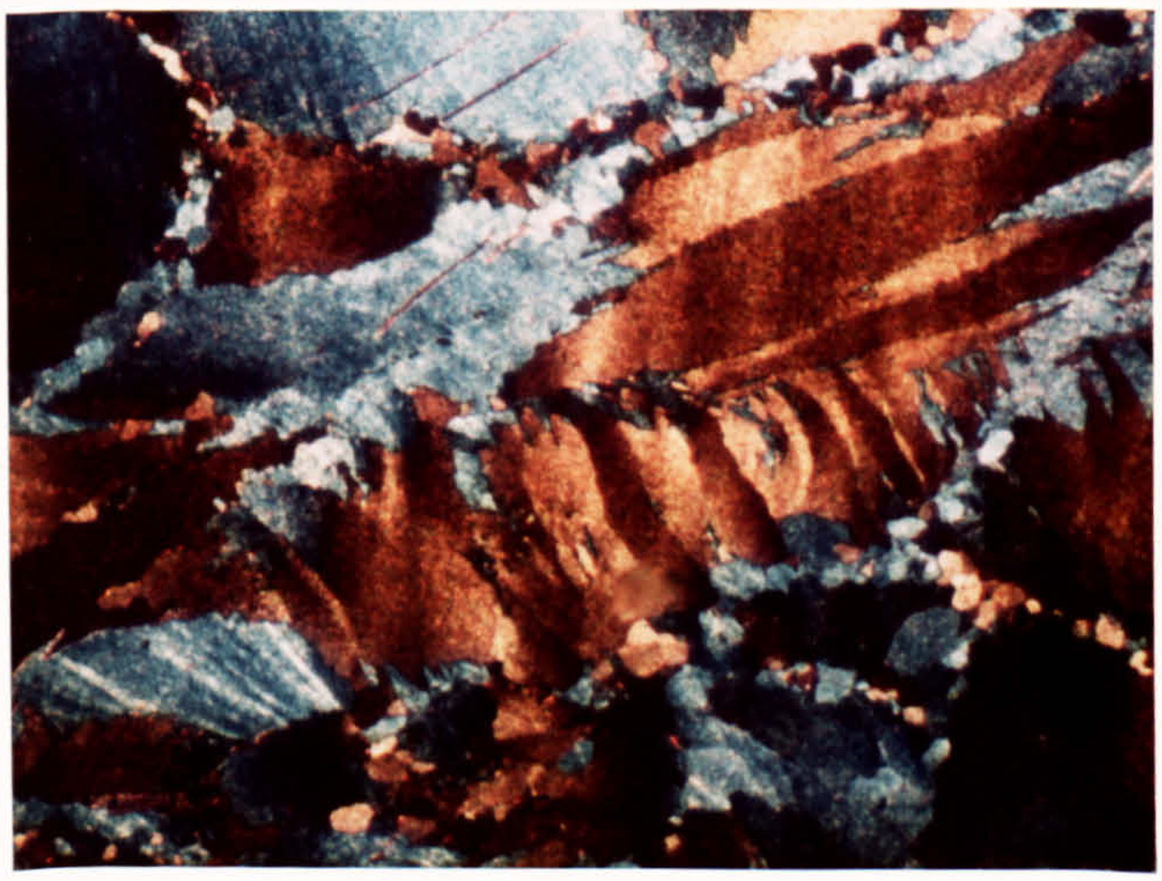
15°

d



20°

e

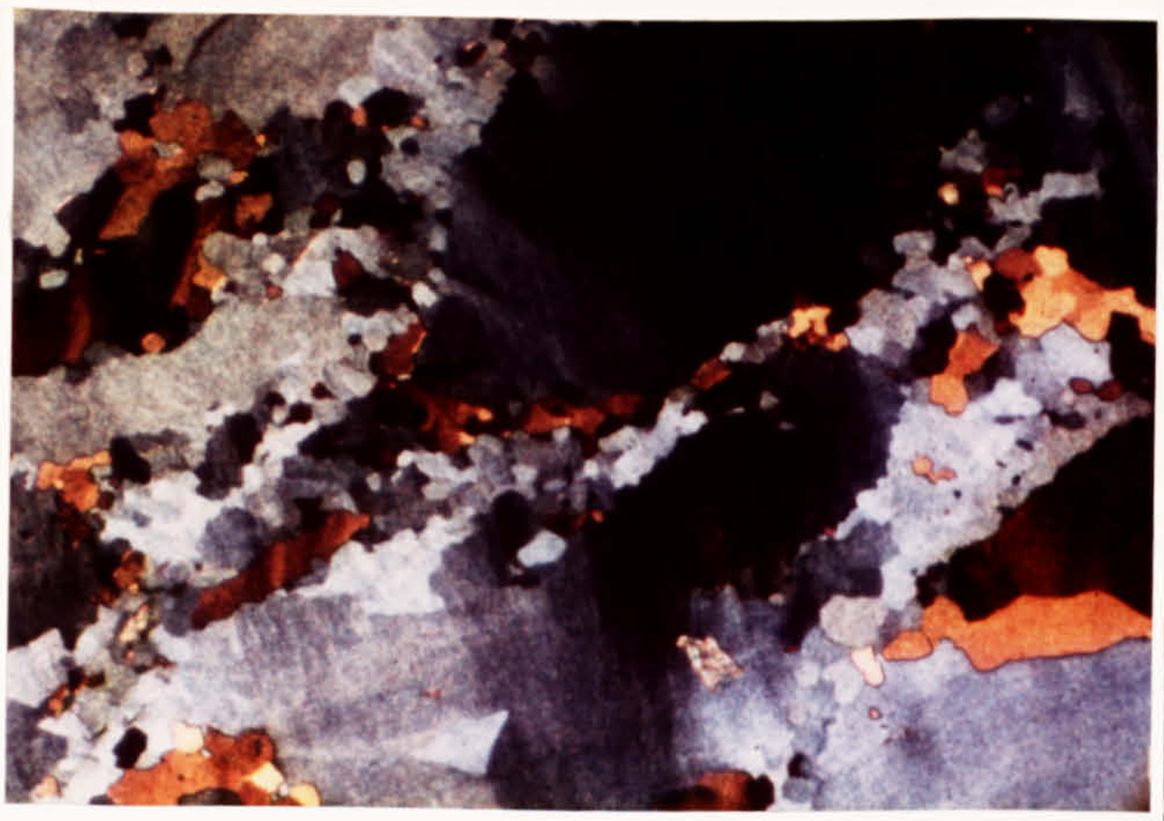


25°

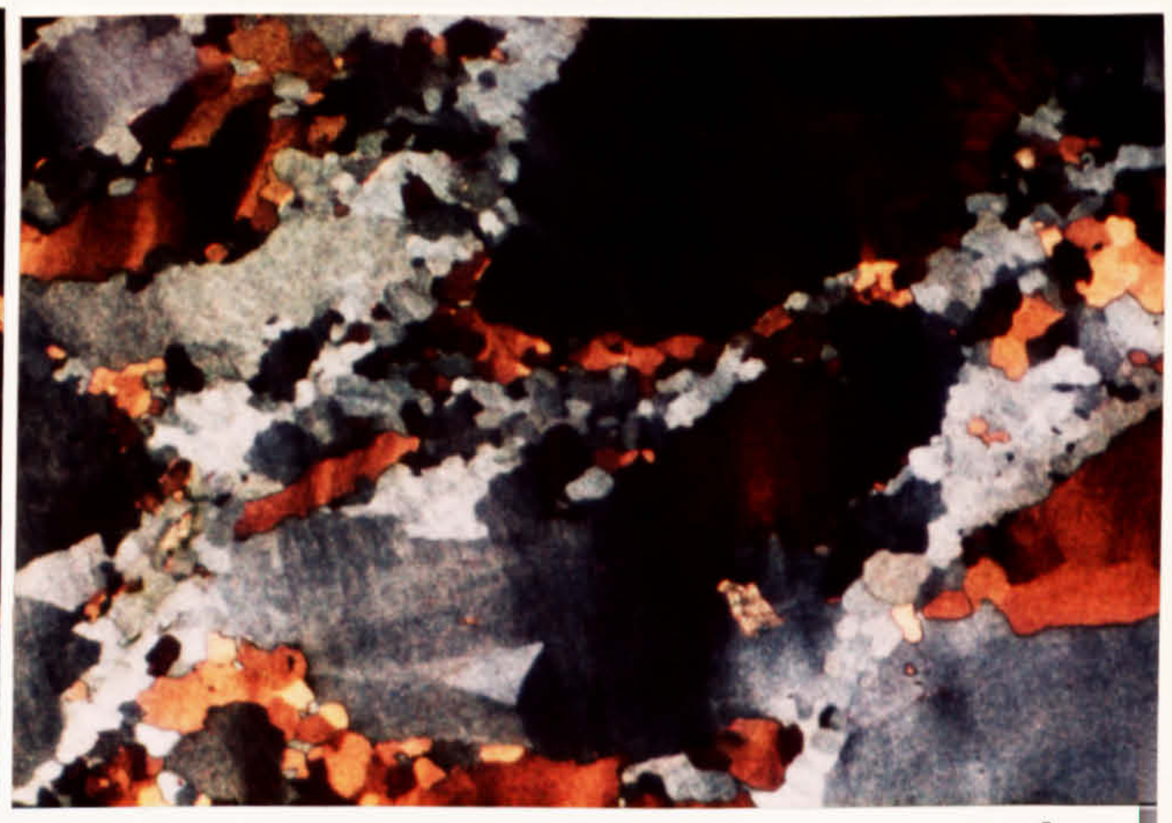
f

100μm

Figure 3.41 55% strain at 230°C.

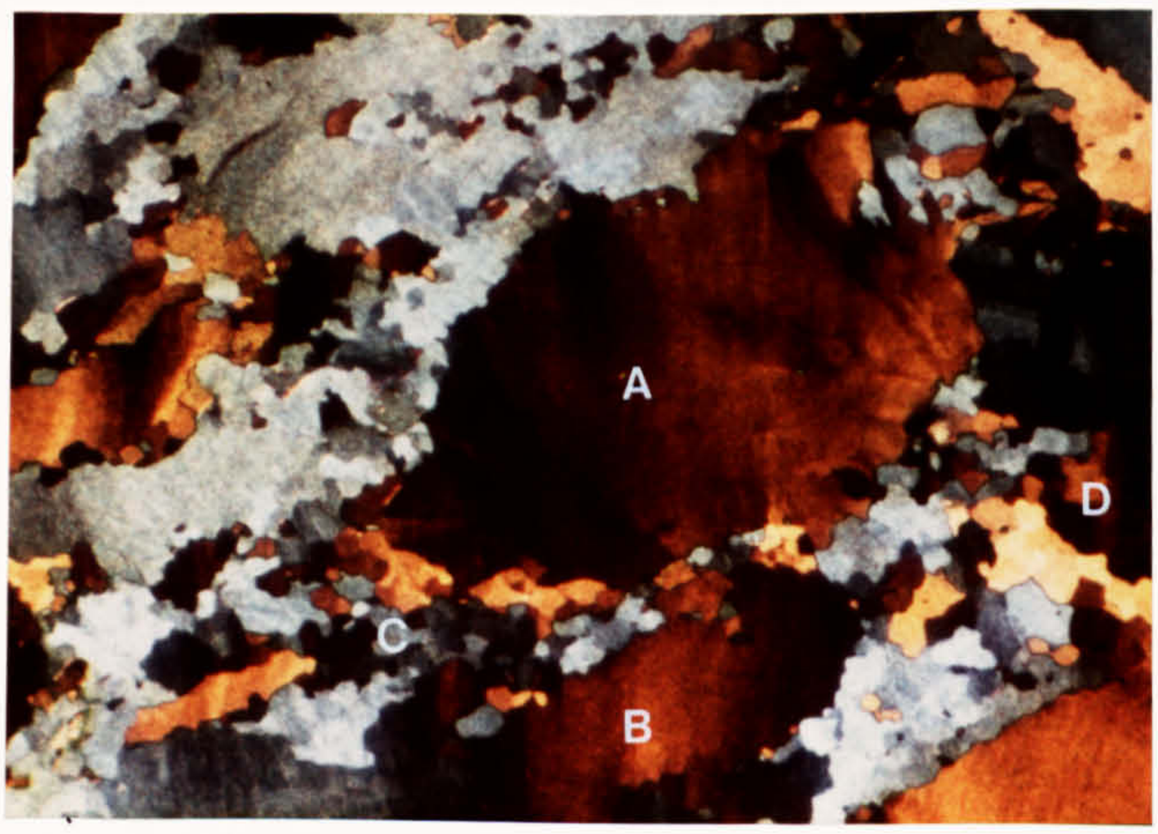


a



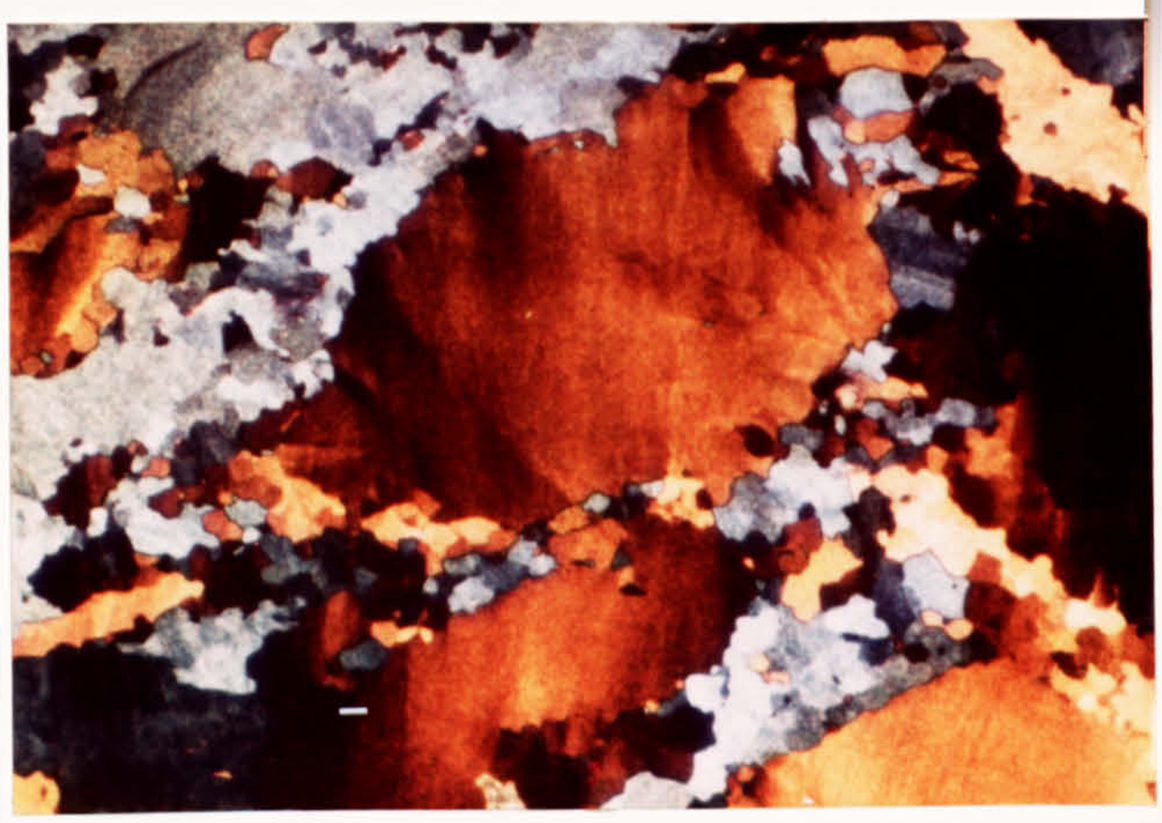
5

b



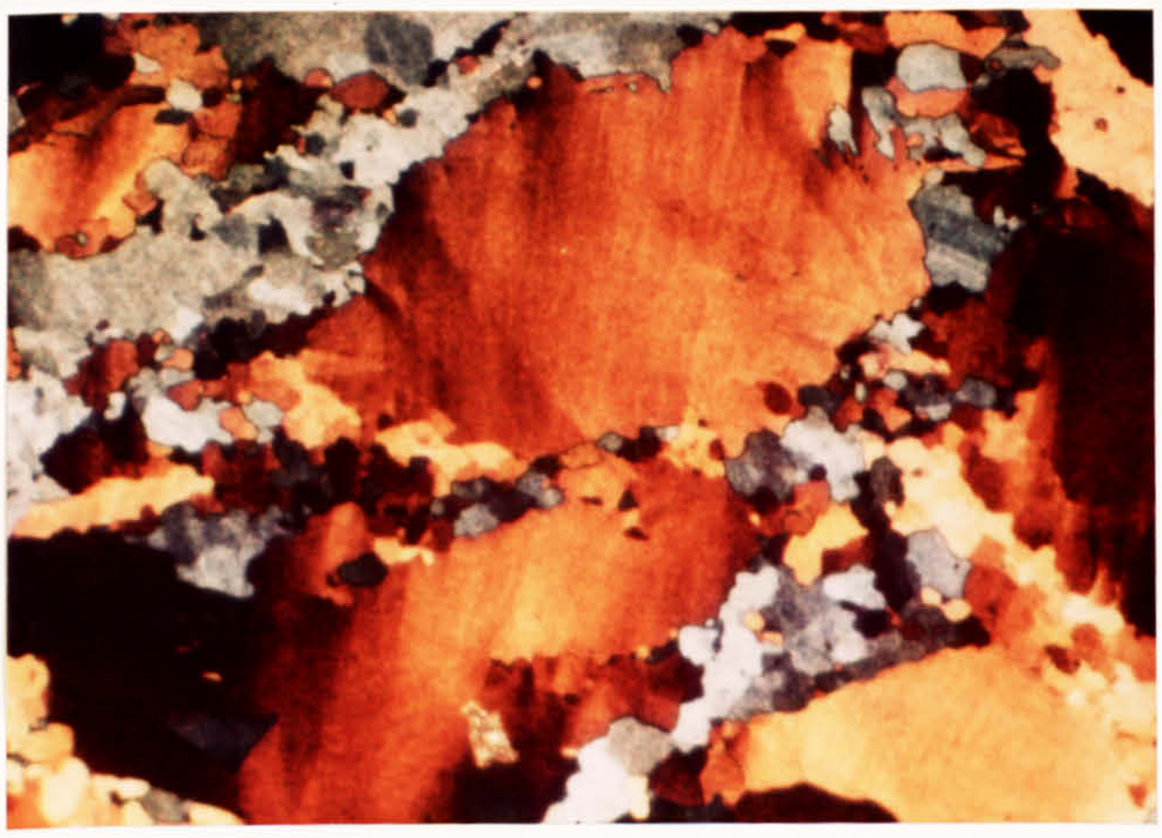
10°

c



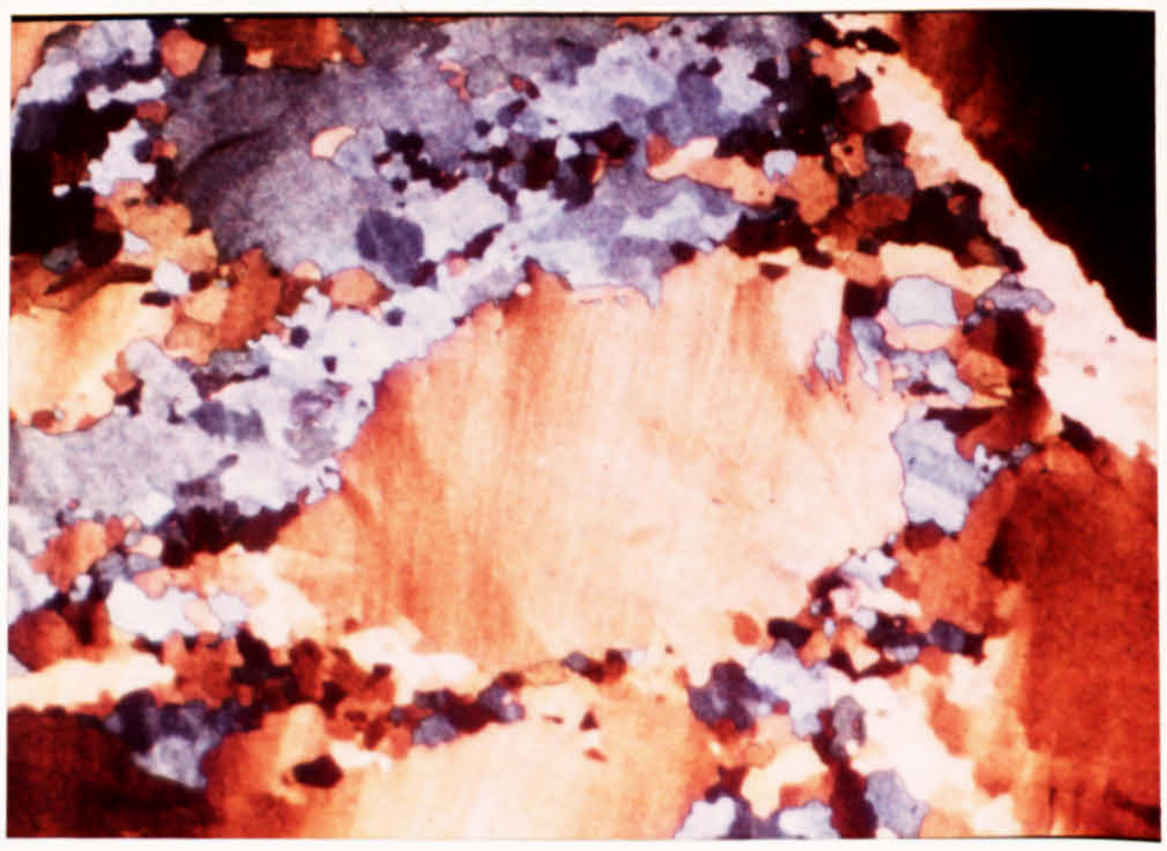
15°

d



20°

e



25°

f

Figure 3.42 55% strain at 300°C.

100µm

ground on each cylinder to a depth of 3 mm from the outside circumference. This surface was carefully mechanically polished to a 1μm finish but was not chemically polished. A gold grid was then evaporated onto each sample which was then carefully repositioned in the deformation rig to be given a further 10 or 15% ε. The deformed surfaces were examined in the optical microscope and in the S.E.M. The sample was then sectioned parallel to the deformed surface and the microstructure examined to ascertain whether a) the surfaces represented the bulk behaviour, b) removing the sample and re-deforming it affected the microstructure in any way. The behaviour of the sample pre-strained 9% which was representative will be presented in detail.

i) Optical microscopy

Although it was possible to image the grid after deformation, the 1μ scratches left on the specimen after polishing proved to be the better strain markers. Standard B.F. microscopy and also Nomarski interferometry were used. It was possible to obtain information about the deformation behaviour in this way but the lack of depth of focus on the deformed samples which had a rumpled surface made the recording of this information on photographic film difficult. One of the better examples can be seen in Figure 3.43a. It could clearly be seen that severe deformation had taken place at the grain boundaries, but that there were no sharp offsets at the boundaries. The marker lines were kinked by $\sim 25^{o}$ in the vicinity of the grain boundary indicated. This result is in accord with the rotations measured optically on the underlying microstructure.

ii) Scanning electron microscopy

The S.E.M. proved to be the better instrument for imaging the grid and obtaining adequate depth of focus. In Figure 3.43b the grid was relatively undeformed in the grain centres but was severely distorted in the vicinity of grain boundaries. A technique developed by Spiers (1979a) was used to quantify this information. It involved the use of a Sonic Digitizer to record the relative positions of each corner of each grid square in a defined area as data points. This data was input to a computer program which compared the shape of each deformed grid 'square' to a standard square.
The program superimposed the rigid body rotation and shear strain components of the deformation on a schematic outline of the micrograph (Figure 3.44). A second example of the procedure is shown in Figures 3.45 and 3.46 where the behaviour in the vicinity of a single grain

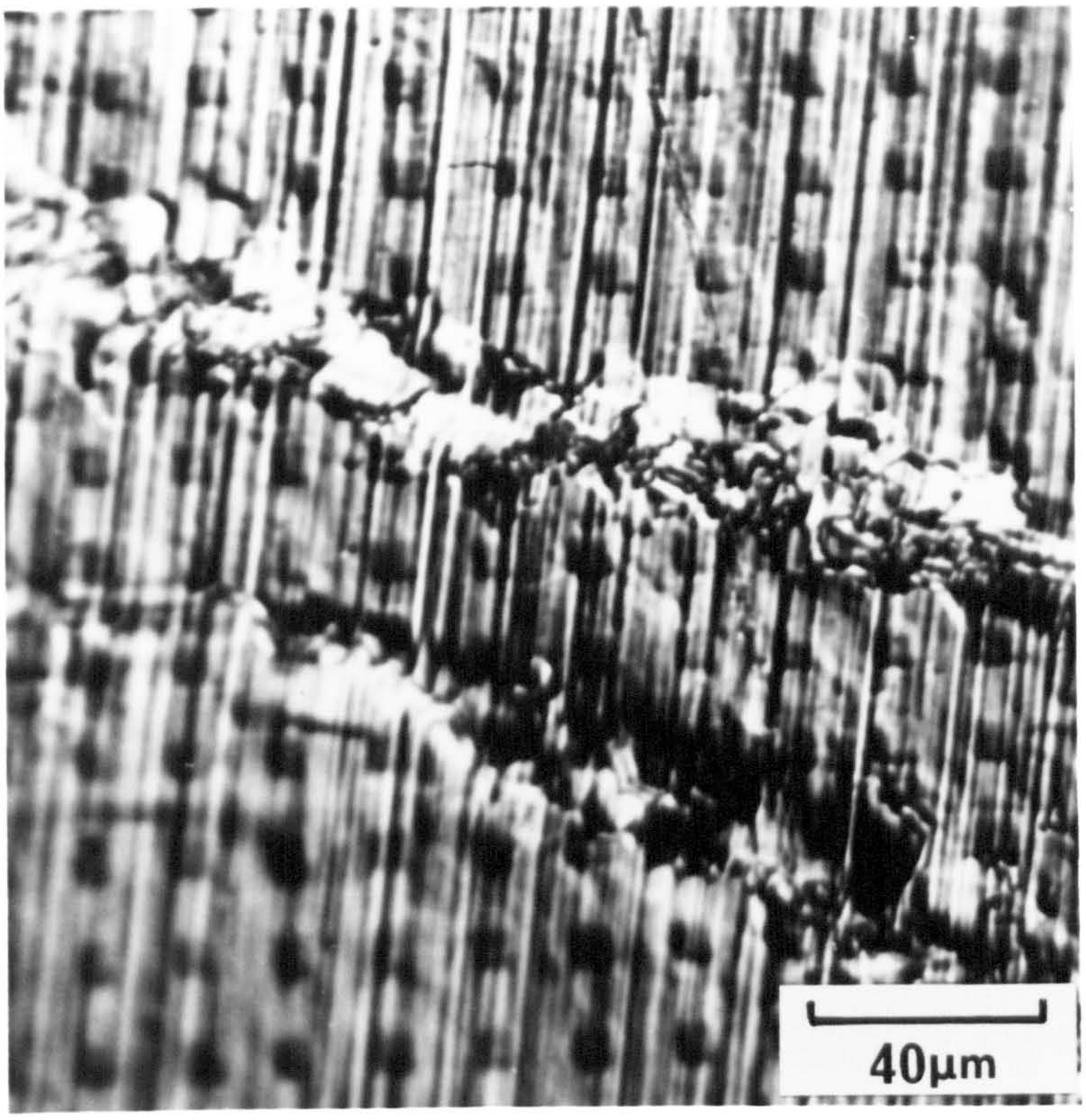


Figure 3.43a. Zone of deformation in the region of a grain boundary imaged using the Nomarski interference technique. The scratch lines can be seen to be severely distorted across the boundary but there is no planar offset. The specimen had been deformed 15%.

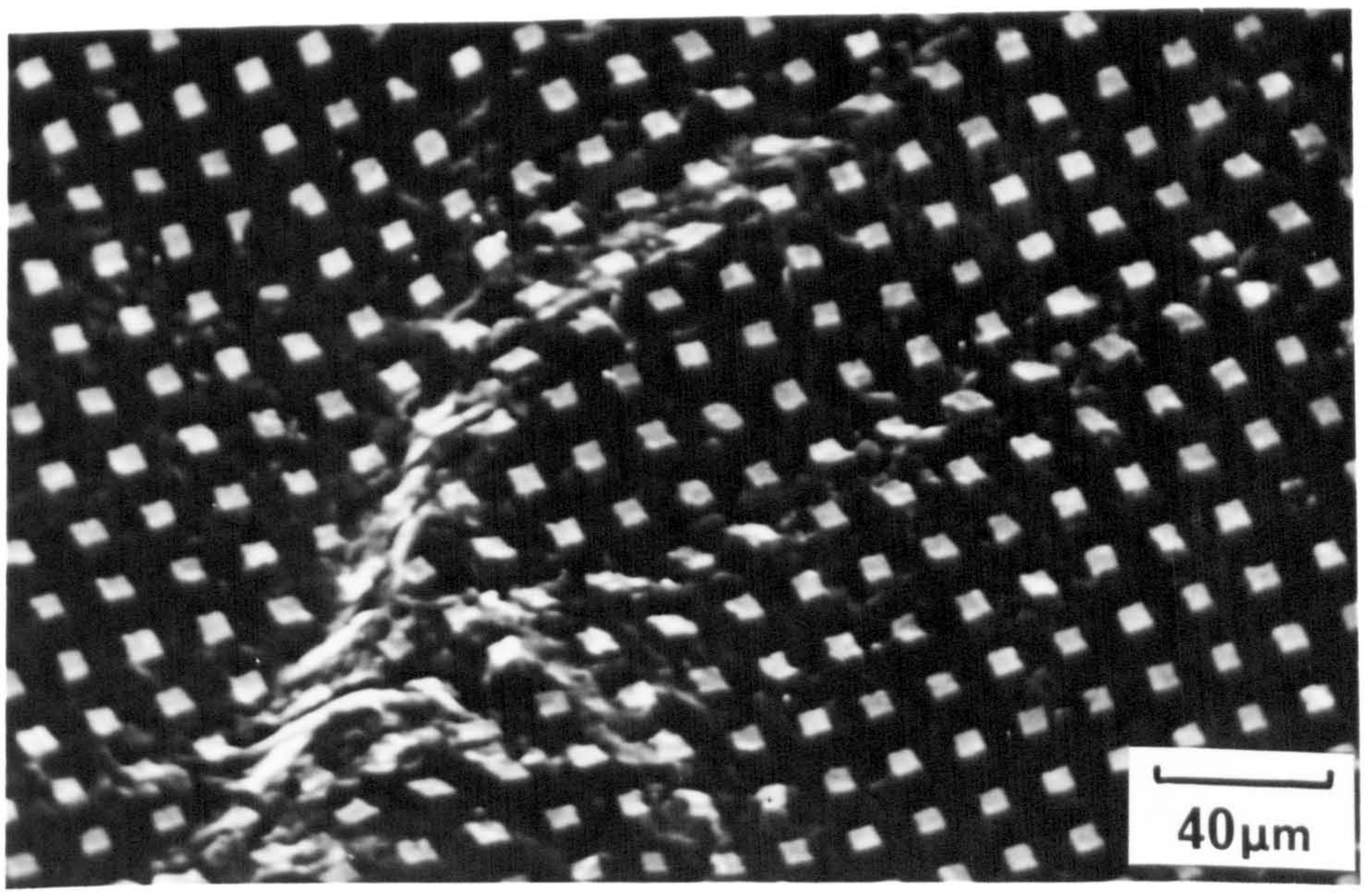
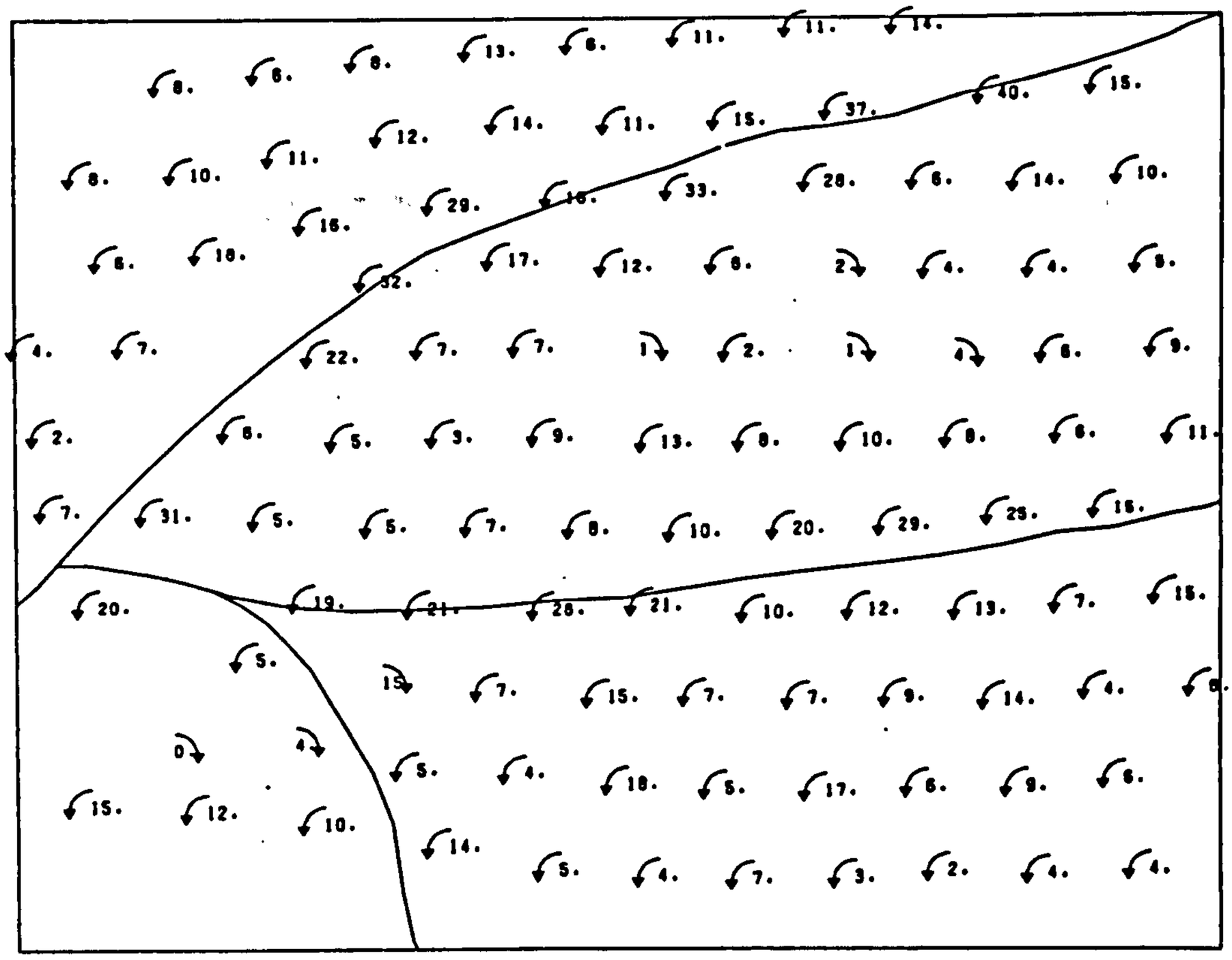


Figure 3.43b. Micrograph of a deformed region in the specimen imaged above. The gold grid shows high rotations in the vicinity of the grain boundaries. The deformation is quantified in Fig. 3.44.



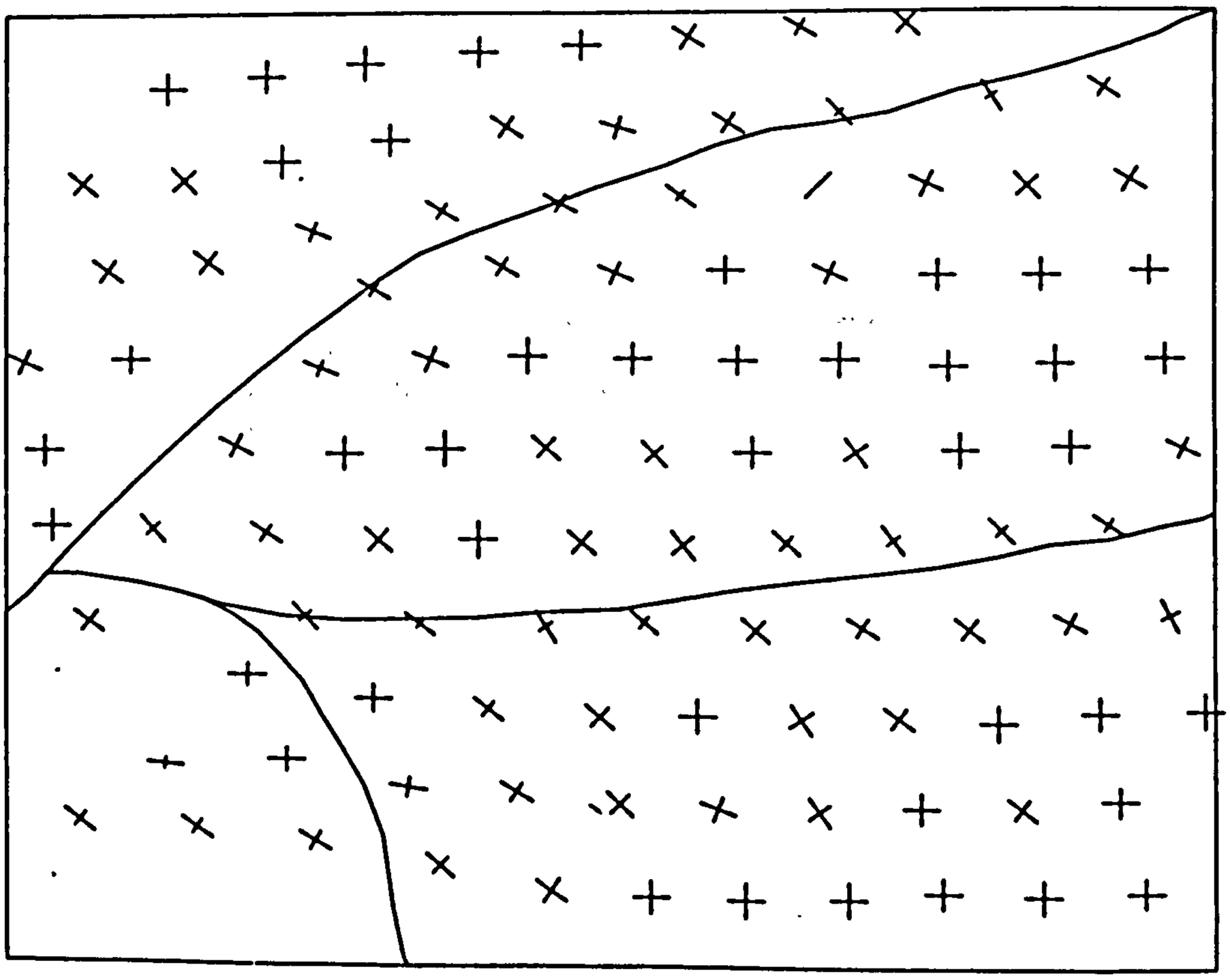


Figure 3.44 Rigid body rotation and shear strain components of the deformation superimposed on a schematic outline of the micrograph in Fig.3.43b.

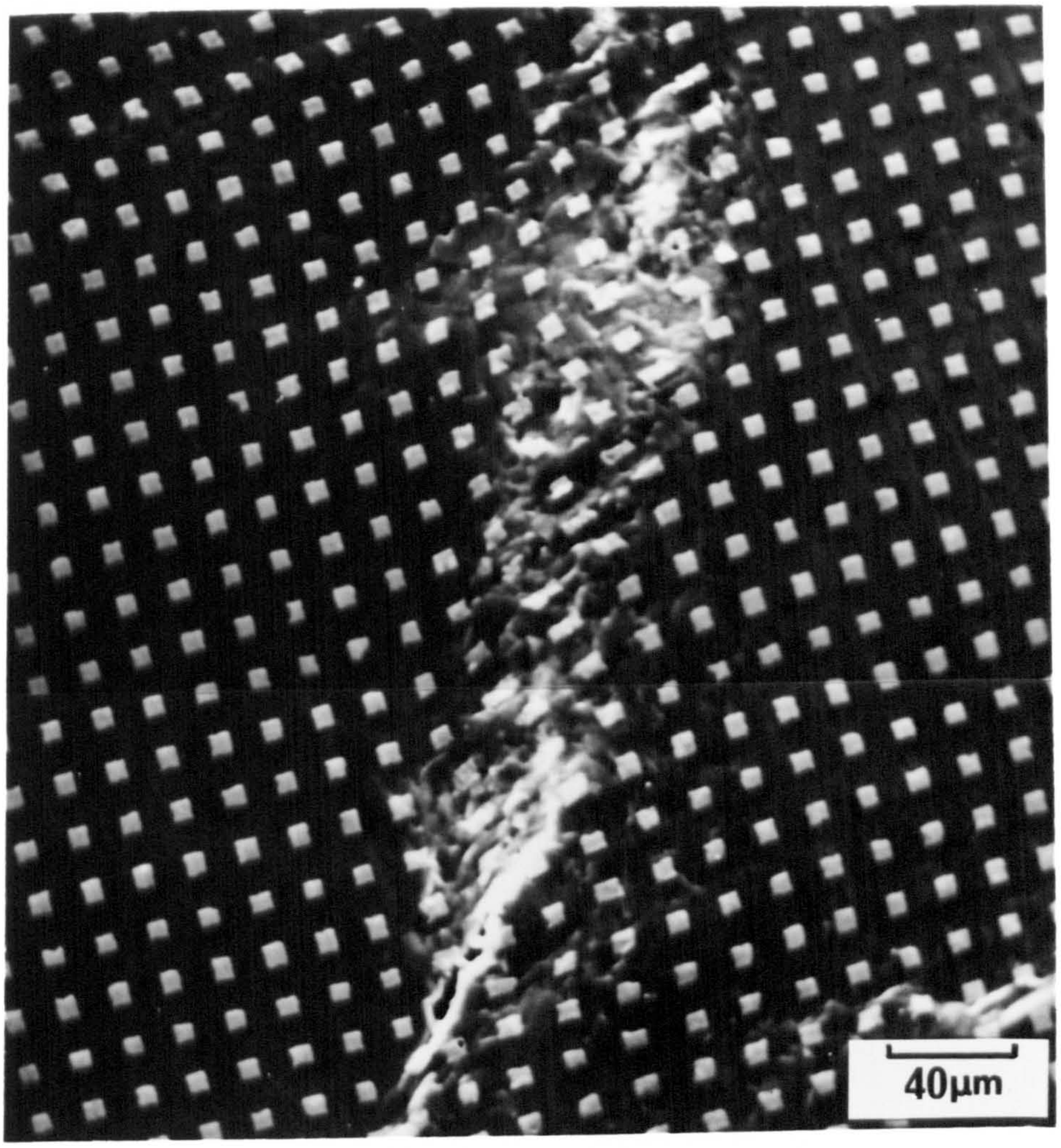
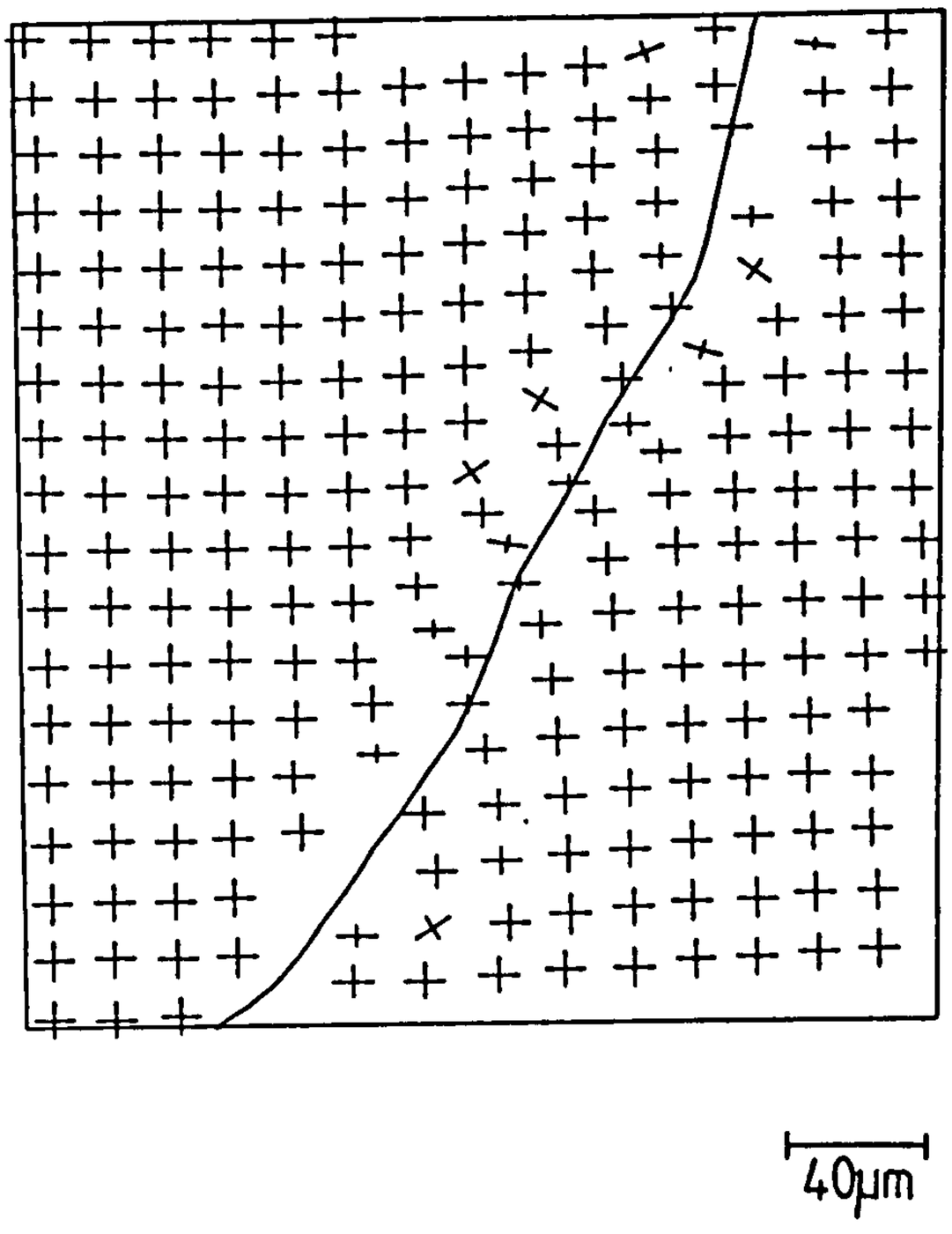


Figure 3.45. Grain boundary in a specimen deformed 15% at 260°C after a gold grid had been deposited on its surface. It can be seen that there was virtually no deformation in the grain centres: all the deformation had been accommodated in a zone adjacent to the grain boundary. The deformation is quantified in Fig. 46.



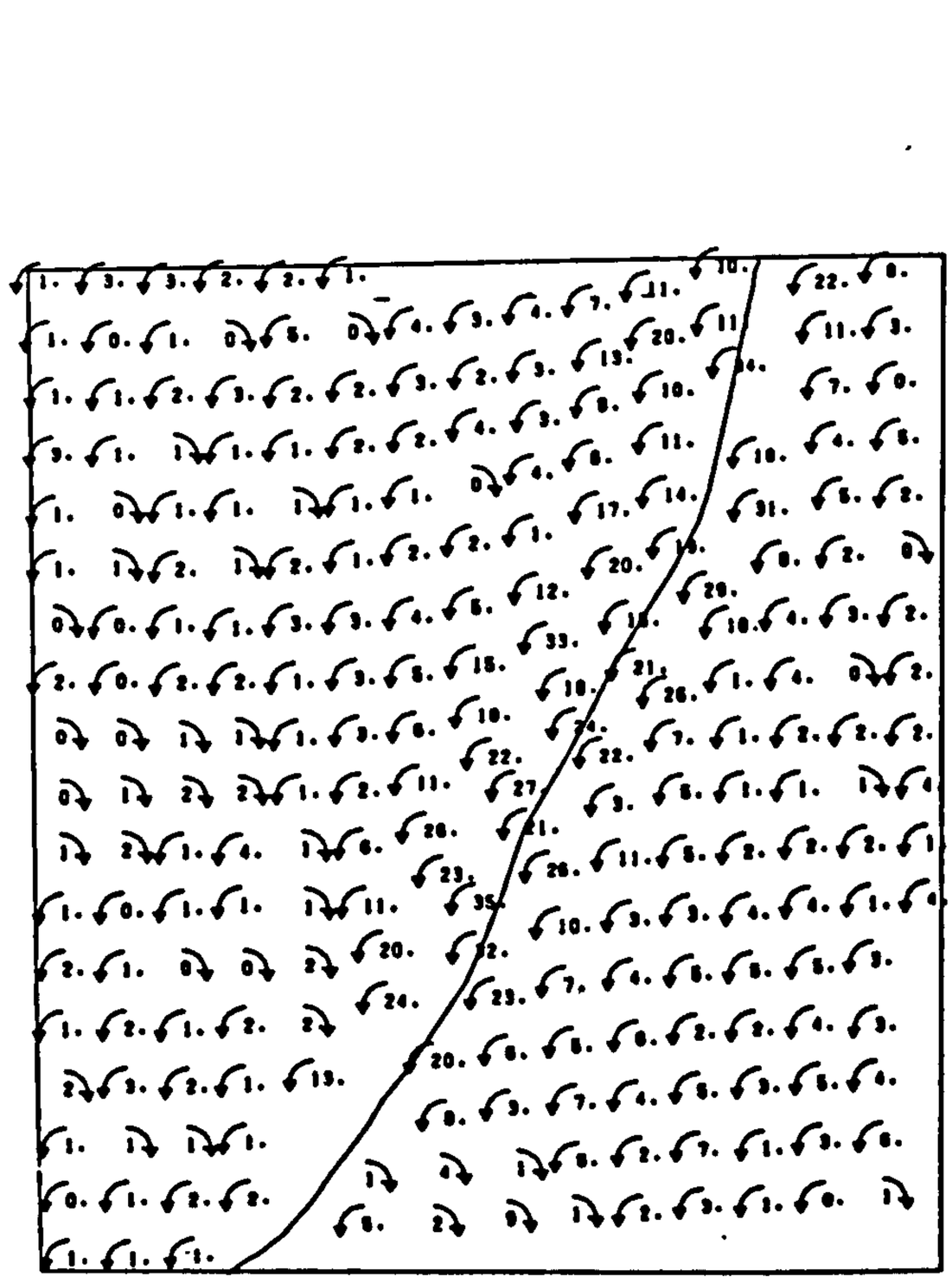


Figure 3.46 Quantified deformation behaviour in the region of the grain boundary in Fig. 3.45.

boundary is well illustrated. The crosses in the upper diagram represent the shear strain component of the deformation the axes of the strain elipsoid being represented by the cross bars. The compression axis ran from top to bottom. The diagram shows that there has been little strain accommodated in the grain centres (apart from a macroscopic bending of the grid as a whole) and that severe straining has occurred at the grain boundaries. The arrows in the lower diagram represent the rigid body rotation and show that large rotations have occurred in regions of high strain. These results agree with the observations made in the optical and E.M. studies.

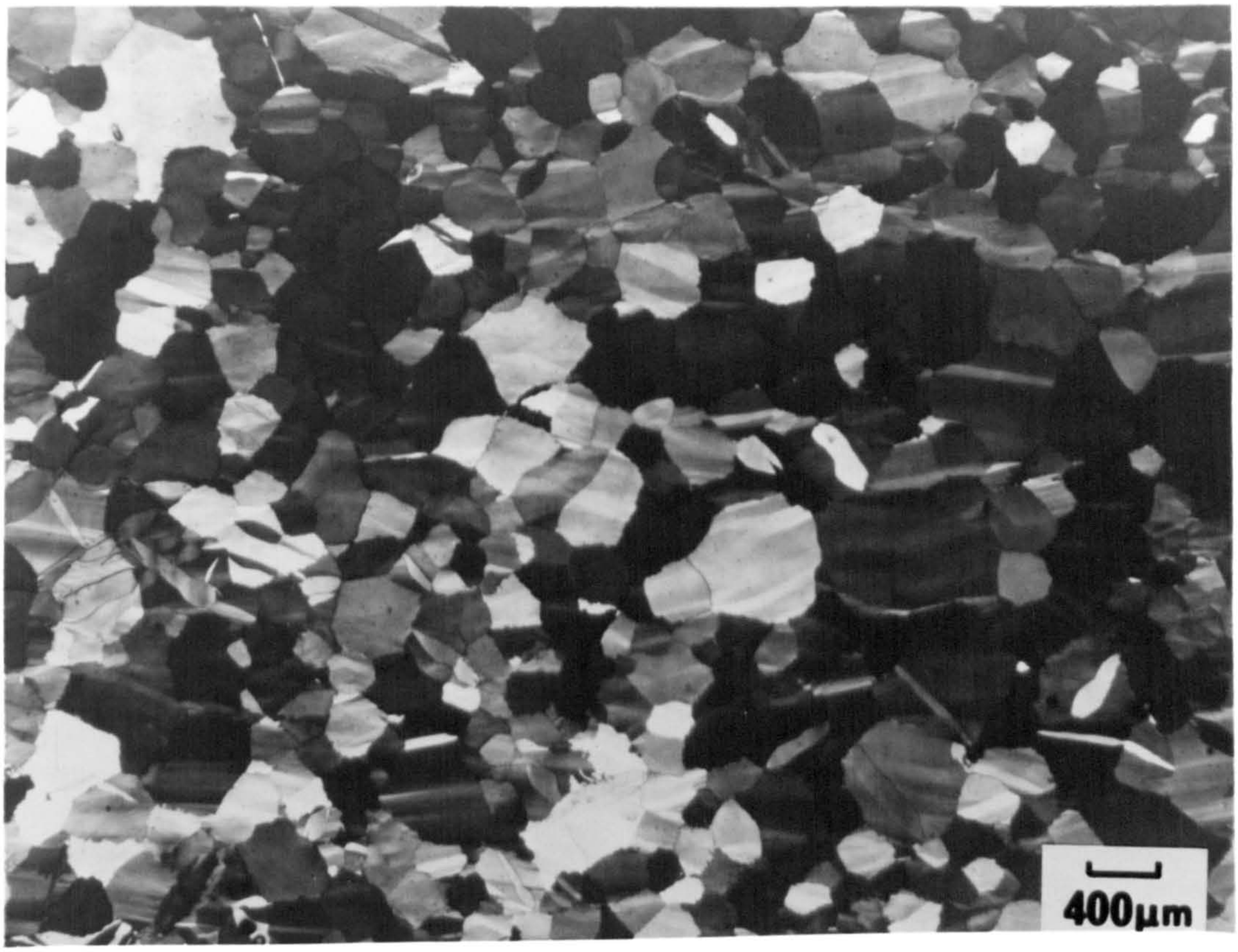
3.3.2.4. Microstructural development at high temperatures

3.3.2.4.1. General observations at $370^{o}C$

At high temperatures the deformation was much more homogeneous. This was a result of the greater degree of recovery and the role of slip on systems other than the basal system in the accommodation of the overall strain. Grain boundary bulging was marked at early strains Figure 3.47, and the bulges were much larger than those in similarly strained samples at lower temperatures, c.f. Figure 3.20.

The fine strain features present at lower temperatures were not observed at $370^{o}C$ and there was no evidence for the Core and Mantle behaviour reported at lower temperatures. E.M. studies of foils from a specimen deformed 25% at $370^{o}C$ showed that the substructure was homogeneous and consisted mainly of well developed equiaxed sub-grains. The subgrains were larger than those formed at $150^{o}C$ and $260^{o}C$ and had an average size of 25μm. The average subgrain sizes at 150 and $260^{o}C$ were 4μm and 8μm respectively. The dislocation density was lower at high temperatures and tended to be in the form of networks and sub-boundaries. The dislocations analysed had $\vec{a}$ and $\overrightarrow{c + a}$ burgers vector (see appendix).

Deformation bands were common at these higher temperatures, Figure 3.48. They occurred within the old grains and using the optical colour technique it was possible to determine the differences in basal plane orientation between them. A typical example of this is shown in Figure 3.49. Angular misorientations as high as 28^{o} have been recorded across individual bands and as is the case in Figure 3.49 the misorientation alternates from band to band. In contrast to the behaviour at lower temperatures the old grains became elongated perpendicular to the compression axis after deformation; the recrystallised



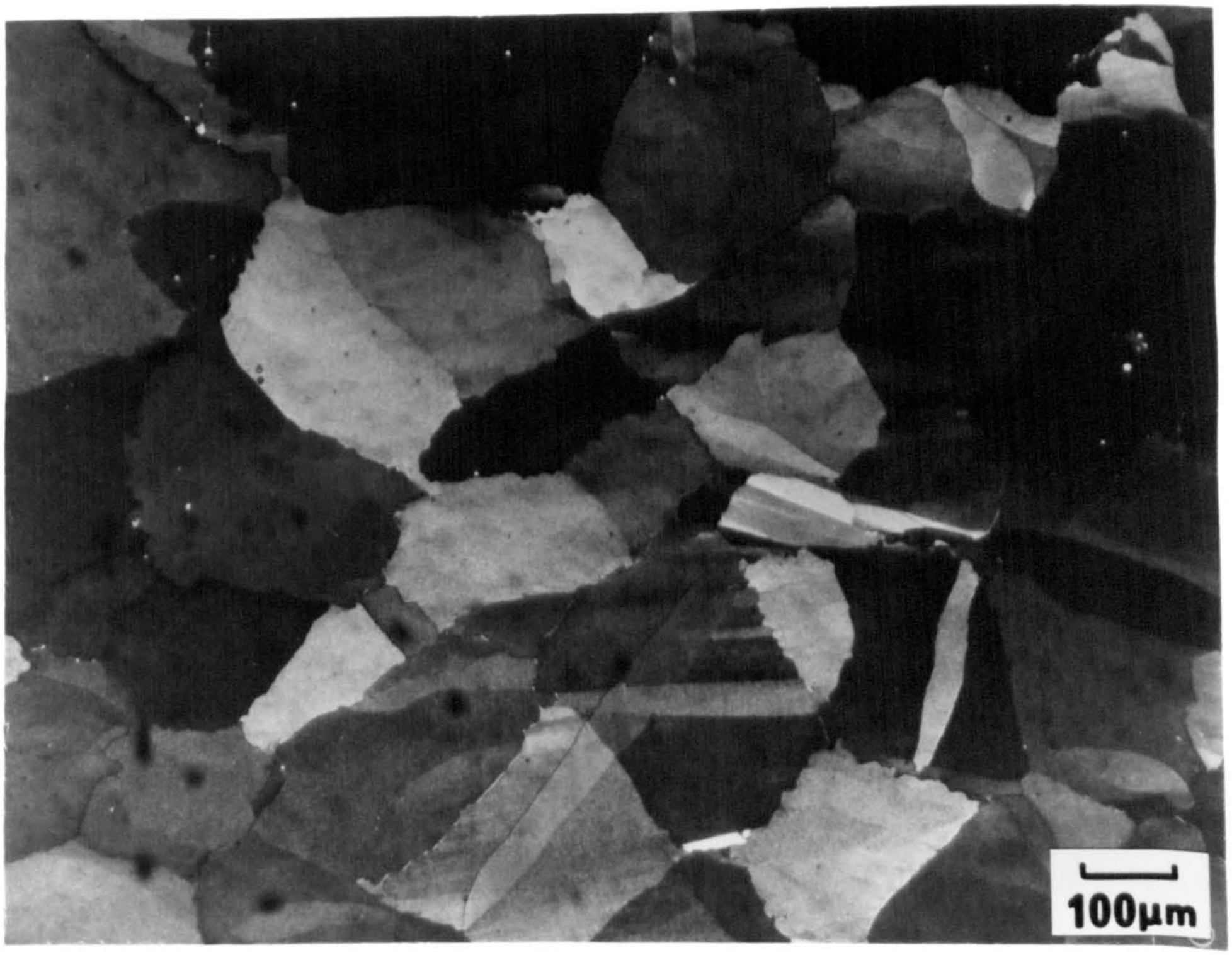


Figure 3.47. This sample was deformed 1.5% at 370°C $\dot{\varepsilon} \sim 10^{-5} s^{-1}$



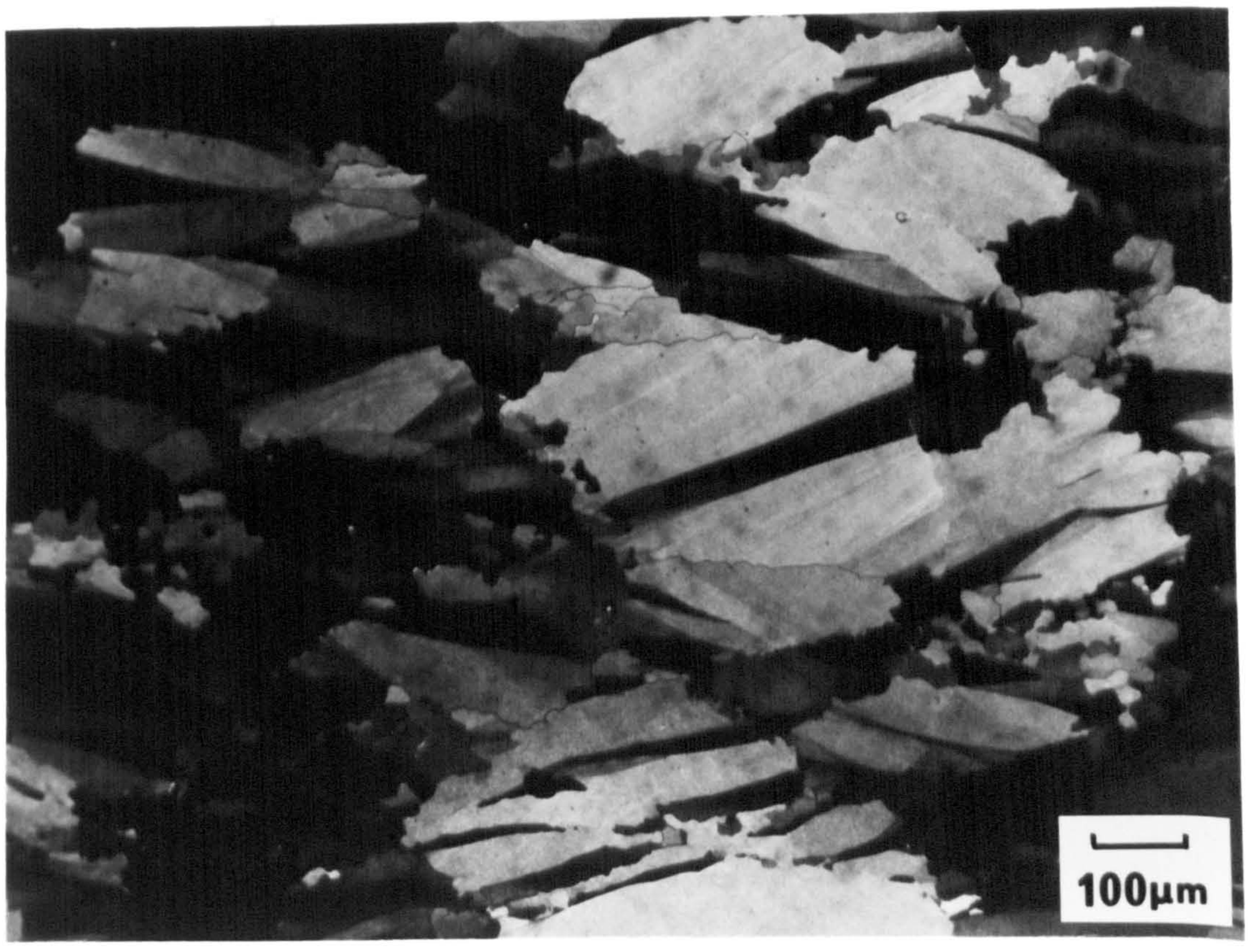
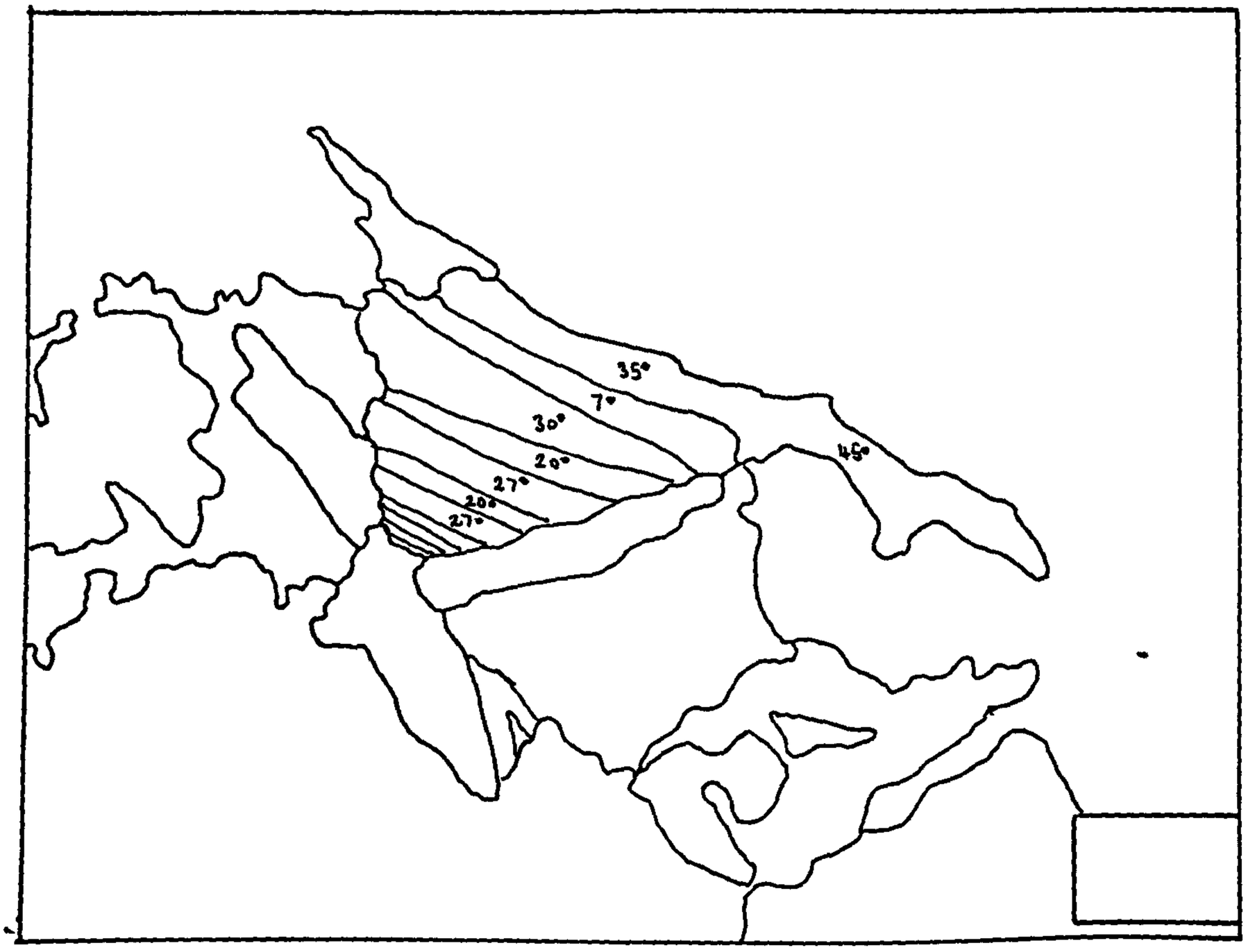


Figure 3.48. Sample deformed to 25% strain at 370^{o}C. Grain boundary bulging and migration was very marked and deformation bands were common within the old grains at this strain. The recrystallised grains appeared to have formed from the bulges in the old grain boundaries.


35°
7°
30°
20°
27°
20°
27°
45°

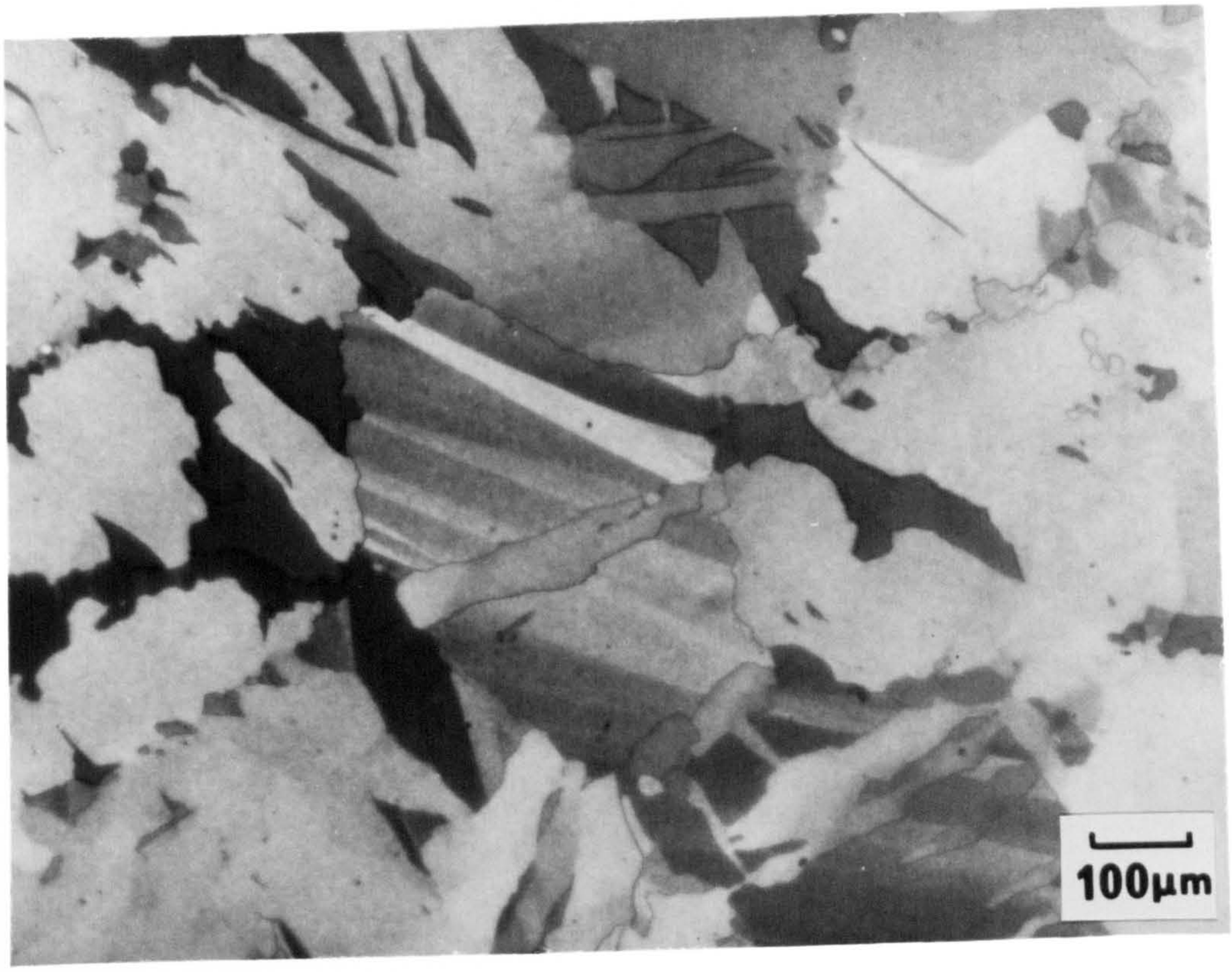


Figure 3.49. Determination of the basal trace direction within the deformation bands in a specimen deformed 25% at 370°C. The misorientation across individual boundaries can be seen to be as high as 28°.

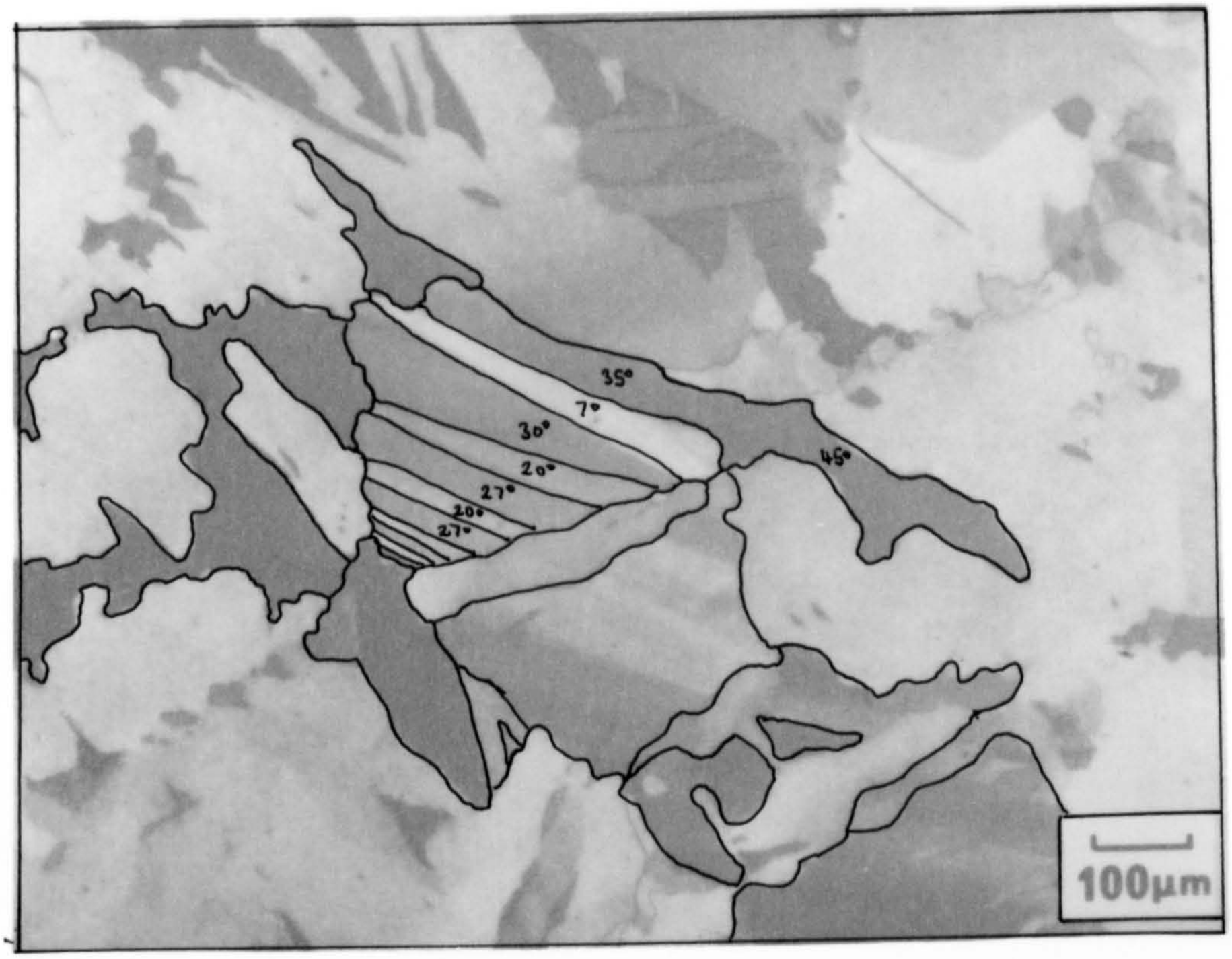


Figure 3.49. Determination of the basal trace direction within the deformation bands in a specimen deformed 25% at 370°C. The misorientation across individual boundaries can be seen to be as high as 28°.

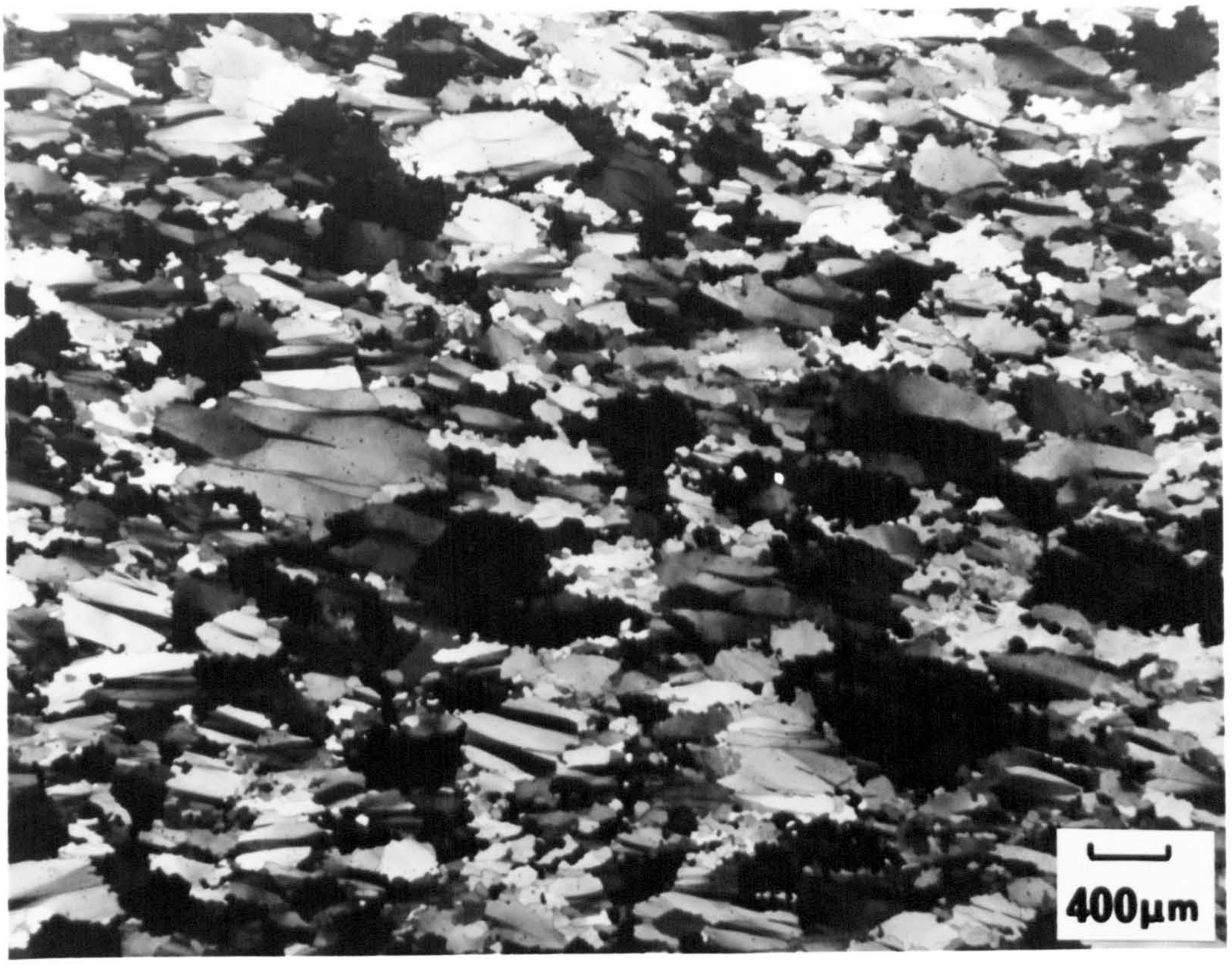
grains were also elongated (Figure 3.50). They appeared to form from the bulges which were common in the grain boundaries. Bulging and migration of grain boundaries were also evident in the recrystallised grains.

3.3.2.4.2. The observation of deformed polished surfaces to investigate the homogeneity of deformation at 370°C

These studies confirmed that the deformation was relatively homogeneous. In agreement with the low temperature behaviour no shear offsets of either grid or scratches could be detected at grain boundaries. However in contrast with the low temperature behaviour the grids showed shortening even in the centres of the grains and the rotations at grain boundaries were much smaller (Figure 3.51a). This was confirmed by comparing the grid after deformation with a standard as before (Figure 3.51b). The area examined revealed that the only major distortion had occurred in the vicinity of the triple point and even then the maximum rotation was 21°. The grid squares showed almost uniform shortening across a grain as determined from the ratios of the bars of the crosses which represent the axes of the strain elipsoid. This shortening which was 9·7% concurred with the bulk shortening of the sample of 10%.

3.3.2.5. Effect of strain rate on microstructural development

A series of specimens was deformed at different strain rates at 260°C to determine the effect of strain rate on microstructure. In the range 10^{-5}-$10^{-1}s^{-1}$ the microstructures were very similar. The specimens deformed at the faster rates 1.5 and 3×10^{-2} exhibited a different type of twinning. In addition to the recrystallised grains at the grain boundaries which were also common at the lower strain rates, recrystallised grains could also be seen in the fine twins which were present in many grains, Figure 3.52. Optical analysis of these twins showed that they were not of the $(10\bar{1}2)$ type (Figure 3.53). The twins were inclined at $58^{\circ} \pm 5^{\circ}$ to the basal plane. It was thought that they occurred as a result of the operation of the $\{10\bar{1}1\}\{10\bar{1}2\}$ double twinning mechanism (see section 1.2.2.1) The $\{10\bar{1}1\}$ bands were consistently recrystallesed and the wide spread of orientations within them made it difficult to obtain an accurate value of the basal plane reorientation when the twin first formed. Measurements on 10 twins with only slight differences in recrystallised orientations revealed a basal plane rotation of $\sim 38^{\circ} \pm 5^{\circ}$.



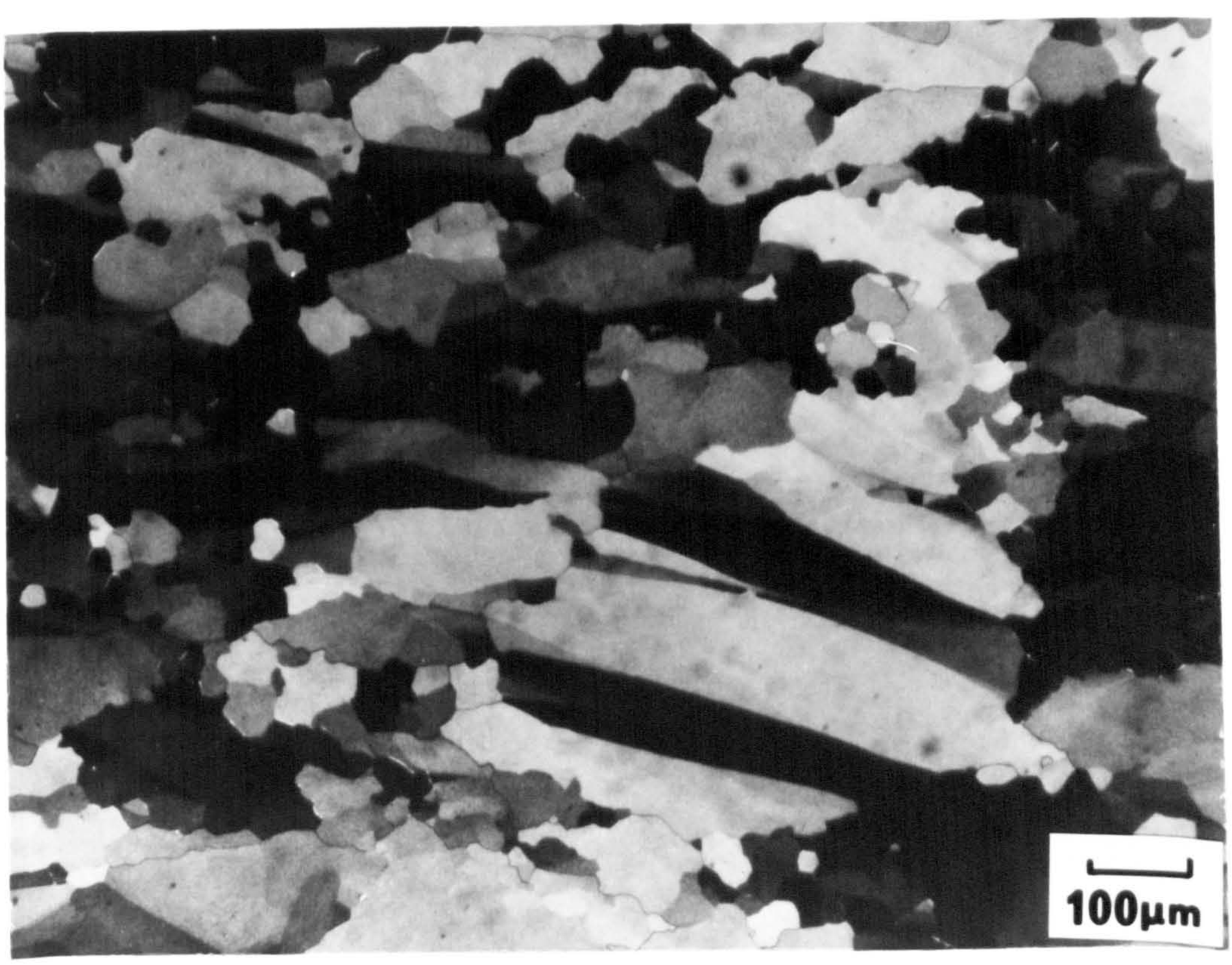
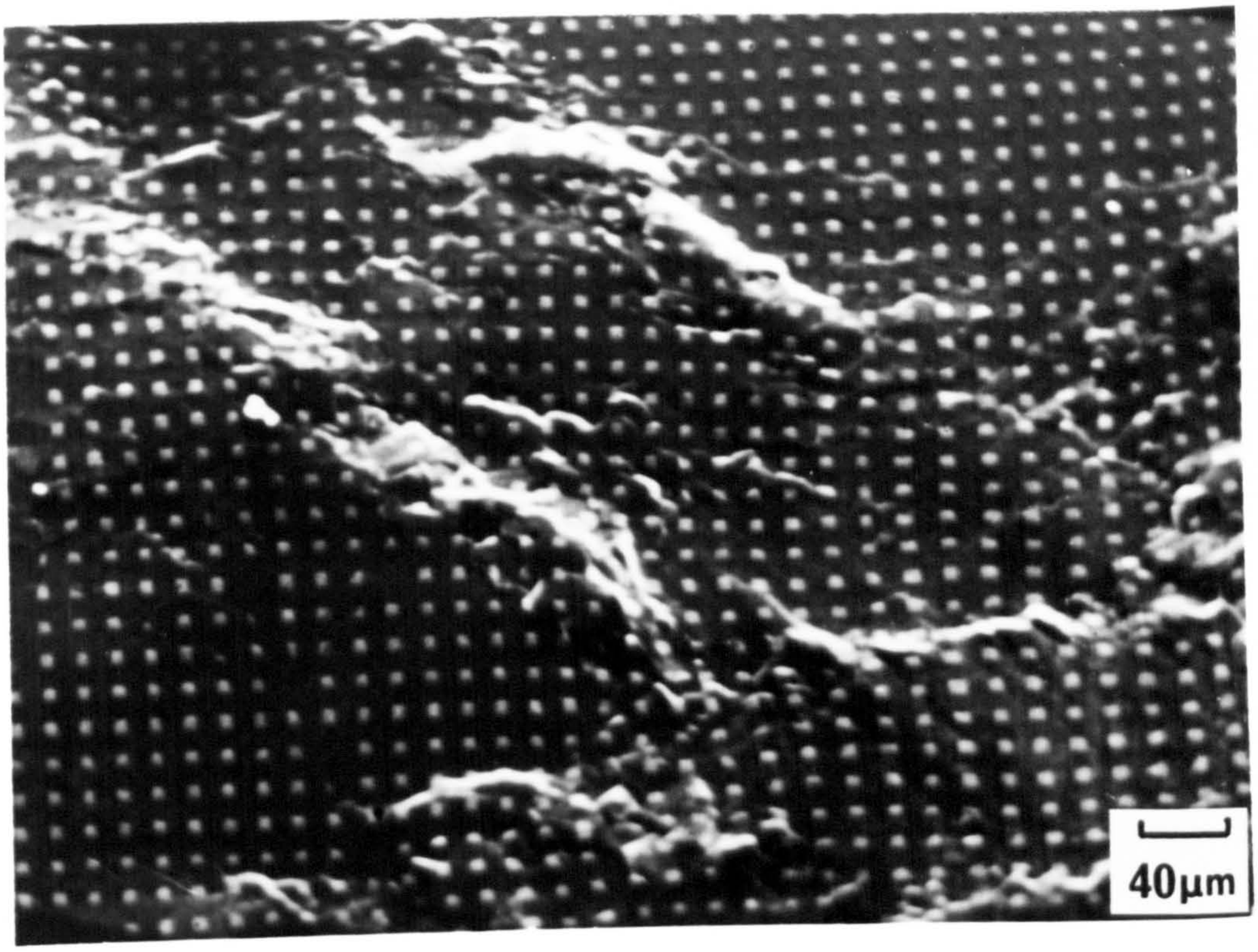
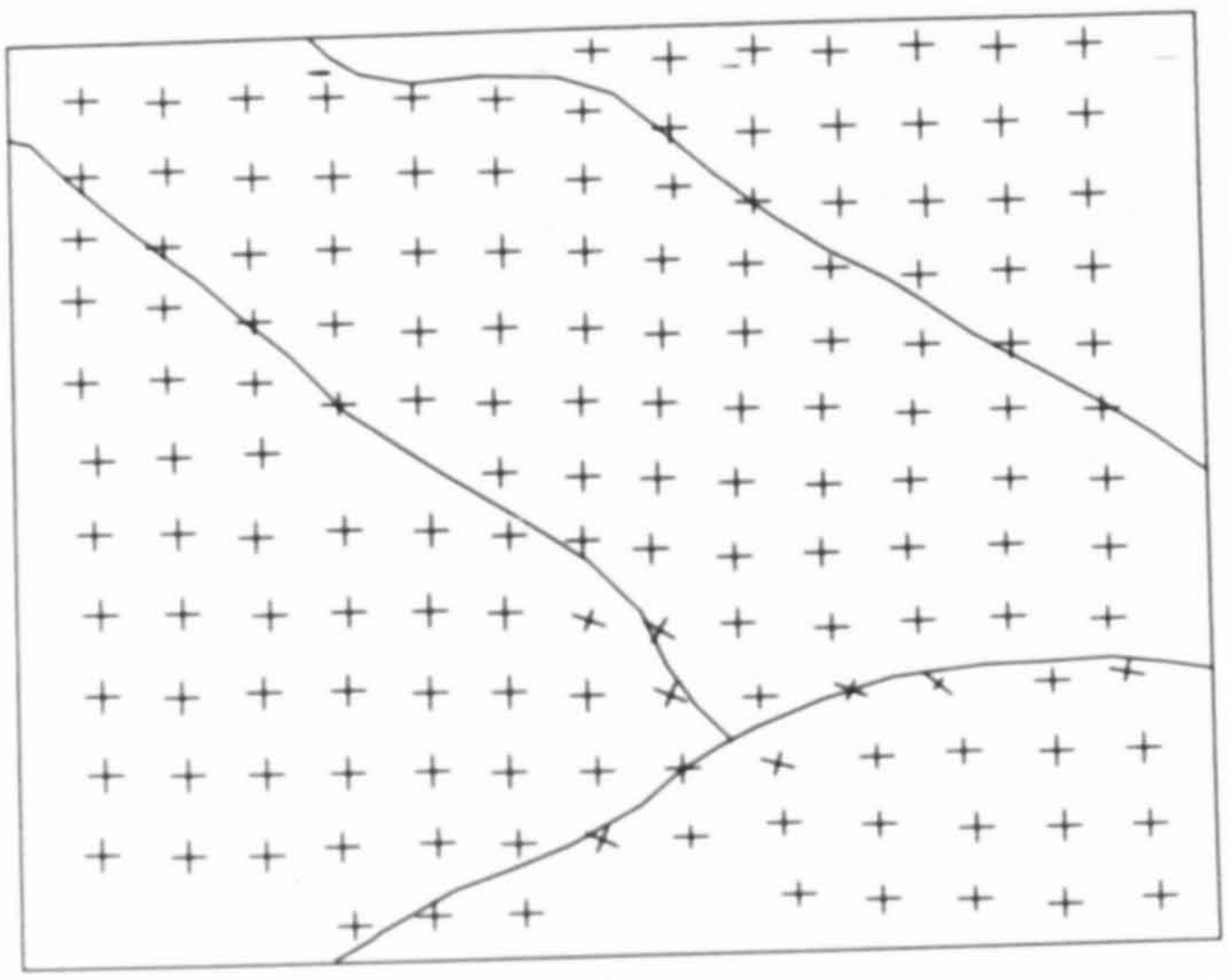
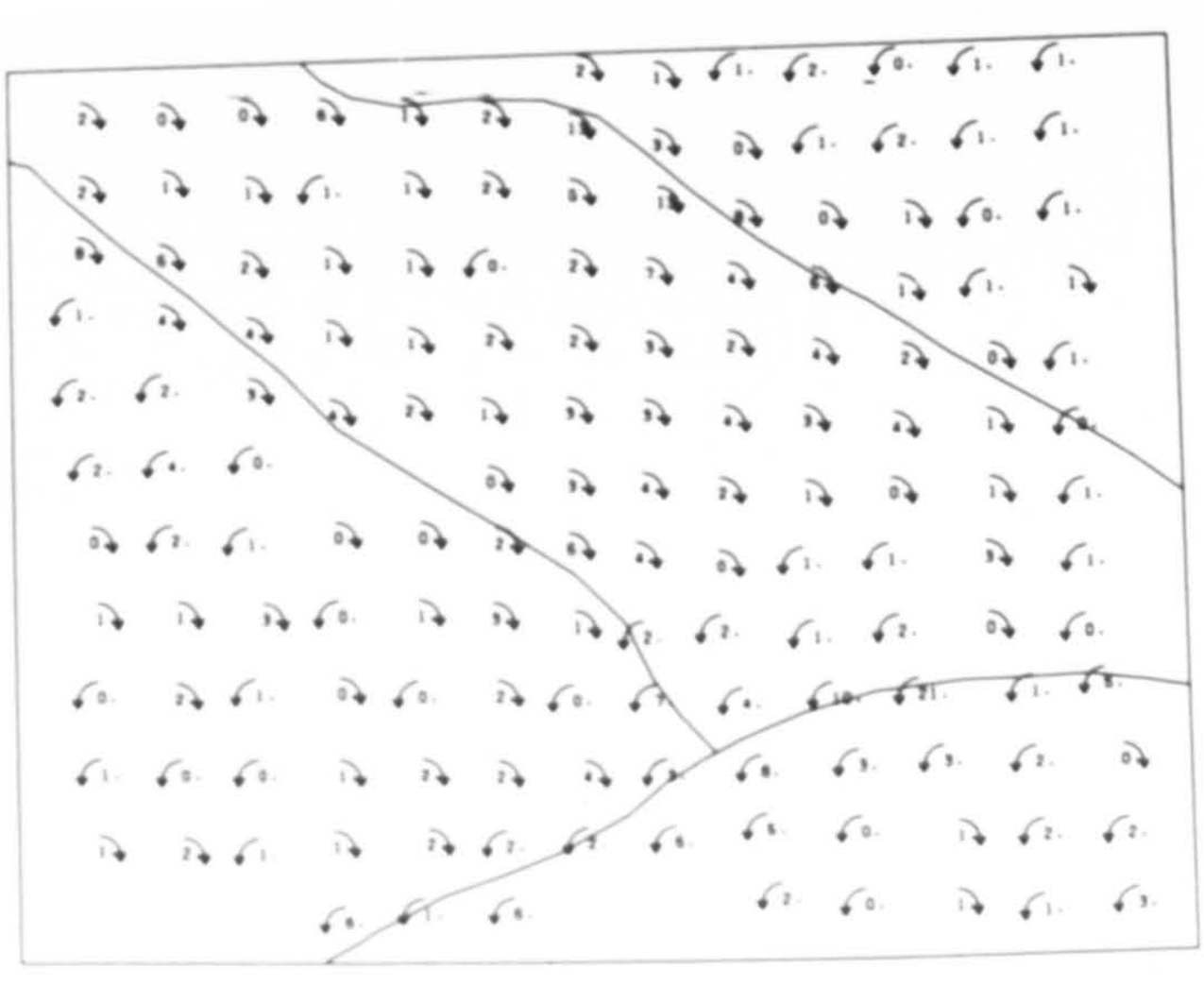


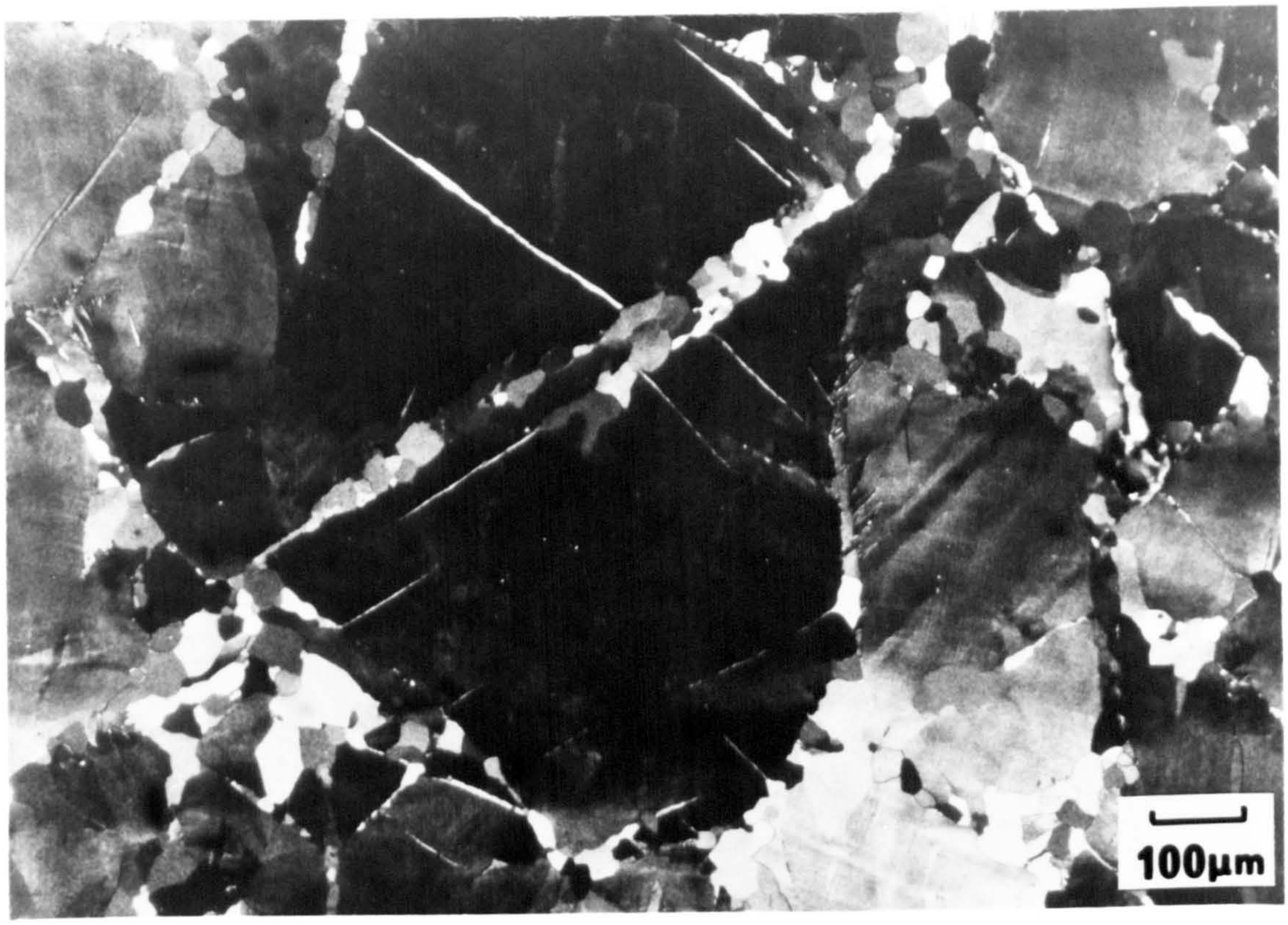
Figure 3.50. Sample deformed 55% at 370^{o}C. Extensive recrystallisation had occurred in this sample. The recrystallised grains appeared to form from bulges in the old grain boundaries and some of these 'new' grains showed bulging and migration.

Figure 3.51. Relative homogeneity of the deformation at 370°C. The grid squares show almost uniform shortening across a grain. The shear strain and rigid body rotation components of the deformation are illustrated in the two line diagrams.


40μm







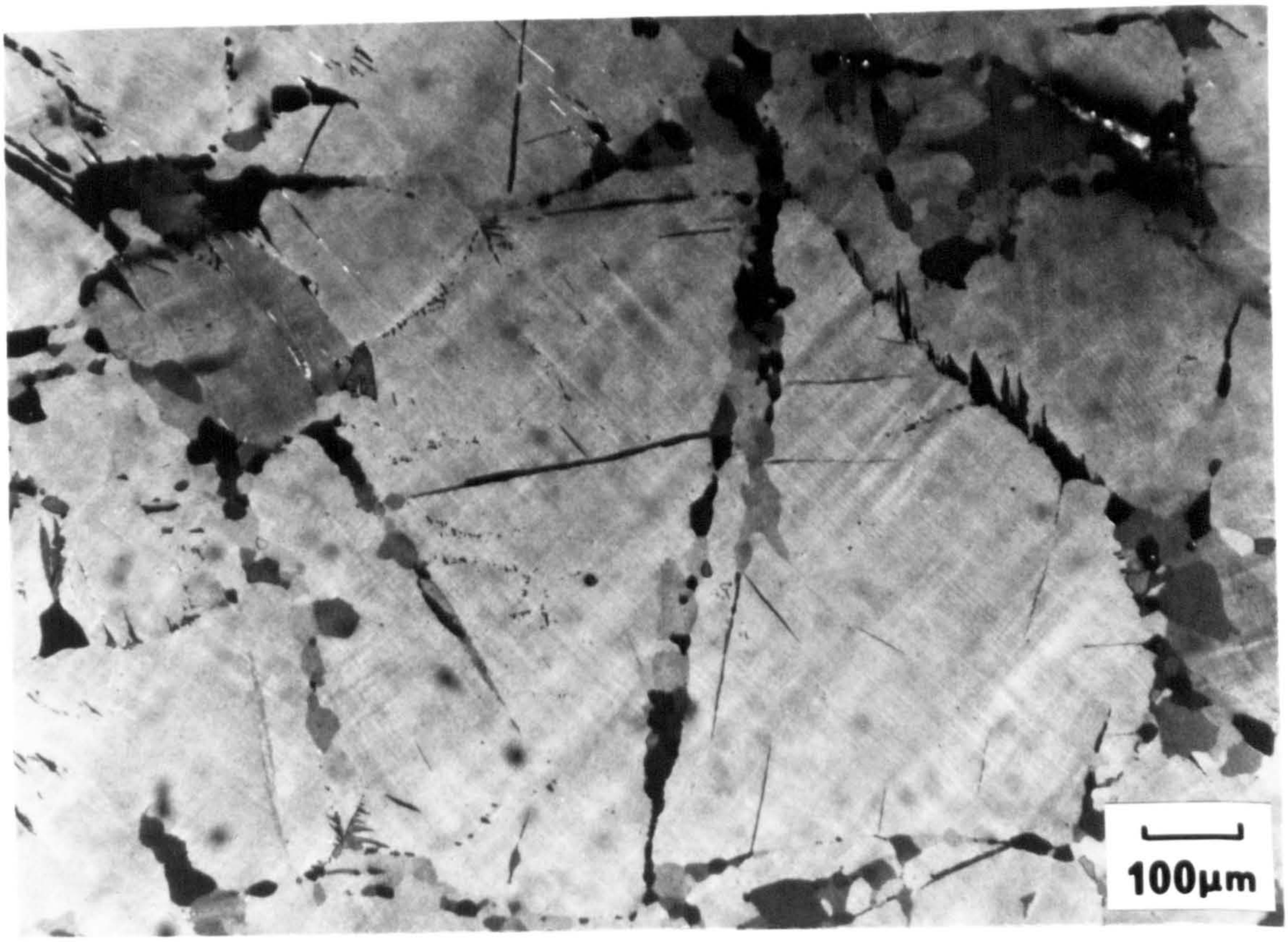


Figure 3.52. This specimen was deformed 35% at a crosshead speed of 0.2 cm min^{-1}, i.e. $\dot{\varepsilon} \sim 10^{-3}s^{-1}$. An example of the fine twins present throughout the sample can be seen in the centre grain. The lower micrograph, taken with the specimen rotated 45° on the microscope stage reveals the slip markings in the old grains.

Compression axis



Figure 3.53. The colour technique was used to determine the direction of the basal plane trace within the old grains and in the recrystallised grains. The rotation measured with respect to the compression axis is indicated on the overlay.

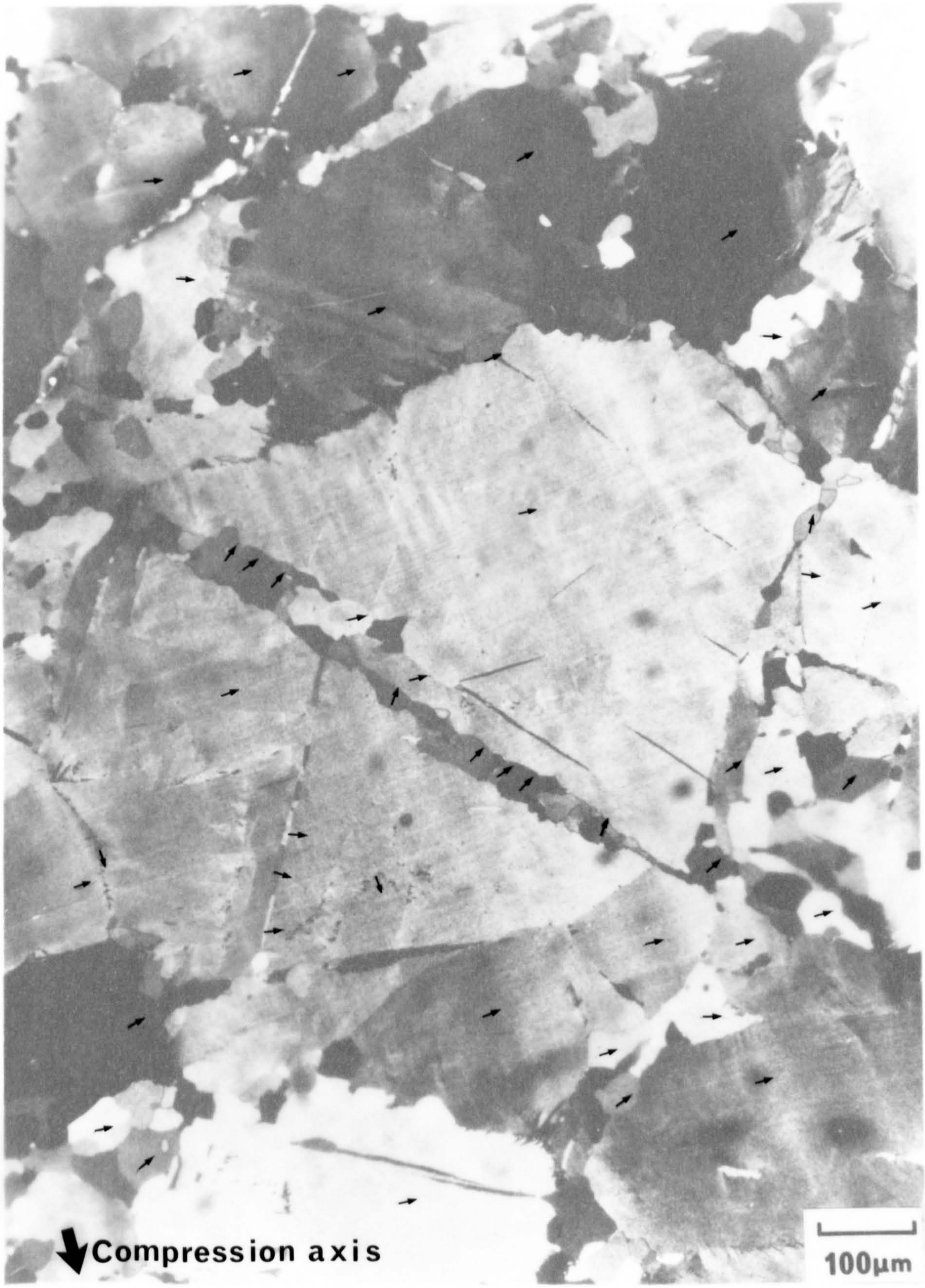


Figure 3.53. The colour technique was used to determine the direction of the basal plane trace within the old grains and in the recrystallised grains. The rotation measured with respect to the compression axis is indicated on the overlay.

3.4. DEVELOPMENT OF TEXTURE WITH INCREASING STRAIN IN SAMPLES UNFAVOURABLY ORIENTED FOR BASAL SLIP

3.4.1. Introduction

The X-ray goniometry revealed the changes in texture of the bulk samples as a function of strain. Instead of representing the data as conventional pole figures it was found useful for purposes of comparison to plot intensity profiles showing the normalised reflected X-ray intensity as a function of ϕ, the angle between the reflecting planes and the compression axis. Figure 3.54 shows both the profile and the pole figure obtained for reflections from the basal planes in the starting material. As expected, it shows that the preferred orientation is very strong, with the majority of basal planes lying within a few degrees of the specimen axis, i.e. the extrusion direction of the as supplied rod. The effect of strain on texture development will be reported for the temperatures 150°C, 260°C, 300°C and 370°C.

3.4.2. Textural development at 150°C

The texture at 22% strain showed that the basal planes had undergone a rotation of $\sim 90^{\circ}$ from their initial position and were aligned perpendicular to the compression axis, Figure 3.55. No intensity could be detected from basal planes in the original orientation.

3.4.3. Textural development at 260°C

In view of the fact that there was such a marked change in the orientation of the basal planes between 0 and 22% strain at 150°C it was decided to examine the texture development at lower strains in greater detail (Figure 3.56). It could be seen that at very early strains (1.5%) there was already evidence for basal planes rotated 90° from their original orientation. As strain increased so did the X-ray intensity of material in the new orientation. The basal plane orientations detected were either parallel or perpendicular to the compression direction the former decreasing at the expense of the latter as strain increased. This supported the view that $\{10\bar{1}2\}$ twinning which causes a basal plane reorientation of 86.3° was an active mechanism at low strains.

Beyond 12% strain the peak in the basal plane distribution became broader.

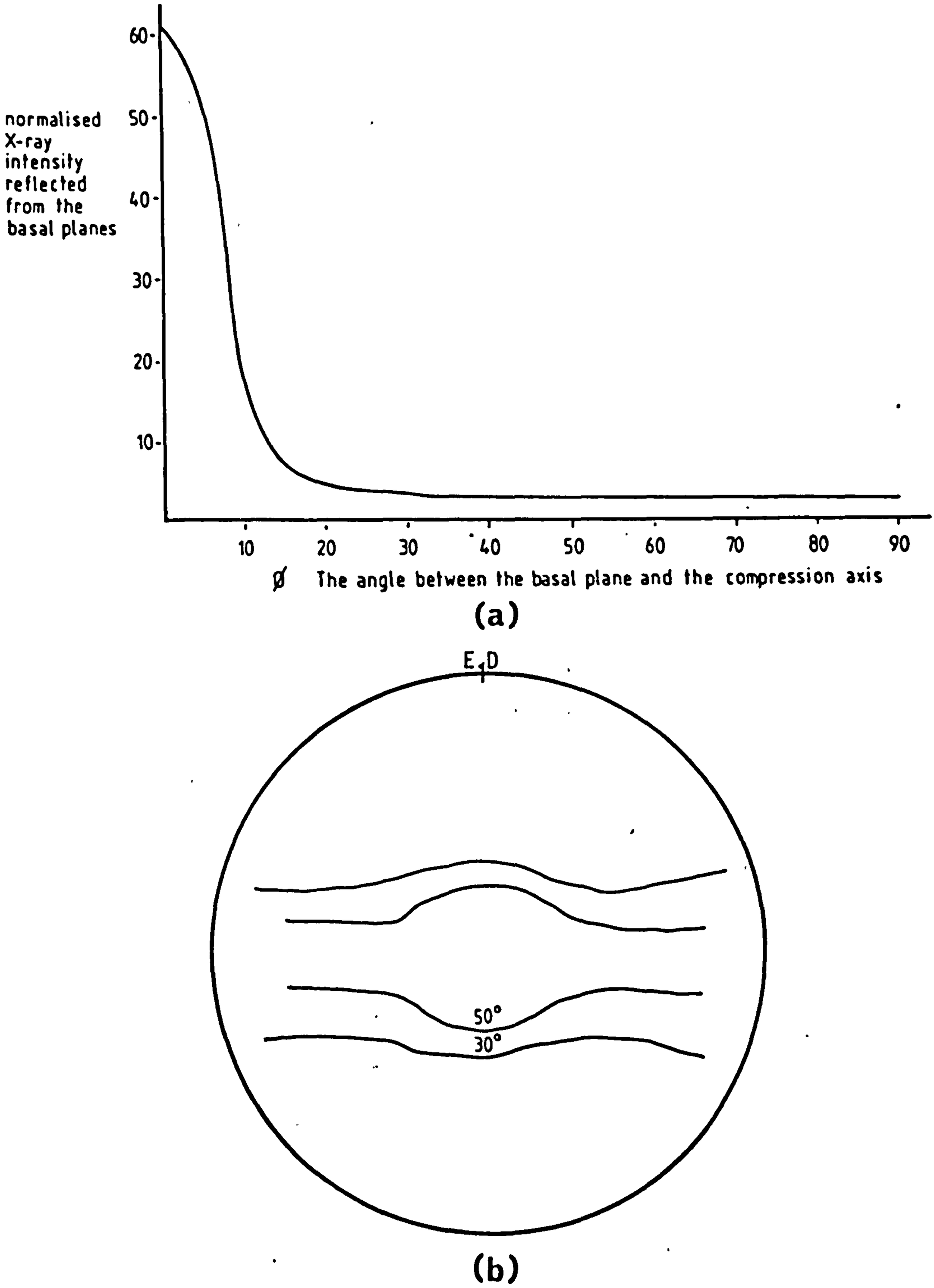


Figure 3.54. The basal plane profile and 0002 pole figure for the starting material.

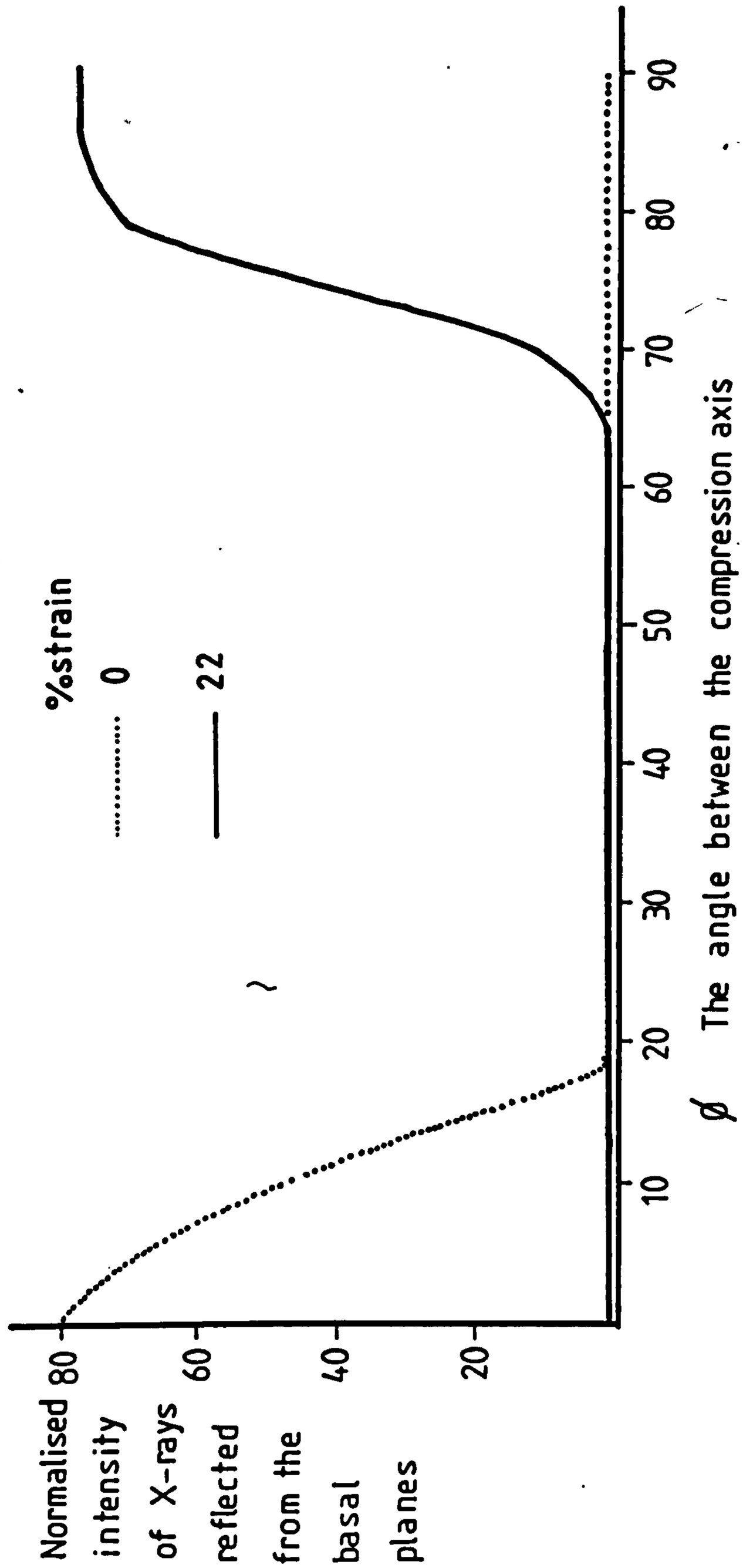


Figure 3.55. 150°C.

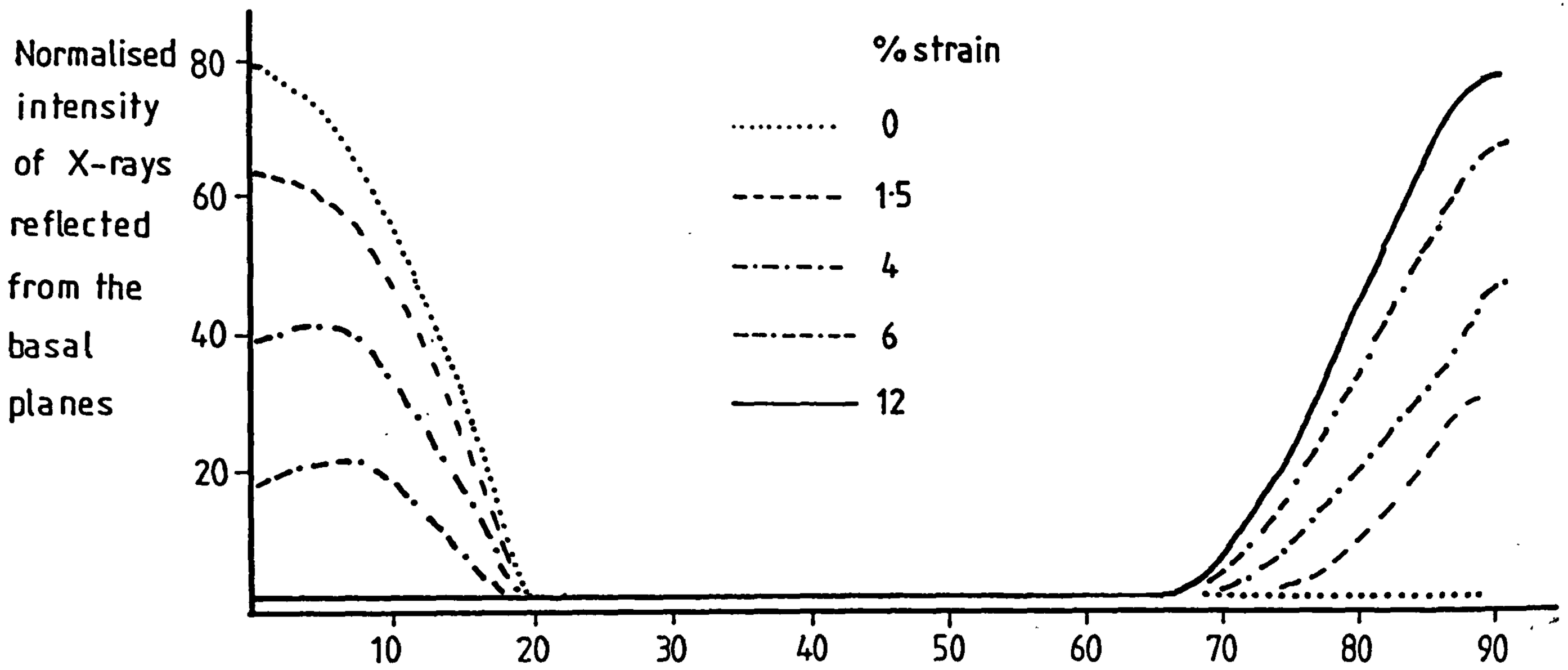


Figure 3.56. 260°C.

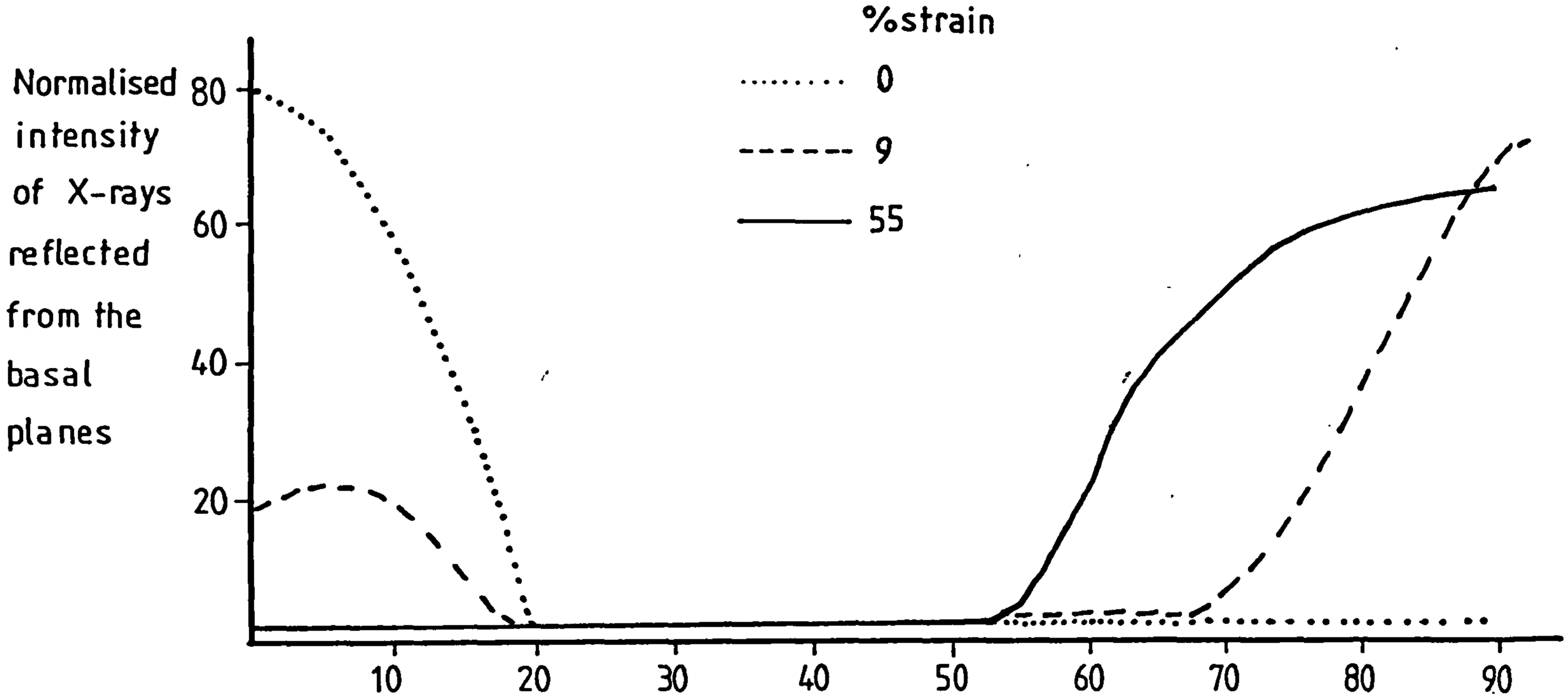


Figure 3.57. 300°C.

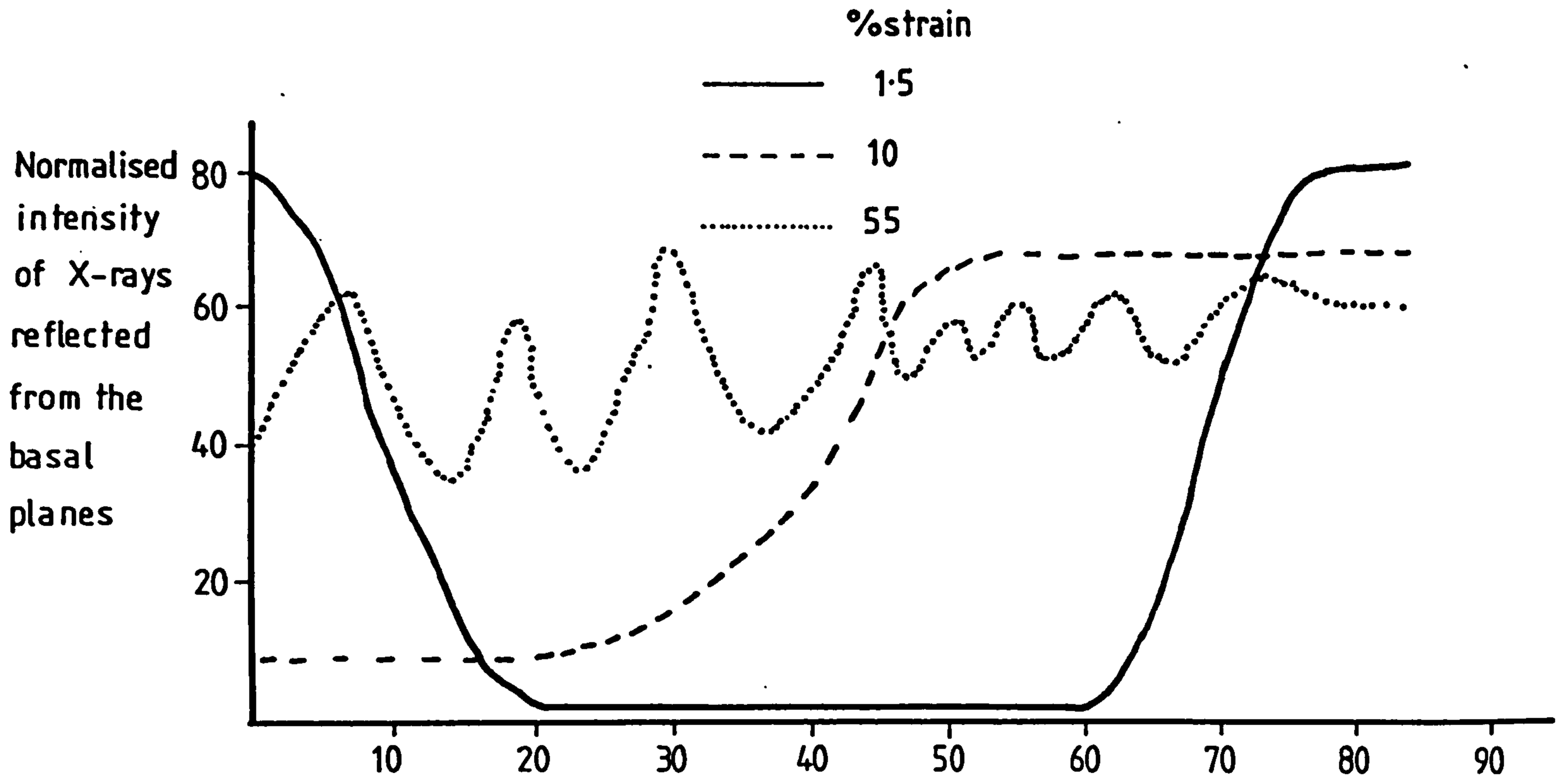


Figure 3.58. 370°C.

PAGE NUMBERING AS ORIGINAL

3.4.4. Textural development at 300°C

Similar results were recorded for specimens deformed at this temperature (Figure 3.57). By 9% strain there was very little of the sample left in the original orientation; the majority of grains were aligned with their basal planes perpendicular to the specimen axis (compression direction). By 20% strain there was no detectable intensity reflected from basal planes in the original orientation. Beyond this strain there were no marked changes in the intensity profile which merely became broader.

3.4.5. Textural development at 370°C

The distribution of basal planes from samples deformed at 370°C was much more diffuse (Figure 3.58). At low strains (1.5% ε) two peaks - parallel and perpendicular to the compression direction - could be detected cf low temperatures but in this case they were much broader. The distribution became more diffuse with increasing strain until at 55% strain a preferred orientation was barely discernible.

3.5. SUMMARY OF MICROSTRUCTURAL AND TEXTURAL DEVELOPMENT IN SAMPLES UNFAVOURABLY ORIENTED FOR BASAL SLIP

A summary of the results of experiments on material unfavourably oriented for basal slip is presented below in the form of a table to enable comparisons to be made between the different temperatures.

	150°C	260°C	370°C
S/S curve	sharp peak	less sharp peak	broad peak
Peak stress MPa at $\dot{\varepsilon}$ - $10^{-5}s^{-1}$	12.75	9.0	2.2
Strain at peak stress	17%	16%	6%
Old grains			
slip lines	very prominent	prominent	none detected
fine periodicity	very prominent	prominent	none detected
deformation bands	none detected	none detected	present
$\{10\bar{1}1\}\{10\bar{1}2\}$ twins	present	present at $\dot{\varepsilon}>10^{-3}s^{-1}$	none detected
$\{10\bar{1}2\}$ twins	common	common	rare
mantle width	10μ	50μ	no detectable difference between core and mantle
Final texture	very strong	strong	weak
boundary migration	rare	marked	very marked

	150°C	260°C	370°C
shear zone	narrow	becoming broader	No shear zones
voids	present	present	none detected
average recrystallised grain size just beyond peak in s/s curve	10μ	20μ	60μ
average subgrain size core	4μ	8μ	)25μ
mantle	3μ	6μ	)
homogeneity of deformation	very hetero-geneous	hetero-geneous	relatively homogeneous

3.6. MICROSTRUCTURAL DEVELOPMENT WITH INCREASING STRAIN AT 260°C IN MATERIAL FAVOURABLY ORIENTED FOR BASAL SLIP

The stress strain curve shows a longer period of work hardening to a higher value of strain than the specimens previously mentioned, and the peak in the curve is not as marked. This is presumably because the preferred orientation is such that many of the grains are initially favourably oriented for basal slip which is the means whereby the deformation is preferably accommodated. The specimens examined in the optical microscope had undergone 5%, 10%, 30% and 70% strain.

At 5% ε slip lines could be detected in the old grains, Figure 3.59 (arrowed). These lines were the traces of the basal planes as determined using the colour technique. The light coloured grains in the micrograph were favourably oriented for basal slip. It is noticeable that twinning had occurred in the less favourably oriented darker grains.

At 10% strain (Figure 3.60) twinning was more prolific and the slip lines were more pronounced (arrowed). The grain boundaries exhibited bulging and migration. Periodicity could also be detected perpendicular to the basal plane. This is also arrowed on the micrograph. The spacing between these less regular lines corresponded to the bulge size. By 30% strain (Figure 3.61) the old grains were noticeably elongated perpendicular to the compression direction and recrystallisation had occurred at some of the old grain boundaries, particularly where there was evidence of heterogeneous strain. Bulging was more extensive in this sample (arrowed).

At 70% strain the macroscopic deformation had become heterogeneous (Figure 3.62). The deformation was concentrated in a zone at 45° to



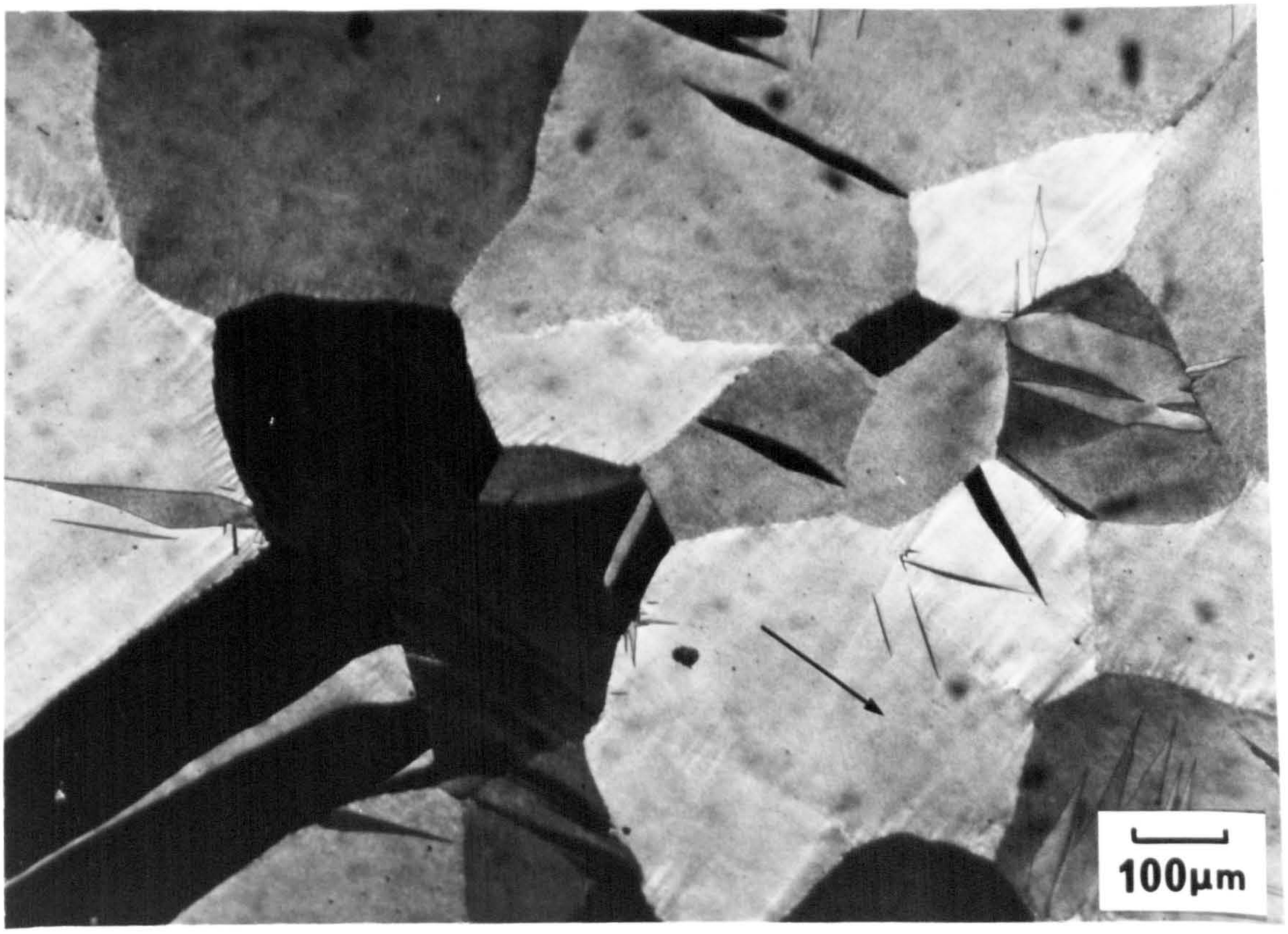


Figure 3.59. The polarised light microscopy revealed that most grains were favourably oriented for basal slip (light in colour), and consequently twinning was much less prolific at this strain than in material unfavourably oriented for slip. The traces of the basal planes can be seen in many grains (arrowed) as can more pronounced periodicity perpendicular to these traces.





Figure 3.60. The slip lines were more pronounced in this specimen (single arrow) and a small amount of grain boundary migration could be detected. Periodicity could also be detected perpendicular to the slip lines (double arrow). Twins were present in some grains.



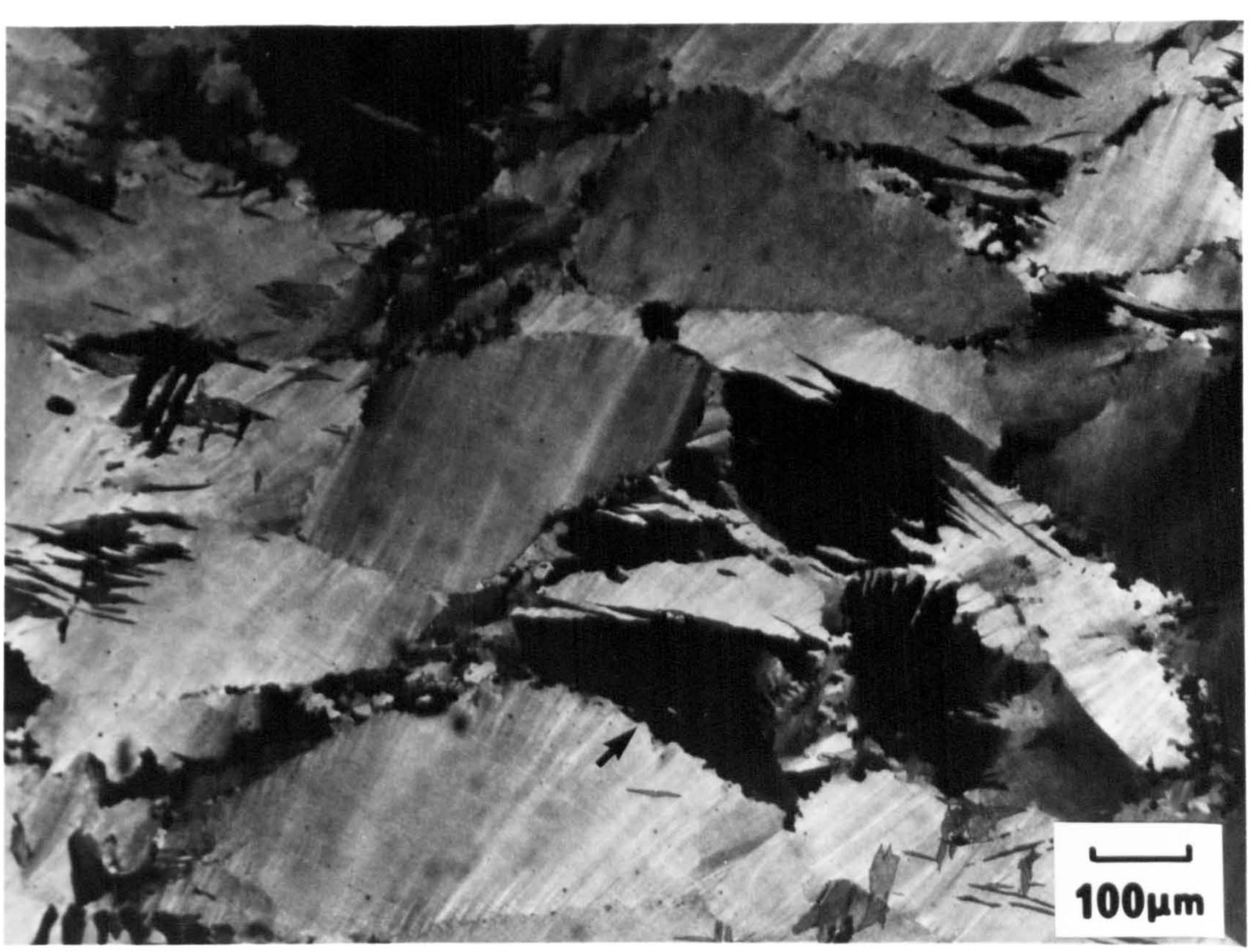


Figure 3.61. Grain boundary bulging was more marked in this sample. The wavelength of the bulges seemed to be related to the periodicity perpendicular to the basal slip trace. This feature is arrowed in the lower micrograph.



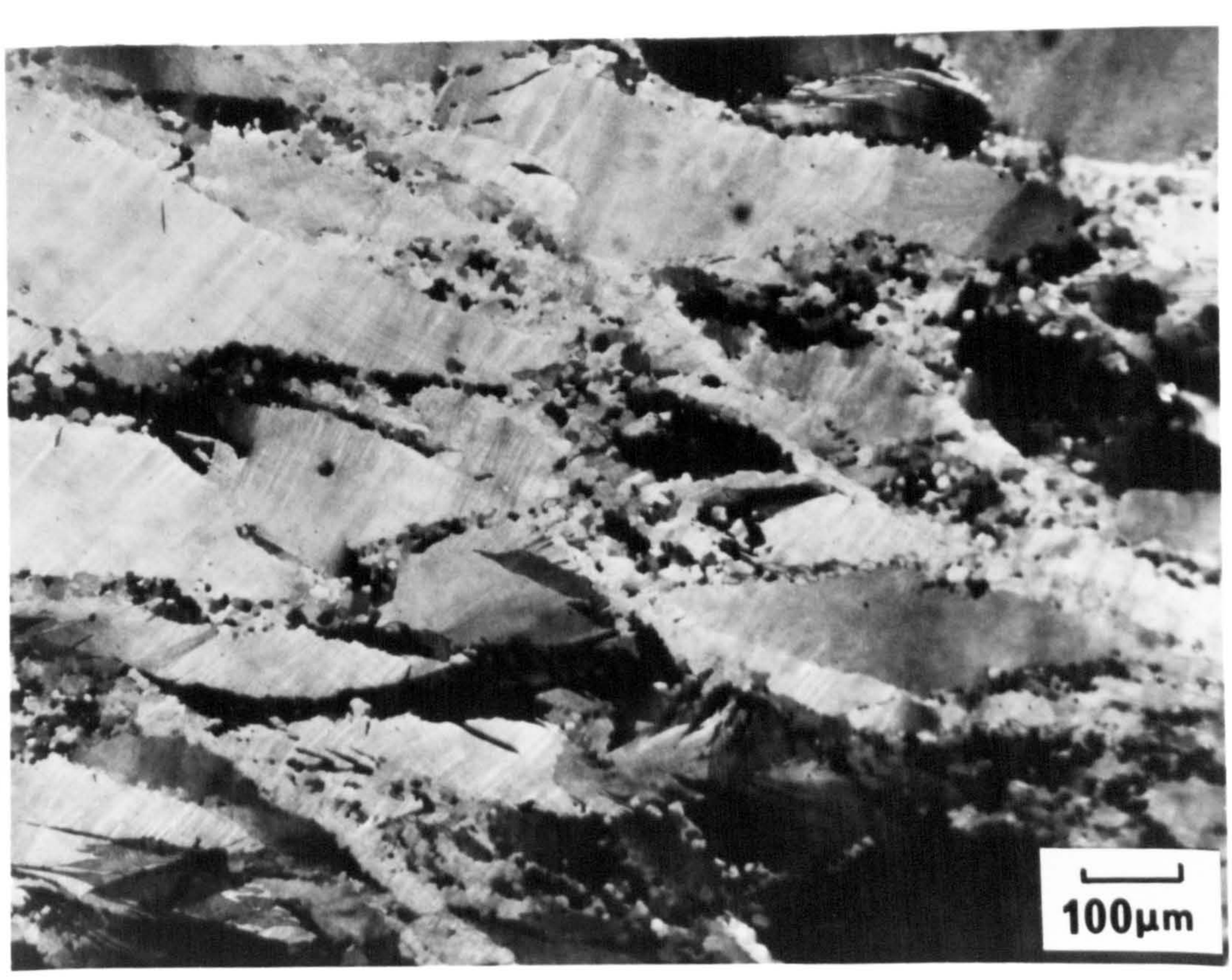


Figure 3.62. Specimen deformed 70% at 260°C. The deformation was more heterogeneous in this sample and there was a zone of higher strain at 45° to the compression direction: this is indicated by the markers on the upper micrograph.

the compression axis. This is indicated on the micrograph. The old grains in this region were elongated parallel to the zone, i.e. parallel to the basal slip planes. There was a higher density of recrystallised grains particularly in the region exhibiting a higher strain.

3.7. SHEAR ZONES IN MAGNESIUM

3.7.1. Introduction

The microstructural studies carried out on the samples deformed at temperatures below 320°C in an orientation unfavourable for basal slip showed that once the peak in the stress strain curve had been passed then the deformation became very heterogeneous on a bulk scale. A macroscopic view of a sample deformed 94% at 260°C is shown in Figure 3.63. It can be seen that the strain is heterogeneous being greater within a shear zone which occupies approximately 50% of the sample volume. The volume of recrystallised grains was much higher in the shear zone. In the samples deformed in the orientation favourable for basal slip the deformation did not become macroscopically heterogeneous until much higher strains had been attained.

X-ray goniometry, optical microscopy and electron microscopy have been utilized to undertake a detailed investigation into the micro-structure of shear zones. The results presented in the following paragraphs were derived mainly from specimens unfavourably oriented for basal slip deformed at 260°C. Some data is presented in the final paragraph to show the effect of temperature on the microstructure in shear zones.

3.7.2. Study of shear zones at 260°C

3.7.2.1. Stress strain behaviour

Figure 3.64 shows two stress-strain curves. Curve A represents the behaviour of a sample which contained a well-developed shear zone. Marked softening occurred once the peak in the stress strain curve had been reached, i.e. once the shear zone had been initiated. Curve B represents the behaviour of a sample deformed at the same temperature and strain rate, but which did not develop a shear zone. The peak in the stress strain curve occurred at a higher strain and the value of the stress at the peak was also higher. The softening which occurred beyond the peak was not as marked as for curve A.

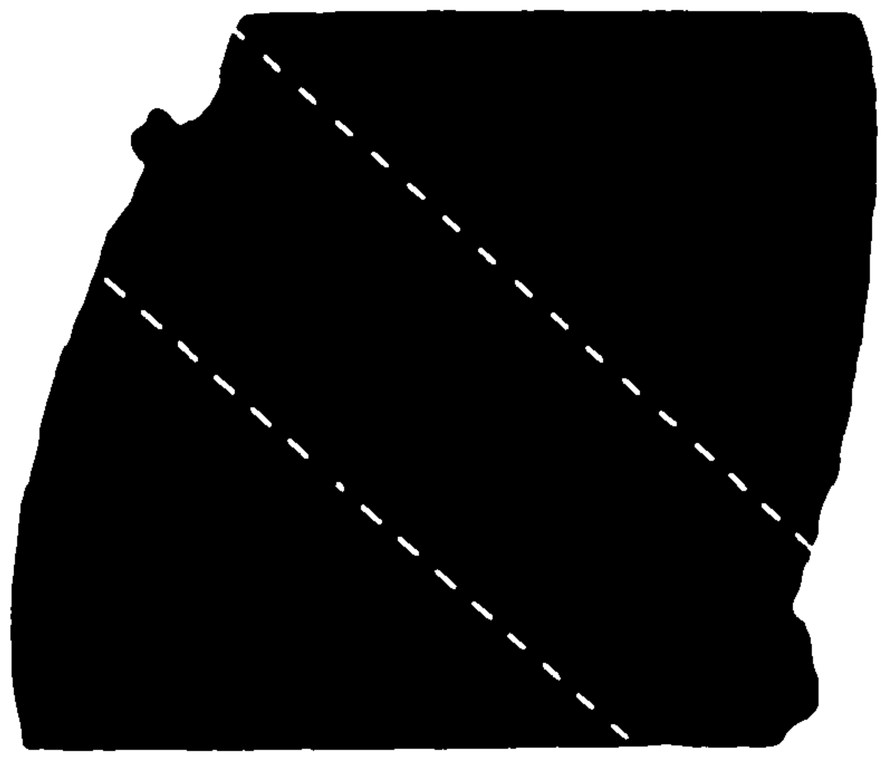


Figure 3.63. Crossection of a specimen containing a shear zone at 260°C.

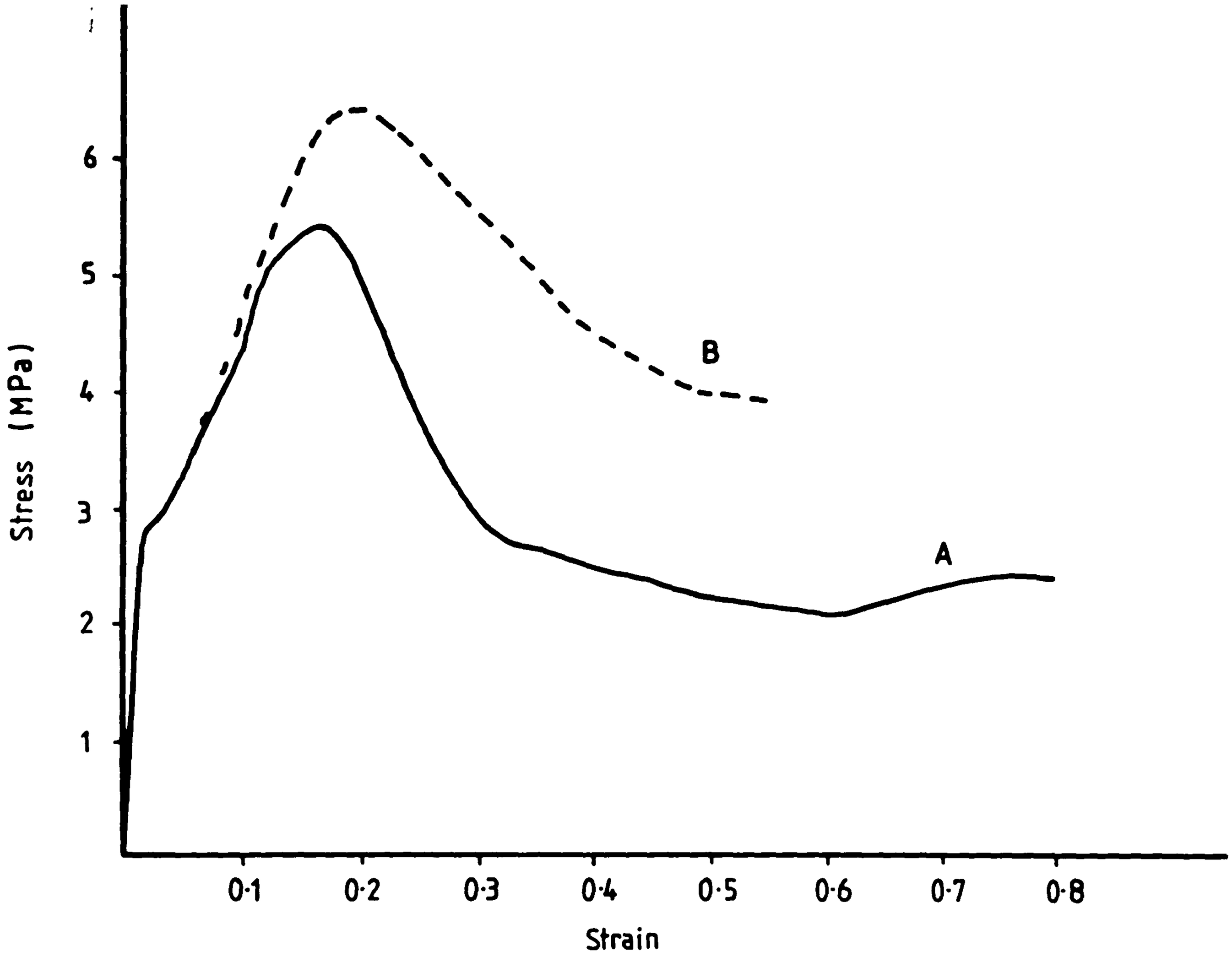


Figure 3.64. Effect of shear zone formation on stress strain behaviour at 260^{o}C.

3.7.2.2. X-ray goniometry

The texture work carried out on the sample exhibiting the shear zone revealed a fairly large spread in basal plane distribution, Figure 3.65. Optical microscopy of the sample as a whole had shown that basal planes of the grains within the shear zone tended to lie parallel to the direction of the zone rather than perpendicular or parallel to the compression axis. Two samples were taken from the specimen for further X-ray goniometry: one from the centre of the shear zone and one from part of the specimen away from the shear zone. The results showed that the overall texture was due to two components - one from the shear zone and the second from the lesser deformed regions away from the zone. These are shown as dotted lines in Figure 3.65: together the two components account for the diffuse nature of the distribution as a whole.

3.7.2.3. Optical microscopy

The way in which data is collected on a standard X-ray goniometer prevents the examination of specific areas less than 2000μm in width i.e. over several grain diameters, so only a general impression of the texture could be obtained by this method. A close examination of the shear zone under the optical microscope revealed detail on a much finer scale, Figure 3.66. The zone consisted mainly of small recrystallised grains.

Two types of periodicity could be detected optically. Perpendicular to the shear zone there was a banding effect. The recrystallised grains had straight well aligned boundaries, the alignment being strongest perpendicular to the zone. Parallel to the zone there was also a regular variation in basal plane orientation. In the micrograph (Figure 3.66) this is manifested as a lightening and darkening of the shade of the recrystallised grains. Within the lighter bands (A) the orientation difference between the individual grains was one or two degrees in clusters of 4 or 5 grains. The misorientation between clusters was slightly higher being 7 or 8^{o}. This is shown schematically in Figure 3.67. These lighter bands had their basal planes aligned parallel with the shear zone edges at $52^{o} \pm 8^{o}$ to the compression axis. The darker regions (e.g. B and C) on the other hand had a greater orientation spread but the orientations lay within 20^{o} of the compression plane.

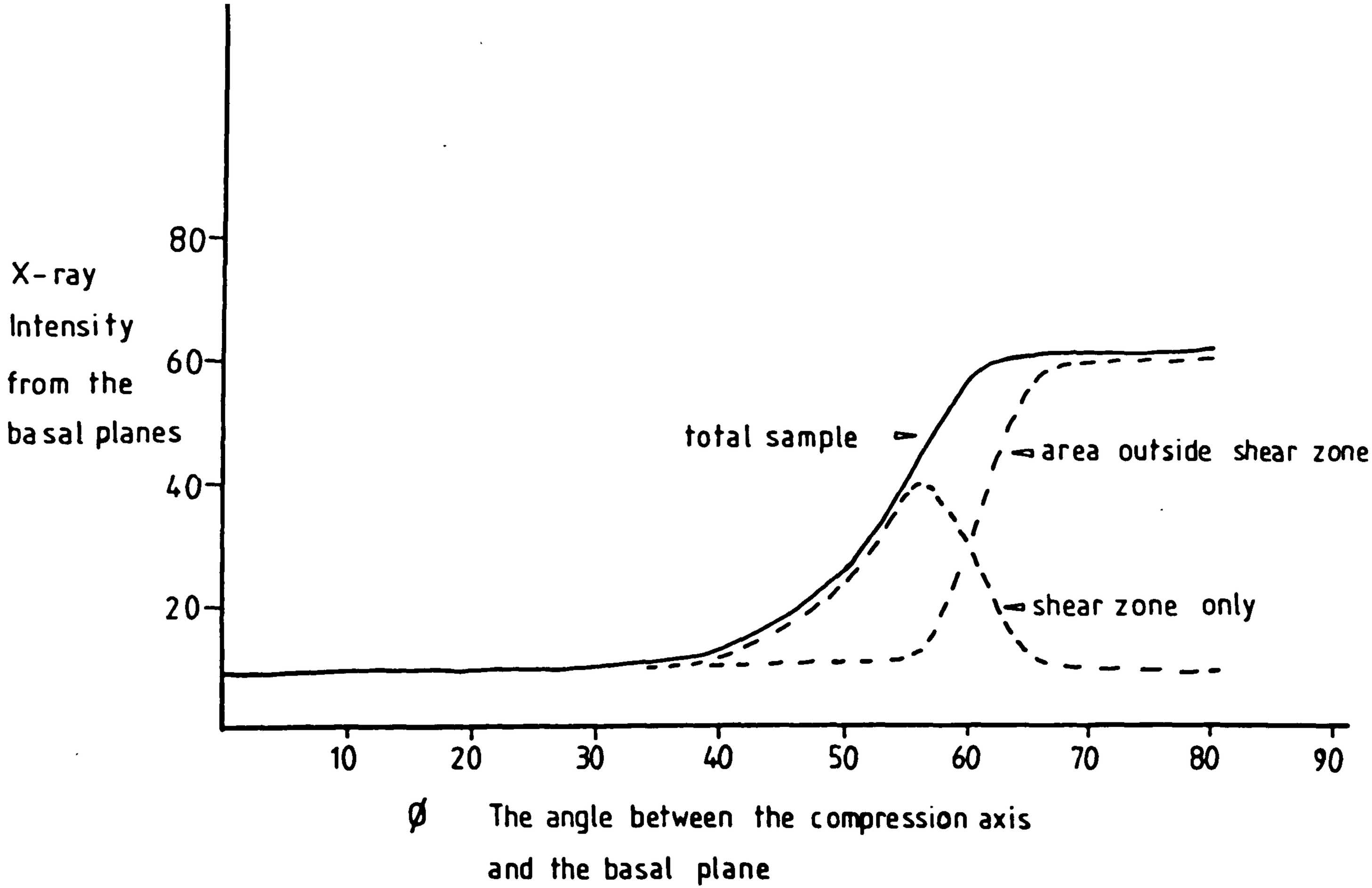


Figure 3.65 Distribution of basal planes in a sample containing a well developed shear zone. The broad distribution recorded from the total sample was found to be made up of two components :- i) from the area of sample outside the shear zone
ii) from the shear zone only

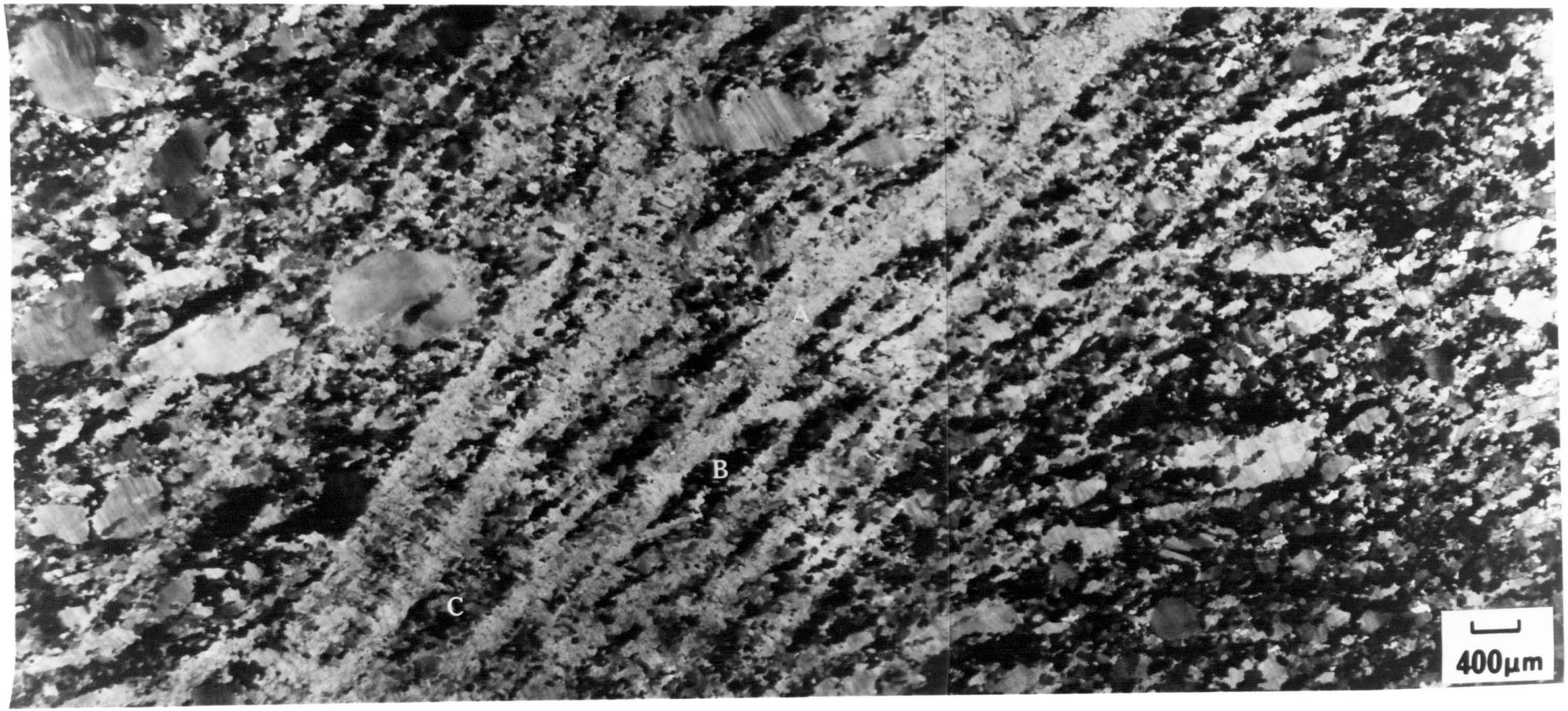
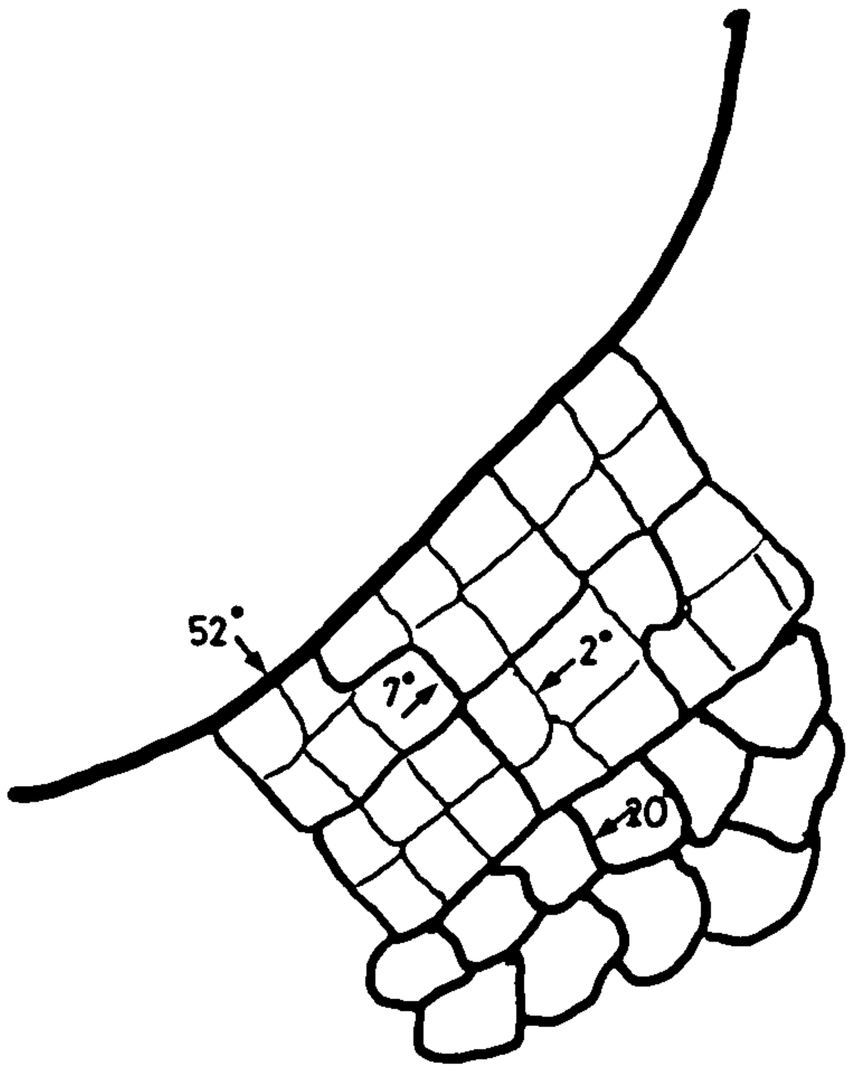


Figure 3.66. Macroscopic view of a shear zone. The lighter coloured areas (A) were closely related in orientation. The basal planes lay parallel to the zone at $52^{o} \pm 8$ to the compression axis. The areas marked B anc C had a greater orientation spread and the basal planes were aligned at $90^{o} \pm 20^{o}$ to the compression axis. The recrystallised grains in A had an average size of 20µm ± 3, whilst those in B and C were 30µm ± 3 in size.



BOUNDARY TYPE		MISORIENTATION
———	major boundary between old and new grains	52°
———	recrystallised grains similar to those from areas B and C (Fig. 3·66)	20° (max)
———	boundaries between clusters	7°
———	boundaries between individual recrystallised grains	2°

Figure 3.67 Schematic diagram of the misorientations within the shear zone

The two classifications of recrystallised grains had different grain sizes. Those grains within A were 20μm in size whilst those within B and C were 30μm in size.

3.7.2.4. Electron microscopy

Numerous foils have been examined and the general results are presented here. Two types of structure will be described; firstly the structure found within the centre of the shear zone and secondly the structure at the edge of the zone where remnants of the old grains can still be detected.

a) Structure within centre of shear zone

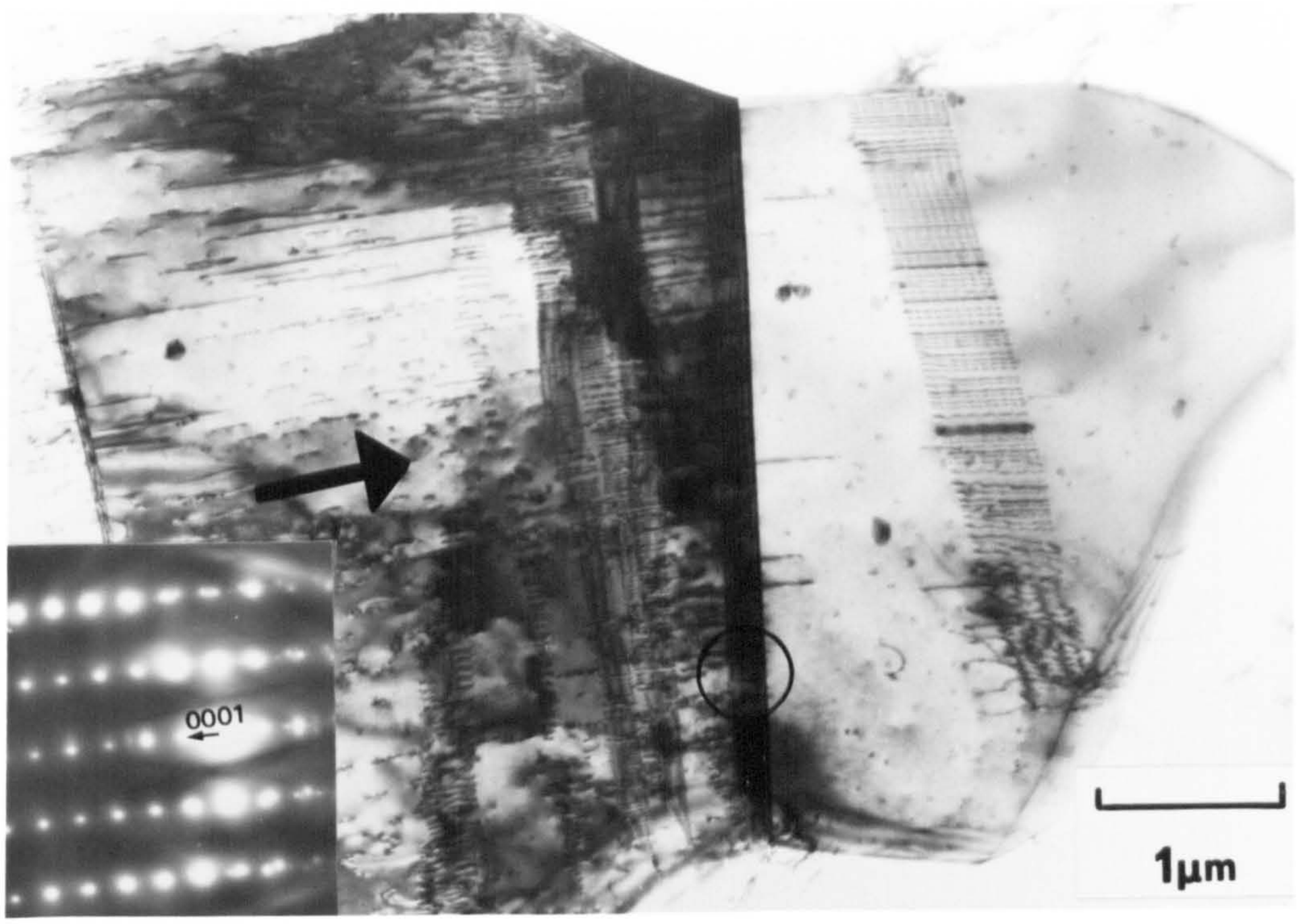
The grains within the shear zone had very straight boundaries and there was no evidence of bulging and migration of the boundaries which tended to lie parallel to or perpendicular to the axis of the shear zone. The grains were closely related in orientation to their neighbours. The dislocation walls lay parallel to the traces of the basal or prism planes and consisted mainly of dislocations with $\vec{a}$ burgers vector in the form of tilt boundaries as can be seen in Figure 3.68.

b) Structure in the old grains at the edge of the shear zone

The structure typically found at the edge of a shear zone is shown in Figure 3.69. The boundaries were better developed perpendicular to the direction of the shear zone. The misorientation across these boundaries was measured: the results are presented for the boundaries in Figure 3.69 which were representative of the behaviour. The misorientations were determined from Kikuchi line analysis and also from rotations in the diffraction patterns taken across the boundaries. They were as high as 10^{o} across some of the boundaries agreeing with the optical analysis (Figure 3.70). The arrow on the micrograph points to the edge of an old grain where the misorientations are similar to those observed in the electron micrograph (Figure 3.69). The change in colour of the recrystallised grains within the major zone is small indicating that misorientations are no greater than 10^{o} in agreement with the E.M. observations in (a).

3.7.3. Macroscopic heterogeneous deformation due to the operation of a shear zone

A study of the deformed surface similar to the ones undertaken to investigate the deformation at lower strains was carried out. A sample was deformed at $\dot{\varepsilon} \sim 10^{-5} s^{-1}$ at $260^{o}C$ to 25% ε, i.e. beyond the peak in



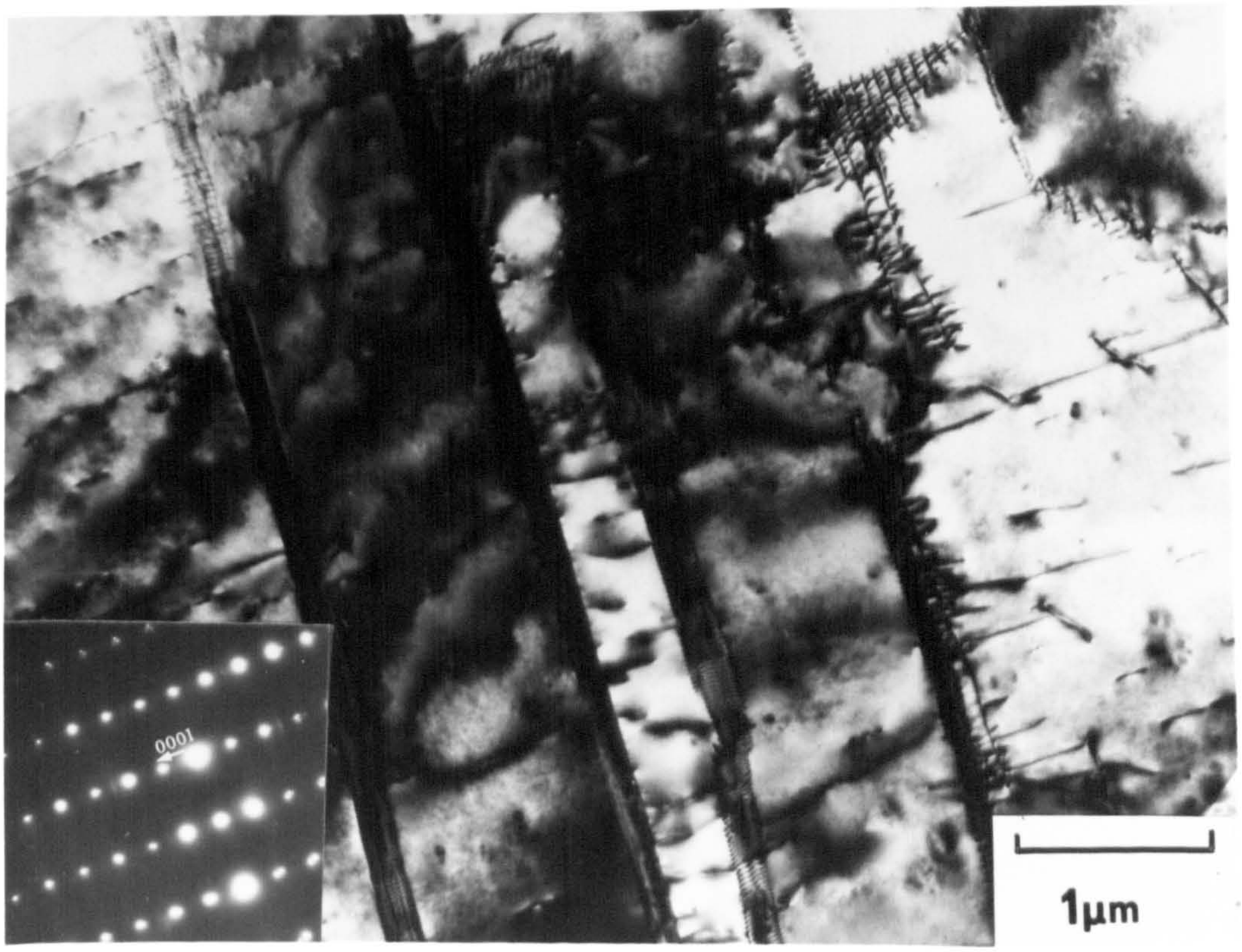


Figure 3.68. These two electron micrographs illustrate the tilt boundaries commonly found in the recrystallised grains within the shear zone.



Figure 3.69. Structure in an old grain at the edge of the shear zone. The direction of the zone is indicated by the arrow. The rotation about the $|2\bar{1}\bar{1}0|$ zone axis is $\sim 12^{o}$ across the boundaries which have developed perpendicular to the shear zone.

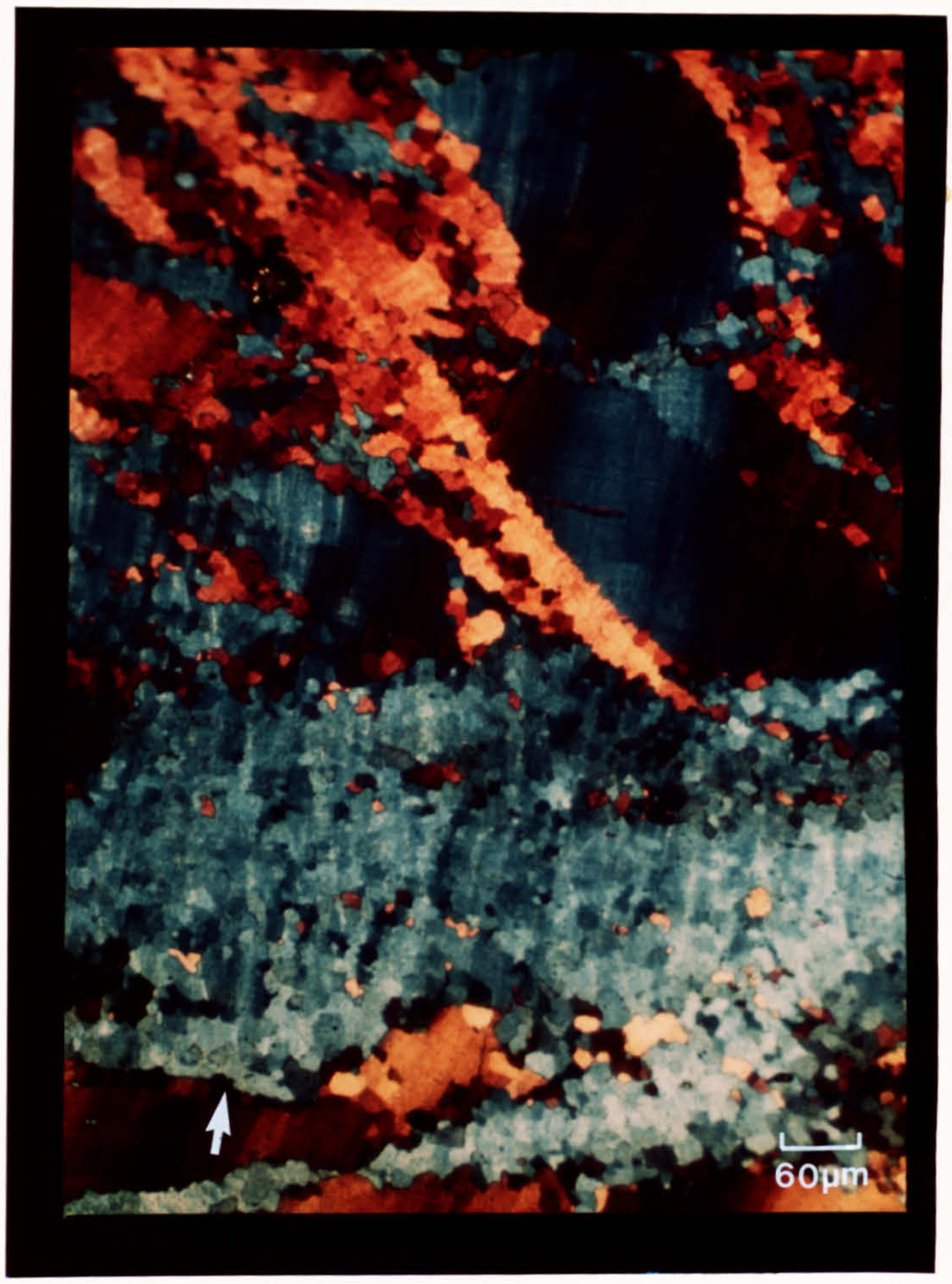


Figure 3.70. Colour metallograph of a well developed shear zone (blue) and a narrow second zone (orange). The narrow zone is highly misoriented ($45^{o} \pm 5^{o}$) from adjacent old grain. The arrow points to a zone of misoriented subgrains in the mantle of an old grain adjacent to the 'blue' zone.

the stress strain curve. It could be seen by inspection of the bulk specimen that a shear zone had been initiated (Figure 3.71a). The surface parallel to the compression axis was ground flat such that the cross section of the shear zone was revealed (Figure 3.71). The sample was prepared and deformed for a further 10% as before. A schematic diagram (Figure 3.71b) illustrates the behaviour since neither the S.E.M. or the optical micrographs showed the overall behaviour satisfactorily. The bulk of the deformation appeared to have taken place at the edges of the shear zone where both the evaporated grid and polishing scratches were rotated 45^{o}. The grid and scratches were relatively undeformed and exhibited little rotation across the zone with the exception of one discontinuity which coincided with a line of elongated voids. The voids were elongated in the direction of the zone and the behaviour of the grid in their vicinity is illustrated in Figure 3.72 where it can be seen to be very distorted. The microstructure of the voids was reminiscent of that found in ductile shear fractures. A typical example is presented in Figure 3.72 where the fracture surface appeared to have been a result of microvoid coalescence.

The microstructure of the material after a section had been cut parallel to the deformed surface is shown in Figure 3.73. The upper micrograph which is taken away from the shear zone exhibits a microstructure typical of 18% strain, even though the bulk sample has undergone 35% strain. The lower micrograph which is taken in the shear zone shows the massive lattice rotations which have occurred in this region. Old grains remaining in the zone have been rotated with respect to the compression axis and there has been more recrystallisation. These observations are similar to those reported in section 3.3.2.3.4., so the behaviour of this sample and the information obtained from its deformed surface are therefore thought to be representative results.

3.7.4. Effect of temperature on shear zone development

As temperature was decreased the heterogeneity of deformation increased both on the microscopic and macroscopic scale. In the latter case heterogeneity is easily recognised in the form of sharp offsets on the specimen profiles (Figure 3.74). In the former case at $150^{o}C$ lattice bending and rotations were confined to $\sim 10\mu m$ within a grain boundary whereas at $260^{o}C$ bending was common throughout a $300\mu m$

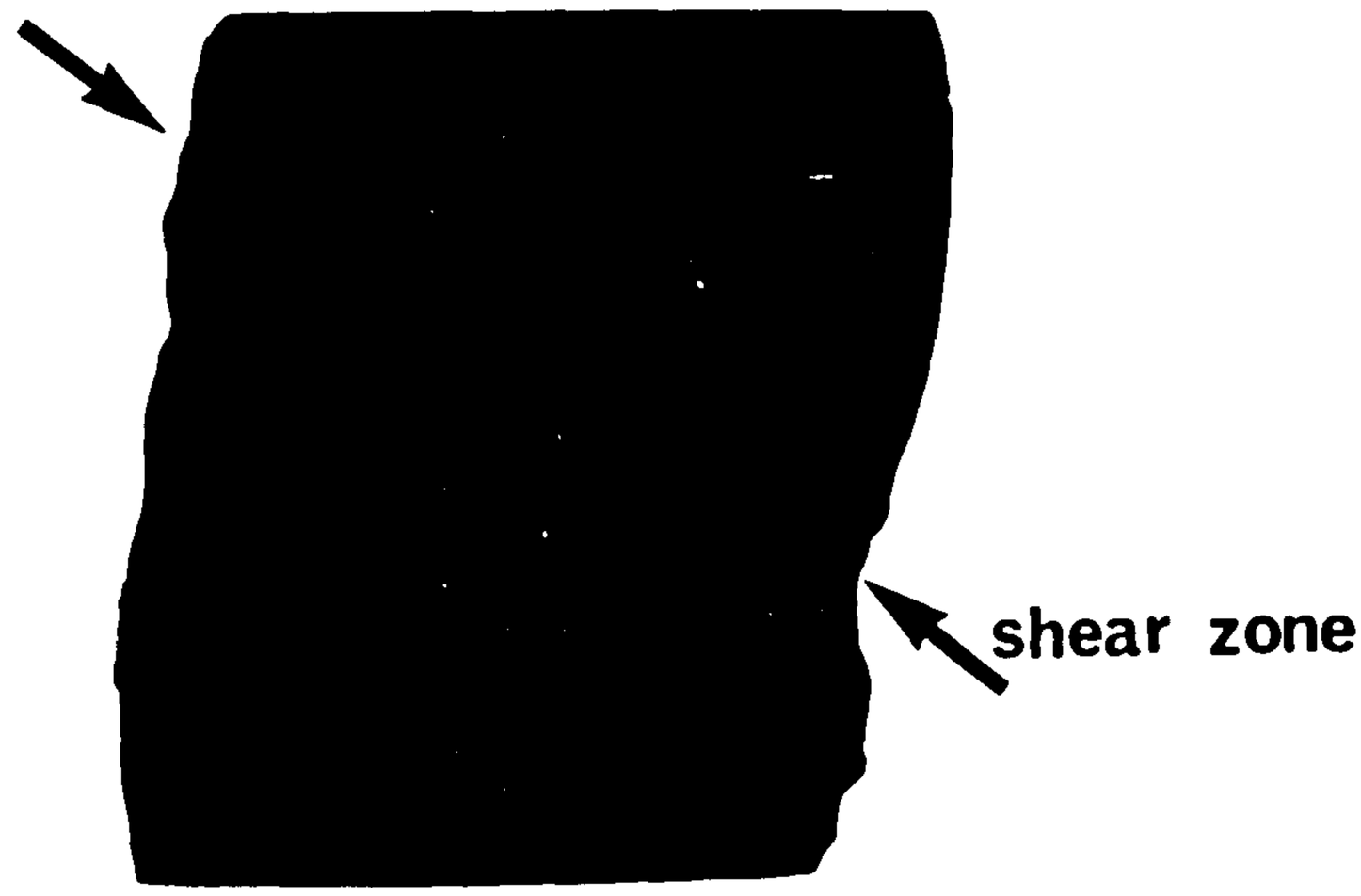


Figure 3.71a Macroscopic view of a sample in which a shear zone had been initiated.

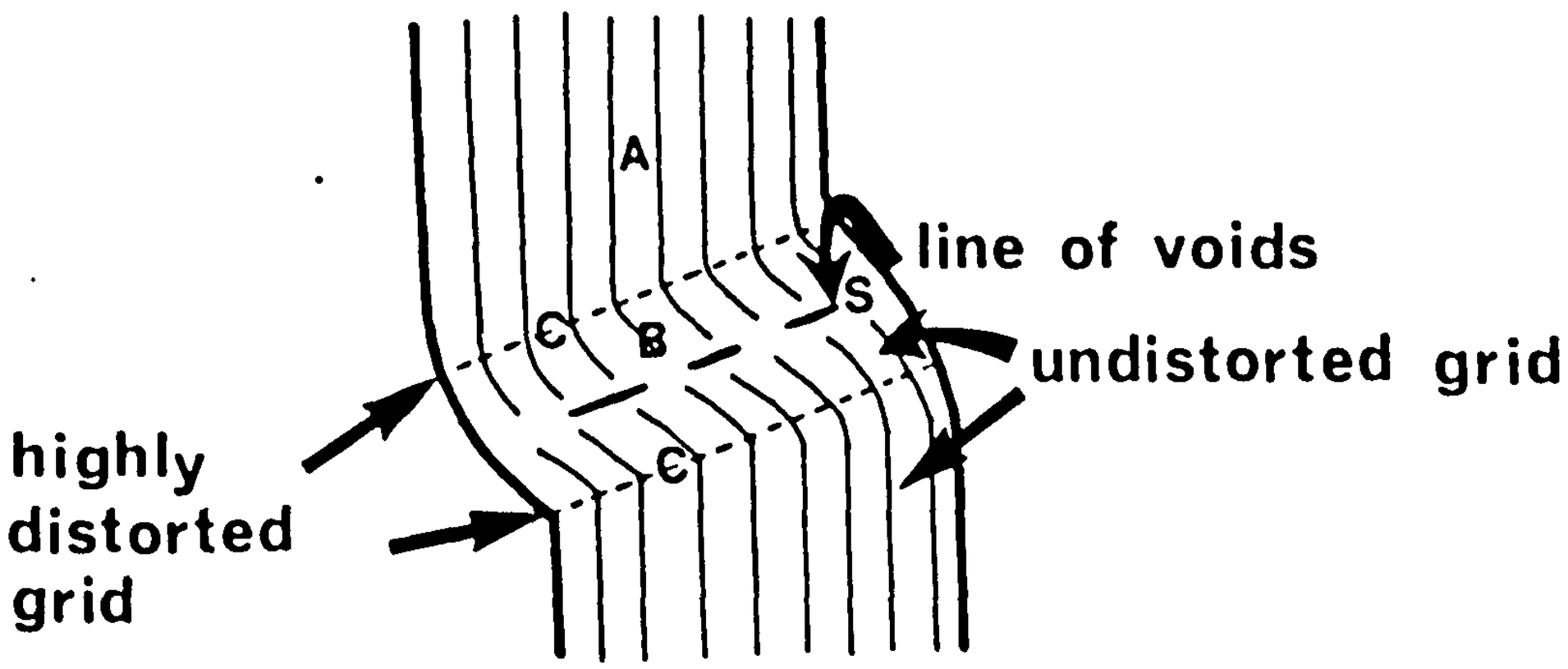


Figure 3.71b Schematic illustration of the behaviour of the grids on the surface of the sample. The grids were undeformed in areas A and B and showed high rotations at the edges of the shear zone C. They were discontinuous in the vicinity of the voids in the centre of the zone S.

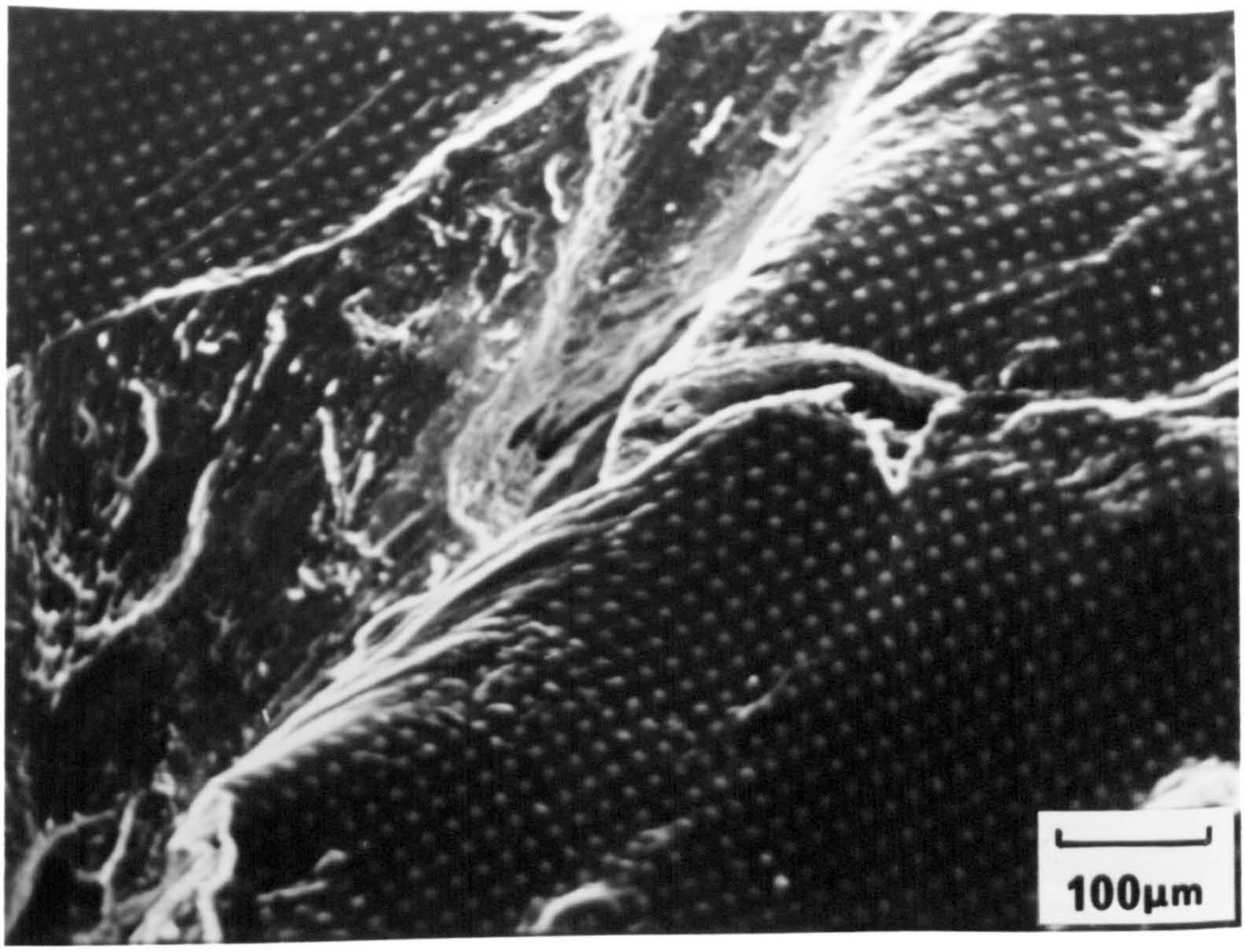


Figure 3.72a. Severe shearing in the vicinity of a grain boundary in a shear zone. Note the heavy deformation recorded by the grid.

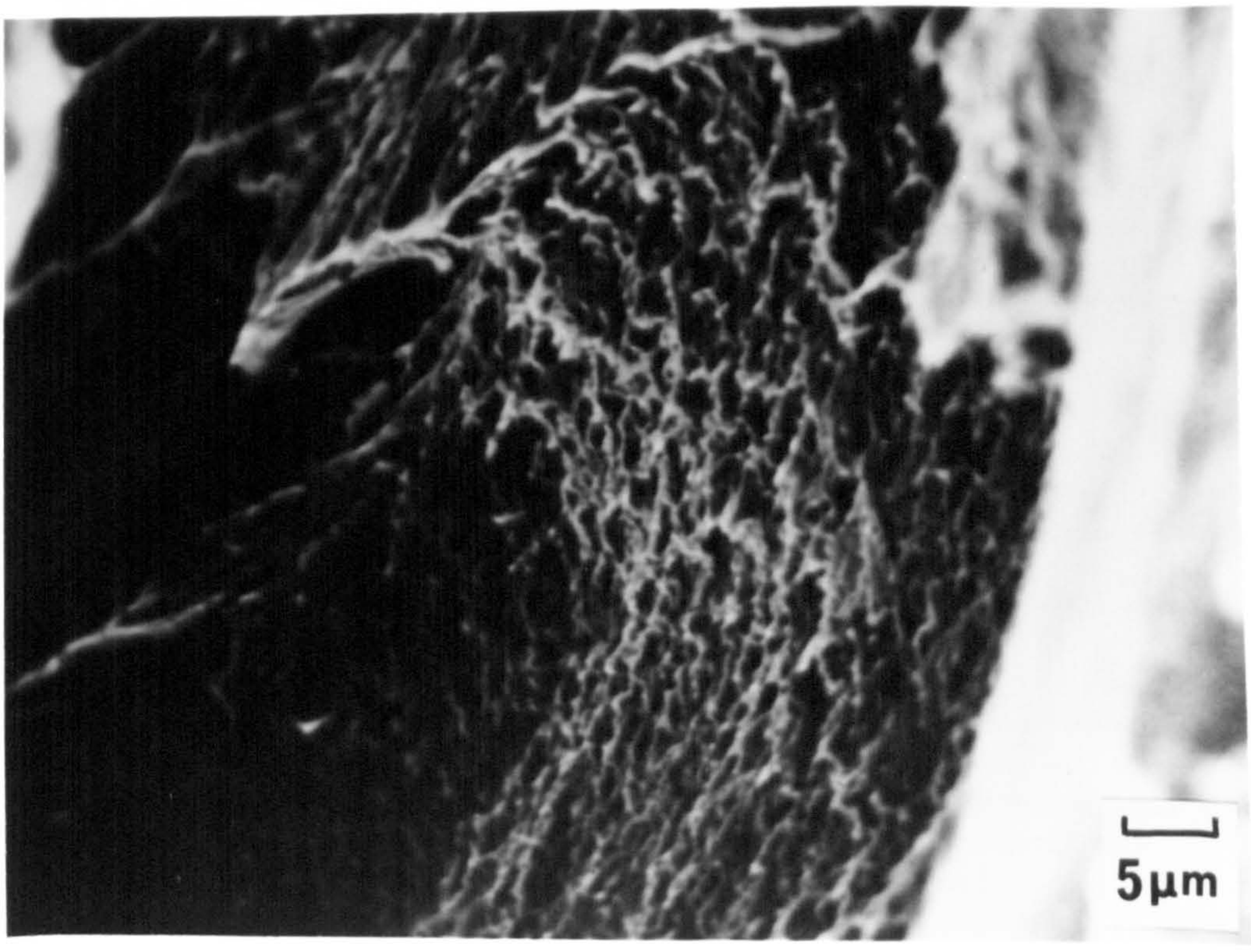
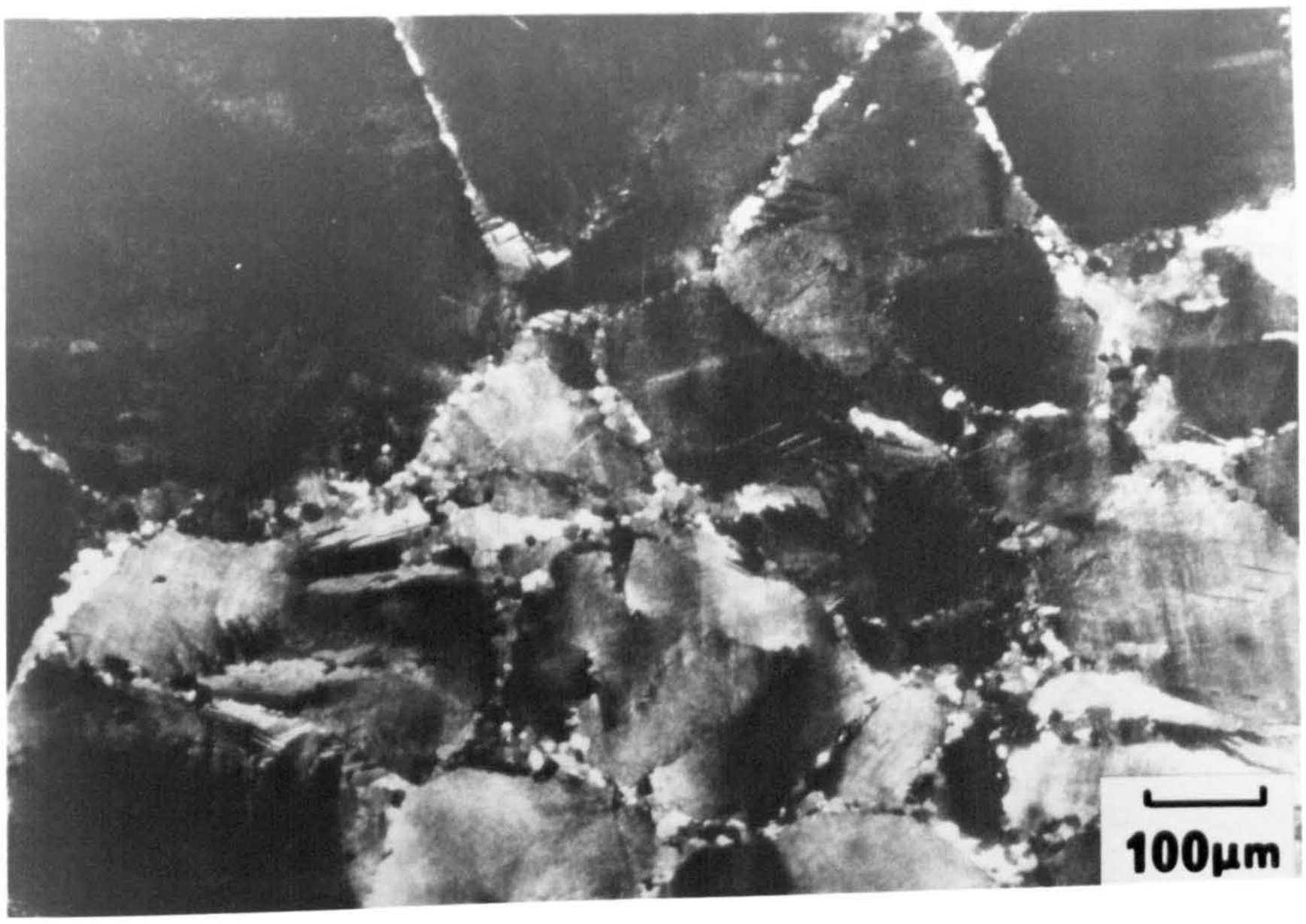


Figure 3.72b. Surface of sheared grain boundary similar to the one illustrated above. The micrograph is typical of one showing creep fracture by microvoid coalescence.



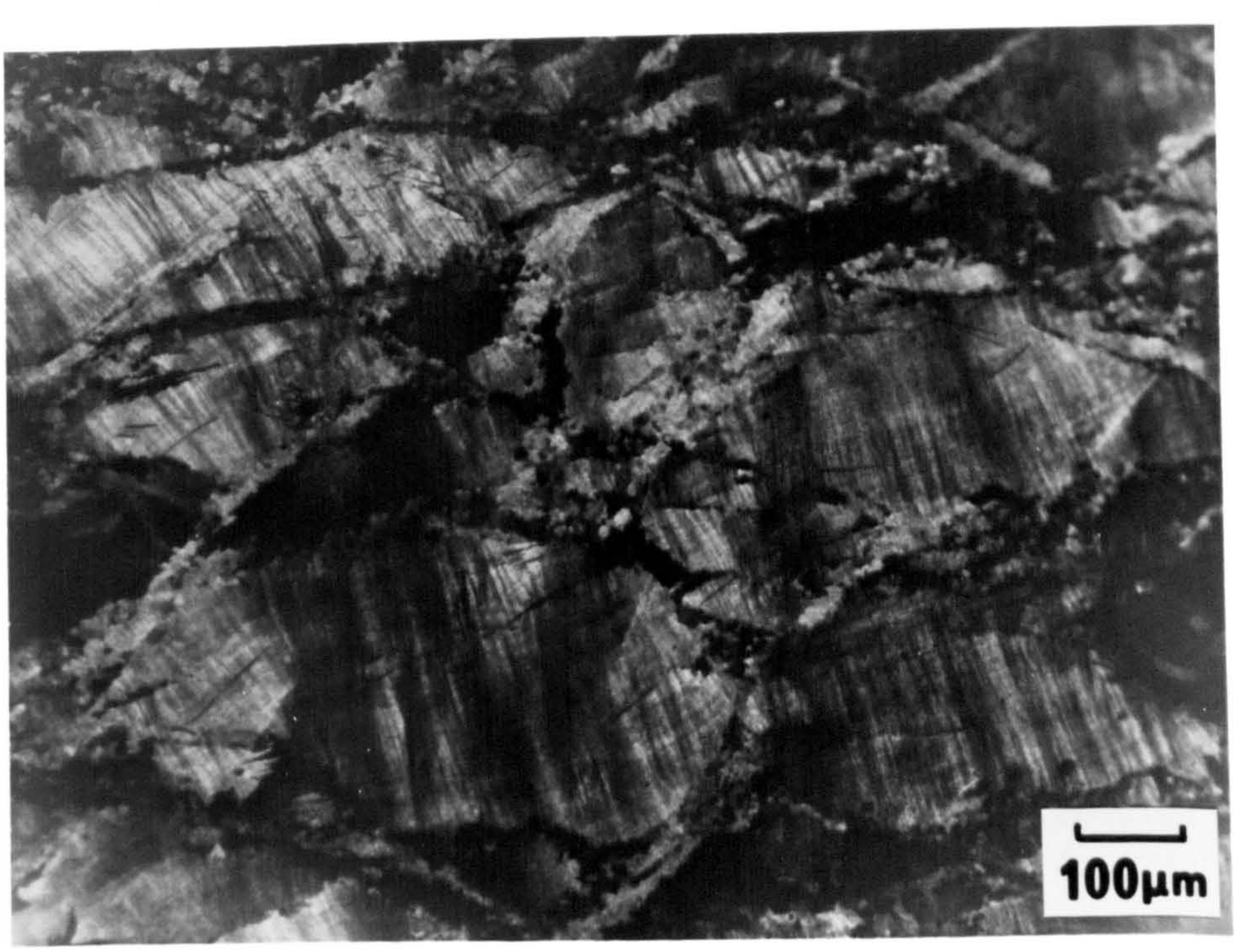


Figure 3.73. Internal microstructure of the sample on which the gold grid had been deposited. The upper micrograph is from an area away from the shear zone whilst the lower micrograph is taken in the centre of the zone. It can be seen from the substructure within the old grains that the deformation had obviously been concentrated in the shear zone.



Figure 3.74 Effect of temperature on the macroscopic deformation behaviour. Shadow masks of five specimens deformed 55% at temperatures in the range 150°-320°C illustrate the way in which the deformation becomes progressively more homogeneous as the test temperature is raised. At low temperatures, the deformation is so heterogeneous that macroscopic shearing occurs, resulting in visible offsets at the specimen surface.

grain. On the macroscopic scale at 150°C, the incidence of voiding was marked along the shear zone and parts of the specimen along the zone had undergone shear fracturing. Very fine recrystallised grains barely resolvable at x400 in the optical microscope were present in the areas of specimen between the elongated voids in the shear zone (Figure 3.75). The specimen had undergone a bulk strain of 55%, but the microstructure outside the shear zone resembled that at 22% strain.

The size of the recrystallised grains within the shear zone increased with ihcreasing temperature and hence decreasing peak stress and the width of the zone of heterogeneous deformation also increased. At 260°C this zone of heterogeneous strain was composed of several impinging shear zones, (Figure 3.66). Voids tended to form preferentially along the shear zones, (see for example Figure 3.76)- although as the temperature of testing was increased they were less catastrophic. In all cases the recrystallised grains within the shear zones were favourably oriented for basal slip. Old grains which were found in the centre of the individual shear zones at 260°C also had their basal planes favourably oriented for slip. Slip lines could usually be detected within these grains which were elongated parallel to the slip plane and the zone. At lower temperatures the volume occupied by the old grains within the shear zone was greater, but once again they had undergone rotation such that their basal planes were parallel to the zone.

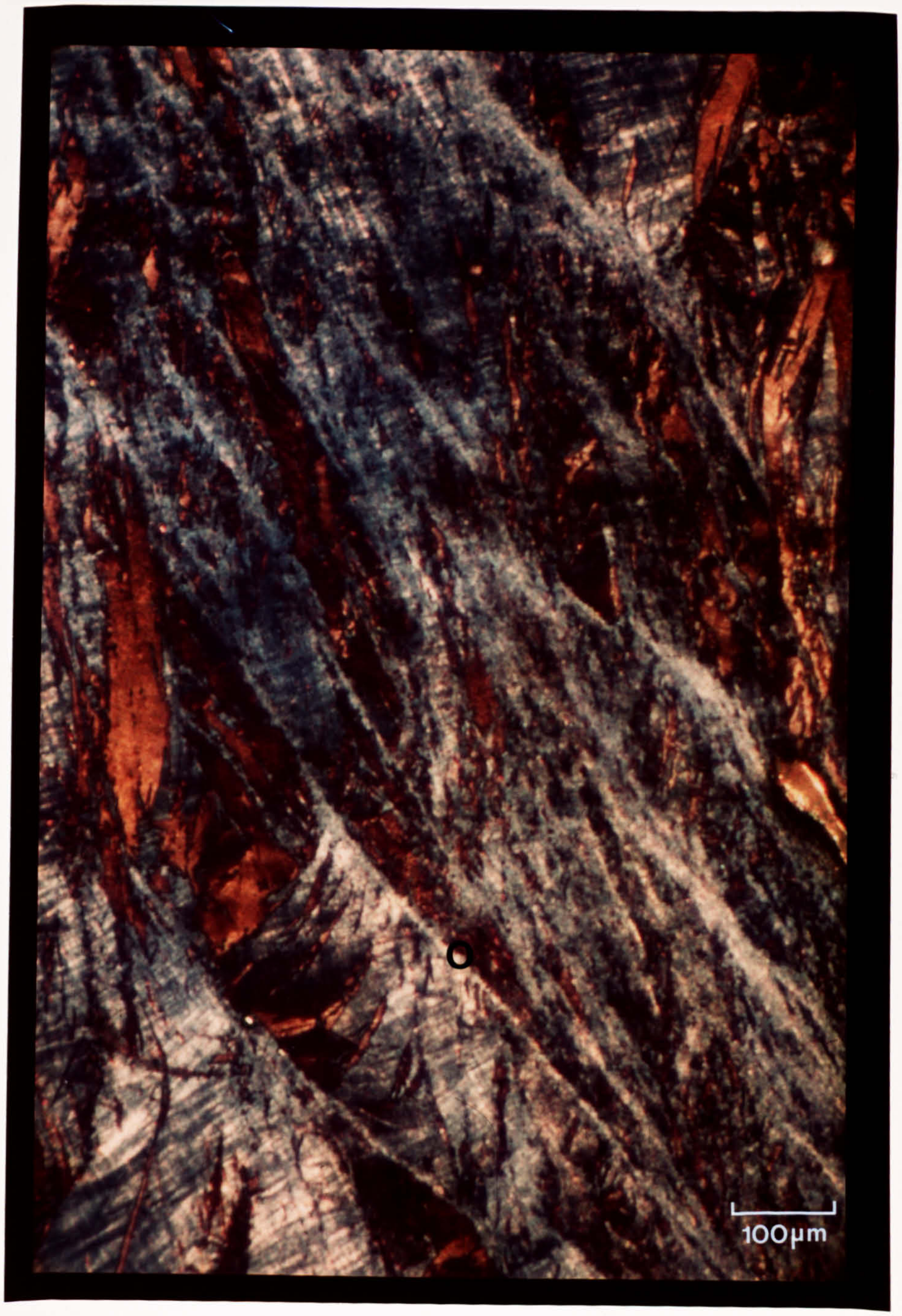


Figure 3.75 Region of very fine recrystallised grains between elongated voids in a specimen which had undergone a bulk strain of 55% at 150°C. The circled area is similar to the area from which the E M foil photographed in Fig. 3.17 was taken.

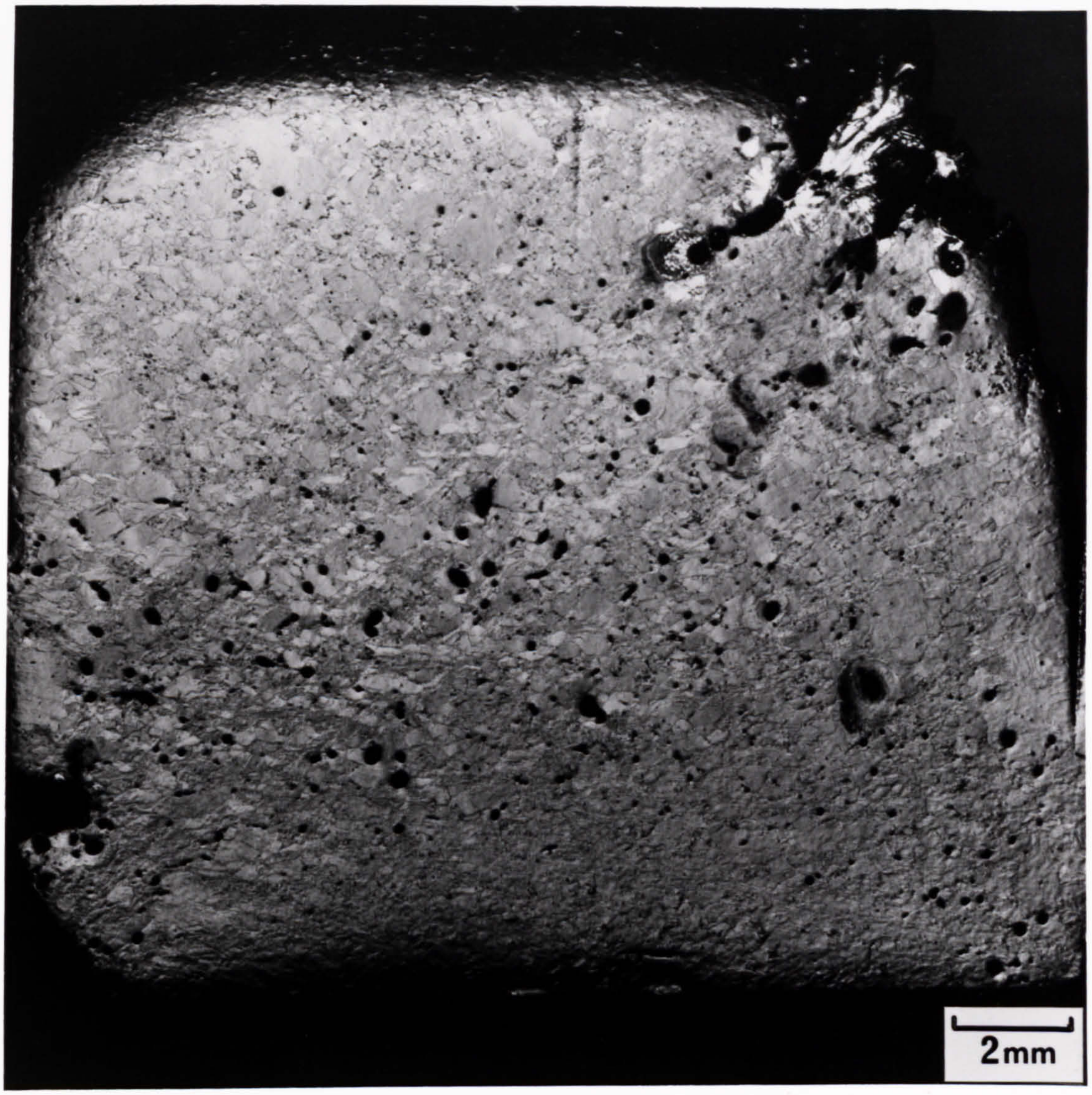


Figure 3.76. Macroscopic view of sample deformed 55%. Voids had formed preferentially along a zone of higher strain.

CHAPTER 4

Discussion

4.1. INTRODUCTION

The results have shown that dynamic recrystallisation is important in Magnox A180 and that it has a marked effect on mechanical properties and microstructural development. The deformation behaviour of the metal has been studied in depth and will be discussed in detail after the mechanisms for dynamic recrystallisation reported in the literature have first been considered.

4.2. MECHANISMS OF DYNAMIC RECRYSTALLISATION REPORTED IN THE LITERATURE

The present theories for dynamic recrystallisation are based mainly on studies designed to explain the stress-strain behaviour of the material under consideration. Microstructural observations have tended to play a secondary role and little attention has been paid to nucleation: static mechanisms have been assumed. Two mechanisms of nucleation are cited:-

a) Nucleation from bulges which have formed during deformation in the old grain boundaries.
b) The progressive misorientation of subgrains until the sub-boundaries become high angle grain boundaries.

In the former case all reports of dynamic recrystallisation nucleated from bulges invoke the Bailey and Hirsch (1962) mechanism of strain induced boundary migration, but as pointed out in Chapter 1 this paper deals mainly with the kinetics of static recrystallisation. Most of the references to bulge nucleation are based on optical microscopy of materials which undergo dynamic recrystallisation. Luton and Sellars (1969) examined dynamic recrystallisation in Ni and Ni-Fe alloys at high temperatures and found that the old grain boundaries were markedly irregular and that there was evidence of localised bulging and the formation of recrystallised grains in the boundary regions. Thin foil microscopy indicated the presence of a substructure in the recrystallised samples. It was poorly developed and the authors noted its similarity with the substructure in pure Ni deformed in creep conditions (Richardson et al 1966). Similar observations have also been reported for α-iron (Glover and Sellars 1974), austenitic stainless steel (Roberts and Ahlblom 1978,) and also for copper (Bromley and Sellars 1973).

The second mechanism of recrystallisation was reported in copper deformed in hot torsion at high strain rates (McQueen and Bergerson 1972). Small patches of high perfection slightly larger than subgrains were thought to be regions which had just recrystallised and were thus more

lightly deformed than the surrounding matrix. It was suggested that the high angle boundaries formed from cell walls through the accumulation of dislocations.

A study of the microstructures produced as a result of compressive deformation of single crystals of halite (NaCl) revealed that two mechanisms of dynamic recrystallisation were operative in the material (Guillopé and Poirier 1979). Firstly a mechanism of subgrain rotation whereby the misorientation of the subgrains increased until it was sufficiently high for them to be termed recrystallised grains and secondly by bulging and migration of the sub-boundaries to form recrystallised grains. The former mechanism occurred below a critical temperature which depended on stress and the latter mechanism resulted from the growth of one of several subgrains or grains already obtained by the rotation mechanism. It was suggested that migration recrystallisation would only occur if the temperature and stress conditions were such that the boundaries would migrate rapidly enough to allow the growing grains to remain relatively substructure free.

The mechanism of subgrain rotation has often been reported for deformed minerals (see e.g. White 1976) but strain induced boundary migration is the mechanism normally reported for metals and it is this mechanism which is invoked in models to explain the kinetics of dynamic recrystallisation. The models proposed make one important assumption, viz; that the dynamically recrystallised grains when they first form are strain free, or at least have an appreciably lower dislocation density than surrounding material. For example, it was found that good qualitative agreement could be obtained between stress strain curves predicted for pure Ni and those obtained experimentally (Luton and Sellars 1969) if dynamic recrystallisation was assumed to follow similar kinetics to those of static recrystallisation, i.e. at any time (t) measured from the time that the critical strain was reached the volume recrystallised (x) would be given by

$$x = 1 - \exp(-kt^n)$$

where k and n are constants.

In order to calculate the flow stress, the increment of recrystallisation x_i occurring in uniform increment time was measured from the recrystallisation curves. The assumption made was that as each increment recrystallised, the flow stress σ_i would fall instantaneously to zero and then would follow a work hardening curve identical with that of the

initial curve. The flow stress of the remaining old grains σ_e would be determined by extrapolating the initial work hardening curve. Thus the nett flow stress would be given by

$$\sigma = \sum_o^i x_i \sigma_i + (1 - \sum_o^i x_i) \sigma_e$$

The model also assumed that further recrystallisation could occur when each increment of volume reached the critical strain and that the flow stress at the critical strain was the maximum value.

Similar assumptions have been made in a model based on the relationship of dislocation density to flow stress (Stuwe and Ortner 1974) in that the new grains are assumed to be initially dislocation free and a critical dislocation density must be attained to initiate recrystallisation.

More sophisticated treatments which take into account dynamic recrystallisation accompanied by dynamic recovery have been proposed (Roberts and Ahlblom 1978, 1979). They also invoke the Bailey and Hirsch mechanism of bulge nucleation and assume recrystallisation will occur when a bulge of critical size is formed.

The preceding paragraphs emphasise the point that the theoretical studies proposed in the literature invoking dynamic recrystallisation have resulted from considerations of the kinetics of bulge formation and the assumption that the new grains are initially strain free in attempts to explain the stress strain behaviour of metals and alloys during creep and hot working. This study of the behaviour of magnesium has been different in that the microstructural development has been examined in detail in an attempt to elucidate the microscopic mechanisms occurring during dynamic recrystallisation in the material.

The microstructures found experimentally in the magnesium will now be discussed and a mainly qualitative model put forward to account for them.

The specimens deformed at temperatures below 320^{o}C in the orientation which was unfavourable for basal slip have been studied in detail since it was these specimens which showed marked changes of stress strain behaviour on dynamic recrystallisation. For a given strain rate the behaviour can be divided into two categories depending on the temperature. The division arises because of the heterogeneous nature of the deformation at low temperatures compared with the relatively homogeneous nature of the deformation at high temperatures. The latter will be considered first.

4.3. HIGH TEMPERATURE DEFORMATION BEHAVIOUR

4.3.1. The homogeneous nature of the deformation

At high temperatures (>320^{o}C) the deformation is relatively homogeneous. This is reflected in both the optical and electron microscopy and in the shape of the stress strain curve where a steady state is reached at fairly low strains (∿25%). The final texture is diffuse as indicated by the X-ray goniometry (Figure 3.58) and the quantitative reflected polarised light microscopy. The shape of the samples after deformation reveals macroscopic homogeneous strain. It is thought that additional slip systems and recovery processes rather than lattice bending play a much greater role in the accommodation of deformation. The relative ease of basal slip compared with slip on other systems decreases with increasing temperature and climb and cross slip are much easier at higher temperatures. Evidence for this was found in the EM work where the substructure was better developed and relatively homogeneous. The subgrains at 370^{o}C contained well developed substructures in the form of networks and tilt boundaries. There was extensive evidence for the operation of $\overrightarrow{c + a}$ as well as $\vec{a}$ burgers vectors. The subgrains were larger and more equiaxed than those found at lower temperatures.

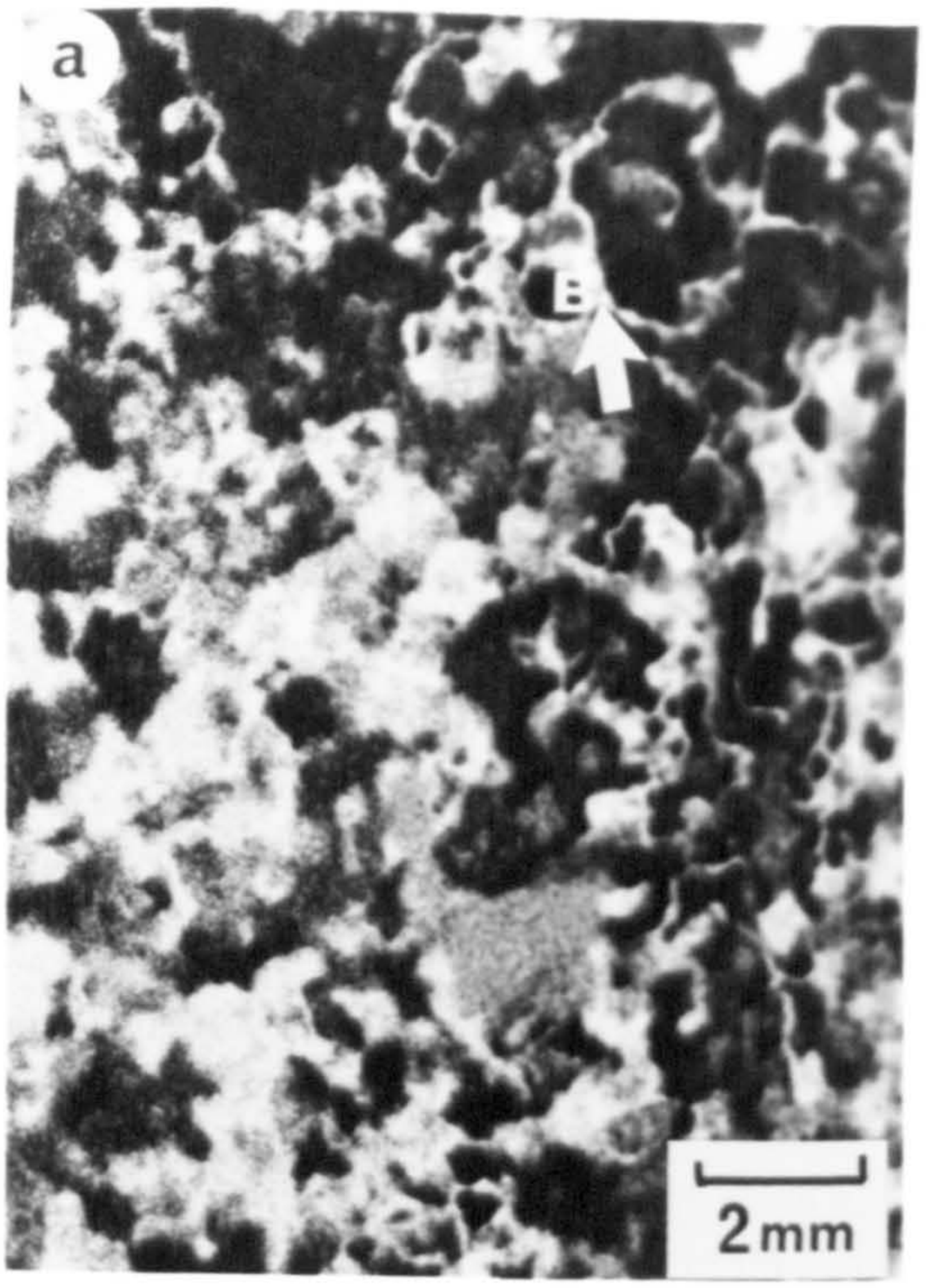
The experiments carried out on samples with the superimposed grids also confirmed that the deformation was more homogeneous at high temperatures (Figure 3.51). The grids tended to show uniform shortening and although there were some rotations in the grain boundary regions they were on a much smaller scale than those found at low temperatures.

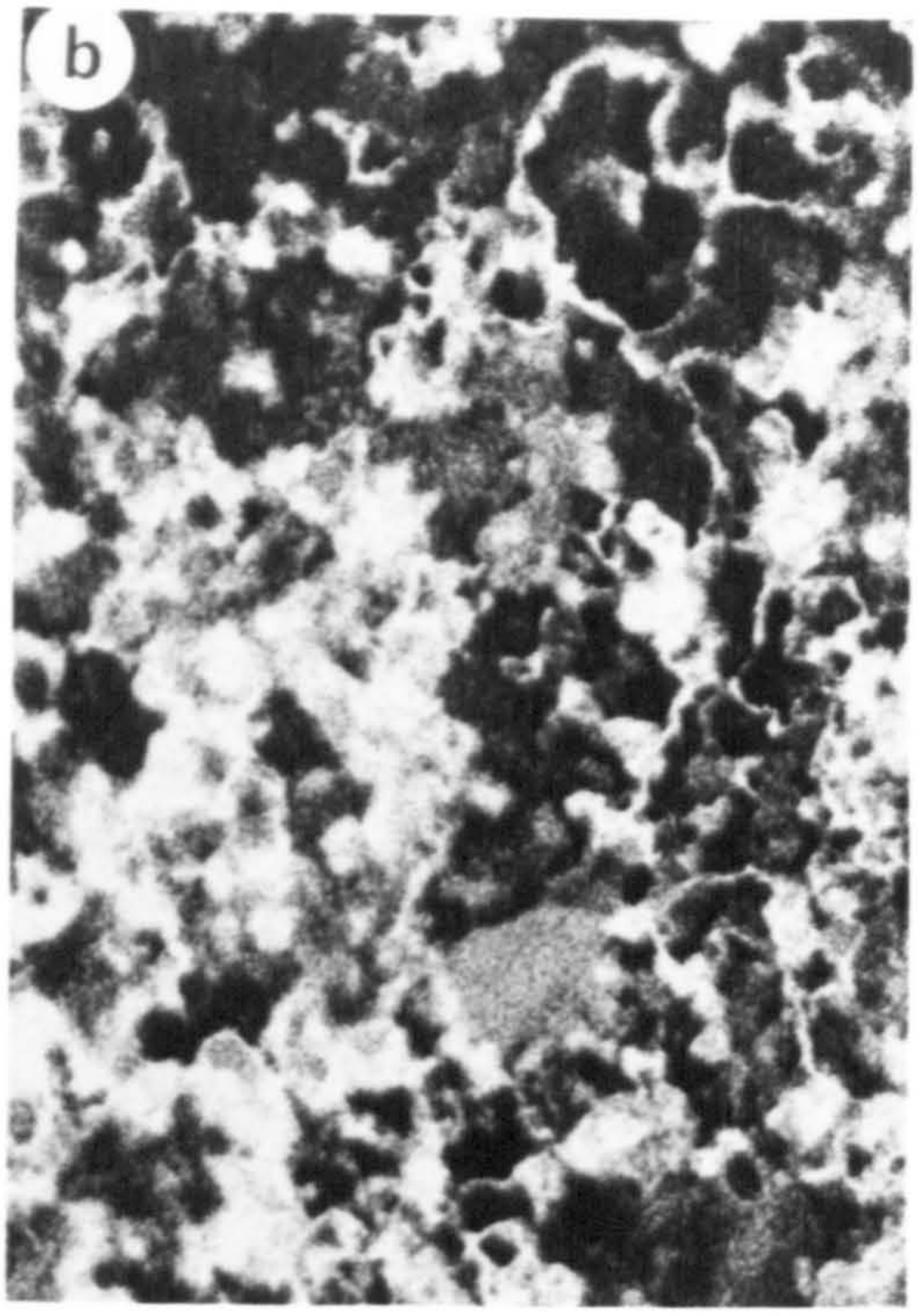
A few experiments were carried out on the magnesium alloy Zr55 to see whether or not internal markers behaved in the same way as the grids on deformation (for experimental details see Appendix D). The only large rotations occurred at deformation band boundaries (Figure D4) which is in agreement with the studies carried out optically, cf. Figure 3.49.

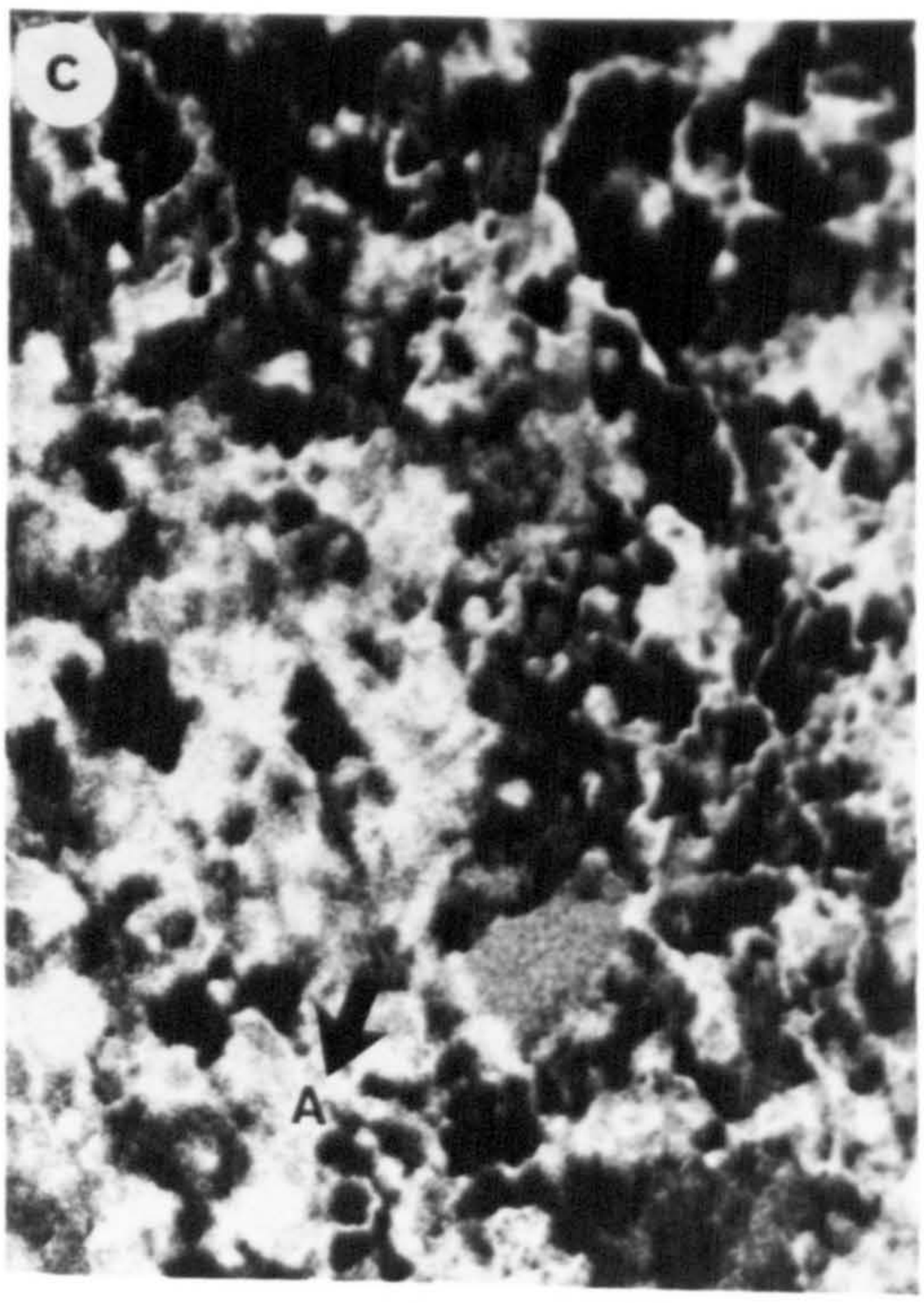
4.3.2. The Mechanism of Dynamic Recrystallisation

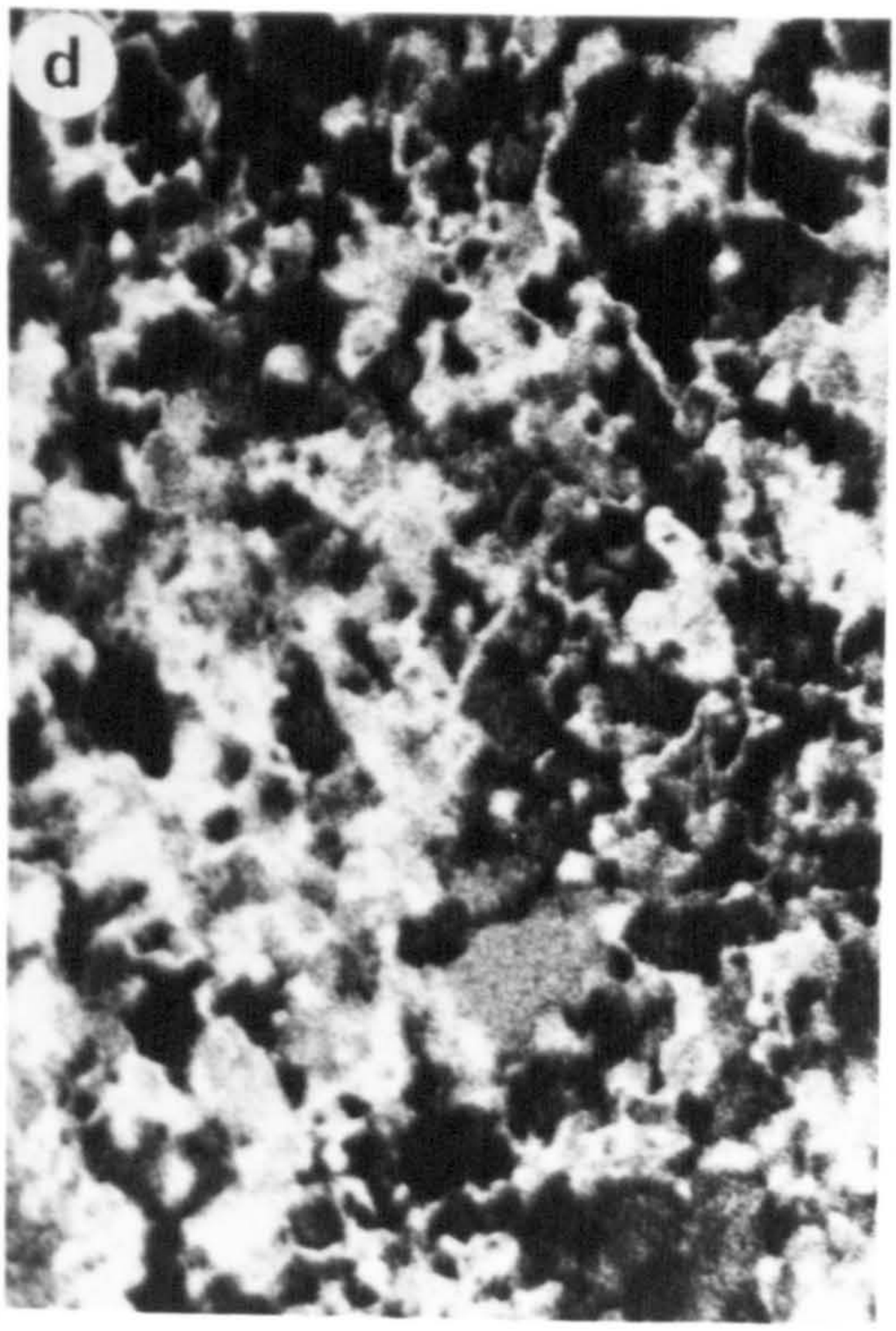
The microstructures of the strained samples showed extensive bulging and migration of the old grain boundaries which appeared to result in recrystallisation. The recrystallised grains were similar in size to the boundary bulges and they also showed bulging and migration. These observations implied that recrystallisation was taking place by a continuous process of migration and bulging and when the flow curve had reached a steady state a homogeneous microstructure was maintained by

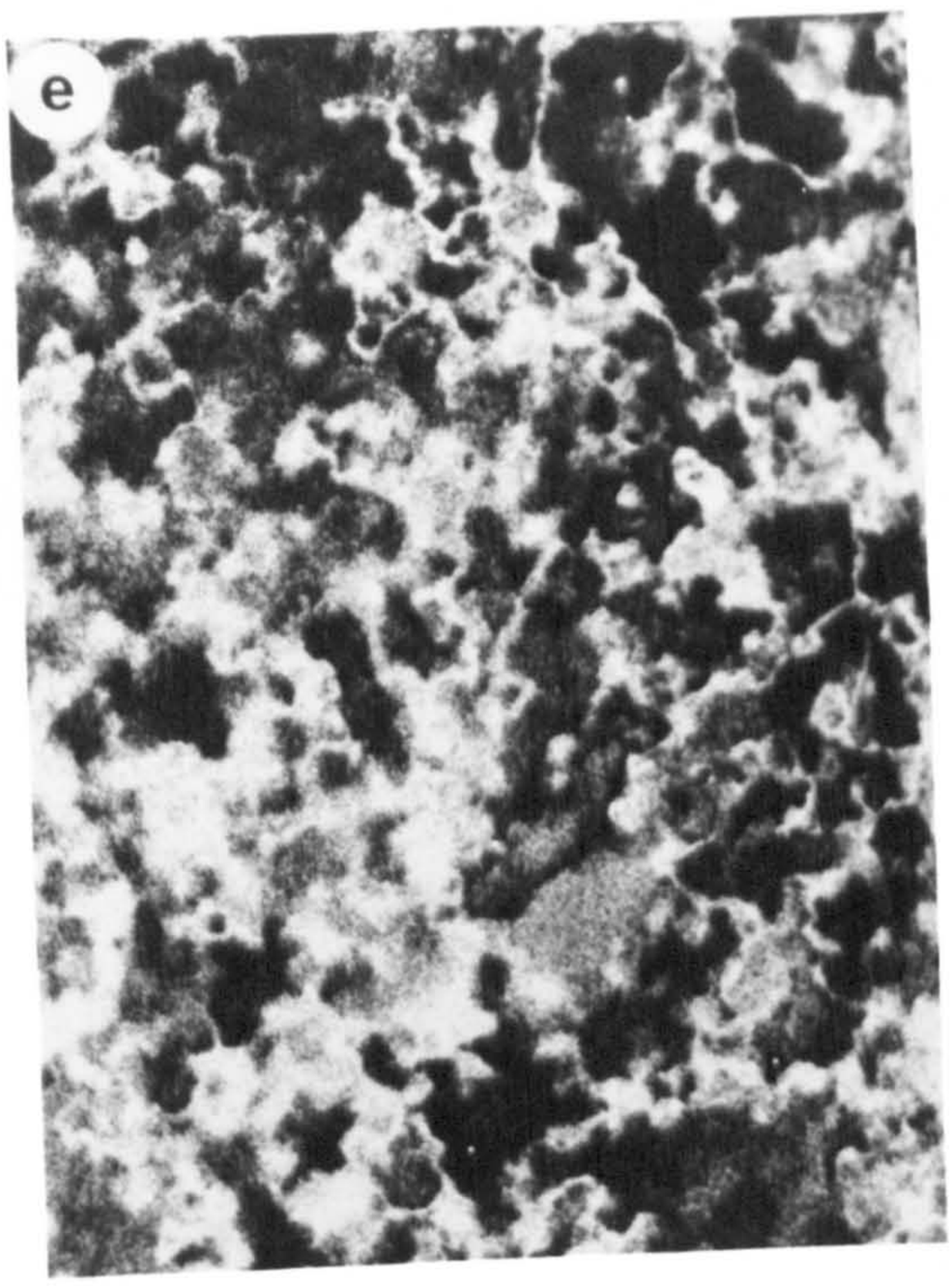
Figure 4·1

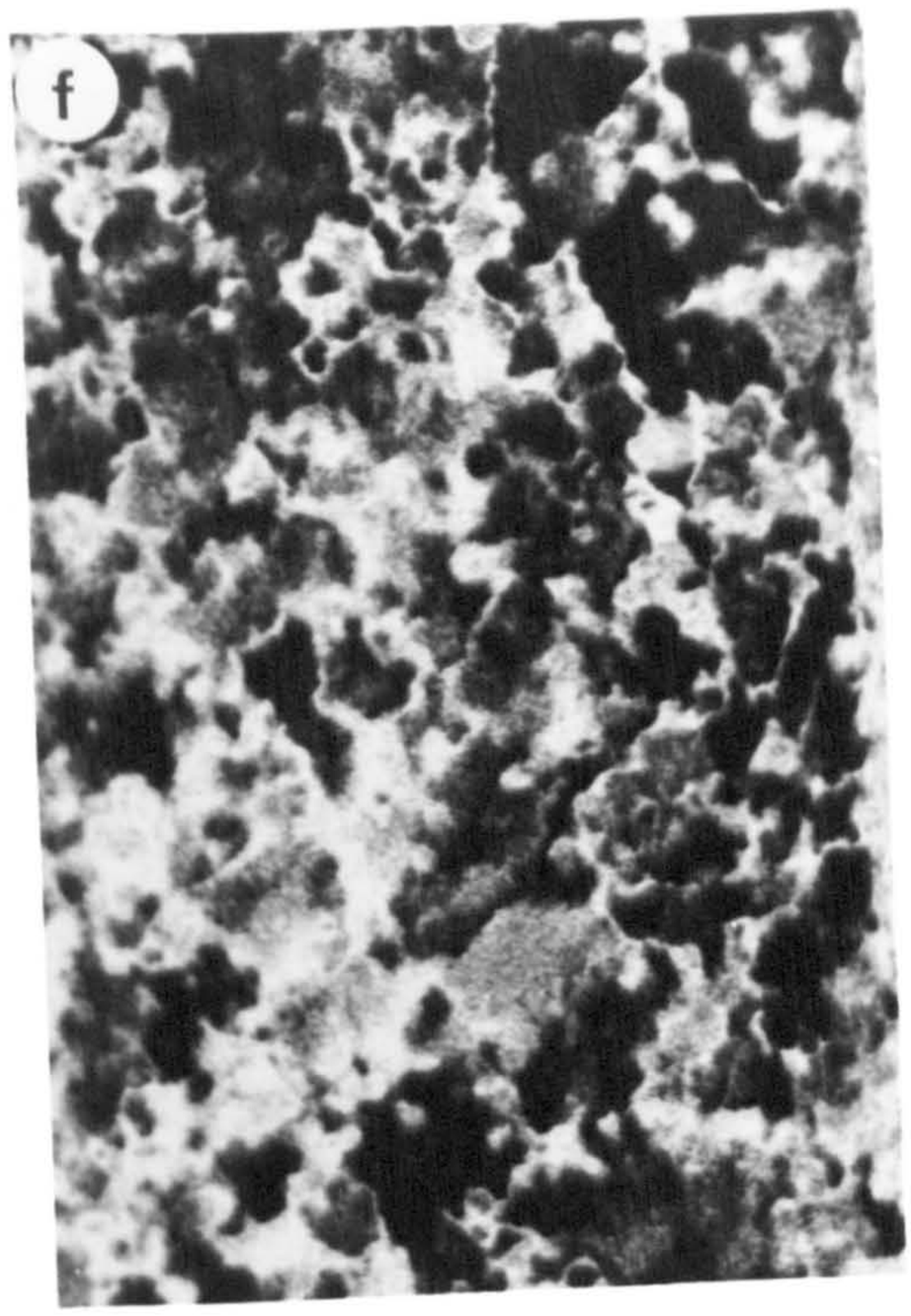

a
B
2mm

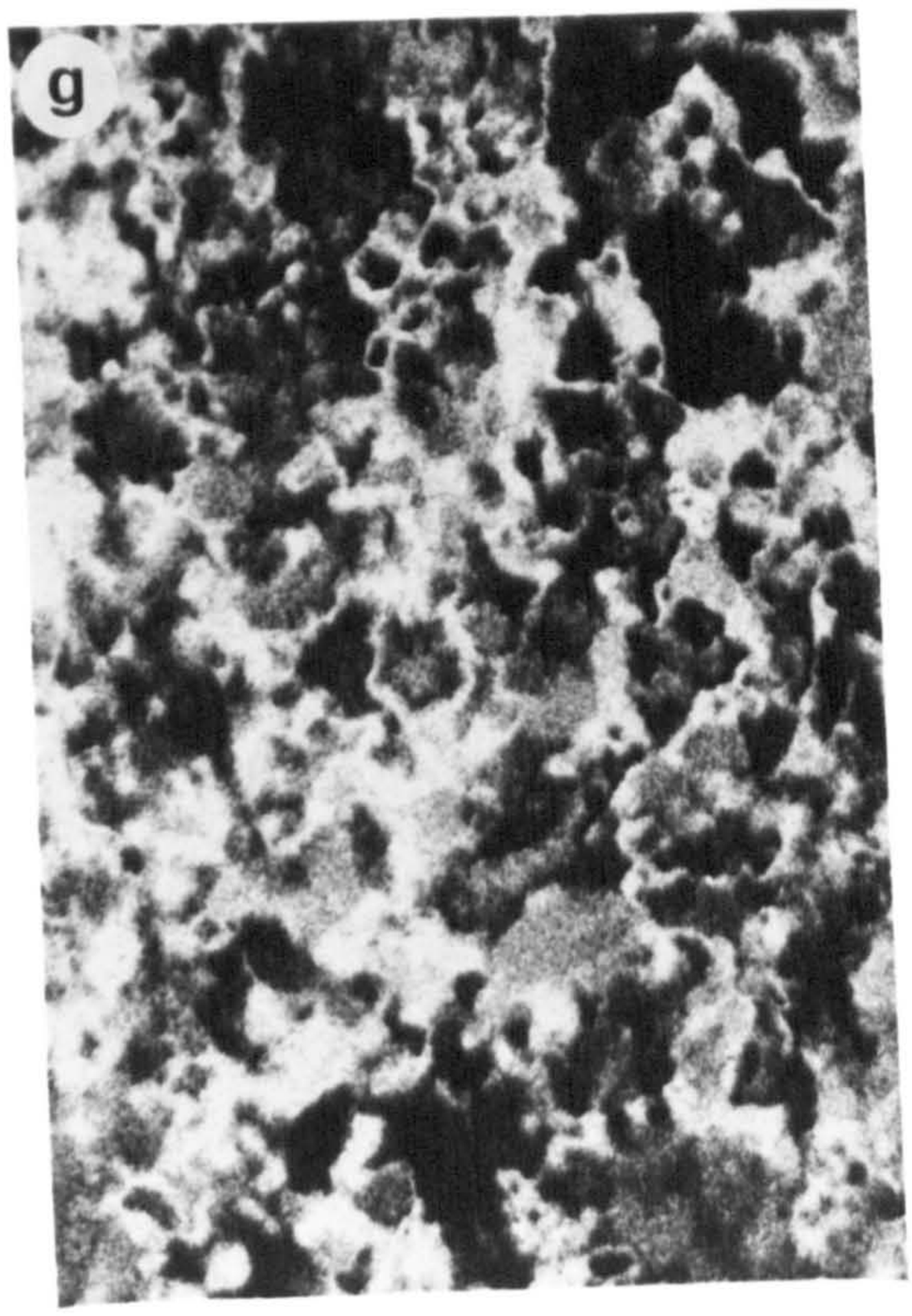

b

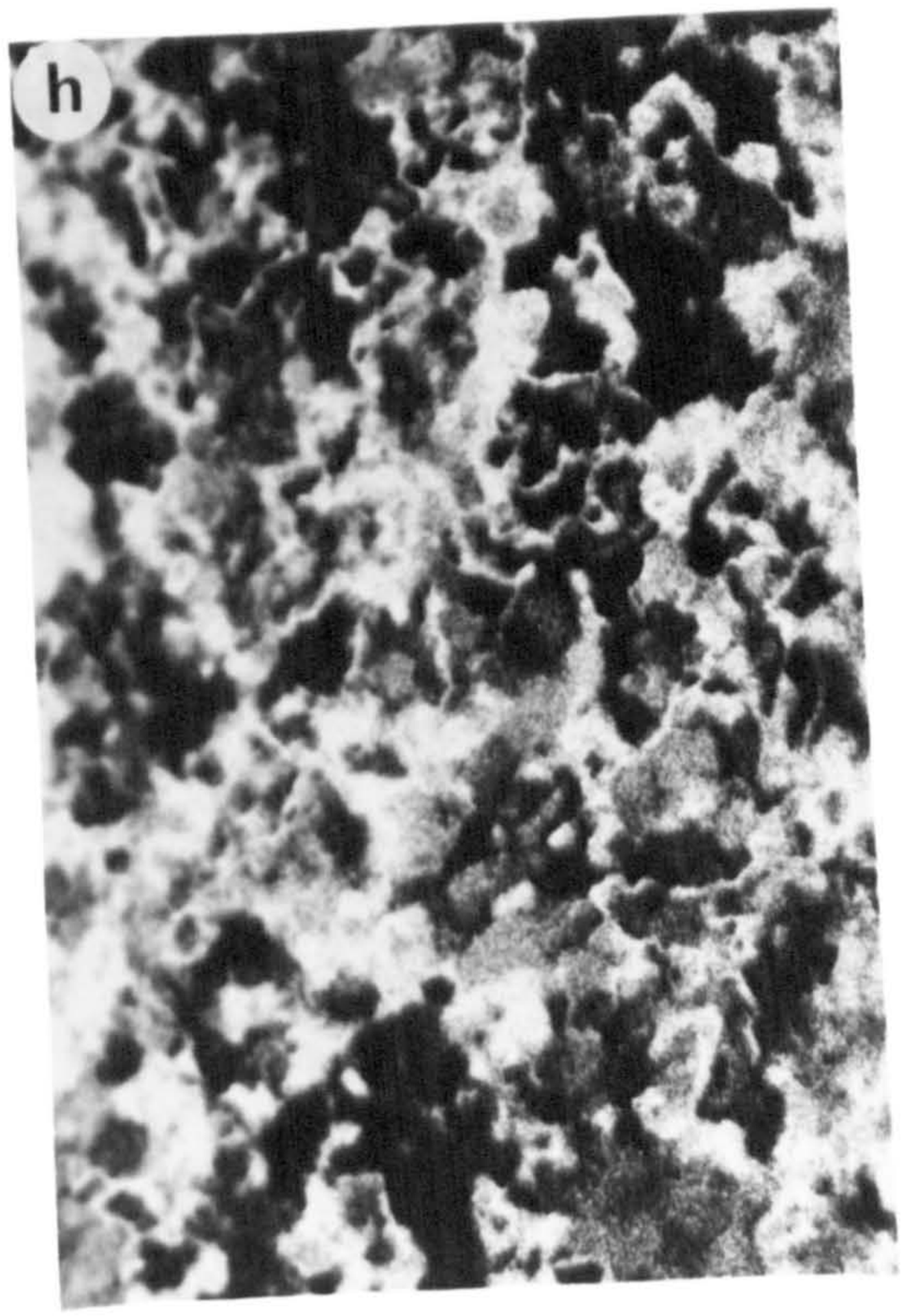

c
A


d


e


f


g


h

this continuous process. However, without direct observations of bulging, migration and misorientation and subsequent recrystallisation the mechanism of strain induced boundary migration (SIGBM) can only be suggested to account for the bulging and the maintenance of a constant microstructure beyond 35% strain. In-situ experiments would verify the process but on a macroscopic scale these have not been possible in the metal. However, model materials have been used in the past as analogues to illustrate processes such as solidification and grain growth so experiments have been carried out on the transparent organic solid camphor to obtain further information about dynamic recrystallisation and are reported in Appendix E. One important result to have come from the work is that the material exhibits dynamic recrystallisation by SIGBM and it is possible to record the results on video or 16 mm film. Figure 4.1 shows 8 stills reproduced from a 16 mm film, which clearly illustrate the process. The boundaries repeatedly migrate and the bulged regions misorientate to form recrystallised grains which then exhibit migration and bulging, resulting in a dynamic equilibrium caused by continuous recrystallisation.

4.4. LOW TEMPERATURE DEFORMATION BEHAVIOUR

4.4.1. Mechanical Properties

4.4.1.1. Effect of temperature

In agreement with the vast amount of published experimental data on the mechanical properties of Magnox A180 (see e.g. Jones and Harris 1963), the peak stress decreases with increasing temperature. This is attributed to the decrease in the critical resolved shear stress (CRSS) on systems other than the basal slip system as temperature increases and to the greater amount of recovery at higher temperatures.

4.4.1.2. Effect of orientation

The high coefficient of strain hardening in part (i) of the stress strain curve A shown schematically in Figure 4.2. is attributed to the fact that the starting material was unfavourably oriented for basal slip. Since the loading system (compression parallel to the extrusion direction) was favourable $\{10\bar{1}2\}$ twinning occurred. However this resulted in little change in the resolved shear stress on the basal system and the overall stress continued to rise until dynamic recrystallisation occurred just before the peak in the stress strain curve was reached. In common with other anisotropic materials which have one easy slip system the flow stress is very dependent on the orientation of the starting material with respect

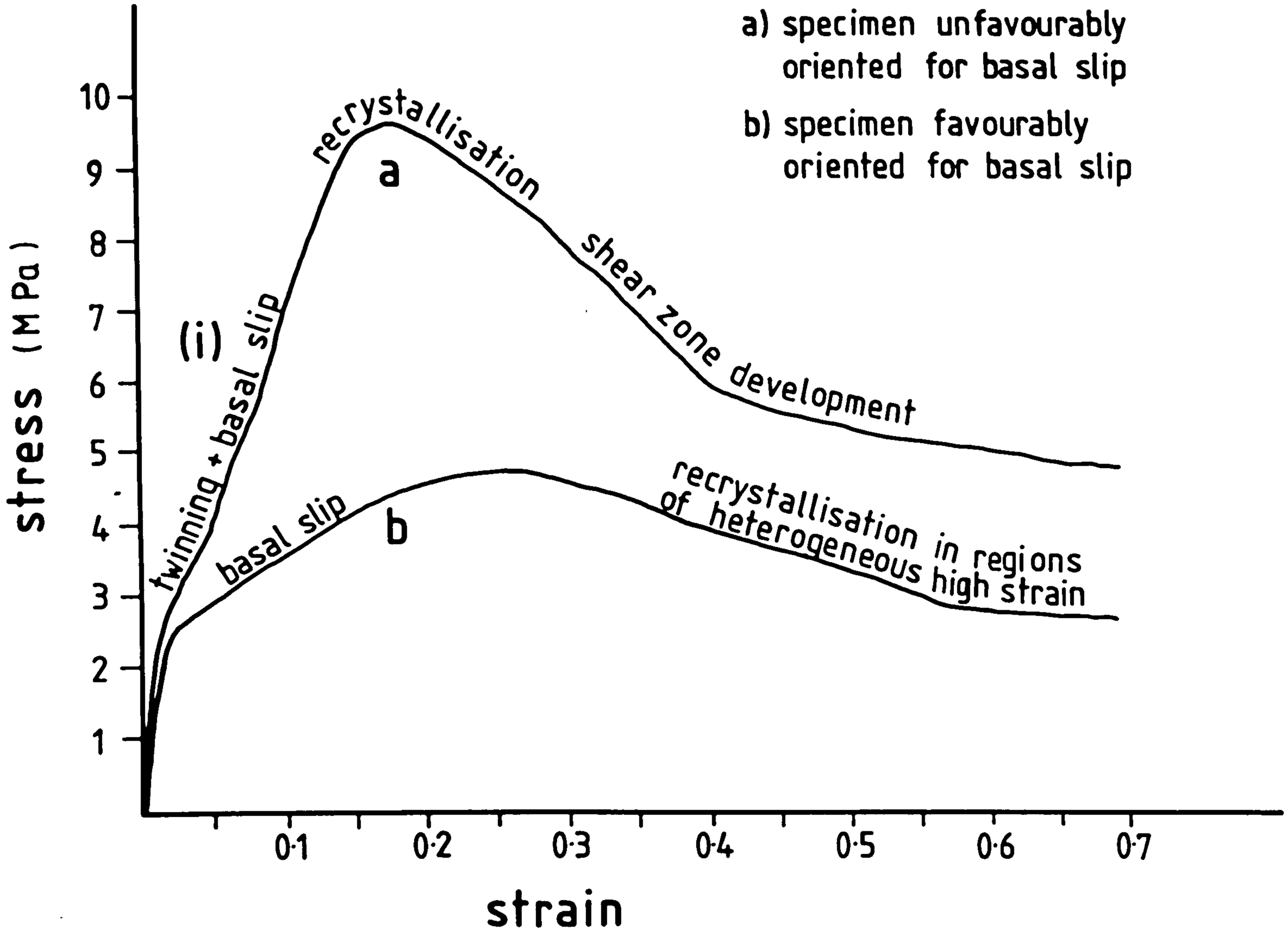


Figure 4.2. Variation in stress strain behaviour of polycrystalline samples of Magnox A180 with the preferred orientation of the starting material, at a temperature of 260°C and a strain rate of $10^{-5}s^{-1}$.

to the axis of deformation. Curve B, Figure 4.2, which illustrates the behaviour of material favourably oriented for basal slip has a much lower peak stress at the same temperature and strain rate for this very reason. Figure 4.3., reproduced from the work of Burke and Hibbard (1952), who studied the orientation dependence of the flow stress on magnesium single crystals, shows the behaviour of two single crystals deformed in different orientations; the first crystal being favourably oriented for basal slip and the second unfavourably oriented for basal slip. It can be seen that these two curves exhibit similar work hardening behaviour to the two curves for the polycrystalline material shown schematically in Figure 4.2. The strong preferred orientation of the starting material means that it can be treated as a quasi single crystal. The CRSS has been shown to be strongly orientation dependent (Figure 4.3.); the morphologies of the polycrystalline stress strain curves are a direct result of this fact.

4.4.1.3. Estimation of Q and n from mechanical data

The value of Q - the activation energy of the creep process, estimated from the stress-strain curves (section 3.2.2.) was 25 Kcal/mol. This is significantly lower than the activation energy for self diffusion (32 Kcal/mol) required by theoretical analyses of creep, but is in agreement with experimental studies by Jones and Harris (1963) and Tegart (1961). The disparity was thought to arise from a contribution due to dislocation pipe diffusion since the value of Q was close to that for grain boundary diffusion (Crossland and Jones 1972).

The value of the stress exponent n, calculated in the current work was 7, which differs from the theoretical values of 3, for glide, and 4.5 for climb, in an analysis by Weertman (1968). Once again this deviation from the predicted values has been recorded during other experimental studies on magnesium (Jones and Harris 1963, Crossland and Jones 1972). The reasons for the disparity are not known, other than the fact that the constant microstructure and steady state required in theory are not found in practice. However, the fact that n has a high value supports the view that the mechanisms taking place must involve slip and dislocation processes, rather than processes involving diffusive mass transfer which give low values.

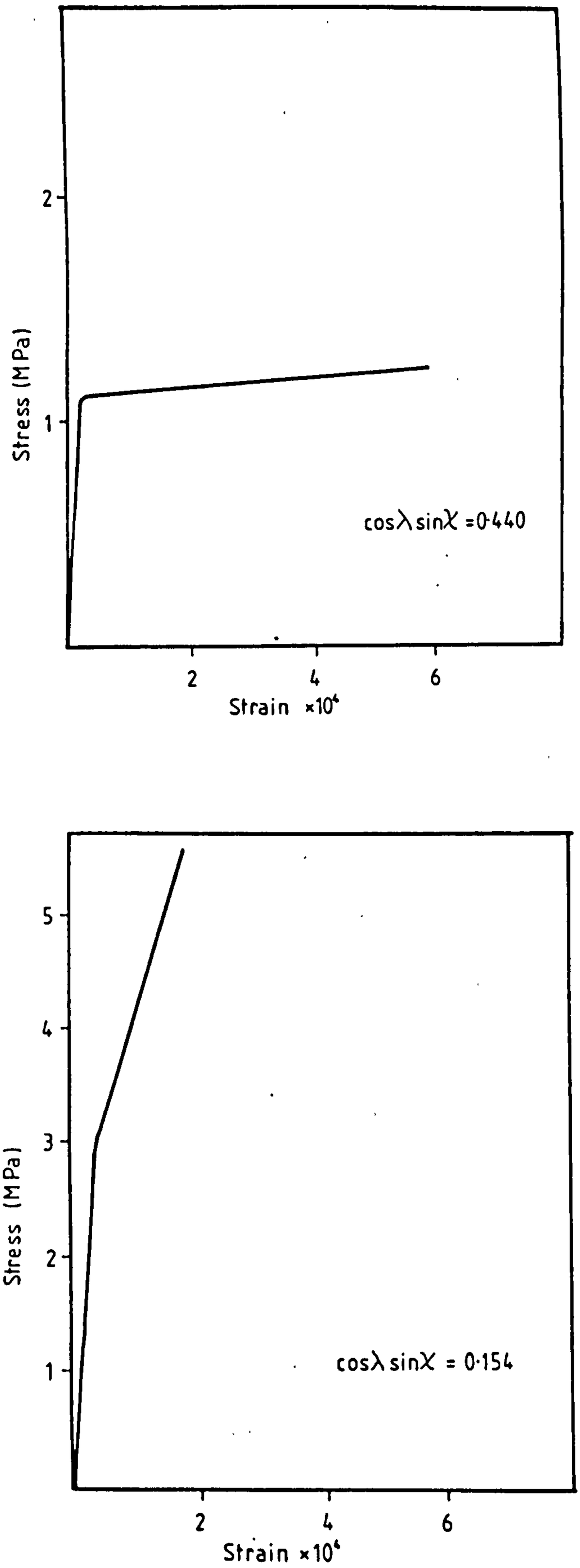


Figure 4.3 Orientation dependence of the flow stress of magnesium (after Burke and Hibbard 1952).

4.4.2. Twinning

The most common form of twinning in magnesium deformed in compression parallel to the basal plane is $\{10\bar{1}2\}$, as described in section 1. Since the preferred orientation of the starting material under study was such that the basal planes were oriented close to parallel to the extrusion direction of the supplied rod, it was expected that compressive deformation along this axis would result in $\{10\bar{1}2\}$ twinning, and a strong final texture. This was confirmed both optically and with X-ray goniometry. Figure 3.22 shows that virtually all the grains in the micrograph are twinned with only small patches of material in the original orientation at the old grain boundaries. The X-ray profile, Figure 3.36 shows that at 12% strain the twinned orientation is the only one detected. Twinning had resulted in a swing of $\sim 90^{o}$ in basal plane orientation which is in accord with the $(10\bar{1}2)$ mechanism. The mechanism was also confirmed in the EM work, Figure 3.23.

Specimens deformed at higher strain rates and lower temperatures exhibited a different type of twinning mechanism which was found to be $\{10\bar{1}1\}$-$\{10\bar{1}2\}$, Figure 3.52. Twinning on $\{10\bar{1}2\}$ results in a basal plane reorientation of 86.3^{o}, which means that the resolved stress on the basal slip system is not changed significantly and therefore slip within the twinned volume is not likely to contribute much to the overall strain. Thus the strain accommodated by $(10\bar{1}2)$ twinning is small. However, once this type of twinning has occurred it is thought that at the higher strain rates and lower temperatures, since other strain relief mechanisms cannot keep pace with the deformation, another type of twinning could occur. The double twinning mechanisms $\{10\bar{1}1\}$ followed by $\{10\bar{1}2\}$ reported by Couling et al (1959) and $\{10\bar{1}3\}$ followed by $\{10\bar{1}2\}$ reported by Reed-Hill (1960) occur under an opposite system of loading to $(10\bar{1}2)$ twinning, so once the specimen had twinned in the normal way it would be suitably oriented for either double twinning mechanism to occur. The $\{10\bar{1}1\text{–}10\bar{1}2\}$ mechanism was confirmed and many of these twins were found to contain recrystallised grains with high misorientations. In agreement with Wonsiewicz and Backofen (1967) this basal plane rotation in the recrystallised grains is thought to be induced by slip following the double twinning sequence. Wonsiewicz and Backofen suggested that intense basal plane shear would be likely to occur as a result of the double twinning process since the basal plane is rotated as it slips into alignment with the habit plane of the band, thus accounting for the voids present in some of the twins.

Adenis and Couling 1964 reported this type of twinning in Mg3%Al-1%ZnO.4%Mn sheet. When the material was deformed by alternate tension and compression there was a tendency for some grains to recrystallise with basal plane positions midway between the initial and twinned orientations. The authors speculated that this texture was formed by the double twinning mechanism $\{10\bar{1}1\}$ followed by $\{10\bar{1}2\}$.

4.4.3. Voids

At temperatures below 320°C the onset of recrystallisation was accompanied by the appearance of voids at triple points and along grain boundaries oriented parallel to the maximum shear stress. In the tests at 150°C and at the faster strain rates of 10^{-2} s^{-1} at 260°C they also occurred along $(10\bar{1}1)(10\bar{1}2)$ twins. Cavitation has been studied extensively in Magnox alloys because of the detrimental effect on the behaviour of reactor fuel element cans. The three main mechanisms of nucleation as cited in Section 1 are particle induced nucleation, cavities induced by grain boundary sliding and vacancy condensation. Irrespective of the initial nucleating mechanism cavity growth must occur by either vacancy condensation or by grain boundary sliding or a combination of the two. No attempt has been made to investigate the nucleation mechanism on a submicroscopic scale but certain conclusions about the formation of voids and their subsequent growth can be drawn from the microstructural studies in the current work. Both vacancy condensation and grain boundary sliding have been put forward as explanations for experimental rates of intergranular cavity growth. A detailed analysis of vacancy condensation was originally proposed by Hull and Rimmer, 1959 and it was suggested that the creep-ductility relationship of Magnox AL80 could be explained if cavity growth occurred by this mechanism (Harris 1965). On the other hand it has been concluded that void growth occurs by grain boundary sliding since it is not affected by temperature or grain size, Evans (1969), and the maximum percentage of voids coincides with the maximum number of grain boundaries regardless of strain rate (Byrne 1963).

The fact that the intergranular cavities assumed an elongated shape with increasing strain suggested that grain boundary sliding was contributing to the process. The irregular nature of the grain boundaries however would not favour this mechanism. The results of the experiments to illustrate the behaviour of grids on the surfaces of specimens have shown that sliding in the strict sense of the word is not responsible for

the voids in the current work, but neither is the mechanism one of vacancy condensation. The microstructural studies clearly point to a process more akin to ductile tearing in grain boundary regions. It must be remembered that in a dislocation creep regime grain boundary sliding is not simply the relative motion of two perfectly flat smooth surfaces. Real grain boundaries are uneven and any movement in their vicinity must involve migration and slip. This means that there will be a zone of accommodation and markers used to detect grain boundary sliding will not necessarily show the sharp offsets normally associated with the phenomenon. Whilst grain centres may have moved relative to one another, the zone of accommodation can be fairly wide and in this case grain boundary shearing would be a more appropirate terminology. The studies of the deformed polished surfaces showed that the lattice was severely bent and distorted in the vicinity of grain boundaries - particularly at triple points and along boundaries oriented obliquely with the compression axis. The behaviour is a direct result of the heterogeneous nature of the deformation because of the lack of available slip systems. At certain points in the specimen it becomes impossible to maintain compatibility across a boundary due to local constraints and grain boundary shearing is observed. The resulting voids elongate with increasing strain and coalesce to produce shear fractures typical of those observed in ductile rupture by a process of void coalescence. (Figure 3.72).

The intragranular voids which formed along $\{10\bar{1}1\}\{10\bar{1}2\}$ twins at low temperatures and high strain rates were thought to occur as a result of the intense basal plane shear which results from the twinning process, as suggested by Wonsiewicz and Backofen (1967).

Voids were absent in the high (>320^{o}C) temperature tests in agreement with other work on magnesium (Byrne 1963). This was to be expected as the deformation was more homogeneous and its accommodation in grain boundary regions was easier because of the operation of additional slip systems and the greater ease of recovery.

4.4.4. Dynamic Recrystallisation

4.4.4.1. Microstructural observations of dynamic recrystallisation at low temperatures

In agreement with other workers who have investigated dynamic recrystallisation (Sellars 1978, Roberts 1978), recrystallised grains can be detected in the microstructures of specimens deformed to just below the peak in the stress strain curve. They are found at grain

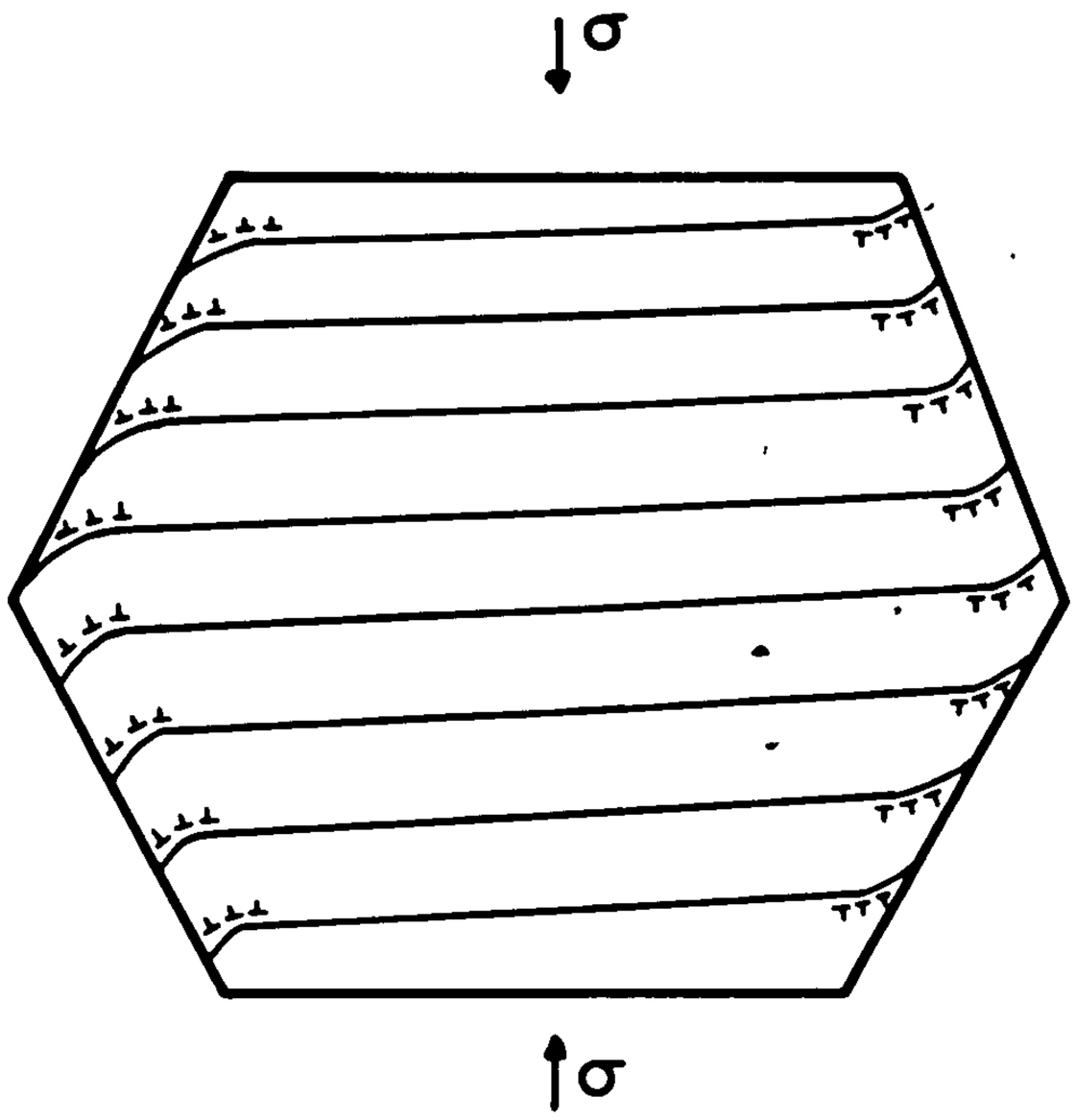
boundaries initially in regions where there are remnants of material in the old orientation (untwinned) or at triple points where one of the grains has been better oriented for slip. In the former case the accommodation difficulties at twin/grain boundary intersections result in these being preferred sites for recrystallisation and in the latter case recrystallisation is a result of the accommodation difficulties when slip is severely constrained.

Recrystallised grains eventually surround the old grains. As observed under the optical microscope they fall into two categories - firstly those recrystallised grains which are closely related in basal plane orientation to either twin or matrix being rotated by 4 or 5^{o} from these host orientations when they first appear. These recrystallised grains occur mainly on horizontally disposed boundaries with respect to the external compression axis. The second category of recrystallised grains have a high basal plane misorientation with respect to adjacent old grain and occur on boundaries oblique to the compression axis. In both cases recrystallisation is preceded by bulging of the old grain boundaries. The bulges are similar in size to the recrystallised grains and are misoriented from adjacent lattice. The mechanism of recrystallisation then is not solely one of strain induced boundary migration (SIGBM) since other processes must take place to account for the high misorientations which occur about a single axis at the old/new interface.

4.4.4.2. A qualitative model for dynamic recrystallisation below $320^{o}C$

The preferred orientation of the starting material is such that even when twinning ($\{10\bar{1}2\}$ type) has occurred the resolved shear stress on the basal system remains virtually unchanged. However, basal slip is by far the easiest means of accumulating strain but this results in severe accommodation problems in the grain boundary regions which are likely to become points of stress concentration. The constraints imposed at the grain boundaries and slip on only the basal system generates an excess of dislocations of one sign at opposite ends of the slip plane and this results in lattice rotations in the mantles leading to dynamic recrystallisation. Where the rotations are high which is along boundaries obliquely inclined to the stress axis the process is more akin to kinking. Schematic diagrams of the process are shown in Figures 4.4 and 4.5.

It is assumed in the mechanism that slip occurs on one system - in this case the basal system. Slip within a grain generates dislocations which move towards the boundaries and result in pile ups. Strain energy



Lattice rotations which occur as a result of boundary constraints and limited slip are accommodated by geometrically necessary dislocations.

Figure 4.4. Schematic diagram to illustrate the kinking process.

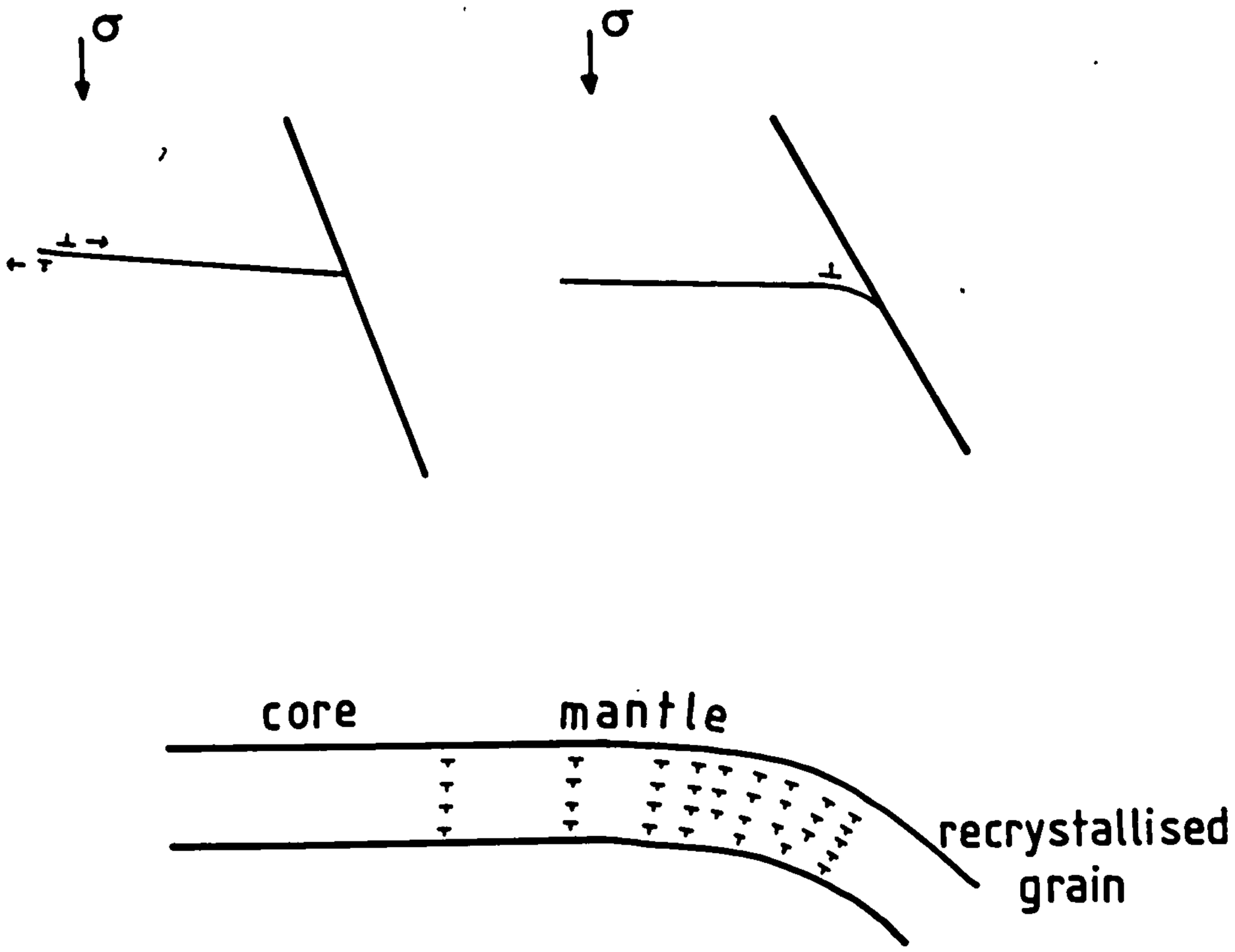
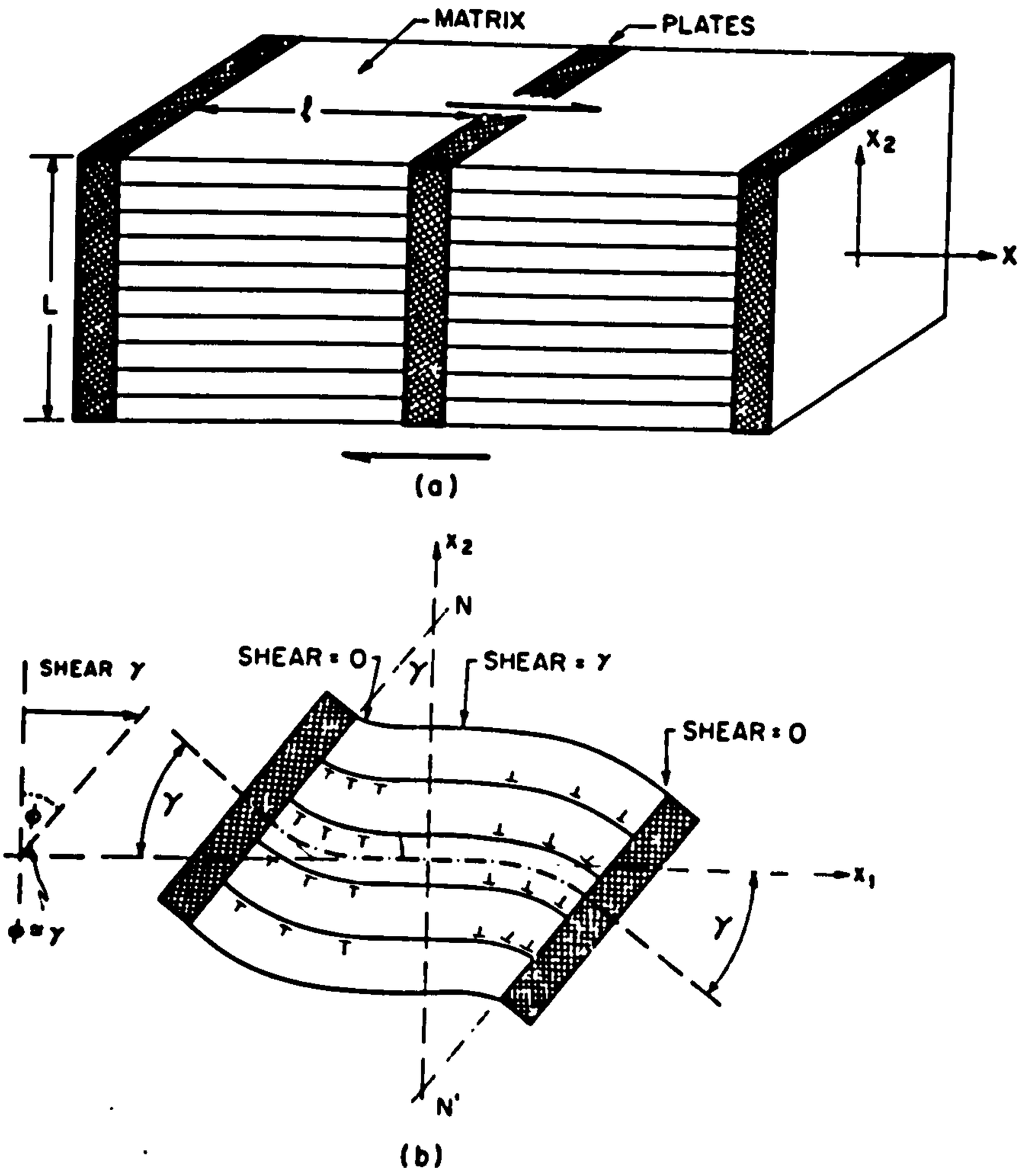


Figure 4.5. Schematic diagrams of the recrystallisation process. The constraints imposed at the grain boundaries and limited slip result in lattice rotations in the mantles. Where the rotations are high, this process, together with limited recovery, leads to dynamic recrystallisation at the old grain boundaries.

is relieved by the kinking of the lattice and is accommodated by an excess of dislocations of one sign and by dynamic recovery, the amount depending on the temperature. The angle of kinking increases to a point where the kinked material can no longer be called a subgrain but is recognised as a grain in its own right.

The process is somewhat similar to that put forward by Ashby (1970) who considered the deformation of plastically non-homogeneous materials. The deformation of a model composite consisting of non-deforming plates strongly bonded to a single crystal was investigated. A diagram of the process is shown in Figure 4.6.. Ashby assumed that the plates were rigid (i.e. non-deforming) and that the matrix was strongly bonded to them. Thus no dislocations could enter the particle matrix interface and no sliding could occur in the plane of the interface. It was assumed that the composite sheared by slip in the matrix on a single system in a direction normal to the plate surface as shown in the diagram. The central part of each slip plane sheared by an amount γ but since its ends were bonded to the plate they were prevented from shearing. The shear in the matrix immediately adjacent to a plate would therefore be zero and there would be a gradient of shear on the slip system of γ/Ll_2. This gradient would result in a rotation of the plates through an angle relative to the original slip plane normal and a curvature of the matrix lattice.

In polycrystalline magnesium where compressive deformation results in slip on the basal planes and the majority of the grains are unfavourably oriented then the grain boundaries act as similar barriers to the slip process as the plates to the shear in the model described above. The interior of each grain deforms by basal slip and the lattice is rotated in a region on either side of a grain boundary. If a single grain in the polycrystalline aggregate is considered the amount of rotation at the boundaries will depend not only upon the strain accommodated by slip in that grain but also upon the behaviour of its neighbours. If it is easy to propagate slip across a grain boundary (as will be the case when an adjacent grain is favourably oriented for slip) then the rotations will be smaller, whereas in grains where adjacent neighbours are unfavourably oriented and themselves not deforming then the rotations will be high. If adjacent grains are unfavourably oriented for slip to propagate across the boundary but are themselves deforming then implicit in this the rotations will necessarily be of a complex nature. These latter two are likely to result in incompatibilities at the boundaries and eventual



(*a*) A model composite consisting of non-deforming plates strongly bonded to a single-crystal matrix. At (*b*) the matrix is sheared on a single slip system; close to the plates it cannot shear and must therefore rotate.

Figure 4.6. Deformation of a model composite. (Ashby 1970).

boundary shearing.

The operation of these mechanisms would result in the following microstructural observations.

1. Evidence for extensive activity on the basal slip system.
2. High lattice misorientations along boundaries parallel and oblique to the stress axis in unfavourably oriented old grains.
3. Low lattice misorientations along boundaries normal to the stress axis and those where adjacent old grains are favourably oriented for basal slip.
4. A high proportion of subgrain walls in the form of straight tilt boundaries lying normal to (0001).

4.4.4.3. Experimental evidence for the model

Evidence in support of these predictions has been sought and confirmed. The extensive electron microscopy showed that a Core and Mantle structure was frequently observed in that the centres (cores) of the old grains had high dislocation densities consisting mainly of dislocations with basal burgers vectors lying in the slip plane and little evidence for subgrain formation. The mantles showed more evidence of subgrain formation mainly in the form of straight tilt boundaries trending along planes normal to basal glide planes.

Both the optical and the transmission and scanning electron microscopy have verified predictions 2 and 3. The misorientations measured at grain boundaries in the transmission electron microscope agreed with those determined optically. The misoriented regions coincided with bulges in the old grain boundaries. The reflected polarised light microscopy enabled easy determination of the relative orientations of the basal planes in old and new grains. The highest misorientations were recorded along boundaries oblique to the stress axis and TEM showed that they often occurred across a single boundary of edge dislocations. (Figure 3.34).

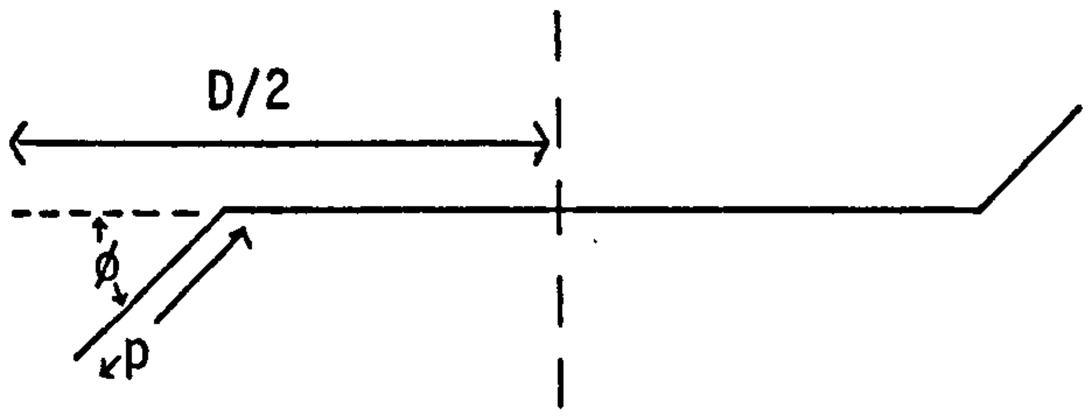
The scanning electron microscopy and optical microscopy of the deformed surfaces provided convincing evidence for the kinking mechanism in that boundaries oriented other than normal to the compression axis showed severe lattice bending whilst those normal to the applied compression direction showed little evidence of distortion.

It is suggested then that the kinked (or rotated) regions form the nuclei in the dynamic recrystallisation in magnesium. In effect the mechanism is one of SIGBM (to account for the bulges in the old grain boundaries) combined with large lattice rotations in the mantles to

accommodate slip in the grain centres. The model has obvious limitations in that it is essentially qualitative and it assumes that basal slip and glide polygonisation are the only operative mechanisms.

Semi quantitative estimates of the contribution of the kinking process to the overall strain can be made but they are really only applicable below 260°C as above this temperature the deformation is not as heterogeneous and other mechanisms such as slip on other systems and recovery play a greater role in strain accommodation. The greater activity of other systems and recovery at higher temperatures is manifested in the width of the mantles which are wider at higher temperatures and contain larger subgrains. The major component of the rotation still tends to occur across a single boundary as from energy considerations one boundary with a high misorientation has a lower energy than several boundaries with low misorientations.

If kinking is assumed to be the only mechanism accommodating strain then it is possible to calculate its contribution to the overall deformation.



If the kinked region at the edge of a grain has a width p and the process is assumed to take place in two dimensions

Then for a single grain

$$\gamma = \frac{2p \sin \phi}{D}$$

where γ is the shear strain

D is the grain diameter

p is the normal width of the kinked region

ϕ is the angle through which the mantle is kinked.

If this is typical of all grains then γ represents the shear strain of the whole specimen.

Taking as an example a grain size of 400μm and a mantle width of 20μ and a kinking angle of 45° (which is common at 260°C)

Then $\gamma_T = 0.07$.

This gives a shear strain of 7% and since the kinking angle assumed was 45° a shortening of 7%.

This value is realistic as the sample which was chosen in the example had undergone a bulk strain of 25%. Recrystallisation was only evident beyond 16% strain so the bulk strain and the strain relieved by kinking and consequent recrystallisation together accounted for 92% of the imposed strain. The anomaly can be accounted for in that the assumptions made to carry out the calculation grossly oversimplify the situation.

4.4.4. Kinking

In view of the importance of the kinking process, it is worthwhile diverging at this stage to review the literature investigating kinks. Kinking is an inhomogeneous mode of deformation which is observed on both a macro and micro-scopic scale (Gilman 1954). The phenomenon is well known in long single crystals of hexagonal metals such as zinc and cadmium which are grown with the glide plane (0001) nearly parallel to the wire axis. In this orientation the usual glide mechanism is unfavoured under the action of tensile or bending loads. If compressive loads are applied, the crystals suddenly collapse forming kinks with sharp ridges and regular curvatures (Gilman,1969). Orowan 1942 was one of the first workers to study kinking. He carried out X-ray metallography on single crystals of cadmium and showed that the kink had the structure shown in Figure 4.7a. In the curved regions the lattice is subjected to flexural glide and the deformed crystals contain the planes KK^1 in which the glide lamellae are so sharply bent that they appear broken. The plane of kinking K need not be a crystallographic plane.

Most of the information about kinks arises from ancilliary observations associated with studies of slip and twinning, and until recently, little experimental work has been carried out specifically to elucidate the properties of kinks. After the first observations about kinks by Orowan, similar features were recorded in materials with other crystals structures, but there is some confusion in terminology since "kink band" has often been included in the more general phenomenon of "deformation band". Honeycombe 1968 discusses kinking in hexagonal crystals and states the strict geometrical conditions necessary for their formation. These are summarized below.

i) Kinks form gradually during compression of the crystal by a progressive rotation of the lattice. The rotations may be as little as a few degrees or as high as 80^{o}.

ii) In general kinking does not occur in compression if the angle between the slip plane and the axis is $<2.5^{o}$ but it does occur readily in the range $2.5 - 24^{o}$. The form of the kinks is not well defined at the higher angles.

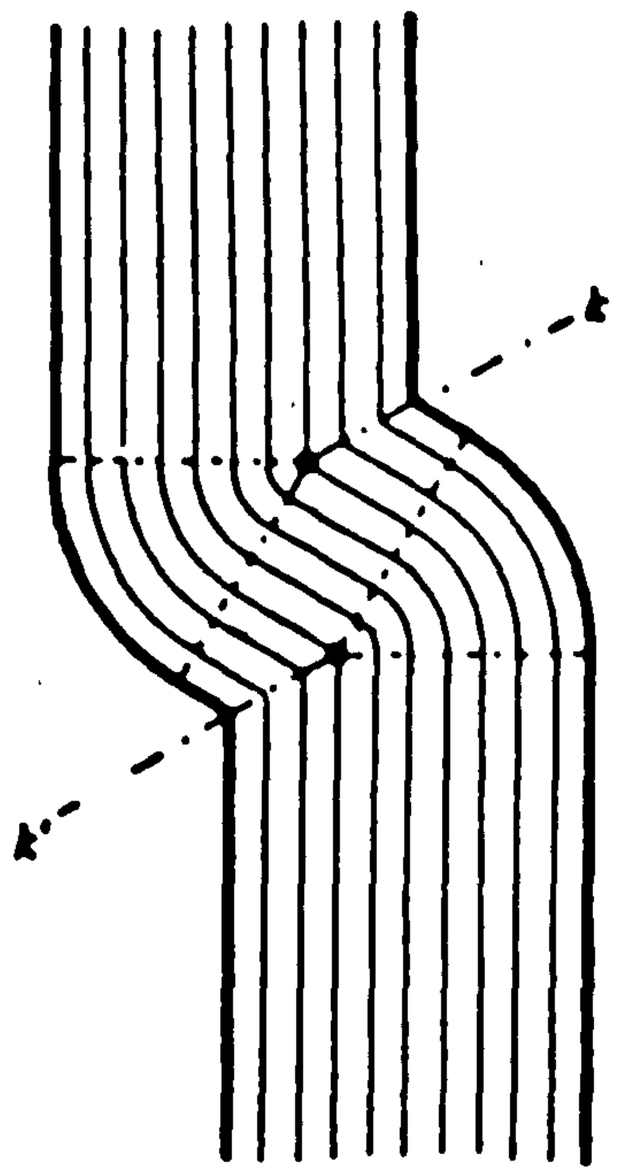


Figure 4.7a. The mechanism of kinking (from Orowan 1942). The thin parallel lines represent the glide planes. On compressing parallel to the glide planes the crystal suddenly collapses in the way shown so that the planes of kinking (dash-dotted lines K and K'), the slip planes are sharply bent. The broken lines indicate the boundary of wedge shaped regions of flexural glide.

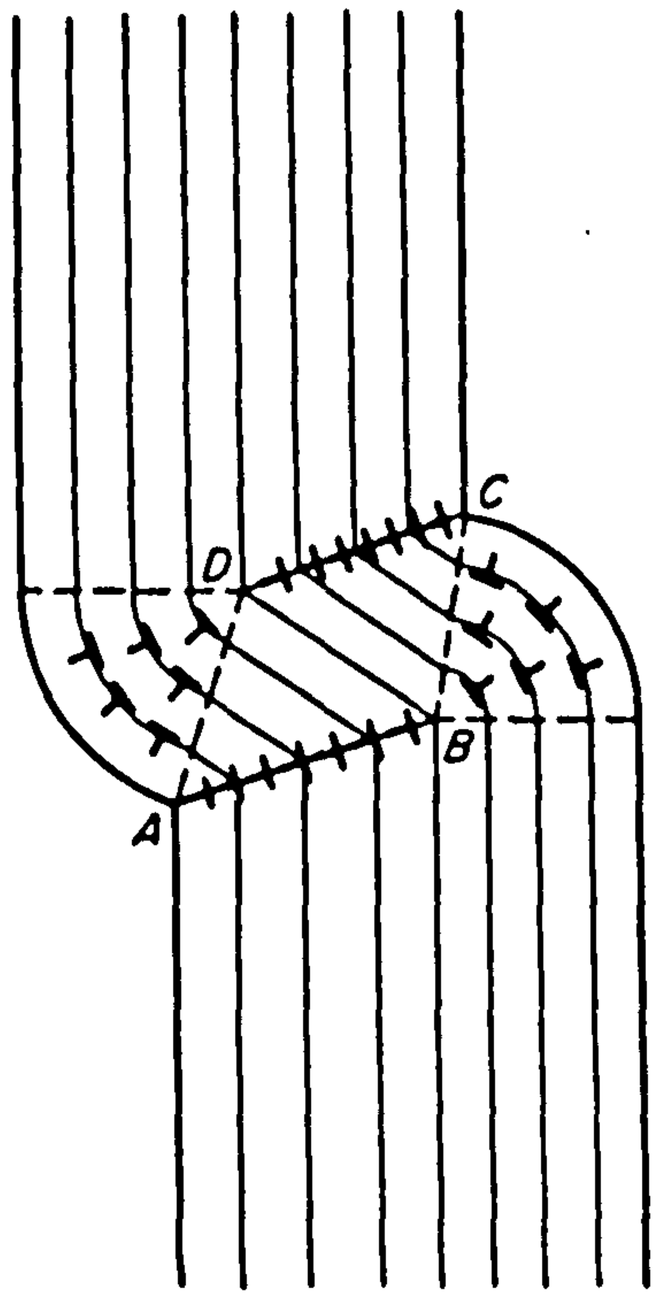


Figure 4.7b. Schematic diagram to illustrate the dislocation distribution in a kinked crystal (Honeycombe 1968).

iii) The process is reversed on application of a tensile stress to the kinked crystal.

iv) Referring to the schematic diagram illustrating the dislocation distribution in a kinked crystal, two regions of severe lattice curvature are separated from each other and the unkinked crystal by well defined kink planes AB and CD which are walls of edge dislocations. The curved regions contain an excess of dislocations of one sign. This causes the marked X-ray asterisms observed in Laue photographs. They are also preferred sites for polygonisation and recrystallisation on annealing.

v) Kink bands also occur during tensile deformation of hexagonal metals particularly in regions near the grips or in the vicinity of heavy scratches.

vi) The bands are thought to nucleate at inhomogeneities which block dislocations on several adjacent slip lines, leading to local curvatures which in turn interact with dislocations on other slip planes and cause the lateral growth of the band.

It was suggested that the dislocation structure in a kink band is similar to that of a tilt polygonisation boundary with the exception that kinks can form and cause large misorientations at temperatures where rapid climb of dislocations is not possible (Honeycombe 1968). Thus kink planes are formed by the rapid feeding in and planar arrangement of glide dislocations on the basal slip plane, in other words by glide polygonisation. The formation of these kink planes also helps to relieve stresses set up by twin formation.

The recent investigations into the formation of kinks has involved the use of a range of experimental techniques including HVEM. One or two of the more relevant papers will be reviewed below. The formation of kinks has been explained in terms of geometrical softening of the active slip systems and the results are consistent with an analysis by Crocker and Abell (1976) who developed a scheme to classify kinking in all crystalline materials. Fraser, Smallman and Loretto (1973), studied kinking of single crystals of NiAl stressed along <001> and showed it to be a result of geometrical softening of the <001> {110} slip systems. Later work by Tapetado and Loretto (1976) on single crystals of Zn also discussed the factors governing the deformation behaviour in terms of geometrical softening of the slip systems. These authors found that crystals compressed along directions close to $<1\bar{1}00>$ and $<11\bar{2}0>$ deformed in two ways. Firstly by kinking without significant prior plastic deformation;

these crystals contained only dislocations of $\underline{b} = \frac{1}{3}\langle 11\bar{2}0\rangle$. Secondly by plastic buckling (or kinking after a high strain) in which case dislocations of $\underline{b} = \frac{1}{3}\langle 11\bar{2}0\rangle$, $\frac{1}{3}\langle 11\bar{2}3\rangle[0001]$, were analysed. When the compression direction is sufficiently far away from the basal plane and kinking occurs the only dislocations involved have $b = \frac{1}{3}\langle 11\bar{2}0\rangle$. Also the rotation of the crystal within the kinked region is such that the angle between the compression direction and the basal plane increases and hence the stress on the $\langle 11\bar{2}0\rangle(0001)$ slip systems increases. Tapetado and Loretto (1974) interpreted the kinking behaviour in the following way.

Assuming that the only slip system operative in zinc is $\langle 11\bar{2}0\rangle(0001)$ the fraction of the applied stress τ/σ acting on the $\langle 11\bar{2}0\rangle(0001)$ system increases as the angle between the slip plane and the compression direction increases. Hence if a zinc crystal is aligned in such a way that the angle between the compression direction and the slip plane is close to zero, the deformation can occur under a falling load as the compression axis rotates towards [0001]: geometrical softening can occur. Tapetado and Loretto thus concluded that if kinking is due to the operation of $\langle 11\bar{2}0\rangle(0001)$ slip a load drop may be expected during the formation of the kink and the deformation would tend to become localised.

Kinking in single crystals occurs because the constraints imposed by the deformation conditions result in a special kind of accommodation problem, i.e. immovable ends and the operation of only one slip system oriented close to parallel with the compression direction force kinking to occur as a means of relieving strain energy.

In the case of the magnesium polycrystals with a strong preferred orientation such that the basal planes are aligned close to parallel or perpendicular to the compression direction then the constraints imposed by similarly oriented neighbouring grains and the high strain hardening due to the orientation of the basal planes result in high rotations of the lattice at grain boundaries. The mechanism operates to relieve strain energy in the absence of other means. Although the geometry of the process with respect to external stress axes may not be the same the reasons for their operation are thought to be similar in both cases, i.e. the lack of independent slip systems and constrained deformation, cause high lattice rotations produced as a result of slip on one system and its internal accommodation.

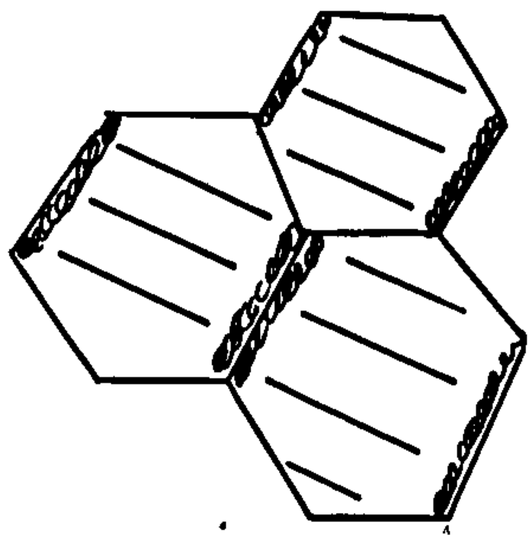
4.4.5. Shear Zones

4.4.5.1. The formation of shear zones

After dynamic recrystallisation has occurred, the stress strain curve of the bulk sample exhibits a negative strain hardening with increasing strain. This is particularly marked in samples which have developed a macroscopic shear zone. The shear zones in the magnesium are zones of mainly fine recrystallised grains favourably oriented for basal slip and shear. A schematic diagram of the process is shown in Figure 4.8. The recrystallised grains at the old grain boundaries form as a consequence of the kinking and lattice bending which occurs at the old grain boundaries. The new grains are favourably oriented for basal slip, and shear - particularly along those boundaries supporting a high shear stress. These processes are prevented from playing a major part in the overall deformation by the constraints imposed by neighbouring grains (a). The major activity continues to take place in the old grains causing further lattice rotations and consequent recrystallisation at the old grain boundaries until sufficient recrystallised grains have been nucleated to form a continuous line across the specimen. Any discontinuities in the line will be overcome by high local stresses which must be concentrated at the tip of each recrystallised section (b). Catestrophic shearing is then able to occur (c). Most of the further deformation imposed on the sample is accommodated in the zone. The evidence for this is threefold:

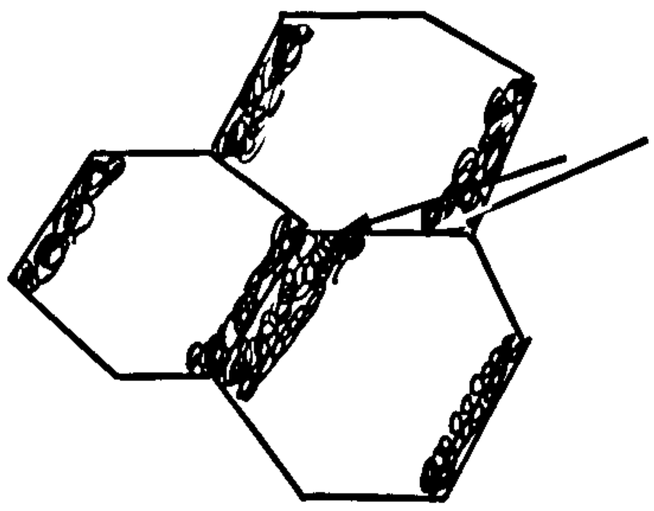
1. The shape of the old grain (allowing for the recrystallised grains at the boundaries) does not reflect the overall strain.

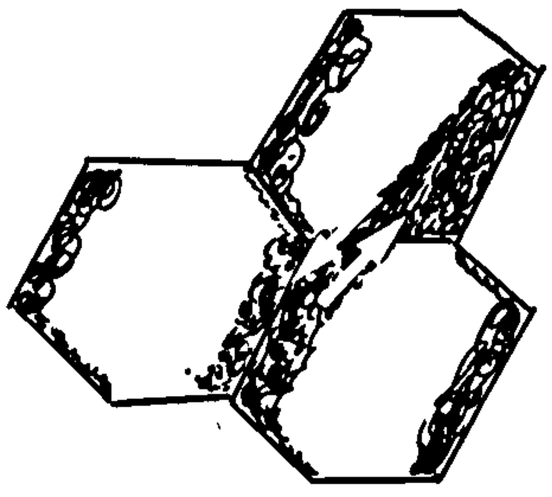
2. The volume of kinked material in the sample cannot alone account for the remainder of the strain accommodated. As an example a sample which had undergone a total strain of 65% at 260^{o}C has been considered. There was more than one layer of recrystallised grains around many of the old grains so it was assumed that the sample had undergone 5 kinking events (an overestimation since the recrystallised grains were not 5 deep at each old grain boundary). The initial old grain size was 400μm and the recrystallised grain size 20μm. The kinking angle was assumed to be 45^{o} for the purposes of the calculation although there was a variation of ±15^{o} at many boundaries. Recrystallisation as determined from other tests at the same temperature could be detected at 16% strain. Thus the sum of the strain accommodated by kinking and that accommodated prior to recrystallisation was 35% + 16%, i.e. 51% in total. (i.e. a shortfall of 14%).



(a)

(b)





(c)

Figure 4.8. Schematic diagram to illustrate the formation of a shear zone in magnesium.

3. The concentration of deformation in the shear zones, particularly at lower temperatures, is high enough to result in macroscopic shearing of one half of the sample with respect to the other and visible offsets at the specimen surface (Figure 3.74).

It can be concluded that the deformation is concentrated in the shear zones once they have been initiated and therefore there must be a strain rate acceleration within them.

4.4.5.2. Strain rate acceleration in shear zones

An order of magnitude calculation has been carried out to estimate the strain rate acceleration in a shear zone in a typical sample deformed at 260°C, Figure 3.66

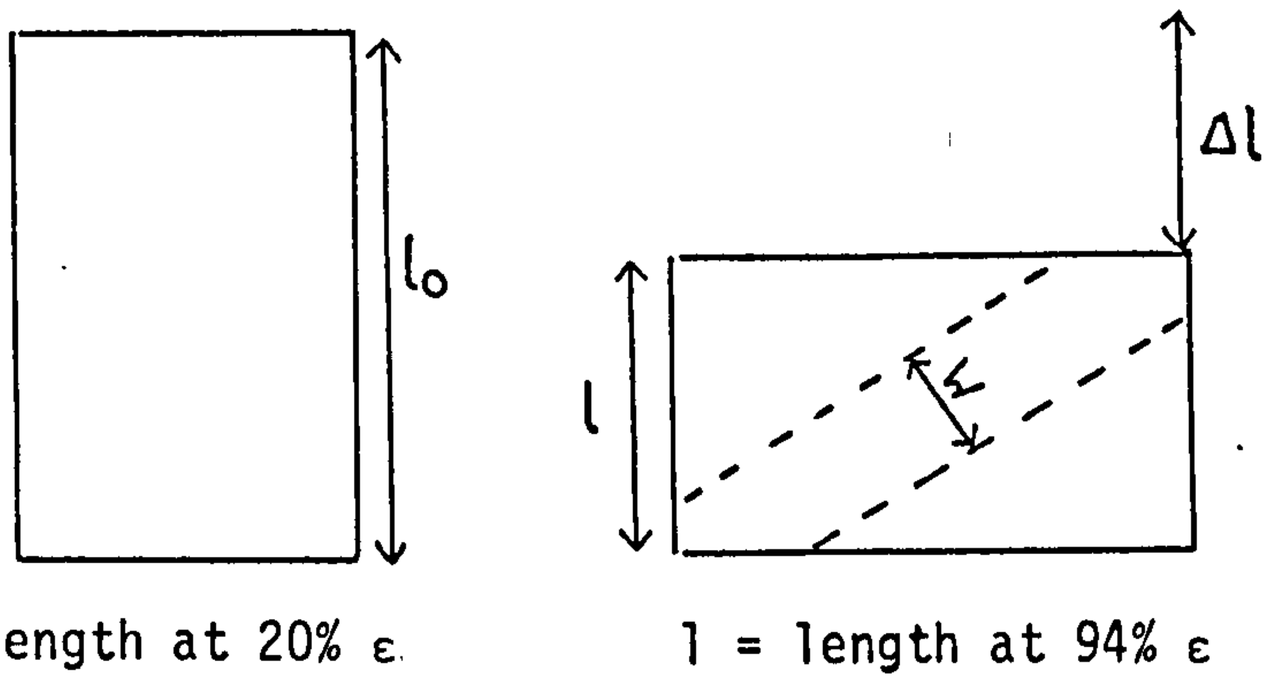
The overall strain on the sample was 94%. It was assumed that the shear zone had taken up most of the deformation beyond 20% strain. The angle the macroscopic zone made with respect to the compression axis was 45°.

$$\text{Thus } \frac{d\gamma}{dt} \text{ shear zone} = \frac{d\varepsilon}{dt} \text{ shear zone} = \frac{\frac{\sqrt{2}\,\Delta l}{w}}{t} = 4 \times 10^{-4}\ s^{-1}$$

where Δl = the change in length of the specimen once the shear zone formed = 13 mm

w = the width of the shear zone = 3 mm

t = time



l_o = length at 20% ε l = length at 94% ε

The duration of the test was 6.3 hrs which meant that the average plastic strain rate was $4 \times 10^{-5}\ s^{-1}$.

This meant that the strain rate in the shear zone was an order of magnitude higher than that imposed on the bulk sample by the motion of the crossheads of the test rig.

This calculation obviously gives only a rough estimate of thestrain rate acceleration since it assumes that the deformation was all being accommodated by the shear zone whereas some, albeit small, will have been accommodated in the remainder of the sample. It also assumes that the zone was uniform whereas as pointed out in Section 3, mostwere in fact 'composites' and consisted of several smaller zones which had impinged on one another. Thus there is likely to have been a variation in strain rate a) across the macroscopic zone b) during the duration of the test.

4.4.5.3. Mechanisms of deformation within the shear zones

The shear zones are geometrically softer than the old grains in that they are favourably oriented for basal slip and shear which are likely to be the dominant processes. The shape of the recrystallised grains in the shear zones however did not reflect the high strains accommodated in these regions. This indicated that either continuous dynamic recrystallisation was occurring in addition to slip and shear, or that the deformation mechanism had changed to a mechanism similar to that found in superplasticity where grain boundary sliding was contributing to the accommodation of deformation. This possibility has been considered. Although the high incidence of voids along samples containing single well developed zones pointed to grain boundary sliding as a contributory mechanism of strain accumulation the studies of the behaviour of grids on specimen surfaces rules this mechanism out. As was discussed in Section a sample was pre-strained to initiate a shear zone: a grid was then superimposed on the polished surface and the sample strained a further 20%. Most of the deformation was accommodated in the shear zone, the grid was virtually undistorted elsewhere in the sample. Macroscopic shear had occurred in the centre of the shear zone resulting in a line of elongated voids along its length and grid discontinuity in their vicinity. The behaviour of the grid is shown schematically in Figure 4.9. No offsets could be detected at grain boundaries within the zone, the only large distortions occurring at the edges of the shear zone where the grid units showed high rotations, and adjacent to the voids where shearing was evident. The microstructure of the voids was typical of that observed in ductile tearing. Planar offsets indicative of grain boundary sliding have not been detected in these experiments: this observation together with the very strong texture present in the shear zones would seem to indicate that a 'superplastic' type of mechanism where a weakening of texture would be expected is not operative. Experiments were also carried out on the alloy Zr55 where the presence of zirconium hydride precipitates

in the form of stringers acted as internal markers. The details of the experiments are reported in Appendix D but the main result is discussed here. The main purpose of the work was to see whether or not the markers showed evidence for grain boundary sliding and to determine if the surface markers presented a realisaic picture of the internal deformation. Figure D2 shows a macroscopic view of a sample which had developed a shear zone. The material in the zone is rotated by 45^{o} with respect to the outside of the zone, the major rotation occurring at the zone boundaries in agreement with the surface studies.

It is suggested that basal slip and shear are the main mechanisms operating in the shear zones but since the boundaries are not smooth and the texture imperfect then climb and the operation of other slip systems, e.g. $\overrightarrow{c + a}$ must contribute to the deformation process if compatibility is to be maintained. Continuous dynamic recrystallisation must also occur to maintain the constant equiaxed grain sixe throughout the zone.

4.4.5.4. Effect of temperature

It has been observed that the shear zones are narrower at lower temperatures and contain a high volume fraction of voids. The shear zones in magnesium are 'soft' compared with the rest of the sample and the strain rate acceleration which occurs within them should be reflected in the microstructure. If it can be assumed that for a thermally activated deformation process an increase in strain rate is equivalent to a decrease in temperature then it is possible to calculate this decrease approximately given that the standard flow law

$$\dot{\varepsilon} = A\sigma^{n} \exp(-\frac{Q}{RT})$$

applies.

The pre-exponential term is assumed to be constant.

The activation energy Q is assumed to be that calculated for the deformation process in magnesium (Section 2.1), i.e. 25 Kcal/mol.

R, the universal gas constant = 2 cal/g^{o}K.

Now

$$\ln \frac{\dot{\varepsilon}_1}{\dot{\varepsilon}_2} = \frac{Q}{R} \left(\frac{T_2 - T_1}{T_2 T_1}\right)$$

The value of T_2 is taken as $260^{o}C = 533K$

The strain rate acceleration at this temperature is assumed to be an order of magnitude (as estimated in the preceding paragraph).

$$\therefore \quad T_1 = 485K$$

Thus a strain rate increase of an order of magnitude at 260°C would be equivalent microstructurally to a temperature decrease of 48°C. This calculation, although an approximation, does reveal that a significant effect on microstructure can be expected in shear zones due to strain rate acceleration. It explains the high incidence of voids along the shear zones since climb and slip mechanisms other than basal will be more difficult and macroscopic shearing is more likely to occur.

At low temperatures, e.g. 150°C, where climb and other slip mechanisms are difficult before the shear zones form, there is already a high incidence of voiding and cracking at the old grain boundaries due to incompatibilities at early stages in the deformation process. Thus when a path for shear eventually forms across the sample since it already contains a high volume fraction of voids, the strain rate acceleration in the zone accentuates the voiding and catastrophic shear results.

In conclusion, shear zones in magnesium form as a consequence of the heterogeneous deformation forced to occur, as a result of crystal anisotropy and the lack of independent deformation modes necessary to accommodate the strain. Kinking of the lattice at grain boundaries leads to the formation of closely related recrystallised grains favourably oriented for basal slip and shear. Once a shear zone has been initiated by a local stress concentration it propagates across the sample and offers a virtually unrestricted path for basal glide and shear resulting in a strain rate acceleration and concentration of further deformation in the zone. The width of a particular zone will depend on local heterogeneities within a sample for a given temperature and strain rate. At low temperatures the zones are narrow because the lack of means to accommodate the lattice bending at the boundaries results in a high incidence of voids, preferential development of one zone and eventual specimen failure.

4.4.5.5. Effect of external constraints

It is worthwhile mentioning the effect of deformation conditions on the initiation and development of shear zones in Magnox AL80. The formation of the zone is a result of the very heterogeneous deformation which occurs as samples are compressed uniaxially. It is particularly marked in samples unfavourably oriented for slip where the zones develop at ~20% strain. The relative ease of basal slip in magnesium means that polycrystalline deformation is forced to be heterogeneous. Some grains are always more favourably oriented for slip than others - even in a highly textured sample - which means that slip is able to occur within them at

lower stresses. If surrounding grains are in harder orientations then stress concentrations arise at the boundaries. The strain is accommodated by lattice rotations which are highest along boundaries parallel to the maximum shear stress. The rotated regions are geometrically softer than surrounding material and are therefore preferred zones of deformation. Once a zone of 'softer' material has propagated through the sample extensive slip and shear is able to occur within it. The operation of these processes depends upon the constraints applied to the specimen. If the ends of the sample are friction free then a shear zone does not develop. This condition is achieved by placing PTFE tape between the sample and the pistons. If the specimen has a length:diameter ratio greater than ∿1.2:1, then it physically rotates between the pistons of the test rig as the crosshead descends until it reaches the most favourable orientation for basal slip (Figure 4.9). If the length:diameter ratio is less than ∿1.2:1 then extrusion occurs at the piston contacts with the sample (Figure 4.10). In both these cases recrystallisation at the old grain boundaries is limited and in the former case in particular the microstructure after 55% strain is similar to that reported in Section 3 for a sample initially oriented favourably for basal slip.

Shear zones develop in the magnesium

a) Because uniaxial compression of samples unfavourably oriented for basal slip when this is the dominant deformation mechanism results in a heterogeneous microstructure containing zones of texturally softer material.

b) Only if there is sufficient friction at the pistons deforming the sample to prevent it rotating between them or flowing preferentially at the interface between them and its ends.

c) When local stress concentrations (often but not always, at the specimen-piston contacts) are high enough to cause the zone of favourably oriented material to propagate across the sample.

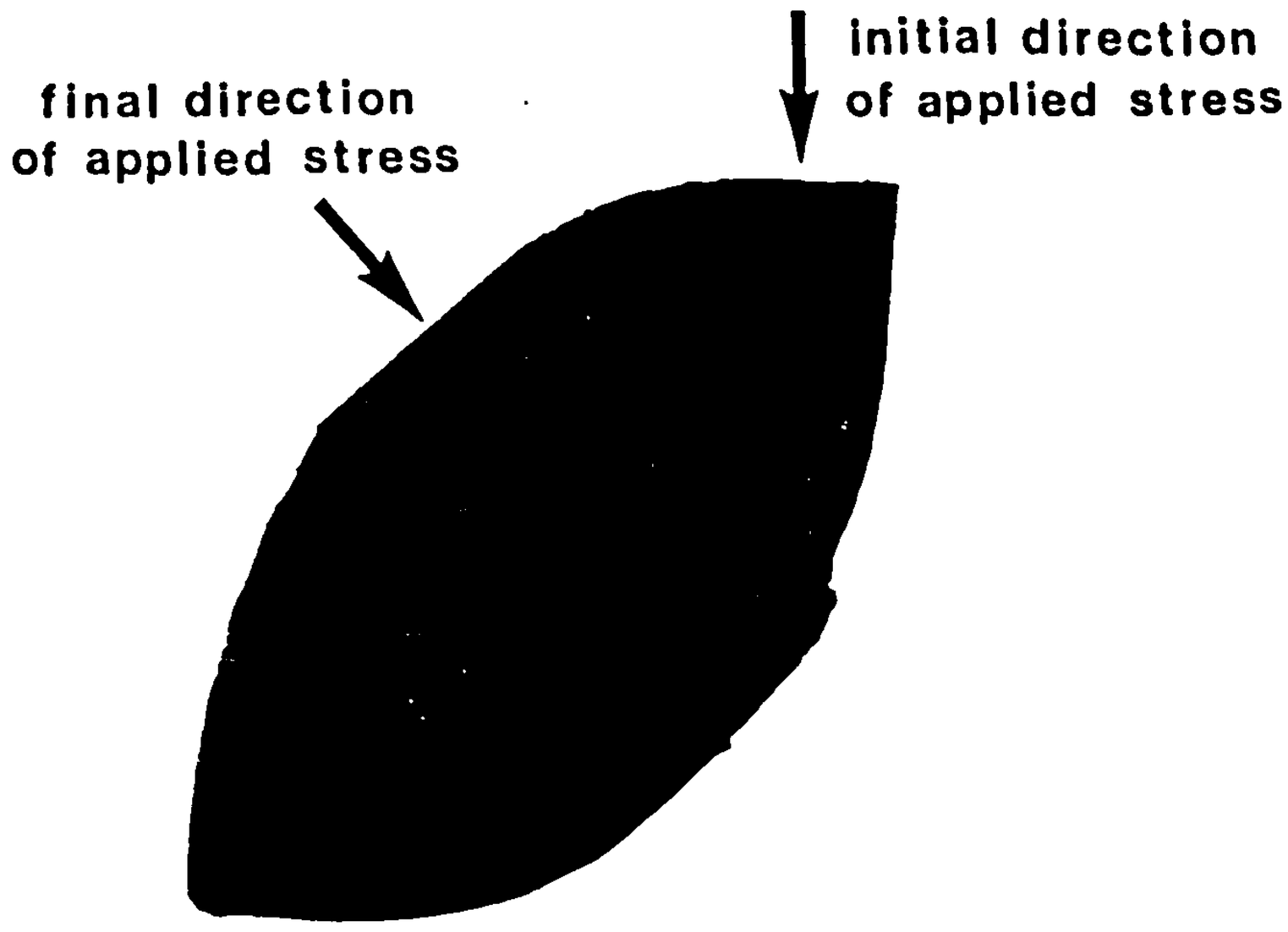


Figure 4.9. Enlarged shadow mask of a specimen deformed at a strain rate of $10^{-5}s^{-1}$ at $260^{o}C$. The ends of the specimen were lubricated with P.T.F.E. It can be seen that it rotated between the pistons of the test rig as it was being deformed.



Figure 4.10. Enlarged shadow mask of a specimen deformed under the same conditions as that in Fig.4.9. The difference in this case was that the length : diameter ratio of the sample was less than 1.2 : 1. The specimen has extruded at the piston contacts during deformation.

CHAPTER 5

Geological Implications of the Deformation Behaviour of Magnesium

5.1. INTRODUCTION

The study of the mechanical behaviour of rocks under stress and of the processes on an atomic scale responsible for their behaviour is becoming increasingly important to geologists. A knowledge of the deformation behaviour of rocks is necessary before any interpretation or predictions can be made concerning the mechanisms responsible for the observed large scale tectonic movements which have taken place in the past and are still occurring today. The deformations of interest range over many orders of magnitude in strain rate; from the high strain rates of 10^{7} - 10^{9} s^{-1} associated with meteorite impact to the slow tectonic deformations of 10^{-10} - 10^{-15} s^{-1} associated with mountain building.

The importance of plastic deformation, which is well documented in the metallurgical literature, has been recognised in the deformation of both crustal and mantle rocks and in recent years there has been extensive interaction between structural geologists and physical metallurgists. This is evidenced by the interdisciplinary nature of three recent international meetings in London (Phil. Trans. Royal Soc. Lond. A 288 1-236 1978) Leiden (Tectonophys 39 no 3-4 1977) and Perros Guirec (Bull Mineral 102 no 2-3 1979). In many respects the aims of the two disciplines are similar: the crystallographer and mineralogist attempt to determine crystal structure whilst the physical metallurgist and geologist explain microstructures and these two inputs are used by the engineer and tectonophysicist to formulate constitutive equations. The engineer seeks to predict the behaviour of components and the tectonophysicist seeks to predict future Earth movements and to explain those that have taken place in the past. There is however one major difference and that is that geologists cannot perform experiments at the strain rates of 10^{-10} - 10^{-15} s^{-1} known to be responsible for many naturally deformed structures and they therefore have to adopt a forensic approach to their studies. Once ties between microstructural observations and macroscopic behaviour had been well established, geologists were quick to notice similarities between minerals and metals deformed in conditions of creep and hot working. As a result metallurgical analogues have been used to explain geological observations and techniques developed primarily by metallurgists have been adopted in studies of microstructures and textures (fabrics) of deformed rocks e.g. X-ray goniometry (Baker et al 1969) and transmission electron microscopy (White 1976). Whilst much relevant data can be obtained from studies of naturally deformed rocks this data must be evaluated with reference to controlled laboratory experiments. This

poses many problems not the least of which is that laboratory experiments must be accelerated such that events which would actually occur in millions of years are simulated in time spans of less than one year. Thus, higher pressures and temperatures are employed, where phase transformations permit, to achieve strains comparable to those found in the field, but in a much shorter time period. The results are then extrapolated to correspond to rates of deformation occurring in natural conditions, i.e. an adjustment of 5-6 orders of magnitude. Whether or not this is realistic is a matter for debate. For some rock types, e.g. those containing substantial amounts of calcite and galena, which are soft minerals and therefore relatively easy to deform experimentally, the similarity between deformation processes occurring in nature and those simulated in the laboratory has enabled reasonable correlation between the two to be made. However it is with the mineral quartz that most problems occur and this mineral is one of the most common in the Earth's crust. It is a weak mineral in nature and therefore controls the deformation of many quartz-rich rocks. There are severe difficulties associated with the laboratory deformation of quartz and in spite of extensive research satisfactory correlation between field and experimental results has yet to be achieved. It is for this reason that suitable analogues have been sought, particularly in the metallurgical literature to elucidate deformation mechanisms which have been responsible for the microstructures observed in naturally deformed quartzites.

Whilst analogues have proved useful in helping to interpret geological structures there are still large areas in which knowledge is lacking, mainly due to the differences in approach by geologists and metallurgists to the two disciplines. In the former case strains of the order of tens of percent are not uncommon but mechanical data is often unavailable. In the latter case the metallurgist usually has a good knowledge of the mechanical properties of his material, but with the exception of metal forming and hot working he is mainly concerned with the tailoring of components for low strain engineering applications and for this reason much of the metallurgical literature is devoted to low strain studies. In addition, in spite of the substantial amount of literature published on hot deformation of metals very few serious attempts have been made to systematically characterize microstructures with increasing strain. This is particularly true of lower symmetry structures, for example hexagonal close packed metals, which would be of more interest to the geologist. For this reason it was thought that the study of microstructural development with increasing strain in the magnesium would be useful to geologists whose main aim is to show whether or not present day

microstructures are good indicators of past deformation conditions and mechanisms. The mechanism of dynamic recrystallisation and the formation of shear zones in the metal were thought to be particularly worthy of note.

Two different types of crustal rock will be examined in detail - quartzite because of the well known difficulties associated with laboratory deformation and calcite because of the heterogeneous deformation which occurs in polycrystalline aggregates and the consequent rapid fabric (texture) development. Numerous attempts have been made in the past to correlate the microstructures of these two minerals with metallurgical deformation mechanisms, e.g. Barber and Wenk (1973) on calcite and Tullis et al (1973) and White (1976) on quartz. A review of the 'state of the art' for each mineral will be made; this will be followed by a comparison of each with the relevant work on the magnesium. Particular attention will be paid to the initiation and development of shear zones in quartz rich rocks and to the practice of estimating stresses at the time of deformation from present day microstructures. Calcite will be discussed first.

5.2. CALCITE

5.2.1. Introduction

As pointed out in the preceding paragraphs calcite is a soft mineral and relatively easy to deform in the laboratory at moderate temperatures and pressures (for a review see Carter 1976 or Nicolas and Poirier 1976). Satisfactory correlation between field and experimental studies has been found for calcite: (Wenk et al 1973 carried out an extensive study of uniaxial deformation in fine grained limestones and correlated the results with naturally occurring rocks) consequently much of the experimental effort on the mineral has been directed towards rheological studies with a view to determining its flow laws (Heard and Raleigh 1972, Rutter 1974, Schmid 1976).

Experimental Deformation

5.2.2. Single crystal studies

The experiments carried out on single crystals have produced the following results:

1) The most prominent mechanism is twin gliding on $\{01\bar{1}2\}$ (Turner et al 1954, Griggs et al 1960, Turner and Heard 1965). The reorientation of the c axis in the twinned volume is 52^{o} and the shear accomplished is 0.69. This means that small strains can produce large fabric (texture) changes.

2) $\{10\bar{1}1\}$ slip is more important at higher temperatures in suitably oriented crystals (Carter 1976). The mechanism commonly causes kink bands to form by rotation during inhomogeneous slip.
3) Other minor mechanisms such as $(02\bar{2}1)[f: r_3]$ or $[f: r_2]$ and r slip parallel to $<21\bar{3}\bar{2}>$ (Weiss and Turner 1972) and twinning on $\{10\bar{1}1\}$ parallel to $[r_1:f_2]$ with positive shear (Borg and Handin 1967) have also been reported in experimental studies of calcite single crystals.[1*]

It is the first two mechanisms which are important in naturally deformed calcite.

5.2.3. Polycrystalline aggregates

Experiments on polycrystals of calcite have centred in the main on three types of calcite rock viz Yule marble, Carrara marble and Solenhofen limestone: most effort has been concentrated on Yule marble, which has a moderate grain size 400 μm, which facilitates optical studies and a homogeneous fabric (Texture) and on Solenhofen limestone which is strong and brittle in laboratory conditions, very fine grained - 5 μm and has mainly been examined to determine macroscopic failure criteria.

Calcite deforms by a combination of intracrystalline plastic deformation and diffusive mass transfer below 250-300°C. The diffusive processes are favoured by fine grain sizes, slower strain rates, lower differential stresses and the presence of phyllosilicates. A phenomenon called pressure solution (Ramsay 1967, Rutter 1976) which involves water assisted diffusive transfer around grain boundaries has also been documented.
At temperatures above 250-300°C the operation of power law creep has been inferred from the experimental results of Heard and Raleigh (1972).
The microstructural aspects of pressure solution and power law creep will now be summarized.

Pressure solution

This is thought to be similar to the Coble creep which has been reported in metals (Coble 1963). Deformation is achieved by mass transfer from points at high stress to points at low stress along grain boundaries. The difference is that the grain boundary diffusion is enhanced by the presence of a fluid phase. Grain boundary sliding also occurs to fulfil strain compatibility requirements. A model, based on that for Coble creep, put forward by Raj and Ashby (1971) has been suggested by Rutter (1976) to describe the kinetics of rock deformation by pressure solution.

1* In the geological literature it is common to use the following terminology when referring to slip and twinning systems
r $\{10\bar{1}1\}$, f $\{0\bar{2}21\}$, a $\{11\bar{2}0\}$ and e $\{01\bar{1}2\}$

Power law creep

A study of steady state flow in Yule marble (Heard and Raleigh 1972) revealed that for differential stresses below 1100 bar in the temperature range 500-800°C the strain rate followed the relationship

$$\dot{\varepsilon} = A\sigma^n \exp\left(-\frac{Q}{RT}\right)$$

Microstructural observations of the experimentally deformed samples led to the suggestion that dislocation climb was operative and resulted in the formation of polygonised subgrains, the substructure being better developed athigher temperatures. Intergranular and intragranular recrystallisation were also found to occur. The intergranular recrystallisation was associated with bulges at the old grain boundaries. The intragranular nucleation was observed at higher strain rates but was not closely investigated and the features described have since been attributed to kink bands (Nicolas and Poirier 1976).

Schmid (1976) investigated the steady state flow of Solenhofen limestone and distinguished three regions of rheological/microstructural behaviour

1) Exponential flow
2) Power law flow a) and
3) Power law flow b).

He calculated the stress exponent n in the two power law regimes and obtained values of 4.5 in (a) and 1.7 in (b). These values were lower than that of n = 8 determined by Heard and Raleigh, and the discrepancy was attributed to the greater contribution of grain boundary sliding and of diffusion accommodated flow to the deformation in the fine grained material.

Other mechanisms such as Nabarro-Herring creep have also been put forward to account for higher temperature deformation behaviour in experimentally deformed calcite (Heard and Raleigh 1972) but under conditions commonly found in the Earth's crust it is thought that power law creep should predominate (Rutter 1974, Carter 1976).

5.2.4. The effect of preferred orientation on the deformation of calcite

The strong preferred orientation which develops in calcite rocks at moderate homologerus temperatures is caused mainly by reorientation due to e $(01\bar{1}2)$ twinning. Thus there is a rapid development of texture below 20% strain when all crystals which are favourably oriented for twinning do so. Thereafter the texture does not alter significantly as the grains continue to deform by r slip. The large part played by e

twinning has been recognised for several years (Wenk et al 1973) and numerous attempts have been made to theoretically predict fabric development (see e.g. Lister 1978) but it is only recently that the exact path of its development has been ascertained (Spiers 1979). Split cylinder tests were carried out so that the homogeneity on a grain scale could be investigated and it was found that the deformation was very heterogeneous. Grains suitably oriented for twinning would deform preferentially producing rapid host grain rotation thus accounting for the well developed fabric at relatively low strains. It was concluded that predictions of fabric development when twinning is important should be based on models assuming homogeneous stress rather than homogeneous strain.

In higher temperature experiments where other slip mechanisms can compete more efficiently with twinning then deformation is more homogeneous and final textures are weaker (Nicolas, Poirier 1976, Spiers 1979).

5.2.5. Comparison between Mg and experimentally deformed calcite

There are some basic similarities between the behaviour of magnesium and that of calcite: they are a result of the influence of crystal anisotropy and the operation of a limited number of slip systems on the homogeneity of deformation. A table of comparable features is presented below.

	Mg	Calcite
Crystal structure	hcp	trigonal
Twinning plane	$(10\bar{1}2)$	$(01\bar{1}2)$
shear	0.13	0.69
Major low temp. accommodating mechanism	basal slip	twin gliding on $(01\bar{1}2)$ (Fig. 5.25.1a)
Dynamic recrystallisation by rotation	at low T	at moderate T where twinning is less important (Fig. 5.25.1b)
Dynamic recrystallisation by extensive migration and bulging	at high T	at high T in the absence of twinning (Fig. 5.25.1c)

The similarities between the magnesium and the calcite are due to the operation of one 'easy' means of accommodating the deformation at low temperatures. In the magnesium the 'easy' slip system is the basal system. The twinning in magnesium, although of the same type as that in calcite, is relatively unimportant as a deformation mechanism as the shear it accommodates is small. In common with calcite, it is important in fabric development in that it results in rapid reorientation of the



experimentally deformed at: $600^{o}C/10^{-4}s^{-1}$, 3kb
differential stress: 1435 bar. strain: 16%.



experimentally deformed at: $600^{o}C/10^{-5}s^{-1}$, 3kb
differential stress: 300 bar. strain: 30%.



experimentally deformed at: $1000^{o}C/10^{-5}s^{-1}$, 3kb
differential stress: 150 bar. strain: 20%.

Figure 5.25.1. These micrographs of deformed carrara marble were reproduced courtesy of Schmid (1976). The deformation conditions are indicated below each micrograph.

basal planes at low strains. As explained in the discussion (Section 4.4.4.2.) the operation of the basal slip system results in heterogeneous deformation and kinking of the lattice at grain boundaries. In the calcite e $(01\bar{1}2)$ twinning as well as being important in fabric development is also the softest mechanism at low strains and accomplishes large shears. Grains which are suitably oriented for twinning are 'weak' and thus undergo large strains forcing the deformation which is then heterogeneous to be accommodated in the form of kink bands and lattice bending: rotations of up to 15^{o} have been observed for only 10% overall strain (Spiers 1979). The two micrographs in Fig. 5.25.2 illustrate the heterogeneous deformation in calcite. Figure 5.25.2a shows the lattice bending and preferred deformation of a twinned grain which is partly accommodated by grain boundary cracking. Figure 5.25.2b illustrates the geterogeneity revealed by scratches on the specimen face. The vertical lines have bulged around the twinned grain in the centre.

At moderate temperatures in experimentally deformed calcite twinning is less important and other mechanisms - r and f slip have been detected. Dynamically recrystallised grains have been reported at twin-grain boundary intersections and at the old grain boundaries where there are large lattice misorientations (Shaw 1979).

At high temperatures grain boundary migration and grain growth is marked and recrystallisation appears to occur by bulging and migration of the old grain boundaries although the mechanisms are poorly understood.

In summary then, both materials exhibit very heterogeneous deformation at low temperatures as a consequence of boundary constraints in a polycrystalline sample and the operation of one easy mechanism: in magnesium the rotations at the grain boundaries are sufficiently high for dynamic recrystallisation to occur: in calcite dynamic recrystallisation becomes evident at moderate temperatures when twinning is less important.

5.3. QUARTZITE

5.3.1. Introduction

Features found in the microstructures of naturally deformed quartz aggregates such as deformation lamellae and undulatory extinction prompted geologists to try and reproduce the same effects under laboratory conditions.

There are two types of apparatus used in the experimental deformation of rocks:

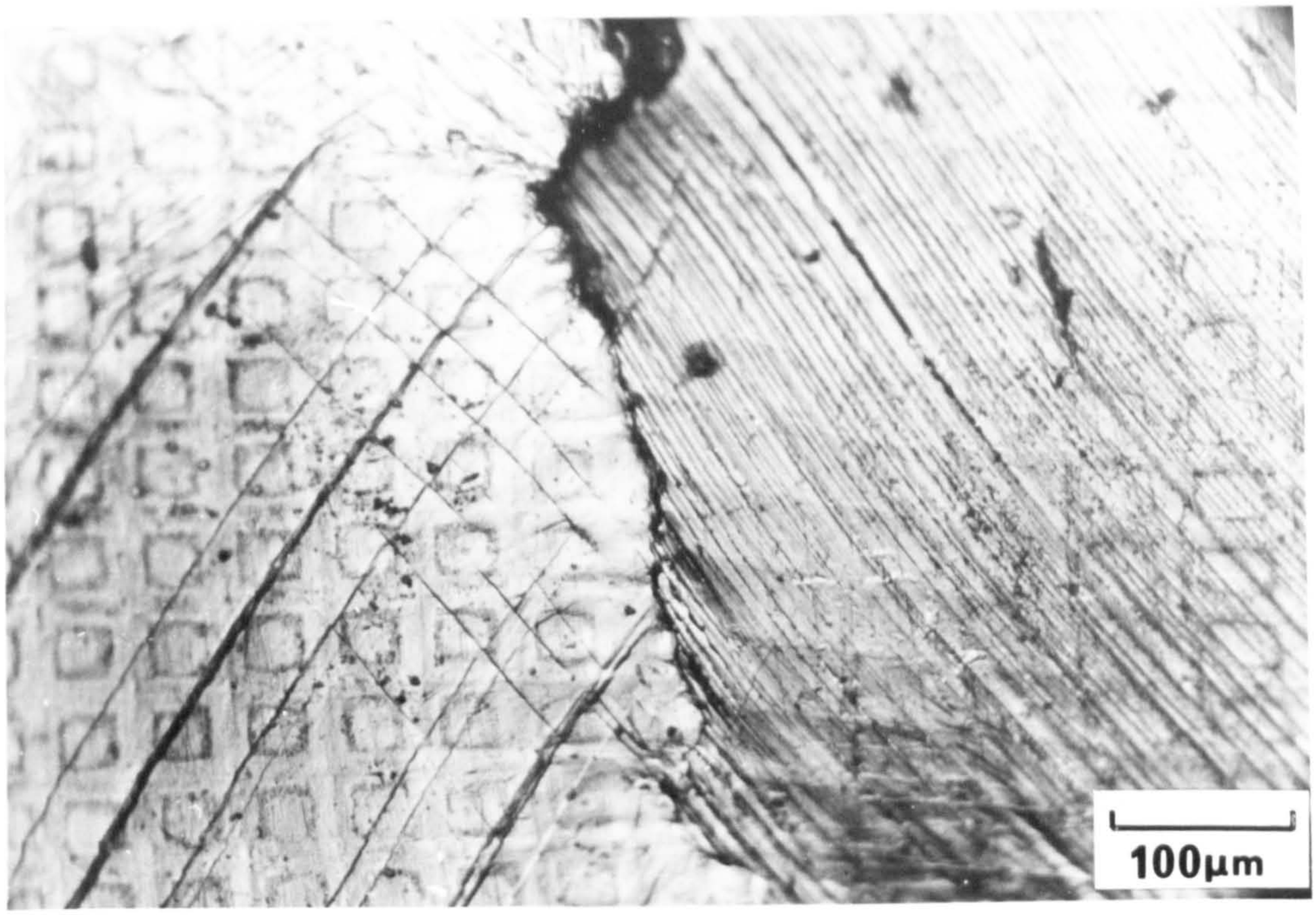


Figure 5.25.2a. Preferred deformation of a grain in twinning orientatio (right) compared with the deformation of a crystal in a non-twinning orientation. Strain is marked by a 50µm grid Heterogeneity is accommodated partly by grain boundary cracking. (Compression axis vertical)

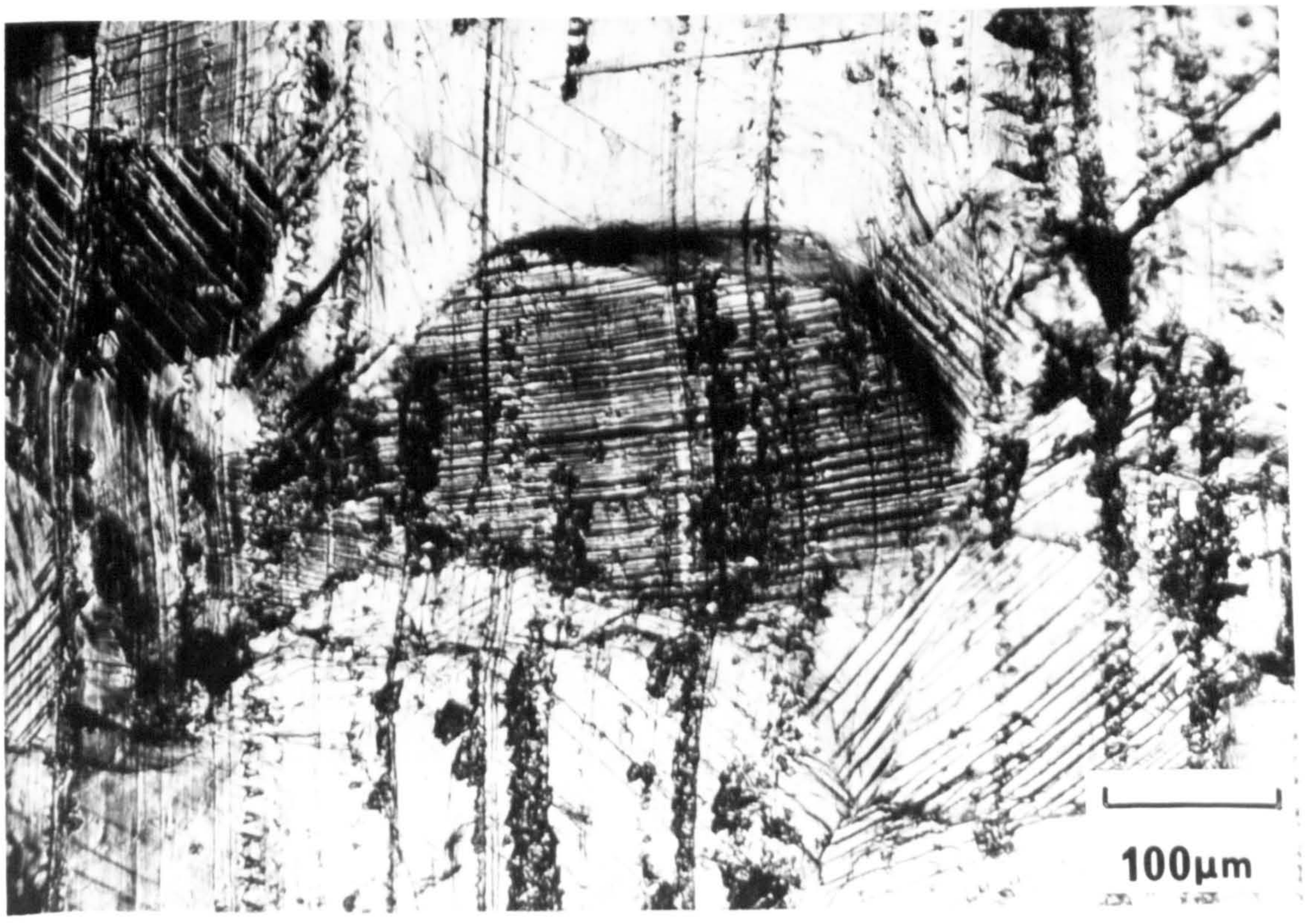


Figure 5.25.2b. Heterogeneous deformation associated with a twinned crystal in a split cylinder of Carrara marble. Note the bulging of the vertical scratch lines around the twinned crystal. (Compression axis vertical)

Both of these micrographs were reproduced courtesy of Spiers (1979).

a) The solid medium apparatus which was developed to overcome the early difficulties of maintaining pressure at high temperatures in apparatus with gas as a confining medium. The solid medium apparatus employs weak solids such as talc as confining media. Strains of up to 60% can be obtained but the stress is not accurately known.

b) Apparatus which utilizes gas or oil as confining media and which can now apply pressures of 3kb. Although the stresses are known the strains which can be achieved in the gas apparatus are low; high strains can only be reached in the solid medium apparatus where there is a distinct disadvantage in that it is impossible to obtain reliable stress strain data.

However although there is widespread evidence for plastic deformation of quartz in tectonic environments, the mineral has been found to be exceedingly strong when tested under dry laboratory conditions. Even as late as 1960 (Griggs et al) fracture and cataclasis (brittle failure and rigid body rotation) were the dominant modes of deformation found experimentally. It was found that only under very high confining pressures could plastic deformation be achieved (Carter et al 1964, Christie et al 1964, Griggs and Blacic 1964, 1965, Griggs 1967, Blacic 1971).

5.3.2. Single crystal studies

The most significant work on natural single crystals was by Griggs and Blacic (1964) using a solid pressure medium, constant strain rate apparatus. They were the first to determine the dominant slip systems. The flow mechanism up to 700^{o}C was basal slip and above 700^{o}C predominantly prismatic slip. In the next year Griggs and Blacic found that when the temperature of the system was raised to the dehydration temperature of the talc confining medium the strength of the quartz dropped markedly. They postulated hydrolytic weakening to account for the change in mechanical behavious. A further important result was that synthetic quartz crystals were easily deformable compared with the natural material. As a consequence of these two results the literature over the past 14 years has been dominated by attempts to explain the role of water in the plastic deformation of quartz and in particular to explain the behaviour of OH-rich synthetic crystals (for a review see Carter 1976 and Paterson and Kekulawala 1979). Although the experiments performed on synthetic and natural quartz single crystals have provided much information about the operating slip systems (e.g. Baeta and Ashbee 1969) there is some doubt as to their general applicability - in particular some of the experiments on synthetic crystals have revealed features which are not

found in the natural rock (see Paterson and Kekulawala 1979 for a summary).

5.3.3. Experimental deformation of quartz aggregates

It is the deformation of quartz aggregates which is of particular interest since studies of this kind are more applicable to the deformation undergone by quartz bearing rocks.

The table below lists the features commonly observed in naturally deformed quartz aggregates and indicates those which have also been found in experimentally deformed quartzites.

Environment	Natural	Experimental	Strain rate
natural tectonic	subgrains - evidence for climb and recovery	-	
mylonite	climb, recovery, sub-grain development and also recrystallisation	Tullis et al (1973) P = 15kb Ardell et al (1973)	$10^{-5} s^{-1}$ - $10^{-7} s^{-1}$
cataclastic	grain boundary fracture, fragmentation resulting in flow. Still some evidence for dislocation motion in the form of undulatory extinction and large dislocation densities in cases near the ductile brittle transition	Hobbs et al (1972) 500°C P = 3kb No evidence of subgrains, straining beyond 10% resulted in fracture	10^{-6} - 10^{-7} s^{-1}
pseudotachylite	structures consist mainly of glass due to frictional sliding		

The results obtained from experimentally deformed quartzites have been very inconsistent. A wide variety of submicroscopic structures have been recorded in experiments between 600-900°C at strain rates of 10^{-5} - 10^{-7} s^{-1}. Ardell et al (1973) compared dislocation structures in natural quartzites with those deformed experimentally and concluded that natural quartzites generally showed lower dislocation densities and more extensive recovery. This was in spite of the fact that the natural material was deformed at lower temperatures than the experimental

material but is an expected result when the slower strain rates and lower stresses of the natural deformation are taken into consideration. In agreement with observations by other workers such as Tullis et al 1973 (experimental); and Hobbs, McLaren and Paterson 1972; McLaren and Hobbs 1972; White 1971, 1973 and White et al 1971 (natural) it would appear that the submicroscopic structures of quartzites deformed experimentally at the highest temperatures and slowest strain rates resemble those of quartz mylonites whereas those structures resembling quartz tectonites have not yet been achieved experimentally. For this reason geologists engaged in the study of naturally deformed quartzites have frequently sought analogues in the metallurgical and materials science literature to aid with the interpretation of observed microstructural features.

5.3.4. Microstructures of naturally deformed quartz aggregates

Naturally deformed quartzites examined in thin section exhibit undulatory extinction, deformation bands, deformation lamellae, subgrains and recrystallised grains. It has been suggested (White 1975) that they develop sequentially with increasing strain. Direct correlation is possible between these optically visible features and the dislocation substructures which produce them as revealed by HVEM. In addition HVEM enables comparisons to be made between seemingly similar features in experimentally deformed and naturally deformed quartzites.

i) Undulatory Extinction

This effect is caused by lattice bending due to constraints during deformation imposed by neighbouring grains and EM work has indicated that it can be produced by two structures:

a) Very narrowly spaced subgrain walls $\sim 1\mu m$ in width which accommodate the lattice bending in small steps;
b) An anisotropic dislocation density which is common in experimentally deformed quartz but not in nature (Hobbs et al 1972).

Banded undulatory extinction observed in the optical microscope can be due in (a) to a variation in the subgrain spacing as the misorientation across individual walls is too small to be resolved in the optical microscope and in (b) to a variation in the dislocation density.

ii) Deformed Bands

In the metallurgical literature similar features are sometimes referred to as transition bands or kink bands as well as deformation bands.

In quartz most deformation bands develop parallel and perpendicular to the most active slip plane (White 1976). Optical microscopy indicates the spacing between the bands is ∿50μm but electron microscopy reveals further bands of lower misorientations which are ∿10μm apart and have been shown to be closely spaced subgrains (White 1973).

iii) Deformation Lamellae

Considerable controversy exists as to the origins of deformation lamellae. White (1973) showed that in naturally deformed quartzites deformed in tectonic conditions the features were in fact narrow subgrains often decorated by bubbles. In high stress environments the lamellae were straight planar features due to shear fractures or deformation twins decorated by glass.

Optical examination of deformation lamellae produced experimentally led to the belief that they were slip planes (Carter et al 1964). This has since been shown to be incorrect (McLaren et al 1970). TEM of experimentally produced deformation lamellae has revealed that the features can be caused by several different structures, e.g.:-

1) Fractures decorated by glass (Christie and Ardell 1974)
2) Planes and zones of bubbles do.
3) Very narrow zones of high dislocation density (Hobbs et al 1972)
4) Subgrains - produced in creep experiments (McLaren et al 1970)

iv) Subgrains

Subgrain formation is indicative of recovery processes and has been used as a criterion for the recognition of deformation by dislocation creep (White 1971, 1976). Elongate and equidimensional subgrains can be detected by both optical and electron microscopy but in the EM it is possible to resolve dislocation walls with smaller misorientations and smaller subgrains, i.e. subgrains can be observed within the optically visible subgrains. In the optical microscope only subgrains with misorientations greater than 1^{o} can be seen. A feature commonly found in naturally deformed quartzites is the 'Core and Mantle' structure (White 1973, 1976). The cores (central areas of grains) contain deformation bands and lamellae whilst the mantles (grain boundary regions) contain small highly misoriented subgrains.

Recrystallised grains

Recrystallised grains are commonly found along old grain boundaries and deformation bands. They exhibit optical strain features similar to the old grains indicating they are formed dynamically and often have a

crystallographic relationship similar to the old grains (McLaren and Hobbs 1972, White 1973, White and Wilson 1978). There is still controversy over the exact mechanism of nucleation but sufficient evidence exists to suggest that in some areas the recrystallised grains form by subgrain rotation (White 1973 - natural; Hobbs 1968 - experimental).

5.3.5. Comparison between magnesium and naturally deformed quartzites

It has been stated in the preceding paragraphs that the structures commonly observed in quartzite rocks deformed in tectonic environments have not been reproduced in controlled laboratory conditions. This has meant that geologists have been forced to rely on very limited laboratory data and more importantly on metallurgical analogues to explain microstructures in naturally deformed rocks. In particular dynamic recrystallisation is thought to have played an important part in the microstructural development of quartz rich rocks. However, the metallurgical knowledge of dynamic recrystallisation is still in its infancy as far as mechanisms are concerned and studies have been limited to creep and hot working of cubic metals where the behaviour is likely to be different as they are isotropic and slip is not as limited. For this reason the study carried out on magnesium is thought to be particularly useful since the metal is hexagonal and therefore anisotropic with limited slip systems and more likely to behave in a similar way to quartzite. Dynamic recrystallisation has also been shown to play an important role in microstructural development in magnesium and the mechanisms have been thoroughly investigated. The similarities between the metal and the mineral are tabulated below.

	Mg	Quartzite
crystal structure	hcp	trigonal
major low temp. accommodating mechanism	basal slip	prism slip
dynamic recrystallisation at low T	by subgrain rotation	by subgrain rotation
dynamic recrystalliation at high temps.	by boundary bulging & migration	by boundary bulging & migration
Structure within old grains	Core and Mantle	Core and Mantle
	long elongated sub-boundaries	long elongated sub-boundaries
	large subgrain rotations and some evidence for $\vec{c + a}$	large sub-grain rotations & the operation of additional slip systems

Both materials readily undergo inhomogeneous deformation and develop shear zones.

In the case of the magnesium and the quartz slip on one system at low temperatures is relatively easy: for magnesium it is the basal system and for quartz the prism system. This forces the deformation to be heterogeneous if compatibility is to be maintained at grain boundaries. The core and mantle structure has frequently been observed in both materials. Narrow elongated subgrains formed in the cores and had walls parallel to the basal or prism planes (Fig. 5.35.1). In the mantles the constraints imposed by neighbouring grains modified the pattern of deformation. The lattice was rotated with respect to the core and there was evidence at some boundaries in the magnesium for the operation of a second slip system. In the quartz additional slip systems have also been found in the mantles and the subgrains are smaller and more misoriented than those in the cores (White et al 1978). It was suggested that this was a reflection of stress intensification in the mantles and a consequence of the accommodation difficulties caused by the boundary constraints and easy operation of only one slip system. In both mateials then the high misorientations which build up at grain boundaries lead to dynamic recrystallisation - effectively by subgrain rotation.

The series of micrographs (Figs. 5.35.2-4) illustrates the similarity in microstructure of the metal and the mineral.

i) Both materials exhibit undulatory extinction which is due to lattice bending (Fig. 5.35.2).

ii) Both materials exhibit dynamic recrystallisation at the old grain boundaries by a mechanism involving lattice rotations (Fig. 5.35.3).

iii) A duplex microstructure (or bimodal grain distribution) typical of that found in naturally deformed quartzites is frequently observed in the magnesium (Fig. 5.35.4).

5.4. SHEAR ZONES

5.4.1. Introduction

There has been a great deal of interest in the formation and development of shear zones: this is evidenced by the volume of geological literature on this subject currently in print and in press. Of particular interest to the geologist are mylonite zones which are narrow regions in the earth's crust and upper mantle where high strains have been accommodated by ductile flow. The mylonite zones often have

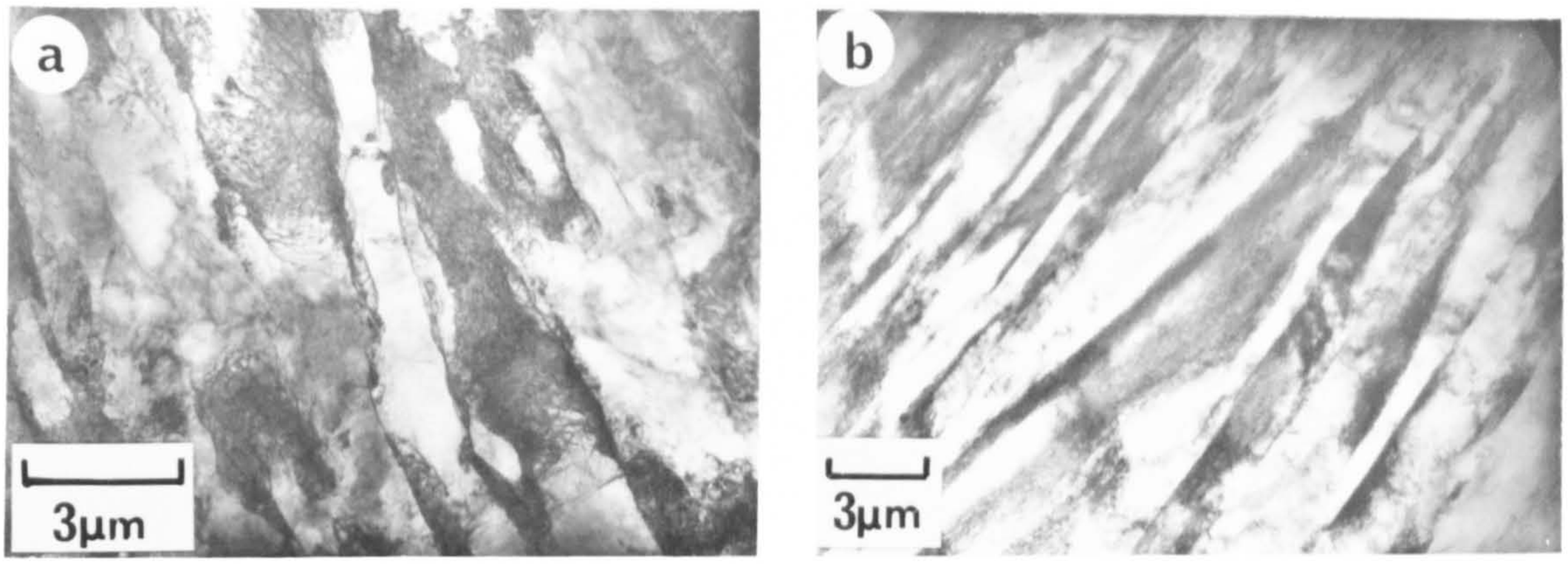


Figure 5.35.1. Elongated subgrains in quartzite (a) magnesium (b). The micrograph of the quartz was taken by S.H. White.

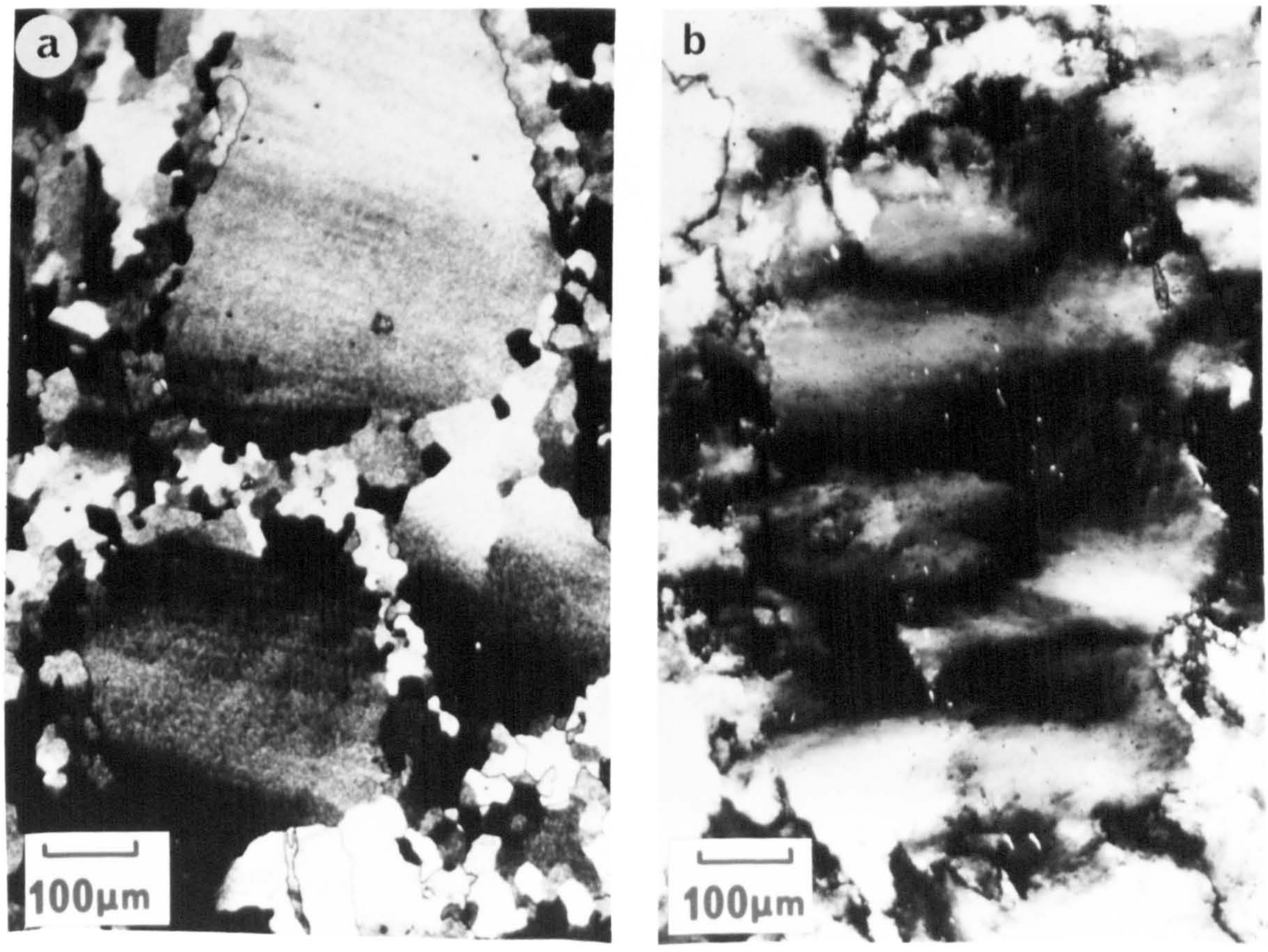


Figure 5.35.2. Undulatory extinction in magnesium (a) and quartz (b). The micrograph of the quartzite was taken by S.H. White



Figure 5.35.3a. Dynamic recrystallisation at the old grain boundaries is clearly illustrated in this deformed quartzite. Sub-grains can also be seen within the characteristic 'ribbon' grains.

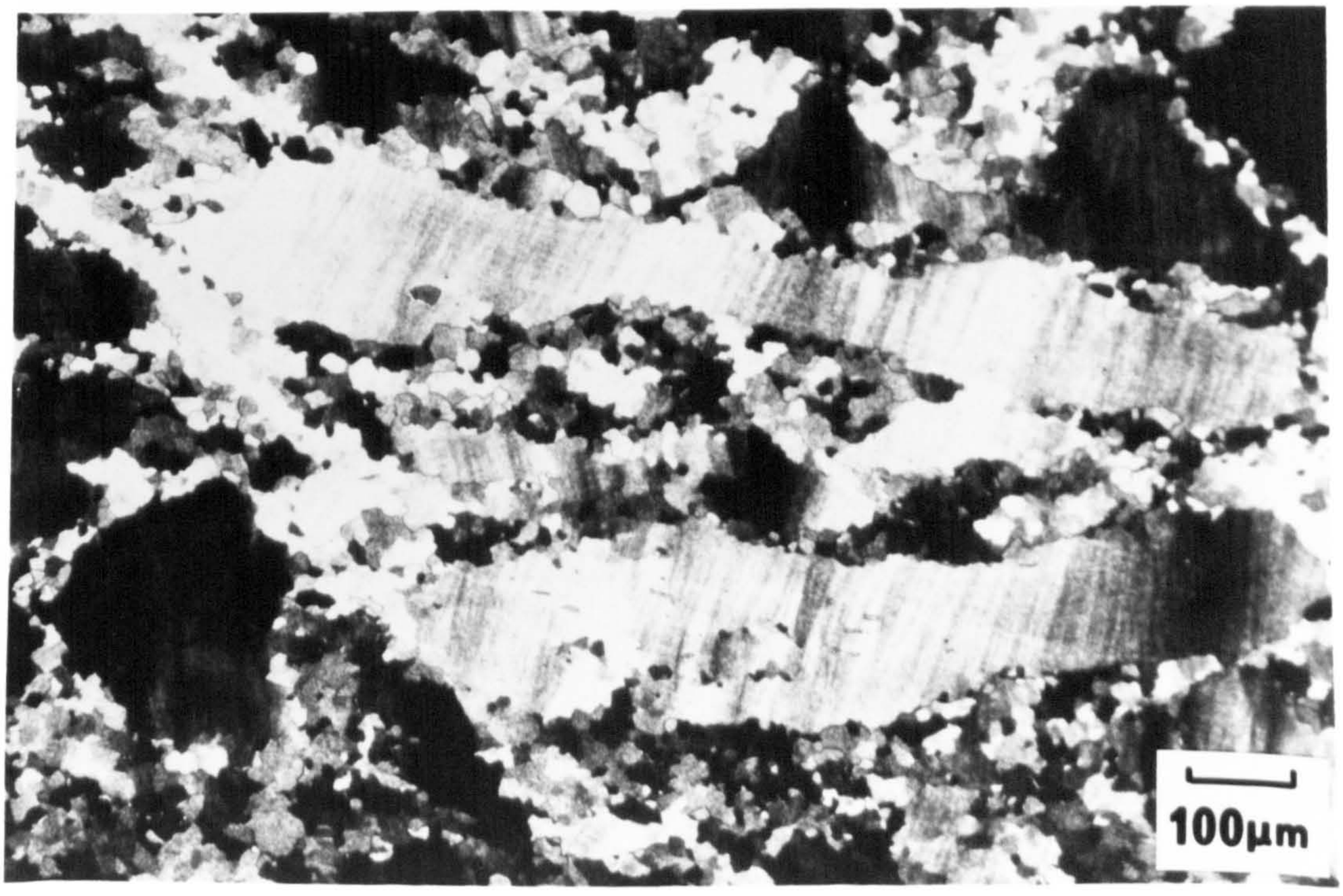
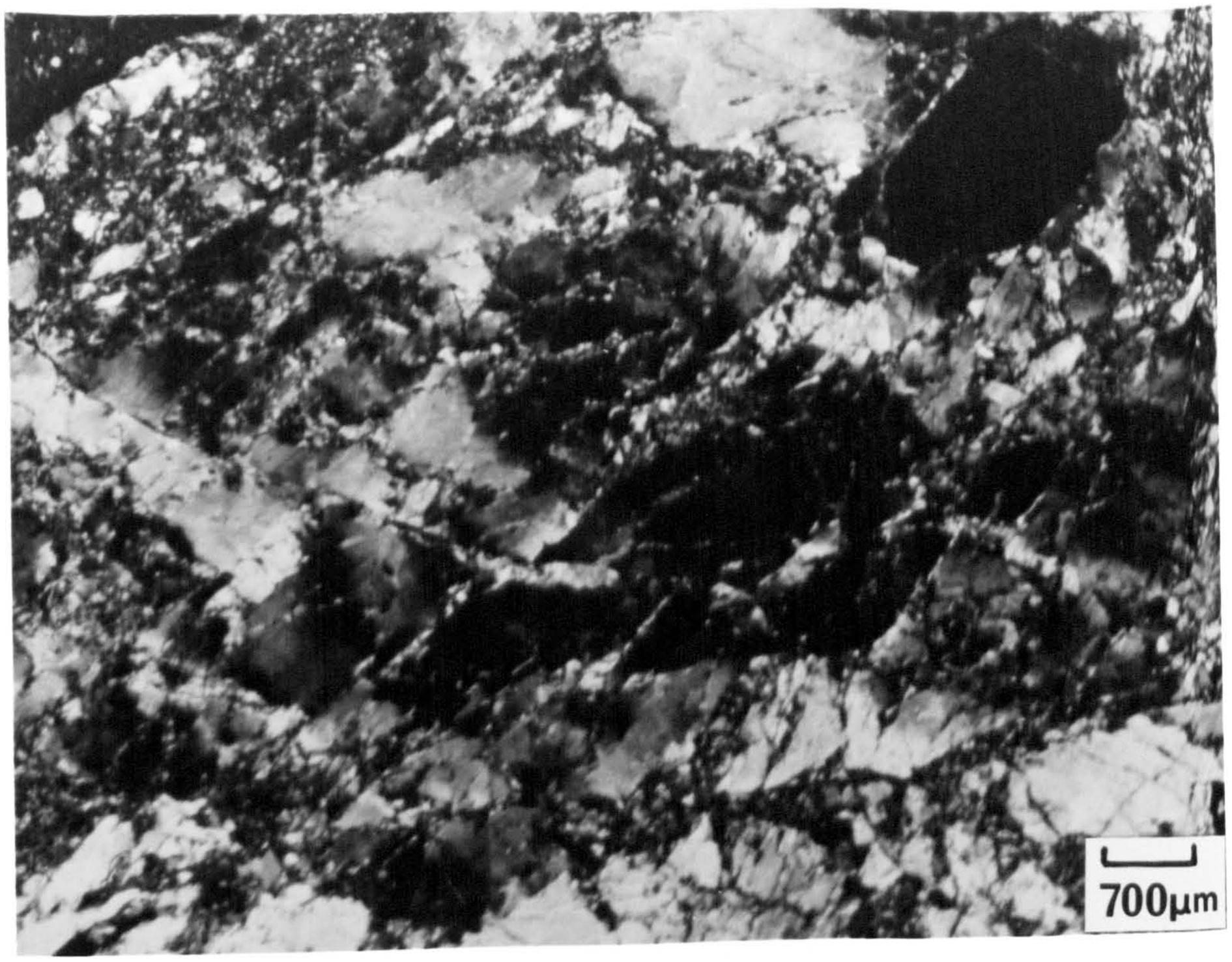


Figure 5.35.3b. Dynamic recrystallisation at the old grain boundaries in the magnesium illustrates the similarity in deformation microstructure with the quartzite. Substructure can be detected in the elongated old grains in the metal.



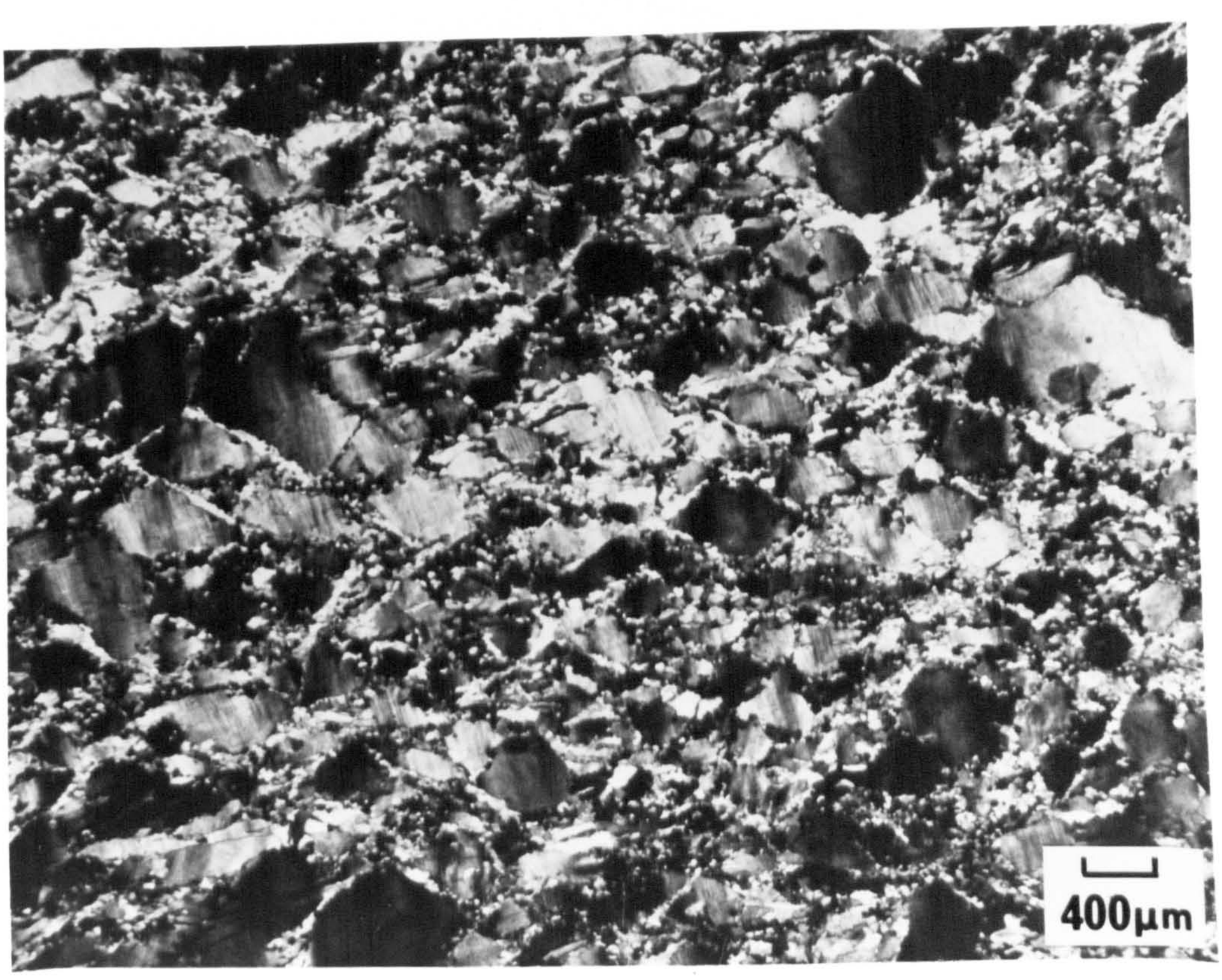


Figure 5.35.4. These micrographs illustrate the similarity in microstructure of a quartz mylonite (upper micrograph) and magnesium deformed 35% at 260°C. Both materials exhibit dynamic recrystallisation at the old grain boundaries.

a fine grain size compared with surrounding rock. Deformation is concentrated in the zones and it has been suggested (White 1977) that the development of a mylonite microstructure must lead to strain softening. It has been suggested that the microscopic processes in the shear zone involve one or more of the following.

a) Continuous dynamic recrystallisation (White 1973, 1976, Bell and Etheridge 1973,1976, Mercier et al 1977).
b) Texture (fabric softening).
c) Mechanical softening involving grain boundary sliding (Etheridge and Wilkie 1979).
d) Chemical weakening (Ramsay and Graham, 1960, White and Knipe, 1978)
e) Shear heating.

These processes have been discussed at length in the literature and an up to date view of the state of the art can be found in the Barcelona Shear Zone Conference volume (1979).

5.4.2. Comparison of shear zones in Mg with geological shear zones

The experiments carried out on the magnesium have proved to be useful in view of the lack of data on mineral and rock deformation. They have confirmed that texture (fabric) softening is an important factor to be considered. In common with the data obtained for the magnesium, there is strong evidence for the importance of dislocation flow in fine grained mylonites and it has often been observed that quartz mylonite zones exhibit strong preferred orientations which are favourable for prism slip (see e.g. Carreras 1974) - the easy slip mechanism in naturally deformed quartzites. Another similarity between the metal and the mineral is the difference in recrystallised grain size inside and outside the shear zone, it being smaller in the shear zone. It has been suggested that this implies that mylonite zones were regions of high stress either at initiation or during flow but the work on the magnesium has shown that the zones in the metal are regions of high strain rate. In agreement with Schmid (1979) it is thought that mylonite zones are more likely to be zones of high strains and strain rates deformed at stresses of the same order of magnitude as the coarser grained material outside the zone and that grain size gradients observed in mylonite zones are due to strain rate rather than stress gradients.

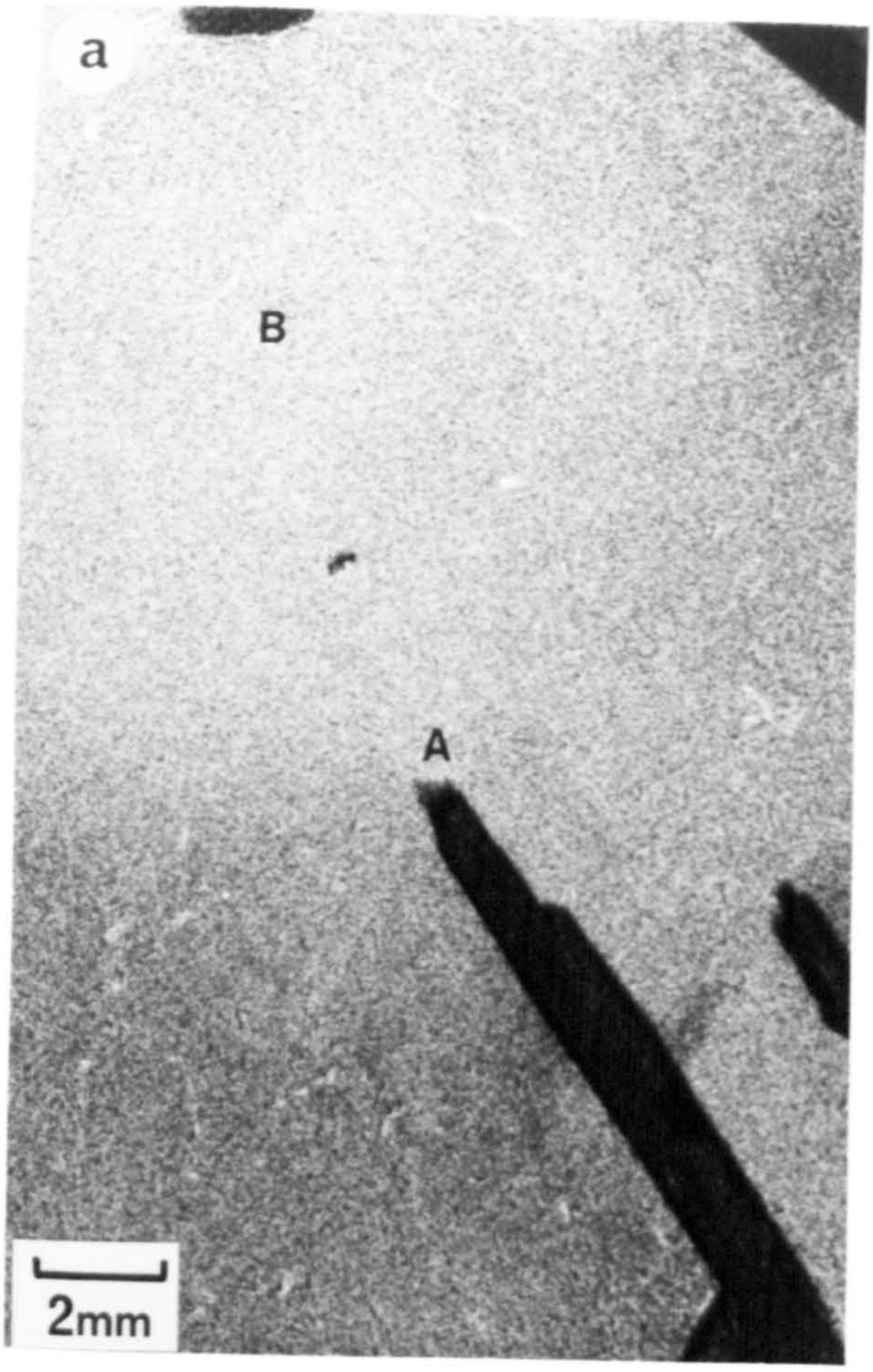
Although the experimental deformation of magnesium produced some interesting results which could help to ascertain the mechanisms operating in geological shear zones, it should be pointed out that the

interpretations made in section 4 are to some extent speculative and that the mechanismsoperating in the metal are still far from clear. It is very difficult to interpret microstructures of samples which have deformed heterogeneously on a macroscopic scale as no two specimens behave in exactly the same way and therefore a series of samples deformed at constant temperature to different strains will not provide information on the development of a particular shear zone. In-situ deformation would obviously provide some of the answers but this was not possible for the metal. For this reason it was decided to examine the behaviour of the transparent organic solid camphor in-situ. The reasons for the choice of material, its characteristics and the experimental details are reported in Appendix E. Suffice it to say that the camphor dynamically recrystallised during deformation and developed shear zones at high strains. The results which are presented below were thought to be particularly important in view of their potential in the interpretation of geological shear zones. They concern the behaviour of a typical sample which underwent macroscopic heterogeneous deformation.

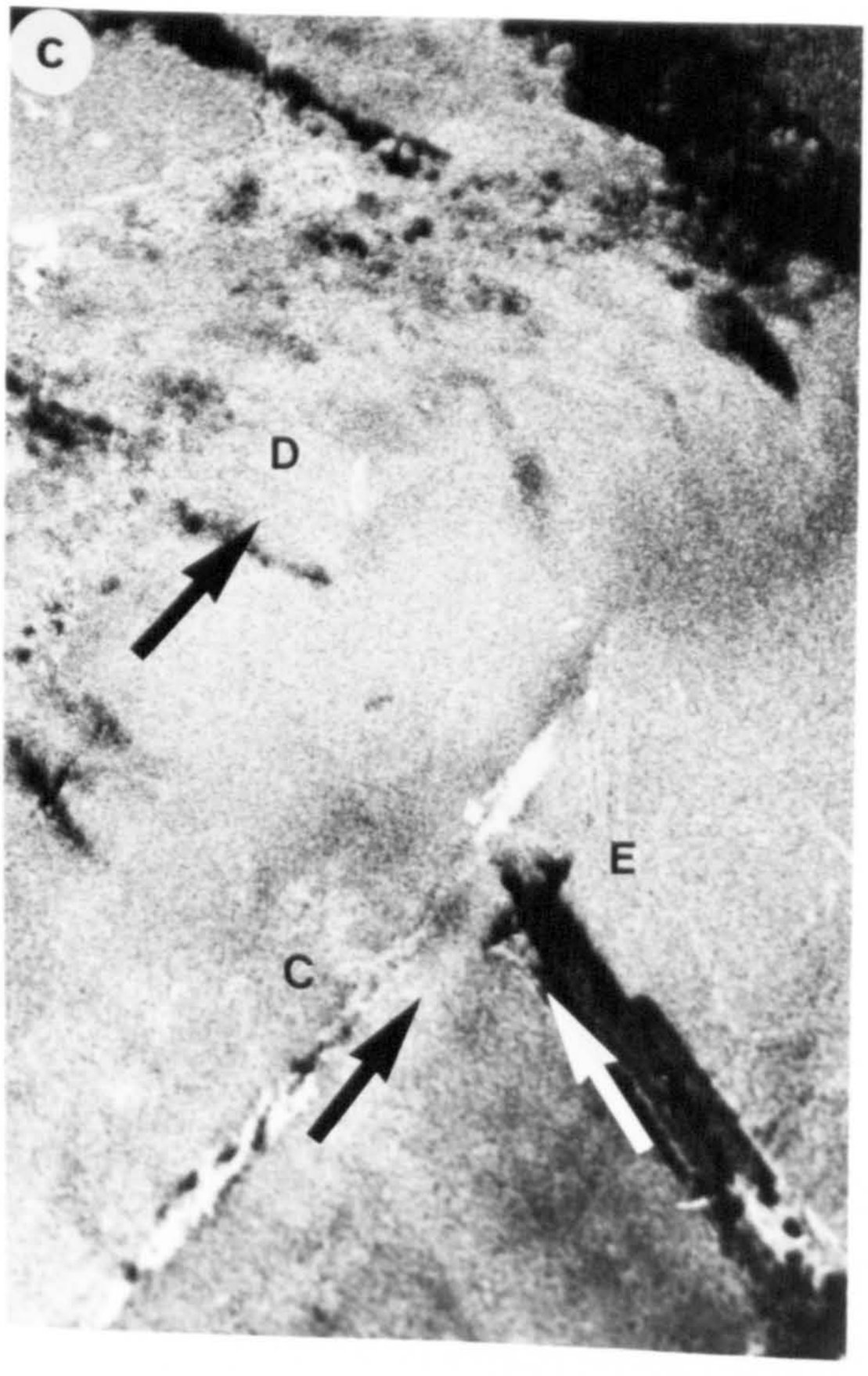
5.4.3. Shear zone development during in-situ deformation of camphor

The series of 8 micrographs in Figure 5.4.3.1. were reproduced from a 16 mm colour cine film of a specimen deformed at $20^{o}C$ at $\dot{\varepsilon} \sim 10^{-4}s^{-1}$. The light areas in the micrographs were unfavourably oriented for slip whilst the dark areas were favourably oriented for slip. Misorientations of the lattice built up in areas A and B (Figure a) until a large amount of slip occurred along the line arrowed in Figure b. At this stage the strain rate accelerated markedly in the zones marked in Figure c where macroscopic shear began to occur (the white region in the centre of the micrograph was caused by an air bubble forming between the camphor and the upper glass slide of the deformation rig). Deformation along what was effectively two shear zones C and D resulted in the macroscopic rotation of E as indicated by the arrow. A good indication of the movement along zone D can be obtained by noting a secondary zone F-F' in Figure d which ceased to operate and quickly became offset, Figure c. The only major activity was taking place in zones C and D which were effectively undergoing simple shear. Zone G had ceased to operate and was undergoing rotation. The rest of the sample appeared to be relaxing - note the grain growth which had occurred in zone G (cf. Figures d and f). It was difficult to confirm the exact mechanisms operating in the two zones owing to

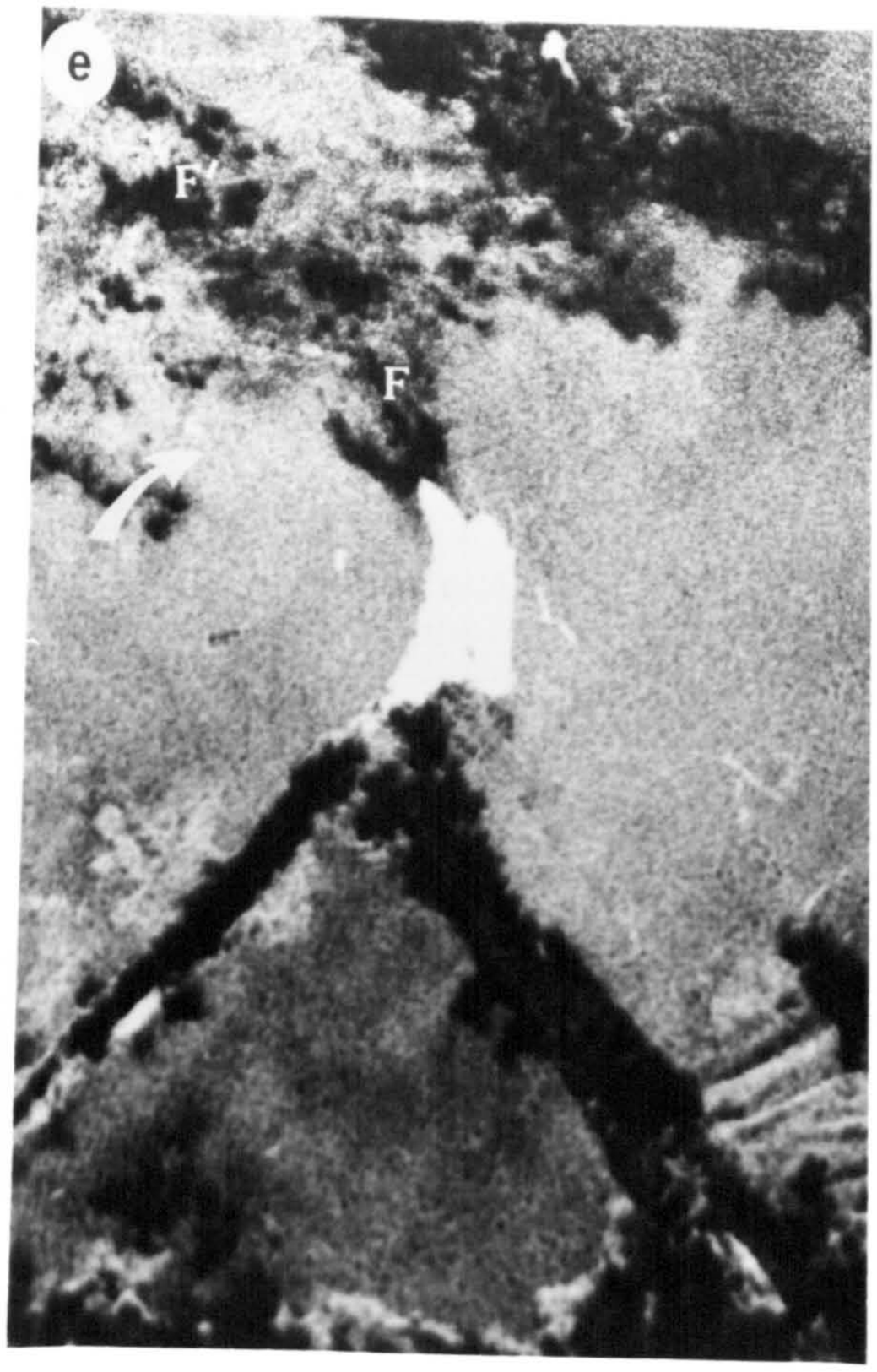
Figure 5·4·3·1

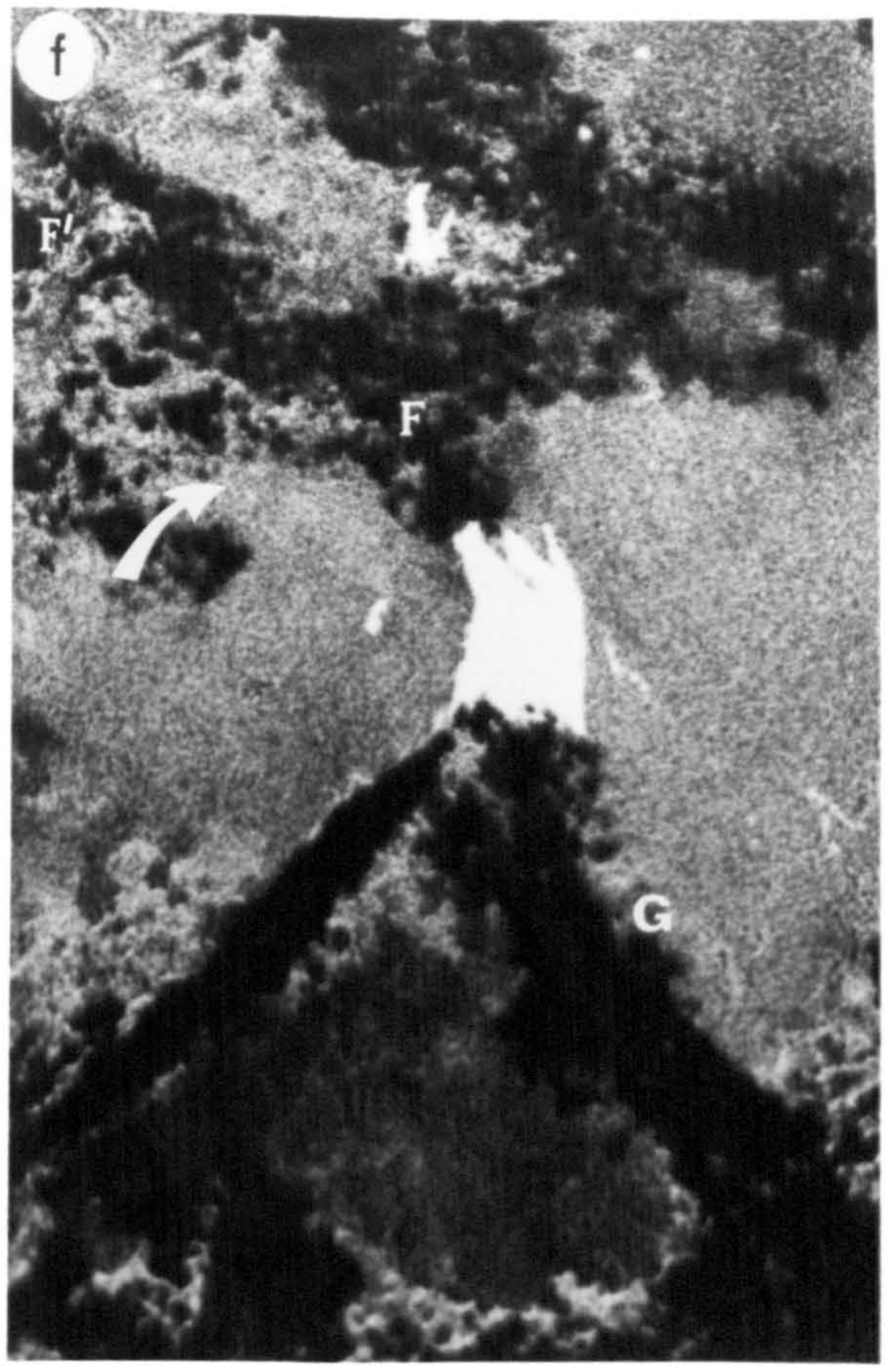

a
B
A
2mm

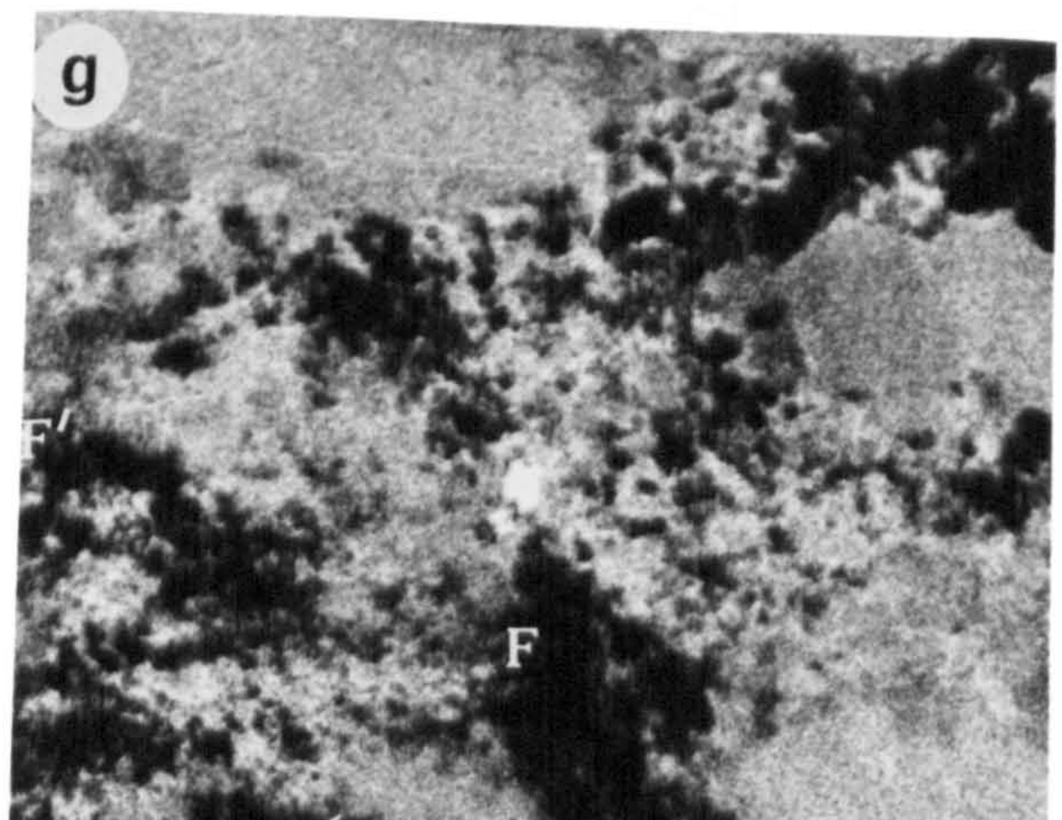

b


c
D
E
C


d


e
F'
F


f
F'
F
G


g
F'
F


h

the small grain size, but it appears that the deformation was essentially in simple shear conditions accompanied by continuous dynamic recrystallisation.

5.5. PALEO STRESS ESTIMATES

5.5.1. Introduction

In view of the difficulties associated with the laboratory deformation of rocks and in particular quartzites, geologists have used microstructural features in an attempt to estimate paleo stresses and strain rates in naturally deformed rocks. However, it must be shown that final microstructures are good indicators of past deformation conditions before any reliance can be placed on the results. There are numerous difficulties in applying paleo stress estimates to naturally deformed rocks some of which will now be discussed (Nicolas and Poirier 1976, White 1979). One of the major objections to the technique is that in estimating microstructures in naturally deformed rocks, geologists have relied heavily on data from the metallurgical literature which is not without controversy itself. Features commonly measured with a view to calculating the stress dependency include dislocation density, subgrain size and recrystallised grain size. All the equations which have been formulated to describe the relationships between stress and the above parameters assume constant microstructure and steady state and implicit in these, homogeneous deformation. In the geological situation if palaeo stress estimates are to be made then the specific relationships of dislocation density subgrain size and recrystallised grain size will have to be determined for each mineral and mineral assemblage, and it will have to be shown that extrapolation to natural deformation conditions are realistic. The relationships used to estimate stresses will now be discussed in more detail.

5.5.2. Relationships commonly used in paleo stress estimates

5.5.2.1. Dislocation density

A relationship commonly cited in the metallurgical literature (McQueen and Jonas 1975, Takeuchi and Argon 1976, Sellars 1978) is that

$$\sigma = K\mu b\rho^{\frac{1}{2}}$$

where K is a constant μ is the shear modulus, b the most common Burgers vector under study and ρ the free dislocation density.

In spite of the severe criticisms of the use of dislocation density to estimate stresses (Nicolas and Poirier, 1976, White 1979) it is still used by many geologists as a technique. Clearly this must be recognised as being unreliable as it is now well known that ρ is subject to alteration during uplift (White 1979) and there is no evidence to support the inherent assumption that final dislocation densities are representative of the original deformation conditions.

Not only is ρ the parameter most sensitive to changes during uplift but the methods of measuring ρ tend to be less reliable. Decoration techniques are dependent to some extent on the orientation of the dislocations and there are problems of resolution if adjacent dislocations are less than 1μm apart. The dislocation density is often heterogeneous and the population as determined from T.E.M. which is necessarily representative of only small areas is unlikely to be accurate.

5.5.2.2. Subgrain size

It has been recognised (White 1973, Nicolas and Poirier 1976) that the size of subgrains recorded for given deformation conditions depends on the technique used to measure them. When stating subgrain sizes the technique used to measure them must also be recorded as for a given set of conditions the subgrain size measured by T.E.M. is much smaller than that recorded by optical microscopy (Green and Radcliffe 1972, White 1973).

The stress has been found to be empirically related to the subgrain size in the following way

$$\sigma = \frac{K\mu}{d} \qquad \text{(Weertman 1968)}$$

Subgrains visible optically have misorientations of $\geq 1^{o}$ whilst those with misorientations of only a few minutes are visible in the T.E.M. White (1979) has pointed out that the Weertman relationship should still hold but that the value of the constant K will depend on the measuring technique. Subgrain structures contain geometrically necessary dislocations which accommodate the bending of the lattice and it has been argued that although the unbound dislocation density will alter during subsequent deformation cycles, subgrain structures should reflect the original deformation. However, it is the timing of the subgrain formation which is important. Subgrains are developed as a result of climb or glide polygonisation, i.e. during high temperature deformation and therefore they could be a result of post deformation

anneals and thus untypical of the original deformation process (Nicolas and Poirier 1976). It has been argued that most subgrains formed during dynamic recovery and therefore may be of use in determining deformation conditions (White 1976), for example undulatory extinction, deformation bands, deformation lamellae and subgrains are all due to subgrain structures which develop sequentially with increasing strain.

5.5.2.3. Recrystallised grain size

Reports of dynamic recrystallisation in the metallurgical literature usually record an empirical relationship of the form

$$\sigma = K D^{-n} \qquad \text{(Jonas et al 1969)}$$

where K is a constant and n has a value between 0.7 → 0.8. However, as reported in section 1, the theoretical investigations of dynamic recrystallisation in metals have been confined mainly to the kinetics of bulge formation (Luton and Sellars 1969, Roberts et al 1979). Mercier et al (1977) showed that the dynamically recrystallised grain size in olivine varied with stress and in view of the potential for using grain size to infer stress geologists have attempted to derive theoretical equations to describe the processes taking place (Twiss 1977, Mercier et al 1977). However, these theoretical relations are severely limited (Poirier and Guillope, 1979, and Brodie 1979) in that they

a) invoke nucleation theories formulated for static recrystallisation,
b) take no account of compositional variations in the rock under consideration.

Whilst nucleation of dynamically recrystallised grains is still the subject of controversy classical homogeneous nucleation has been shown to be thermodynamically impossible for recrystallisation processes except where phase transformations are involved. Other mechanisms are likely to be important. For example, subgrain rotation has frequently been observed in quartzites (White 1976, 77, 79) and two mechanisms have been observed in halite (Guillopé and Poirier 1979). In the latter case the mechanisms were rotation of subgrains and boundary migration. The mechanisms yielded different grain sizes and their operation depended on the position of a critical curve in the σT plane, i.e.the value of the constants in any equation would depend upon the mechanism of recrystallisation.

Clearly any theory involving dynamic recrystallisation must take into account the nucleation mechanisms observed experimentally.

Secondly the compositional variations which occur in rocks must be taken into consideration. The effect of precipitates in pinning grain boundaries is well known in metallurgy: the presence of impurity phases at grain boundaries in minerals must have a similar effect. The role of water in grain boundary mobility must also be understood if the kinetics of boundary migration are to be determined.

5.5.3. Estimation of the flow stress in magnesium using paleo-stress Techniques

5.5.3.1. Introduction

Recrystallised grain sizes have often been measured in rock microstructures in order to infer the stresses at the time of deformation. As pointed out in the preceding section the idea has its foundations in the well proven empirical relationship

$$\sigma = K D^{-n}$$

formulated for cubic metals (i.e. metals of high structural symmetry) where the stress can be related to a homogeneous recrystallised grain size once steady state flow has been reached. Since rock microstructures are not usually homogeneous and steady state has not always been achieved, it was thought useful to examine the magnesium microstructures where similar problems arise, to see whether or not recrystallised grain sizes could be related to specific points along a stress strain curve.

Two effects will first of all be considered in samples deformed at $260^{o}C$, $\dot{\varepsilon} = 10^{-5}s^{-1}$

1) Preferred orientation of the old grains
2) Increase in strain in specimens unfavourably oriented for basal slip.

This will be followed by a discussion of recrystallised grain size in specimens which contain well developed shear zones.

5.5.3.2. Effect of the preferred orientation of the old grains

The preferred orientation of the old grains is largely responsible for the morphology of the initial part of the stress strain curves, and the strain at which dynamic recrystallisation occurs in deformed magnesium. In samples unfavourably oriented for basal slip dynamically recrystallised grains 25μm in size were present around the old grains at 35% strain. The bulk stress at this point was 5.5 MPa. Dynamic recrystallisation did not occur until much higher strains had been reached in samples where the old grains were favourably oriented for

basal slip. In this case dynamically recrystallised grains 20μm in size were present around the old grains at 70% strain. The stress strain curve had registered steady state beyond 25% strain and the stress on the bulk sample at this point was 2.75 MPa. Thus two samples record completely different microstructures and bulk stresses by virtue of their initial orientations. The two are completely inconsistent since the specimen with the smaller recrystallised grain size registered a lower stress.

5.5.3.3. Effect of increase in strain in specimens unfavourably oriented for basal slip

Two samples deformed at $\dot{\varepsilon} = 10^{-5}s^{-1}$, $T = 260^{o}C$ contained dynamically recrystallised grains 25μm in size both at 35% strain and at 47% strain but the bulk stresses at these two strains were 5.50 MPa and 3.50 MPa respectively. Thus samples with a duplex microstructure do not show a simple relationship between bulk stress and recrystallised grain size.

The above two paragraphs have shown that in magnesium when the microstructure is heterogeneous the size of the recrystallised grains will depend to a large extent on the past structural history of the specimen and on the preferred orientation of the old grains.
As the formation of dynamically recrystallised grains depends on the stresses and strains at the old grain boundaries it will be difficult to relate the grain size to the macroscopic applied stress.

5.5.3.4. Recrystallised grain sizes in specimens which contain well developed shear zones

i) Grain sizes in the shear zone.

The microstructure within the shear zone formed at $260^{o}C$ and a bulk strain rate of $10^{-5}s^{-1}$ was relatively speaking homogeneous, the average grain size being 20μm. The shear zone (as discussed in section 4.4.5) had accommodated most of the strain imposed by the crosshead motion of the deformation rig. It was suggested that the microstructure within the shear zone was maintained by a combination of basal slip, shear and continuous dynamic recrystallisation. It would appear to be reasonable to suppose that the recrystallised grain size in the shear zone would reflect the load being felt by the specimen as a whole. Obviously the area over which the load is supported would have to be taken into account and there would only be a simple relationship provided that the grain size in the shear zone was homogeneous and that substantial voiding had not occurred.

ii) Grain sizes outside the shear zone.

It is difficult to see how the recrystallised grains outside the shear zone can be simply related to a given applied stress since most of the deformation is accommodated in the shear zone and the areas outside the shear zone are in effect undergoing relaxation. Since the microstructure is also heterogeneous then the implications of (1) and (2) discussed above will also apply.

5.6. CONCLUSIONS

The preceding sections have shown that the hexagonal close packed metal magnesium is a useful analogue in a broad sense when considering geological deformation. Whilst there are no doubt many similarities between metals and minerals in general, care must be taken when making comparisons and interpreting geological microstructures in terms of metallurgical models which may be too simplistic and not fully understood. The fact that magnesium is anisotropic and therefore deforms heterogeneously exhibiting recrystallisation by lattice rotation and shear zone formation would seem to indicate that its behaviour is more relevant than that of cubic metals normally referred to by geologists.

CHAPTER 6

Conclusions and Suggestions for Further Work

CONCLUSIONS AND SUGGESTIONS FOR FURTHER WORK

6.1. CONCLUSIONS

1. The deformation of polycrystalline Magnox A180 below 320^{o}C is heterogeneous.
2. The heterogeneous deformation is a result of the lack of five independent modes of deformation. Grain boundary constraints and limited slip force lattice rotations to occur at grain boundaries.
3. Dynamic recrystallisation at the old grain boundaries occurs as a consequence of the heterogeneous deformation. The mechanism is more akin to the mechanism of subgrain rotation reported in minerals than to the bulge nucleation and growth mechanism normally reported in metals.
4. The lack of independent slip systems is thought to be more important than stacking fault energy as a criterion for dynamic recrystallisation in this material. Normally dynamic recrystallisation is reported in materials with a low stacking fault energy whereas the reported value for this parameter in magnesium is high.
5. The preferred orientation of the starting material is important in influencing the development of microstructure.
6. Dynamic recrystallisation leads to texture softening and the development of shear zones in magnesium.
7. The comparison of the microstructures of the deformed metal with deformed minerals has shown that the mechanisms operating in magnesium may be similar to those in minerals such as quartzite and calcite. It is thought that the heterogeneous behaviour of this anisotropic metal renders it more useful as an analogue in interpreting deformation mechanisms in minerals than the cubic metals normally referred to by geologists.

6.2. SUGGESTIONS FOR FUTURE WORK

The study undertaken of the magnesium alloy has emphasised the importance of dynamic recrystallisation in microstructural development with increasing strain. Whilst a broad picture of the deformation behaviour has been obtained there are still areas where further research would provide a greater understanding of the microstructural mechanisms, firstly in magnesium and secondly in other materials.

6.2.1. Magnesium

a) Detailed electron microscopy of the mantles of old grains would provide a more complete picture of the mechanism of dynamic recrystallisation and the relationships between old and new grains.

b) The split cylinder method (Spiers 1979), utilizing Electron Back Scattered Patterns and Channel Patterns, could be used to determine the orientations of grains before and after deformation and thereby to ascertain their relative movement during deformation.

c) In-situ deformation of macroscopic specimens of magnesium in a scanning electron microscope should be possible. This would be particularly useful in further studies of the initiation and development of shear zones in the material.

d) The studies of shear zones in this thesis have mainly been confined to their initiation: investigations of the development of microstructure at high strains would ascertain whether or not the deformation is accommodated within a single zone at high strain or whether secondary zones are activated and if so enable the consequent interaction between them to be studied.

e) Deformation of the metal in conditions of pure shear should also provide further information about the development of shear zones.

f) Other experiments such as a study of the effect of initial grain size and a more detailed investigation of the effect of preferred orientation on microstructural development could also be carried out as an extension of the present work.

6.2.2. Other Materials

a) Experiments on other anisotropic materials could be carried out to investigate the effect of crystallography on dynamic recrystallisation.

b) Detailed studies of the microstructural development in cubic metals in conditions similar to those used for the magnesium would provide a clearer picture of the mechanisms operating in these materials, as microstructural aspects of dynamic recrystallisation have tended to play a secondary role in the past.

c) The in-situ experiments on the transparent organic solid camphor have proved useful in suggesting mechanisms of strain accommodation: this work could be extended to other similar materials.

Finally it should be possible to derive quantitative models of the processes which occur during dynamic recrystallisation. These models must take into account the experimentally observed mechanisms.

REFERENCES

Adenis, D.J.P. and Couling, S.L. (1964)
Formation of recrystallisation within {10$\bar{1}$2} twin bands in a polycrystalline Mg alloy.
Trans AIME 230, 554.

Agar, A.W. (1974)
Future developments of the electron microscope
in Practical methods in electron microscopy, p.301, Vol. 2
Ed. A.M. Glauert, North-Holland, Amsterdam.

Ardell, A.J., Christie, J.M. and Tullis, J. (1973)
Dislocation substructure in deformed rocks.
Crystal Lattice defects 4 275.

Ashby, M.F. (1970)
The deformation of plastically non-homogeneous materials.
Phil. Mag. 21, 399.

Ashby, M.F. (1972)
A first report on deformation-mechanism maps.
Acta Met. 20, 887-897.

Ashby, M.F. and Verrall, R.A. (1973)
Diffusion accommodated flow and superplasticity.
Acta Met. 21, 149-163.

ASTM Book of standards E-81
1963 part 31.

Baeta, R.D. and Ashbee, K.H.G. (1969)
Slip systems in quartz: I, Experiments.
Amer. Mineralogist 54, 1551.

Slip systems in quartz: II, Interpretation.
Amer. Mineralogist 54, 1574.

Bailey, J.E. and Hirsch, P.B. (1962)
The recrystallisation process in some polycrystalline metals.
Proc. Royal Soc. 267A, 11.

Bakarian, P.W. and Mathewson, C.H. (1943)
Slip and twinning in magnesium single crystals at elevated temperatures.
Trans. Amer. Inst. Min. (Metall) Engrs. 152, (1943) 226.

Baker, D.W., Wenk, H.R. and Christie, J.M. (1969)
X-ray analysis of preferred orientations in fine grained quartz aggregates.
J. Geol. 77, 144.

Ball, A. and Hutchinson, M.M. (1969)
Superplasticity in the Al-Zn eutectoid.
Met. Sci. J. 3, 1-7.

Barber, D.J. and Wenk, H.R. (1973)
The microstructure of experimentally deformed limestones.
J. Mater. Sci. 8, 500.

Barrett, C.R. (1965)
A note on the creep substructure of pure copper.
Acta Met. 13, 1088.

Barrett, C.S. and Sherby, O.D. (1964)
Steady-state creep characteristics of polycrystalline copper in the temperature range 400 to 950°C.
Trans. Met. Soc. AIME 230, 1322.

Barrett, C.R., Nix, W.D. and Sherby, O.D. (1965)
A model for steady state creep based on the motion of jogged screw dislocations.
Acta Met. 13, 1247.

Barrett, C.R., Muehleisen, E.C.and Nix, W.G. (1972)
Low temperature - low stress creep of Al and Al + 0.5%Fe.
Mat. Sci. Eng. 10 (1) 33.

Beck, P.A. and Sperry, P.R. (1950)
Strain induced grain boundary migration in high purity aluminium.
J. Appl. Phys. 21, 150.

Beere, W. (1978)
Stress and deformation at grain boundaries.
Phil. Trans. R. Soc. Lond A, 288, 177.

Bell, R.L. and Langdon, T.G. (1967)
An investigation of grain boundary sliding during creep.
J. Mat. Sci. 2, 313.

Bell, T.H. and Etheridge, M.A. (1973)
Microstructure of mylonites and their descriptive terminology.
Lithos 6, 337.

Bell, T.H. and Etheridge, M.A. (1976)
The deformation and recrystallisation of quartz in a mylonite zone, Central Australia.
Tectonophysics, 32, 238.

Bellier, S.P. and Doherty, R.D. (1977)
The structure of deformed aluminium and its recrystallisation.
Investigation with transmission Kossel diffraction.
Acta Met. 25, 521.

Bird, J.E., Mukherjee, A.K. and Dorn, J.E. (1969)
Correlations between high-temperature creep behaviour and structure.
in Quantitative relation between properties and microstructure, University Press, Jerusalem, 1969.

Blacic,J.D. (1971)
Plastic deformation mechanisms in quartz: the effect of water.
Tectonophys. 27, 271.

Borg, I.Y., and Handin, J. (1967)
Torsion of calcite single crystals.
J. Geophys. Res. 72, 641.

Briers, G.W., Dawe, D.W., Dewey, M.A.P. and Brammar, I.S. (1963)
A technique for the rapid preparation of thin foils for electron microscopy from bulk materials.
J. Inst. Metals 1964-65, 93, 77.

Brodie, K.H. (1979)
Microstructural and geochemical studies of some deformed ultramafic rocks.
Ph.D. thesis, University of London.

Bromley, R. and Sellars, C.M. (1973)
High temperature deformation of copper and copper-aluminium alloys.
in The microstructure and design of alloys, Third Int. Conf. on Strength of metals and alloys, Vol. 1, 380, London: Inst. of Metals; Iron and Steel Inst.

Brookes, P.E., Kirby, N. and Burke, W.T. (1959-60)
The creep and high temperature fatigue properties of the Mg based canning alloy Magnox A12.
J. Inst. Met. 88, 500.

Burke, E.C. and Hibbard, W.R. (1952)
Plastic deformation of Mg single crystals.
J. Metals 4, 295.

Burton, B. (1972)
The low stress creep of aluminium near to the melting point: the influence of oxidation and substructural changes.
Phil. Mag. 25, 645.

Byrne, J.G. (1963)
Recrystallisation and void formation during elevated temperature deformation of magnesium alloys.
Trans. A.S.M. 56, 68.

Carreras, J. (1974)
Progressive mylonitization in quartzitic and quarto-feldspathic rocks in the shear belts of the Cabo de Creus E-Pyrenees, Spain.
M.Sc. thesis, Imperial College of Science and Technology, 1974.

Carter, N.L. (1976)
Steady state flow of rocks.
Rev. of geophys + space physics, 14, 301.

Carter, N.L., Christie, J.M. and Griggs, D.T. (1964)
Experimental deformation and recrystallisation of quartz.
J. Geol. U.S.A. 72, 687.

Chaudhari, P. (1967)
Deformation behaviour of superplastic Zn-Al alloy.
Acta Met. 15, 1777.

Chaudhuri, A.R., Grant, N.J. and Norton, J.T. (1953)
Metallographic observations of the deformation of high purity Mg in creep at 500°F.
J. Metals 5, 712.

Chaudhuri, A.R., Chang, H.C. and Grant, N.J. (1955)
Creep deformation of magnesium at elevated temperatures by non-basal slip.
Trans. AIME, 203, 682. also J. Metals 7, 682.

Chen, C.W. and Machlin, E.S. (1957)
On a mechanism of high temperature intercrystalline cracking.
Trans AIME 209, 829.

Christie, J.M., Carter, N.L. and Griggs, D.T. (1964)
Experimental evidence of basal slip in quartz.
J. Geol. U.S.A. 72, 734.

Christie, J.M. and Ardell, A.J. (1974)
Substructures of deformation lamellae in quartz.
Geology 1, 405.

Coble, R.L. (1963)
A model for boundary diffusion controlled creep in polycrystalline materials.
J. Appl. Phys. 34, 1679.

Couling, S.L. and Pearsall, G.W. (1957)
Determination of orientation in Mg by polarised light examination.
Trans. AIME, 1957, p.939.

Couling, S.L., Pashak, J.F. and Sturkey, L. (1959)
Unique deformation and ageing characteristics of certain magnesium base alloys.
Trans. Am. Soc. Metals 51, 94.

Crocker, A.G. and Abell, J.S. (1976)
The crystallography of deformation kinking.
Phil. Mag. 33, 305.

Crossland, I.G. and Jones, R.B. (1972)
Dislocation creep in magnesium.
Metal. Sci. J. 6, 162.

Crussard, C. and Friedel, J. (1956)
Creep and fracture of metals at high temperatures
p.255, London, H.M.S.O.

Cullity, B.D. (1959)
Elements of X-ray diffraction.
Addison-Wesley Inc. p.215.

Edelin, G. and Poirier, J.P. (1973)
Etude de la montée des dislocations au moyen d'experiences de fluage par diffusion dans le magnesium.
Phil. Mag. 28, 1203.

Edington, J.W., Melton, K.N. and Cutler, C.P. (1976)
Superplasticity.
Prog. Mater. Sci. 21, 61.

Emley, E.F. (1966)
Principles of magnesium technology.
Pergamon Press, 1966.

Etheridge, M.A. and Wilkie, J.C. (1979)
Grain size reduction, grain boundary sliding and the flow strength of mylonites.
Tectonophysics 58, 1979 (in press).

Evans, H.E. (1969)
The mechanism of void growth and factors affecting the onset of intergranular failure during creep of a Mg-0.8%Al alloy.
Metal Sci. J. 3, 33.

Fleck, R.G., Taplin, D.M.R. and Beevers, C.J. (1975)
An investigation of the nucleation of creep cavities by IMV electron microscopy.
Acta. Met. 23, 415.

Fraser, H.L., Smallman, R.E. and Loretto, M.H. (1973)
The plastic deformation of NiAl single crystals between 300°K and 1050°K.
I. Experimental evidence on the role of kinking and uniform deformation in crystals compressed along <001>. Phil. Mag. 28, 651.
II. The mechanism of kinking and uniform deformation. Phil. Mag. 28, 667.

Friedel, J. (1964)
Dislocations.
Pergamon Press, London, Chapters V and XI.

Frost, H.J. and Ashby, M.F. (1975)
Deformation-mechanism maps and the creep of tungsten lamp filaments.
in Rate processes in Plastic Deformation of Materials, A.S.M. 4, p.70.

Garafalo, F. (1965)
Fundamentals of creep and creep-rupture in metals.
McMillan Series in Materials Science.

Gardner, K.J. and Grimes, R. (1979)
Recrystallisation during hot deformation of aluminium alloys.
Metal Sci. J. 13 March-April 1979, 216.

Geckinli, A.E. and Barrett, C.R. (1976)
Superplastic deformation of the Pb-Sn eutectic.
J. Mater. Sci. 11, 510.

George, P.F. (1947)
Some special metallographic techniques for magnesium alloys.
Trans A.S.M. 38, 686.

Gibbs, G.B. (1965)
Creep and stress relaxation studies with polycrystalline magnesium.
Phil. Mag. 13, 317.

Gifkins, R.C. (1956)
A mechanism for the formation of intergranular cracks when boundary sliding occurs.
Acta Met. 4, 98.

Gifkins, R.C. (1976)
Activation energies for superplastic materials.
Scripta Met. 10, 433-436.

Gifkins, R.C. (1978)
Grain rearrangements during superplastic deformation.
J. Mater. Sci. 13, 1926-1936.

Gifkins, R.C., Gittins, A., Bell, R.L. and Langdon, T.G. (1968)
The dependence of GBS on shear stress.
J. Mat. Sci. 3, 306-313.

Geckinli, A.E. and Barrett, C.R. (1976)
Superplastic deformation of the Pb-Sn eutectic.
J. Mater. Sci. 11, 510.

Gilman, J.J. (1954)
Mechanism of ortho kink-band formation in compressed zinc monocrystals.
J. Metals, Vol. 7, 621.

Gilman, J.J. (1956)
Etch pits and dislocations in zinc monocrystals.
J. Metals, Vol. 9, 998.

Gilman, J.J. (1969)
Micromechanics of flow in solids.
McGraw-Hill series in materials science and engineering, p.60.

Gleiter, H., Hornbogen, E. and Bard, G. (1968)
The mechanism of grain boundary glide (abs)
Acta Met. 16, 1053.

Glover, G. and Sellars, C.M. (1973)
Recovery and Recrystallisation during high temperature deformation of α-Fe.
Met. Trans. 4, 765-775.

Goods, S.H. and Brown, L.M. (1979)
The nucleation of cavities by plastic deformation.
Acta Met. 27, 1.

Gottstein, G., Zabardjas, D. and Melking, H. (1979)
Dynamic recrystallisation in tension deformed Cu single crystals.
Metal Sci. 13, 223-227.

Green, H.W. and Radcliffe, S.V. (1972)
Deformation processes in the upper mantle.
In Flow and Fracture of Rocks, Geophys. Monogr. Ser. Vol. 16.
Ed. H.C. Heard, I.Y. Borg, N.L. Carter and C.B. Raleigh, p.139
A.G.U. Wahsington, D.C.

Greenwood, J.N. (1952)
Intercrystalline cracking of metals.
J.I.S.I. 171, 380.

Greenwood, J.N., Miller, D.R. and Suiter, J.W. (1954)
Intergranular cavitation in stressed metals.
Acta Met. 2, 250.

Griggs, D.T. (1967)
Hydrolytic weakening of quartz and other silicates.
Geophys. J.R. astr. Soc. 14, 19.

Griggs, D.T., Turner, F.J. and Heard, M.C. (1960)
Deformation of rocks at 500°C - 800°C.
In: Griggs, D.T. and Handin, J. (eds) Rock Deformation, 39-104
Geol. Soc. Am. Mem. 79.

Griggs, D.T. and Blaicic, J.D. (1964)
The strength of quartz in the ductile regime.
Trans. Amer. Geophy. Un. 45, 102.

Griggs, D.T. and Blaicic, J.D. (1965)
Quartz: Anomalous weakness of synthetic crystals.
Science, U.S.A. 147, 292.

Guillope, M. and Poirier, J.P. (1979)
Dynamic recrystallisation during creep of single crystalline halite:
an experimental study.
J. Geophys. Res. (in press).

Hallimond, A.F. (1953)
The polarizing microscope p.116 2nd Edition
York Cooke, Troughton and Simms Ltd.

Harper, J. and Dorn, J.E. (1957)
Viscous creep of aluminium near its melting temperature.
Acta Met. 5, 654

Harper, J.G., Sheppard, L.A. and Dorn, J.E.
Creep of aluminium under extremely small stresses.
Acta. Met. 6, 509.

Harris, J.E. (1963)
Recrystallisation and grain boundary sliding in a magnesium alloy.
Nature 200, 1197.

Harris, J.E. (1965)
An analysis of creep ductility of Magnox A180 and its implications.
J. Nucl. Mat. 15, 201.

Harris, J.E. (1965)
Nucleation of creep cavities in magnesium.
Trans. Met. Soc. AIME 233, 1509.

Harris, J.E. and Masters, B.C.
The annealing of faulted loops in magnesium and zinc.
Proc. Royal Soc. Lond. A 292, 240

Harris, J.E., Jones, R.B., Greenwood, G.W. and Ward, M.J. (1969)
The inhibition of Nabarro-Herring creep by second phase particles.
Proc. Int. Conf. on 'Interfaces' Melbourne Aug. 1969
also J. Aust Inst. Metals 14, 154.

Hartt, W.H. and Reed-Hill, R.E. (1967)
The irrational habit of second-order $\{10\bar{1}1\}$-$\{10\bar{1}2\}$ twins in magnesium.
Trans. AIME 239, 1511.

Hauser, F.E., Landon, P.R. and Dorn, J.E. (1956)
Deformation and fracture mechanisms of polycrystalline Mg at low temperature.
Trans. Am. Soc. Metals 48, 986.

Hauser, F.E., Landon, P.R. and Dorn, J.E. (1958)
Deformation and fracture of alpha solid solution of lithium in magnesium.
Trans ASM 50, 856.

Hausselt, J. and Blum, W. (1976)
Dynamic recovery during and after steady state deformation of Al-11wt%Zn.
Acta Met. 24 p.1027-1039.

Heard, H.C. and Raleigh, C.B. (1972)
Steady-state flow in marble at 500-800^{o}C.
Geol. Soc. Amer. Bull. 83, 935.

Hearing, C. (1950)
Diffusional viscosity of a polycrystalline solid.
J. Appl. Phys. 21, 437.

Higgins, G.T. (1963)
Secondary recrystallisation in Magnox A180.
J. Nucl. Mat. 8, 153.

Hobbs, B.E. (1968)
Recrystallisation of single crystals of quartz.
Tectonophysics 6, 353.

Hobbs, B.E., McLaren, A.C. and Paterson, M.S. (1972)
Plasticity of single crystals of synthetic quartz.
in Flow and Fracture of rocks (ed. H.C. Heard, I.Y. Borg, N.L. Carter and C.B. Raleigh) Amer. Geophys. Union, Geophys Monogr. Ser. 16, 29.

Honeycombe, R.W.K. (1968)
The plastic deformation of metals.
Arnold.

Honeycombe, R.W.K. and May, M.J. (1960-61)
Discussion on magnesium alloys for fuel-element components.
J. Inst. Metals 89, p.397.

Horton, C.A.P. (1975)
The interdependence between grain boundary sliding and grain creep deformation.
In "Grain Boundaries in Engineering Materials" Proc. A.S.M. 4th Bolton Landing Conference p.355. ed. J.L. Walter, J.H. Westbrook and D.A. Woodford, Claitor, Baton Rouge.

Hull, D. and Rimmer, D.E. (1959)
The growth of grain-boundary voids under stress.
Phil. Mag. 4, 673.

Intrater, J. and Machlin, E.S. (1959-60)
Grain boundary sliding in copper bicrystals.
J. Inst. Metals, 88, 305.

Ishida, Y. and McLean, D. (1967)
The formation and growth of cavities in creep.
Met. Sci. J. 1, 171.

Jaffe, N. and Dorn, J.E. (1962)
Effect of stress on the creep rate of high-purity aluminium in the cross-slip region.
Trans. AIME 224, 1167.

Johanneson, T. and Tholen, A. (1970)
On the influence of grain boundaries on mechanical properties.
Phil. Mag. 21, 1223.

Johannesson, T. and Tholen, A. (1972)
The role of grain boundaries in creep deformation.
Metal. Sci. J. 6, 189.

Johnson, R.H. (1970)
Superplasticity.
Met. Rev. 146, 115.

Jonas, J.J., Sellars, C.M. and Tegart, W.J.McG. (1969)
Strength and structure under hot working conditions.
Met. Rev. 14, 1-24.

Jones, R.B. (1965)
Diffusion creep in polycrystalline magnesium.
Nature 207, 70.

Jones, R.B. and Harris, J.E. (1963)
Creep deformation of polycrystalline magnesium.
Proc. Joint Int. Conf. on Creep, Inst. Mech. Eng. p.1-1-1.8.

Karim, A. (1969)
On the nature of superplastic deformation in the Mg-Al eutectic.
Scripta Met. 3, 887.

Karim, A., Holt, D.L. and Backofen, W.A. (1969)
Diffusional creep and superplasticity in a Mg-6Zn-0.5Zr alloy.
Trans. AIME 245, 1131.

Kestenback, H.J., Krause, W. and Silveira, T.L. da (1978)
Creep of 316 stainless steel under high stress.
Acta Met. 26, 661.

King, A.H. and Smith, D.A. (1979)
Nucleation of recrystallisation - model for strain-induced grain boundary migration.
Met. Sci. J. 13, Nos. 3-4, 113.

Kocks, U.F. (1975)
The recovery glide theory of creep.
J.E. Dorn Memorial Symposium ASM 8, 356.

Lagnesborg, R. (1972)
Dislocation mechanisms in creep.
Int. Met. Rev. 17, 130.

Langdon, T.G. (1965)
The role of grain boundary sliding in creep.
Ph.D. Thesis, University of London.

Langdon, T.G. (1975)
Grain boundary processes during creep.
in J.E. Dorn Memorial Symp. ASM 410.

Langdon, T.G. (1975)
The enhancement of creep rates in engineering materials due to grain boundary processes.
In "Grain Boundaries in Engineering Materials" Proc. ASM 4th Bolton Landing Conference p.339. ed. J.L. Walter, J.H. Westbrook and D.A. Woodford, Claitor, Baton Rouge.

Leed (1969)
Reply to: On the nature of superplastic deformation in the Mg-Al eutectic.
Scripta Met. 3.

Lister, G.S. (1978)
Texture transitions in plastically deformed calcite rocks.
Proc. 5th Int. Conf. on Textures, Aachen, April 1978.

Lubahn, J.D. (1961)
Plasticity and creep of metals.
John Wiley and Sons.

Luton, M.J. and Sellars, C.M. (1969)
Dynamic recrystallisation in Ni-Fe alloys during high temperature deformation.
Acta Met. 17, 1033-1043.

Lytton, J.L., Barrett, C.R. and Sherby, O.D. (1965)
Substructure formation during high temperature creep of (110)[001] - oriented polycrystalline Fe-3.1%Si.
Trans. AIME 233, 1399.

McLaren, A.C., Turner, R.G., Boland, J.N. and Hobbs, B.E. (1970)
Dislocation structure of the deformation lamellae in synthetic quartz: a study by electron and optical microscopy.
Contr. Mineral and Petrol. 29, 104.

McLaren, A.C. and Hobbs, B.E. (1972)
Transmission electron microscope investigation of some naturally deformed quartzites.
A.M. Geophys. Union Geophys. Monograph Ser. 16, 55.

McLean, D.L. (1963)
J. Aust. Inst. Met. 8, 45.

McQueen, H.J. (1977)
The production and utility of recovered disc substructures.
Met. Trans. 8A, 807.

McQueen, H.J., Wong, W.S. and Jonas, J.J. (1967)
Deformation of alumijium at high temperatures and strain rates.
Can. J. Phys. 45, 1225-1235.

McQueen, H.J. and Bergerson, S. (1972)
Dynamic Recrystallisation of Cu during hot torsion.
Met. Sci. J. 6, 25-29.

McQueen, H.J. and Jonas, J.J. (1975)
Recovery and recrystallisation during high temperature deformation.
Treatise on Materials Science and Technology 6, 393. ed. Arsenault, R.J.

McQueen, H.J. and Baudelet, B. (1979)
Comparison and contrast of mechanisms, microstructures ductilities in superplasticity and dynamic recovery and recrystallisation.
in Strength of metals and alloys, ed. Haasen, P., Gerold V, and Kostorz, G. Vol. 1, p.329, Pergamon Press.
Proc. 5th Int. Conf. on Strength of Metals and Alloys, Aachen, W. Germany, Aug. 27-31, 1979.

McQueen, H.J. (1979)
Metallography and the mechanisms related to the hot working of metals.
Microstructural Science, Vol 7, p.71, Elsevier North Holland, Inc.

Machlin, E.S. (1956)
Creep rupture by vacancy condensation.
Trans. AIME 206, 106.

Meching, H. and Kirch, F. (1971)
Recovery and recrystallisation during deformation.
in Recrystallisation of metallic materials, 1st ed. 257, ed. Haessner.

Mercier, J.C.C., Anderson, D.A. and Carter, N.L. (1977)
Stress in the lithosphere. Inferences of steady state flow of rocks.
Pageophys. 115, 199.

Mohamed, F.A., Murty, K.L. and Morris, J.W. Jr. (1973)
Harper-Dorn Creep in Al, Pb and Sn.
Met. Trans. 4, 935.

Mohamed, F.A. and Langdon, T.G. (1974)
Deformation mechanism maps based on grain size.
Met. Trans. 5, 2339.

Mohamed, F.A., Murty, K.L. and Morris, J.W.Jr. (1975)
Harper-Dorn creep of metals at high temperatures.
in Rate Processes in plastic deformation of materials, A.S.M. 4, 459.

Mukherjee, A.K. (1971)
The rate controlling mechanism in superplasticity.
Mater. Sci. Eng. 8, 83.

Mukherjee, A.K. (1975)
High temperature creep.
in Treatise on Mater. Sci. and Technol. 6, 163, ed. R.J. Arsenault,
Academic Press, New York, 1975.

Nabarro, F.R.N. (1948)
Rep. Bristol Conf. Strength of Solids, p.75,
Phys. Soc. Lond.

Naziri, H., Pearce, R., Henderson-Brown, M. and Halek, F. (1975)
Microstructural-mechanism relationship in the zinc/aluminium eutectoid superplastic alloy.
Acta Met. 23, 489.

Nicolas, A. and Poirier, J.P. (1976)
Crystalline plasticity and solid state flow in metamorphic rocks,
Wiley-Interscience.

Orowan, E. (1942)
A type of plastic deformation new in metals.
Nature, Lond. 149, 643.

Orowan, E. (1947)
'Discussion' Symposium on Internal Stresses, p.451.
Inst. Metals, London.

Paterson, M.S. and Kekulawala, K.R.S.S. (1979)
The role of water in quartz deformation.
Bull. Mineral. 102, nos. 2-3, 92.

Pickles, B.W. (1967)
The creep behaviour of heat treated Magnox ZR55 in the temperature range 350-450°C.
J. Inst. Met. 95, 333.

Poirier, J.P. (1978)
Is power-law creep diffusion controlled?
Acta Met. 26, p.629-637.

Poirier, J.P. and Nicolas, A. (1975)
Deformation induced recrystallisation by progressive misorientation of subgrain boundaries, with special reference to mantle peridotites.
J. Geology, 83, 707.

Poirier, J.P. and Guillope, M. (1979)
Deformation-induced recrystallisation of minerals.
Bull. Mineral. 102, Vol. 2-3, 1.

Raj, R. and Ashby, M.F. (1971)
On grain boundary sliding and diffusional creep.
Met. Trans. 2, 1113.

Ramsay, J.G. (1967)
Folding and fracturing of rocks.
McGraw-Hill, New York.

Ramsay, J.G. and Graham, R.H. (1970)
Strain variation in shear belts.
Can. J. of Earth Sci. 7, 786.

Raraty, L.E. (1966)
A comment on "Diffusion creep deformation" in a magnesium reactor component.
J. Nucl. Mat. 20, 344.

Raynor, G.V. (1959)
The physical metallurgy of magnesium and its alloys.
International series of monographs on metal physics and physical metallurgy
Vol. 5, Pergamon Press, 1959.

Reed-Hill, R.E. (1960)
A study of the $\{10\bar{1}1\}$ and $\{10\bar{1}3\}$ twinning modes in magnesium.
Trans AIME 218, 554.

Reed-Hill, R.E. and Robertson, W.D. (1957)
Additional modes of deformation twinning in magnesium.
Acta Met. 5, 717.

Richardson, G.J., Sellars, C.M. and Tegart, W.J.McG. (1966)
Recrystallisation during creep of nickel.
Acta Met. 14, 1225.

Roberts, C.S. (1953)
Creep behaviour of extruded electrolytic magnesium.
Trans. AIME, J. Metals Sept. 1953, p.1121.

Roberts, C.S. (1960)
Magnesium and its alloys.
John Wiley and Sond, 1960, New York.

Roberts, W. and Ahlblohm, B. (1978)
A nucleation criterion for dynamic recrystallisation during hot working.
Acta Met. 26, p.801-813.

Roberts, W., Boden, H. and Ahlblom, B. (1979)
Dynamic recrystallisation kinetics.
Metal Sci. J. 13, Nos. 3-4, 195.

Rutter, E.H. (1974)
The influence of temperature, strain rate and interstitial water in the experimental deformation of calcite rocks.
Tectonophysics 22, 311.

Rutter, E.H. (1976)
The kinetics of rock deformation by pressure solution.
Phil. Trans. R. Soc. Lond. A, 283, 203.

Sah, J.P., Richardson, G.J. and Sellars, C.M. (1974)
Grain size effects during dynamic recrystallisation of nickel.
Metal Sci. J. 8, 325.

Sestak, B. (1979)
Plasticity and crystal structure.
in Strength of metals and alloys, Vol. 3 (in press), ed. Haasen P, Gerold, V. and Kosborz, G. Proc. 5th Int. Conf. on Strength of metals and alloys, Aachen, W. Germany, August, 27-31, 1979.

Schmid, S.M. (1976)
Rheological evidence for changes in the deformation mechanism of Solenhofen limestone towards low stress.
Tectonophysics 31, T21.

Schmid, S. (1976)
Steady state flow of Solenhofen limestone.
Unpublished data presented at Tectonic Studies Meeting University of Leeds, December 1976.

Schmid, S. (1979)
Discussion on "Difficulties associated with paleo-stress estimates" by S.H. White.
Bull. Mineral 162, 215.

Schmid, S.M., Boland, J.N. and Paterson, M.S. (1977)
Superplastic flow in fine-grained limestone.
Tectonophysics 43, 257.

Schulz, L.G. (1949)
Determination of preferred orientation in flat transmission samples using a Geiger counter X-ray spectrometer.
J. Appl. Phys. 20, 1033.

Sellars, C.M. (1978)
Recrystallisation during hot deformation.
In Creep in Engineering Materials and of the Earth. Proc. Royal Soc.
Phil. Trans. R. Soc. Lond. A288, 147-58.

Servi, I.S. and Grant, N.J. (1951)
Structure observations of aluminium deformed in creep at elevated temperatures.
Trans. AIME, 191, 917.

Shaw, N.D. (1979)
Field and experimental studies of deformation and recrystallisation in carbonate rocks.
Ph.D. thesis, University of London (in press).

Sherby, O.D. and Burke, P.M. (1968)
Mechanical behaviour of crystalline solids at elevated temperatures.
Prog. Mater. Sci. 13, 325-390.

Sherby, O.D., Klundt, R.H. and Miller, A.K. (1977)
Flow stress, subgrain size and subgrain stability at elevated temperatures.
Met. Trans. A, 8A, 843.

Shewmon, P.G. and Rhines, F.N. (1954)
Rate of self diffusion in polycrystalline magnesium.
Trans. AIME, 200, 1021.

Smallman, R.E. and Ashbee, K.H.G. (1966)
Modern metallography p.74.
Pergamon Press.

Speight, M.V. (1976)
The role of GBS in the creep of polycrystals.
Acta. Met. 24, 725-729.

Spiers, C.J. (1979)(a)
Experimental deformation of polycrystalline calcite.
Ph.D. Thesis, University of London.

Spiers, C.J. (1979)
Fabric development in calcite polycrystals deformed at 400°C.
Bull Mineral. 102, 282.

Squires, R.L., Weiner, R.T. and Phillips, M. (1963)
Letter to editor Grain boundary denuded zones in a Mg-½wt%Zr alloy.
J. Nucl. Mat. 8, 77.

Stacey, R.D. (1958)
Deformation mechanisms in Mg and some Mg-Al alloys.
Metallurgia, 58, 125.

Stohr, J.F., Poirier, J.P. (1972)
Etude en microscope electronique du glissement pyramidal {11$\bar{2}$2} <11$\bar{2}$3>
dans le magnesium.
Phil. Mag. 25, 1313.

Stuwe, H.P., and Ortner, B. (1974)
Recrystallisation in hot working and creep.
Metal. Sci. 8, 161.

Suiter, J.W. and Wood, W.A. (1952/53)
Deformation of magnesium at various rates and temperatures.
J. Inst. Metals 81, 181.

Takeuchi, S. and Argon, A.S. (1976)
Steady state creep of single-phase crystalline matter at high temperatures.
J. Mat. Sci. 11, 1542.

Tapetado, E.G. and Loretto, M.H. (1974)
A study of kinking and buckling in zinc single crystals.
Phil. Mag. 30, 515.

Taplin, D.M.R. and Wingrove, A.L. (1967)
Study of intergranular cavitation in iron by electron microscopy of
fracture surfaces.
Acta Met. 15, 1231.

Taylor, G.I. (1938)
Plastic strain in metals.
J. Inst. Metals, 62, 307.

Tegart, W.J. McG. (1961)
Activation energies for high temperature creep of polycrystalline Mg.
Acta Met. 9, 614-616.

Tegart, W.J. Mc.G. (1963)
Independent Slip systems and ductility of hexagonal polycrystals.
Phil. Mag. 4, 339.

Tegart, W.G. McG. and Sherby, O.D. (1958)
Activation energies for high temperature creep of polycrystalline zinc.
Phil. Mag. 3, 1287.

Tullis, J.A., Christie, J.M. and Griggs, D.T. (1973)
Microstructures and Preferred orientations of experimentally deformed quartzites.
Geol. Soc. Amer. Bull. 84, 297.

Turner, F.J., Griggs, D.T. and Heard, H.C. (1954)
Experimental deformation of calcite crystals.
Geol. Soc. Amer. Bull. 65, 883.

Turner, F.J. and Heard, H.C. (1965)
Deformation of calcite crystals at different strain rates.
Geol. Sci. Publ. 46, 103, Univ. of Calif. Los Angeles.

Twiss, R.J. (1977)
Theory and applicability of recrystallised grain size paleopiezometer.
Pure Appl. Geophys. 115, 227.

Tyler, S.J. and Whittaker, V.N. (1963)
The use of intermediate strain rates to study creep cavitation in Magnox A12.
Metallurgia, 68, 17.

Vickers, W. and Greenfield, P. (1967)
Diffusion creep in magnesium alloys.
J. Nucl. Mat. 24, 249.

Von Mises, (1928)
Z. angew. Math. Mech., Dtsch. 8, 161.

Weertman, J. (1968)
Dislocation climb theory of steady state creep.
Trans. ASM 61, 681.

Weertman, J. (1972 and 1975)
High temperature creep produced by dislocation motion.
Proc. J.E. Dorn memorial symp. Cleveland October 1972, also in A.S.M. 4 (1975) p.315.

Weiss, L.E. and Turner, F.J. (1972)
Some observations on translation gliding and kinking in experimentally deformed calcite and dolomite.
in Flow and Fracture of Rocks, Geophys. Monogr. Ser. Vol. 16, ed. H.C. Heard, I.Y. Borg, N.L. Carter and C.B. Raleigh, p.95, A.G.U. Washington D.C. 1972.

Wenk, H.R., Venkitasubramanyan, C.S. and Baker, D.W. (1973)
Preferred orientation in experimentally deformed limestone.
Contrib. Mineral. Petrol. 38, 81.

White, S. (1971)
Natural creep deformation of quartzites.
Nature Phys. Sci. 234, 175.

White, S. (1973a)
Syntectonic recrystallisation and texture development in quartz.
Nature 244, 276.

White, S. (1973)
The dislocation structures responsible for the optical effects in some naturally deformed quartzites.
J. Mat. Sci. 8, 490.

White, S. (1975)
Estimation of strain rates from microstructural features.
Quart. J. Geol. Soc. Lond. 131, 577.

White, S.H. (1976)
The effects of strain on the microstructures, fabrics and deformation mechanisms in quartzites.
Phil. Trans. R. Soc. Lond. A 283, 69.

White, S. (1977)
Geological significance of recovery and recrystallisation processes in quartz.
Tectonophysics, 39, 143.

White, S.H. (1979)
Difficulties associated with paleo-stress estimates.
Bull Mineral. 102, 210.

White, S., Crosby, A. and Evans, P.E. (1971)
Dislocations in naturally deformed quartzite.
Nature Phys. Sci. 231, 85.

White, S.H., Burrows, S.E. and Carreras, J. (1978)
Textural and microstructural development in a naturally deformed quartzite - a metallurgical approach.
Proc. Int. Conf. on Textures, Aachen, April, 1978.

White, S.H. and Knipe, R. (1978)
Transformation and reaction enhanced ductility in rocks.
J. Geol. Soc. Lond. 135, 513.

White, S. and Wilson, C.J.L. (1978)
Microstructure of some quartz pressure fringes.
N. Jb. Miner. Abh. 134, 33.

Williams, R.J., Brown, A.F. and Healey, T. (1969)
Basal pole orientation determination in Magnox AL80 using polarised light microscopy.
CEGB Report RD/B/N1375.

Wonsiewicz, B.C. and Backofen, W.A. (1967)
Plasticity of Mg crystals.
Trans. TMS-AIME 239, 1422.

ACKNOWLEDGEMENTS

Firstly I would like to thank my supervisors Drs. F.J. Humphreys and S.H. White for all their advice and encouragement during the course of this project. Secondly I am indebted to my colleagues in the Electron Microscopy and Stuctural Geology groups, in particular to R.A.H. Edwards and C.J. Spiers, for their friendship and participation in stimulating discussions.

The technical expertise of Mr. G.W. Briers has been gratefully appreciated. Messrs. J. Woodall and R. Holloway are also thanked for their assistance. Miss P. Martins and Messrs. J. Rossdale and B. Bishop are thanked for their assistance with the photographic work.

The excellent typing of Mrs. G. Flower is gratefully appreciated

I would also like to express my thanks to Professor J.G. Ball for providing the laboratory facilities and to the Science Research Council for their financial support.

Finally I would like to express my gratitude to my parents for all their help and encouragement and to my fiancé John for his patience and understanding.

Appendices

APPENDIX A

ANALYSIS OF MECHANICAL DATA

INTRODUCTION

The mechanical data obtained from the compression tests was output from the Instron in the form of load-time curves. It was processed into stress-strain data by means of the following simple Fortran program. The program assumed that the area on which the load was acting remained circular and that it increased uniformly with strain. It also assumed that no barrelling or buckling of the specimen occurred during the duration of the test.

```
00100 PROGRAM SUE1(INPUT,OUTPUT,TAPE5=INPUT,TAPE6=OUTPUT,TAPE62)
00110 COMMON STRESS(100),STRAIN(100)
00120 DIMENSION FORCE(100),ALOAD),TIME(100),COMP(100),AREA(100)
00130 PRINT,"TYPE IN THE NUMBER OF DATA ENTRIES"
00140 READ,N
00150 IF(N.GT.100)STOP
00160 PRINT,"WHAT ARE THE VALUES OF THE ORIGINAL LENGTH,RADIUS,TEMP&SRATE"
00170 READ,ALENGTH,RADIUS,TEMP,SRATE
00180 PRINT,"    ALENGTH    RADIUS    TEMPERATURE    SRATE"
00190 WRITE(6,200)ALENGTH,RADIUS,TEMP,SRATE
00200 200 FORMAT(5X,F8.3,2X,F8.3,2X,F8.3,2X,F8.5)
00210 PRINT,"TYPE IN THE LOAD AND TIME AFTER EACH  ? "
00220 DO 100 I=1,N
00230 READ,ALOAD(I),TIME(I)
00240 FORCE(I)=9.807*ALOAD(I)
00250 COMP(I)=SRATE*TIME(I)
00260 AREA(I)=(RADIUS**2)*3.142*ALENGTH/(ALENGTH-COMP(I))
00270 STRESS(I)=FORCE(I)/AREA(I)
00280 STRAIN(I)=-ALOG((ALENGTH-COMP(I))/ALENGTH)
00290 100 CONTINUE
00300 PRINT,"TIME(MINS)        STRESS      STRAIN"
00310 WRITE(62,600)N
00320 600 FORMAT(I3)
00330 DO 300 I=1,N
00340 WRITE(6,400)TIME(I),STRESS(I),STRAIN(I)
00350 WRITE(62,500) STRESS(I),STRAIN(I)
00360 300 CONTINUE
00370 400 FORMAT(5X,F5.1,9X,F8.4,5X,F8.5)
00380 500 FORMAT(F8.4,F8.5)
00390 STOP
00400 END
```

APPENDIX B

Burgers Vector Analysis

Elastic strain fields which are produced by dislocations enable them to be imaged in the electron microscope. If the crystal is set near the Bragg condition for (hkl) planes the strain in these planes may bend them locally into or out of the Bragg condition. This alters the transmitted and hkl diffracted beam intensities and renders the dislocations visible.

If the strain field of the dislocation does not bend the (hkl) plane which is producing diffraction then the dislocation will remain invisible. For elastically isotropic crystals this occurs when the burgers vector of the dislocation lies in the hkl plane.

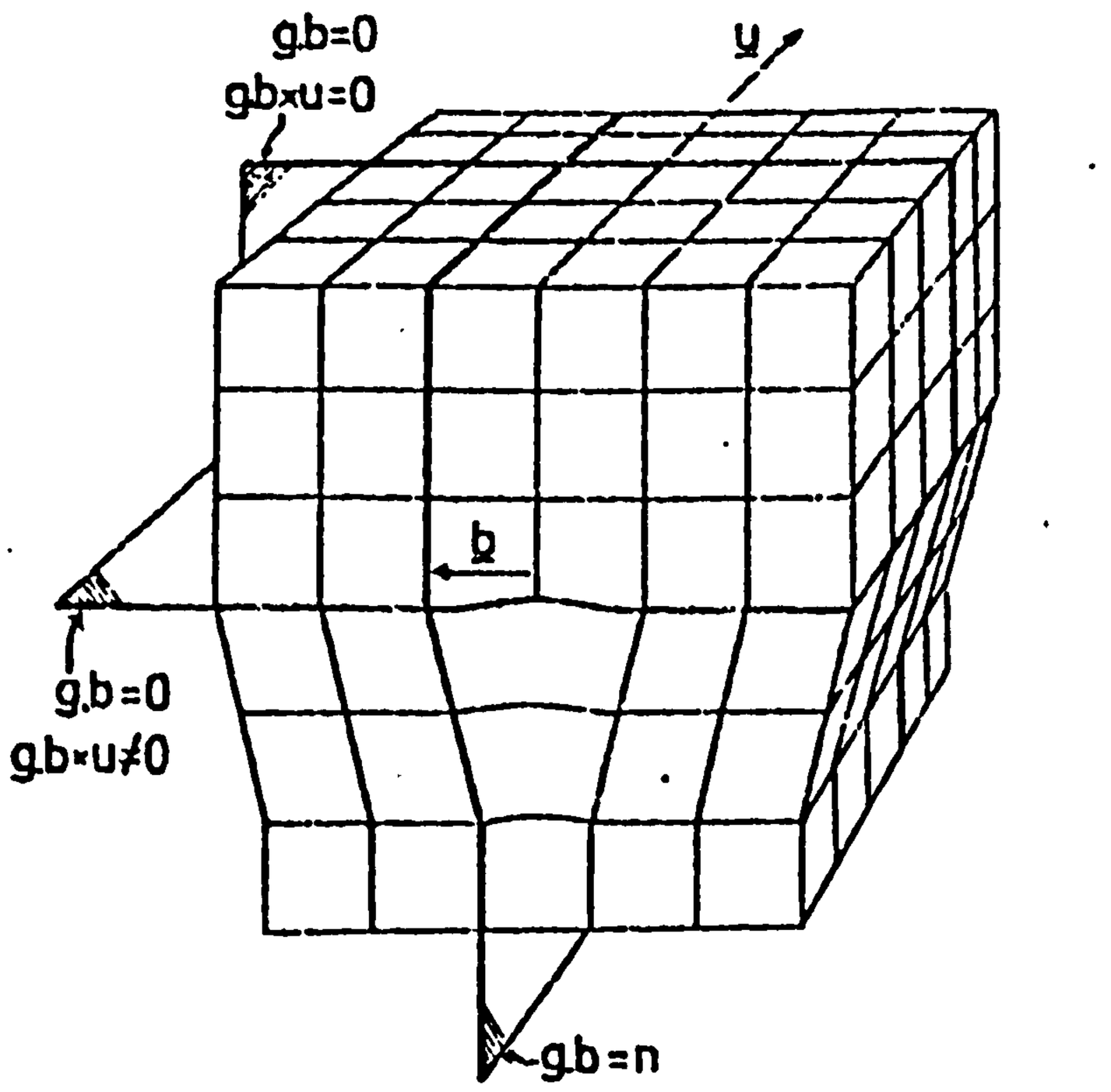
i.e. for screw dislocations invisibility occurs when

$$\underline{g}.\underline{b} = 0$$

where $\underline{g}$ is the vector of the reflecting planes (hkl) and $\underline{b}$ the burgers vector of the dislocations.

For edge dislocations dislocation images can sometimes be seen even when $\underline{g}.\underline{b} = 0$ as there is a small dilation perpendicular to the plane containing both the dislocation line $\underline{u}$ and the burgers vector $\underline{b}$ (see above). For an edge dislocation to be invisible

$$\underline{g}.\underline{b} \times \underline{u} = 0$$



In hcp metals stable perfect dislocations are limited to a, c and (c + a) from self energy considerations.

This means that all $\vec{a}$ type are invisible under an 0002 reflection and all c type are invisible under $11\bar{2}0$. A table giving the value of g.b for the first seven reflections and 1/3<$11\bar{2}0$> 1/3<$11\bar{2}3$> and (0001) type Burgers vectors is given below (Partridge 1964).

Reflection		Burgers vectors of perfect dislocations (× ⅓)									
		±[$11\bar{2}0$]	±[$\bar{1}2\bar{1}0$]	±[$\bar{2}110$]	±[$11\bar{2}3$]	±[$\bar{1}2\bar{1}3$]	±[$\bar{2}113$]	±[$11\bar{2}3$]	±[$\bar{1}2\bar{1}3$]	±[$\bar{2}113$]	±[0003]
1	$10\bar{1}0$ $01\bar{1}0$ $\bar{1}100$	±1 ±1 0	0 ±1 ±1	∓1 0 ±1	±1 ±1 0	0 ±1 ±1	∓1 0 ±1	±1 ±1 0	0 ±1 ±1	∓1 0 ±1	0 0 0
2	0002	0	0	0	±2	±2	±2	∓2	∓2	∓2	±2
3	$10\bar{1}1$ $10\bar{1}\bar{1}$	±1 ±1	0 0	∓1 ∓1	±2 0	±1 ∓1	0 ∓2	0 ±2	∓1 ±1	∓2 0	±1 ∓1
	$01\bar{1}1$ $01\bar{1}\bar{1}$	±1 ±1	±1 ±1	0 0	±2 0	±2 0	±1 ∓1	0 ±2	0 ±2	∓1 ±1	±1 ∓1
	$\bar{1}101$ $\bar{1}\bar{1}0\bar{1}$	0 0	±1 ±1	±1 ±1	±1 ∓1	±2 0	±2 0	∓1 ±1	0 ±2	0 ±2	±1 ∓1
4	$10\bar{1}2$ $10\bar{1}\bar{2}$	±1 ±1	0 0	±1 ±1	±3 ∓1	±2 ∓2	±1 ∓3	∓1 ±3	∓2 ±2	∓3 ±1	±2 ∓2
	$01\bar{1}2$ $01\bar{1}\bar{2}$	±1 ±1	±1 ±1	0 0	±3 ∓1	±3 ∓1	±2 ∓2	∓1 ±3	∓1 ±3	∓2 ±2	±2 ∓2
	$0\bar{1}12$	±1	±1	0	∓1	∓1	∓2	±3	±3	±2	∓2
	$\bar{1}102$ $\bar{1}10\bar{2}$	0 0	±1 ±1	±1 ±1	±2 ∓2	±3 ∓1	±3 ∓1	∓2 ±2	∓1 ±3	∓1 ±3	±2 ∓2
5	$11\bar{2}0$ $\bar{1}2\bar{1}0$ $\bar{2}110$	±2 ±1 ∓1	±1 ±2 ±1	∓1 ±1 ±2	±2 ±1 ∓1	±1 ±2 ±1	∓1 ±1 ±2	±2 ±1 ∓1	±1 ±2 ±1	∓1 ±1 ±2	0 0 0
6	$10\bar{1}3$ $10\bar{1}\bar{3}$	±1 ±1	0 0	∓1 ∓1	±4 ∓2	±3 ∓3	±2 ∓4	∓2 ±4	∓3 ∓3	∓4 ±2	±3 ∓3
	$01\bar{1}3$ $01\bar{1}\bar{3}$	±1 ±1	±1 ±1	0 0	±4 ∓2	±4 ∓2	±3 ∓3	∓2 ±4	±4 ∓2	∓3 ±3	±3 ∓3
	$\bar{1}103$ $\bar{1}10\bar{3}$	0 0	±1 ±1	±1 ±1	±3 ∓3	±4 ∓2	±4 ∓2	∓3 ±3	±4 ∓2	∓2 ±4	±3 ∓3
7	$11\bar{2}2$ $11\bar{2}\bar{2}$	±2 ±2	±1 ∓1	∓1 ∓1	±4 0	±3 ∓1	±1 ∓3	0 ±4	∓1 ±3	∓3 ±1	±2 ∓2
	$\bar{1}2\bar{1}2$ $\bar{1}2\bar{1}\bar{2}$	±1 ±1	±2 ±2	±1 ±1	±3 ∓1	±4 0	±3 ∓1	∓1 ±3	0 0	∓1 ±3	±2 ∓2
	$\bar{2}112$ $\bar{2}11\bar{2}$	∓1 ∓1	±1 ±1	±2 ±2	±1 ∓3	±3 ∓1	±4 0	∓3 ±1	±3 ±1	0 ±4	±2 ∓2

An example of the determination of the burgers vector of some dislocations observed in the current work is shown in Figure B1. It was found that good contrast was difficult to obtain and the use of the H.V.E.M. to obtain added penetration rendered two beam conditions also difficult to achieve.

References

Partridge, P.G. (1964) Metals and Materials, vol 1, 11, p 169.

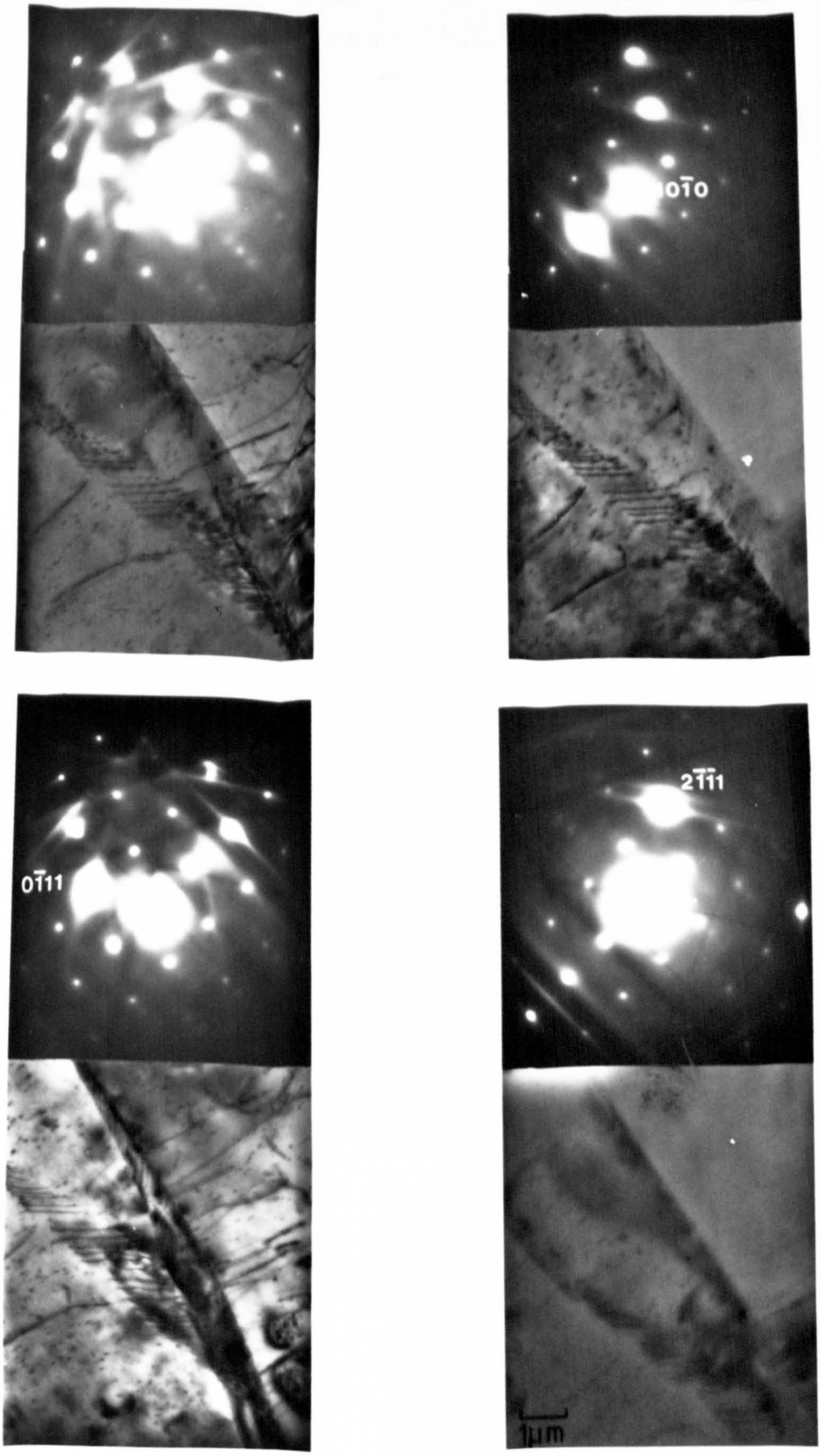


Figure B1. Burgers vector analysis.

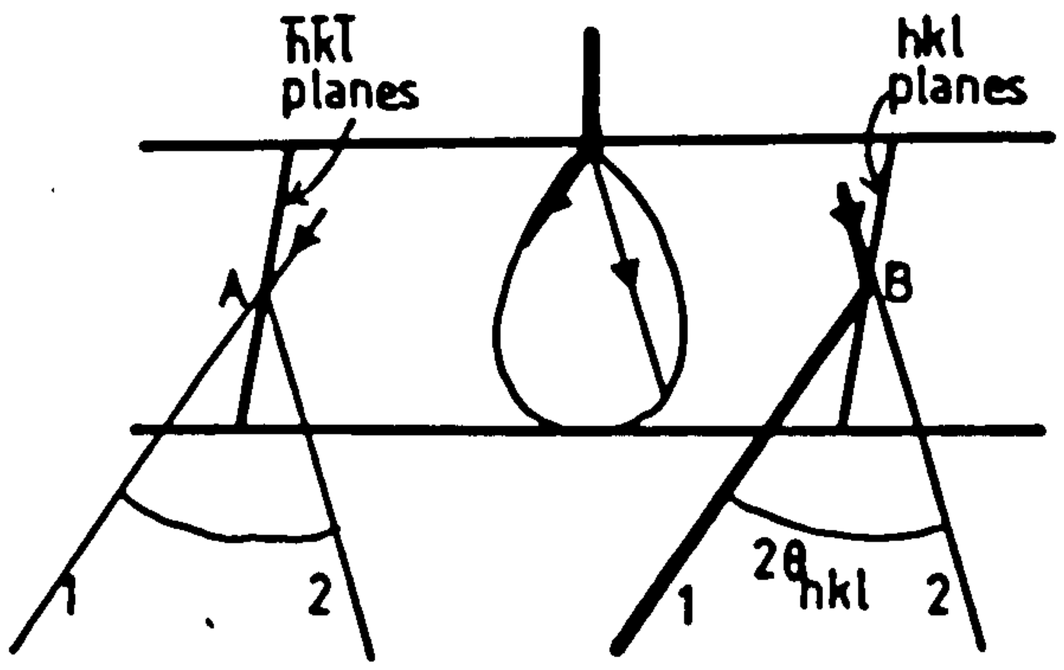
The dislocations are present under the $10\bar{1}0$ and $0\bar{1}11$ reflections but invisible under the $2\bar{1}\bar{1}1$ reflection; Therefore $b = \frac{1}{3}[11\bar{2}\bar{3}]$.

APPENDIX C

KIKUCHI LINE ANALYSIS

Kikuchi lines result from inelastic scattering of electrons in the foil; they provide a means of determining local crystal orientations accurately.

Electrons are inelastically scattered in all directions within the crystal (although the intensity decreases sharply with increasing angle of scattering).



The intensity of inelastic scattering is shown at the centre of the sketch as a function of the angle of scattering. The length of the line joining the incident beam to the edge of the pear shaped region is proportional to the intensity of the beam scattered at that angle. Hence the intensity scattered at the Bragg angle for ($\bar{h}\bar{k}\bar{l}$) planes is much lower than that scattered at the Bragg angle for (hkl) planes.

after Flower and Staton-Bevan (1976)

At (A) elecrons inelastically scattered through a large angle are exactly at the Bragg angle for diffraction by the planes ($\bar{h}\bar{k}\bar{l}$). This produces a decrease in the inelastically scattered intensity along direction (1) and an increase along direction (2).

At (B) electrons inelastically scattered through a small angle are exactly at the Bragg angle for diffraction by planes (hkl). This This produces an excess background intensity along direction (1) and a deficiency along direction (2), i.e. exactly the converse of that produced at (A). However, since the electron intensity involved at (B) is greater than that at (A) the nett result is an excess background intensity along direction (1) and a deficiency along direction (2).

In the diffraction pattern this results in a line of lower than average background intensity and a parallel line of excess intensity. These defect and excess lines are the Kikuchi lines. Their separation is the same as that between the 000 spot and the hkl reflection since both spacings correspond to angular separations of twice the Bragg angle.

As the crystal is rotated, the Kikuchi lines move across the diffraction pattern. They can be used to determine angular mis orientations in a crystal. Unlike diffraction spots which either fade or increase in intensity with misorientation, when two regions of a crystal are misoriented, the Kikuchi patterns are displaced with respect to each other. The displacement is directly proportional to the angular misorientation of the two regions. An example of the way in which this has been used in the current work is shown in Figure C1.

In grain A there is an angular misorientation across the subgrain boundary. The value of the misorientation was determined by measuring the displacement of the Kikuchi lines from one side of the subboundary to the other. The constant of proportionality for the system was determined by measuring a distance on the pattern corresponding to a known Bragg reflection and Bragg angle.

$$K = 2\theta_{hkl} / r_{hkl}$$

For the $01\bar{1}1$ diffraction spot r= 8.55mm

Using Bragg's Law $\theta = \sin^{-1} \frac{\lambda}{2d}$

Now for 500kv electrons $\lambda = 0.01432$

and $d_{01\bar{1}1} = 2.452$

Thus $K = 0.08^{o}mm^{-1}$

The displacement of the Kikuchi lines across the subboundary due to the angular misorientation is 8mm on the photograph indicating an angular misorientation of 0.64^{o}.

References

Flower, H.M. and Staton-Bevan, A. (1976). A laboratory notebook in Electron Microscopy, Department of Metallurgy and Materials Science, Imperial College, Internal Publication.



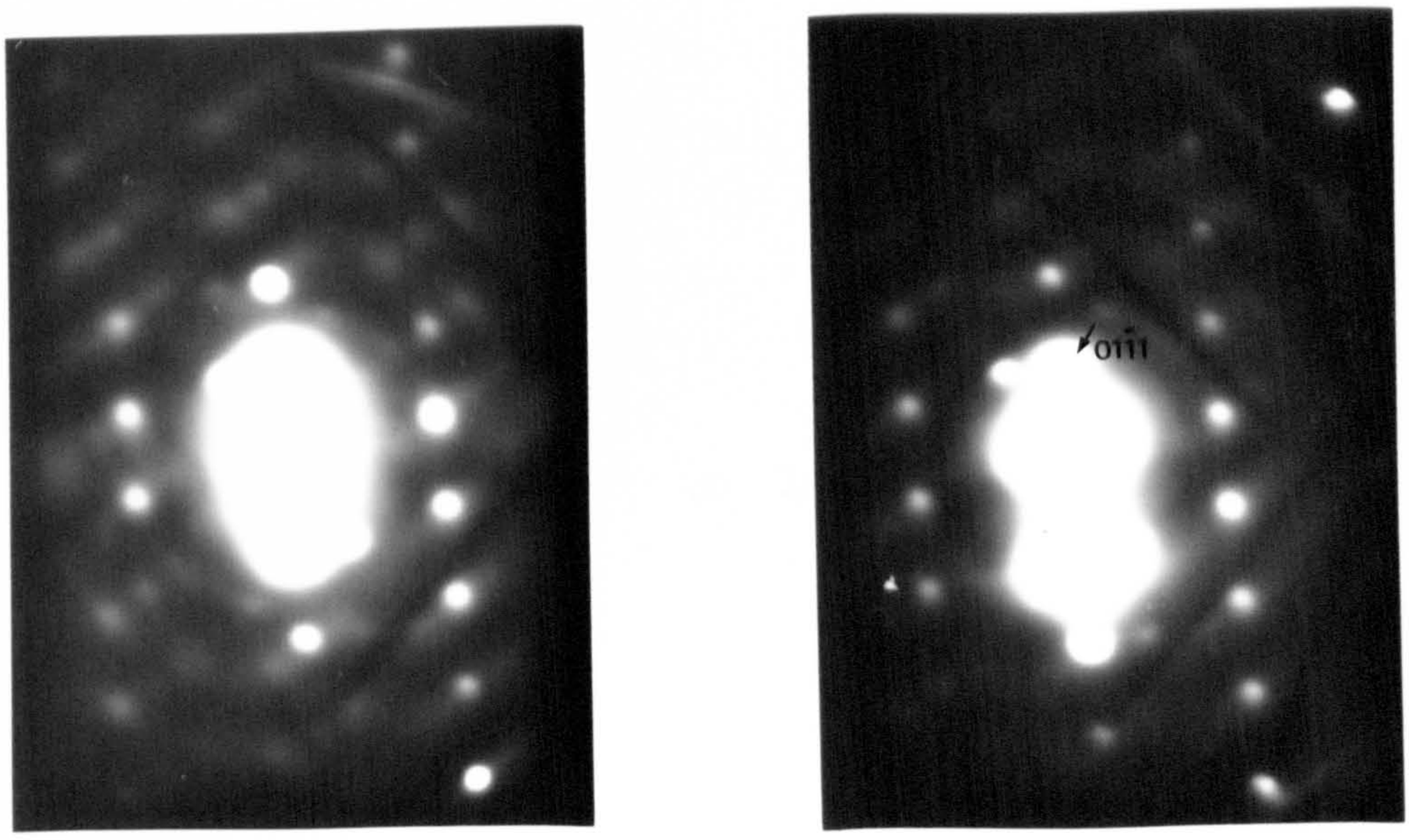


Figure C1. Determination of misorientation from Kikuchi line shift.

APPENDIX D

EXPERIMENTS CARRIED OUT ON THE ALLOY Zr55

D.1. INTRODUCTION

It was recognised that the experiments carried out to examine the behaviour of a grid on a polished surface had their limitations since a free surface is not the most ideal when searching for evidence of grain boundary sliding. The Magnox alloy Zr55 has been used in the past in investigations of grain boundary sliding - mainly connected with diffusion creep. This is because annealing the material in a hydrogen atmosphere results in extensive precipitation of zirconium hydride in the form of stringers, (Squires et al 1963) which can act as internal markers.

D.2. THE MATERIAL

Zr 55 is a binary alloy Mg-0.5wt%Zr (manufacturers specification) It was supplied by Magnesium Elektron Ltd. in the form of extruded rod 9/16" in diameter.

D.3. EXPERIMENTAL METHODS

Cylinders 1/8" were cut from the supplied rod. The ends of the cylinders were polished using standard metallographic techniques including a final polish in 10% HNO_3 to remove mechanically induced deformation. Each specimen was annealed in a hydrogen atmosphere at $500^{o}C$ for 24 hours. This greatment resulted in extensive precipitation of zirconium hydride in the form of stringers as shown in Figure D.1 and a grain size of 100 μm.

The specimens were compressed uniaxially at a rate of $\dot{\varepsilon} \sim 10^{-5}s^{-1}$ and a temperature of $260^{o}C$ in the same apparatus as the Magnox A180. It was found however that these conditions resulted in a stress strain curve similar to that obtained in the high temperature tests on the A180 alloy. The microstructure was also reminiscent of the A180 high temperature microstructures. Decreasing the temperature to $200^{o}C$ resulted in similar mechanical behaviour as exhibited by A180 at $260^{o}C$, i.e. marked strain hardening followed by a sharp peak in the stress strain curve and a period of softening. The reasons for the differences in mechanical behaviour are outside the scope of this thesis and will not therefore be dealt with here. The purpose of the change in material was to find out whether or not internal markers recorded similar behaviour to the grids and scratch lines in the surface experiments on A180.

This has been found to be the case and the results are reported below. The behaviour at 200°C will be presented first, followed by the behaviour at 260°C. Optical microscopy was used to investigate the microstructures: the sample preparation and polishing techniques employed were identical to those used for the Magnox A180 (see section 2.).

D.4. RESULTS AND DISCUSSION

D.4.1. Low Temperature Behaviour

A specimen deformed 55% confirmed the kinking which had been suggested for the Magnox A180. A macroscopic view of the sample (Figure D.2) shows that there are 2 zones of kinking (a and b). These are defined by the macroscopic rotations undergone by the zirconium hydride stringers. The microstructure within the better developed kinked region is shown in Figure D.3. The upper micrograph (Figure D.3a) was taken under ordinary bright field illumination since the markers were difficult to discern in polarised light (Figure D.3b). The original direction of the markers is indicated on the micrograph. The whole microstructure has rotated (old and new grains alike) with respect to its original orientation so that the basal planes are aligned parallel with the zone. The major rotations of the markers had occurred at the edges of the zone with minor fluctuations within the zone.

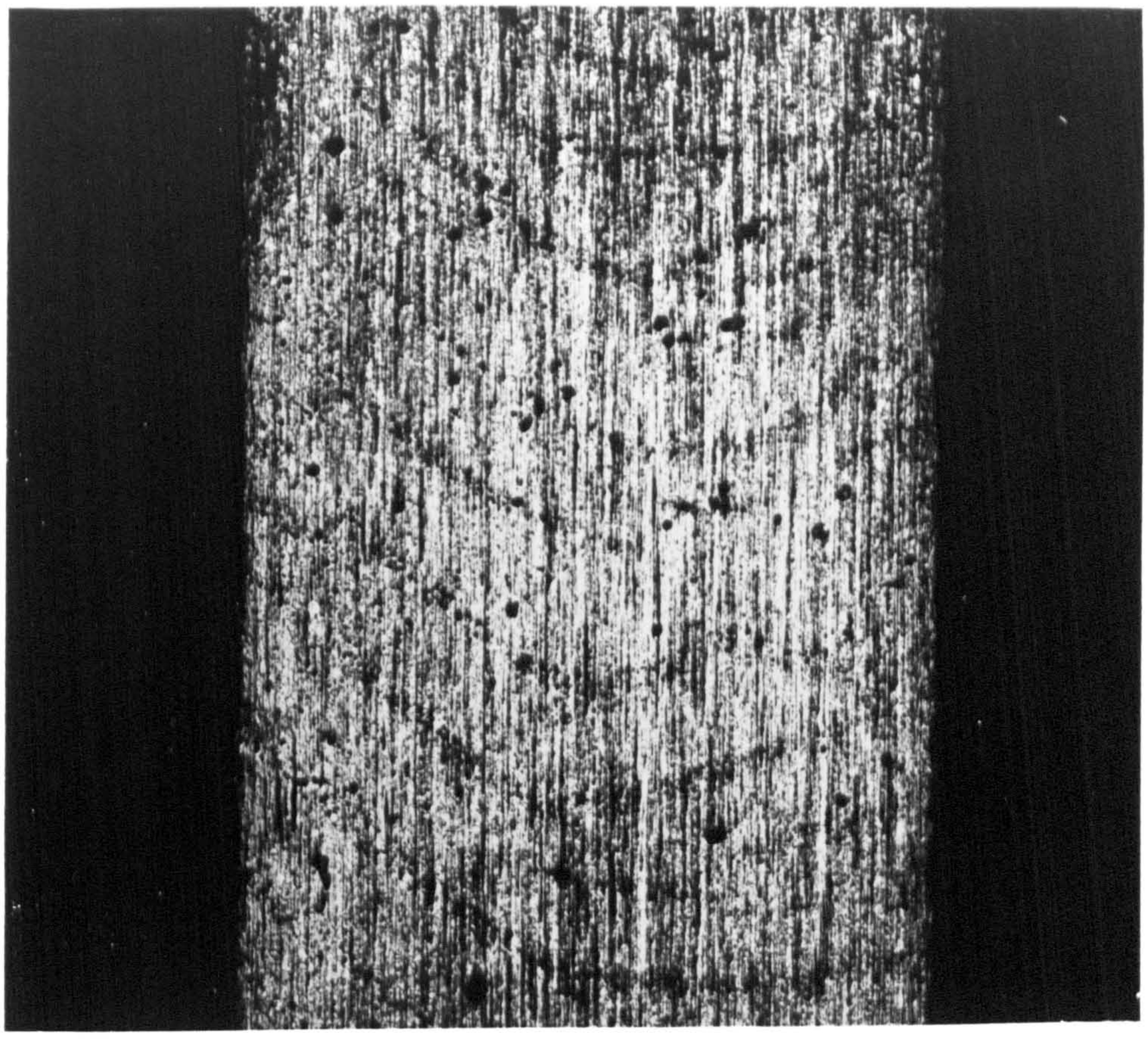
D.4.2. High Temperature Behaviour

The zirconium hydride markers revealed that the deformation was relatively homogeneous at higher temperatures. The sharp direction changes of the markers in Figure D4a can be seen to coincide with deformation band boundaries.

The results obtained from these experiments then suggested that the behaviour of the internal markers was similar to that of the surface markers on the Magnox A180 thus indicating that the behaviour of the grids and scratches did give a representative view of internal behaviour.

References

Squires, R.L., Weiner, R.T. and Phillips, M. (1963) J. Nucl. Mat. 8, 77.



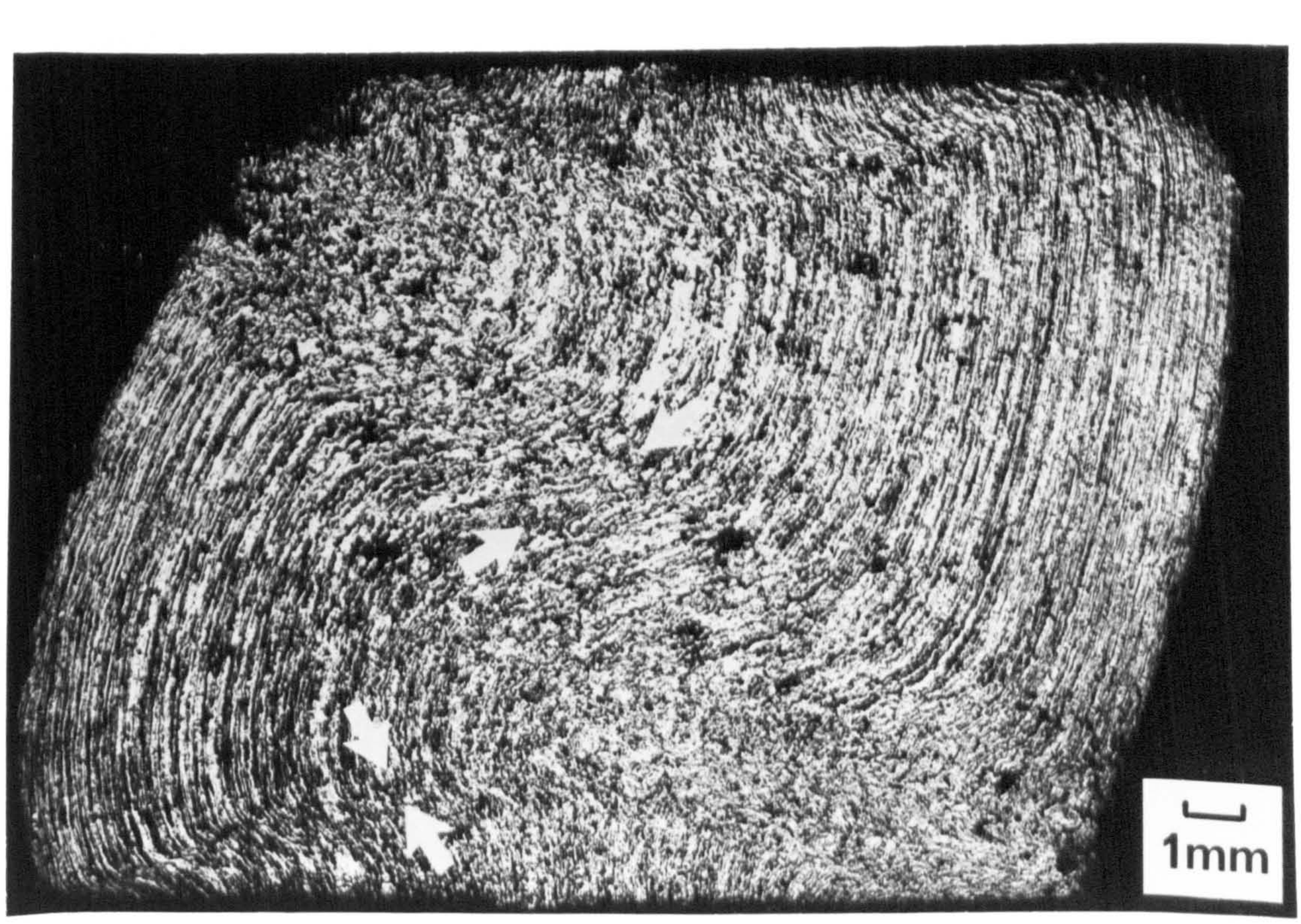
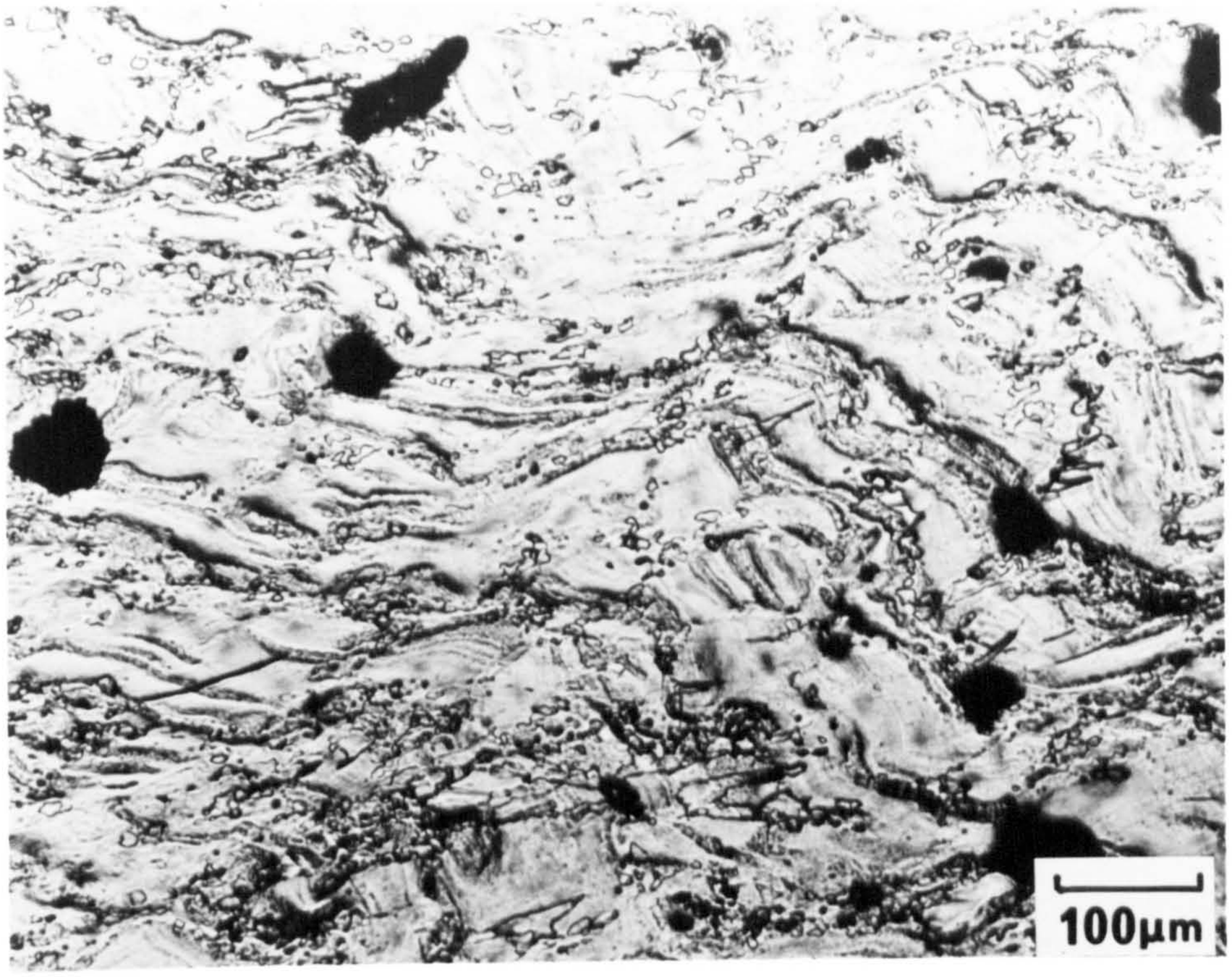


Figure D1/2. The upper micrograph is of an undeformed sample. It illustrates the lines of zirconium hydride precipitate which act as internal markers. The lower micrograph shows the inhomogeneous deformation which has occurred as revealed by the behaviour of the precipitates.



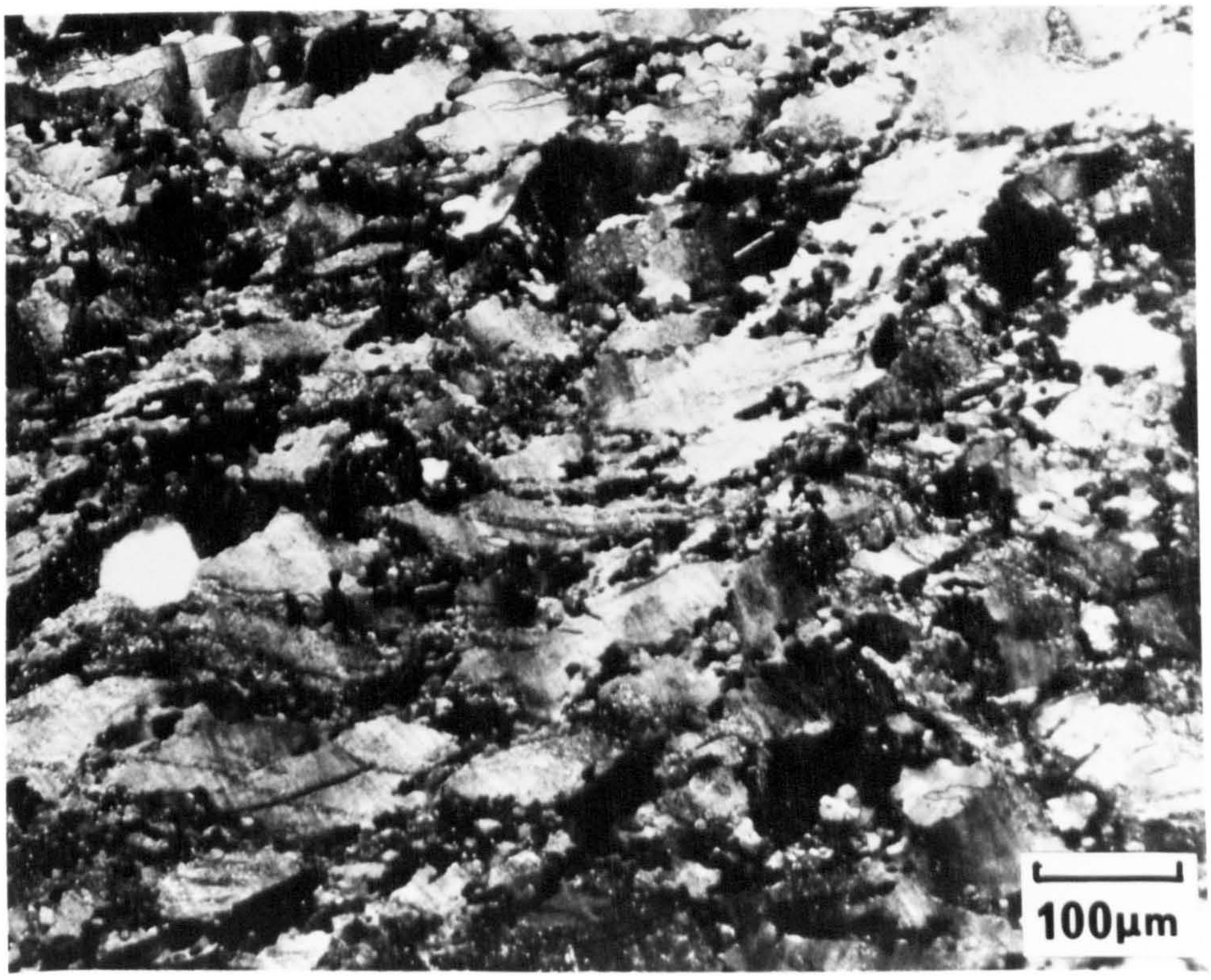
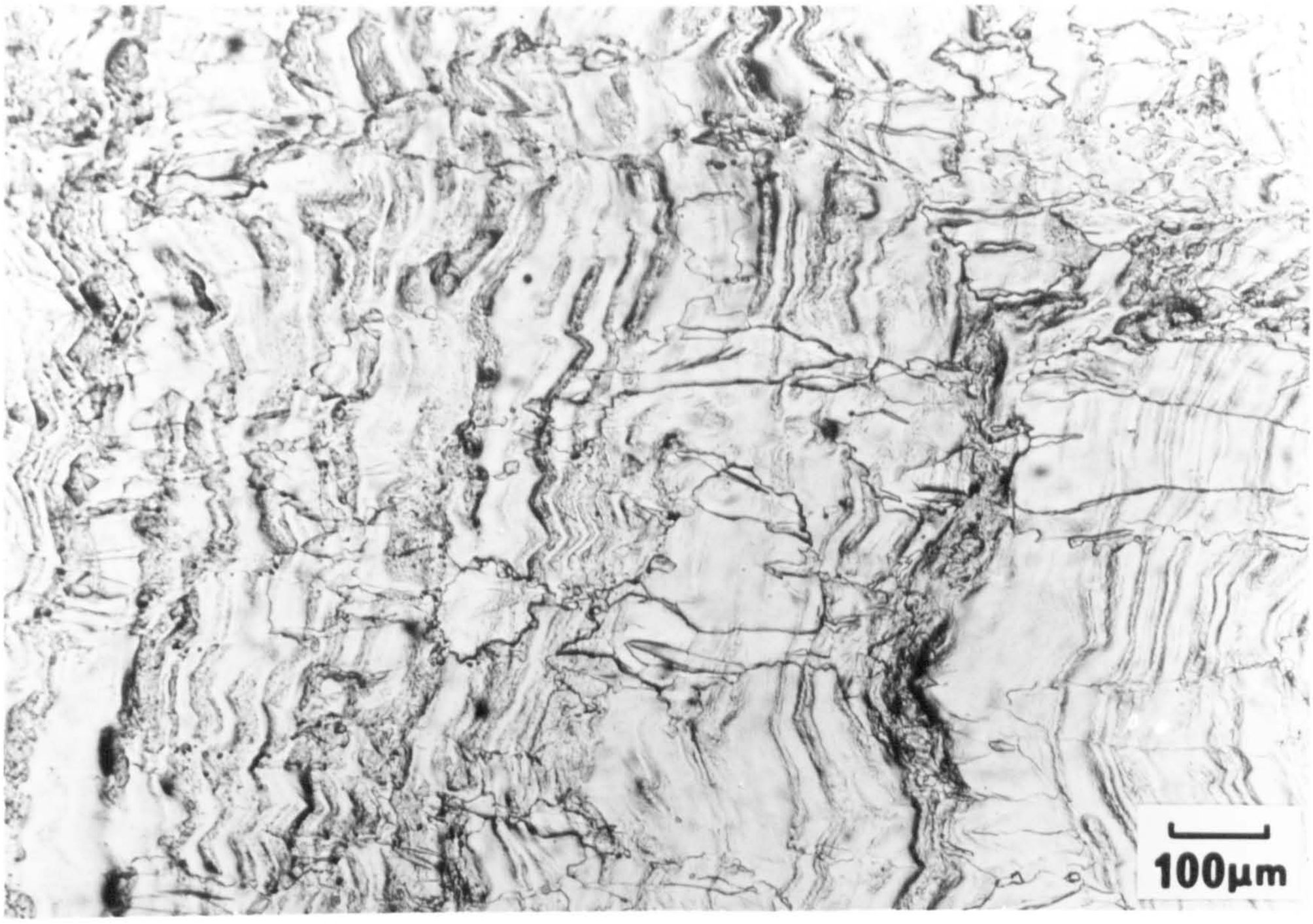


Figure D3. Micrographs illustrating the behaviour in the kinked region of the sample of Zr55. Both photographs are of the same area: the upper one exhibiting the behaviour of the lines of precipitate in bright field illumination whilst the microscopic detail is revealed in polarised light in the lower micrograph.



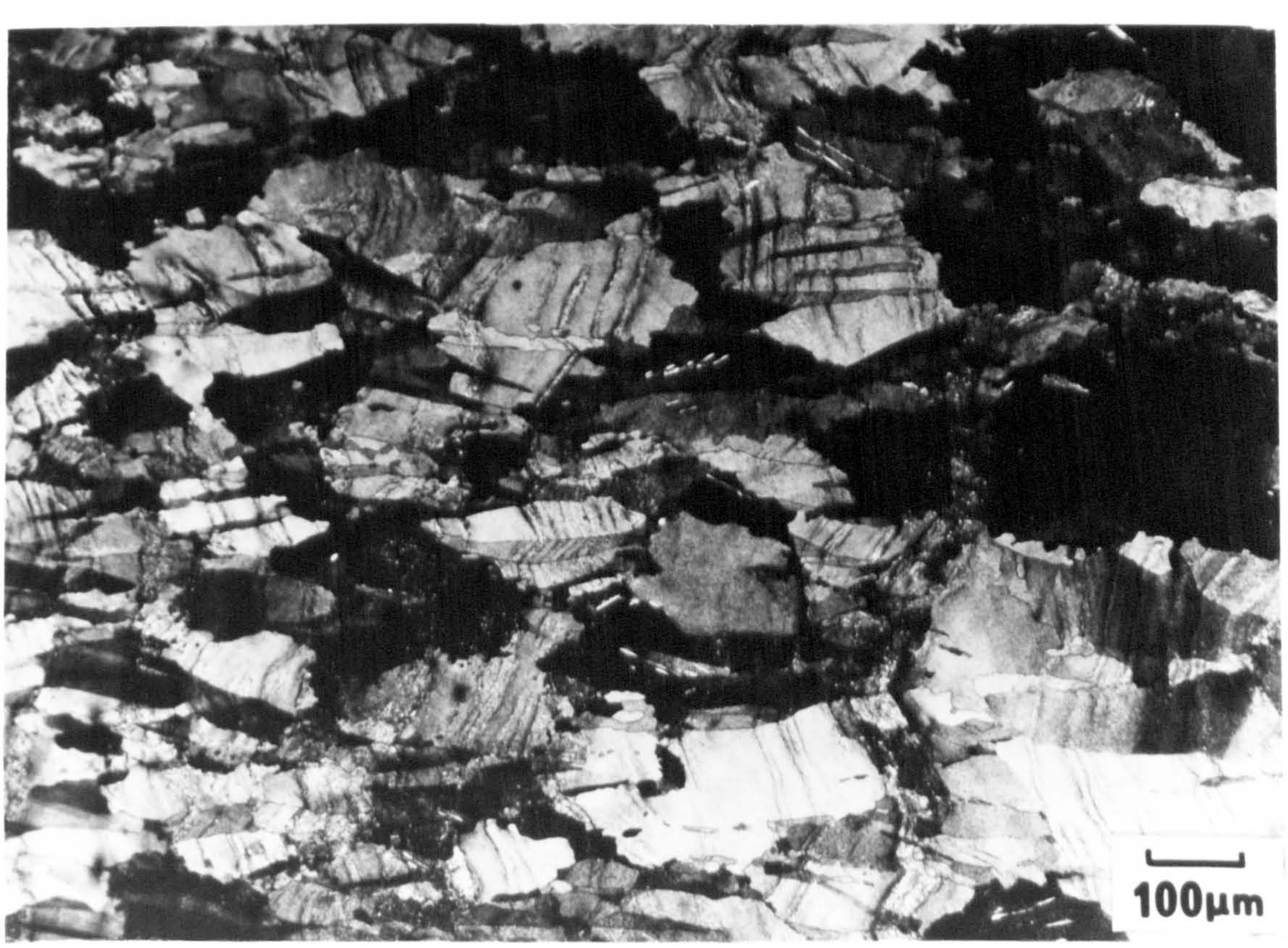


Figure D4. High temperature deformation bands in Zr55. The behaviour of the precipitates which change direction at the deformation band boundaries indicates the high rotations which occur across them.

APPENDIX E

IN-SITU STUDIES OF THE DEFORMATION AND DYNAMIC RECRYSTALLISATION OF RHOMBOHEDRAL CAMPHOR.

E.1. INTRODUCTION

The work reported in the following paragraphs constitutes part of a joint project carried out in conjunction with Mr. J. Urai and Dr. F.J. Humphreys.

The deformation processes which occur when crystalline materials are deformed to large strains at high temperatures are of importance in both the industrial hot working of materials, and in the natural deformation of minerals as studied by the structural geologist. Although differing greatly in terms of the rates of strain and in the types of material involved, there is little doubt that many of the microstructural deformation processes which occur are common to both (Nicolas and Poirier 1976, Kelly et al 1977).

These processes, the relationship between them, and the way in which inhomogeneous microstructures develop at high strains are not well understood. Work on minerals is hampered by the difficulties of laboratory deformation experiments, and interpretatiin of the behaviour of metals, so far confined mainly to cubic materials, is restricted by the difficulties of preserving the unstable microstructures of rapidly hot worked metals. The present work was undertaken to try and obtain some insight into the processes of high strain deformation and dynamic recrystallisation by using polycrystalline specimens of a transparent organic compound as an analogue for either minerals or metals of low symmetry.

Similar materials have been used previously as analogues of metals in studies of solidification (Hunt and Jackson 1956) and grain growth (Simpson et al 1969), and deformation cells viewed in transmitted light have been used to study the deformation of ice (Wilson 1968) and aggregates of granular minerals (Means 1977).

E.2. THE MATERIAL

Materials known as "plastic organic crystals" have been studied for some time, and a historical review has been presented by Timmermans (Timmermans 1961). Many of these molecular crystals have, immediately

below their melting point, a cubic structure in which the molecules are free to rotate (Rotator Phase). In this condition the materials are soft and ductile; and in a series of experiments, Hawthorne and Sherwood (1970) have shown that the mechanical behaviour is controlled by similar deformation processes to those in metals. Although the transformations to phases of lower symmetry at lower temperatures are well documented, little attention has been paid to the mechanical behaviour of these phases.

Camphor ($C_{10}H_{16}O$) occurs in several forms, the actual transformation temperatures being dependent both on the purity of the material, and the proportions of d and l isomers present (Yager and Morgan 1935).

The phase transformations are as follows (Powles 1952, Dunning 1961):

LIQUID $\overset{452K}{\rightleftharpoons}$ f.c.c. $\overset{370K}{\rightleftharpoons}$ Rhombohedral I $\overset{243K}{\rightleftharpoons}$ Rhombohedral II (more birefringent)

The details of the rhombohedral phases have not been reported. Rhombohedral I Camphor was chosen for the present investigation because, being birefringent, changes in the microstructure during deformation and recrystallisation could conveniently be followed in the polarizing optical microscope over a range of easily obtainable temperatures.

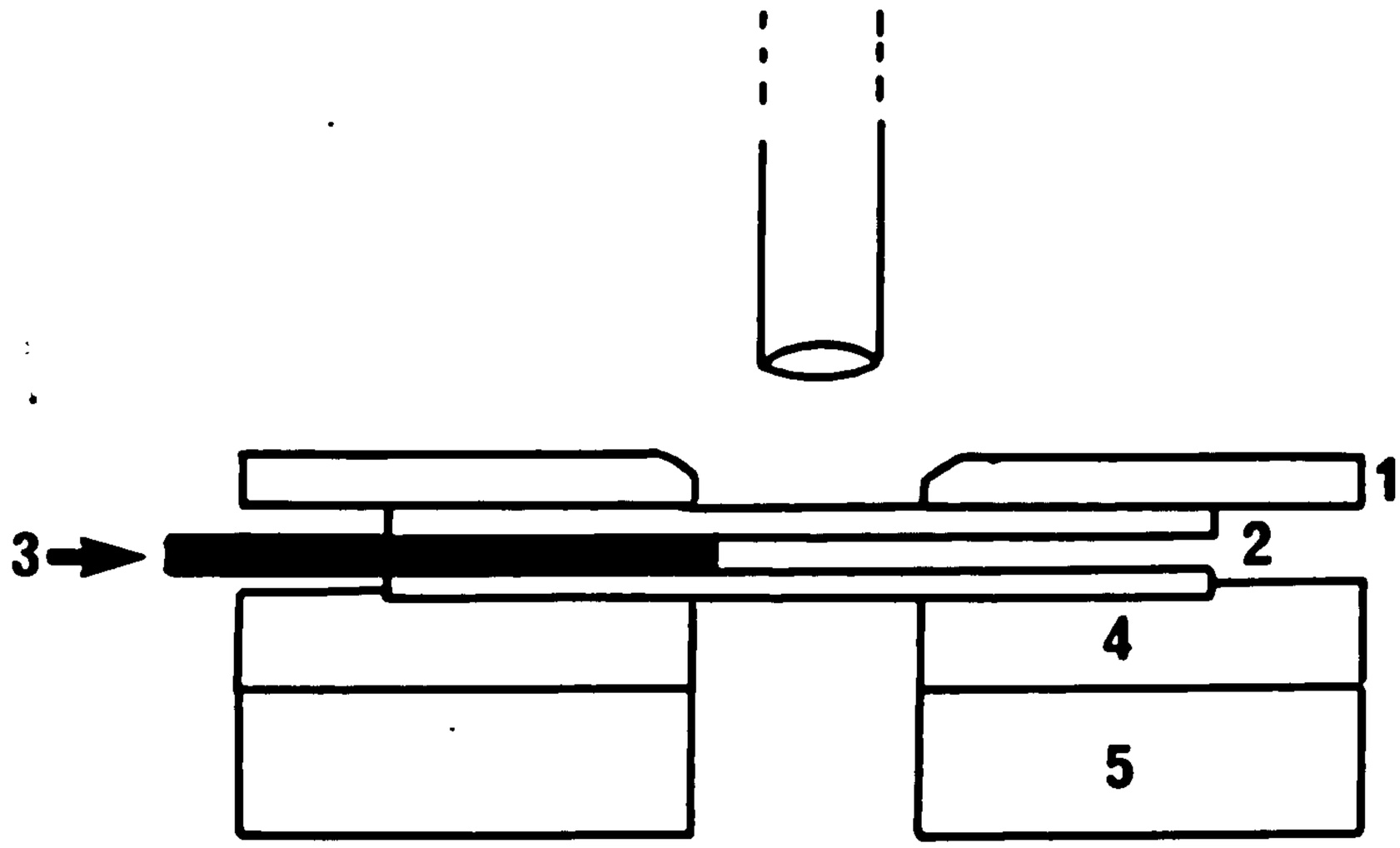
E.3. EXPERIMENTAL METHODS

E.3.1. Apparatus

Deformation experiments were carried out in the simple stage shown schematically in Figure E1. The specimen was contained in a glass cell, 0.15 mm thick, and was deformed by driving an 0.15 mm thick piston into the cell at a constant rate. The temperature, monitored in the cell, could be varied by resistance heating, and was controlled to $\pm 2^{o}C$. Tests were carried out between 283K and 343K. The deforming specimen was viewed in transmitted polarized light. Use of a quartz sensitive tint plate enabled orientation information to be obtained from the colours of the grains (see e.g. Stoiber and Morse 1972). The dynamic events were recorded either on 35 mm film, or by using a time lapse camera, on 16 mm colour cine film (Urai et al 1980).

E.3.2. Specimen Preparation

Camphor of commercial purity was cold pressed into sheets ~0.15 mms thick, and specimens ~7 x 7 mms were placed in the deformation cell. Preliminary experiments showed that, without affecting the nature of the deformation processes, silicone oil minimised friction between specimen



1 Cover plate
2 Cell
3 Piston
4 Heated block
5 Insulation

Figure E1. Schematic diagram of the deformation cell.

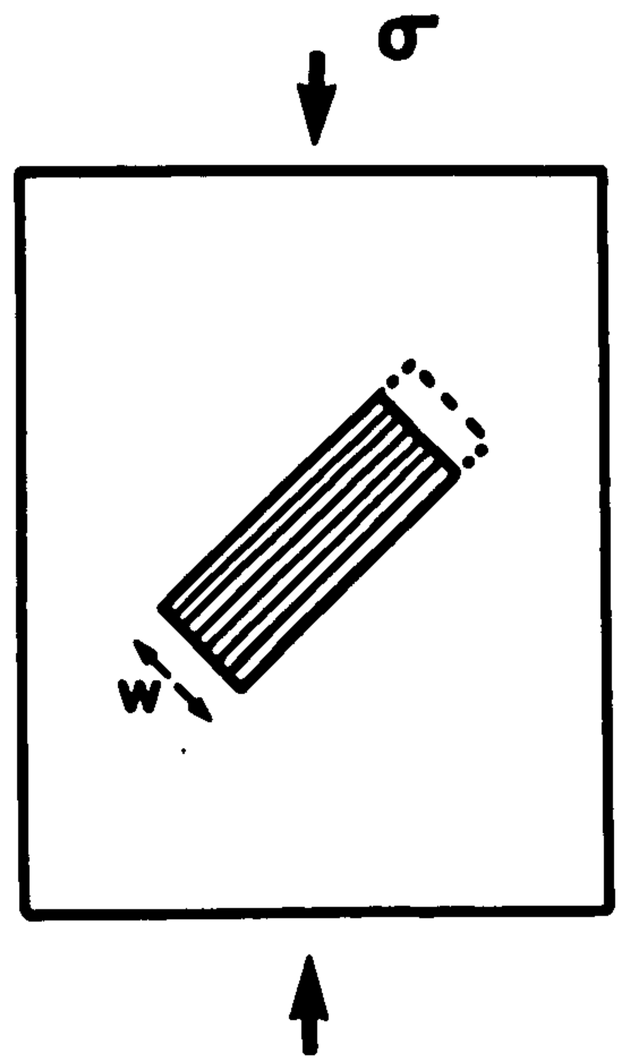


Figure E9. Schematic diagram to illustrate the high temperature deformation process.

and glass during the test, resulting in more homogeneous deformation of the specimen. The camphor was heated into the f.c.c. phase field and slowly cooled. This produced grains of the rhombohedral phase which were generally elongated (Figure E7a) and up to 1 mm long. At room temperature the grains tended to become equiaxed, but the process was slow, some elongation being apparent even after 500 hrs.

E.3.3. Reproducibility and Validity of the Tests

The reproducibility of the experiments was good, and, with experience, the various deformation processes in a particular specimen could generally be predicted. The deformation behaviour of a thin constrained specimen as used in the present work will clearly differ from that of a bulk specimen, and thus caution must be exercised in interpreting the results. Nevertheless, the behaviour is more likely to represent that of a bulk polycrystalline specimen, particularly at high strains, than in-situ observations of free surfaces of either bulk or thin specimens. In order to investigate the effect of specimen thickness, some 0.5 mm thick samples were tested. These showed similar deformation processes to those observed in the thin specimens, and by focussing the microscope at points through the specimen it could be seen for example that dynamic recrystallisation, producing grains of ∿1/10 specimen thickness, occurred in the middle of the specimen, and was not confined to the surface regions. However, the considerable overlap of information in such thick specimens was a bar to their wider use for tests.

Camphor from two sources was used, Hopkin and Williams and BDH. Although the deformation mechanisms were similar in both, the transition, rhombohedral to cubic occurred at ∿358K for the H and W material, and ∿373K for the BDH. This could be due either to impurity effects, or to differences in the proportion of d and l isomers present.

E.4. RESULTS AND DISCUSSION

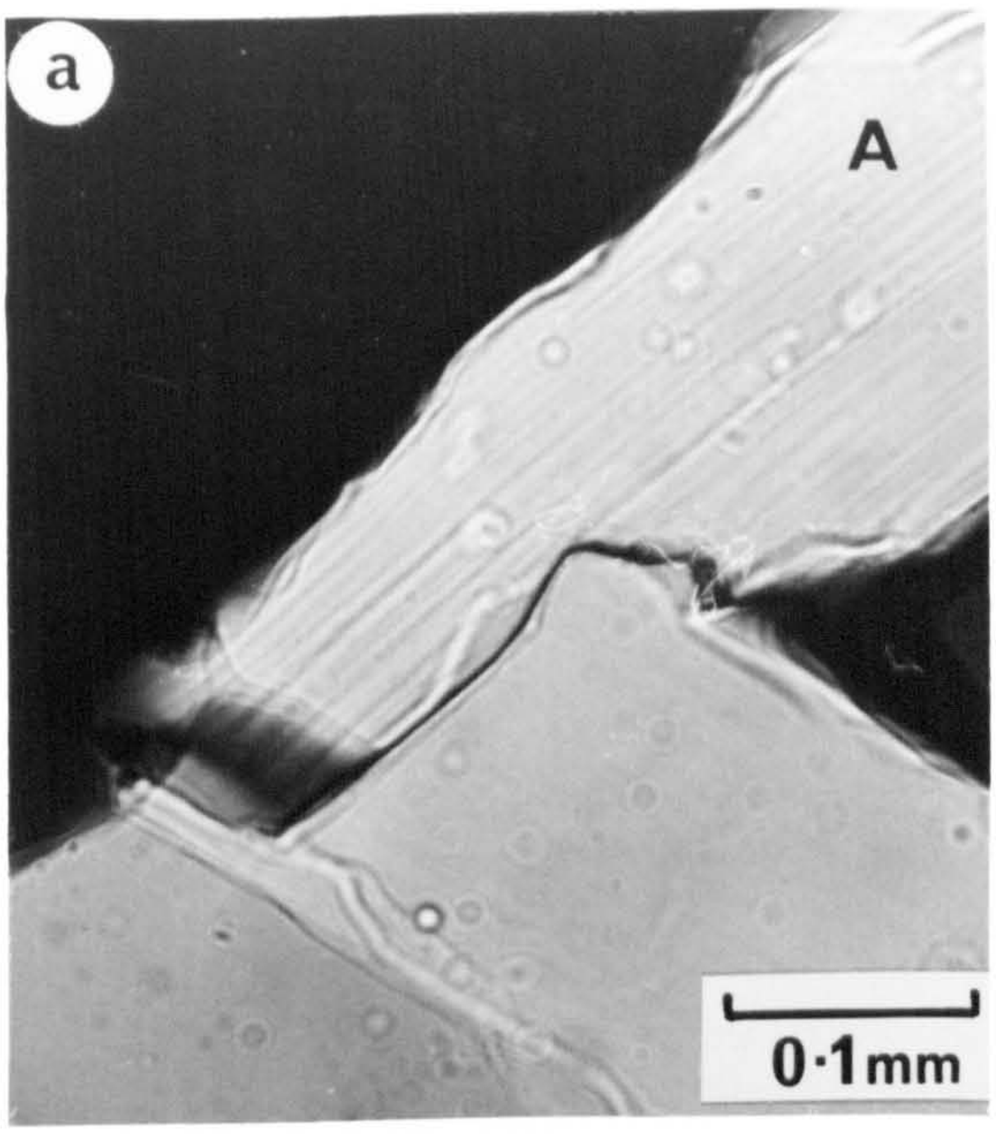
Some 40 tests were carried out as described above, generally at a strain rate of $\sim 10^{-4}$ sec^{-1}. The mechanical behaviour was dependent on the temperature, and there was a marked change in the mode of dynamic recrystallisation at ∿310K (H and W) or ∿320K (BDH). The results for the high and low temperature regimes will be presented separately.

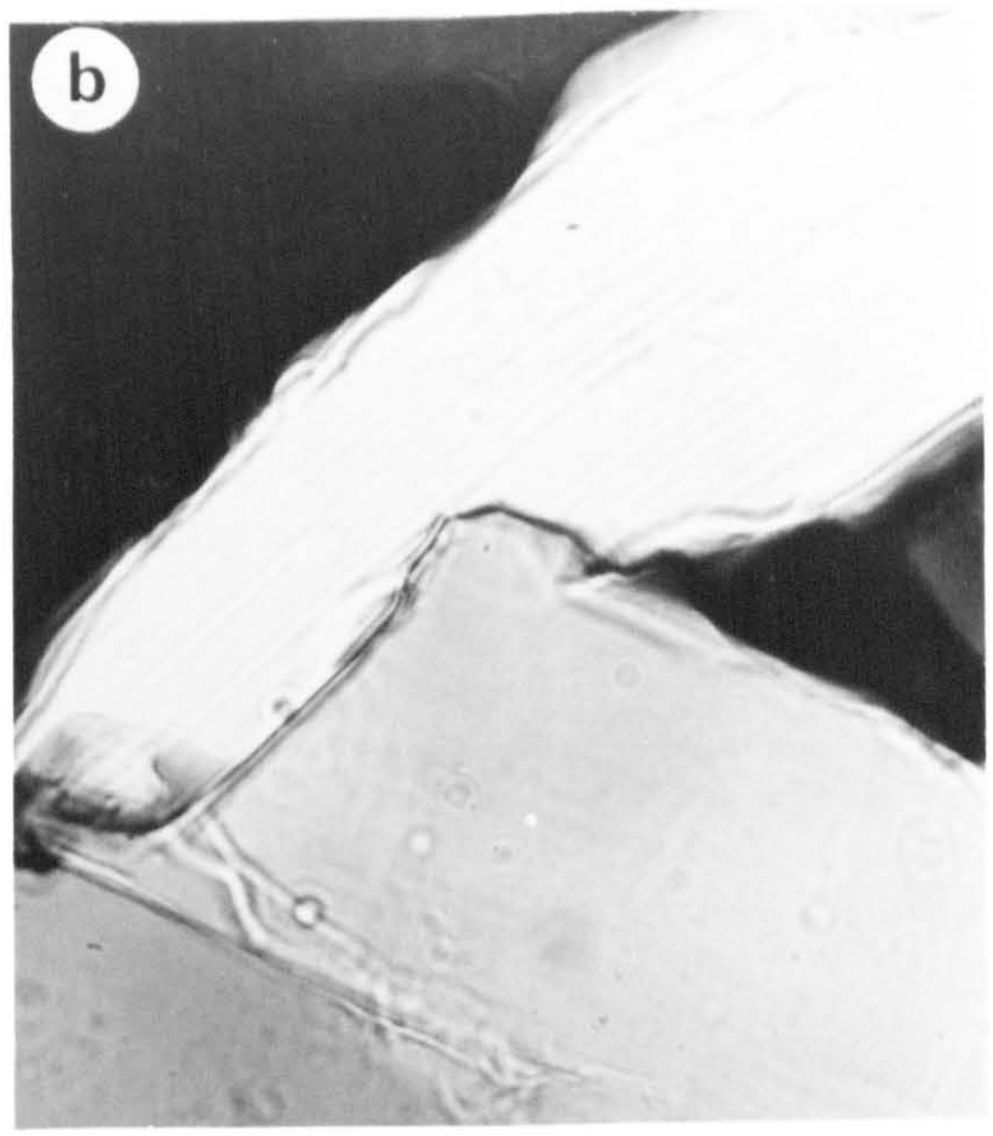
E.4.1. Low Temperature Tests

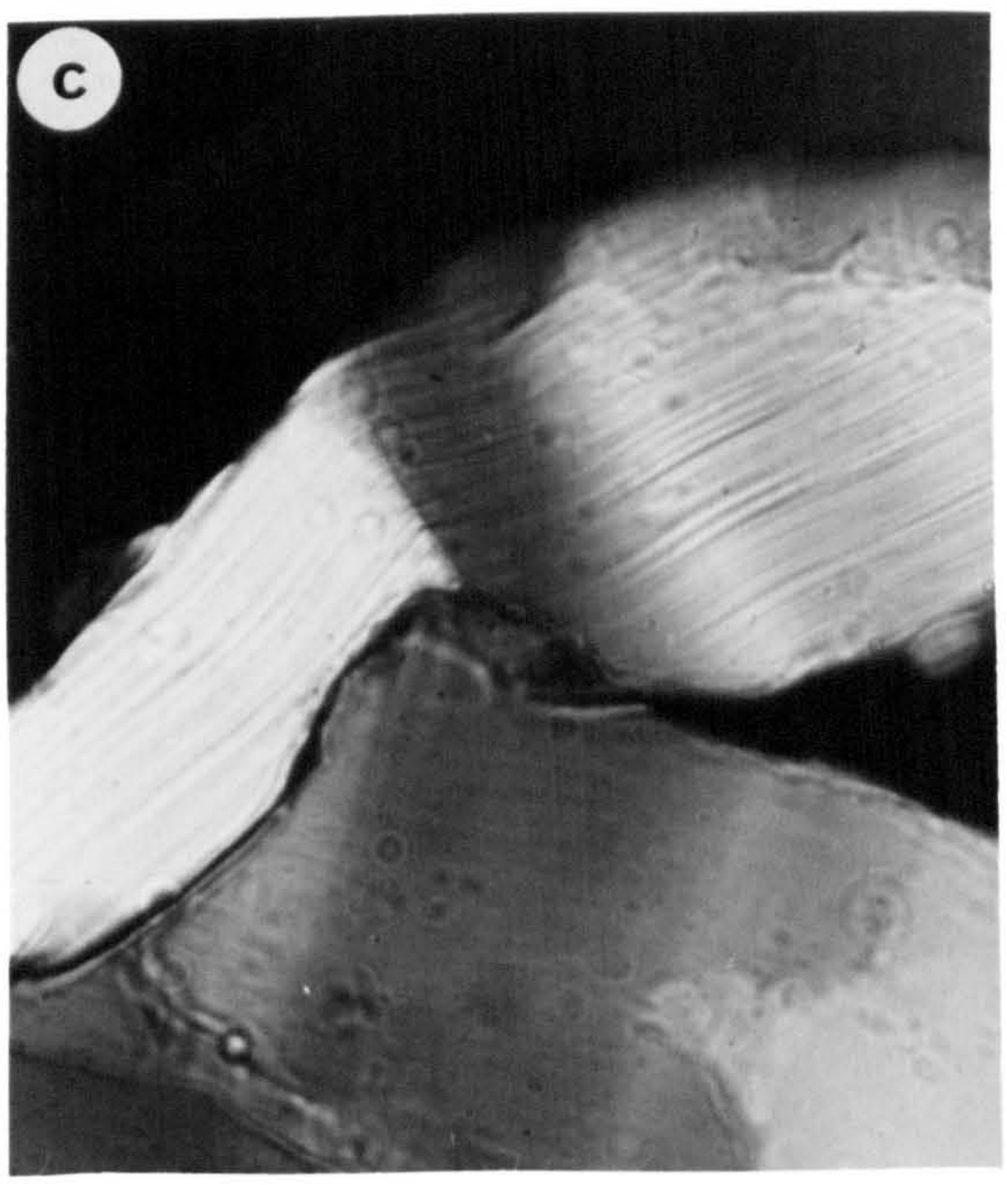
E.4.1.1. Slip

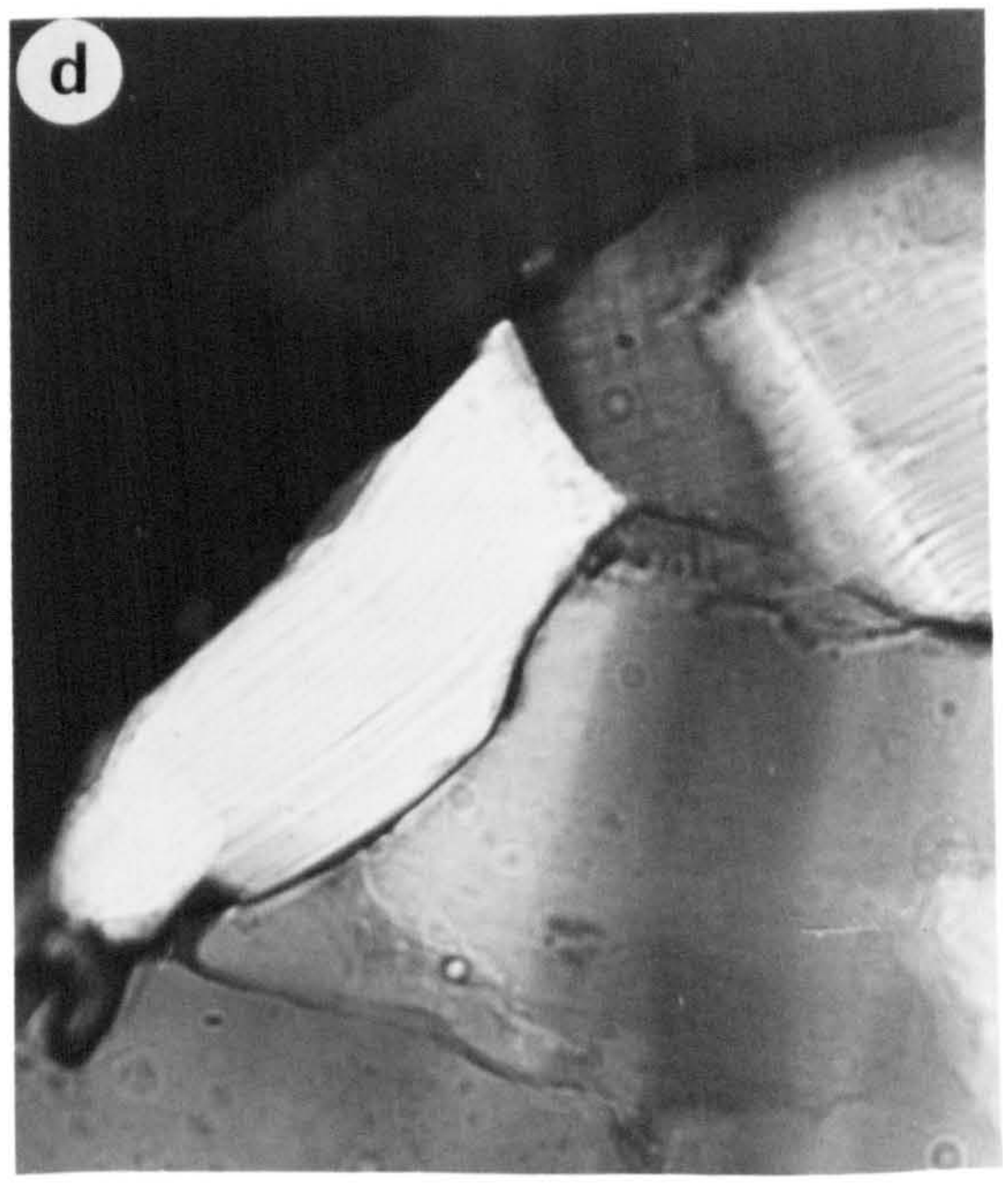
Slip was found to occur easily on only one plane of the camphor

Figure E2. Deformation sequence at 300K showing slip, lattice bending, kinking and dynamic recrystallisation in the kink bands. (compression axis vertical).


a
A
0·1mm


b


c


d


e


f

grains, and this was generally the first indication of plastic deformation (FigureE2a). Polarizing microscopy showed this to be the basal plane (0001). Although the full crystal structure of camphor has yet to be determined, it is probable that the benzene rings are aligned parallel to this plane, thus making it a preferred slip plane. Support for this model was obtained by universal stage microscopy which showed the camphor to be uniaxial negative. Other materials of similar crystal structure which are optically negative also have their planar molecules aligned in this way (Stoiber and Morse 1972).

E.4.1.2. Kinking

In grains oriented with the (0001) plane perpendicular to the specimen plane, e.g. grain A in Figure E2, if the local deformation was such as to cause bending of the slip planes (Figure E2b), then slip was frequently followed by the development of kink bands as shown in Figure E2. The process is gradual, lattice bending being followed by the formation of a sharp kink band (Figure E2c) starting at one edge of the grain and propagating in a direction approximately normal to the slip plane. Migration of the kink bands was seen to occur (Figure E2d) and continued deformation resulted in the formation of further kink bands (Figure E2d-f) to accommodate the strain. Although kinking was more likely to occur in those grains whose slip planes were at small angles to the compression axis, because of the locally inhomogeneous strain as illustrated by Figure E2, kinking occurred in grains of many orientations.

The above observations are similar to the results obtained for suitably oriented crystals of hexagonal metals (Hess and Barrett 1949) and are consistent with the proposed dislocation mechanism of kink formation, which is essentially one of glide polygonisation.

E.4.1.3. Deformation Twinning

Deformation twinning was frequently observed, particularly at high strain rates. It differed from kinking in that it was a rapid process. Part of a deformation sequence is shown in Figure E3, where twins of two orientations can be seen. The instability of the deformed microstructure did not allow the crystallography of the twins to be determined. Figure E4 shows a characteristic twinned microstructure. The parallel twins are in grains with their basal planes almost parallel to the specimen plane, and the chevron twins are in a thin grain with the slip plane perpendicular to the specimen and parallel to the axis of compression.





Figure E3. Deformation twinning at room temperature (Compression axis vertical)

This grain is thus poorly oriented for slip or kinking.

E.4.1.4. Dynamic Recrystallisation

During the later stages of the deformation, dynamic recrystallisation became increasingly important. The new grains were easily identifiable, being equiaxed, and much smaller than the original grains under all conditions of deformation. The grains originated at various sites in the specimen:-

(a) Kink band boundaries.

Although many kink bands remained stable and unchanged throughout the deformation, recrystallisation occurred at kink bands in regions of severe lattice bending, and this is clearly shown in Figure E2e,f.

(b) Twins.

Twinned regions invariably recrystallised, and an example is shown in Figure E5. The twin boundaries developed irregularities (5b) and eventually formed new grains (5c).

(c) Old Grain Boundaries.

Dynamic recrystallisation frequently originated at the old grain boundaries, and this was most clearly seen in specimens which initially had an equiaxed grain structure. Such a microstructure could be achieved by stopping deformation after a small strain and allowing the newly recrystallised grains to grow for ∿24 hrs. Figure E6 shows the subsequent development of the microstructure on straining. Dynamic recrystallisation at the grain boundaries results in a duplex microstructure similar to that found in metals or minerals undergoing dynamic recrystallisation (Roberts et al 1979, Burrows et al 1979).

In all the above cases, the mechanism of dynamic recrystallisation appears to involve the migration of previously existing boundaries. This is most clearly seen in the time lapse cine sequences in which the action is speeded up by a factor of between 50 and 100. Regions near grain boundaries can be seen to develop misorientation, the boundary then begins to bow out to form a new grain, in the manner envisaged for static recrystallisation of metals, see e.g. Doherty 1974.

The size of the dynamically recrystallised grains remained approximately constant during a test, and this was achieved by a process of continual recrystallisation in the zone of dynamic recrystallisation, the new grains regularly forming, and being consumed, the grain size being determined by the dynamic balance between the rates of nucleation and growth.

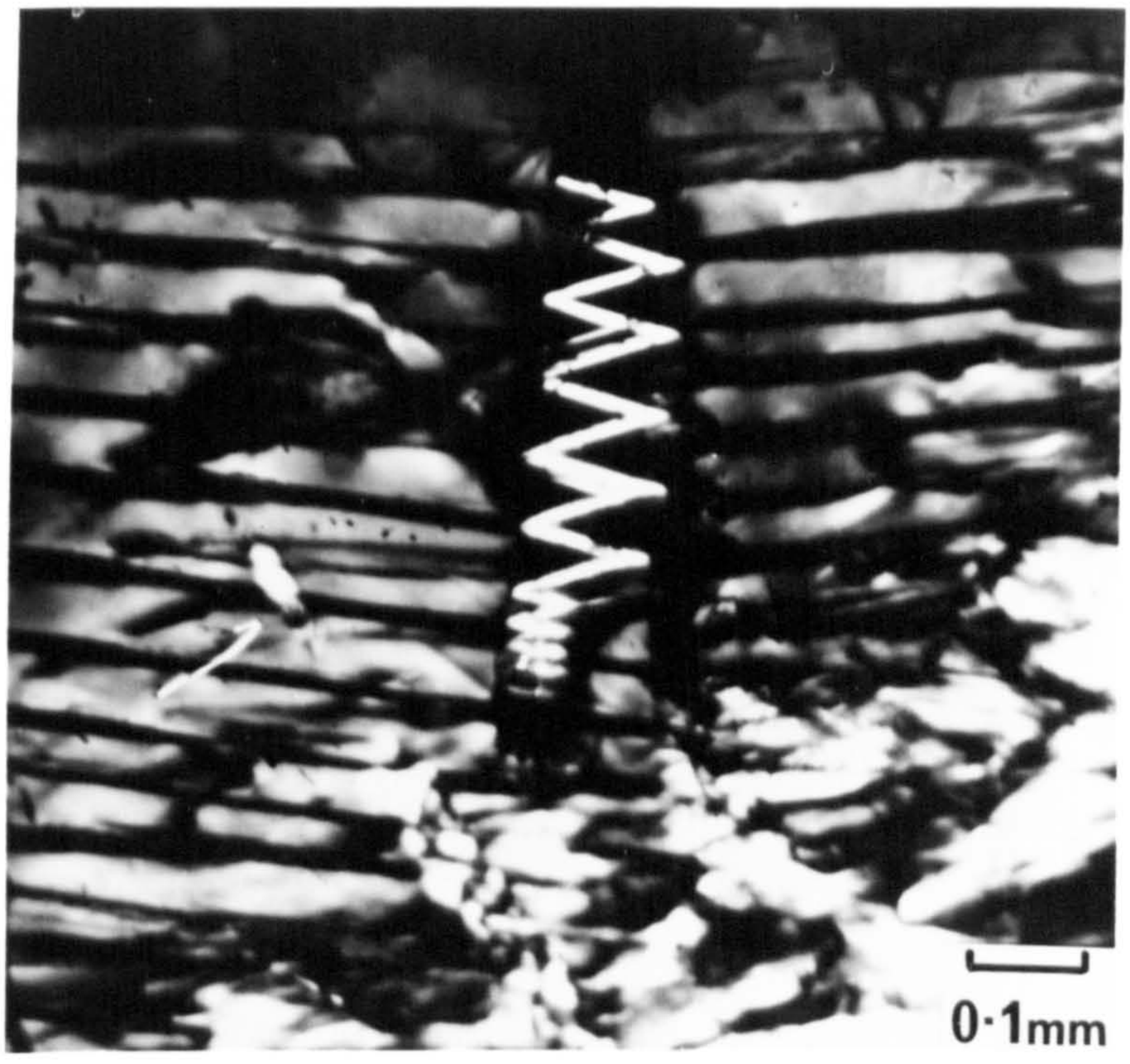
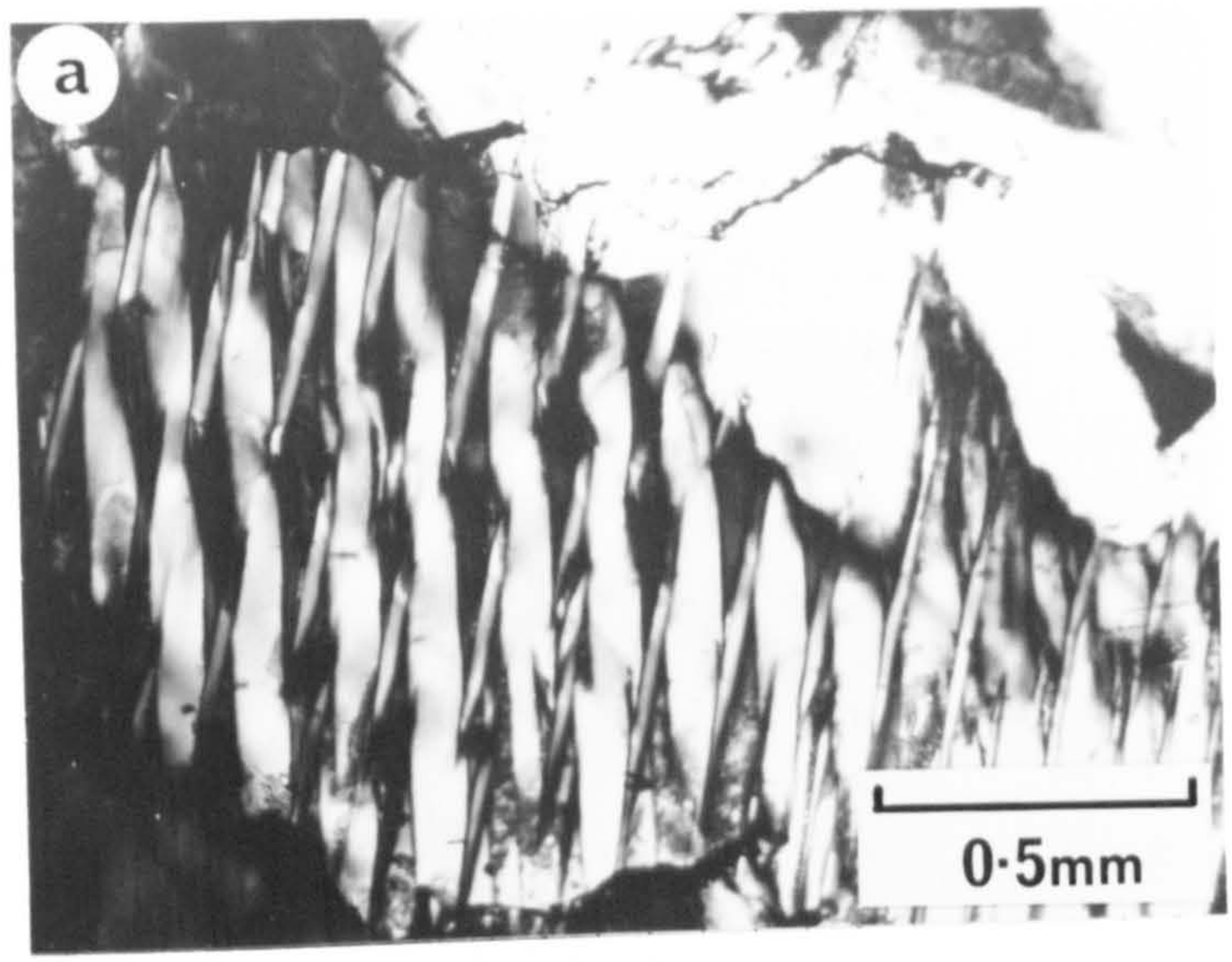


Figure E4. Twinned microstructure after deformation at 319K. The 'chevron' twins are in a narrow grain running from top to bottom of the micrograph. (Compression axis vertical)



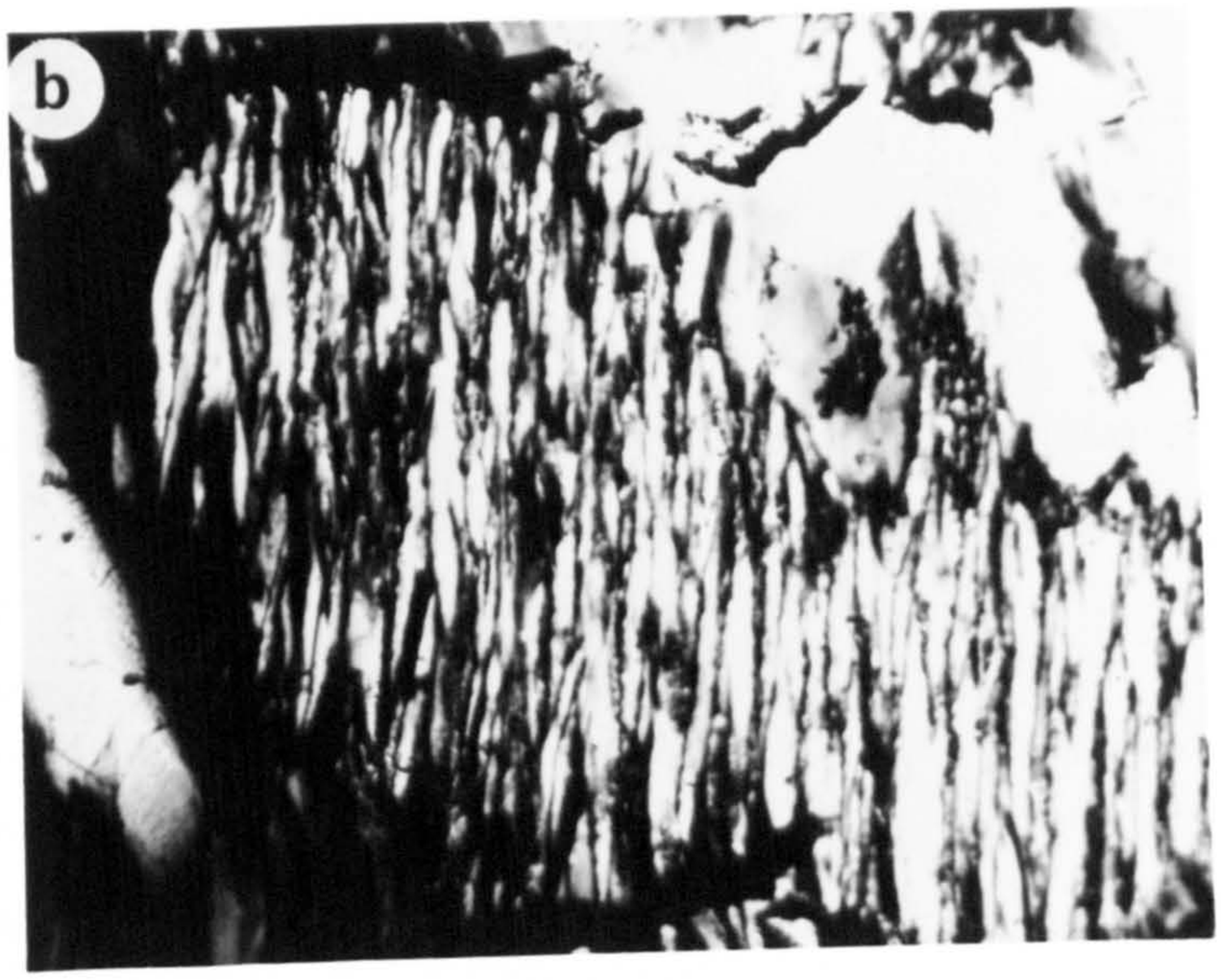




Figure E5. Dynamic recrystallisation originating at deformation twins during room temperature deformation. (Compression axis horizontal)

The size of the dynamically recrystallised grains was found to be dependent on the strain rate and temperature of deformation, being smallest for low temperatures and rapid strain rates as is found for metals (see e.g. Sellars 1978). Measurement of the grain size was difficult as the new grains were considerably smaller than the specimen thickness, thereby giving overlapping images. However, at room temperature the variation of grain size (d) with strain rate was found to be approximately as given below:-

$\dot{\varepsilon}$ 10^{-2} sec^{-1}	10^{-3} sec^{-1}	10^{-4} sec^{-1}
d 20 μm	30 μm	50 μm

E.4.1.5. The Development of Microstructure with Strain

The overall microstructure which developed in a specimen during straining was a result both of the individual mechanisms discussed above, and their inter-relationship. This depended on the size, shape and orientation of the grains as well as on the strain rate. A good example of the development of structure is shown in Figure E7. Grains A, B and C are oriented with the (0001) planes parallel to their lengths and perpendicular to the specimen plane. Grains D and E have their (0001) planes approximately parallel to the specimen plane. Although grain A is favourably oriented with respect to the compression axis for slip, this form of deformation is limited by contact with grain C, and kinks develop (Figure E7b). At the same time, grain B is riding into grain A, causing high local deformation, resulting in dynamic recrystallisation. (Figure E7b and c). At a later stage, grain E twins (Figure E7c) and begins to recrystallise. It can be seen that grain D has undergone little deformation and survives almost intact (Figure E7d). Similarly the regions of grain A which have undergone slip survive, whilst the inhomogeneously deformed parts of the grain recrystallise. The phenomenon of relic old grains remaining in a matrix of dynamically recrystallised grains even after high strains is commonly observed in minerals (Nicolas and Poirier 1976) and has also been shown in the preceding chapters to be common in magnesium.

Thus, because of the anisotropic deformation of this material, an inhomogeneous microstructure is formed, particularly in specimens with a non-equiaxed initial grain structure. At high strains the deformation becomes concentrated in bands of dynamically recrystallised grains at angles of $\sim 30\text{-}50^{o}$ to the compression axis which spread across the specimen to form shear zones. These are discussed in more detail in Chapter 5.

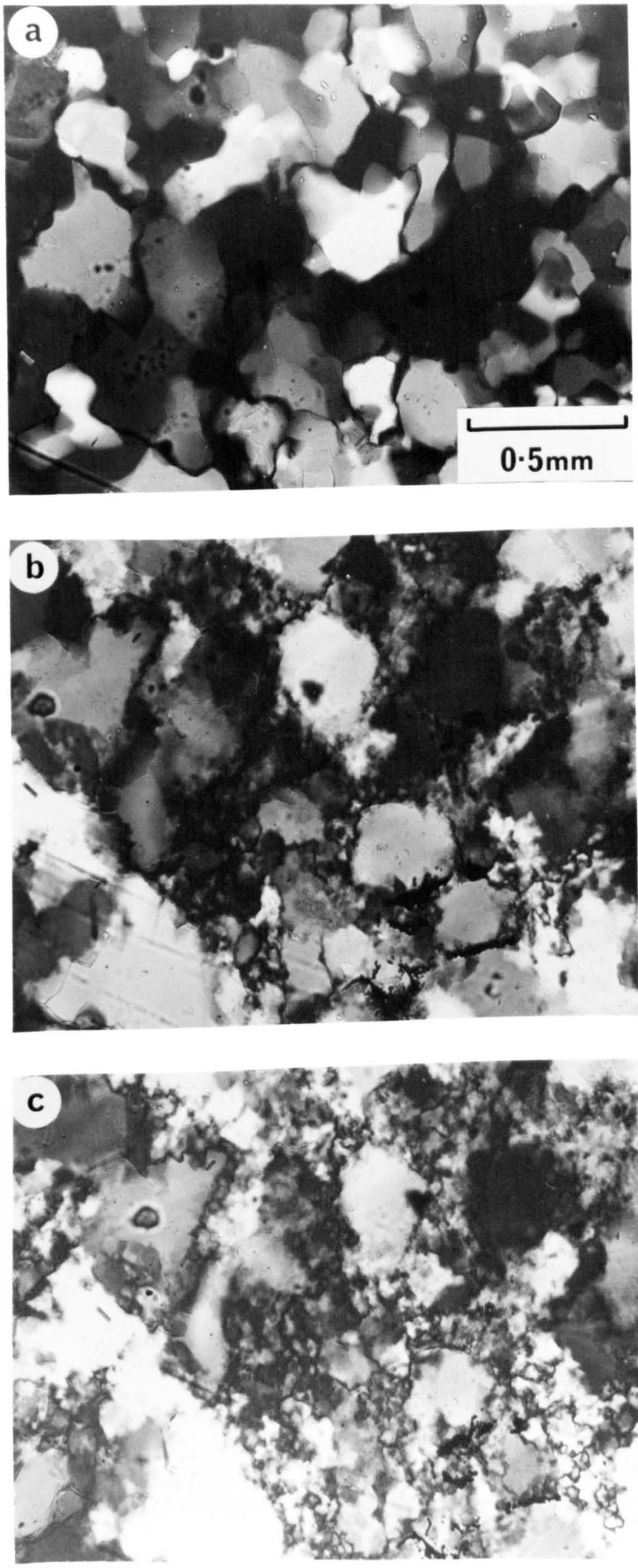


Figure E6. Dynamic recrystallisation at the old grain boundaries during deformation at 310K in a specimen with initially equiaxed grains. (Compression axis horizontal)

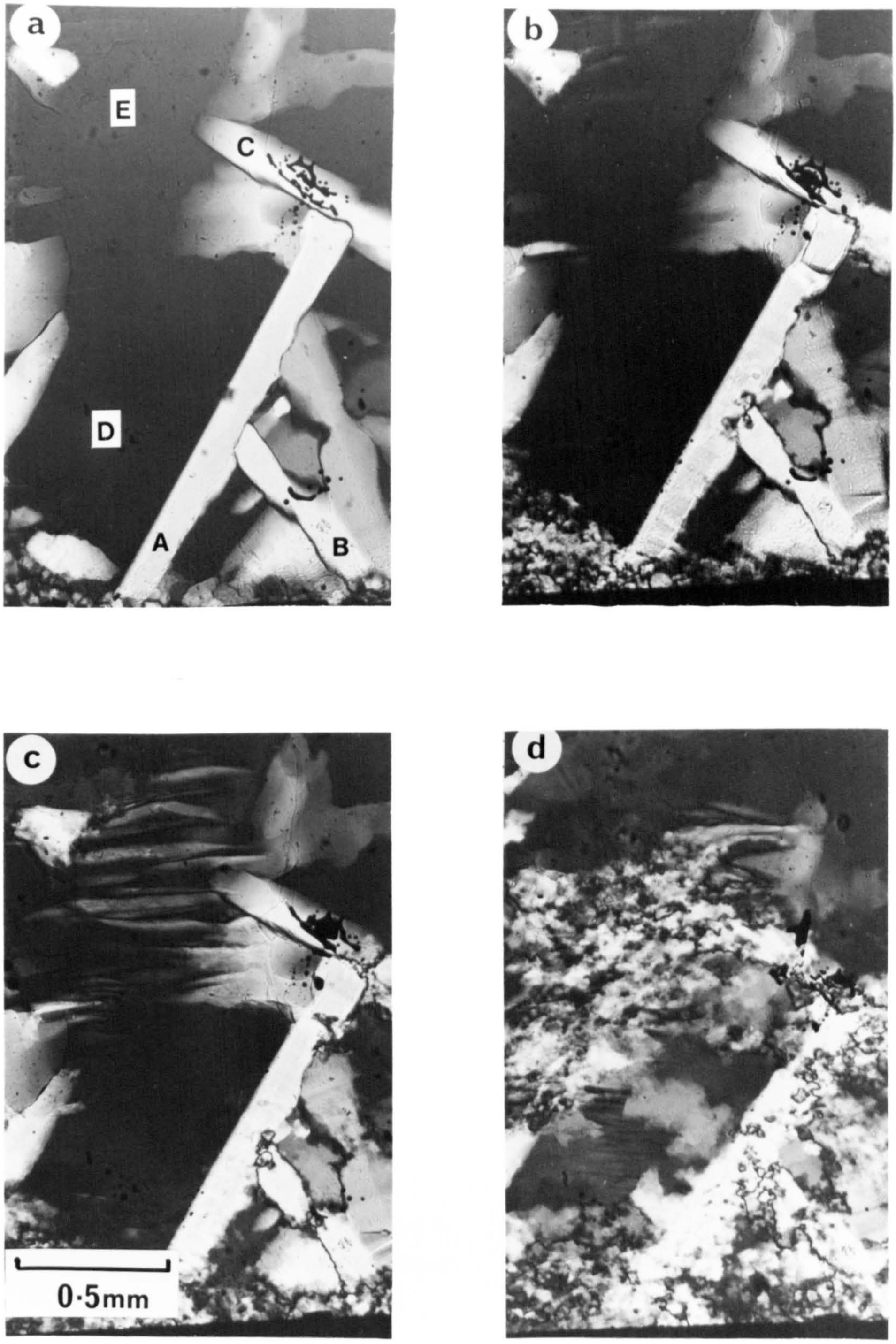


Figure E7. Development of microstructure with increasing strain at 310K. (Compression axis vertical).

E.4.2. High Temperature Tests

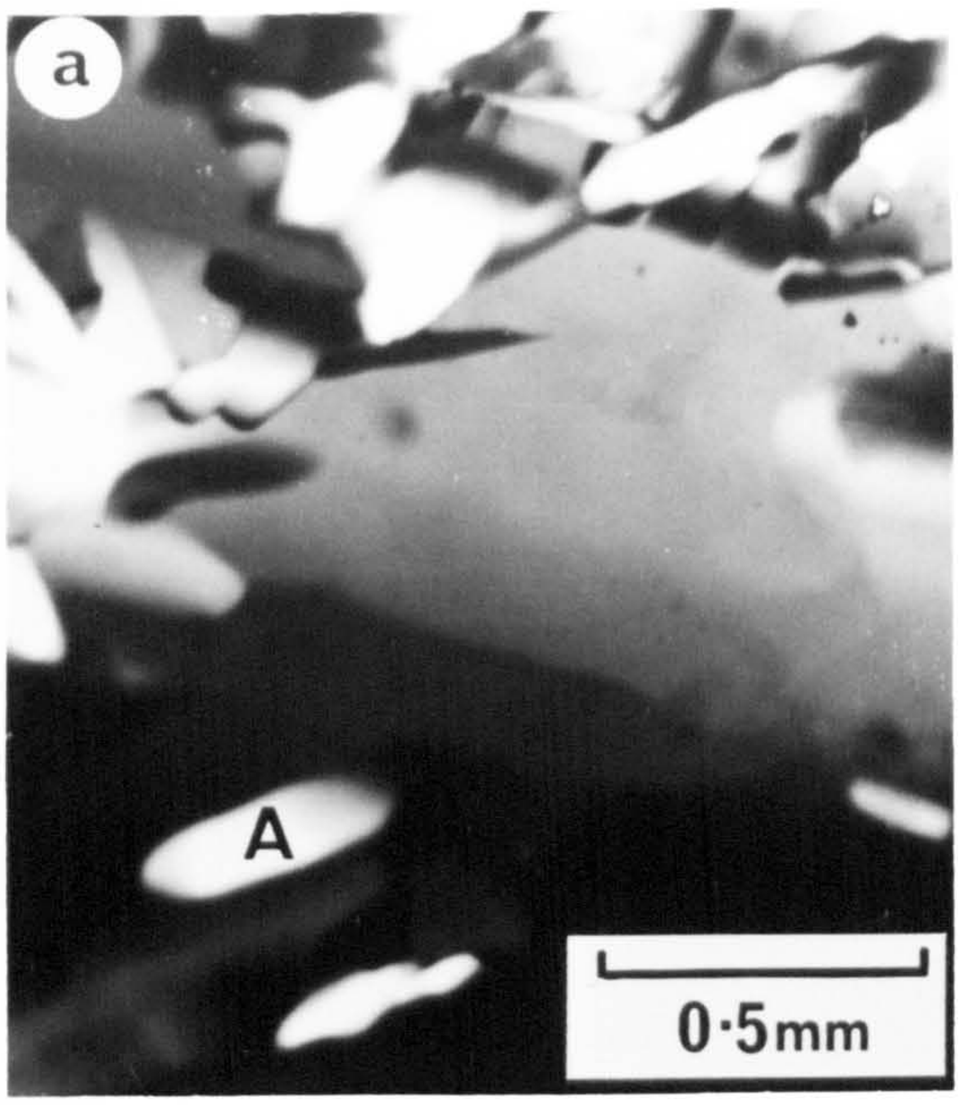
As discussed earlier, above ∿310-320K there was a marked change in the mechanism of dynamic recrystallisation, and the high temperature behaviour is shown in Figure E8. At an early stage of the deformation, certain grains, particularly those favourably oriented for slip (A and B) grew rapidly. In many cases the regions into which these grains grew appeared at least initially, to be undeformed, e.g. grain C. The driving force for this migration is not clear and would appear to be different to that of strain induced boundary migration such as is found at lower temperatures. It is possible that elastic anisotropy in the material leads to stress induced boundary migration. Kamb (1959) proposed such a mechanism (piezocrystallisation) to account for textural development in minerals, but as discussed by Nicolas and Poirier (1976) there has been, as yet, no experimental support for this model. An alternative approach is to consider the effect of the anisotropy of plastic deformation as follows. Consider a grain with one slip plane, favourably oriented for slip with respect to the compression axis (Figure E9), embedded in another grain unfavourably oriented for slip. On applying a compressive stress σ, the large grain will deform elastically, with stored energy/unit volume $\sim\sigma^2/2E$, whilst the small grain will deform plastically on one slip system storing negligible energy. Thus there will be a driving force for the small grain to grow, although this creates interfacial energy γ/unit area, and for the 2-dimensional core of Figure E9, growth will occur if

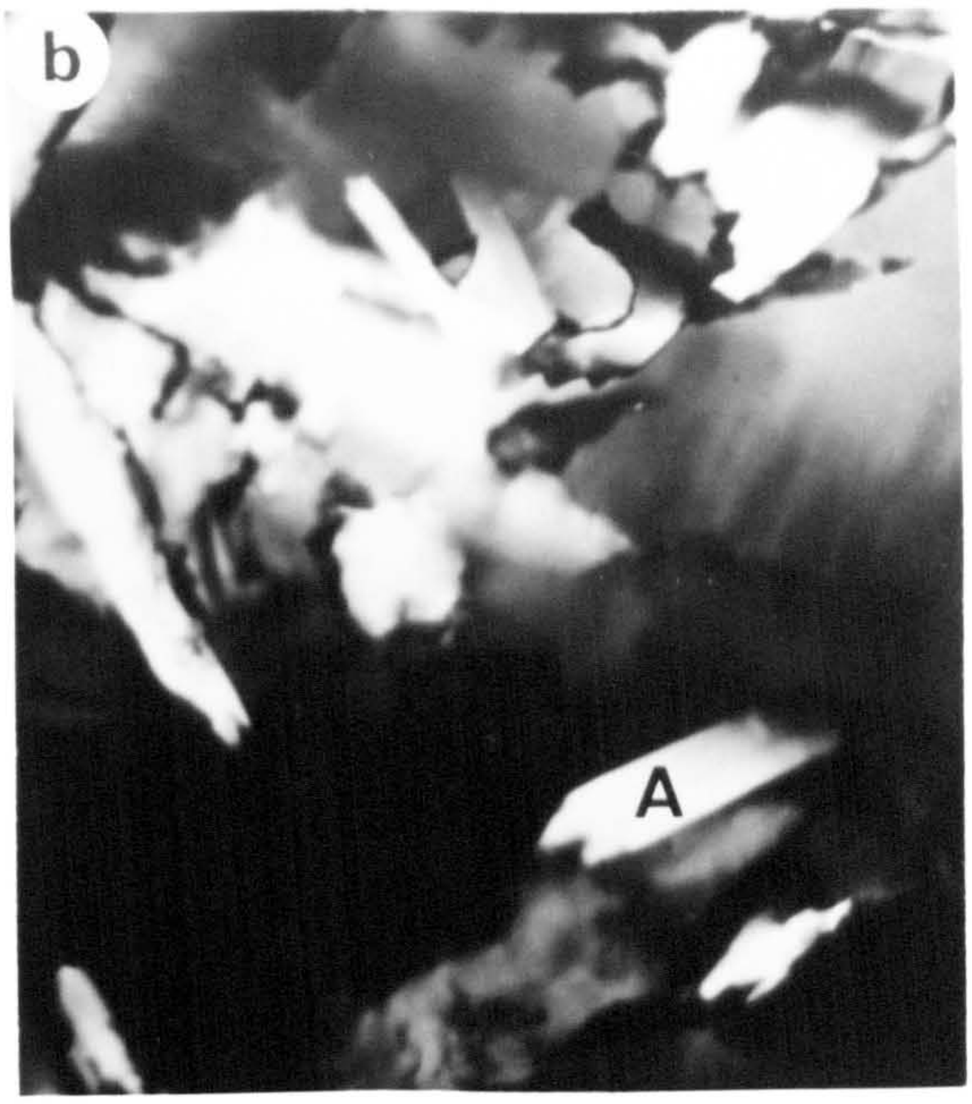
$$\sigma \lesssim \sqrt{\frac{4E\gamma}{w}}$$

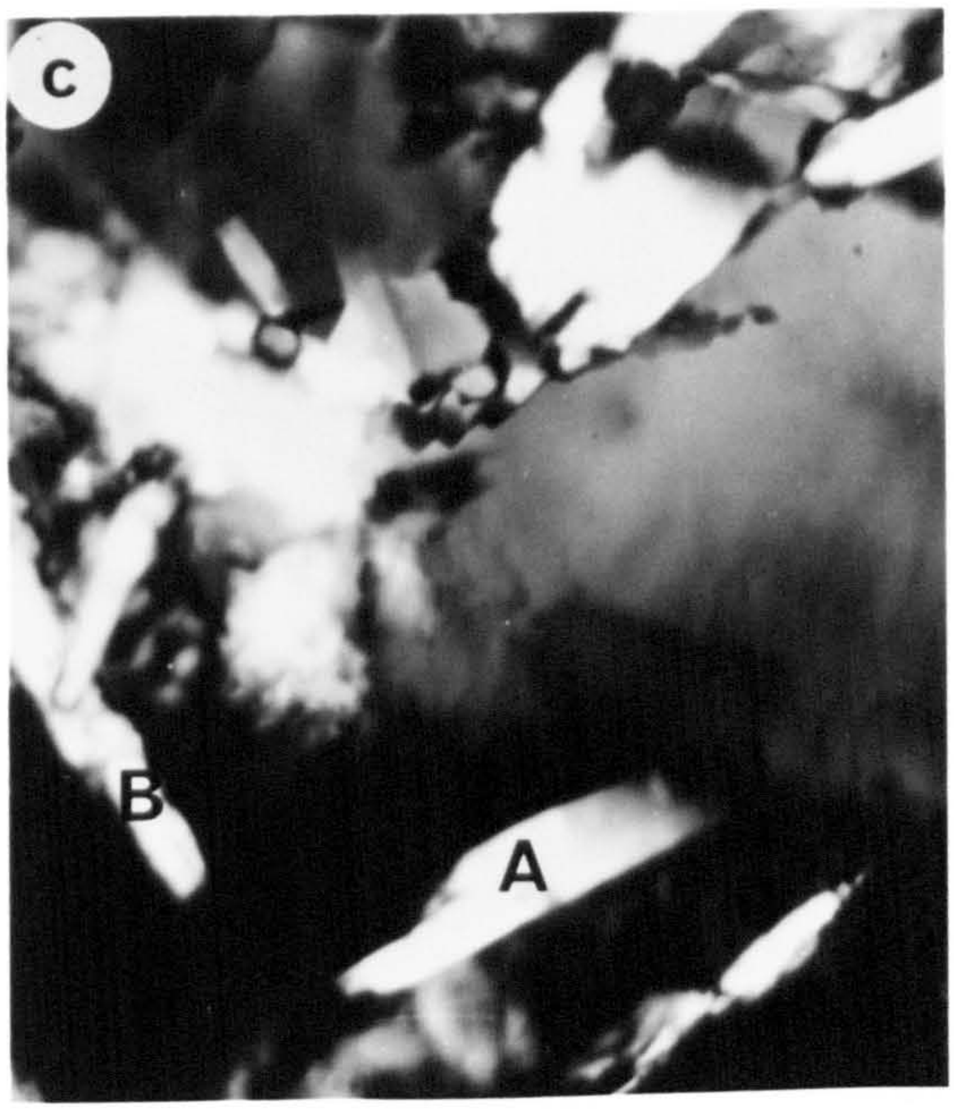
This simple calculation neglects the strain incompatibility at the ends of the grain, but at elevated temperatures these can be accommodated by local diffusion. Thus, if the crystal has limited systems of easy slip, and has a low grain boundary energy on at least one plane, as would seem to be the case for camphor, then this type of mechanism could account for the observed phenomenon.

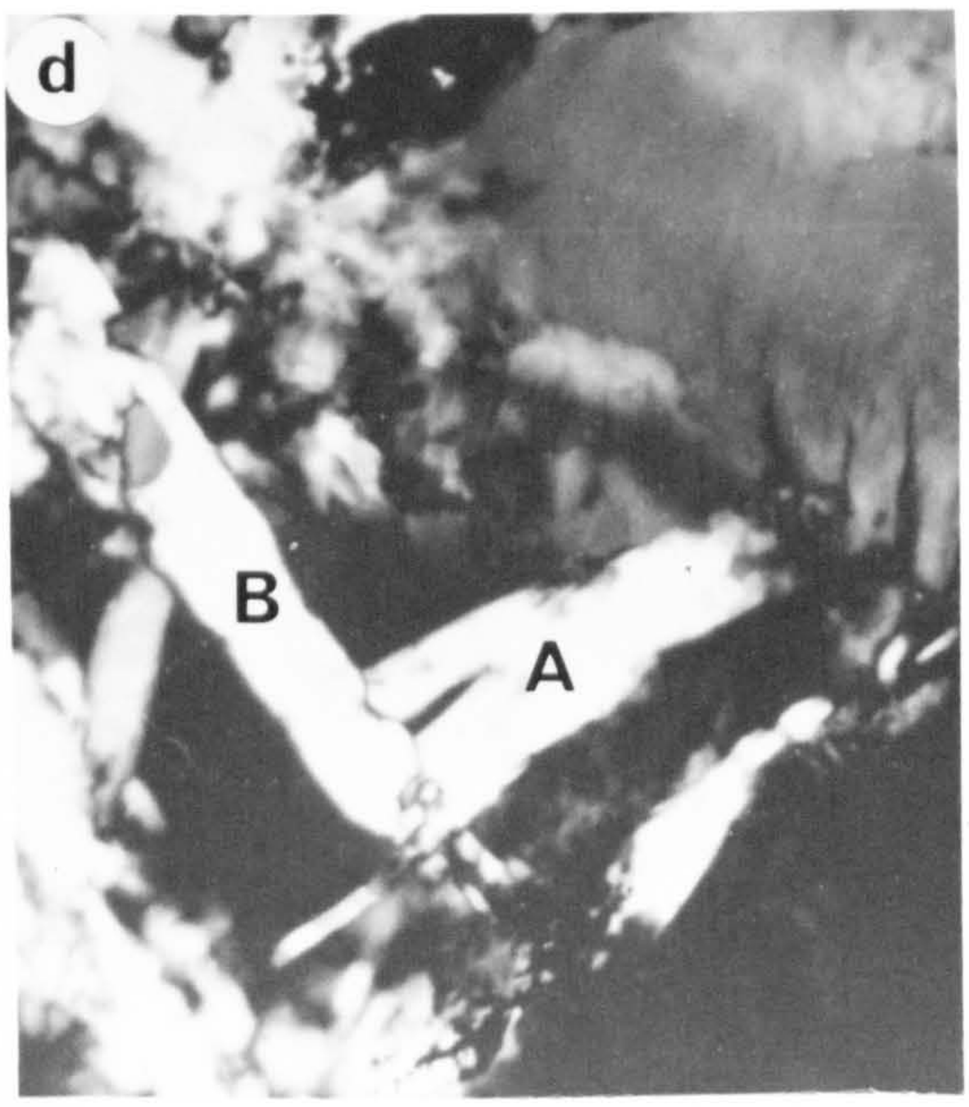
The elongated grains formed as a result of this process, are seen to deform readily, and where two such sets of grains interact, e.g. Figure E8d-e, smaller recrystallised grains form, and some of these may in turn elongate. In other regions of the specimen, recrystallisation occurs by the same means as at lower temperatures, although there is a tendency for those new grains with favourable slip orientations to elongate as described above.

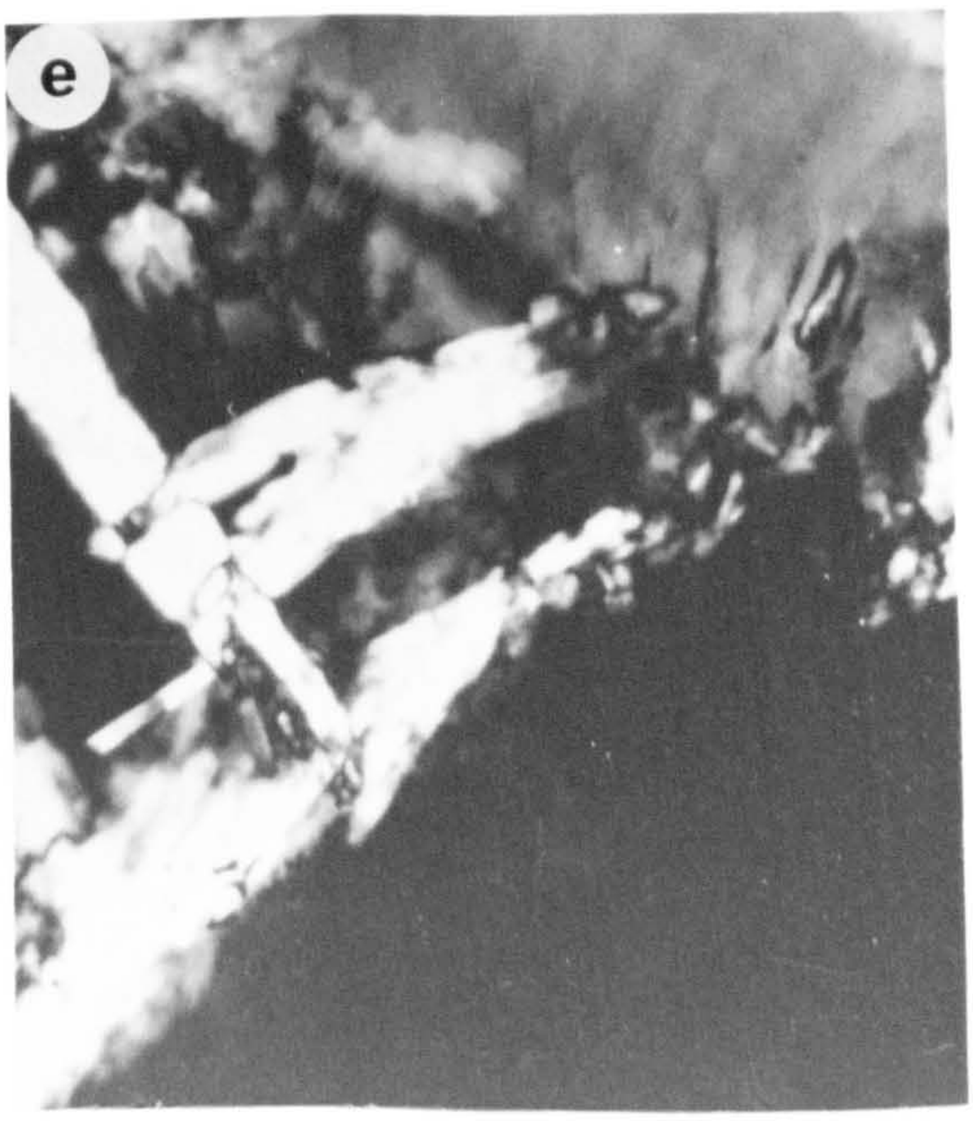
Figure E8. Deformation in the high temperature regime at 325K showing growth of elongated grains (compression axis vertical).


a
A
0·5mm


b
A


c
B
A


d
B
A


e

Thus, either by the growth of favourably oriented old grains, or by the selected growth of dynamically recrystallised grains, a crystallographic texture develops in the specimen, with the (0001) planes being parallel to the planes of high shear stress. This is an example of the 'oriented growth' method of texture formation long discussed by metallurgists (see e.g. Cahn 1970).

Further deformation is then confined to the textured regions which then form shear zones extending through the specimen. The formation of elongated grains during dynamic recrystallisation has not been reported for metals, but there is evidence of somewhat similar microstructures in quartz mylonites (Ribbon quartz) (Boullier and Bouchez 1978).

E.5. CONCLUSIONS

The deformation of polycrystalline specimens of rhombohedral camphor has been shown to involve processes of deformation and dynamic recrystallisation such as are found in metals and minerals deformed at elevated temperatures. There are many points of similarity between the behaviour of camphor and metals and minerals of low symmetry, and although the use of such analogues must be treated with caution, the ability to study the deformation processes and the development of microstructure directly is valuable. Not only may events which would not be revealed by conventional post-deformation examinations (e.g. the continuous renewal of grains in regions of dynamic recrystallisation) be detected, but also, direct observations may by providing clues, stimulate new ways of interpreting the very complex microstructure of naturally deformed minerals.

REFERENCES

Boullier, A. and Bouchez, J. (1978) Bull. Soc. Geol. France 7 253.

Burrows, S.E., Humphreys, F.J. and White, S.H. (1979) Bull. Mineral. 102 75.

Cahn, R.W. (1970) in "Physical Metallurgy" (ed. R.W. Cahn) 2nd ed. North Holland, Amsterdam. p1129.

Doherty, R.D. (1974) Met. Sci. J. 8 132

Dunning, W.J. (1961) J. Phys. Chem. Solids, 18 21.

Hawthorne, H.M. and Sherwood, J.N. (1970) Trans. Faraday Soc. 66 1793.

Hess, J.B. and Barrett, C.S. (1949) Trans. A.I.M.E. 185 599.

Hunt, J.D. and Jackson, K.A.(1966) Trans. Met. Soc. AIME. 236 843.

Kamb. W.B. (1959) J. Geol. 67 153.

Means. W.D. (1977) Earth and Plan. Sci. Letters, 35 169.

References (cont.)

Nicolas, A. and Poirier, J.P. (1976) "Crystalline Plasticity and Solid state flow in metamorphic rocks", Wiley.

Powles, J.G. (1952) J. Chem. Phys. 20 1648.

Roberts, W., Boden,H. and Ahlblom, B. (1979) Metal Science, 13 195.

Sellars, C.M.(1978) in "Creep of Engineering Materials and of the Earth". (eds. A. Kelly, G.W. Greenwood and A.H. Cook) Royal Soc. Also in Phil. Trans. Royal Soc. A. 288

Simpson, C.J., Aust, K.T. and Winegard, W.C. (1969) Scripta. Met. 3 171.

Stoiber, R.E. and Morse, S.A. (1972) "Microscopic identification of crystals", Ronals Press, New York.

Timmermans, J. (1961) J. Phys. Chem. Solids, 18 1.

Urai, J., Humphreys, F.J. and Burrows, S.E. (1980) Paper and Cine film to be presented at the International Conference on "The Effect of Deformation on Rocks", Gottingen. also J. Materials Science (in press).

Wilson, C.J. (1968) Unpublished Cine Film.

Yager, A. and Morgan, S.O. (1935) J. Am. Chem. Soc., 57 2071.